

EARLY AVIAN EVOLUTION

EDITED BY: Jingmai Kathleen O'Connor, Corwin Sullivan and Daniel J. Field

PUBLISHED IN: *Frontiers in Earth Science* and *Frontiers in Ecology and Evolution*



frontiers

Frontiers eBook Copyright Statement

The copyright in the text of individual articles in this eBook is the property of their respective authors or their respective institutions or funders. The copyright in graphics and images within each article may be subject to copyright of other parties. In both cases this is subject to a license granted to Frontiers.

The compilation of articles constituting this eBook is the property of Frontiers.

Each article within this eBook, and the eBook itself, are published under the most recent version of the Creative Commons CC-BY licence.

The version current at the date of publication of this eBook is CC-BY 4.0. If the CC-BY licence is updated, the licence granted by Frontiers is automatically updated to the new version.

When exercising any right under the CC-BY licence, Frontiers must be attributed as the original publisher of the article or eBook, as applicable.

Authors have the responsibility of ensuring that any graphics or other materials which are the property of others may be included in the CC-BY licence, but this should be checked before relying on the CC-BY licence to reproduce those materials. Any copyright notices relating to those materials must be complied with.

Copyright and source acknowledgement notices may not be removed and must be displayed in any copy, derivative work or partial copy which includes the elements in question.

All copyright, and all rights therein, are protected by national and international copyright laws. The above represents a summary only. For further information please read Frontiers' Conditions for Website Use and Copyright Statement, and the applicable CC-BY licence.

ISSN 1664-8714

ISBN 978-2-88971-302-8

DOI 10.3389/978-2-88971-302-8

About Frontiers

Frontiers is more than just an open-access publisher of scholarly articles: it is a pioneering approach to the world of academia, radically improving the way scholarly research is managed. The grand vision of Frontiers is a world where all people have an equal opportunity to seek, share and generate knowledge. Frontiers provides immediate and permanent online open access to all its publications, but this alone is not enough to realize our grand goals.

Frontiers Journal Series

The Frontiers Journal Series is a multi-tier and interdisciplinary set of open-access, online journals, promising a paradigm shift from the current review, selection and dissemination processes in academic publishing. All Frontiers journals are driven by researchers for researchers; therefore, they constitute a service to the scholarly community. At the same time, the Frontiers Journal Series operates on a revolutionary invention, the tiered publishing system, initially addressing specific communities of scholars, and gradually climbing up to broader public understanding, thus serving the interests of the lay society, too.

Dedication to Quality

Each Frontiers article is a landmark of the highest quality, thanks to genuinely collaborative interactions between authors and review editors, who include some of the world's best academicians. Research must be certified by peers before entering a stream of knowledge that may eventually reach the public - and shape society; therefore, Frontiers only applies the most rigorous and unbiased reviews.

Frontiers revolutionizes research publishing by freely delivering the most outstanding research, evaluated with no bias from both the academic and social point of view. By applying the most advanced information technologies, Frontiers is catapulting scholarly publishing into a new generation.

What are Frontiers Research Topics?

Frontiers Research Topics are very popular trademarks of the Frontiers Journals Series: they are collections of at least ten articles, all centered on a particular subject. With their unique mix of varied contributions from Original Research to Review Articles, Frontiers Research Topics unify the most influential researchers, the latest key findings and historical advances in a hot research area! Find out more on how to host your own Frontiers Research Topic or contribute to one as an author by contacting the Frontiers Editorial Office: frontiersin.org/about/contact

EARLY AVIAN EVOLUTION

Topic Editors:

Jingmai Kathleen O'Connor, Field Museum of Natural History, United States

Corwin Sullivan, University of Alberta, Canada

Daniel J. Field, University of Cambridge, United Kingdom

Citation: O'Connor, J. K., Sullivan, C., Field, D. J., eds. (2021). Early Avian Evolution. Lausanne: Frontiers Media SA. doi: 10.3389/978-2-88971-302-8

Table of Contents

- 05 Editorial: Early Avian Evolution**
Jingmai Kathleen O'Connor, Daniel J. Field and Corwin Sullivan
- 08 A New Enantiornithine (Aves) Preserved in Mid-Cretaceous Burmese Amber Contributes to Growing Diversity of Cretaceous Plumage Patterns**
Lida Xing, Jingmai K. O'Connor, Kecheng Niu, Pierre Cockx, Huijuan Mai and Ryan C. McKellar
- 19 New Information on the Keratinous Beak of Confuciusornis (Aves: Pygostylia) From Two New Specimens**
Xiaoting Zheng, Jingmai O'Connor, Yan Wang, Xiaoli Wang, Yin Xuwei, Xiaomei Zhang and Zhonghe Zhou
- 33 An Exceptionally Preserved Specimen From the Green River Formation Elucidates Complex Phenotypic Evolution in Gruiformes and Charadriiformes**
Grace Musser and Julia A. Clarke
- 51 Erratum: An Exceptionally Preserved Specimen From the Green River Formation Elucidates Complex Phenotypic Evolution in Gruiformes and Charadriiformes**
Frontiers Production Office
- 52 Multiple Functional Solutions During Flightless to Flight-Capable Transitions**
Ashley M. Heers, Stephanie L. Varghese, Leila K. Hatier and Jeremiah J. Cabrera
- 69 Investigating Possible Gastroliths in a Referred Specimen of Bohaiornis guoi (Aves: Enantiornithes)**
Shumin Liu, Zhiheng Li, Alida M. Bailleul, Min Wang and Jingmai O'Connor
- 82 Intraskkeletal Osteohistovariability Reveals Complex Growth Strategies in a Late Cretaceous Enantiornithine**
Jessie Atterholt, Ashley W. Poust, Gregory M. Erickson and Jingmai K. O'Connor
- 98 Osteohistology of the Scapulocoracoid of Confuciusornis and Preliminary Analysis of the Shoulder Joint in Aves**
Qian Wu, Alida M. Bailleul, Zhiheng Li, Jingmai O'Connor and Zhonghe Zhou
- 114 A Juvenile Specimen of Archaeorhynchus Sheds New Light on the Ontogeny of Basal Euornithines**
Christian Foth, Shiyang Wang, Frederik Spindler, Youhai Lin and Rui Yang
- 133 The True Identity of Putative Tooth Alveoli in a Cenozoic Crown Bird, the Gastornithid Omorhamphus**
Antoine Louchart, Bhart-Anjan Bhullar, Ségolène Riamon and Daniel J. Field
- 143 Comments on the Morphology of Basal Paravian Shoulder Girdle: New Data Based on Unenlagiid Theropods and Paleognath Birds**
Fernando E. Novas, Matías J. Motta, Federico L. Agnolín, Sebastián Rozadilla, Gastón E. Lo Coco and Federico Brissón Egli

157 Exploring the Ecomorphology of Two Cretaceous Enantiornithines With Unique Pedal Morphology

Alexander D. Clark and Jingmai K. O'Connor

176 Quantitative Analysis of Morphometric Data of Pre-modern Birds: Phylogenetic Versus Ecological Signal

Alyssa Bell, Jesús Marugán-Lobón, Guillermo Navalón, Sergio M. Nebreda, John DiGiuldo and Luis M. Chiappe



Editorial: Early Avian Evolution

Jingmai Kathleen O'Connor^{1,2*}, Daniel J. Field^{3,4} and Corwin Sullivan^{5,6}

¹Field Museum of Natural History, Chicago, IL, United States, ²Institute of Vertebrate Paleontology and Paleoanthropology, Chinese Academy of Sciences, Beijing, China, ³Department of Earth Sciences, University of Cambridge, Cambridge, United Kingdom, ⁴Museum of Zoology, University of Cambridge, Cambridge, United Kingdom, ⁵Department of Biological Sciences, University of Alberta, Edmonton, AB, Canada, ⁶Philip J. Currie Dinosaur Museum, Wembley, AB, Canada

Keywords: Aves, stem birds, paleornithology, evolution, avian flight

Editorial on the Research Topic

Early Avian Evolution

The study of early avian evolution—how birds evolved from dinosaurs and radiated into the most diverse group of amniotes on the planet—is one of the most dynamic areas of research in paleontology, fueled not only by the rapid rate of discovery of new specimens (see Foth et al.; Musser and Clarke; and Xing et al.) and sheer volume of available material (see Zheng et al.) but also by the innovative application of new analytical methods to key evolutionary questions (see Heers et al.; Liu et al.). Also critical to our understanding is the exceptional level of preservation of many Mesozoic and early Cenozoic bird fossils, which not uncommonly preserve soft tissues and other indicators that may provide key insights into the biology of these organisms (see articles by Clark and O'Connor; Foth et al.; Xing et al.; Zheng et al.). In putting together this research topic, our aim was to further expand our understanding of early avian evolution by gathering a body of work highlighting the diversity of research currently being undertaken in this area. As such, articles published in this topic have augmented our understanding of a variety of important areas related to early avian evolution, including the recognition of new taxonomic diversity (see Clark and O'Connor and Musser and Clarke), insights into the evolution of key avian traits such as flight (Heers et al.) and a toothless beak (see Louchart et al. and Zheng et al.), and the piecemeal evolution of crown avian biology (see Atterholt et al. and Heers et al.).

Fossil specimens examined in this research topic come from Lagerstätten around the world, sampling strata that range in age from Early Cretaceous to early Eocene and thus capture over 70 million years of avian evolutionary change. The contributing researchers are globally distributed, hailing from Argentina, Canada, China, France, Germany, Switzerland, the United Kingdom and the United States. Lead authors represent the complete spectrum of career stages, from Master's and PhD students to well-established scientists. This speaks to the importance of multiple forms of diversity in science and perhaps especially in paleontology, in which we rely on a comprehensive view of the global fossil record in order to understand broad evolutionary questions. The immense benefit of bringing together young minds from diverse backgrounds clearly shines throughout the entirety of this research topic.

Two articles in this research topic address the origins of the unique, rapid development that characterizes modern birds. Atterholt et al. use histology to document a previously unrecognized level of developmental complexity in Late Cretaceous enantiornithines, and Foth et al. describe the first known Early Cretaceous ornithuromorph representing an early ontogenetic stage, revealing in the process a primitive pattern of development comparable to that observed in other basal, non-neornithine avian lineages and non-avian dinosaurs. While the vast majority of living birds grow to adult size rapidly, well within the first year of growth and in some cases within mere weeks (Lovette and Fitzpatrick, 2004), non-neornithine birds grew slowly, fledging well before skeletal maturity in a manner similar to non-volant theropods (Chinsamy et al., 2020). Accordingly, ontogimorphs may have occupied distinct ecological niches at different ontogenetic stages. Although it seems clear that

OPEN ACCESS

Edited and reviewed by:

André Jasper,
Universidade do Vale do Taquari -
Univates, Brazil

*Correspondence:

Jingmai Kathleen O'Connor
jingmai.oconnor@gmail.com

Received: 24 June 2021

Accepted: 30 June 2021

Published: 12 July 2021

Citation:

O'Connor JK, Field DJ and Sullivan C
(2021) Editorial: Early Avian Evolution.
Front. Earth Sci. 9:730214.
doi: 10.3389/feart.2021.730214



FIGURE 1 | Illustration of the Early Cretaceous Jehol avifauna depicting *Confuciusornis* (Wu et al. and Zheng et al.) together with a bohaiornithid enantiornithine (Liu et al.). Artwork by Michael Rothman.

enantiornithines achieved locomotor independence and sexual maturity prior to skeletal maturity, the histology of *Mirarce* described by Atterholt et al. reveals startling variation in enantiornithine growth strategies in the Late Cretaceous, also strongly highlighting the necessity of sampling multiple elements in histological studies in order to more accurately capture growth patterns.

In their description of two new *Confuciusornis* (Figure 1) specimens with rarely preserved traces of the keratinous rhamphotheca, Zheng et al. observe features suggesting that independent origins of a toothless beak in non-neornithines yielded distinctive morphologies contrasting with those found in extant birds. Similarly, Bell et al. document clear differences in hind limb proportions between ornithuromorph and non-ornithuromorph birds. These studies add to the rapidly accumulating evidence that non-neornithine birds were very different from those alive today.

Two new taxa are erected in this research topic. Clark and O'Connor name *Fortipesavis prehensens*, a probable enantiornithine preserved in 100 Ma Burmese amber, and Musser and Clarke name *Nahmavis grandei* from the ~50 Ma old Green River Formation. Both taxa are incomplete, limiting interpretations, yet still shed light on important events in avian evolution. Clark and O'Connor's ecological insights into the ethology of unusual Burmese enantiornithines, arising from

careful comparisons with extant analogues, suggest that enantiornithines adapted to specific niches on the basis of unique anatomical traits different from those seen in crown birds, possibly due to developmental limitations imposed by their precocial development. Xing et al. report on a new, unnamed specimen, also preserved in Burmese amber, that increases the diversity of this mid-Cretaceous avifauna with regard to both skeletal proportions and plumage patterns. Musser and Clarke observe that *Nahmavis*, despite potentially being the first Green River charadriiform, also exhibits characteristics of gruiforms, rendering its phylogenetic position uncertain. Such early diverging neornithines are critical for understanding the early diversification of extant avian clades.

In our call for articles we noted that despite the enormous wealth of new data bearing on avian evolution that continues to accrue, numerous controversies exist and major gaps in our understanding remain. In this research topic two lingering controversies are addressed: Liu et al. tackle the purported ingestion of gastroliths for digestive purposes by at least some enantiornithines (Li et al., 2014; O'Connor, 2019), and Louchart et al. investigate the purported retention of teeth in some early Cenozoic crown birds (Lambrecht, 1930). In both cases, numerous analytical methods justify rejection of the original hypotheses, suggesting that bohaiornithid enantiornithines did not ingest gastroliths, and that putative tooth alveoli in young gastornithids are in fact the openings of large vascular canals—supporting the apparent irreversibility of transitions to toothlessness among total-group birds. In addition, the work of Heers et al. speaks to controversies surrounding flight capabilities in basal avian lineages (Olson and Feduccia, 1979; Gatesy and Dial, 1996), strongly supporting the interpretation that despite their relatively plesiomorphic anatomy, basal birds likely achieved about the same level of flight capability as anatomically derived crownward birds (ornithurines) through compensatory features such as the proportionately large deltopectoral crest present in *Confuciusornis*, *Sapeornis*, *Jeholornis*, and enantiornithines. While Novas et al. provide an in-depth look at the morphology of the scapulocoracoid complex, Heers et al. point out the necessity of whole system research for understanding locomotor behaviors as complex as dinosaurian flight.

Even as long-standing controversies are resolved, others continue to arise, as in the case of the unusual pattern of fusion observed by Wu et al. in the basal pygostylian *Confuciusornis*. In exploring the transition early in avian evolution from a fused scapulocoracoid complex to an unfused scapula and coracoid, Wu et al. detect a strange pattern in *Confuciusornis*, and more questions are raised than are answered. Similarly, although the purported gastroliths in *Bohaiornis* are shown by Liu et al. to be something other than ingested stones, the precise nature of these traces remains uncertain and Bell et al. find that phylogenetic influences on skeletal proportions can overshadow ecological ones, complicating morphometrically-based ecological inferences. These articles strongly indicate the need for continuing research as we ask increasingly complex questions about avian evolution and dig deeper using new methods. Together, the collection of articles published in this research topic exemplifies the exciting diversity of research currently being conducted on the early evolution of birds.

AUTHOR CONTRIBUTIONS

All authors listed have made a substantial, direct, and intellectual contribution to the work and approved it for publication.

REFERENCES

- Chinsamy, A., Marugán-Lobón, J., Serrano, F. J., and Chiappe, L. M. (2020). Osteology and Life History of the Basal Pygostylian *Confuciusornis Sanctus*. *Anatomical Record* 303, 949–962.
- Gatesy, S. M., and Dial, K. P. (1996). From Frond to Fan: *Archaeopteryx* and the Evolution of Short-Tailed Birds. *Evolution* 50 (5), 2037–2048. doi:10.2307/2410761
- Lambrecht, K. (1930). Studien über fossile Riesenvögel. *Institutum Regni Hungariae Geologicum* 7, 1–37. doi:10.1159/000397953
- Li, Z., Zhou, Z., Wang, M., and Clarke, J. A. (2014). A New Specimen of Large-Bodied Basal Enantiornithine *Bohaiornis* from the Early Cretaceous of China and the Inference of Feeding Ecology in Mesozoic Birds. *J. Paleontol.* 88 (1), 99–108. doi:10.1666/13-052
- Lovette, I. J., and Fitzpatrick, J. W. (2004). *The Handbook of Bird Biology*. New Jersey: Princeton University Press.
- O'Connor, J. K. (2019). The Trophic Habits of Early Birds. *Palaeogeogr. Palaeoclimatol. Palaeoecol.* 513, 178–195. doi:10.1016/j.palaeo.2018.03.006
- Olson, S. L., and Feduccia, A. (1979). Flight Capability and the Pectoral Girdle of *Archaeopteryx*. *Nature* 278, 247–248. doi:10.1038/278247a0

ACKNOWLEDGMENTS

We are grateful to our contributors who have conducted exceptional work truly making this a special topic.

Conflict of Interest: The authors declare that the research was conducted in the absence of any commercial or financial relationships that could be construed as a potential conflict of interest.

Copyright © 2021 O'Connor, Field and Sullivan. This is an open-access article distributed under the terms of the Creative Commons Attribution License (CC BY). The use, distribution or reproduction in other forums is permitted, provided the original author(s) and the copyright owner(s) are credited and that the original publication in this journal is cited, in accordance with accepted academic practice. No use, distribution or reproduction is permitted which does not comply with these terms.



A New Enantiornithine (Aves) Preserved in Mid-Cretaceous Burmese Amber Contributes to Growing Diversity of Cretaceous Plumage Patterns

OPEN ACCESS

Edited by:

K. Christopher Beard,
The University of Kansas,
United States

Reviewed by:

Chad Eliason,
Field Museum of Natural History,
United States
Federico Agnolin,
Museo Argentino de Ciencias
Naturales Bernardino Rivadavia,
Argentina

*Correspondence:

Jingmai K. O'Connor
jingmai@ivpp.ac.cn;
jingmai.oconnor@gmail.com

† These authors have contributed
equally to this work

Specialty section:

This article was submitted to
Paleontology,
a section of the journal
Frontiers in Earth Science

Received: 10 February 2020

Accepted: 12 June 2020

Published: 16 July 2020

Citation:

Xing L, O'Connor JK, Niu K,
Cockx P, Mai H and McKellar RC
(2020) A New Enantiornithine (Aves)
Preserved in Mid-Cretaceous
Burmese Amber Contributes
to Growing Diversity of Cretaceous
Plumage Patterns.
Front. Earth Sci. 8:264.
doi: 10.3389/feart.2020.00264

Lida Xing^{1,2,3†}, Jingmai K. O'Connor^{4,5*†}, Kecheng Niu³, Pierre Cockx^{6,7}, Huijuan Mai^{8,9}
and Ryan C. McKellar^{6,7,10}

¹ State Key Laboratory of Biogeology and Environmental Geology, China University of Geosciences, Beijing, China, ² School of the Earth Sciences and Resources, China University of Geosciences, Beijing, China, ³ Yingliang Stone Nature History Museum, Nan'an, China, ⁴ Key Laboratory of Vertebrate Evolution and Human Origins, Chinese Academy of Sciences, Institute of Vertebrate Paleontology and Paleoanthropology, Beijing, China, ⁵ CAS Center for Excellence in Life and Paleoenvironment, Beijing, China, ⁶ Royal Saskatchewan Museum, Regina, SK, Canada, ⁷ Department of Biology, University of Regina, Regina, SK, Canada, ⁸ Yunnan Key Laboratory for Palaeobiology, Yunnan University, Kunming, China, ⁹ MEC International Laboratory for Palaeobiology and Palaeoenvironment, Yunnan University, Kunming, China, ¹⁰ Department of Ecology and Evolutionary Biology, University of Kansas, Lawrence, KS, United States

Recent discoveries of enantiornithine birds trapped in amber have decreased the lower size limit of members of this clade, increased their morphological diversity, and provided significant new data regarding their plumage. Here, we describe a new specimen that consists of the distal extremities of both forelimbs and hindlimbs. Size and morphology suggest the specimen represents an immature individual. Although the skeletal morphology is poorly preserved, the new specimen most probably represents a member of the Enantiornithes based on the sum of its preserved morphologies, including its small size, elongate penultimate pedal phalanges, and large recurved unguals. Based on the lengths of the metatarsals, the new specimen is even smaller than previously described enantiornithines that preserve these elements; however, the forelimb elements are longer than those in the only other specimen preserving comparable overlapping skeletal material. This is suggestive of a diversity of limb proportions in the Burmese enantiornithine fauna, similar to that observed in the Jehol avifauna, in which intermembral indices range from approximately 1 to 1.5. The wing appears to consist of eight primaries, less than that of neornithines, contributing to mounting data that suggests the flight apparatus of enantiornithines was unique from that of other basal birds and neornithines. The well-preserved flight feathers are ornamented with pale basal bands, further adding to the diversity of Cretaceous plumage patterns revealed by Burmese amber specimens.

Keywords: enantiornithes, remiges, flight feathers, plumage patterns, limb proportions, intermembral index, albian – cenomanian, mesozoic

INTRODUCTION

Scientific understanding of Mesozoic birds has grown enormously over the past three decades (O'Connor et al., 2011). For the first two decades, new information primarily came from the rich Lower Cretaceous deposits in northeastern China that yield the celebrated Jehol Biota (Chang et al., 2003; Zhou et al., 2003). Although the diversity reported from these deposits continues to increase, specimens are heavily compressed, limiting and obscuring the morphological data they contain (Wang and Zhou, 2019; Wang et al., 2019). In 2016, the first avian skeletal remains preserved encased in Albian-Cenomanian age Burmese amber were described (Xing et al., 2016). Since these two partial wings were reported, two partial skeletons (Xing et al., 2017, 2018a), another partial wing (Xing et al., 2020), and three partial hindlimbs have been described (Xing et al., 2019a,b,c). Together, these have revealed new details of enantiornithine plumage, such as the bizarre body feathers present in hatchlings and the presence of enigmatic scutellate scale filaments (Xing et al., 2017), as well as previously unknown skeletal morphologies such as the bizarrely elongated third pedal digit of *Elektorornis chenguangi* (Xing et al., 2019c).

Particularly with regards to skeletal remains, the quality of preservation varies depending on the unique taphonomic conditions of each individual specimen. These include differences in whether the bird was alive or dead when it became trapped in the amber, whether it was partially scavenged, and how long it took for the remains to be fully encapsulated in the resin. As a result, skeletal preservation varies from excellent (Xing et al., 2019a) to absent, as in one specimen that preserves only a mold of the soft tissues (Xing et al., 2019b).

The new piece of Burmese amber YLSNHM00813 is from the Angbamo site, Tanai Township, Myitkyina District, Kachin State of northern Burma (Myanmar). Biostratigraphic evidence suggests that Burmese amber dates back to the middle-upper Albian based on ammonites (Wright et al., 1996), Albian-Cenomanian based on palynology (Davies, 2001), or Cenomanian-Turonian based on arthropods (Grimaldi et al., 2002). Radiometric dating using U-Pb from zircons found in the volcanoclastic matrix surrounding the amber has refined this age, providing an absolute estimate of 98.8 ± 0.6 Ma (Shi et al., 2012). This means that these amber specimens help to fill an important gap between the well-known Early Cretaceous avifaunas from China and Spain that are Barremian to Aptian (Sanz and Ortega, 2002; Pan et al., 2013) and Late Cretaceous specimens from North and South America that range from the Coniacian to Maastrichtian (Chiappe, 1993; Atterholt et al., 2018).

The new specimen YLSNHM00813 preserves the distalmost portions of two forelimbs and two feet all belonging to the same individual making it one of the relatively more complete specimens known so far (Figure 1). Feathers associated with both forelimbs are also preserved. The amber piece measures $127.34 \times 88.04 \times 44.52$ mm, and weighs 284 g. We describe the skeletal and integumentary remains and compare them to previously described specimens.

MATERIALS AND METHODS

Micro-CT Scanning and 3D Reconstruction

YLSNHM00813 was scanned with an X-ray micro-CT: Xradia 520 Versa (Carl Zeiss X-ray Microscopy, Inc., Pleasanton, CA, United States) at the Yunnan Key Laboratory for Palaeobiology, Yunnan University, Kunming, China. Without scanning it is impossible to view the morphology of the skeletal elements obscured both by the preservation of soft tissue and the amber itself, which includes numerous inclusions. The entire piece was scanned with a beam strength of 50 kV/4W for 168 min, with a voxel size of 26.59 μ m. A total of 1,014 radiographs were registered in the scan and saved as TIFF stacks and used to reconstruct the specimen with the Amira 5.4 software (Visage Imaging, San Diego, CA, United States). The subsequent volume rendering and animations were performed using VG StudioMax 2.1 (Volume Graphics, Heidelberg, Germany) (Supplementary Figures 1–4). Final figures were prepared with Photoshop CS5 (Adobe, San Jose, CA, United States) and Illustrator CS5 (Adobe, San Jose, CA, United States).

Terminology and Abbreviations

Osteological terminology primarily follows Baumel and Witmer (1993) using the English equivalents for the Latin terms, while plumage is described with the terminology of Lucas and Stettenheim (1972). Institutional abbreviations for specimens used as comparative material include: DIP – Dexu Institute of Palaeontology, Chaozhou, China; HPG – Hupoge Amber Museum, Tengchong City China; YLSNHM – Yingliang Stone Nature History Museum, Nan'an, China.

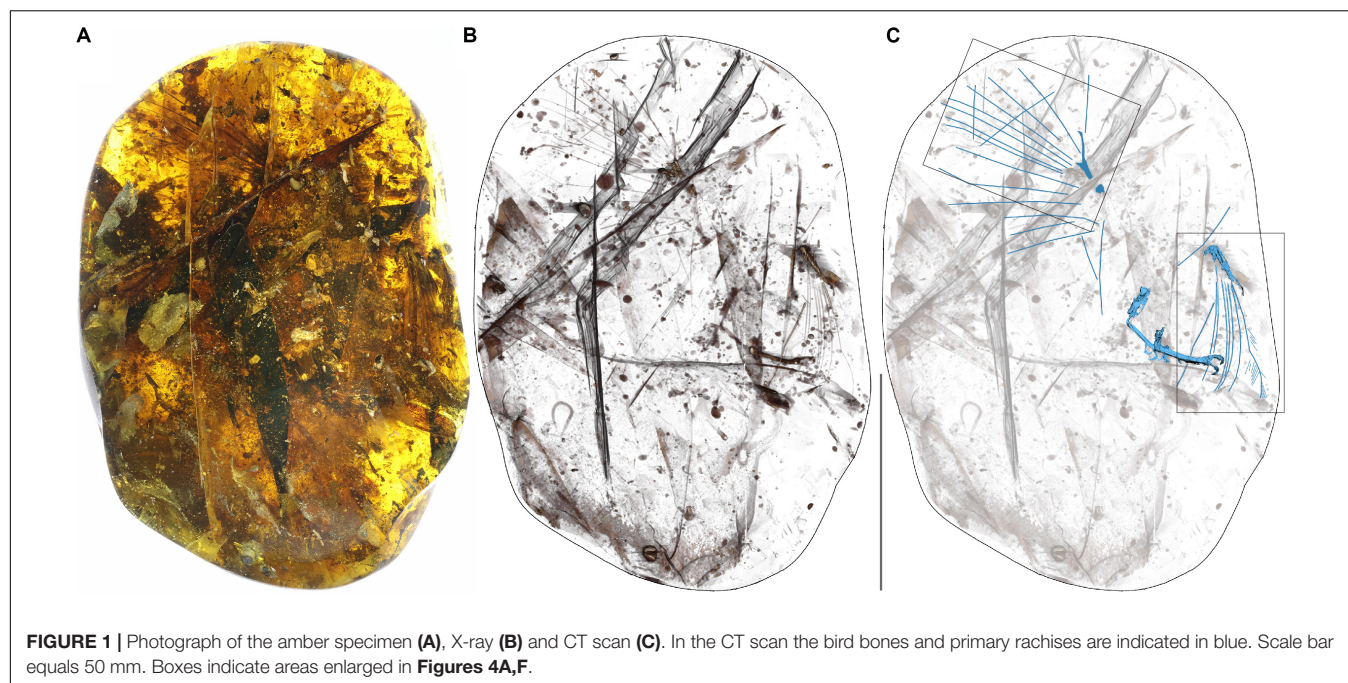
RESULTS

Skeletal Description

The new specimen YLSNHM00813 preserves the distal portions of both wings and hindlimbs, although most of the skeletal elements are poorly preserved due to various degrees of dissolution and decay, thus preventing detailed morphological observations (Figure 1 and Supplementary Figures 1–4).

Forelimbs

The left wing is the better preserved of the two (Figures 1–3). The distal epiphyses of the radius and ulna are preserved in articulation with the hand, which is complete and nearly in full articulation. The cortex of the ulna appears to be very thin and the element is hollow. The condyles on the ulna extend from the distal to caudal surface; the intercondylar sulcus is only weakly developed. The radius appears to have a ventral aponeurosis tubercle, which is bordered by the tendinal sulcus. Three free carpals are preserved; the largest is interpreted as the ulnare, which is preserved ventrocaudal to the ulna (Figure 3A). It is wedge-shaped with the thicker end oriented toward the metacarpals. The radiale, preserved between the radius and the alular metacarpal, is smaller (approximately one-third the size



of the alular metacarpal), has a blunt triangular shape in profile, and is dorsoventrally compressed. The third carpal appears to be “carpal x” (Chiappe et al., 2007) and is preserved at the proximal end of the minor metacarpal, level with the major metacarpal such that the minor metacarpal is displaced distally. It is wedge-shaped, with the tapered end directed toward the minor metacarpal. The proximal end is dorsoventrally thicker than the distal end.

The alular digit is slightly disarticulated away from the rest of the hand, so that the alular metacarpal is not preserved in contact with the major metacarpal, indicating that these two elements were unfused (**Figure 3A**). The alular metacarpal is roughly rectangular, about twice as tall craniocaudally as it is dorsoventrally wide and 2.5 times as long as it is tall. The first phalanx of the alular digit is proximally robust and tapers distally, so that the craniocaudal thickness is twice proximally what it measures distally; it is more than twice the length of the alular metacarpal. The alular ungual phalanx is curved and dorsoventrally compressed, measuring nearly the same length as the alular metacarpal. Were the alular digit in articulation, it would extend distally to the level of the distal margin of the major digit.

The proximal end of the major metacarpal is thickened relative to the shaft, especially in the dorsal direction (**Figure 3A**). It is possible the semilunate carpal was fused to the major metacarpal. Otherwise, this element is not preserved. The shaft of the major metacarpal is only slightly more robust than that of the minor metacarpal. As preserved, the two bones end distally at the same level. The distal end of the major metacarpal is weakly ginglymous. The major digit consists of three phalanges; the two non-ungual phalanges are roughly equal in length although the proximal phalanx is the longest. The major digit ungual phalanx is much larger than that of the alular digit, recurved, and with

a well-developed flexor tubercle. The articulations between the major digit phalanges appear to all be weakly ginglymous.

The highly reduced minor digit consists of two small phalanges, both strongly dorsoventrally compressed. The first is rectangular in profile and nearly twice as long as the second, which is triangular and sharply tapered distally (**Figure 3A**).

Hindlimbs

The two hindlimbs are poorly preserved (**Figures 2B,C**). Morphological details can be best observed on the left limb (**Figure 3B**). The left hindlimb preserves the distal half (or more) of the tibiotarsus and the nearly complete foot in full articulation. The right preserves approximately the distal one-third of the tibiotarsus in articulation with the foot. The exposed cross section of the tibiotarsus shows the bone had thin cortical walls and was hollow. Soft tissue obscures the tibiotarsus and tarsometatarsus so that very few morphological details can be gleaned. The proximal tarsals appear to be fused to the tibia, but this is most likely an artifact due to poor preservation, given that the carpal bones are unfused. It appears the distal end of the tibiotarsus is expanded slightly relative to the shaft and slightly bowed cranially (**Figure 3B**). The latter morphology may be a product of poor preservation (the potentially unfused proximal tarsals may be deflected cranially beneath the soft tissue). The tarsometatarsus is proportionately long and narrow. The metatarsals are clearly unfused to each other on the right limb, although they are preserved in tight articulation on the left. The first metatarsal is preserved on the plantar surface of the tarsometatarsus, but it may be displaced. It is approximately 20% of the length of metatarsal III, as in most enantiornithines with the exception of the Pengornithidae (Wang et al., 2014). Metatarsal III is the longest, followed by metatarsal II and metatarsal IV, the latter of which is the shortest of the

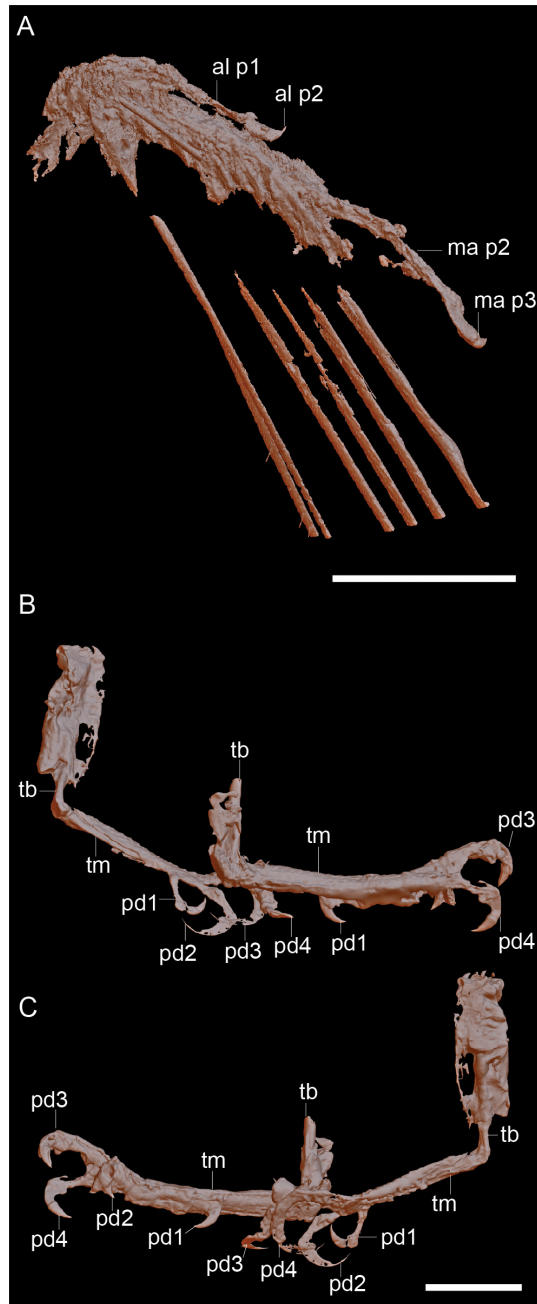


FIGURE 2 | Raw CT data of the right hand (A) and the feet viewed from the right (B) and viewed from the left (C). Scale bars equal 5 mm. Anatomical abbreviations: al p1, alular digit phalanx 1; al p2, alular digit phalanx 2; ma p2, major digit phalanx 2; ma p3, major digit phalanx 2; pd1-4, pedal digits 1-4; tb, tibiotarsus; tm, tarsometatarsus.

three. The trochleae are narrow, not expanded relative to the metatarsal shafts.

The pedal phalangeal formula is 2-3-4-5-x. The third digit is the longest, closely followed by the fourth digit. The hallux is preserved in a fully reversed position in both the right and the left feet (Figures 2B,C). The first digit is short, with the

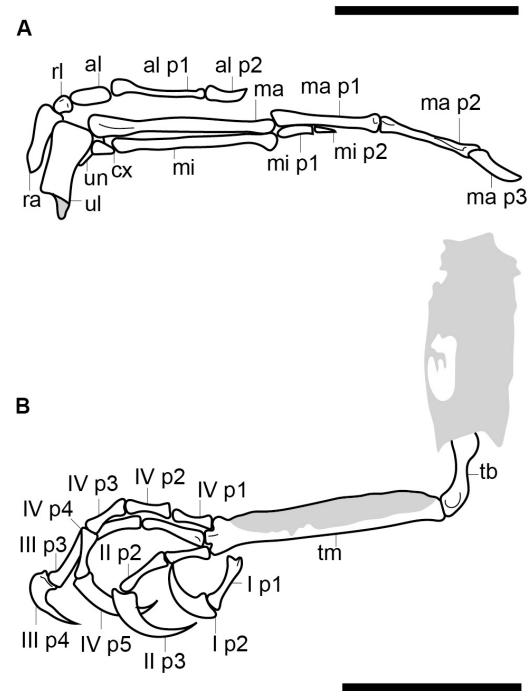


FIGURE 3 | Reconstruction of the right hand (A) and the left foot (B). Scale bars equal 5 mm. Anatomical abbreviations not listed in the Figure 2 caption: al, alular metacarpal; ma, major metacarpal; mi, minor metacarpal; ma p1, major digit phalanx 1; mi p1, minor digit phalanx 1; minor digit phalanx 2; ra, radius; rl, radiale; ul, ulna; un, ulnare.

first phalanx similar in length to the claw, which is curved and sharply tapered with a small but distinct flexor tubercle. The first phalanx of the second digit is shorter than the penultimate phalanx, which is subequal to the first phalanx in the hallux but slightly more delicate. The second digit claw is longer and more robust (although it is slightly less recurved) than that of the hallux. The keratinous sheath remains in articulation on the pedal claws. The first phalanx of the third digit is the longest in the foot and subequal in length to the penultimate phalanx of the same digit. The second phalanx is approximately 75% the length of the preceding and following phalanges. The ungual phalanx of the third digit is larger, more robust, and more recurved than that of the second digit. The first phalanx of the fourth digit is the shortest in the foot. The following two phalanges are subequal in length and shorter than the penultimate phalanx. The claw is slightly smaller and less recurved than those of digits I–III (Figure 3B).

Ontogeny and Taxonomy

So far, only enantiornithines have been unequivocally recovered from the Hukwang avifauna. The very small body size and unfused proximal carpometacarpus suggest that YLSNHM00813 is an immature individual. Similar to the immature holotype of *Iberomesornis romerali* (Sanz and Ortega, 2002), the minor metacarpal does not project farther distally than the major metacarpal as it does in most of the other enantiornithines

(Chiappe and Walker, 2002). Given the preservational state of the left manus, in YLSNHM00813 it is possible that this morphology is due to slight disarticulation of the metacarpals. The two non-ungual phalanges of the major digit are subequal, whereas in most enantiornithines the penultimate phalanx is shorter than the proximal one. The penultimate phalanx is longer in the basalmost enantiornithine *Protopteryx* (Zhang et al., 2001) and notably, the minor metacarpal only projects slightly farther than the major metacarpal in this taxon as well (Chiappe et al., 2019). The pedal phalanges are elongated distally so that the penultimate phalanx is the longest in each digit, as in all known enantiornithines. The claws are large and recurved as in all known enantiornithines, whereas in Cretaceous ornithuromorphs the pedal claws are short and unrecurved (O'Connor, 2012). Based on these morphological characteristics, the most parsimonious inference is that YLSNHM00813 represents an immature and fairly basal enantiornithine.

Integument

Feathers from both the right and left wing are preserved, including what is interpreted as the complete set of primaries on both sides (Figures 1, 4). The left wing preserves eight primaries and four secondaries, with the two feather tracts separated by a small gap (Figure 4A). The primaries are truncated apically by the polished surface of the amber (Figures 4B–E). The exposed cross-sections of the primary rachises are subcylindrical basally and ovoid distally and are hollow and pith filled. The ventral rachis margins are slightly wider than the dorsal margins. The blade-shaped barb rami are deep (extending ventrally from the barbs) and dorsolaterally attached along the rachis (Figures 4B,C). Both the rachises and the barbs are preserved with a dark gray color due to pyrite infiltration. Proximal barbs are straight and blade-shaped, whereas the distal barbs have a slightly angled pennulum with hooklets that is poorly distinguished from the base. Primaries are strongly asymmetric, with barbs in the leading vane being approximately 0.4 times the length of the barbs in the trailing vane. Furthermore, the barbs differ in the angle of divergence from the rachis forming an angle of approximately 17° (standard error of about 0.66) in the leading-edge vane, versus approximately 28° (standard error of 0.98) in the trailing-edge vane.

In cross-section, the rachises of the secondaries are subcircular and are hollow and pith filled. Although less clear, it appears that the secondaries were also asymmetric, but less so than observed in the primary remiges (ratio of about 0.7). Primary coverts are sparsely preserved. They are short, restricted to the very base of the primaries. No secondary coverts can be identified but this region of the wing does not appear to be preserved.

The right wing also consists of eight primaries, together with three alular coverts and a sparse row of primary coverts (Figure 4F). The sparse distribution of the primary coverts in both wings is interpreted as due to taphonomic loss. Some feathers have been displaced and damaged (e.g., one secondary remex is strongly displaced anterior to the leading edge of the wing). Coverts from either the leading edge of the manus or the propatagium are preserved as a clump that has been offset ventral to the wing.

The right wing is structurally consistent with the left, but with slightly better visibility through the amber allowing better observation of color. In the right wing, the preserved primaries and coverts have pale rachises and barb rami. The barbs are medium brown with a grayish tinge. A pale band extends transversely along the basal quarter of the primary remiges and in the primary coverts (Figure 4F). A second pale band extends transversely across the primary coverts and partly into the alular coverts. The coverts are preserved with a darker brown coloration (Figures 4F, 5A).

CT-scan data show three rows of scutellae on the dorsal surface of the right leg (Figure 2B). No scutes are present. It was not possible to observe if scutellate scale filaments are present due to the delicate nature of these features and the large amount of overlapping plant material also trapped in the amber in YLSNHM00813 (Figure 1A).

Taphonomy

The decay products and breaks within the preserved material suggest that the bird fell into the resin with its belly up, and that the dominant taphonomic processes were decay and drift (no signs of predation or scavenging). YLSNHM00813 is dominated by a scatter of large, strap-like leaves that are more than twice the size of the primary flight feathers (Figure 1A). The surrounding amber is also rich in wood particulates, plant detritus, insect frass, and contains representatives of multiple orders of arthropods (e.g., Coleoptera, Diptera, Hemiptera, Hymenoptera, Araneae, and Blattoidea), including forest floor dwelling groups, such as Diplopoda and Collembola. Altogether, this evidence suggests the resin mass formed on or near the forest floor, capturing a litter assemblage (Perrichot, 2004). Visibility is restricted by a combination of plant material on the dorsal side of the avian inclusion, and thick overlying amber full of particulates and fractures on the ventral surface. However, the dorsal surfaces of the wings are clearly visible, along with an assortment of detached feathers that are adrift within the resin flow. It may be a function of limited visibility, but no sheets of skin are visibly present within the amber mass, and most of the covert feathers that surround the primaries and secondaries appear to have been lost in the surrounding resin.

The preserved distal portions of the forelimbs are generally in the correct anatomical orientation, but they appear to have drifted relative to one another (Figure 1A). The jagged and irregular margins of the broken edges of the right radius and ulna suggest that these breaks occurred postmortem. Combined with the high number of isolated contour feathers in seemingly random orientations, the fractures and limb displacements indicate a high degree of decay and resin mobility before the limbs were fully engulfed and the resin began to polymerize. Bubbles emanating from the broken ends of bones, as well as those emanating from decaying plant material, have risen toward the ventral surface of the bird inclusion. Bent feathers and plant material indicate that the surrounding resin flowed toward the right side of the bird. Together, these observations indicate that the bird fell into the resin mass with its ventral surface exposed upward, where it proceeded to decay and weather extensively. The limbs were the only parts of the body deeply entombed in the

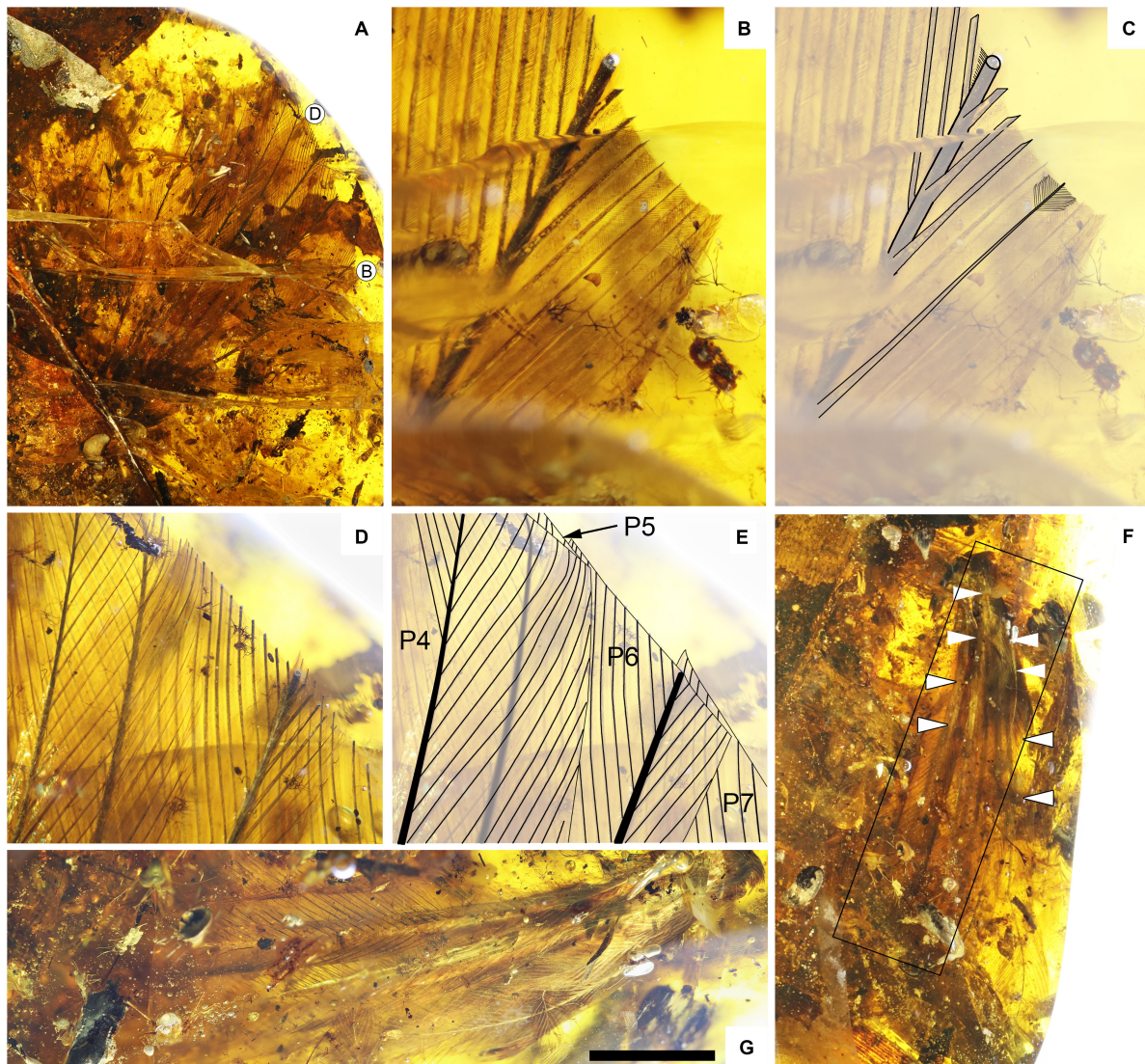


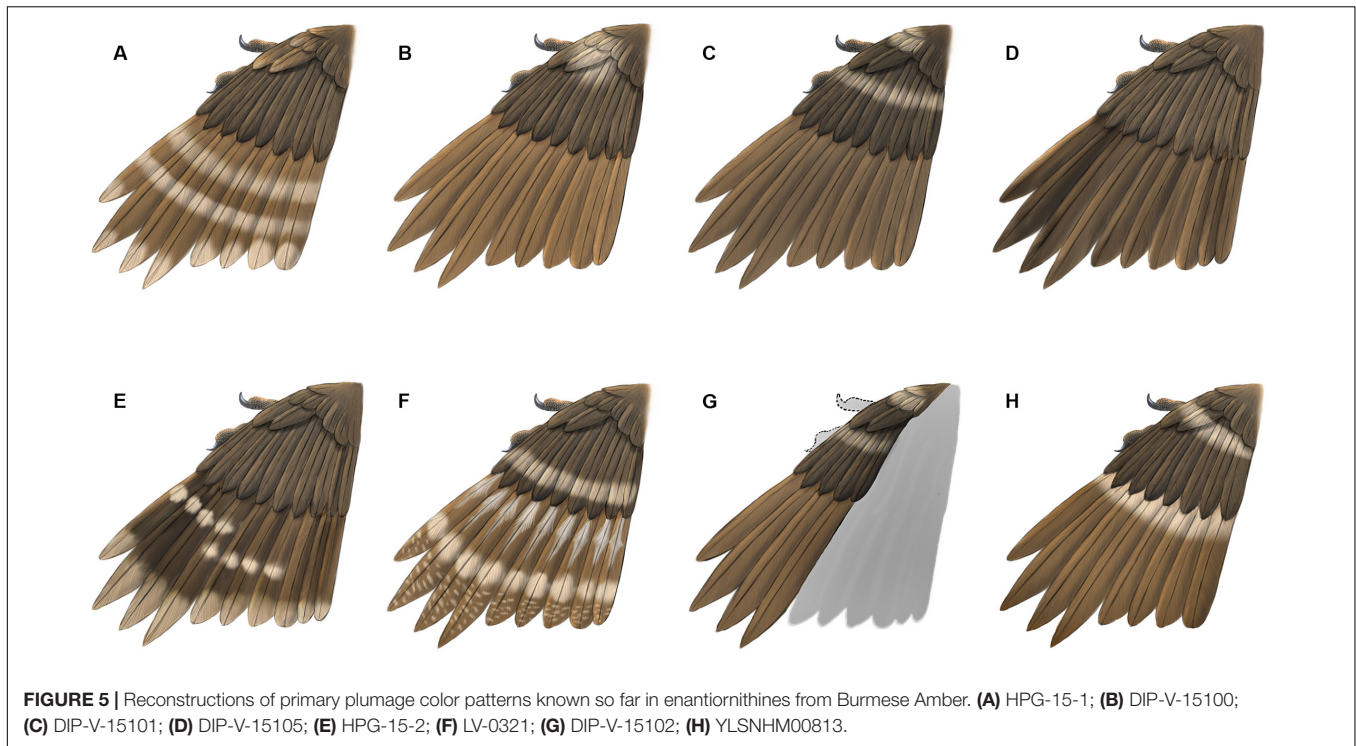
FIGURE 4 | Plumage of YLSNHM00813. **(A)** Overview of the left wing; **(B)** close-up of a barb truncated at the amber surface; **(C)** interpretive diagram of **(B)** with examples of barb rami position and barbule position; **(D)** close-up of remiges superimposed and truncated by the surface of amber; **(E)** interpretive diagram of **(D)** highlighting the outline of the vanes as well as the position of the rami and the rachises; **(F)** overview of the right wing with arrowheads (white and white with a black contour) highlighting the position of two white bands; **(G)** close-up of the left wing. Scale bars = **A**: 10 mm; **B**: 1 mm; **D**: 3 mm; **F,G**: 5 mm.

resin, leading to their preferential preservation and subsequent drift within the fluid resin. The limbs do not have a heavy coating of milky amber surrounding them, and the skin around the feet adheres tightly to the underlying bones. This likely indicates that the body parts dried on the surface prior to encapsulation, but it is possible that decay products may have been swept away from the feet by resin flows (Martínez-Delclòs et al., 2004).

DISCUSSION

The specimen described here, YLSNHM00813, is the ninth reported Burmese amber specimen preserving avian skeletal remains. Although the skeletal remains are poorly preserved,

the cumulative morphological features (e.g., penultimate pedal phalanges longest, pedal ungual phalanges long and recurved) suggest referral to the Enantiornithes, the dominant clade of Cretaceous land birds (O'Connor et al., 2011) and so far the only clade identified with certainty in Burmese amber (Xing et al., 2016, 2017, 2018a, 2019a,b,c). The position of the forelimbs and hindlimbs in the amber block suggests that these remains belong to a single individual (Figure 1). As in other specimens thus far preserved in amber, YLSNHM00813 is very small with the metatarsals measuring less than one centimeter (Table 1). The only specimen in which both forelimb and hindlimb measurements can be compared is the hatchling HPG-15-1 (Xing et al., 2017). Compared to HPG-15-1, the foot is slightly smaller in YLSNHM00813, yet the hand is larger (Table 1). This suggests



that YLSNHM00813 would have had a higher intermembral index and proportionately larger wingspan than HPG-15-1. Such diversity is unsurprising: enantiornithines from the Jehol avifauna show considerable variation in limb proportions, with species ranging from subequal forelimbs and hindlimbs (e.g., *Monoenantiornis*, *Rapaxavis*) to taxa with forelimbs considerably elongated relative to the hindlimbs (e.g., *Longipteryx*, *Pengornis*) (O'Connor et al., 2009; Hu and O'Connor, 2017). Mesozoic birds with elongated hindlimbs are so far only definitively known in the Ornithuromorpha (O'Connor et al., 2010). Differences in limb proportions between Burmese amber enantiornithines likely reflect subtle ecological differences between species. The better preserved and more complete specimen HPG-15-1 has been interpreted as a hatchling, and YLSNHM00813 is also likely an immature individual, as suggested by the apparently unfused proximal carpometacarpus (Figure 3A).

The primary wing feathers are well preserved in YLSNHM00813. The number of preserved primaries is eight on both sides, which suggests the tract is complete (Table 2). Eight remiges are also preserved in HPG-15-1, but it is unclear if the tract is complete in the latter specimen (Xing et al., 2017). Nine primaries are preserved in DIP-V-15100, which also preserves secondaries and thus is likely complete (Xing et al., 2016), and ten primaries are reported in DIP-V15105 (Xing et al., 2019a). Specimen HPG-15-2 may have ten or perhaps 11 primaries, but it is difficult to distinguish between the primaries and secondaries due to feather overlap within this specimen (Xing et al., 2019c). When wings are preserved, the number of primary feathers usually cannot be accurately estimated in lithic specimens due to overlap but in amber specimens the remige count is aided by CT data that clearly reveals the rachis of each

flight feather. The data from the Hukawng avifauna indicates intraclade diversity in the number of primary feathers in the wing in enantiornithines, as in neornithines (Gill, 2007). This diversity hints at potential differences in wing shape and flight style between species. In neornithines the number of primaries ranges from nine to 12 (Lovette and Fitzpatrick, 2004); *Archaeopteryx* falls in the modern range with 11 primaries (Elzanowski, 2002). Currently available data suggests the number of primaries in enantiornithines ranged from eight to 11. This contributes to the numerous lines of evidence that the flight apparatus of enantiornithines was unique from that of other basal birds and neornithines (Chiappe and Walker, 2002). The rest of the wing plumage in YLSNHM00813 is poorly preserved due to extensive postmortem decay. The most valuable information lies in the preserved coloration, adding to the known diversity of plumage patterns recognized among Mesozoic birds.

Diversity of Plumage Patterns

As specimens accumulate so has the diversity of plumage color patterns observed in enantiornithines in Burmese amber (Figure 5 and Table 2). Although in very rare instances patterns such as stripes and spots are preserved directly in some lithic specimens (Chen et al., 1998; Ji et al., 1998; de Souza Carvalho et al., 2015; Zheng et al., 2017; Li et al., 2018), these do not necessarily reflect color differences and may indicate areas of increased melanization (Zheng et al., 2017). It is possible to determine the original melanosome-based coloration in well preserved lithic fossils by sampling the preserved traces and viewing them using a scanning electron microscope (SEM) to look for preserved melanosomes; however, getting a clear picture of the entire wing coloration would require extensive destructive

TABLE 1 | Comparative measurements of enantiornithines from the Hukawng avifauna.

| | YLSNHM00813 | DIP-V-15100 | DIP-V-15101 | HPG-15-1 | DIP-V-15102 | YLSNHM01001 | DIP-V-15105a | HPG-15-2 | LV-0321 |
|-------------------|-------------|-------------|-------------|----------|-------------|-------------|--------------|----------|---------|
| Ulna | (2.55) | (7.94) | | (5.22) | 14.38 | | | | |
| Radius | (1.91) | (6.5) | | (5.48) | 12.93 | | | | |
| Alular metacarpal | 1.08 | 1.00 | | | | | | | |
| Alular phalanx-1 | 2.36 | 1.83 | (2.95) | 1.68 | | | | | |
| Alular phalanx-2 | 1.13 | 1.28 | 1.81 | 0.94 | | | | | |
| Major metacarpal | 5.2 | 4.17 | (4.95) | 3.88 | | | | | |
| Major phalanx-1 | 3.03 | 2.22 | 3.10 | 1.85 | | | | | (2.41) |
| Major phalanx-2 | 2.73 | 1.78 | 2.57 | 1.23 | | | | | 4.51 |
| Major phalanx-3 | 1.49 | 1.28 | 2.14 | 1.00 | | | | | 2.21 |
| Minor metacarpal | 4.55 | 4.72 | (6.24) | 3.85 | | | | | |
| Minor phalanx-1 | 1.09 | 1.00 | 1.38 | 1.07 | | | | | |
| Metatarsal I | | | | | | | 1.57 | 1.87 | |
| Metatarsal II | 6.95 | | | 7.50 | | | (2.67) | 6.75 | |
| Metatarsal III | 7.02 | | | 8.00 | | (5.2) | (2.39) | 7.55 | |
| Metatarsal IV | 6.71 | | | 7.17 | | | (2.29) | 6.97 | |
| Digit I-1 | 1.49 | | | | | | 2.17 | 2.95 | |
| Digit I-2 | 1.59 | | | | | | 2.57 | 1.71 | |
| Digit II-1 | 1.25 | | | | | | 1.20 | 1.24 | |
| Digit II-2 | 1.49 | | | | | | 2.44 | 2.31 | |
| Digit II-3 | 2.09 | | | | | 4.50 | 3.10 | 1.84 | |
| Digit III-1 | 2.02 | | | 2.10 | | | 1.57 | 1.97 | |
| Digit III-2 | 1.49 | | | | | | 1.56 | 2.35 | |
| Digit III-3 | 1.95 | | | | | | 2.04 | 2.95 | |
| Digit III-4 | 1.95 | | | | | | | 1.81 | |
| Digit IV-1 | 1.18 | | | | | | 0.84 | 0.98 | |
| Digit IV-2 | 1.32 | | | | | | 0.85 | 1.33 | |
| Digit IV-3 | 1.2 | | | | | | 0.91 | 1.24 | |
| Digit IV-4 | 1.35 | | | | | | 1.59 | 1.65 | |
| Digit IV-5 | 2.12 | | | | | | 1.36 | 1.78 | |

Measurements represent lengths in mm; parentheses indicate incomplete elements. Measurements of pedal unguals do not include the keratinous sheath.

TABLE 2 | Wing plumage characteristics in Hukawng enantiornithines.

| Collection No. | Publication | Ontogeny | Primaries | Secondaries | Plumage pattern |
|----------------|--------------------------------|----------------|-----------|-------------|--------------------------------------------------------------------------------------------------------------------------------------------------------------------------------------------------------------------------------|
| HPG-15-1 | Xing et al., 2017 | Hatchling | (8) | 9 | Each primary feather with walnut brown color with pale feather apex and two pale transverse bands in distal half. Single preserved alular feather with trailing edge paler than the leading edge. |
| DIP-V-15102 | Xing et al., 2018a | Juvenile | (4) | (10)/(11) | In primaries, barbules, rami and rachises all preserved a diffuse, pale brown color. |
| HPG-15-2 | Xing et al., 2019c | Subadult/Adult | 10/11 | 4/3 | Wing preserved overall dark brown color; two large-scale pale wing spots; barb apices in trailing edge vane of primaries pale or white |
| DIP-V-15100 | Xing et al., 2016 | Juvenile | 9 | 5 | Overall dark brown coloration with pale or white spot basal to the alula, which extends on to some of the primary coverts |
| DIP-V-15101 | Xing et al., 2016 | Juvenile | 9 | (5) | Overall dark brown coloration with pale or white spot basal to the alula; second pale band present extending across the dorsal surface of the wing apical to the alula. |
| LV-0321 | Xing et al., 2020 | ? | 8/9 | — | Overall dark, walnut brown color; longitudinal pale stripe in basal half of each primary extending along the rachis; more diffuse transverse pale patch located subapically |
| DIP-V-15105b | Xing et al., 2019a | Juvenile | 10 | — | Overall dark diffuse brown color. |
| YLSNHM00813 | Xing et al. (this publication) | Juvenile | 8 | 4 | Primaries preserved a pale brown color with a pale band extending transversely along the basal quarter of their length; a second pale band extends transversely across the primary coverts and partly into the alular coverts. |

A “/” indicates an uncertainty and parentheses indicate that the tract is incomplete or might be incomplete.

sampling given how much color can vary even within a single feather (Zhang et al., 2010). Therefore, melanosome-based color research can only provide a general idea of the coloration and not a detailed reconstruction of the color patterning (Zheng et al., 2017). Furthermore, feathers in lithic specimens are typically only preserved forming a halo around the skeleton because most often a majority of the feathers are prepared away where they overlap the bones themselves. Therefore, even if all preserved feathers were sampled for SEM analysis in such specimens, the plumage color and patterns revealed would still be incomplete.

In contrast, the large-scale color patterns of light and dark areas can be observed directly in all known feathered specimens preserved in amber in which presumably the whole feather (including the keratin matrix) is preserved and not just the decay resistant melanosomes. Although also limited by incomplete preservation, in this case because only portions of the skeleton and their associated soft tissues are preserved, the detailed color patterns revealed in several complete wings preserved in amber represent a major source of data concerning plumage patterns, but perhaps not true coloration, in enantiornithines in at least one ecological environment (wet tropical forest) (Xing et al., 2018b).

Although in tropical forests today we typically envision birds that are brightly colored, in most Burmese amber specimens the feathers are preserved with various shades of brown and this base coloring is supplemented with pale markings (inferred to represent areas of reduced or absent pigmentation) (Xing et al., 2017). Observed markings include transverse bands (LV-0321, HPG-15-1, DIP-V-15101) (Xing et al., 2016, 2017, 2020), spots (LV-0321, HPG-15-1, HPG-15-2, DIP-V-15100 and DIP-V-15101) (Xing et al., 2016, 2019a,c, 2020) and possibly longitudinal stripes (LV-0321) (Xing et al., 2020). The brownish appearance of the feathers may be somewhat due to the yellow of the amber itself. The fact that all specimens known so far reveal brown coloration may additionally suggest that the color of the feathers is somehow altered by the chemistry and preservational history of the resin. While the shade of brown color itself may prove not to be reliable, the distinct spots and bands are most likely features indicative of original plumage patterning – if due to degradation, a more random pattern would be expected. Although spots and stripes have been identified in a few exceptional feathered dinosaurs from the Jehol including some birds (Chen et al., 1998; Zheng et al., 2017; Li et al., 2018) and the ornamental tail feathers in one juvenile enantiornithine from Brazil preserve unusual spots that may represent remnants of original coloring (de Souza Carvalho et al., 2015), all currently available information on plumage patterning in the wings of enantiornithines is from specimens preserved in Burmese amber (O'Connor, 2020).

The presence of pale bands and spots is not unique to YLSNHM00813. However, the combination of features present in this specimen is distinct from all previously described specimens (Figure 5). In HPG-15-1 the primaries are preserved with an overall walnut brown color interrupted by two transverse bands in the distal half with pale apices, while the alula feathers showed a paler color in the trailing edge vane (Xing et al., 2017; Figure 5A). In YLSNHM00813 the transverse pale bands are located in the basal (proximal) quarter of the remiges, not in the distal section of the feathers as in HPG-15-1, and the feather apices lack the

paler coloration, somewhat resembling the pattern in the wings of a Northern Mockingbird (*Mimus polyglottos*) (Figure 5H). However, these two specimens are similar in that the coverts have an overall darker pigmentation in the barbules with the rachis and barb rami being relatively paler (Figure 4). The feathers in the two well-preserved wings DIP-V-15100 and DIP-V-15101 have an overall darker brown coloration than that of YLSNHM00813, and show a pale spot basal to the alula (Xing et al., 2016). In DIP-V-15100, this pale spot extends on to some of the primary coverts, whereas in DIP-V-15101 a secondary pale band is also present extending across the dorsal surface of the wing apical to the alula (Xing et al., 2016). A diffuse brown coloration is present throughout the wing plumage in DIP-V-15102 and DIP-V-15105b, but the barbs have paler cores in DIP-V-15102 (Xing et al., 2018a, 2019a). The holotype of *Elektorornis chenguangi* (HPG-15-2) also preserves some wing feathers with two large-scale pale wing spots halfway down the length of the primaries, and the trailing edge vane of each primary has a pale margin (Xing et al., 2019c). Another partial wing specimen, LV-0321, consisting of the distal portion of a manus with attached primaries, preserves a pattern that is also unique from all other specimens (Xing et al., 2020). The barbs in the primaries are mostly a dark brown color, whereas the rachis is pale or white. Along the length of each primary rachis there are three patches of barbs in which the inner portions are white forming three spots on each feather that together form three transverse bands on the wing as a whole. The basal two spots somewhat grade into each other and this has been described as forming a longitudinal stripe (Xing et al., 2020).

Ecological Implications of Observed Plumage Patterns

The plumage patterns observed in avian specimens preserved in Burmese amber have certainly been affected by taphonomic processes although to what degree is currently not understood. Interpretations regarding the plumage provided here are preliminary, and would certainly be affected by new data in the future should these specimens be subject to chemical analyses and or high resolution imaging capable of identifying additional pigments or melanic microstructure (Thomas et al., 2014). Furthermore, most of the avian specimens recovered from Burmese amber, including the specimen described here, are inferred to represent juveniles or even hatchlings and therefore the preserved plumage patterns may at least partially reflect this early ontogenetic stage and may also be subject to pronounced changes later in ontogeny. So far, all of the Burmese amber specimens appear to have generally cryptic color patterns and palettes that would have made the individuals inconspicuous in forest habitats. Solely based on this patterning, it is not possible to make absolute statements about ecology given the competing selective pressures acting on modern birds (Baker and Parker, 1979). In general, birds feeding at night, spending significant time on the ground, and or employing poorly concealed incubation sites and reduced parental care for juveniles, tend to have less conspicuous dorsal wing surface coloration (Baker and Parker, 1979). The few spots and bands of pale or white color

that are present on the Burmese enantiornithine wings also seem to be consistent with disruptive camouflage, and if they were bright white, they may have been useful in visual signaling, or predator and prey startling strategies (Jabłoński, 1996; Smithwick et al., 2017).

In comparison to modern birds, Burmese enantiornithines fall at the small end of the avian spectrum. The color patterns found in their wing feathers show a mixture of the patterns observed in extant birds from varying ecologies. Among Passeriformes, some taxa with relatively monotonous dark plumage have pale apices or bands running through their coverts, or pale spots near the alula or within the propatagium that are reminiscent of the patterns observed in amber enantiornithines. A few thrushes, grosbeaks, creepers, and warblers (e.g., *Ixoreus naevus*, *Pheucticus ludovicianus*, *Certhia americana*, and *Setophaga caerulescens*) even have broad pale bands among the primary and secondary feathers that are composed of spots similar to those in the amber specimens. However, the repetition of relatively broad pale bands in the primaries and secondaries of some amber specimens is also somewhat reminiscent of modern Falconiformes, such as kestrels (e.g., *Falco sparverius*). With the currently available data, these patterns are not clearly indicative of a particular ecology, but probably relate to crypsis. Cryptic color patterns in these juvenile enantiornithines may relate to ontogeny or to trophic ecology, since enantiornithines have been compared to raptorial birds based on their pedal morphology (O'Connor, 2019).

CONCLUSION

The new specimen YLSNHM00813 most likely represents a juvenile enantiornithine, like a majority of previously described specimens from Burmese amber. The limb proportions differ from that of the most complete enantiornithine previously reported in amber suggesting some ecological diversity among the enantiornithines in this fauna. In all specimens the feathers are preserved with a visible brown color, suggesting this may not be indicative of *in vivo* coloration. Pale spots and bands are considered to be true features. Although obscured by preservation and other inclusions in the amber,

it appears that the plumage pattern differs in all specimens uncovered so far.

In the future, novel chemical analyses may help to further elucidate how color patterns observed in feathers preserved within amber would actually translate to *in vivo* coloration. As we gain a better understanding of these color patterns, they may eventually improve our understanding of species-level diversity in the Hukawng avifauna.

DATA AVAILABILITY STATEMENT

All the raw data generated from the CT scans for this study are included in the MorphoSource and available at: https://www.morphosource.org/Detail/ProjectDetail/Show/project_id/1067.

AUTHOR CONTRIBUTIONS

LX, JO'C, PC, and RM designed the project. LX, JO'C, PC, RM, KN, and HM performed the research. JO'C, PC, RM, and LX wrote the manuscript. All authors contributed to the article and approved the submitted version.

FUNDING

This research was funded by the Natural Sciences and Engineering Research Council of Canada (2015-00681); the National Geographic Society, United States (EC0768-15); and the National Natural Science Foundation of China (Nos. 41790455 and 41772008). This research was also supported by "The Foreign Cultural and Educational Experts Employment Program" from Foreign Experts Service Division, Ministry of Science and Technology of China (G20190001245).

SUPPLEMENTARY MATERIAL

The Supplementary Material for this article can be found online at: <https://www.frontiersin.org/articles/10.3389/feart.2020.00264/full#supplementary-material>

REFERENCES

- Atterholt, J. A., Hutchison, J. H., and O'Connor, J. (2018). The most complete enantiornithine from North America and a phylogenetic analysis of the avosauridae. *PeerJ* 6:e5910. doi: 10.7717/peerj.5910
- Baker, R. R., and Parker, G. A. (1979). The evolution of bird coloration. *Trans. R. Soc. Lond.* 287, 63–130. doi: 10.1098/rstb.1979.0053
- Baumel, J. J., and Witmer, L. M. (1993). "Osteologia," in *Handbook of Avian Anatomy: Nomina Anatomica Avium*, Second Edition, eds J. J. Baumel, A. S. King, J. E. Breazile, H. E. Evans and J. C. Vanden Berge (Cambridge: Nuttall Ornithological Club), 45–132.
- Chang, M.-M., Chen, P.-J., Wang, Y.-Q., Wang, Y., and Miao, D.-S. (eds) (2003). *The Jehol Fossils: The Emergence of Feathered Dinosaurs, Beaked Birds and Flowering Plants*. Shanghai: Shanghai Scientific & Technical Publishers.
- Chen, P.-J., Dong, Z., and Zhen, S. (1998). An exceptionally well-preserved theropod dinosaur from the yixian formation of China. *Nature* 391, 147–152. doi: 10.1038/34356
- Chiappe, L. M. (1993). Enantiornithine (Aves) tarsometatarsi from the cretaceous lecho formation of northwestern argentina. *Am. Museum Novit.* 3083, 1–27.
- Chiappe, L. M., Ji, S., and Ji, Q. (2007). Juvenile birds from the Early cretaceous of China: implications for enantiornithine ontogeny. *Am. Museum Novit.* 3594, 1–46.
- Chiappe, L. M., Liu, D., Serrano, F. J., Zhang, Y.-G., and Meng, Q.-J. (2019). Anatomy and flight performance of the early enantiornithine bird *Protopteryx fengningensis*: information from new specimens of the early cretaceous huajiyi formation of China. *Anatom. Record* 303, 716–731. doi: 10.1002/ar.24322
- Chiappe, L. M., and Walker, C. A. (2002). "Skeletal morphology and systematics of the cretaceous euenantiornithes (Ornithothoraces: Enantiornithes)," in *Mesozoic Birds: Above the Heads of Dinosaurs*, eds L. M. Chiappe and L. M. Witmer (Berkeley: University of California Press), 240–267.
- Davies, E. H. (2001). *Palynological Analysis And Age Assignments Of Two Burmese Amber Sample Sets*. Calgary: Branta Biostratigraphy Ltd.

- de Souza Carvalho, I., Novas, F. E., Agnolin, F. L., Isasi, M. P., Freitas, F. I., and Andrade, J. A. (2015). A mesozoic bird from gondwana preserving feathers. *Nat. Commun.* 6, 1–5.
- Elzanowski, A. (2002). “Archaeopterygidae (upper Jurassic of Germany),” in *Mesozoic Birds: Above the Heads of Dinosaurs*, eds L. M. Chiappe and L. M. Witmer (Berkeley: University of California Press), 129–159.
- Gill, F. B. (2007). *Ornithology*, 3rd Edn, New York, NY: W.H. Freeman and Company.
- Grimaldi, D. A., Engel, M. S., and Nascimbene, P. C. (2002). Fossiliferous cretaceous amber from Myanmar (Burma): its rediscovery, biotic diversity, and paleontological significance. *Am. Museum Novit.* 2002, 1–71. doi: 10.1206/0003-0082(2002)361<0001:fcaimb>2.0.co;2
- Hu, H., and O'Connor, J. K. (2017). First species of enantiornithines from sihedang elucidates skeletal development in early cretaceous enantiornithines. *J. Syst. Palaeontol.* 15, 909–926. doi: 10.1080/14772019.2016.1246111
- Jabłoński, P. (1996). Dark habitats and bright birds: warblers may use wing patches to flush prey. *Oikos* 75, 350–352.
- Ji, Q., Currie, P. J., Norell, M. A., and Ji, S.-A. (1998). Two feathered dinosaurs from northeastern China. *Nature* 393, 753–761. doi: 10.1038/31635
- Li, Q.-G., Clarke, J. A., Petey, J. A., and Shawkey, M. D. (2018). Elaborate plumage patterning in a Cretaceous bird. *PeerJ* 6:e5831. doi: 10.7717/peerj.5831
- Lovette, I. J., and Fitzpatrick, J. W. (2004). *The Handbook Of Bird Biology*. New Jersey: Princeton University Press.
- Lucas, S. G., and Stettenheim, P. R. (1972). *Avian Anatomy: Integument Part I*. Washington, DC: U.S. Department of Agriculture.
- Martínez-Delclòs, X., Briggs, D. E. G., and Peñalver, E. (2004). Taphonomy of insects in carbonates and amber. *Palaeogeogr. Palaeoclimatol. Palaeoecol.* 203, 19–64. doi: 10.1016/S0031-0182(03)00643-646
- O'Connor, J. (2012). A revised look at *Liaoningornis longidigitrus* (Aves). *Verteb. Palasiat.* 5, 25–37.
- O'Connor, J. (2020). “The plumage of basal birds,” in *The Evolution of Feathers*, eds C. Foth and O. W. M. Rauhut (Cham: Springer), 147–172. doi: 10.1007/978-3-030-27223-4_9
- O'Connor, J. K. (2019). The trophic habits of early birds. *Palaeogeogr. Palaeoclimatol. Palaeoecol.* 513, 178–195. doi: 10.1016/j.palaeo.2018.03.006
- O'Connor, J. K., Chiappe, L. M., and Bell, A. (2011). “Pre-modern birds: avian divergences in the mesozoic,” in *Living Dinosaurs: the Evolutionary History of Birds*, eds G. D. Dyke and G. Kaiser (Hoboken, NJ: J. Wiley & Sons), 39–114. doi: 10.1002/9781119990475.ch3
- O'Connor, J. K., Gao, K.-Q., and Chiappe, L. M. (2010). A new ornithuromorph (Aves: Ornithothoraces) bird from the Jehol group indicative of higher-level diversity. *J. Verteb. Paleontol.* 30, 311–321. doi: 10.1080/02724631003617498
- O'Connor, J. K., Wang, X.-R., Chiappe, L. M., Gao, C.-H., Meng, Q.-J., Cheng, X.-D., et al. (2009). Phylogenetic support for a specialized clade of cretaceous enantiornithine birds with information from a new species. *J. Verteb. Paleontol.* 29, 188–204. doi: 10.1080/02724634.2009.10010371
- Pan, Y.-H., Sha, J.-G., Zhou, Z.-H., and Fürsich, F. T. (2013). The Jehol biota: definition and distribution of exceptionally preserved relicts of a continental early cretaceous ecosystem. *Cretaceous Res.* 44, 30–38. doi: 10.1016/j.cretres.2013.03.007
- Perrichot, V. (2004). Early cretaceous amber from south-western france: insight into the mesozoic litter fauna. *Geol. Acta* 2, 9–22.
- Sanz, J. L., and Ortega, F. (2002). The birds from las hoyas. *Sci. Prog.* 85, 113–130. doi: 10.3184/003685002783238843
- Shi, G., Grimaldi, D. A., Harlow, G. E., Wang, J., Wang, J., Yang, M., et al. (2012). Age constraint on burmese amber based on U-Pb dating of zircons. *Cretaceous Res.* 37, 155–163. doi: 10.1016/j.cretres.2012.03.014
- Smithwick, F. M., Nicholls, R., Cuthill, I. C., and Vinther, J. (2017). Countershading and stripes in the theropod dinosaur sinosauropteryx reveal heterogeneous habitats in the early cretaceous Jehol biota. *Curr. Biol.* 27, 3337–3343.
- Thomas, D. B., Nascimbene, P. C., Dove, C. J., Grimaldi, D. A., and James, H. F. (2014). Seeking carotenoid pigments in amber-preserved fossil feathers. *Sci. Rep.* 4, 1–6.
- Wang, M., O'Connor, J., Zhou, S., and Zhou, Z.-H. (2019). New toothed early cretaceous ornithuromorph bird reveals intraclade diversity in pattern of tooth loss. *J. Syst. Palaeontol.* 18, 631–645. doi: 10.1080/14772019.2019.1682696
- Wang, M., and Zhou, Z.-H. (2019). A new enantiornithine (Aves: Ornithothoraces) with completely fused premaxillae from the early cretaceous of China. *J. Syst. Palaeontol.* 17, 1299–1312. doi: 10.1080/14772019.2018.1527403
- Wang, X.-L., O'Connor, J. K., Zheng, X.-T., Wang, M., Hu, H., and Zhou, Z.-H. (2014). Insights into the evolution of rachis dominated tail feathers from a new basal enantiornithine (Aves: Ornithothoraces). *Biol. J. Linnean Soc.* 113, 805–819. doi: 10.1111/bij.12313
- Wright, C. W., Callomon, J. H., and Howarth, M. K. (1996). “Cretaceous ammonioidea,” in *Treatise on Invertebrate Paleontology. Part I. Mollusca 4 (Revised)*, ed. R. L. Kaesler (Boulder: Geological Society of America), 362.
- Xing, L.-D., McKellar, R. C., and O'Connor, J. (2020). An unusually large bird wing in mid-cretaceous burmese amber. *Cretaceous Res.* 110:104412. doi: 10.1016/j.cretres.2020.104412
- Xing, L.-D., McKellar, R. C., O'Connor, J., Bai, M., Tseng, K.-W., and Chiappe, L. M. (2019a). A fully feathered enantiornithine foot and wing fragment preserved in mid-cretaceous burmese amber. *Sci. Rep.* 9, 1–9.
- Xing, L.-D., McKellar, R. C., O'Connor, J. K., Niu, K.-C., and Mai, H.-J. (2019b). A mid-cretaceous enantiornithine foot and tail feather preserved in Burmese amber. *Sci. Rep.* 9, 1–8.
- Xing, L.-D., O'Connor, J., Chiappe, L. M., McKellar, R. C., Carroll, N., Hu, H., et al. (2019c). A new enantiornithine with unusual pedal proportions found in amber. *Curr. Biol.* 29, 2396–2401.
- Xing, L.-D., McKellar, R. C., Wang, M., Bai, M., O'Connor, J. K., Benton, M. J., et al. (2016). Mummified precocial bird wings in mid-cretaceous burmese amber. *Nat. Commun.* 7:12089.
- Xing, L.-D., O'Connor, J. K., McKellar, R. C., Chiappe, L. M., Bai, M., Tseng, K.-W., et al. (2018a). A flattened enantiornithine in mid-cretaceous burmese amber: morphology and preservation. *Sci. Bull.* 63, 235–243. doi: 10.1016/j.scib.2018.01.019
- Xing, L.-D., Stanley, E. L., Bai, M., and Blackburn, D. C. (2018b). The earliest direct evidence of frogs in wet tropical forests from cretaceous burmese amber. *Sci. Rep.* 8:8770.
- Xing, L.-D., O'Connor, J. K., McKellar, R. C., Chiappe, L. M., Tseng, K.-W., Li, G., et al. (2017). A mid-Cretaceous enantiornithine (Aves) hatchling preserved in Burmese amber with unusual plumage. *Gondwana Res.* 49, 264–277. doi: 10.1016/j.gr.2017.06.001
- Zhang, F., Zhou, Z., Hou, L., and Gu, G. (2001). Early diversification of birds: evidence from a new opposite bird. *Chin. Sci. Bull.* 46, 945–949. doi: 10.1007/bf02900473
- Zhang, F.-C., Kearns, S. L., Orr, P. J., Benton, M. J., Zhou, Z.-H., Johnson, D., et al. (2010). Fossilized melanosomes and the colour of cretaceous dinosaurs and birds. *Nature* 463, 1075–1078. doi: 10.1038/nature08740
- Zheng, X.-T., O'Connor, J. K., Wang, X.-L., Pan, Y.-H., Wang, Y., Wang, M., et al. (2017). Exceptional preservation of soft tissue in a new specimen of eoconfuciusornis and its biological implications. *Natl. Sci. Rev.* 4, 441–452. doi: 10.1093/nsr/nwx004
- Zhou, Z., Barrett, P. M., and Hilton, J. (2003). An exceptionally preserved lower cretaceous ecosystem. *Nature* 421, 807–814. doi: 10.1038/nature01420

Conflict of Interest: The authors declare that the research was conducted in the absence of any commercial or financial relationships that could be construed as a potential conflict of interest.

Copyright © 2020 Xing, O'Connor, Niu, Cockx, Mai and McKellar. This is an open-access article distributed under the terms of the Creative Commons Attribution License (CC BY). The use, distribution or reproduction in other forums is permitted, provided the original author(s) and the copyright owner(s) are credited and that the original publication in this journal is cited, in accordance with accepted academic practice. No use, distribution or reproduction is permitted which does not comply with these terms.



New Information on the Keratinous Beak of *Confuciusornis* (Aves: Pygostylia) From Two New Specimens

Xiaoting Zheng^{1,2*}, Jingmai O'Connor^{3,4*}, Yan Wang^{1,2}, Xiaoli Wang^{1,2}, Yin Xuwei², Xiaomei Zhang² and Zhonghe Zhou^{3,4}

¹ Institute of Geology and Paleontology, Linyi University, Linyi, China, ² Tianyu Natural History Museum of Shandong, Pingyi, China, ³ Key Laboratory of Vertebrate Evolution and Human Origins of the Chinese Academy of Sciences, Institute of Vertebrate Paleontology and Paleoanthropology, Beijing, China, ⁴ Chinese Academy of Sciences (CAS) Center for Excellence in Life and Paleoenvironment, Beijing, China

OPEN ACCESS

Edited by:

Daniel J. Field,
University of Cambridge,
United Kingdom

Reviewed by:

Valentina Rossi,
University College Cork, Ireland
Christian Foth,
Université de Fribourg, Switzerland

*Correspondence:

Xiaoting Zheng
ty4291666@163.com
Jingmai O'Connor
jingmai@ivpp.ac.cn;
jingmai.oconnor@gmail.com

Specialty section:

This article was submitted to
Paleontology,
a section of the journal
Frontiers in Earth Science

Received: 17 April 2020

Accepted: 07 August 2020

Published: 16 September 2020

Citation:

Zheng X, O'Connor J, Wang Y,
Wang X, Xuwei Y, Zhang X and
Zhou Z (2020) New Information on
the Keratinous Beak of *Confuciusornis*
(Aves: Pygostylia) From Two New
Specimens. *Front. Earth Sci.* 8:367.
doi: 10.3389/feart.2020.00367

The keratinous beak is inferred to have evolved multiple times in the Archosauria and in Aves. Unfortunately, this feature rarely preserves in the fossil record. Here we examine a collection of 603 specimens belonging to the *Confuciusornithiformes*, a clade of edentulous basal avians, only two of which preserve visible traces of the rhamphotheca. Preservation is very different between the two specimens, offering no clues as to the taphonomic conditions that are conducive to preservation of this feature. These differences suggest that preservation of the rhamphotheca is not limited to a very narrow set of specific chemical conditions. We suggest the more common preservation of feathers over rhamphotheca is due to the higher melanin content in the former. The well-preserved traces in one specimen described here suggests that the rhamphotheca covering the upper and lower jaws each may consist of a pair of right and left elements, thus differing from the condition in neornithines in which the premaxillary nail and mandibular nail covering the rostral half of the upper and lower jaws respectively each form a single unit.

Keywords: rhamphotheca, keratin, beak, soft tissue, Jehol avifauna, Early Cretaceous, avian evolution, *Confuciusornithiformes*

INTRODUCTION

The beaked rostrum is one of the most distinctive features of birds, present in all living species and exhibiting an enormous diversity of form and size relative to the body (Lovette and Fitzpatrick, 2004; Gill, 2007). Although this morphological diversity is commonly associated with various feeding strategies, the actual relationship between shape and function is far more complex (Bright et al., 2016; Navalón et al., 2019). In some extant birds the rhamphotheca, the keratinous sheath that covers the edentulous bony rostrum and together form the beak, forms specialized structures such as filters (e.g., flamingos) and “teeth” (e.g., mergansers) that facilitate

certain feeding behaviors (Storer, 1960). In addition to its primary role in feeding, the beak has evolved a myriad of other functions including sound production (e.g., bill-clattering/culmen knocking in Storks) (Han et al., 1999), warfare (e.g., Toucans, Long-billed hermit hummingbird) (Rico-Guevara and Araya-Salas, 2015), thermoregulation (e.g., Toucans) (Tattersall et al., 2016), and inter and intraspecific signaling (e.g., Toucans, American goldfinches, King penguins) (Murphy et al., 2009; Nolan et al., 2010; Guaraldo et al., 2019). The keratinous beak is a dynamic feature – it grows continuously as it is also constantly worn away through use and can change in size, shape, and color in response to seasonal differences in functional requirements (Stettenheim, 1972; Matthysen, 1989; Bonser and Witter, 1993; Tattersall et al., 2016).

A keratinous beak was absent in the earliest bird, *Archaeopteryx*, which had a fully toothed rostrum (Elzanowski, 2002; Mayr et al., 2005; Rahut et al., 2018). Tooth reduction and an edentulous rostrum evolved numerous times during the Mesozoic evolution of Aves given the phylogenetic distribution of edentulous clades and clades containing edentulous taxa (O'Connor et al., 2011, 2016; O'Connor and Zhou, 2013; Wang M. et al., 2018). The oldest and most basal occurrence of a toothless rostrum in Aves is in the Early Cretaceous basal pygostylian clade, the Confuciusornithiformes, in the oldest and most primitive member of this clade – *Eoconfuciusornis* from the 131 Ma Huajiyang Formation (Hou et al., 1995b; Zhang et al., 2008). Tooth loss also evolved independently at least once in the diverse ornithothoracine clade, the Enantiornithes, as evidenced by the edentulous *Gobipteryx minuta* (Elzanowski, 1974; Chiappe et al., 2001). Tooth loss is far more common in the enantiornithine sister-clade the Ornithuromorpha, the clade that includes modern birds nested within (O'Connor et al., 2011). Several Early Cretaceous ornithuromorphs preserve edentulous rostra: *Archaeorhynchus* (Zhou and Zhang, 2006; Zhou et al., 2013), *Eogranivora* (Zheng et al., 2018), *Xinghaiornis* (Wang et al., 2013), *Schizoura* (Zhou et al., 2012), and *Dingavis* (O'Connor et al., 2016). The phylogenetic distribution of these taxa strongly suggests that tooth loss most likely evolved independently in each lineage and thus numerous times in this clade alone (O'Connor et al., 2016; Wang M. et al., 2018). Complete tooth loss in Mesozoic birds has been linked to herbivory (Louchart and Viriot, 2011; O'Connor, 2019), which is also suggested in some data from non-avian dinosaurs (Zanno and Makovicky, 2011; Wang et al., 2017).

In addition, some ornithuromorphs (e.g., *Yanornis*, *Yixianornis*) possess a rostrum that is only edentulous at the tip of the premaxillae, caudally followed by teeth (Zhou and Zhang, 2001). This edentulous tip, which ventrally articulates with the edentulous avian premaxilla, is inferred to have been covered by a small rhamphotheca (Bailleul et al., 2019). The entire premaxilla is edentulous in the Early Cretaceous *Iteravis* (Zhou et al., 2014) and in the Late Cretaceous ornithurines *Ichthyornis* (Field et al., 2018) and the Hesperornithiformes (Gingerich, 1973). However, the pattern of tooth loss in the Ornithuromorpha was not a straight-forward rostro-caudal reduction as previously hypothesized (Louchart and Viriot, 2011). *Mengciusornis*, a schizourid ornithuromorph closely related to the edentulous

Schizoura, possesses teeth only in the premaxilla, indicating that tooth loss in ornithuromorphs proceeded both rostro-caudally and caudo-rostrally (Wang et al., 2019a).

Like an edentulous rostrum, presumably rhamphothecae also evolved multiple times during the Cretaceous evolution of birds associated with each new occurrence of tooth loss or reduction (Hieronymus and Witmer, 2010). Although the absence of teeth is readily identifiable, actual traces of the rhamphothecae are rarely preserved in the fossil record (O'Connor, 2019). So far among Mesozoic Aves traces of the rhamphotheca have only been reported in four specimens referable to the Early Cretaceous basal pygostylian clade, the Confuciusornithiformes: the holotype of *Eoconfuciusornis zhengi*, the holotype of *Confuciusornis dui*, and two referred specimens of *Confuciusornis sanctus* (Hou et al., 1999; Zhang et al., 2008; Chiappe and Meng, 2016; Falk et al., 2019). More avian specimens from the Jehol Group are referable to the Confuciusornithiformes than to any other clade (Hou et al., 1995a,b, 1996, 1999, 2002; Chiappe et al., 1999, 2008; de Ricqlès et al., 2003; Dalsätt et al., 2006; Zhang et al., 2008, 2009; Li L. et al., 2010; Li et al., 2018; Marugán-Lobón et al., 2011; Chinsamy et al., 2013, 2019; Zheng et al., 2013, 2017; Falk et al., 2016; Jiang et al., 2017; Elzanowski et al., 2018; Wang and Zhou, 2018). A large number of described specimens boast well-preserved soft tissues most commonly in the form of feathers and keratinous ungual sheaths (e.g., Chiappe et al., 1999 – Figure 8, Falk et al., 2016 – Figure 1, Li et al., 2018 – Figure 1, Zheng et al., 2017 – Figure 1). Most specimens are recovered from the Yixian Formation and referred to *C. sanctus* (Wang et al., 2019b). *Confuciusornis sanctus* is without a doubt the fossil bird known from the greatest number of specimens in the world, with thousands reportedly known and scattered throughout collections primarily in China but also elsewhere (Elzanowski et al., 2018; Wang et al., 2019b). Most other Jehol birds with fully edentulous rostra are known from a single specimen (e.g., *Xinghaiornis*, *Eogranivora*) with the definite exception of *Archaeorhynchus*, which is known from five specimens, none of which preserve traces of the rhamphotheca (Zhou and Zhang, 2006; Zhou et al., 2013; Wang and Zhou, 2016; Wang X. et al., 2018).

The largest single collection of Confuciusornithiformes is that of the Shandong Tianyu Museum of Nature (STM) in Pingyi, China. The collection boasts 603 specimens, all of which consist of partial to nearly complete mostly articulated skeletons. It has been reported that 273 of these specimens preserve soft tissue in the form of feathers (Zheng et al., 2013). A survey of this collection identified only two specimens preserving traces of the soft tissue of the beak (Figures 1, 2). These specimens are described here and compared to other specimens preserving traces of the rhamphotheca with regards to shape and mode of preservation (Falk et al., 2019).

MATERIALS AND METHODS

603 specimens belonging to the Confuciusornithiformes in the collection of the STM were surveyed for preserved rhamphothecae. This feature was identified in two previously undescribed specimens, STM13-133 and STM13-162. As in

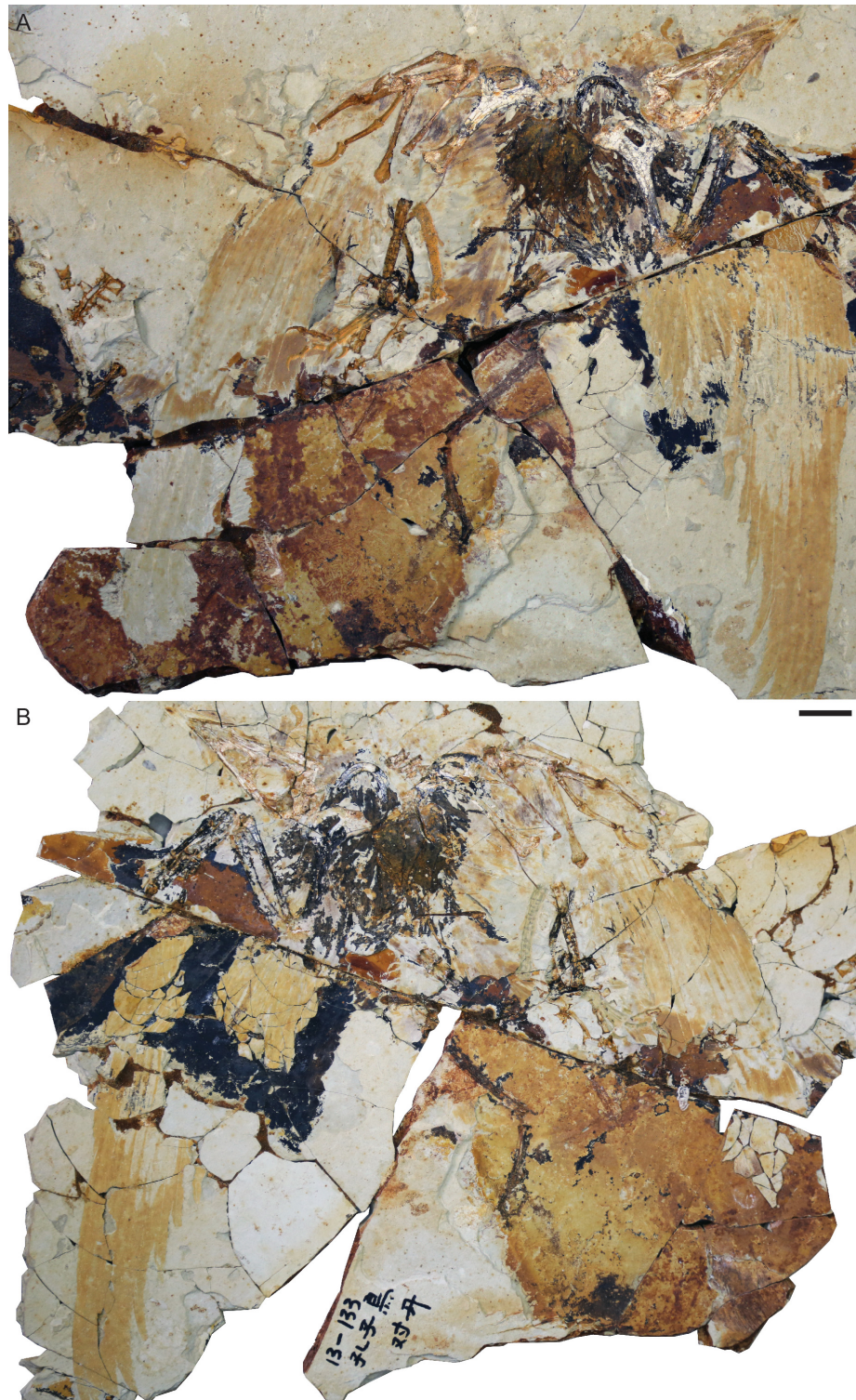


FIGURE 1 | *Confuciusornis* sp. STM13-133: **(A)** main slab; **(B)** counter-slab. Scale bar equals two centimeters.

all specimens preserving this feature, the traces are visible under normal light. These two specimens were studied using a Leica binocular microscope and photographed using a

Canon EOS 5DS. Measurements were taken using Fiji (ImageJ) 2.0. Figures and illustrations were generated using Adobe CC 2018.

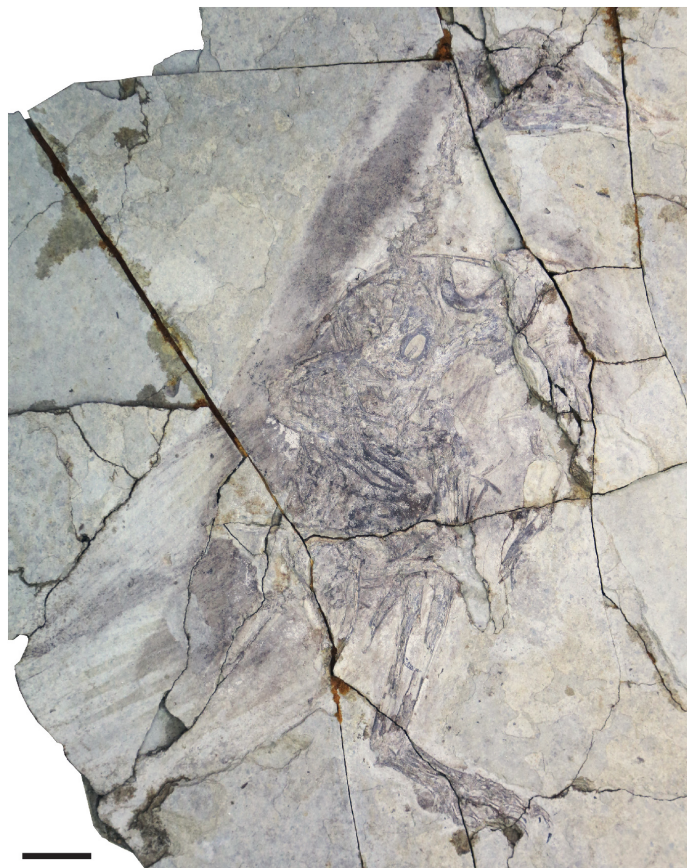


FIGURE 2 | *Confuciusornis* sp. STM13-162 (main slab). Scale bar equals two centimeters.

Terminology and Abbreviations

Osteological terminology primarily follows Baumel and Witmer (1993) using the English equivalents for the Latin terms (Baumel and Witmer, 1993). For terminology concerning the rhamphothecae we follow Hieronymus and Witmer (2010). Institutional abbreviations for other specimens preserving rhamphothecae: BMNHC, Beijing Museum of Natural History Collection, Beijing, China; IVPP, Institute of Vertebrate Paleontology and Paleoanthropology, Beijing, China.

DESCRIPTION

STM13-133

This specimen consists of a nearly complete and articulated individual preserved with feather impressions in a slab and counter-slab (**Figure 1**). STM13-133 can be readily identified as *Confuciusornis* based on the robust edentulous rostrum, stout boomerang shaped furcula lacking a hypocleidium, massive perforated deltopectoral crest on the humerus, and characteristic manual morphology with reduced major digit ungual (Chiappe et al., 1999). Where unbroken, the bones are preserved white with cracks distinctly visible in black. Where the bones are broken they reveal a reddish coloration indicative of iron oxidative

taphonomic processes. The feathers are preserved primarily as reddish impressions with the rachis clearly visible as a gap in some primaries. In the distal half of the left wing the barbs are preserved a pale white-pink color. In addition to the wings, in which impressions of the primaries, secondaries, and some coverts are fairly well-preserved, body feathers are preserved on the dorsal and ventral margins of the skull, ventral surface of the neck, left lateral surface of the body, and near the right knee. The keratinous sheaths covering the manual and pedal claws are mostly not preserved although the sheath covering the left minor digit ungual is partially preserved as a reddish stain.

The skull is preserved in left lateral view (**Figures 1, 3**). Although the general shape of the skull is well-preserved, the cranial bones themselves are very poorly preserved, with most elements preserved as reddish voids or elements torn in half between the slab and counter-slab. The traces of the rhamphotheca appear to consist of four distinct parts, suggesting that the rhamphotheca covering the upper jaw and the rhamphotheca covering the lower jaw each consisted of two elements. This is evident from the morphology of the preserved traces themselves and further suggested by the fact that short feathers appear to extend nearly to the rostral tip of the rostrum (approximately, only the rostral 4 mm of the premaxillary corpus lack feathers) and toward the tip of the mandibular symphysis

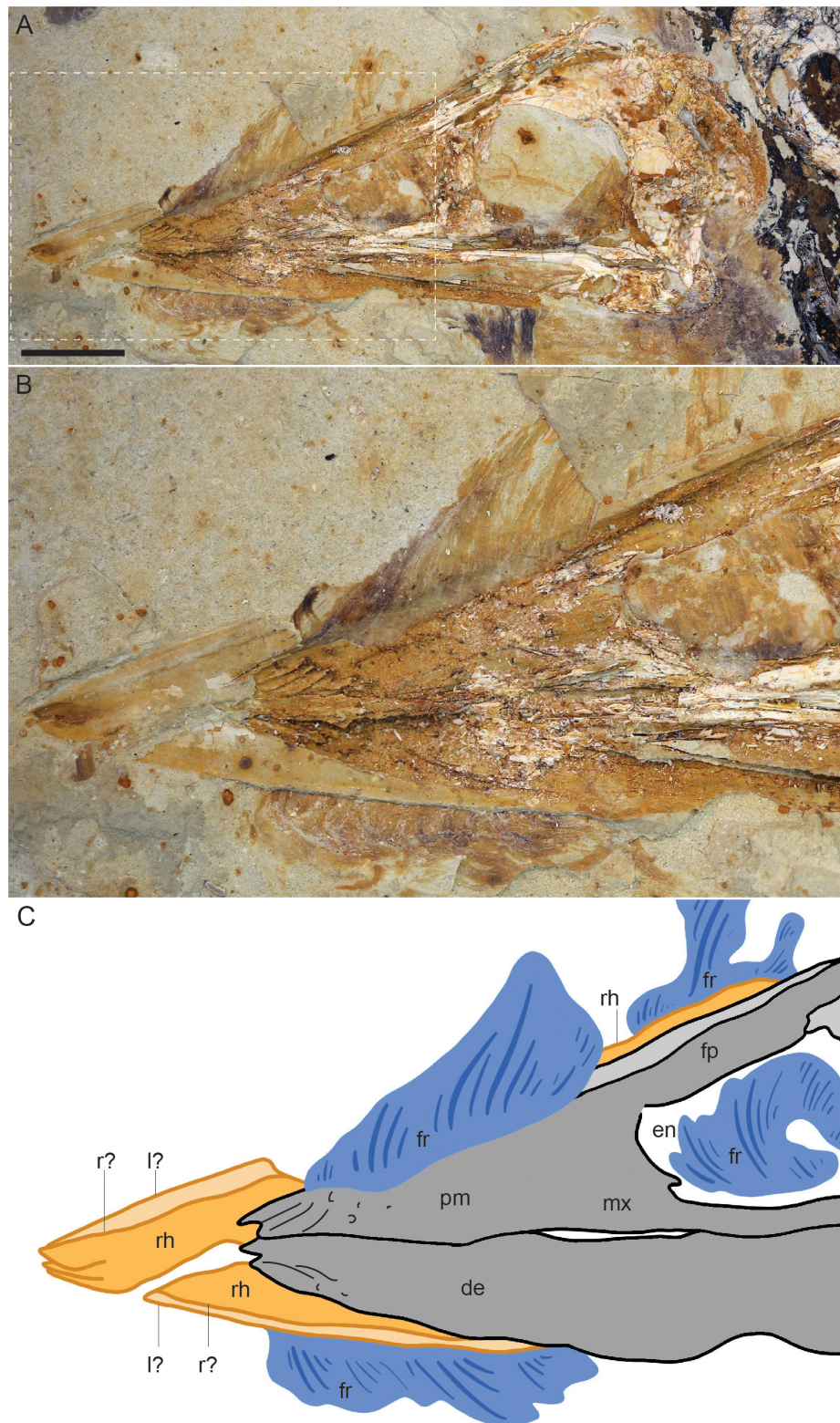


FIGURE 3 | Close up of the skull of *Confuciusornis* STM13-133: **(A)** photograph; **(B)** close up of the ramphothecal traces **(C)**, interpretative drawing of **(B)**. Dark gray indicates poorly preserved bone, light gray indicates bone preserved as voids, orange indicates the traces of the ramphothecae, and blue indicates feather traces. Anatomical abbreviations: de, dentary; en, external nares; fp, frontal process of the premaxilla; fr, feathers; l?, possible left side of the ramphotheca; mx, maxilla; pm, premaxilla; r?, possible right side of the ramphotheca; rh, ramphotheca.

(Figure 3). However, it cannot be ruled out that these “separate parts” of the rhamphothecae are not the result of post-mortem breakage (Foth and Rauhut, 2017).

The dorsal feathers are short, extend caudodorsally, and increase in height caudally until they disappear due to poor preservation (the layer of matrix preserving the soft tissue is chipped away in this region) just rostral to the level of the caudal margin of the external nares. From their rostral-most point until the cranial margin of the external nares the feathers appear to overlap the right frontal process of the premaxilla, however, it is likely that the basal portions of the feathers are not complete. Caudal to this point portions of the feather apices are preserved but not their basal portions, exposing a caudal portion of the rhamphotheca extending along the dorsal margin of the frontal process of the right premaxilla (Figure 3). This trace extends for approximately the length of the dorsal margin of the external nares with a fairly even thickness of 2.8 mm and ends rather abruptly just cranial to the caudal margin of the external nares suggesting it may be caudally incomplete.

The rhamphothecae extend rostrally from the premaxillae and dentaries just over 9 mm (Table 1). From the rostral position of the feathers and the pre-rostral length of the rhamphothecal traces it may be that both the rhamphothecae and the feathers are displaced rostrally. The traces of the upper and lower rhamphothecae overlap obscuring the dorsoventral thickness of these traces although the tips of each can be distinguished, preserved very close to each other consistent with the closed morphology of the jaws. The upper rhamphotheca appears to consist of two separate parts. The dorsal margin of each part can be distinctly observed due to the fact these margins are preserved a darker color than the remaining rhamphothecal traces (Figure 3). The dorsal margins of the right and left portions depart from a single point, approximately demarcating an angle of 8°. For most of their preserved length cranial to the premaxilla the dorsal margins extend caudally nearly parallel to each other, separated by a distance of 0.86 mm. Both traces are interrupted by the feathers on the dorsal (or dorsolateral) margin of the skull.

The rhamphothecae covering the mandible also appears to be formed by left and right parts, the tips of which are clearly preserved slightly offset from each other (Figure 3). This could be due to the notched morphology of the tip of the mandible itself (Chiappe et al., 1999). However, a faint line of darker reddish color extends through the lower rhamphothecal traces parallel to the ventral margin, continuous with the offset tip of the presumably right half of the mandibular rhamphotheca. The mandibular rhamphothecae extend rostrally to approximately the same level as the premaxillary rhamphothecae. As preserved the traces have a maximum thickness of 2.47 mm just rostral to the mandibular symphysis. Caudally it steadily decreases in thickness disappearing just rostral to the level of the cranial margin of the external nares. Similar to the upper jaw, the presence of left and right elements forming the mandibular rhamphothecae is supported by submalar feathers that extend far rostrally, presumably extending between the two halves of the mandibular rhamphothecae. These ventral feathers begin just caudal to the rostral tip of the mandibular bones and are separated from the

TABLE 1 | Comparative measurements of the rhamphothecae traces and body size in the six published confuciusornithiform specimens preserving this trace.

| Taxon | Specimen no. | Femur length | Skull length | Skull:femur | Upper rhamphotheca | | | | Lower rhamphotheca | | | | Feathers | Claws |
|--------------------------------|--------------|--------------|--------------|-------------|--------------------|----------------|---------------|-----------------------------------------------------------------|--------------------|----------------|---------------|-------------------|----------|-------|
| | | | | | Length total | Length rostral | Depth rostral | Depth dorsal (at level of rostral margin of the external nares) | Length total | Length rostral | Depth rostral | Depth ventral | | |
| <i>Confuciusornis dui</i> | IIPP V11553 | 33.8 | 42.58 | 1.259763314 | 16.75 | 6.8–7.9 | 1.7 | 0.6 | 10.42 | 5.88 | unknown | – | x | |
| <i>Confuciusornis sanctus</i> | IIPP V12352 | 41.9 | 60.64 | 1.44725537 | 29.48 | 6–7 | 2.8 | 0.9 | 3.2 | 1.2 | 0.64 | – | | x |
| <i>Confuciusornis</i> sp. | STM13-133 | 37.21 | 58.43 | 1.570276807 | 35.86 | 9.13 | 1.77 | 0.736 | 17.7 | 9.04 | 2.47 | Tapers constantly | x | x |
| <i>Confuciusornis</i> sp. | STM13-126 | – | 55.85 | | 26.8 | 5.9 | 5.09 | Tapers constantly | 19.02 | 6.66 | 1.52 | Tapers constantly | x | x |
| <i>Eoconfuciusornis zhengi</i> | IIPP V11977 | 35 | 41.46 | 1.184571429 | 2.16 | 1.3 | 0.83 | – | 6.57 | 3.07 | 1.6 | – | x | |
| <i>Confuciusornis sanctus</i> | BMNH-C-PH986 | 54.1 | 75.1 | 1.388170055 | 20.51 | 6.79 | 2.92 | Tapers constantly | 9.81 | 6.81 | 2.27 | – | x | x |

dentary by the preserved trace of the mandibular rhamphothecae. The feather traces are interrupted by poor preservation (the layer preserving the soft tissue is clearly not preserved, exposing a lower level of sediment) at the level of the external nares, but appear again at the level of the antorbital fenestra and continue caudally, continuous with feathers along the ventral surface of the neck.

STM13-162

STM13-162 represents a complete specimen preserved in lateral view in a slab and counter-slab (**Figure 2**). The specimen is preserved in an unusual position with all the limbs folded close to the body. Faint traces of feathers are visible around the skeleton including traces of the wings. The keratinous sheaths covering the manual and pedal unguals are preserved. Dark material in the orbit may be soft tissue traces of the eye. Like STM13-133, STM13-162 is referable to *Confuciusornis* based on the robust edentulous rostrum, stout boomerang shaped furcula lacking a hypocleidium, massive perforated deltopectoral crest on the humerus, and characteristic manual morphology with hypertrophied alular ungual and reduced major digit ungual (Chiappe et al., 1999).

The skull is preserved in lateral view (**Figures 2, 4**). Although the skull is complete and it retains its general shape the bones are crushed with little to no clearly preserved anatomical details. Notably, the tip of the fused premaxillae are slightly but distinctly downturned (**Figure 4**). Traces of the rhamphothecae from both the upper and lower jaws are visible in both slabs but more clearly observed in the main slab. These traces appear to be slightly displaced from their natural positions. The upper rhamphotheca trace is displaced dorsally so that the ventral margin is not level with the ventral margin of the premaxilla (**Figure 4**). The traces extend 5.9 mm from the premaxillae with a total length of 26.8 mm, dorsally ending near the caudal margin of the external nares. The pre-rostral portion of the traces form a triangular impression, divided dorsally and ventrally by the fact the dorsal portion that is continuous with the trace extending caudally over the frontal processes of the premaxillae is much darker. The margin dividing the darker (dorsal) and lighter (ventral) traces is interpreted as the ventral margin of the trace of either the right or left upper rhamphotheca, with the opposing trace somewhat displaced ventrally, forming the lighter portion of the pre-rostral impression of the rhamphothecae (**Figure 4**).

The trace of the mandibular rhamphotheca extends 6.66 mm from the dentaries and has a total length of 19.02 mm. The traces have a fairly even thickness of 1.52 mm except where they taper away caudally.

DISCUSSION

Due to the rare preservation of the rhamphotheca in the fossil record, very little is known about this feature in extinct organisms. As such, each new specimen has the potential to provide new information. So far among Mesozoic birds, data has only been recovered for the Cretaceous *Confuciusornithiformes* (Hou et al., 1999; Zhang et al., 2008; Chiappe and Meng, 2016;

Falk et al., 2019). Most birds collected in deposits corresponding to the Lower Cretaceous Yixian Formation are referable to this clade. Counter intuitively, the horny sheath or rhamphotheca that covers the rostrum in edentulous birds is less likely to preserve than the more pliable feather integument (Falk et al., 2019). In a collection of 603 specimens of *confuciusornithiformes* nearly half preserve feathers on some part of the body (273 specimens, 45%) (Zheng et al., 2013). In contrast, only two specimens preserve some trace of the beak – that is 0.33% of the collection. This percentage is likely exaggerated by at least two factors. First, most fossils in the STM collection are not fully prepared and what preparation has been done was conducted prior to being placed in the collections of the STM and was not done by professionals. This may make it more difficult to identify the subtle traces of the preserved rhamphothecae, which are proportionately small compared to traces of the plumage. Furthermore, these subtle traces may also have been lost during cursory non-professional preparation attempts. The rhamphothecal traces preserved in *Confuciusornis* IVPP V12352 are surrounded by clear marks of preparation (Falk et al., 2019 – **Figure 1A**) – unfortunately, there is not enough data currently available to assess to what extent the morphology of these and other soft tissue traces are affected by the work of preparators. Second, as the collection was aggregated an emphasis may have been placed on acquiring feathered specimens, which are visually striking, but not on specimens preserving the rhamphotheca, a soft tissue feature that is less obvious and easily overlooked. Unsurprisingly, the two specimens preserving beak traces described here also preserve feathers. Of the two new specimens, STM13-133 is the better preserved and offers the most significant new morphological information.

Confuciusornithiform Beak Traces Compared

The appearance of the two new specimens STM13-133 and STM13-162 suggests very different modes of preservation, presumably contributing to the diversity of taphonomic processes that apparently lead to the preservation of rhamphothecae in Jehol specimens. Preservation is very different in all six known specimens that record these traces, among these differences varying with respect to the quality of bone preservation (excellent in *E. zhengi* IVPP V11977 and *C. sanctus* IVPP V12352) and preservation of feathers (preserved in all but *C. sanctus* IVPP V12352). Notably, several specimens appear to preserve some non-keratinous soft tissue (e.g., probable eye tissue in STM13-162; abdominal tissues in *E. zhengi* IVPP V11977) indicative of exceptional preservation.

In STM13-133 the mandibular rhamphothecae extend rostrally to approximately the same level as the premaxillary rhamphothecae as in *C. dui* IVPP V11553 and *C. sanctus* BMNHC-PH986, whereas the premaxillary traces extend farther in *C. sanctus* IVPP V12352 and STM13-162 and the mandibular traces extend farther in *E. zhengi* IVPP V11977. With the limited information available it is impossible to determine to what degree this is due to taphonomy vs. actual interspecific differences. The

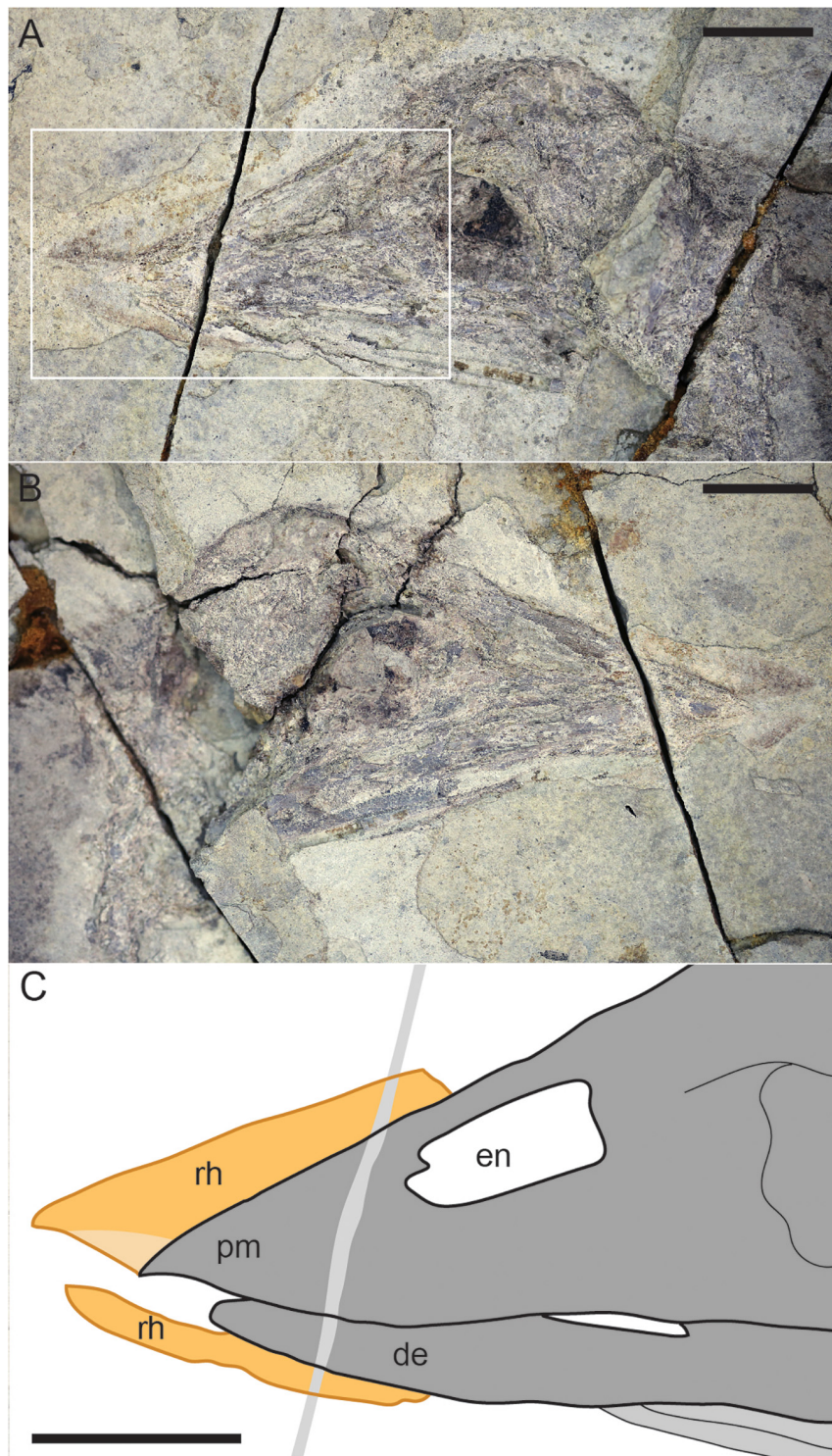


FIGURE 4 | Close up of the skull of *Confuciusornis* STM13-162: **(A)** photograph of slab; **(B)** photograph of counter slab; **(C)** interpretative drawing. Scale bars equal one centimeter. For anatomical abbreviations see **Figure 3** caption.

traces in the two STM specimens are much more comparable to those in *C. sanctus* IVPP V12352 – so far *C. dui* IVPP V11553 is unique in having a ramphotheca that is rostrally upturned

and this may be a diagnostic feature of this taxon. However, the holotype and only known specimen has been lost making *C. dui* a nomen dubium.

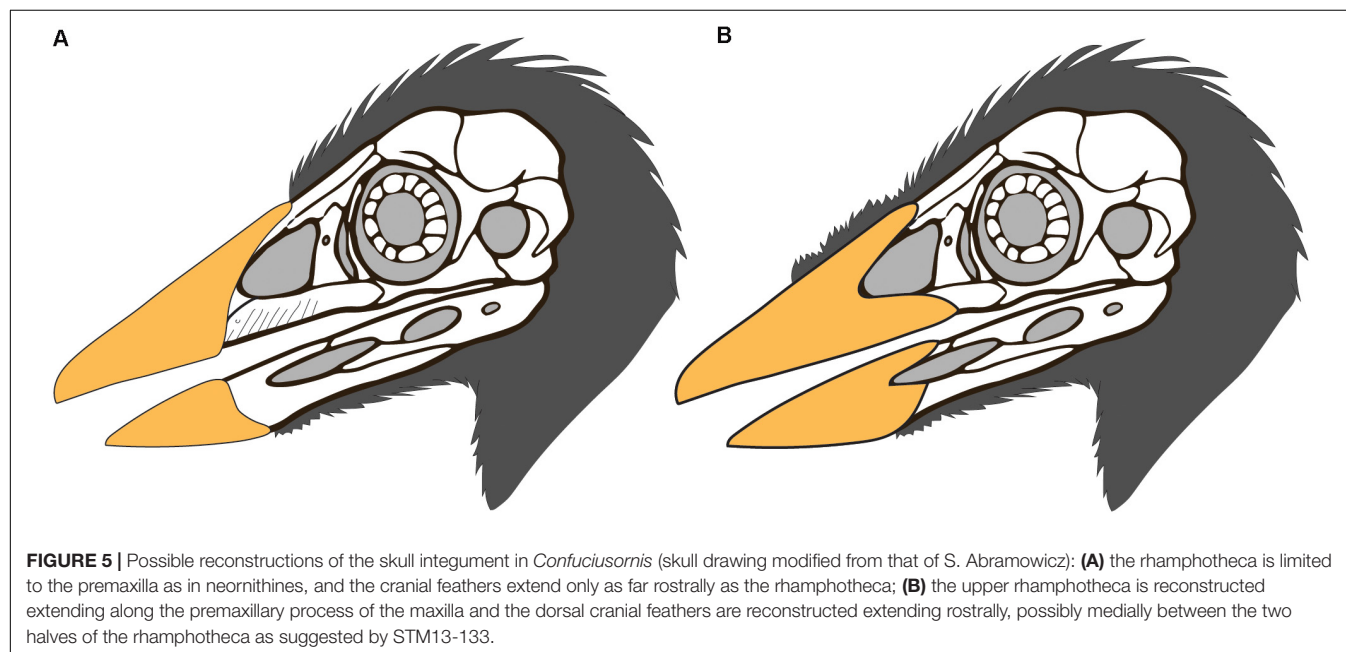
Notably, in the five specimens in which both skull and femur length can be measured the skull is proportionately much larger in specimens of greater body size (Table 1). Interpretations are obscured by the taxonomic diversity of these confuciusornithiforms. However, at least *E. zhengi* IVPP V11977 is regarded as a subadult. This may suggest that the skull becomes proportionately longer in mature individuals. A proportionately short rostrum is a common indicator of ontogenetic immaturity (Bhullar et al., 2016). This also suggests that ontogeny is not a factor that plays into preservation of the rhamphotheca since this feature is preserved in both subadult and adult specimens.

Non-ornithurine Rhamphothecal Morphology

Ichthyornis and *Hesperornis* were described as having osteological correlates that indicate the presence of compound rhamphothecae with the upper jaws covered by a premaxillary nail, culmicorn and paired latericorns and the lower jaw rhamphothecae consisting of a mandibular nail and paired ramicornes (Hieronymus and Witmer, 2010). This in turn was used to infer that the presence of compound rhamphothecae covering the rostrum is plesiomorphic to the crown clade (Hieronymus and Witmer, 2010). However, a recent comprehensive description of the skull of *Ichthyornis* based on multiple new specimens indicates that osteological features of compound rhamphothecae, i.e., a nasolabial groove on the upper jaw and mentolabial grooves on the mandibles (Hieronymus and Witmer, 2010), are in fact absent (Field et al., 2018). Only a premaxillary nail is inferred to be present in this taxon based on the presence of numerous neurovascular foramina on the rostral portion of the edentulous premaxilla, presumably accentuating the hooked morphology of this element (Field et al., 2018). A mandibular nail was absent but a small keratinous sheath likely

covered the outer surface of the prementary bone present in these non-neornithine ornithurines (Zhou and Martin, 2011; Bailleul et al., 2019), thus the condition in *Hesperornis* and *Ichthyornis* represents a primitive rhamphothecal morphology not present in neornithines (the prementary being a feature restricted to non-neornithine ornithuromorphs).

An edentulous rostrum covered by rhamphothecae in the Confuciusornithiformes evolved independently from that in ornithurines like *Ichthyornis*, enantiornithines like *Gobipteryx*, basal ornithuromorphs like *Archaeorhynchus* and *Eogranivora*, and other stem lineages that display some form of tooth reduction and thus may have had small beaked portions of the rostrum similar to *Ichthyornis* (e.g., *Jeholornis*, *Sapeornis*) (Hieronymus and Witmer, 2010). Therefore, it would not be unexpected to find morphological differences in this feature between Cretaceous avian clades. In most neornithines the caudal extent of the rhamphothecae of the upper jaw is approximated by the caudal extent of the maxillary process of the premaxilla (Hieronymus and Witmer, 2010). If confuciusornithiforms shared this condition with neornithines it would suggest that the ventral and lateral portion of the rhamphotheca below the external nares would be rostrally limited due to the fact that the maxilla makes up a majority of the facial margin (Figure 5A). It cannot be determined if the ventral margin of the rhamphotheca ends level with the premaxillomaxillary contact since the ventral margin below the premaxilla is not preserved in any specimen and similarly the lateral portions of the rhamphotheca are also not preserved (presumably lost during preparation). However, we suggest it is more likely that confuciusornithiforms differed from neornithines in this feature and that the rhamphotheca extended onto the maxilla in confuciusornithiforms (Figure 5B). This is supported by the fact that the maxilla, like the premaxilla and dentary, also bears pits and grooves indicative of neurovasculature (Figure 6).



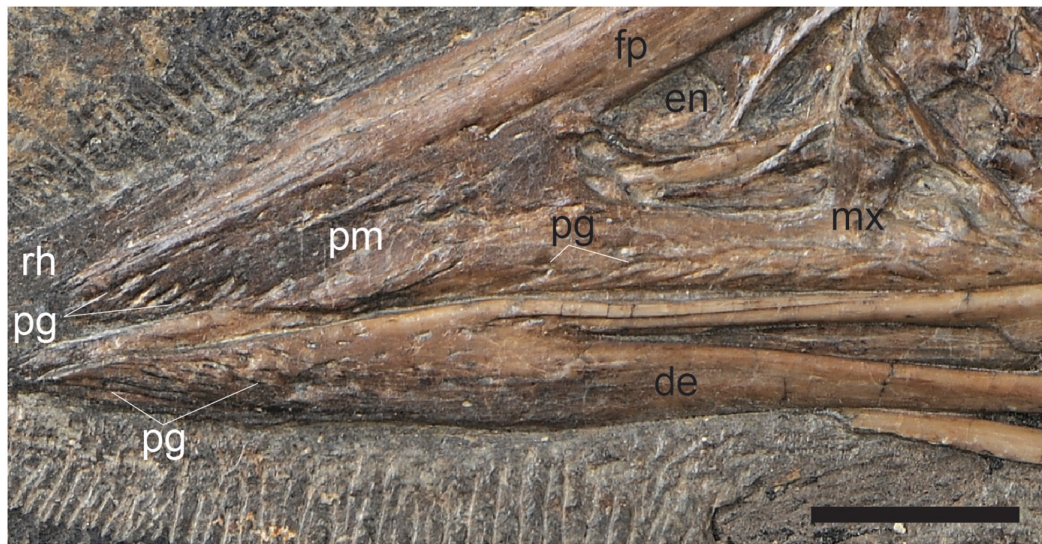


FIGURE 6 | A close up of the cranial half of the rostrum in *C. sanctus* IVPP V12352 showing the pits and grooves that cover the premaxillary body, premaxillary process of the maxilla, and the rostral portion of the dentaries, inferred to reflect neurovasculature related to the presence of a keratinous beak. Scale bar equals five millimeters. Anatomical abbreviations not listed in **Figure 3** caption: pg, pits and grooves.

Compared to the premaxillary body and the rostral portion of the dentary, the maxilla is dominated by grooves and pits are less common. These pits and grooves are only present on the premaxillary process of the maxilla suggesting the caudal-most extension of the rhamphotheca on the upper jaw was the caudal margin of the external nares, which is partially enclosed caudally by the nasal process of the maxilla that divides this element into premaxillary and jugal processes. Notably there are no osteological correlates (pits, grooves) that support the caudal extension of the rhamphotheca along the dorsal surface of the skull although the presence of the rhamphotheca is demonstrated by direct evidence in several specimens (IVPP V12352, STM13-133).

Nasolabial, culminolabial, and mentolabial grooves, features that indicate the divisions between the compound rhamphothecal elements in neornithines, are not visible in the skull bones of *Confuciusornis*. The premaxillary nail, the only portion of the neornithine rhamphotheca considered present in *Ichthyornis*, is rostrally restricted (Hieronymus and Witmer, 2010). At least along the dorsocranial margin the rhamphotheca is caudally extensive in *Confuciusornis* (Falk et al., 2019). The absence of a culminolabial groove may suggest that the rhamphotheca covering the tip of the premaxilla and frontal processes of the premaxilla were not separated into a premaxillary nail and culminocorn as in neornithines with compound rhamphothecae. This is also supported by the morphology of the traces in IVPP V12352 in which the dorsal margin of the preserved rhamphothecal traces are smooth along their entirety (Falk et al., 2019). This suggests the condition in confuciusornithiforms was more reminiscent of the simple rhamphotheca in many living birds in which the compound elements are entirely fused and grooves are absent (Hieronymus and Witmer, 2010). However, unlike in neornithines, in

which the premaxillary nail and mandibular nail are single elements (Kingsbury et al., 1953), evidence from STM13-133 may suggest that the rhamphotheca covering the upper and lower jaws including the rostral-most portions may have been compound elements medially divided into left and right components.

Although STM13-133 is the only specimen to preserve evidence suggesting the confuciusornithiform rhamphotheca was divided into right and left halves, it may be that only one side, presumably the side still buried in matrix (for example, the right in IVPP V12352), is preserved in most specimens due to the lateral exposure of the skull and or taphonomy, or that the two halves were tightly attached rostrally. The morphology in STM13-162 somewhat supports the interpretation at least that the upper rhamphotheca consisted of left and right halves but the weakly preserved traces provide no definitive information. However, without additional data it is impossible to rule out the alternative that the appearance of right and left components forming the rhamphotheca in STM13-133 is an artifact of preservation. Potentially the upper and lower rhamphothecae were crushed and broken giving the appearance of consisting of two parts. Crushed, two-dimensional fossils often preserve fractures than can be misinterpreted as true morphologies (Foth and Rahhut, 2017).

Considerations Regarding Preservation of the Rhamphotheca

Falk et al. (2019) discussed the differential preservation of various keratinous integumentary structures in the numerous described specimens of confuciusornithiforms. Despite evidence that the rhamphotheca is the hardest of the beta-keratin integumentary structures (Bonser, 1996), it is the least commonly preserved

and notably there appears no pattern in the preservation of specific keratin structures (Table 1). STM13-133 and STM13-162 offer no information that elucidates this issue. Superficially, preservation appears very different between these two specimens, offering no clues as to the taphonomic conditions that are conducive to preservation of this feature. Differences in bone coloration hint at different mineralization processes (iron oxidative processes were clearly part of the taphonomic history of STM13-133 as indicated by the reddish color where the bones are broken and the reddish stains forming the feather traces, but not STM13-162). Differences in preservation of the plumage also point to different modes of preservation; a large portion of the plumage is preserved in STM13-133 and these are mostly preserved as reddish stains, whereas the feathers in STM13-162 are only faintly preserved. The stark contrasting modes of preservation (evident from comparing the quality of preservation of structures such as bone and feathers and differences in mineral composition as superficially determined by differences in color) between the two specimens confirms previous observations that preservation of the rhamphotheca is not limited to a very narrow set of specific chemical conditions (Falk et al., 2019). In the future, chemical analyses of specimens preserving rhamphothecal traces may shed light on the specific taphonomic processes and geochemical conditions conducive to the preservation of these traces.

Given the differential preservation of keratinous structures in various specimens, we hypothesize that the preservation of keratinous integumentary structures may not be related to properties of the keratin itself. The common preservation of feathers compared to the rhamphotheca may be due to the fact that the former is commonly melanized in confuciusornithiforms, as demonstrated in multiple specimens (Zhang et al., 2010; Zheng et al., 2017; Li et al., 2018). The addition of melanin to keratinous structures increases their relative hardness (Bonser and Witter, 1993). Melanin is extremely resistant to decay and most preserved feathers in Jehol specimens that have been studied using SEM have been described as remnants of the melanosomes rather than the keratinous matrix (Zhang et al., 2010; Li et al., 2012, 2018; Vinther, 2015; Peteya et al., 2017; Zheng et al., 2017). A survey of SEM studies conducted on feathers preserved in Jehol paravians reveals that most commonly melanosomes are preserved together with their impressions (Li Q. et al., 2010; Zhang et al., 2010; Peteya et al., 2017; Zheng et al., 2017; Hu et al., 2018). This may be related to the fact that most Jehol specimens are preserved split between a slab and counter-slab; the act of splitting may be responsible for the formation of impressions of melanosomes in the surrounding matrix (whether consisting of degraded or petrified remnants of the feather keratin or sediment) just as voids are left by bones that remain in the opposite slab. The few studies in which only imprints (Li et al., 2012) or melanosomes (O'Connor et al., 2020) were recovered may reflect limited sampling. However, even where only impressions of melanosomes were recovered, keratin was reportedly not preserved (Li et al., 2012). Although understanding of feather preservation in the Jehol and other deposits is currently incomplete, available studies strongly suggest that a majority

of feather traces contain preserved melanosomes. The rare preservation of the rhamphothecae in confuciusornithiforms may suggest this structure was not melanized in most members of this clade (in neornithines both melanic and non-melanic beak morphologies are present). The only known specimen of *C. dui* preserves traces of the rhamphotheca (Hou et al., 1999) and thus hypothetically it is possible the bill may have been melanized in this species. Unfortunately, this hypothesis cannot be tested since the specimen is lost. Alternatively, the bill may be seasonally melanized, like that of some extant birds (Bonser and Witter, 1993), and only preserved in individuals that died during this particular season. Although the overall scarcity of such traces (now six specimens reported out of purportedly thousands) suggests that the rhamphotheca was simply not melanized, it is possible to test these two hypotheses by sampling bill traces preserved in specimens of *Confuciusornis* and studying them using scanning electron microscopy (SEM) in order to determine the presence or absence of preserved melanosomes. However, the rarity of these traces and their relatively limited surface area (compared to feathers) make it unlikely that this will be possible due to the destructive nature of SEM sampling. If confuciusornithiforms had non-melanic rhamphothecae this would indicate the bill was lightly colored, thus providing new data that will translate to more accurate reconstructions of this important clade of Cretaceous birds (Figure 5).

CONCLUSION

A total of six confuciusornithiforms preserving traces of the rhamphothecae have now been identified. Preservation is very different between all six specimens, thus providing no information pertaining to the specific taphonomic conditions that are conducive to the preservation of this feature. In the future, chemical analyses on all six specimens will hopefully elucidate the different diagenetic pathways that are conducive to preservation of the rhamphotheca, at least in confuciusornithiforms. The rare preservation of rhamphothecae may suggest that the beak in confuciusornithiforms was non-melanic and thus lightly colored. Although it was reasonable to assume that the rhamphothecae would have a different morphology in each independent evolutionary origin of this feature, this study provides the first discussion of the differences between the rhamphothecae in non-neornithine ornithurines, confuciusornithiforms, and neornithines. In addition to having rhamphotheca that extends onto the maxilla, one specimen suggests that the *Confuciusornis* rhamphotheca may have been a compound structure consisting of right and left halves on both the upper and lower jaws. Osteological and soft tissue evidence suggests that the rhamphothecae covering the upper jaw extended dorsally and laterally to the caudal margin of the external nares. Notably, evidence from several specimens indicates that although pits and grooves may indicate the presence of a rhamphotheca, they do not correlate strictly with the extent of this feature as the frontal processes of the premaxilla lack pits and grooves but were clearly covered in rhamphotheca in confuciusornithiforms.

DATA AVAILABILITY STATEMENT

All datasets generated for this study are included in the article/**Supplementary Material**, further inquiries can be directed to the corresponding authors.

AUTHOR CONTRIBUTIONS

XTZ, JO'C, ZZ, YW, and XW designed the project. JO'C wrote the manuscript. YW photographed the specimen. All authors examined the collection for rhamphothecae.

FUNDING

This research was supported by the National Natural Science Foundation (Grant Nos. 41688103, 41402017, and 41372014)

REFERENCES

- Bailleul, A. M., Li, Z.-H., O'Connor, J. K., and Zhou, Z.-H. (2019). Origin of the avian prehendatory and evidence of a unique form of cranial kinesis in Cretaceous ornithuromorphs. *Proc. Natl. Acad. Sci. U.S.A.* 116, 24696–24706. doi: 10.1073/pnas.1911820116
- Baumel, J. J., and Witmer, L. M. (1993). "Osteologia," in *Handbook of Avian Anatomy: Nomina Anatomica Avium*, 2nd Edn, eds J. J. Baumel, A. S. King, J. E. Breazile, H. E. Evans, and J. C. Vanden Berge (Cambridge, MA: Nuttall Ornithological Club), 45–132.
- Bhullar, B.-A., Hanson, M., Fabbri, M., Pritchard, A., Bever, G. S., and Hoffman, E. (2016). How to make a bird skull: major transitions in the evolution of the avian cranium, paedomorphosis, and the beak as a surrogate hand. *Integr. Comp. Biol.* 56, 389–403. doi: 10.1093/icb/icw069
- Bonsler, R. H. (1996). Comparative mechanics of bill, claw and feather keratin in the Common Starling *Sturnus vulgaris*. *J. Avian Biol.* 27, 175–177.
- Bonsler, R. H., and Witter, M. S. (1993). Indentation hardness of the bill keratin of the European starling. *Condor* 95, 736–738. doi: 10.2307/1369622
- Bright, J. A., Marugán-Lobón, J., Cobb, S. N., and Rayfield, E. J. (2016). The shapes of bird beaks are highly controlled by nondietary factors. *Proc. Natl. Acad. Sci. U.S.A.* 113, 5352–5357. doi: 10.1073/pnas.1602683113
- Chiappe, L. M., Ji, S., Ji, Q., and Norell, M. A. (1999). Anatomy and systematics of the Confuciusornithidae (Theropoda: Aves) from the Late Mesozoic of northeastern China. *Bull. Am. Mus. Nat. Hist.* 242, 1–89.
- Chiappe, L. M., Marugán-Lobón, J., Ji, S., and Zhou, Z. (2008). Life history of a basal bird: morphometrics of the early cretaceous *Confuciusornis*. *Biol. Lett.* 4, 719–723. doi: 10.1098/rsbl.2008.0409
- Chiappe, L. M., and Meng, Q.-J. (2016). *Birds of Stone*. Baltimore, MD: JHU Press.
- Chiappe, L. M., Norell, M., and Clark, J. (2001). A new skull of *Gobiapteryx minuta* (Aves: Enantiornithes) from the cretaceous of the Gobi desert. *Am. Mus. Novit.* 3346, 1–15. doi: 10.1206/0003-0082(2001)346<0001:ansogm>2.0.co;2
- Chinsamy, A., Chiappe, L. M., Marugán-Lobón, J., Gao, C.-H., and Zhang, F.-J. (2013). Gender identification of the Mesozoic bird *Confuciusornis sanctus*. *Nat. Commun.* 4:1381. doi: 10.1038/ncomms2377
- Chinsamy, A., Marugán-Lobón, J., Serrano, F. J., and Chiappe, L. M. (2019). Osteohistology and life history of the basal pygostylian, *Confuciusornis sanctus*. *Anat. Rec.* 303, 949–962. doi: 10.1002/ar.24282
- Dalsätt, J., Zhou, Z., Zhang, F., and Ericson, P. G. P. (2006). Food remains in *Confuciusornis sanctus* suggest a fish diet. *Naturwissenschaften* 93, 444–446. doi: 10.1007/s00114-006-0125-y
- de Ricqlès, A. J., Padian, K., Horner, J. R., Lamm, E.-T., and Myhrvold, N. (2003). Osteohistology of *Confuciusornis sanctus* (Theropoda: Aves). *J. Vertebr. Paleontol.* 23, 373–386. doi: 10.1671/0272-4634(2003)023[0373:oocta]2.0.co;2
- Elzanowski, A. (1974). Preliminary note on the palaeognathous bird from the Upper Cretaceous of Mongolia. *Palaeontol. Pol.* 30, 103–109.
- and the Taishan Scholars Program of Shandong Province (Grant No. Ts20190954).

ACKNOWLEDGMENTS

We thank Y. O'Connor for assistance with figures and L. Chiappe and S. Abramowicz for providing images of the BMNH specimen and allowing use of their reconstruction of the skull of *Confuciusornis*.

SUPPLEMENTARY MATERIAL

The Supplementary Material for this article can be found online at: <https://www.frontiersin.org/articles/10.3389/feart.2020.00367/full#supplementary-material>

- Elzanowski, A. (2002). "Archaeopterygidae (Upper Jurassic of Germany)," in *Mesozoic Birds: Above the Heads of Dinosaurs*, eds L. M. Chiappe and L. M. Witmer (Berkeley, CA: University of California Press), 129–159.
- Elzanowski, A., Peters, D. S., and Mayr, G. (2018). Cranial morphology of the early cretaceous bird *Confuciusornis*. *J. Vertebr. Paleontol.* 38:e1439832. doi: 10.1080/02724634.2018.1439832
- Falk, A. R., Kaye, T. G., Zhou, Z.-H., and Burnham, D. A. (2016). Laser fluorescence illuminates the soft tissue and life habits of the early cretaceous bird *Confuciusornis*. *PLoS One* 11:e0167284. doi: 10.1371/journal.pone.0167284
- Falk, A. R., O'Connor, J., Wang, M., and Zhou, Z.-H. (2019). On the preservation of the beak in *Confuciusornis* (Aves: Pygostylia). *Diversity* 11, 1–8.
- Field, D. J., Hanson, M., Burnham, D. A., Wilson, L. E., Super, K., Ehret, D., et al. (2018). Complete *Ichthyornis* skull illuminates mosaic assembly of the avian head. *Nature* 557, 96–100. doi: 10.1038/s41586-018-0053-y
- Foth, C., and Rauhut, O. W. M. (2017). Re-evaluation of the Haarlem *Archaeopteryx* and the radiation of maniraptoran theropod dinosaurs. *BMC Evol. Biol.* 17:236. doi: 10.1186/s12862-017-1076-y
- Gill, F. B. (2007). *Ornithology*, 3rd Edn. New York, NY: W.H. Freeman and Company.
- Gingerich, P. D. (1973). Skull of *Hesperornis* and early evolution of birds. *Nature* 243, 70–73. doi: 10.1038/243070a0
- Guaraldo, A. C., Antequeras, L. M. C., and Manica, L. T. (2019). Beyond a feeding and thermoregulatory structure: toucan's bill as a sword and pincer. *Rev. Bras. Ornitol.* 27, 145–148. doi: 10.1007/bf03544462
- Han, X.-D., Wu, Z.-G., Tian, F.-M., and Sun, F. (1999). Observation on behavior of adult oriental white stork in nesting period. *J. For. Res.* 10, 118–120. doi: 10.1007/bf02855541
- Hieronymus, T. L., and Witmer, L. M. (2010). Homology and evolution of avian compound rhamphothecae. *Auk* 127, 590–604. doi: 10.1525/auk.2010.09122
- Hou, L., Martin, L. D., Zhonghe, Z., Feduccia, A., and Zhang, F. (1999). A diapsid skull in a new species of the primitive bird *Confuciusornis*. *Nature* 399, 679–682. doi: 10.1038/21411
- Hou, L., Martin, L. D., Zhou, Z., and Feduccia, A. (1996). Early adaptive radiation of birds: evidence from fossils from northeastern China. *Science* 274, 1164–1167. doi: 10.1126/science.274.5290.1164
- Hou, L., Zhou, Z., Gu, Y., and Zhang, H. (1995a). *Confuciusornis sanctus*, a new late Jurassic sauririne bird from China. *Chin. Sci. Bull.* 40, 1545–1551.
- Hou, L., Zhou, Z.-H., Martin, L. D., and Feduccia, A. (1995b). A beaked bird from the Jurassic of China. *Nature* 377, 616–618. doi: 10.1038/377616a0
- Hou, L., Zhou, Z., Zhang, F., and Gu, Y. (2002). *Mesozoic Birds from Western Liaoning in China*. Shenyang: Liaoning Science and Technology Publishing House.

- Hu, D.-Y., Clarke, J. A., Eliason, C. M., Qiu, R., Li, Q.-G., Shawkey, M. D., et al. (2018). A bony-crested Jurassic dinosaur with evidence of iridescent plumage highlights complexity in early paravian evolution. *Nat. Commun.* 9:217.
- Jiang, B.-Y., Zhao, T., Regnault, S., Edwards, N. P., Kohn, S. C., Li, Z.-H., et al. (2017). Cellular preservation of musculoskeletal specializations in the Cretaceous bird *Confuciusornis*. *Nat. Commun.* 8:14779.
- Kingsbury, J. W., Allen, V. G., and Rotherham, B. A. (1953). The histological structure of the beak in the chick. *Anat. Rec.* 116, 95–115. doi: 10.1002/ar.1091160109
- Li, L., Wang, J.-Q., and Hou, S.-L. (2010). A new species of *Confuciusornis* from lower cretaceous of Jianchang, Liaoning, China. *Glob. Geol.* 29, 183–187.
- Li, Q., Gao, K.-Q., Vinther, J., Shawkey, M. D., Clarke, J. A., D'Alba, L., et al. (2010). Plumage color patterns of an extinct dinosaur. *Science* 327, 1369–1372. doi: 10.1126/science.1186290
- Li, Q.-G., Clarke, J. A., Peteya, J. A., and Shawkey, M. D. (2018). Elaborate plumage patterning in a Cretaceous bird. *PeerJ* 6:e5831. doi: 10.7717/peerj.5831
- Li, Q.-G., Gao, K.-Q., Meng, Q.-J., Clarke, J. A., Shawkey, M. D., D'Alba, L., et al. (2012). Reconstruction of Microraptor and the evolution of iridescent plumage. *Science* 335, 1215–1219. doi: 10.1126/science.1213780
- Louchart, A., and Viriot, L. (2011). From snout to beak: the loss of teeth in birds. *Trends Ecol. Evol.* 26, 663–673. doi: 10.1016/j.tree.2011.09.004
- Lovette, I. J., and Fitzpatrick, J. W. (2004). *The Handbook of Bird Biology*. Princeton, NJ: Princeton University Press.
- Marugán-Lobón, J., Chiappe, L. M., Ji, S.-A., Zhou, Z.-H., Gao, C.-H., Hu, D.-Y., et al. (2011). Quantitative patterns of morphological variation in the appendicular skeleton of the early cretaceous bird *Confuciusornis*. *J. Syst. Palaeontol.* 9, 91–101. doi: 10.1080/14772019.2010.517786
- Matthysen, E. (1989). Seasonal variation in bill morphology of Nuthatches *Sitta europaea*: dietary adaptations or consequences? *Ardea* 77, 117–125.
- Mayr, G., Pohl, B., and Peters, D. S. (2005). A well-preserved *Archaeopteryx* specimen with theropod features. *Science* 310, 1483–1486. doi: 10.1126/science.1120331
- Murphy, T. G., Rosenthal, M. F., Montgomerie, R., and Tarvin, K. A. (2009). Female American goldfinches use carotenoid-based bill coloration to signal status. *Behav. Ecol.* 20, 1348–1355. doi: 10.1093/beheco/arp140
- Navalón, G., Bright, J. A., Marugán-Lobón, J., and Rayfield, E. J. (2019). The evolutionary relationship among beak shape, mechanical advantage, and feeding ecology in modern birds. *Evolution* 73, 422–435. doi: 10.1111/evo.13655
- Nolan, P. M., Dobson, F. S., Nicolaus, M., Karels, T. J., McGraw, K. J., and Jouventin, P. (2010). Mutual mate choice for colorful traits in King Penguins. *Ethology* 116, 635–644.
- O'Connor, J. K. (2019). The trophic habits of early birds. *Palaeogeogr. Palaeoclimatol. Palaeoecol.* 513, 178–195. doi: 10.1016/j.palaeo.2018.03.006
- O'Connor, J. K., Chiappe, L. M., and Bell, A. (2011). “Pre-modern birds: avian divergences in the Mesozoic,” in *Living Dinosaurs: the Evolutionary History of Birds*, eds G. D. Dyke and G. Kaiser (Hoboken, NJ: John Wiley & Sons), 39–114. doi: 10.1002/9781119990475.ch3
- O'Connor, J. K., Wang, M., and Hu, H. (2016). A new ornithuromorph (Aves) with an elongate rostrum from the Jehol Biota, and the early evolution of rostralization in birds. *J. Syst. Palaeontol.* 14, 939–948. doi: 10.1080/14772019.2015.1129518
- O'Connor, J. K., Zheng, X.-T., Pan, Y.-H., Wang, X.-L., Wang, Y., Zhang, X.-M., et al. (2020). New information on the plumage of *Protopteryx* (Aves: Enantiornithes) from a new specimen. *Cretac. Res.* 116:104577. doi: 10.1016/j.cretres.2020.104577
- O'Connor, J. K., and Zhou, Z.-H. (2013). A redescription of *Chaoyangia beishanensis* (Aves) and a comprehensive phylogeny of Mesozoic birds. *J. Syst. Palaeontol.* 11, 889–906. doi: 10.1080/14772019.2012.690455
- Peteya, J. A., Clarke, J. A., Li, Q.-G., Gao, K.-Q., and Shawkey, M. D. (2017). The plumage and coloration of an enantiornithine bird from the early cretaceous of China. *Palaeontology* 60, 55–71. doi: 10.1111/pala.12270
- Rauhut, O. W. M., Foth, C., and Tischlinger, H. (2018). The oldest *Archaeopteryx* (Theropoda: Avialae): a new specimen from the Kimmeridgian/Tithonian boundary of Schamhaupten, Bavaria. *PeerJ* 6:e4191. doi: 10.7717/peerj.4191
- Rico-Guevara, A., and Araya-Salas, M. (2015). Bills as daggers? A test for sexually dimorphic weapons in a lekking hummingbird. *Behav. Ecol.* 26, 21–29. doi: 10.1093/beheco/aru182
- Stettenheim, P. R. (1972). The integument of birds. *Avian Biol.* 2, 1–63. doi: 10.1016/b978-0-12-249402-4.50010-3
- Storer, R. W. (1960). “Adaptive radiation in birds,” in *Biology and Comparative Physiology of Birds*, ed. A. J. Marshall (New York, NY: Academic Press), 15–55. doi: 10.1016/b978-1-4832-3142-6.50007-0
- Tattersall, G. J., Arnaout, B., and Symonds, M. R. E. (2016). The evolution of the avian bill as a thermoregulatory organ. *Biol. Rev.* 11:e0154768.
- Vinther, J. (2015). A guide to the field of palaeo color. *Bioessays* 37, 643–656.
- Wang, M., O'Connor, J., Zhou, S., and Zhou, Z.-H. (2019a). New toothed early cretaceous ornithuromorph bird reveals intraclade diversity in pattern of tooth loss. *J. Syst. Palaeontol.* 18, 631–645. doi: 10.1080/14772019.2019.1682696
- Wang, M., O'Connor, J., and Zhou, Z.-H. (2019b). A taxonomical revision of the Confuciusornithiformes (Aves: Pygostylia). *Vertebrata Palasiatica* 57, 1–37.
- Wang, M., Stidham, T. A., and Zhou, Z.-H. (2018). A new clade of basal early cretaceous pygostylia birds and developmental plasticity of the avian shoulder girdle. *Proc. Natl. Acad. Sci. U.S.A.* 115, 10708–10713. doi: 10.1073/pnas.1812176115
- Wang, X., O'Connor, J., Maina, J. N., Pan, Y.-H., Wang, M., Wang, Y., et al. (2018). *Archaeorhynchus* preserving significant soft tissue including probable fossilized lungs. *Proc. Natl. Acad. Sci. U.S.A.* 115, 11555–11560. doi: 10.1073/pnas.1805803115
- Wang, M., and Zhou, Z.-H. (2016). A new adult specimen of the basalmost ornithuromorph bird *Archaeorhynchus spathula* (Aves: Ornithuromorpha) and its implications for early avian ontogeny. *J. Syst. Palaeontol.* 15, 1–18. doi: 10.1080/14772019.2015.1136968
- Wang, M., and Zhou, Z.-H. (2018). A new confuciusornithid (Aves: Pygostylia) from the early cretaceous increases the morphological disparity of the Confuciusornithidae. *Zool. J. Linn. Soc.* 185, 417–430. doi: 10.1093/zoolinnean/zly045
- Wang, S., Stiegler, J., Amiot, R., Wang, X., Du, G.-H., Clark, J. C., et al. (2017). Extreme ontogenetic changes in a ceratosaurian theropod. *Curr. Biol.* 27, 144–148. doi: 10.1016/j.cub.2016.10.043
- Wang, X.-R., Chiappe, L. M., Teng, F.-F., and Ji, Q. (2013). *Xinghaiernis lini* (Aves: Ornithothoraces) from the early cretaceous of Liaoning: an example of evolutionary mosaic in early birds. *Acta Geol. Sin. Engl. Ed.* 87, 686–689. doi: 10.1111/1755-6724.12080
- Zanno, L. E., and Makovicky, P. J. (2011). Herbivorous ecomorphology and specialization patterns in theropod dinosaur evolution. *Proc. Natl. Acad. Sci. U.S.A.* 108, 232–237. doi: 10.1073/pnas.1011924108
- Zhang, F., Zhou, Z., and Benton, M. J. (2008). A primitive confuciusornithid bird from China and its implications for early avian flight. *Sci. China Ser. D Earth Sci.* 51, 625–639. doi: 10.1007/s11430-008-0050-3
- Zhang, F.-C., Kearns, S. L., Orr, P. J., Benton, M. J., Zhou, Z.-H., Johnson, D., et al. (2010). Fossilized melanosomes and the colour of cretaceous dinosaurs and birds. *Nature* 463, 1075–1078. doi: 10.1038/nature08740
- Zhang, Z.-H., Gao, C.-H., Meng, Q.-J., Liu, J.-Y., Hou, L.-H., and Zheng, G.-M. (2009). Diversification in an early cretaceous avian genus: evidence from a new species of *Confuciusornis* from China. *J. Ornithol.* 150, 783–790. doi: 10.1007/s10336-009-0399-x
- Zheng, X.-T., O'Connor, J. K., Wang, X.-L., Pan, Y.-H., Wang, Y., Wang, M., et al. (2017). Exceptional preservation of soft tissue in a new specimen of *Eoconfuciusornis* and its biological implications. *Natl. Sci. Rev.* 4, 441–452. doi: 10.1093/nsr/nwx004
- Zheng, X.-T., O'Connor, J. K., Wang, X.-L., Wang, Y., and Zhou, Z.-H. (2018). Reinterpretation of a previously described Jehol bird clarifies early trophic evolution in the Ornithuromorpha. *Proc. R. Soc. B Biol. Sci.* 285:20172494. doi: 10.1098/rspb.2017.2494
- Zheng, X.-T., Zhou, Z.-H., Wang, X.-L., Zhang, F.-C., Zhang, X.-M., Wang, Y., et al. (2013). Hind wings in basal birds and the evolution of leg feathers. *Science* 339, 1309–1312. doi: 10.1126/science.1228753
- Zhou, S., O'Connor, J. K., and Wang, M. (2014). A new species from an ornithuromorph dominated locality of the Jehol Group. *Chin. Sci. Bull.* 59, 5366–5378. doi: 10.1007/s11434-014-0669-8

- Zhou, S., Zhou, Z.-H., and O'Connor, J. K. (2012). A new toothless ornithurine bird (*Schizoura lii* gen. et sp. nov.) from the lower cretaceous of China. *Vertebrata Palasiatica* 50, 9–24.
- Zhou, S., Zhou, Z.-H., and O'Connor, J. K. (2013). Anatomy of the early cretaceous *Archaeorhynchus spathula*. *J. Vertebr. Paleontol.* 33, 141–152.
- Zhou, Z., and Zhang, F. (2001). Two new ornithurine birds from the early cretaceous of western Liaoning, China. *Kexue Tongbao* 46, 371–377.
- Zhou, Z.-H., and Martin, L. D. (2011). Distribution of the predentary bone in Mesozoic ornithurine birds. *J. Syst. Palaeontol.* 9, 25–31. doi: 10.1080/14772019.2010.504080
- Zhou, Z.-H., and Zhang, F.-C. (2006). A beaked basal ornithurine bird (Aves, Ornithurae) from the lower cretaceous of China. *Zool. Scr.* 35, 363–373. doi: 10.1111/j.1463-6409.2006.00234.x

Conflict of Interest: The authors declare that the research was conducted in the absence of any commercial or financial relationships that could be construed as a potential conflict of interest.

The handling editor is currently organizing a Research Topic with one of the authors JO'C, and confirms the absence of any other collaboration.

Copyright © 2020 Zheng, O'Connor, Wang, Wang, Xuwei, Zhang and Zhou. This is an open-access article distributed under the terms of the Creative Commons Attribution License (CC BY). The use, distribution or reproduction in other forums is permitted, provided the original author(s) and the copyright owner(s) are credited and that the original publication in this journal is cited, in accordance with accepted academic practice. No use, distribution or reproduction is permitted which does not comply with these terms.



An Exceptionally Preserved Specimen From the Green River Formation Elucidates Complex Phenotypic Evolution in Gruiformes and Charadriiformes

Grace Musser* and Julia A. Clarke

Department of Geological Sciences, The University of Texas at Austin, Austin, TX, United States

OPEN ACCESS

Edited by:

Daniel J. Field,
University of Cambridge,
United Kingdom

Reviewed by:

Gerald Mayr,
Senckenberg Museum, Germany
Junya Watanabe,
University of Cambridge,
United Kingdom

*Correspondence:

Grace Musser
gmusser@utexas.edu

Specialty section:

This article was submitted to
Paleontology,
a section of the journal
Frontiers in Ecology and Evolution

Received: 07 May 2020

Accepted: 09 September 2020

Published: 26 October 2020

Citation:

Musser G and Clarke JA (2020)
An Exceptionally Preserved Specimen
From the Green River Formation
Elucidates Complex Phenotypic
Evolution in Gruiformes
and Charadriiformes.
Front. Ecol. Evol. 8:559929.
doi: 10.3389/fevo.2020.559929

The stem lineage relationships and early phenotypic evolution of Charadriiformes (shorebirds) and Gruiformes (rails, cranes, and allies) remain unresolved. It is still debated whether these clades are sister-taxa. New phylogenetic analyses incorporating Paleogene fossils have the potential to reveal the evolutionary connections of these two speciose and evolutionarily critical neoavian subclades. Although Gruiformes have a rich Paleogene fossil record, most of these fossils have not been robustly placed. The Paleogene fossil record of Charadriiformes is scarce and largely consists of fragmentary single elements. Only one proposed Eocene charadriiform-like taxon, *Scandiavis mikkelsenii* of Denmark, is represented by a partial skeleton. Here, we describe a new species from the early Eocene Green River Formation of North America comprising a partial skeleton and feather remains. Because the skeleton lacks the pectoral girdle and forelimbs as in *S. mikkelsenii*, only features of the skull, axial skeleton, and hind limb are available to resolve the phylogenetic placement of this taxon. These anatomical subregions initially showed features seen in Charadriiformes and Gruiformes. To assess placement of this taxon, we use a matrix consisting of 693 morphological characters and 60 taxa, including *S. mikkelsenii* and the oldest known charadriiform taxa represented by single elements. These more fragmentary records comprise two distal humeri from the earliest Eocene Naranbulag Formation of Mongolia and the early Eocene Nanjemoy Formation of Virginia. Our phylogenetic analyses recover the new taxon and *S. mikkelsenii* alternatively as a charadriiform or as a stem-gruiform; placement is contingent upon enforced relationships for major neoavian subclades recovered by recent molecular-based phylogenies. Specifically, when constraint trees based on results that do not recover Charadriiformes and Gruiformes as sister-taxa are used, the new taxon and *S. mikkelsenii* are recovered within stem Gruiformes. Both Paleogene fossil humeri are consistently recovered within crown Charadriiformes. If placement of these humeri or the new taxon as charadriiforms are correct, this may indicate that recent divergence time analyses have underestimated the crown age of another major crown avian subclade; however, more complete sampling of these taxa is necessary, especially of more complete specimens with pectoral elements.

Keywords: avian phylogeny, Neoaves, Eocene, feathers, fossil, divergence time estimation, morphology

INTRODUCTION

Although there is a growing consensus around the majority of relationships among avian subclades, positions of several subclades have been persistently debated. Charadriiformes (shorebirds) and Gruiformes (rails, cranes, and allies) have both been described as some of the most speciose and phylogenetically enigmatic clades of birds (Livezey, 1998, 2010; Mayr, 2011b). Understanding evolution in both clades is critical to resolving the stem lineage relationships of Neoaves, a group that contains approximately 95% of all living bird species, and to elucidating phenotypic evolution across basal Neoaves. There is a lack of consensus among large-scale phylogenetic studies of Neoaves concerning the relationships of, and early phenotypic evolution in, Charadriiformes or Gruiformes. A Charadriiformes + Gruiformes clade was recovered using a variety of datatypes and analytical approaches including recent large genome-based datasets (e.g., Cracraft, 1988; van Tuinen and Hedges, 2001; Livezey and Zusi, 2007; Bertelli et al., 2011; Jarvis et al., 2014; Musser and Cracraft, 2019, primary analysis of Kimball et al., 2019). However, it is not recovered in other large molecular datasets (Hackett et al., 2008; Prum et al., 2015; Reddy et al., 2017, additional analyses of Kimball et al., 2019).

Assessment of Paleogene fossils can directly inform the timing of key divergences in Neoaves. Although Gruiformes have a rich Paleogene fossil record, these fossils have not been robustly placed despite several attempts to do so across large-scale morphological analyses (Livezey and Zusi, 2007; Mayr, 2009, 2017; Musser and Cracraft, 2019; Musser et al., 2019). Even the Messelornithidae, the most complete and well-preserved Paleogene rail-like fossils that are represented by over 500 specimens (Mayr, 2017), are of debated affinities (Musser et al., 2019). The Paleogene fossil record of Charadriiformes is conversely scarce and largely consists of fragmentary single elements. The only previously proposed Paleogene charadriiform represented by a partial skeleton is *Scandiavis mikkelsenii* (Bertelli et al., 2013) of the earliest Eocene marine Fur Formation of Denmark (~54 Ma, Bertelli et al., 2011). *S. mikkelsenii* is missing the shoulder girdle, forelimbs and sternum but is exceptionally preserved in three dimensions. Despite its preservation, this specimen could not be confidently assigned to Charadriiformes (Bertelli et al., 2013). The oldest-known unambiguous charadriiform fossils are represented by single elements and comprise distal humeri from the earliest Eocene lacustrine Naranbulag Formation of Mongolia (~55 Ma, Hood et al., 2019) and the early Eocene marine Nanjemoy Formation of Virginia (53.6–52.8 Ma, Mayr, 2016). All other charadriiform fossils postdate these specimens, with most being younger than Eocene in age (Smith, 2015; Mayr, 2017). Stem representatives of Alcidae from the late Eocene and Turnicidae and Jacanidae from the early Oligocene remain the earliest charadriiform birds that can be confidently assigned to extant lineages (Mayr, 2011b; Smith, 2015). While the stem turnicids *Turnipax* and *Cerestenia* are represented by partial skeletons (Mayr, 2000b), the jacanid remains are fragmentary (Olson, 1976; Rasmussen et al., 1987), leaving phenotypic evolution at the base of Charadriiformes to remain largely unknown.

Here, we describe a two-dimensionally preserved partial skeleton of a bird from the early Eocene Fossil Butte Member (FBM; 51.97 ± 0.16 Ma, Smith et al., 2010) of the lacustrine Green River Formation of North America with exquisitely preserved plumage. Grande (2013) preliminarily reported that this taxon could be related to the extinct *Salmila robusta* (Mayr, 2000a). It was considered to be possibly flightless due to having what appeared to be small wing feathers (Grande, 2013); however, the sternum, shoulder girdle and forelimbs are missing along with their associated feathers. *Salmila robusta* is a slightly larger taxon of the middle Eocene Messel Formation in Hessen, Germany (Mayr, 2000a). *S. robusta* was originally placed within Cariamae (Seriemas; Mayr, 2000a) and later assigned to its own family (Salmilidae) as the sister-taxon of Cariamae (Mayr, 2002; with Cariamae including *Idiornis*, *Psilopterus*, *Phorusrhacos*, and *Cariama* in this study) after identification of an additional specimen and phylogenetic analysis. Three total specimens of *S. robusta* have been identified (Mayr, 2000a, 2002). *S. robusta* has also been thought to share some similarities with *Psophia* (trumpeters), especially within the tarsometatarsus (Mayr, 2000a). No cariamid, gruoid (crane, limpkin, or trumpeter-like) or charadriiform birds have been described from the Green River Formation (Grande, 2013).

We identify this fossil as the holotype specimen of a new species. New x-ray computed tomography (CT) images allowed us to recover previously hidden morphologies, revealing it to represent a bird from rarely sampled environments of Fossil Lake (Grande, 2013) and to represent a new clade for the Green River Formation. The specimen was found at the mid-lake locality, locality A (Grande and Buchheim, 1994; Grande, 2013), and is one of only two avian skeletons published from this site (the other is that of a coliform or mousebird; Ksepka and Clarke, 2010a). Additional avian remains recovered from Locality A comprise two feathers, one of which may be from the giant *Gastornis* (Grande, 2013). Aquatic birds (e.g., frigatebirds, presbyornithids) are among the most common avian species found in the FBM as well as an array of disparate terrestrial taxa including rail-like birds (messelornithids), paleognathous birds (lithornithids), stem parrots and roller-like birds (primobucconids; Grande, 1984; Hesse, 1992; Ericson, 1997, 1999, 2000; Olson and Matsuoka, 2005; Clarke et al., 2009; Ksepka and Clarke, 2010b, 2012; Weidig, 2010; Ksepka et al., 2011; Grande, 2013; Smith, 2013; Nesbitt and Clarke, 2016). Character analysis and phylogenetic placement of this specimen (FMNH PA778) allows new insight into outstanding issues of phenotypic evolution and divergence timing as well as new perspectives on paleoenvironmental and biogeographic history in Neoaves.

INSTITUTIONAL ABBREVIATIONS

AMNH, American Museum of Natural History, New York, NY, United States; FMNH, Field Museum of Natural History, Chicago, IL, United States; HLMD, Hessisches Landesmuseum Darmstadt, Germany; M, the Texas Memorial Museum,

Austin, TX, United States.; USNM, National Museum of Natural History, Smithsonian Institution, Washington, DC, United States. Specimen numbers are presented in **Table 1**.

SYSTEMATIC PALEONTOLOGY

AVES (Linnaeus, 1758),
NEOGNATHAE (Pycraft, 1900),
Neoaves (Sibley et al., 1988),
Nahmavis grandei, gen. et sp. nov.

Holotype Specimen

FMNH PA778, a partial skeleton with feathers and tracheal rings preserved within a kerogen-rich laminated micrite slab.

Remains of the sternum, pectoral girdle and forelimb are absent (**Figures 1,3**). Measurements are provided in **Table 2**.

Etymology

Nahmavis is Native American in origin (Nahma, used by the Shoshoni Great Basin tribe indigenous to this region) and means “together” or “of two things” (Shoshoni Language Project, 2018). The name references the combination of features in this new taxon. The species honors Dr. Lance Grande, who collected the holotype specimen, in recognition of his premier and extensive research on the Green River Formation.

Type Locality and Horizon

The holotype specimen was collected from Fossil Butte Member (sensu Buchheim, 1994) Locality A (F-1 A in Grande and Buchheim, 1994; Grande, 2013), located in SE¼, SE¼, Sec. 19,

TABLE 1 | Specimen numbers of newly added taxa and skeletal specimens used for comparison during fossil description and phylogenetic analyses.

| Group Name | Species Sampled and Specimen Numbers |
|---------------------|-----------------------------------------------------------------------------------------------------------------------------------------------------------------------------------------------------------------------------------------------------------------------------------------------------------------------------------------------------------------------------------------------------------------------------------------------------------------------------------------------------------------------------------------------------------------------------------------------------------------------------------------------------------------------------------------------------------------------------------------------------------------------------------------------------------------------------------------------------------------------------------------------------------------------------------------------------------------------------------------------------------------------------------------------------------------------------------------------------------------------------------------------------------------------------------------------------------------------------------------------------------------------|
| Tinamiformes | <i>Crypturellus undulatus</i> (AMNH 2751, AMNH 6479), <i>Tinamus solitarius</i> (AMNH 21983, USNM 561269, USNM 345133) |
| Galliformes | <i>Lophura bulweri</i> (AMNH 10962, AMNH 16532), <i>Gallus gallus</i> (AMNH 18555, AMNH 4031, M-12244, USNM 489422) |
| Anseriformes | <i>Chauna torquata</i> (M-10449, USNM 646637), <i>Anas platyrhynchos</i> (USNM 633396, USNM 610643), <i>Mergus serrator</i> (USNM 490105, USNM 634853, USNM 430710) |
| Gaviiformes | <i>Gavia immer</i> (AMNH 15919, USNM 501589) |
| Sphenisciformes | <i>Spheniscus humboldti</i> (AMNH 4921) |
| Phoenicopteriformes | <i>Phoenicopterus chilensis</i> (M-4923, M-5325) |
| Podicipediformes | <i>Podiceps cristatus</i> (AMNH 25241, USNM 502553, USNM 560595) |
| Caprimulgiformes | <i>Caprimulgus carolinensis</i> (USNM 559607) |
| Otidiformes | <i>Chlamydotis macqueenii</i> (USNM 430378, USNM 430485, AMNH 28665) |
| Columbiformes | <i>Columba livia</i> (USNM 555707) |
| Opisthocomiformes | <i>Opisthocomus hoazin</i> (AMNH 12127, AMNH 24230, USNM 612024, USNM 344066, USNM 344065) |
| Charadriiformes | <i>Eudromias ruficollis</i> (AMNH 7013, USNM 322963, USNM 322962), <i>Jacana jacana</i> (FMNH 376137, USNM 560148, USNM 614605, USNM 345812), <i>Haematopus ostralegus</i> (FMNH 338440, USNM 502440, USNM 560934, AMNH 1681), <i>Burhinus bistriatus</i> (AMNH 2630, FMNH 289831, USNM 621089, USNM 626233, USNM 432021), <i>Charadrius semipalmatus</i> (AMNH 9963, FMNH 342530, USNM 489728, USNM 489665, USNM 489599), <i>Vanellus coronatus</i> (USNM 636688, USNM 636689, AMNH 5243), <i>Chionis alba</i> (AMNH 549, AMNH 879, USNM 553253, USNM 490989), <i>Pluvianus aegyptius</i> (FMNH 93449, FMNH 291228, USNM 491870, USNM 500294), <i>Larus atricilla</i> (M-10469, USNM 560290, USNM 227064), <i>Recurvirostra avosetta</i> (USNM 556295, USNM 610452, AMNH 28666), <i>Stercorarius longicaudus</i> (USNM 491644, USNM 491643, AMNH 21036), <i>Thinocorus rumicivorous</i> (USNM 227504, USNM 491022, AMNH 10143), <i>Turnix nigricollis</i> (USNM 488643, USNM 432224, AMNH 1994, AMNH 5381) |
| Gruiformes | <i>Psophia crepitans</i> (AMNH 29322, FMNH 338504, USNM 621709, USNM 429974), <i>Aramus guarauna</i> (AMNH 24194, NC State 18405, FMNH 376076, USNM 612025, USNM 226809), <i>Balearica regulorum</i> (AMNH 10699, USNM 637581, USNM 647263, USNM 631784), <i>Grus japonensis</i> (AMNH 1938, AMNH 1718, AMNH 4252), <i>Podica senegalensis</i> (AMNH 4148, AMNH 4208, AMNH 5268, USNM 562803), <i>Heliornis fulica</i> (FMNH 376129, USNM 623068, USNM 19159, USNM 345807, USNM 321493, YPM 109145), <i>Heliopais personata</i> (USNM 534558, USNM 344532), <i>Sarothrura lugens</i> (AMNH 2417, AMNH 4235), <i>Sarothrura pulchra</i> (FMNH 490196, USNM 291778, USNM 292395, AMNH 4235), <i>Himantornis haematopus</i> (AMNH 4183, UNSM 318391), <i>Habroptila wallacii</i> (USNM 560793, USNM 557026, USNM 557027, USNM 572365, USNM 560792, USNM 557025), <i>Gallicrex cinerea</i> (USNM 319118, USNM 319481, USNM 489266, USNM 292017), <i>Canirallus oceleus batesi</i> (AMNH 4151), <i>Aramides cajanea</i> (AMNH 4343, AMNH 8637, FMNH 105856, USNM 612270*, USNM 612266), <i>Rallus longirostris</i> (M-10359, USNM 499648, USNM), <i>Gallinula chloropus</i> (AMNH 28451, FMNH 105107, USNM 499259), <i>Porphyryla martinica</i> (USNM 611560, USNM 611561) |
| Phaethontiformes | <i>Phaethon aethereus</i> (AMNH 28494, FMNH 348136, FMNH 339435, USNM 558044, USNM 525793) |
| Eurypygiformes | <i>Eurypyga helias</i> (AMNH 3750, AMNH 4293, FMNH 376130, FMNH 106439, USNM 637209, USNM 623251, USNM 344047), <i>Rhynochetos jubatus</i> (AMNH 1326, AMNH 554, FMNH 291228, USNM 612087, USNM 018994) |
| Cariamiformes | <i>Cariama cristata</i> (AMNH 1722, AMNH 8667, AMNH 8646, M-10446, FMNH 105634, USNM 555731, USNM 430173, USNM 631176), <i>Chunga burmeisteri</i> (USNM 431487, AMNH 4250) |
| Accipitriformes | <i>Cathartes burrovianus</i> (AMNH 1264, USNM 623071) |
| Leptosomiformes | <i>Leptosomus discolor</i> (AMNH 10083, USNM 291844, USNM 291845) |
| Extinct Taxa | <i>Nahmavis grandei</i> (FMNH PA778), <i>Scandiavis mikkelsenii</i> (Bertelli et al., 2013), <i>Salmila robusta</i> (Mayr, 2000a, 2002), <i>Pellornis mikkelsenii</i> (MGUH 29278, DK664, FUM 1681a; Bertelli et al., 2011; Musser et al., 2019), <i>Songzia acutunguis</i> (Wang et al., 2012), <i>Messelornis cristata</i> (USNM 462392, Hesse, 1990; Bertelli et al., 2011) |

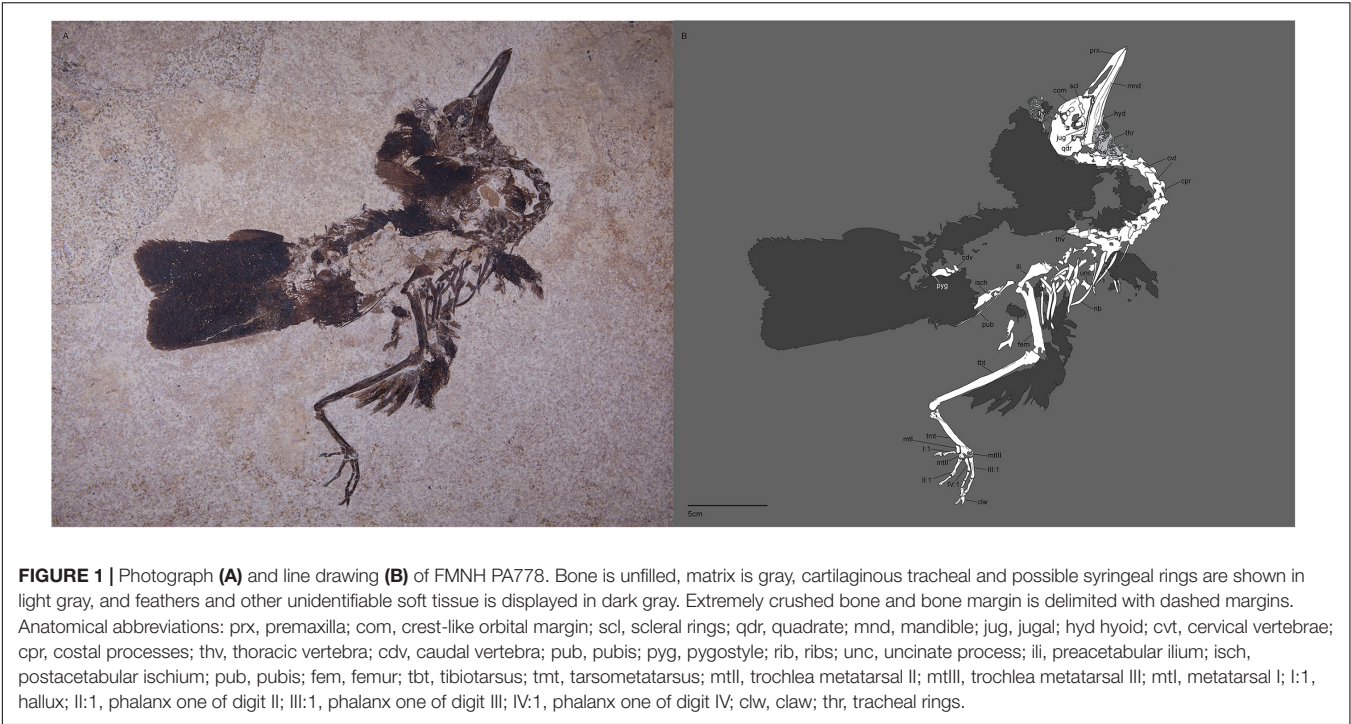


FIGURE 1 | Photograph (A) and line drawing (B) of FMNH PA778. Bone is unfilled, matrix is gray, cartilaginous tracheal and possible syringeal rings are shown in light gray, and feathers and other unidentifiable soft tissue is displayed in dark gray. Extremely crushed bone and bone margin is delimited with dashed margins. Anatomical abbreviations: prx, premaxilla; com, crest-like orbital margin; scl, scleral rings; qdr, quadrate; mnd, mandible; jug, jugal; hyd, hyoid; cvt, cervical vertebrae; cpr, costal processes; thv, thoracic vertebra; cdv, caudal vertebra; pub, pubis; pyg, pygostyle; rib, ribs; unc, uncinat process; ili, preacetabular ilium; isch, postacetabular ischium; fem, femur; tbt, tibiotarsus; tmt, tarsometatarsus; mtII, trochlea metatarsal II; mtIII, trochlea metatarsal III; mtl, metatarsal I; l:1, hallux; II:1, phalanx one of digit II; III:1, phalanx one of digit III; IV:1, phalanx one of digit IV; clw, claw; thr, tracheal rings.

TABLE 2 | Selected measurements of *Nahmavis grandei* in millimeters (mm), taken from surface of slab (does not include CT scan measurements; left/right) compared with previously published measurements of *Salmila robusta* and *Scandiavis mikkelsenii*.

| Measurement (mm) | <i>N. grandei</i> FMNH PA778 | <i>S. robusta</i> SMF-ME 3014 Mayr, 2000a | <i>S. mikkelsenii</i> FU171x (Bertelli et al., 2013) |
|-------------------------|------------------------------|-------------------------------------------|------------------------------------------------------|
| Total skull length | 67.8 | | 49.5 |
| Rostrum length | 35.1 | | |
| Quadrate visible height | /6.5 | | |
| Femur length | /41.0 | /~45 | /33.2 |
| Tibiotarsus length | /60.9 | 69.7/64.4 | 47.7/ |
| Tarsometatarsus length | /32.0 | 42.9/44.7 | 25.5/25.4 |
| I:1 length | /6.6 | 7.6 | |
| I:2 length | /4.9 | 5.0 | |
| II:1 length | /10.0 | 11.8 | |
| II:2 length | /8.5 | 8.2 | |
| III:1 length | /11.4 | 11.2 | |
| III:2 length | /8.9 | 9.3 | |
| III:3 length | /8.1 | 8.4 | |
| IV:1 length | /8.1 | 7.6 | |
| IV:2 length | /5.10 | 4.2 | |
| IV:3 length | /4.80 | 4.2 | |
| IV:4 length | /4.80 | 5.1 | |
| IV:5 length | /4.80 | 5.6 | |

Pedal phalanges are described using the format (digit:phalanx). Measurements are given for holotype specimens only.

T.21N., R.117W., and NE¼, NE¼, Sec. 30, T.21N., R117W., Kemmerer 15 min Quadrangle (USGS). FBM Locality A is a mid-lake locality and is within a 30–40 cm thick horizon representing roughly a few 100 years of the early Eocene (Grande and Buchheim, 1994). The mid-lake fossil-bearing, laminated micrite facies are made up of thin calcite laminae that alternate with almost pure kerogen (Grande and Buchheim, 1994). Few other bird skeletons have been recovered from

the mid-lake locality, with the majority being recovered from the near-shore deposits of FBM locality H (F-2 A in Grande and Buchheim, 1994; Grande, 2013). The mid-lake locality is additionally characterized by a sharp decrease in benthic fauna, perhaps suggesting that bottom conditions were primarily anoxic or dysaerobic as in the avian fossil-bearing deposits of the Fur Formation (Pedersen and Surlyk, 1983; Bertelli et al., 2010).

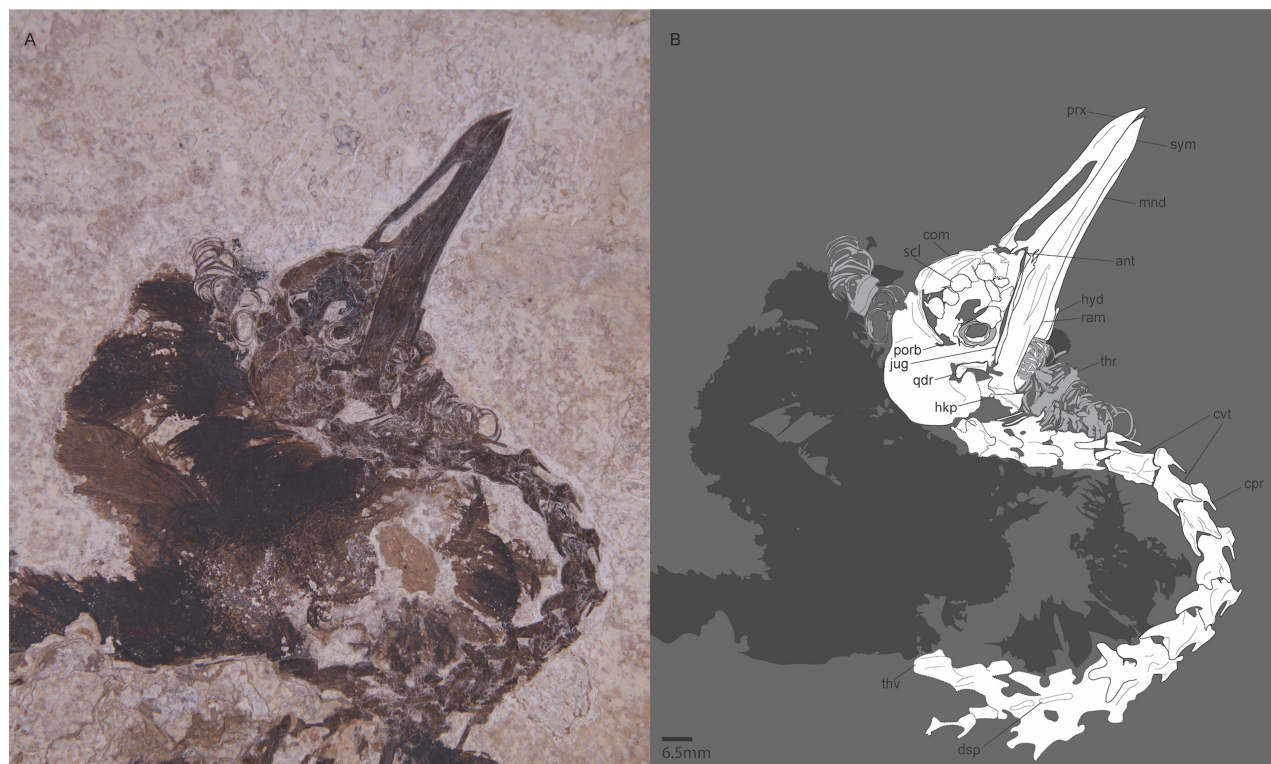


FIGURE 2 | Photograph (A) and line drawing (B) of the head and neck of FMNH PA778. Bone is unfilled, matrix is gray, cartilaginous tracheal and possible syringeal rings are shown in light gray, and feathers and other unidentifiable soft tissue is displayed in dark gray. Extremely crushed bone and bone margin is delimited with dashed margins. Anatomical abbreviations: prx, premaxilla; com, crest-like orbital margin; ant, antorbital angle; scl, scleral rings; porb, postorbital process; qdr, quadrate; mnd, mandible; hkp, hook-like process; ram, mandibular ramus; sym, symphysis; jug, jugal; hyd, hyoid; cvt, cervical vertebrae; cpr, costal processes; thv, thoracic vertebra; dsp, dorsal spinous process; thr, tracheal rings.

Diagnosis

Nahmavis grandei is diagnosed by a proposed unique combination of characters comprising (1) holorhinal nares rostral to the zona flexoria craniofacialis (Figures 1, 2, 6A), (2) a prominent, dorsally protruding crest-like orbital margin (Figures 1, 2, com; see Musser and Cracraft, 2019), (3) a quadrate with apneumatic, well-separated heads (Figures 2, 3A–C, 6D,E), (4) a quadrate with a prominent crista lateralis (Figures 3B,C,L, 6E), (5) a prominent crista tympanica of the quadrate that terminates ventrally within the ventral half of the otic process (Figures 3A,C, ct), (6) a caudally concave otic process of the quadrate (Figures 3C, 6D), (7) a caudal condyle that is confluent with the lateral condyle (Figures 3C,L, 6D), (8) absence of a notarium (Figure 1), (9) preacetabular ilia that are unfused to the synsacrum (Figure 1, ili and Figure 6H), (10) an elongate, thin and recurved pubis (Figure 1, pub) (11) a femur that is over half the length of the tibiotarsus (Figure 1, fem), (12) a prominent crista cnemialis cranialis of the tibiotarsus that is proximally projected above the fossa retropatellares (Figure 3E, ccc), (13) a tarsometatarsus that approximately half the length of the tibiotarsus (Figure 1, tmt), (14) a medial hypotarsal crest that is projected farther plantar than the lateral crest (Figures 3J–L, crm), (15) a deep sulcus extensorius of the tarsometatarsus (Figures 3J,K, ext), (16) plantar alae present on metatarsal

trochleae IV and II (Figures 3J–L), (17) an unbowed pedal digit I: phalanx 1 that is about half the length of pedal digit III:1 (Figures 3J–L, I:1), (18) a lack of a plantomedial flange on proximal margin of pedal digit IV:1 (Figures 3J–L), and (19) a pedal digit IV:4 that is more elongate than pedal digit IV:3 (Figure 3L). Diagnosis for the genus as per the species.

Differential Diagnosis

Nahmavis grandei can be distinguished from earliest Eocene *Scandiavis mikkelsenii* Bertelli et al. (2013) due to possessing (1) less rostrocaudally and dorsoventrally extensive nares (Figures 1, 2), (2) a more acute antorbital angle of approximately 45° (Figure 2, ant), (3) a more caudally elongated cranium (Figures 1, 2), (4) a ventrally oriented postorbital process (Figure 2, porb), (5) a less cranially projected crista cnemialis cranialis of the tibiotarsus (Figures 3D,E, ccc), (6) a crista cnemialis cranialis with a more acuminate distal apex than that of *S. mikkelsenii* (Figures 3D,E; apx), (7) a lack of a notch along the distal rim of the medial condyle of the tibiotarsus (Figures 3G,H), (8) a deeper fossa parahypotarsalis lateralis in the tarsometatarsus (Figure 3L, phl), and (9) a longer femur and tibiotarsus (Figure 1, fem and tbt; Table 2). *N. grandei* is differentiated from the charadriiform-like *Morsoravis sedilis* Bertelli et al. (2010) due to the presence of a zygodactyl foot



FIGURE 3 | Continued

FIGURE 3 | Line drawings (A,D,G,J), segmented CT scan data (B,C,H,I,K), CT scan slice (E), and photographs (F,L) of features in FMNH PA778 recovered by CT scanning and segmentation. (A–C) depicts the quadrates; (D–F) and (G–I) shows the proximal and distal portions, respectively, of the right tibiotarsus; and (J–L) depicts the right tarsometatarsus. Anatomical abbreviations: (A–C) o, otic capitulum; s, squamosal capitulum; ot, otic process; cl, crista lateralis; ct, crista tympanica; c, caudal condyle; l, lateral condyle; qj, quadratojugal site of articulation; (D–F) ccc, crista cnemialis cranialis; apx, distal apex of crista cnemialis cranialis; (G–I) depm, depressio epicondylaris medialis; depl, depressio epicondylaris lateralis; (J–L) tbt, tibiotarsus; tmt, tarsometatarsus; cotm, cotyla medialis; crm, crista medialis; phl, fossa parahypotarsalis lateralis; ext, sulcus extensorius; I:1, hallux; mtl, metatarsal I; mtll, metatarsal II trochlea; mtlll, metatarsal III, trochlea; mtIV, metatarsal IV trochlea; II:1, phalanx 1 of pedal digit II; IV:1, phalanx 1 of pedal digit IV.

in the latter taxon. Presence of this condition is suggested in the holotype due to a wide proximal phalanx of the fourth toe (Mayr, 2011a), and this taxon was recently phylogenetically placed within Pan-Passeriformes (Ksepka et al., 2019). *N. grandei* is distinguished from *Salmila robusta* due to possessing (1) a less decurved and less raptorial anterior terminus of the premaxilla (Figures 1, 2, prx), (2) a more caudally elongate cranium (Figures 1, 2), (3) a truncate postorbital process (Figure 2, porb), (4) a straight and dorsally oriented symphysis of the mandible that is not recurved (Figure 2, sym), (5) a decurved mandibular ramus rostral to the coronoid process (Figure 2, ram), (6) a half-moon shaped pygostyle with a caudal apex that deviates ventrally from the major axis of the pygostyle (Figure 1, pyg), (7) a more elongate pygostyle, (8) a more elongate pubis with at least $\frac{1}{4}$ of the pubis extending caudally beyond the caudal margin of the ischium (Figure 1, pub), (9) a femur that is over half the length of the tibiotarsus (Figure 1, fem), (10) a lateral condyle of the tibiotarsus that is more proximally located than the medial condyle (Figures 3G,H), (11) a deep fossa parahypotarsalis lateralis of the tarsometatarsus (Figure 3L, phl), (12) a metatarsal II trochlea with a plantarly prominent ala (Figures 1, 3J–L, mtII), (13) a metatarsal IV trochlea that is more distally extensive than the metatarsal II trochlea (Figures 3J–L, mtIV), (14) a pedal digit I: phalanx 1 that is approximately half the length of digit III: phalanx 1 (Figures 1, 3, I:1), and (15) a lack of a medially protruding flange at the proximal margin of digit IV: phalanx 1 (Figure 1, IV, see also CT, data in Supplementary Material).

Description and Comparison

Skull

The skull and mandible are preserved in right lateral aspect (Figures 1, 2). The tip of the premaxilla is slightly ventrally deflected, although not as deflected as that of *Salmila robusta* (prx, Figures 1, 2) or *Cariamidae*. Pitting of the rostral terminus of the premaxilla is present as in *Rallidae*. The rostrum is more dorsoventrally limited than that of *Cariamidae*. The cranial length to rostrum length ratio is roughly 1:1, more like that of *Charadriidae* than that of *Haematopodidae* or long-billed rallids such as *Rallus*. The nares are holorhinal and perforate as in *Scandiavis mikkelsenii* (Bertelli et al., 2013), *Cariamidae*, four examined *Charadriiformes* and almost all *Gruiformes* (*Gruiformes* refers to core-*Gruiformes sensu* Hackett et al., 2008). They do not extend caudally beyond the zona flexoria craniofacialis as in *S. mikkelsenii*; *Songzia acutunguis* Hou (1990); *Psophiidae*; *Ralloidea*; *Cariamidae*; and three examined *Charadriiformes*. In contrast, *Pellornis mikkelsenii* exhibits true schizorhiny *sensu* Zusi (1984) in which its caudally acuminate nares extend caudally beyond the zona flexoria craniofacialis

(Hesse, 1990; Musser et al., 2019). The condition of this character in *S. robusta* (Mayr, 2000a, 2002) cannot yet be assessed due to preservation of known specimens. The narial openings are expansive both craniocaudally and dorsoventrally. The suture between the nasals and the frontal process of the premaxilla is visible, as is the midline suture of the frontal process of the premaxilla. The zona flexoria craniofacialis is broken and flattened along the right side of the rostrum but appears to have been most similar to that of *Burhinidae*. The antorbital angle is most similar to that of *Rallus* in that it is markedly acute as in *Cariamidae*, *Heliornithidae* and most examined *Ralloidea* and *Charadriiformes*. In *S. mikkelsenii*, *Psophiidae*, and *S. acutunguis* this angle is larger and approximates a right angle. This cannot be assessed in *S. robusta*. As in *S. acutunguis*, *Heliornithidae*, some *Rallidae*, and most examined *Charadriiformes*, the nasal bar is broader dorsally and tapers ventrally. The dorsal and ventral portions are subequal in *Cariama*. A triangular maxillary process of the palatine extends caudally beyond the nasal bar in *N. grandei*, which is consistent with the condition in *S. mikkelsenii*, *Psophiidae*, *Aramidae*, and several ralloids. This process is absent in *Cariamidae* and most examined *Charadriiformes*. Maxillopalatine processes are visible in the CT scan data (see Supplementary Material). They are triangular and exhibit small foramina, which is most similar to the condition in *Gruoidea* and most *Charadriiformes* and *Ralloidea*. Such foramina are much larger in *Laridae* and *Burhinidae*.

The cranium appears caudally elongate, as in many *Gruiformes*, and is more elongate than that of *S. mikkelsenii* or *S. robusta*. The orbital margin is slightly crushed but forms an extensive, sharp crista that is oriented dorsolaterally as in *S. mikkelsenii*, *Himantornis haematopus* (extant ralloid), *Rhynchoetidae*, *Jacaniidae*, *Charadriidae*, *Burhinidae*, and *Pluvianidae*. CT data show that this crista is also present on the left orbit and is preserved within the slab (see CT data in Supplementary Material). The ectethmoid and lacrimal are too poorly preserved to describe, other than to note that the lacrimals fuse to the skull at about the same craniocaudal location of the zona flexoria craniofacialis. It appears that fonticuli occipitales are absent from the caudal aspect of the skull as in *Ralloidea*, although much of the cranial anatomy cannot be discerned. A thin and linear jugal is present on the surface; with its pair visible beneath the slab in the CT scan data (see CT data in Supplementary Material). It is more slender than that of *S. robusta* (HLMD.Be.161; Mayr, 2002). The postorbital process is moderately small and acuminate like those of most *Ralloidea*. A shallow crista is located along its length to the apex, and its apex is oriented ventrally rather than cranially as in *S. mikkelsenii*. It is smaller and more gracile than that of *S. robusta*. The

zygomatic process appears small and acuminate, but this is difficult to ascertain due to poor preservation. The temporal fossa appears to have been shallow. At least six robust scleral ossicles are preserved. Behind them is a fonticulus interorbitalis which is rostrocaudally expansive as in *S. mikkelsenii*, Gruidae, most Charadriiformes and Ralloidea.

Two well-preserved quadrates are present, with only one being visible above the surface; CT scan data reveal more key features of this element (Figure 3). The orbital processes are too poorly preserved for description. The posterior face between the capitula is apneumatic as in *P. mikkelsenii* and almost all Gruiformes, whereas a foramen is present in almost all examined Charadriiformes. The medial otic capitulum is deflected caudally, as in Charadriiformes and Gruiformes. The capitula of the quadrate are moderately spaced and separated by a deep notch as in examined Rallidae and Laridae. The capitula are best preserved in the right quadrate, where they are robust and rounded like those in Laridae. The capitulum squamosum is rostrocaudally flattened as in all Charadriiformes and Gruiformes, and the capitulum oticum is mediolaterally elongate as in all examined Charadriiformes and Gruiformes. The otic processes of the quadrates are slender and more delicate like those of Ralloidea, and are much less robust than those of Gruoidea. They are recurved toward their dorsal margins. A sharp crista lateralis can be seen along the caudolateral margin of the body of the right quadrate. The prominent crista lateralis is most similar to the condition in examined rallids. A raised crista tympanica is also present as in many Gruiformes and Charadriiformes, and the otic process dorsal to this crista is deeply concave as in many Charadriiformes (e.g., *Vanellus*). A caudal condyle is present and visible in caudal aspect. The caudal condyle is confluent with the lateral condyle as in Gruiformes, Charadriiformes and Cariamidae. The fovea of the cotyla quadratojugalis is deep and laterally directed as in Gruiformes and Charadriiformes. Similarly, as in Ralloidea and many Charadriiformes, a rounded processus lateralis present along the caudodorsal rim projects over the fovea quadratojugalis.

The caudal terminus of the dentary is slightly dorsally convex as in Psophiidae, but this is difficult to ascertain due to breakage. The dorsal ramus of the dentary is short relative to the ventral ramus. The angular is almost in line with the rest of the mandible and not as decurved as that of *S. robusta*, and is more like those of *S. mikkelsenii*, Gruiformes and Charadriiformes. The rostral mandibular fenestrae appear to have been elongate and slit-like, with extremely small caudal mandibular fenestrae if present. The caudal articular area displays neoavian morphology, and a narrow, dorsally projecting hook-like projection is present as in Gruiformes, Charadriiformes and *P. mikkelsenii* (Musser et al., 2019).

Axial skeleton

Crushed remains of what appears to be the atlas in lateral view are located just below the occipital, but the CT scan does not reveal additional diagnostic morphology of the atlas or axis. At least 18 articulated presacral vertebrae are preserved, mostly in lateral aspect. The spinous processes are dorsoventrally truncate and located at approximately the midline of each

cervical vertebra. Elongate costal processes are apparent, as in all examined Charadriiformes and Gruiformes; *S. mikkelsenii*; and *Messelornis cristata* Hesse (1988). They are located relatively rostrally, in contrast to the more caudally located costal processes of Psophiidae. Costal processes are present throughout the series with the exception of the caudal-most cervical vertebrae, although these may be obscured by other bone or matrix. This is similar to the condition in most examined Gruiformes and Charadriidae. The caudal zygapophyses are elongate and taper distally. They are oriented more dorsally than those of Rallidae or Charadriidae, although those of Charadriidae are closer to this condition. Vertebrae preserved in lateral view appear to be laterally concave. A notarium superficially appears to be present; however, CT scan data reveals that it is absent, unlike the condition in Psophiidae. The presence or absence of a notarium is currently unknown in *S. robusta*.

Computed tomography scan data reveal what appear to be fragmented remains of the sternum; however, no diagnostic features can be discerned if this interpretation is correct. Several ribs are preserved in lateral aspect. The cranialmost uncinate process is truncate and broad, but the uncinate processes caudal to that are more elongate and slender. The pygostyle is preserved in lateral aspect along with several poorly preserved caudal vertebrae. It is ventrally recurved and “half-moon” shaped, with the terminus of the pygostyle deviating ventrally from its major axis as in *S. mikkelsenii* and some Charadriidae. It appears to be mediolaterally flattened save for a slight expansion at the dorsocaudal edge. The neural spines of the caudal vertebrae preserved in articulation with the pygostyle are robust, dorsally blunted and angled caudally. One free caudal vertebra is preserved separate from the pygostyle and other caudal vertebrae and is visible in what appears to be posterior aspect underlying the soft tissue. It bears a truncate neural spine and elongate transverse processes that are angled ventrally by approximately 15 degrees from the horizontal position.

Pelvic Girdle

The remains of the pelvis are poorly preserved and obscured by both matrix and preserved plumage. Visible portions comprise the ventral aspect of the right preacetabular ilium, the lateral aspect of the right postacetabular ischium, most of the obturator foramen, the entirety of the right pubis, and a small and broken portion of the midshaft of the left pubis.

The pelvis appears to have been dorsoventrally flattened. The preacetabular ilium is broken along the proximal and medial margins but is proximally expansive and wing-like, as in examined Charadriiformes and *S. mikkelsenii*. The obturator foramen is craniocaudally elongate and ovoid. It is not delimited caudally, but it is uncertain whether this is due to taphonomy. The shape of the obturator foramen is most similar to the condition in Psophiidae and Charadriiformes as it is dorsoventrally wide and broadens caudally, whereas in examined Rallidae the obturator foramen is extremely dorsoventrally flattened. As in many Charadriiformes and Heliornithidae the pubis is extremely long, approximately twice the length of the postacetabular ilium. This is unlike the condition in Sarothruridae, Rallidae and *S. robusta* in which

the postacetabular ischium and pubis are of subequal length (HLMD.Be.161; Mayr, 2002). The pubis tapers to an acuminate point and superficially appears thin and rounded; however, CT scan data reveals that it is broad and flattened as in examined Gruiformes, Cariamidae, and *S. robusta* (SMF-ME 3014; Mayr, 2000a). The fenestra ischiopubica appears to have been dorsoventrally expansive as in examined Charadriiformes and *S. mikkelsenii*. The terminal process of the ischium is caudally elongate and appears to taper caudally as in many Charadriiformes, unlike the condition in Gruiformes and *S. robusta*. The caudolateral vertex of the ilium is present. It is broad at the base, rounded at the terminus and is dorsocaudally directed and truncate. The CT data present this feature as being most similar to that of *S. mikkelsenii* in shape and direction of projection (see **Supplementary Material**). When compared to extant taxa the condition in *N. grandei* is most similar to the condition in Turnicidae and some rallids. The caudal terminus of the ilium is markedly cranial to that of the ischium, as in *S. mikkelsenii* and many charadriiform taxa such as Pluvianidae and Burhinidae.

Hindlimb

An articulated right leg is preserved. The femur is poorly preserved in caudolateral view. It is more robust and elongate compared to the femur of *S. mikkelsenii*. The trochanteric crest and distal condylar area have been obliterated.

The tibiotarsus and articulated fibula are, similarly, poorly preserved in caudo-lateral aspect. The tibiotarsus is approximately twice the length of the tarsometatarsus like in *S. mikkelsenii* and examined Ralloidea. The tarsometatarsus is markedly longer in *S. robusta*, comprising over half the length of the tarsometatarsus (see HLMD.Be.161, Mayr, 2002). The condition in *N. grandei* also differs from that observed in Psophiidae, Burhinidae and Cariamidae in which the tarsometatarsus length is over half the length of the tibiotarsus. The tibiotarsus of *N. grandei* is shorter than that of *S. robusta* as well (see **Table 2**). The fibular head is crushed onto the head of the tibiotarsus. A narrow proximal interosseous foramen can be discerned but its true shape and proximodistal length is unknown due to taphonomic distortion. Morphology of the crista cnemialis has been obliterated on the surface, but CT scan data reveal a prominent, hook-like crista cnemialis cranialis that is limited craniocaudally but proximodistally expansive, as in *S. mikkelsenii* and examined Rallidae. Psophiidae, Cariamidae and Burhinidae also have a well projected crista cnemialis cranialis; however, they are more craniocaudally expansive and are more proximodistally limited in Psophiidae and Burhinidae. The lateral face of the distal condylar area is visible. The depressio epicondylaris lateralis is deep, like that of most Ralloidea and unlike the more shallow depressions of *S. mikkelsenii* and most Gruoidea and Charadriiformes; however, the caudal rim of the condyle is more prominent and laterally extensive than those of Ralloidea. The sulcus m. fibularis appears shallow. CT scan data reveal what appears to be a prominent tubercle latero-distal to the pons supratendineus, like the condition in most Gruiformes. Medial and lateral condyles that exhibit subequal cranial projection are also visible in the CT scan data. The lateral

condyle is proximodistally more elongate and mediolaterally narrower than the medial condyle. As in *S. robusta*, the distal rim of the medial condyle is not notched. This is unlike the condition in *S. mikkelsenii*, Gruoidea, Rallidae, and many Charadriiformes. No ossified tendons are present along the tibiotarsus, which are present in Gruoidea, Sarothruridae and several rallids.

The tarsometatarsus is preserved in caudolateral aspect. CT scan data reveal a prominent eminentia intercotylaris and a deep fossa infracotylaris dorsalis. The cotyla lateralis is distal to the cotyla medialis as in all examined Charadriiformes and Gruiformes. The medial margin of the medial cotyle is prominently projected proximally and forms a sharp crista as in *S. mikkelsenii*, *P. mikkelsenii*, Jacanidae, Pluvianidae, Laridae, Haematopodidae, Recurvirostridae, Thinocoridae, Turnicidae and Gruiformes and unlike the condition in Cariamidae. The hypotarsal crests are moderately projected, with the medial crest being projected farther plantar than the lateral crest. This condition is also present in *S. mikkelsenii*, *S. robusta*, *P. mikkelsenii*, *M. cristata*, and all examined Charadriiformes and Gruiformes. At least one canal appears to be present in the hypotarsus as revealed by the CT scan data, but its homology is uncertain. The fossa parahypotarsalis lateralis is deep as in *M. cristata* and many examined Charadriiformes and Gruiformes. This feature is shallow in *S. mikkelsenii*. The sulcus extensorius is markedly deep along the shaft of the tarsometatarsus. Metatarsal I is truncate and rounded distally. It inserts into a notch in the medial side of the tarsometatarsus, but matrix obscures the articular site. The metatarsal II trochlea is extremely plantarly deflected as in *S. mikkelsenii*, *M. cristata*, *S. acutunguis*, Gruiformes, and all examined Charadriiformes except Burhinidae, Stercorariidae, and Turnicidae. This condition is not present in *S. robusta* or Cariamidae. This trochlea also bears a prominent plantar ala as in *S. mikkelsenii*, *M. cristata*, Gruiformes, and Charadriiformes; this feature is absent in *S. robusta* and Cariamidae. CT scan data reveal a deep central groove that runs along at least the dorsal length of the metatarsal III trochlea. The metatarsal III trochlea extends farther distally than the trochleae for metatarsals II and IV, with the metatarsal IV trochlea extending further distally than that of metatarsal II. This condition is present in *S. mikkelsenii*, *M. cristata*, and most examined Gruiformes; in Cariamidae and *S. robusta*, the condition is similar but differs in that the distal extents of the trochlea for metatarsals II and IV are subequal. No ossified tendons are present along the tarsometatarsus.

All pedal phalanges are preserved with the exception of the unguals of digits II and III. The phalanges are less robust than *S. robusta*. They are shorter and much more delicate than those of Rallidae, and in this way are more similar to those of Charadriidae. In *N. grandei* the first phalanx of each digit is more elongate than the subsequent phalanges. The unguals of digits I and IV are truncate and have deep lateral sulci. At the proximal end, phalanx II:1 (digit: phalanx) has a strong flange at the plantolateral corner. The trochleae appear asymmetrical on both II:1 and II:2, with the lateral rim being farther projected. The robust, medially projected flange seen in *S. robusta* in IV:1 is not present in *N. grandei*.

Possible Syrinx and Trachea

Tracheal rings are pervasive and thick, and a possible syrinx is present above the cranium (Figures 1, 2, see also.stl files in **Supplementary Datasheet 1**). Future imaging and comparison will allow determination of this feature. The tracheal rings appear wider than those of *S. robusta* (HLMD.Be.161; Mayr, 2002), although this is difficult to ascertain in the specimen of *S. robusta*. There is a thick band of rings, a ring with a chevron-like midline connection and then two sets of rings representing bifurcation caudal to the possible syrinx.

Plumage

Individual small contour feather outlines can be seen particularly near the occipital cranium, cervical vertebrae, dorsal body, proximal chest, upper hindlimbs (femur and tibiotarsus), and pygostyle. The tail looks to have been broad and elongate with a shallowly forked tip. The tail comprises large, rectangular feathers largely made up of pars pennacea of vexillum while shorter feathers that appear to comprise pars plumacea of vexillum cover the rest of the body. Rachides and some barbs can be seen, but the number of individual tail feathers cannot be counted due to preservation.

MATERIALS AND METHODS

Comparative Materials

Specimens used for description and phylogenetic analyses came from the Bird Division of FMNH, the Ornithology Department of AMNH, and the Ornithology Department of USNM. Osteological terminology largely follows Baumel and Witmer (1993). Specimen numbers for comparative material are provided in **Table 1**.

CT Scanning

The holotype specimen was scanned using dual tube x-ray computed tomography at the PaleoCT Lab at the University of Chicago, which can scan specimens with a resolution of up to 0.4 μm . As the specimen slab was large, it was scanned using a two-part multiscan that was combined to form one image sequence. The voxel size of the combined scan is 79.0540. The specimen is housed in the Department of Geology of FMNH. CT data generated during the current study are available in the **Supplementary Datasheet 1** via Morphobank (O'Leary and Kaufman, 2012) under Project 3614¹.

Character Matrix

The data matrix is built on that of Musser and Cracraft (2019) following the methodology discussed in that publication, but has expanded since that publication to comprise 693 discrete morphological characters and 60 taxa, eight of which are extinct. Character descriptions are provided in the Appendix and the data matrix has been made publicly available on Morphobank (O'Leary and Kaufman, 2012) under Project 3614

see text footnote 1. In addition to the methods outlined in Musser and Cracraft (2019) and creation of most characters from direct observation of avian skeletons, characters from several previously published morphological datasets (Strauch, 1978; Cracraft and Clarke, 2001; Ferreira and Reginaldo, 2005; Livezey and Zusi, 2006; Mayr, 2008, 2013), especially those that focused on Charadriiformes (Livezey, 2009, 2010; Mayr, 2011b), were evaluated for use in this iteration of the dataset. Specimen numbers for examined taxa are presented in **Table 1**. *Salmila robusta* was added and scored based on Mayr (2000a, 2002) as FMNH PA 778 was previously considered to be closely related to that taxon (Grande, 2013). *Scandiavis mikkelsenii* (Bertelli et al., 2013) and distal humeri IGM 100/1435 (Pan-Charadriiformes, Hood et al., 2019) and SMF AV 619 (Charadriiformes indet., Mayr, 2016) were added and scored from photographs presented in those publications as they have been hypothesized to be extinct exemplars of Charadriiformes and *S. mikkelsenii* shares several features with FMNH PA 778. Two species of *Morsoravis*, *Morsoravis sedilis* (Bertelli et al., 2010; Mayr, 2011a) and an undescribed *Morsoravis* sp. FMNH PA789 (see photograph of specimen published by Grande, 2013) were included in initial analyses as *Morsoravis* was originally hypothesized to be charadriiform (Bertelli et al., 2010); however, we subsequently removed it as *Morsoravis* is now known to be placed within pan-Passeriformes (Ksepka et al., 2019). *Pellornis mikkelsenii*, *Messelornis cristata*, and *Songzia acutunguis* were included as they potentially represent stem Ralloidea (Musser et al., 2019), and FMNH PA778 presented a composite of charadriiform-like and gruiform-like features. The final scorings for each of these taxa are composites of scorings across several specimens from both in-person study and photographs from published studies: Bertelli et al. (2011); Musser et al. (2019) for *P. mikkelsenii*; Hesse (1990); Bertelli et al. (2011) for *M. cristata*; and Wang et al. (2012) for *S. acutunguis*.

Phylogenetic Analyses

We performed unconstrained heuristic parsimony analyses of the dataset in PAUP* (Swofford, 2002); Version 4.0a166, build 164 ($\times 86$) using 10,000 random taxon addition replicates per run. Heuristic search algorithms were used. Tree bisection-reconnection branch swapping was employed and minimum branch lengths valued at zero were collapsed, following Mayr and Clarke (2003), Musser and Cracraft (2019). No character weighting was applied. Characters 245, 320 and 688 were ordered, following Bertelli et al. (2011); Musser et al. (2019). Bootstrap analyses were performed using 500 bootstrap replicates each with 10 random taxon addition replicates as in Mayr and Clarke (2003). In addition to unconstrained analyses, constrained analyses were performed using the topology of recent phylogenomic studies (Prum et al., 2015; Reddy et al., 2017; Kimball et al., 2019) as molecular backbone constraints for the major clades of sampled extant taxa except for *Opisthocomus hoazin* due to current lack of robust placement of that taxon even among these recent molecular studies. Extinct taxa were unconstrained in all analyses.

¹<http://morphobank.org/permalink/?P3614>

Body Size Estimation

Femur length was the best predictor of body mass in extant volant birds ($R^2 = 0.9028$; Field et al., 2013) that could be obtained from FMNH PA778 and *Scandiavis mikkelsenii* (Bertelli et al., 2013).

RESULTS

Unconstrained parsimony analysis resulted in 69 most parsimonious trees (MPTs) of 5,147 steps. This analysis recovered a paraphyletic Gruiformes with respect to Charadriiformes, with *Nahmavis grandei* and *Scandiavis mikkelsenii* being placed as the sister-taxa of all included Charadriiformes (CI = 0.166, RI = 0.475, RC = 0.079, HI = 0.834).

Analysis applying a backbone constraint representing major subclade relationships of Kimball et al. (2019) recovered 56 MPTs of 5,248 steps (Figure 4; CI = 0.163, RI = 0.462, RC = 0.075, HI = 0.838) and a clade containing *N. grandei*, *Turnix nigricollis* and *S. mikkelsenii* as the sister-group of all other included Charadriiformes. Synapomorphies recovered for critical groups across all constrained analyses are displayed in **Supplementary Table 1**. *Pellornis mikkelsenii* was recovered as a messelornithid across all analyses, consistent with prior placements (Bertelli et al., 2011; Musser et al., 2019). Messelornithidae (*Pellornis mikkelsenii* + *Messelornis cristata*) was placed as the sister-taxon of *Songzia acutunguis*. Messelornithidae was within a clade sister to extant Ralloidea across all analyses. This is consistent with the three derived characters described by Mayr (2004) as evidence of a monophyletic (Messelornithidae + (Rallidae + Heliornithidae)) clade and with the phylogenetic analyses of Musser et al. (2019) which recovered a Messelornithidae (including *Pellornis mikkelsenii*) + Ralloidea clade.

Analyses using a backbone constraint based on the major clade relationships of Prum et al. (2015) recovered 75 MPTs of 5,244 steps (Figure 5A; CI = 0.163, RI = 0.463, RC = 0.075, HI = 0.837), and employing a Reddy et al. (2017) constraint yielded 84 MPTs of 5,260 steps (Figure 5B; CI = 0.162, RI = 0.461, RC = 0.075, HI = 0.838). These analyses did not recover Charadriiformes and Gruiformes as sister-groups as in the Kimball et al. (2019) constrained analysis. They resulted in placement of *N. grandei* and *S. mikkelsenii* in a clade containing Messelornithidae that made up the sister-group of extant ralloids, with *S. acutunguis* being placed within crown Ralloidea (Figure 5). When the Messelornithidae were removed, analyses employing the Prum et al. (2015) backbone constraint again placed *N. grandei* and *S. mikkelsenii* as sister-taxa within Charadriiformes, and analyses using the Reddy et al. (2017) constraint resulted in collapse of the relationships of all included Charadriiformes, *N. grandei* and *S. mikkelsenii* into a polytomy at the base of Neoaves. Bootstrap support for placement of extinct taxa was less than 50% across all analyses, with the exception of Messelornithidae earning an 88% bootstrap score in each result.

Salmila robusta was recovered within a clade containing the Cariamidae, *Cathartes burrovianus* and *Leptosomus discolor* under Prum et al. (2015) and Kimball et al. (2019) constraints as the sister-taxon of *L. discolor*. Analyses employing the Reddy et al. (2017) constraints recovered *S. robusta* within a clade containing

the Eurypygiformes, *Caprimulgus carolinensis* and *Columba livia* with *S. robusta* placed as the sister-taxon of the *Eurypygia helias* + *Rhynchoetos jubatus* sister-group. The latter difference in placement may be due to a lack of scorings for *S. robusta* as the specimen was scored from published photographs.

Both Eocene humeri (IGM 100/1435 from Mongolia and SMF AV 619 from Virginia) were recovered within crown Charadriiformes across all analyses, and IGM 100/1435 was placed as the sister taxon of *Chionis alba* under both the Prum et al. (2015) and Kimball et al. (2019) backbone constraints. Messelornithidae is recovered as being within a sister-clade of Ralloidea across all analyses, bolstering evidence for placement of Messelornithidae at the base of Ralloidea as originally recovered by Musser et al. (2019); however, further resolution of taxa such as *S. mikkelsenii* and *N. grandei* must be completed to more confidently place this clade. *S. acutunguis* is consistently recovered as either a sister-taxon of Messelornithidae or as being unresolved within crown Ralloidea, suggesting that it may be more closely related to crown ralloids than the Messelornithidae. Additional fossils still need to be included to more robustly place this taxon (Wang et al., 2012; Musser et al., 2019).

A rough mean body mass estimate for FMNH PA778 is approximately 200g based on published allometric equations using femoral length (Field et al., 2013). This is larger than the estimated body masses for *Scandiavis mikkelsenii* and *Pellornis mikkelsenii* (170.24 g and 133.28 g, respectively). This estimate would make *N. grandei* somewhat smaller than *Dromas ardeola* (325 g), *Ibidoryncha struthersii* (294 g) and roughly similar in size to some members of Laridae, Charadriidae (larger members of *Vanellus*), Recurvirostridae (most consistent with avocets), and Scolopacidae but not approaching the masses of larger shorebirds such as many members of Haematopodidae, Burhinidae, Chionidae, and Stercorariidae (~600 to over 1000 g; Dunning, 2007). The mean mass estimate for *S. mikkelsenii* aligns it more closely in size with Jacanidae, the smallest members of Recurvirostridae (e.g., *Himantopus*), some members of Charadriidae (*Vanellus*), and smaller members of Scolopacidae and Laridae.

DISCUSSION

Nahmavis grandei is recovered as a charadriiform when enforcing avian subclade relationships recovered in Kimball et al. (2019). This result is significant not only because *N. grandei* may be the first known charadriiform from the Green River Formation, but also because the Paleogene record of this group remains globally sparse (Mayr, 2009, 2017). At the same time, recovery of *N. grandei* within basal Gruiformes under the Prum et al. (2015) and Reddy et al. (2017) constraints problematizes that proposed assignment. Specifically, it highlights the sensitivity of the placement of potential stem Charadriiformes to resolution of neoavian subclade relationships. Despite inclusion of well-preserved charadriiform and gruiform fossils with articulated skeletons within a large morphological data matrix, the fine-scale relationships of *N. grandei* and *S. mikkelsenii* remain weakly supported. They are sensitive to phylogenetic placement of extant

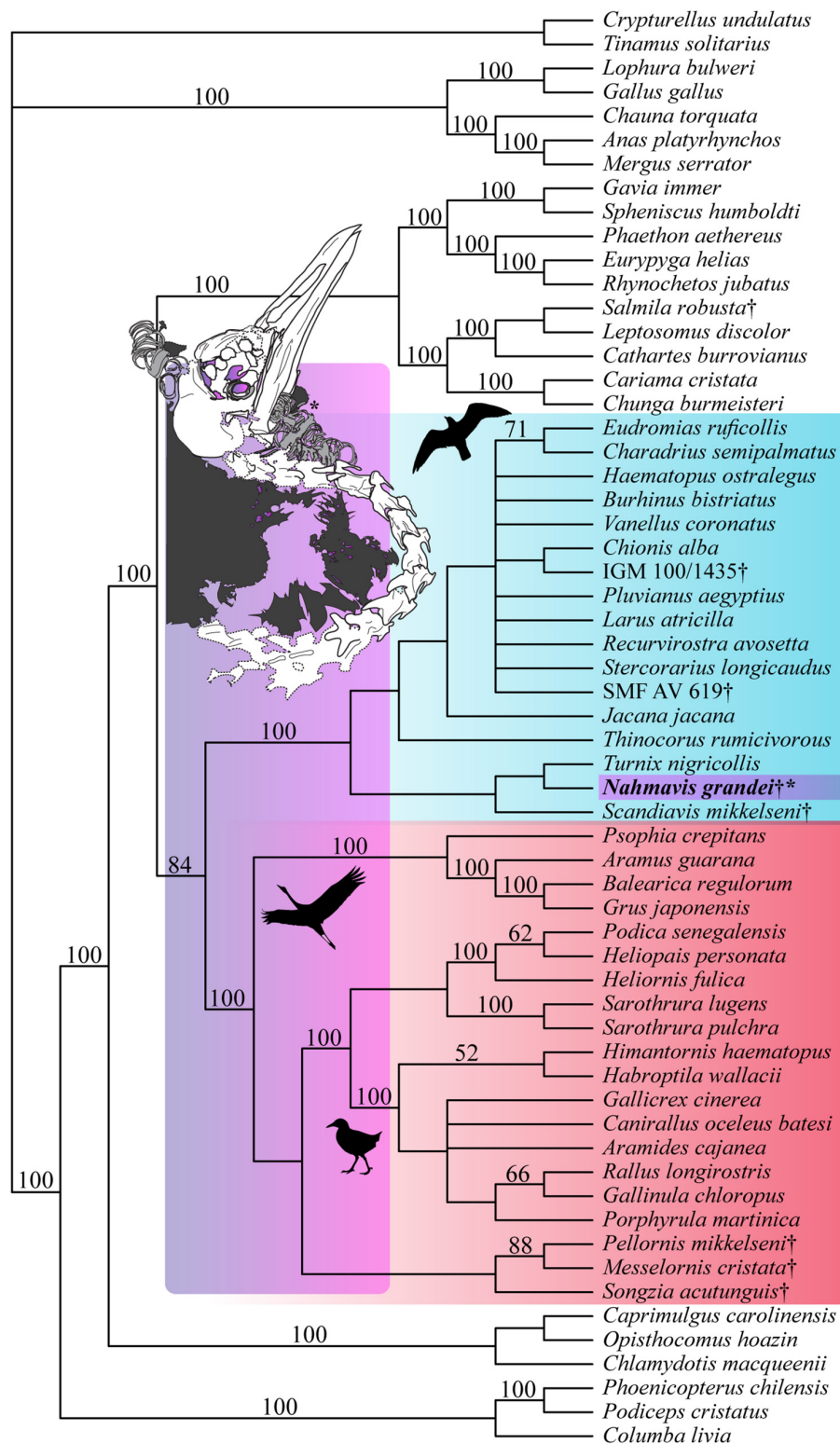
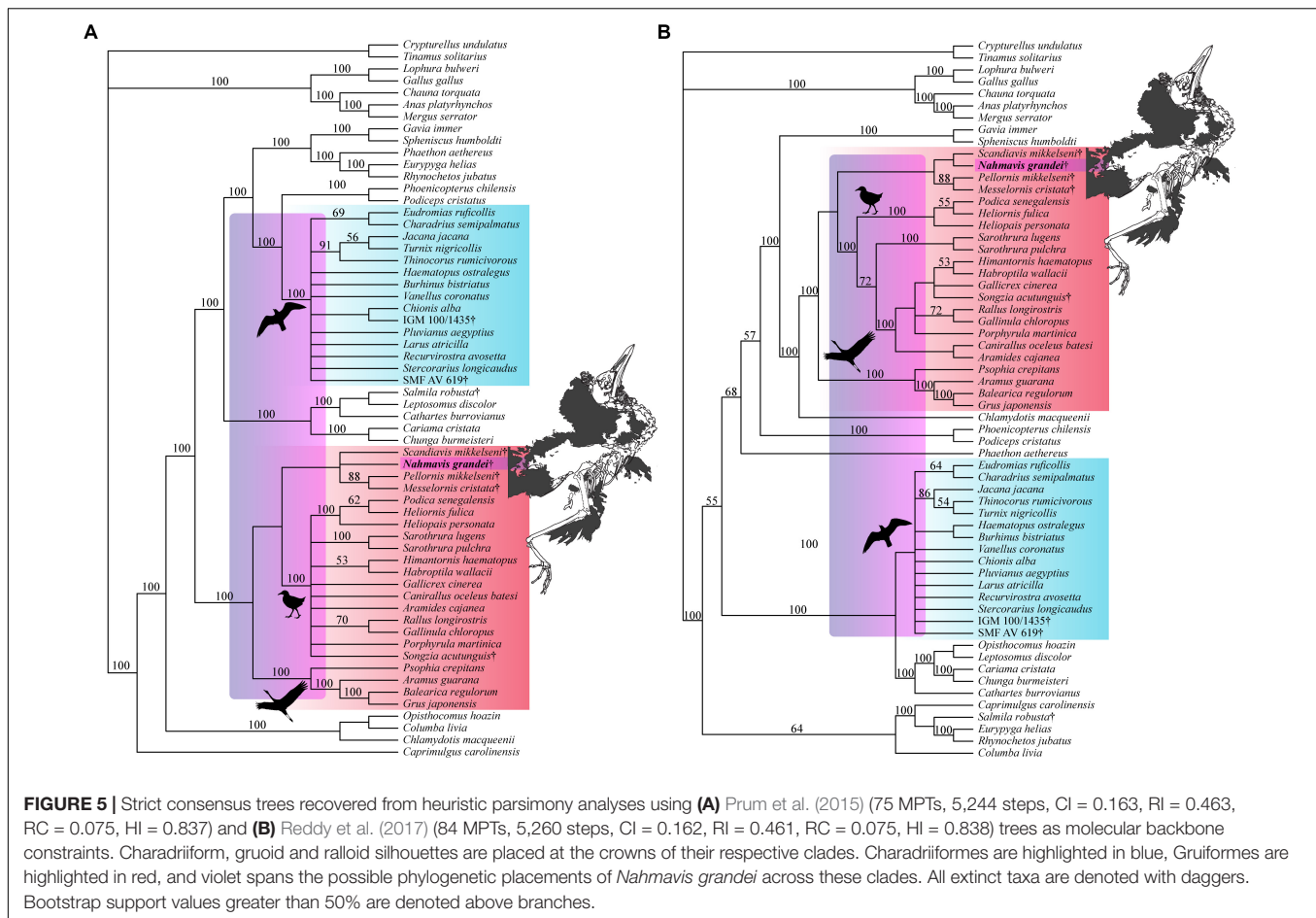


FIGURE 4 | Strict consensus tree of 56 MPTs of 5,248 steps recovered using the most recent Kimball et al. (2019) tree as a molecular backbone constraint (CI = 0.163, RI = 0.462, RC = 0.075, HI = 0.838). Charadriiform, gruoid and ralloid silhouettes are placed at the crowns of their respective clades. Charadriiformes are highlighted in blue, Gruiformes are highlighted in red, and violet spans the possible phylogenetic placements of *Nahmavis grandei* across these clades. All extinct taxa are denoted with daggers. Bootstrap support values greater than 50% are denoted above branches.



clades, especially in phylogenies where Charadriiformes is not recovered as the sister-group of Gruiformes as is the case in the analyses by Prum et al. (2015) and Reddy et al. (2017). A Charadriiformes + Gruiformes sister-taxon relationship has been recovered by phylogenies using a variety of datatypes, including those presented in recent molecular studies (e.g., Cracraft, 1988; van Tuinen and Hedges, 2001; Livezey and Zusi, 2007; Bertelli et al., 2011; Jarvis et al., 2014; Kimball et al., 2019; Musser and Cracraft, 2019). As discussed below, traits such as having a crista tympanica of the quadrate with a terminus within the ventral half of the otic process, unfused iliac blades of the pelvis, and a pedal digit I: phalanx 1 that is half the length of pedal digit III: phalanx 1 are present in parts of both clades.

Six unambiguous and three ambiguous optimized synapomorphies of the skull, cervical vertebrae, pelvis and hallux with CI < 1.0 support placement of *N. grandei* within Charadriiformes using the Kimball et al. (2019) constraint (Figure 6). The nasal bar is rostrocaudally wider at the caudodorsal margin of the nares than at the caudoventral margin in *N. grandei* and many Charadriiformes (character 16: state 2, unambiguous), whereas the opposite is true in most gruoids (16:3) and the margins are subequal in rostrocaudal width in most Ralloidea (16:1). The quadrate in *N. grandei* and most Charadriiformes has a crista tympanica that terminates within

the ventral half of the otic process (180:2, unambiguous), is deeply concave along the caudal face of the otic process dorsal to the crista tympanica (183:2, unambiguous), and has a lateral condyle that terminates well ventral to the ventral margin of the caudal condyle (206:2, ambiguous); in contrast, almost all included Gruiformes have a crista tympanica that terminates at the dorsoventral midpoint or within the dorsal half of the otic process (180:1) and a shallowly excavated or convex caudal face of the otic process (183:1). Most included Gruiformes do share marked ventral location of the ventral margin of the lateral condyle relative to the caudal condyle (206:2). Relative elongation of intermediate cervical vertebrae is lost in *N. grandei* (Figures 1, 2), *S. mikkelsenii*, and most Charadriiformes (253:2, ambiguous), but is present in most Gruiformes (253:1). The iliac blades of the pelvis are not fused to the synsacrum (498:2, unambiguous, Figure 6). Pedal digit I: phalanx 1 is half the length of pedal digit III: phalanx 1 (691:2, unambiguous) in *N. grandei*, *S. mikkelsenii* and almost all Charadriiformes. In all extant Gruiformes, the iliac blades are fused to the synsacrum (498:1) and pedal digit I: phalanx 1 is more elongate (691:1). A medially protruding flange at the proximal margin of pedal digit IV: phalanx 1 is absent in *N. grandei* (692:0, ambiguous, see CT data in **Supplementary Material**) and present in some Gruiformes (692:1). This character could not be assessed for

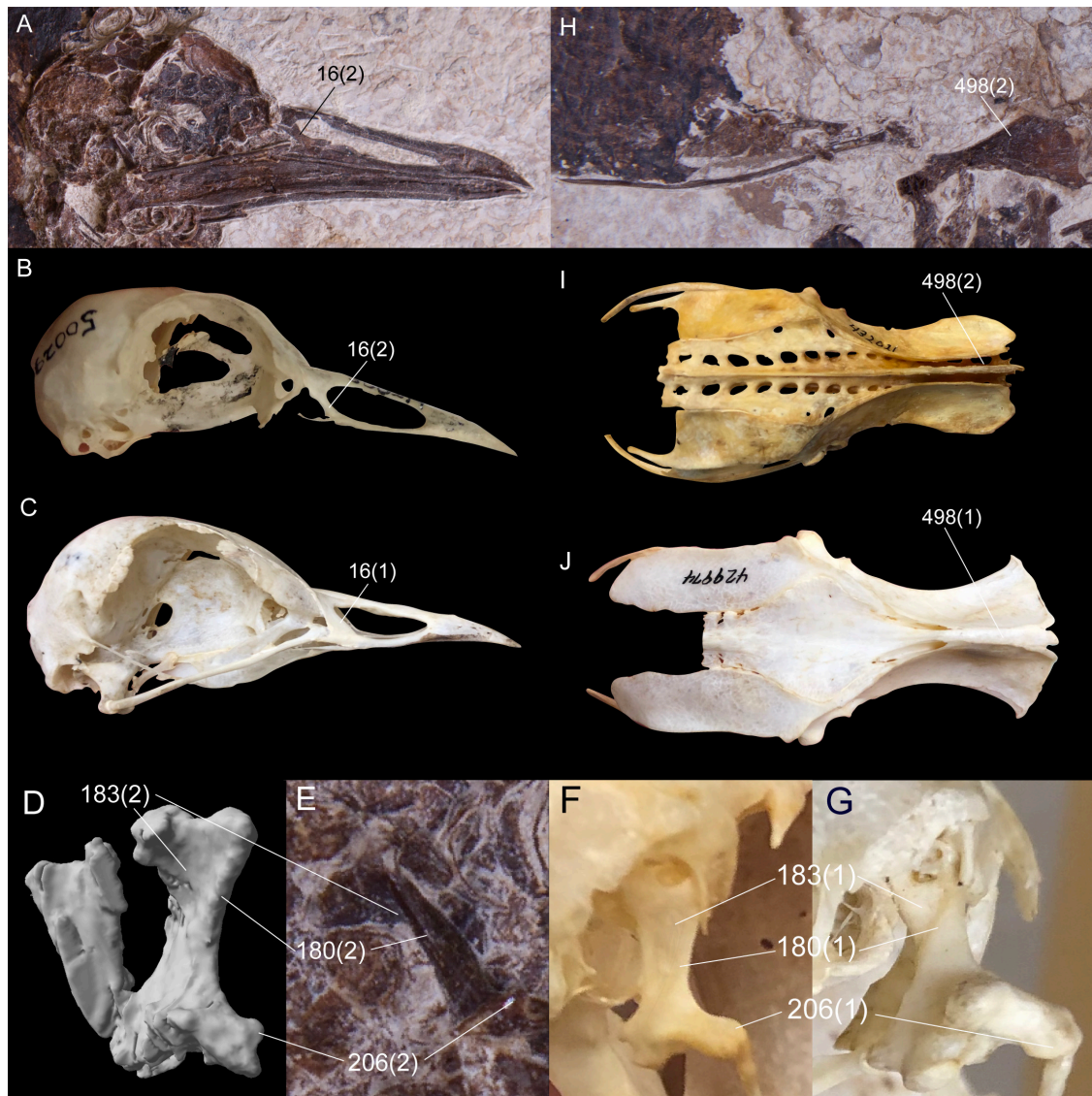


FIGURE 6 | Comparison of selected optimized synapomorphies that place *Nahmavis grandei* within Charadriiformes to the exclusion of Gruiformes under the Kimball et al. (2019) backbone constraints. Synapomorphies are shown with the character number followed by the state in parentheses. **(A–C)** Skulls of *N. grandei*, *Pluvianus aegyptius*, and *Psophia crepitans*. **(D,E)** segmented CT image and photograph of the right quadrate of *N. grandei*. **(F,G)** right quadrates of *Vanellus coronatus* and *P. crepitans*. **(H–J)** pelvises of *N. grandei*, *Burhinus bistriatus* and *P. crepitans*.

included Charadriiformes. The placement of *Turnix nigricollis* as the sister-taxon of *N. grandei* is not consistent with recent phylogenies, which recover *Turnix* as the sister-taxon of a group containing *Glareola*, *Larus*, and *Dromas* (Prum et al., 2015; Reddy et al., 2017; Kimball et al., 2019). In some analyses, this group also contains *Uria*, *Sterna*, *Chroicocephalus*, and *Rynchops* (Prum et al., 2015; Kimball et al., 2019). Incongruous placement of this taxon in our results is likely due to a lack of constraining taxon relationships within major subclades and a need for more taxon and character sampling. *Turnix* is also known to be problematic in morphological analyses; Livezey (2010) similarly recovered *Turnix* as the sister-group to all other Charadriiformes, and Mayr (2011b) recovered

Turnicidae as either within a polytomy in Charadriiformes or as the sister-taxon of a clade containing Jacanidae, Scolopacidae, Rostratulidae, Thinocoridae, and Pedionomidae.

Several characters that were recovered as support for placement of *N. grandei* within Charadriiformes in the analysis employing the Kimball et al. (2019) constraint were also recovered as supporting a clade containing *N. grandei*, *S. mikkelsenii* and the Messelornithidae under the Prum et al. (2015) and Reddy et al. (2017) backbone constraints. Character evidence for placement of *N. grandei* within this group across both analyses comprises a maximum of five unambiguous synapomorphies. As in the placement of *N. grandei* under the Kimball et al. (2019) constraints, the quadrate in *N. grandei*

has a crista tympanica that terminates ventrally within the ventral half of the otic process (180:2, unambiguous), the iliac blades of the pelvis are not fused to the synsacrum (498:2, unambiguous), and pedal digit I: phalanx 1 is half the length of pedal digit III: phalanx 1 (691:2, unambiguous). In addition, a pronounced epicondylus lateralis tubercle of the tibiotarsus is present in *N. grandei* (609:2, unambiguous under the Prum et al. (2015) constraints and ambiguous under the Reddy et al., 2017 constraints) that is diminished in most extant Gruiformes and derived Charadriiformes (609:1). The fossa supratrochlearis plantaris of the tarsometatarsus is distinctly concave as in most examined Charadriiformes (677:1, unambiguous) and to the exclusion of most Gruiformes.

In addition to the issues discussed above, a lack of the pectoral girdle and forelimb in both *N. grandei* and *S. mikkelsenii* may be the cause of these different optimizations under several backbone constraints. Musser et al. (2019) found two out of three synapomorphies for a clade containing Messelornithidae and *Songzia acutunguis* to be located within the humerus and sternum. The direction and development of the dorsal supracondylar tubercle of the humerus is one of the few proposed unambiguous crown traits present in Paleogene material referred to Charadriiformes (Mayr, 2016; Hood et al., 2019).

Shared characters due to a similar ecology in *N. grandei*, *S. mikkelsenii* and the messelornithids cannot be ruled out. The short pedal digit I: phalanx 1 of *N. grandei*, *S. mikkelsenii*, and *M. cristata* (unknown in *P. mikkelsenii*) and the longer pedal digit IV: phalanx 4 than IV:3 observable in both *N. grandei* and *M. cristata* (unknown in *S. mikkelsenii* and *P. mikkelsenii*) suggests some degree of terrestrial or cursorial adaptation (Storer, 1971; Zeffert et al., 2003). In *M. cristata*, specifically, the proximal articulation of the hallux has been proposed to render it immobile (Hesse, 1990). The shorter tarsometatarsus relative to the tibiotarsus in *N. grandei* is distinct from the more subequal elements of *S. mikkelsenii* and *M. cristata*, suggesting that *S. mikkelsenii* could have been more likely to run and wade along the shoreline like a traditional sandpiper than *N. grandei*. Most of the foot is missing in *P. mikkelsenii* and key pedal phalanges are not preserved in *S. mikkelsenii*, again limiting ecological comparison and data for phylogenetic analyses. A high degree of shared plesiomorphy may be expected if Charadriiformes and Gruiformes are sister-taxa or homoplasy may be indicated due to similar ecology if they are not. The scorings for the Messelornithidae and *N. grandei* are nearly identical, with few differences between either *Pellornis* or *Messelornis* and *N. grandei* and even fewer differences between *N. grandei* and both examined Messelornithidae. The differences between *N. grandei* and both examined Messelornithidae comprise the following features: *N. grandei* lacks the pneumatic foramen present on the caudal face of the quadrate between the capitula of *Messelornis* and *Pellornis*, the apices of spinous processes of the cervical vertebrae are more elongate and caudally reaching in the Messelornithidae than in *N. grandei*, the caudal terminus of the pygostyle of *N. grandei* departs ventrally from the craniocaudal axis whereas it departs from this axis dorsally in the Messelornithidae, the mediolateral

thickness of the medial and lateral condyles of the tibiotarsus are subequal in *N. grandei* whereas the medial condyle is mediolaterally thinner in the Messelornithidae, and the ossified retinaculum present in the tibiotarsus in both examined members of Messelornithidae is absent in *N. grandei*. All differences, even those between one examined member of Messelornithidae and *N. grandei*, comprise features that have variable scorings across Gruiformes and Charadriiformes and thus remain cryptic in terms of indicating a more dominant affinity.

A feature of the feathering in *N. grandei* that requires further study and could be alternatively plesiomorphic to a charadriiform-gruiform clade or independently derived in early parts of both clades is the elongate, shallowly cleft tail shape (Figure 1), which appears to be most similar to that of an Oystercatcher or Egyptian Plover. It is unlike that of any extant gruiform (del Hoyo et al., 2020). The tail length may have allowed for additional lift (Thomas, 1993), balance and increased flight maneuverability, perhaps to aid in feeding over-water like a gull (Thomas and Balmford, 1995). The holotype of *P. mikkelsenii* also appeared to have a broad and elongate tail, but its terminal shape is unknown (Bertelli et al., 2011; Musser et al., 2019).

Phylogenetic placement of these Paleogene fossils has implications for the timing of charadriiform diversification. The isolated early Eocene humeri are always recovered as part of that clade. If all specimens are assessed to that clade, they would indicate that both stem and crown taxa were present in both marine and lacustrine environments around the same time across the globe, consistent with a rapid evolutionary radiation. Placement of the two humeri within crown Charadriiformes suggests that they may be useful fossils for calibration, older than even the middle Eocene *Jiliniornis huadianensis* Hou and Ericson (2002) recently proposed as the calibration for crown Charadriiformes by Smith (2015), and that the crown clade is at least as old as the earliest Eocene. Recent studies based on genomes and multiple nuclear genes have provided younger, early Eocene divergence age estimates for crown Charadriiformes (~57 Ma, Ericson et al., 2006; ~56 Ma, Claramunt and Cracraft, 2015; 53.57 Ma, Smith, 2011; ~53 Ma, Kimball et al., 2019; ~48 Ma, Prum et al., 2015) that conflict with the Cretaceous divergence dates (ranging from 67.9 to 93.1 Ma) of the mitochondrial gene sequence and RAG1 nuclear gene sequence based studies reviewed by Smith (2011), (Paton et al., 2002, 2003; Pereira and Baker, 2006; Baker et al., 2007; Brown et al., 2007). Early Eocene and older ages for the crown clade estimated from combined morphological and molecular data (Smith and Clarke, 2015; Smith, 2015) are consistent with the analyses of the fossils assessed here. If correct, some recent divergence time estimates based on nuclear gene and genomic data have underestimated the divergence timing of this group as they have for crown Gruiformes (Musser et al., 2019), although caution needs to be taken in assessing this since the Eocene humeri are isolated, fragmented bones. Only four synapomorphies that were recovered as placing these taxa within crown Charadriiformes

could be scored from these specimens: a fossa olecrani of the humerus with limited depth (469(1)), a proximally elongate supracondylaris dorsalis (470(2)), a deep and extensive fossa *m. brachialis* (474(2)), and a condylus dorsalis that is located distal to the distal terminus of the fossa *m. brachialis* (475(1), only present in IGM 100/1435). Both possible charadriiform skeletons, *N. grandei* and *S. mikkelsenii*, are additionally missing their forelimbs, again suggesting that further studies need to assess the placement of these taxa to identify whether any of these fossils comprise robust calibration points for Charadriiformes.

Our placement of *N. grandei* and the results of our phylogenetic analyses more generally are consistent with a pattern similar to prior proposals for many major avian clades, with possible stem clade origin in Eurasia and rapid expansion into North America. The same pattern has currently been found within the fossil record of Gruiformes (Bertelli et al., 2011; Mayr, 2017; Musser et al., 2019); however, much work remains to be done and morphological data remain key to untangling the role that shifting distributions and ecologies played in avian evolution.

ACCESSION NUMBERS

ZooBank Identifier: urn:lsid:zoobank.org:pub:57238342-B0D2-4764-8F6C-79205EB14F1A

Genus: urn:lsid:zoobank.org:act:8B1CD8D4-6C0F-4535-B1B2-C87286D6234B

Species: urn:lsid:zoobank.org:act:7E917BC1-DCC7-4046-B7FE-14A9537E2F06

DATA AVAILABILITY STATEMENT

The datasets presented in this study can be found in online repositories. The names of the repository/repositories and accession number(s) can be found in the article/**Supplementary Material**.

REFERENCES

- Baker, A. J., Pereira, S. L., and Paton, T. A. (2007). A phylogenetic relationships and divergence times of *Charadriiformes* genera: multigene evidence for the Cretaceous origin of at least 14 clades of shorebirds. *Biol. Lett.* 3:2. doi: 10.1098/rsbl.2006.0606
- Baumel, J. J., and Witmer, L. M. (1993). "Osteologia," in *Handbook of Avian Anatomy: Nomina Anatomica Avium*, eds J. J. Baumel, A. S. King, J. E. Breazile, H. E. Evans, and J. C. Vanden Berge (Cambridge, NY: Publications of the Nuttall Ornithological Club), 45–132.
- Bertelli, S., Chiappe, L. M., and Mayr, G. (2011). A new Messel rail from the early Eocene fur formation of Denmark (Aves, Messelornithidae). *J. Syst. Palaeontol.* 9:4. doi: 10.1080/14772019.2010.538730
- Bertelli, S., Lindow, B. E. K., Dyke, G. J., and Chiappe, L. M. (2010). A well-preserved 'charadriiform-like' fossil bird from the early Eocene Fur Formation of Denmark. *J. Paleontol.* 53:3. doi: 10.1111/j.1475-4983.2010.00950.x
- Bertelli, S., Lindow, B. E. K., Dyke, G. J., and Mayr, G. (2013). Another charadriiform-like bird from the lower Eocene of Denmark. *J. Paleontol.* 47, 1282–1301. doi: 10.1134/S0031030114130024

AUTHOR CONTRIBUTIONS

GM performed the software and funding acquisition, collected most of the data, carried out the data curation, and wrote the original draft of the manuscript. Both authors performed the methodology, carried out the formal analyses and project administration, visualized and supervised the data, did the conceptualization, validated and investigated the data, carried out the resources, and wrote, reviewed, and edited the manuscript.

FUNDING

This project was supported by a National Science Foundation GRFP award (to GM, Grant number DGE-16-4486), an Ornithology Collections Study Grant from the American Museum of Natural History (to GM, 2019) and the Jackson School of Geosciences (GM and JC).

ACKNOWLEDGMENTS

We thank all of the staff of FMNH, especially Lance Grande, William Simpson, Adrienne Stroup, Shannon Hackett, John Bates, and Ben Marks, for specimen access and valuable discussion. We also thank April Neander for scanning the specimen and Matthew Colbert for aid in scan visualization and segmentation. We also thank Daniel Ksepka and Joel Cracraft for valuable discussion. GM would like to thank her recently deceased father, Guy G. Musser, for teaching her to fish and for his guidance throughout her life.

SUPPLEMENTARY MATERIAL

The Supplementary Material for this article can be found online at: <https://www.frontiersin.org/articles/10.3389/fevo.2020.559929/full#supplementary-material>

- Brown, J. W., Payn, R. B., and Mindell, D. P. (2007). Nuclear DNA does not reconcile 'rocks' and 'clocks' in Neoaves: a comment on Ericson et al. *Biol. Lett.* 3:3. doi: 10.1098/rsbl.2006.0611
- Buchheim, P. (1994). "Eocene fossil lake, green river formation, wyoming: a history of fluctuating salinity," in *Sedimentology and Geochemistry of Modern and Ancient Saline Lakes*, eds R. W. Renaut and W. M. Last (Broken Arrow, OK: SEPM Special Publication), 50. doi: 10.2110/pec.94.50.0239
- Caramant, S., and Cracraft, J. L. (2015). A new time tree reveals Earth history's imprint on the evolution of modern birds. *Sci. Adv.* 1:11. doi: 10.1126/sciadv.1501005
- Clarke, J. A., Ksepka, D. T., Smith, N. A., and Norell, M. A. (2009). Combined phylogenetic analysis of a new North American fossil species confirms widespread Eocene distribution for stem rollers (Aves, Coraci). *Zool. J. Linn. Soc.* 157:3. doi: 10.1111/zoj.12181
- Cracraft, J. (1988). "The major clades of birds," in *Phylogeny and Classification of the Tetrapods. Vol. 1. Amphibians, Reptiles, Birds*, ed. J. Benton (Oxford: Systematics Association), 339–361.

- Cracraft, J. L., and Clarke, J. A. (2001). "The basal clades of modern birds," in *New Perspectives on the Origin and Early Evolution of Birds*, eds J. Gauthier and L. F. Gall (New Haven, CT: Peabody Museum of Natural History, Yale University), 143–156.
- del Hoyo, J., Elliott, A., Sargatal, J., Christie, D. A., and de Juana, E. (2020). *Handbook of the Birds of the World Alive*. Barcelona: Lynx Edicions.
- Dunning, J. B. (2007). *Handbook of Avian Body Masses*, 2nd Edn. Boca Raton, FL: CRC Press.
- Ericson, P. (1997). Systematic relationships of the Palaeogene family Presbyornithidae (Aves, Anseriformes). *Zool. J. Linn. Soc.* 121:4. doi: 10.1006/zjls.1997.0098
- Ericson, P. (1999). New material of *Juncitarsus* (Phoenicopteriformes), with a guide for differentiating that genus from the Presbyornithidae (Anseriformes). *Smithson. Contrib. Paleobiol.* 89, 231–234.
- Ericson, P. (2000). Systematic revision, skeletal anatomy, and paleoecology of the New World early Tertiary Presbyornithidae (Aves, Anseriformes). *PaleoBios* 20, 1–23.
- Ericson, P. G. P., Anderson, C. L., Britton, T., Elzanowski, A., Johansson, U. S., Källersjö, M., et al. (2006). Diversification of Neoaves: integration of molecular sequence data and fossils. *Biol. Lett.* 2:4. doi: 10.1098/rsbl.2006.0523
- Ferreira, C. D., and Reginaldo, J. D. (2005). Osteologia craniana de *Platalea ajaja* (Linnaeus) (Aves, Ciconiiformes), comparada com outras espécies de Threskiornithidae. *Rev. Bras. Zool.* 22, 529–551. doi: 10.1590/s0101-81752005000300003
- Field, D. J., Lynner, C., Brown, C., and Darroch, S. A. F. (2013). Skeletal correlates for body mass estimation in modern and fossil flying birds. *PLoS One* 8:e82000. doi: 10.1371/journal.pone.0082000
- Grande, L. (1984). Paleontology of the green river formation, with a review of the fish fauna, 2nd ed. *Geol. Survey Wyom. Bull.* 63, 1–333.
- Grande, L. (2013). *The Lost World of Fossil Lake: Snapshots from Deep Time*. Chicago: The University of Chicago Press.
- Grande, L., and Buchheim, P. (1994). Paleontological and sedimentological variation in early Eocene Fossil Lake. *Rocky Mount. Geol.* 30:33–56. doi: 10.2113/gsrocky.30.1.33
- Hackett, S. J., Kimball, R. T., Reddy, S., Bowie, R. C. K., Braun, E. L., Braun, M. J., et al. (2008). A phylogenomic study of birds reveals their evolutionary history. *Science* 320:5884. doi: 10.1126/science.1157704
- Hesse, A. (1988). Die Messelornithidae—eine neue Familie der Kranichartigen (Aves: Gruiformes: Rhynchoeti) aus dem Tertiär Europas und Nordamerikas. *J. Ornithol.* 129, 83–95. doi: 10.1007/bf01641534
- Hesse, A. (1990). Die Beschreibung der messelornithidae (Aves: Gruiformes: Rhynchoeti) aus dem Alttertiär Europas und Nordamerikas. *Cour. Forsch. Senckenberg.* 128, 1–176.
- Hesse, A. (1992). "A new species of *Messelornis* (Aves: Gruiformes: Messelornithidae) from the middle Eocene Green River Formation," in *Contributions in Science: Papers in Avian Paleontology Honoring Pierce Brodkorb*, ed. K. E. Campbell (Los Angeles, CA: Los Angeles County Museum of Natural History), 171–178.
- Hood, S. C., Torres, C. R., Norell, M. A., and Clarke, J. A. (2019). New fossil birds from the earliest Eocene of Mongolia. *Am. Mus. Novit.* 2019:1. doi: 10.1206/3934.1
- Hou, L., and Ericson, P. G. P. (2002). A middle Eocene shorebird from China. *Condor* 104:4. doi: 10.1093/condor/104.4.896
- Hou, L. H. (1990). An Eocene bird from Songzi, Hubei province. *Vertebrat. Palasiatic.* 28, 34–42.
- Jarvis, E. D., Mirarab, S., Aberer, A. J., Li, B., Houde, P., Li, C., et al. (2014). Whole-genome analyses resolve early branches in the tree of life of modern birds. *Science* 346:6215. doi: 10.1126/science.1253451
- Kimball, R. T., Oliveros, C. H., Wang, N., White, N. D., Barker, F. K., Field, D. J., et al. (2019). A phylogenomic supertree of birds. *Diversity* 11:7. doi: 10.3390/d11070109
- Ksepka, D. T., and Clarke, J. A. (2010a). New fossil mousebird (Aves: Coliiformes) with feather preservation provides insight into the ecological diversity of an Eocene North American avifauna. *Zool. J. Linn. Soc.* 160:4. doi: 10.1111/j.1096-3642.2009.00626.x
- Ksepka, D. T., and Clarke, J. A. (2010b). *Primobucco mcgrewi* (Aves: Coraciiformes) from the Eocene Green River Formation: new anatomical data from the earliest constrained record of stem rollers. *J. Vertebr. Paleontol.* 30:1. doi: 10.1080/02724630903412414
- Ksepka, D. T., and Clarke, J. A. (2012). A new stem parrot from the Green River Formation and the complex evolution of the grasping foot in Pan-Psittaciformes. *J. Vertebr. Paleontol.* 32:2. doi: 10.1080/02724634.2012.641704
- Ksepka, D. T., Clarke, J. A., and Grande, L. (2011). Stem parrots (Aves, Halcyornithidae) from the Green river formation and a combined phylogeny of pan-psittaciformes. *J. Paleontol.* 85:5. doi: 10.1666/10-108.1
- Ksepka, D. T., Grande, L., and Mayr, M. (2019). Oldest Finch-beaked birds reveal parallel ecological radiations in the earliest evolution of Passerines. *Curr. Biol.* 29:4. doi: 10.1016/j.cub.2018.12.040
- Linnaeus, C. (1758). *Systema Naturae per Regna Tria Naturae, Secundum Classes, Ordines, Genera, Species, Cum Characteribus, Differentiis, Synonymis, Locis (Photographic Facsimile)*. London: British Museum of Natural History, doi: 10.5962/bhl.title.542
- Livezey, B. C. (1998). A phylogenetic analysis of the Gruiformes (Aves) based on morphological characters, with an emphasis on the rails (Rallidae). *Philos. Trans. R. Soc. Lond. B Biol. Sci.* 353, 2077–2151. doi: 10.1098/rstb.1998.0353
- Livezey, B. C. (2009). Phylogenetics of modern shorebirds (Charadriiformes) based on phenotypic evidence: characterization. *Bull. Carnegie Mus. Nat. Hist.* 40, 1–95. doi: 10.2992/013.040.0101
- Livezey, B. C. (2010). Phylogenetics of modern shorebirds (Charadriiformes) based on phenotypic evidence: analysis and discussion. *Zool. J. Linn. Soc.* 160, 567–618. doi: 10.1111/j.1096-3642.2010.00635.x
- Livezey, B. C., and Zusi, R. L. (2006). Higher-order phylogeny of modern birds (Theropoda, Aves: Neornithes) based on comparative anatomy (I. Methods and characters). *Bull. Carnegie Mus. Nat. Hist.* 37, 1–544. doi: 10.1111/j.1096-3642.2006.00293.x
- Livezey, B. C., and Zusi, R. L. (2007). Higher-order phylogeny of modern birds (Theropoda, Aves: Neornithes) based on comparative anatomy (II. Analysis and discussion). *Zool. J. Linn. Soc.* 149:1.
- Mayr, G. (2000a). A remarkable new 'gruiform' bird from the Middle Eocene of Messel (Hessen, Germany). *Paläontol. Z.* 74, 187–194. doi: 10.1007/BF02987960
- Mayr, G. (2000b). Charadriiform birds from the early Oligocene of Cereste (France) and the middle Eocene of Messel (Hessen, Germany). *Geobios* 33, 625–636. doi: 10.1016/s0016-6995(00)80034-0
- Mayr, G. (2002). A new specimen of *Salmila robusta* (Aves: Gruiformes: Salmilidae n. fam.) from the Middle Eocene of Messel. *Paläontol. Z.* 76, 305–316. doi: 10.1007/BF02989866
- Mayr, G. (2004). The phylogenetic relationships of the early Tertiary Primoscenidae and Sylphornithidae and the sister taxon of crown group piciform birds. *J. Ornithol.* 145, 188–198.
- Mayr, G. (2008). Avian higher-level phylogeny: well-supported clades and what we can learn from a phylogenetic analysis of 2954 morphological characters. *J. Zool. Syst. Evol. Res.* 46, 63–72.
- Mayr, G. (2009). *Paleogene Fossil Birds*. Berlin: Springer.
- Mayr, G. (2011a). On the osteology and phylogenetic affinities of *Morsoravis sedilis* (Aves) from the early Eocene Fur Formation of Denmark. *Bull. Geol. Soc. Denmark.* 59, 23–35.
- Mayr, G. (2011b). The phylogeny of charadriiform birds (shorebirds and allies) – reassessing the conflict between morphology and molecules. *Zool. J. Linn. Soc.* 161, 916–934. doi: 10.1111/j.1096-3642.2010.00654.x
- Mayr, G. (2013). Parvigruidae (Aves, core Gruiformes) from the early Oligocene of Belgium. *Paleodivers. Paleoenviron.* 93, 77–89. doi: 10.1007/s12549-012-0083-7
- Mayr, G. (2016). The world's smallest owl, the earliest unambiguous charadriiform bird, and other avian remains from the early Eocene Nanjemoy Formation of Virginia (USA). *Paläontol. Z.* 90, 747–763. doi: 10.1007/s12542-016-0330-8
- Mayr, G. (2017). *Avian Evolution: The Fossil Record of Birds and Its Paleobiological Significance*. West Sussex: John Wiley and Sons Ltd.
- Mayr, G., and Clarke, J. A. (2003). The deep divergences of neornithine birds: a phylogenetic analysis of morphological characters. *Cladistics* 19, 527–553. doi: 10.1111/j.1096-0031.2003.tb00387.x
- Musser, G., Ksepka, D. T., and Field, D. J. (2019). New material of paleocene-eocene *Pellornis* (Aves: Gruiformes) clarifies the pattern and timing of the extant gruiform radiation. *Diversity* 11:102. doi: 10.3390/d11070102

- Musser, G. M., and Cracraft, J. (2019). A new morphological dataset reveals a novel relationship for the adzebills of New Zealand (*Aptornis*) and provides a foundation for total evidence neoavian phylogenetics. *Am. Mus. Novit.* 2019, 1–70. doi: 10.1206/3927.1
- Nesbitt, S. J., and Clarke, J. A. (2016). The anatomy and taxonomy of the exquisitely preserved green river formation (Early Eocene) Lithornithids (Aves) and the relationships of lithornithidae. *Bull. Am. Mus. Nat. Hist.* 2016, 1–91. doi: 10.1206/0003-0090-406.1.1
- O'Leary, M. A., and Kaufman, S. G. (2012). *MorphoBank 3.0: Web Application for Morphological Phylogenetics and Taxonomy*. Available online at: <https://morphobank.org> (accessed March 12, 2019).
- Olson, S. L. (1976). A jacana from the Pliocene of Florida (Aves: Jacanidae). *Proc. Biol. Soc. Wash.* 89, 259–264.
- Olson, S. L., and Matsuoka, H. (2005). New specimens of the early Eocene frigatebird *Limnofregata* (Pelecaniformes: Fregatidae), with the description of a new species. *Zootaxa* 1046, 1–15. doi: 10.11646/zootaxa.1046.1.1
- Paton, T. A., Baker, A. J., Groth, J. G., and Barrowclough, G. F. (2003). RAG-1 sequences resolve phylogenetic relationships within charadriiform birds. *Mol. Phylogenet. Evol.* 29:2. doi: 10.1016/S1055-7903(03)00098-8
- Paton, T. A., Haddrath, O., and Baker, A. J. (2002). Complete mitochondrial DNA genome sequences show that modern birds are not descended from transitional shorebirds. *Proc. Biol. Sci.* 269, 839–846. doi: 10.1098/rspb.2002.1961
- Pedersen, G. K., and Surlyk, F. (1983). The Fur Formation, a late Paleocene ash-bearing diatomite from northern Denmark. *Bull. Geol. Soc. Denmark* 32, 43–65.
- Pereira, S. L., and Baker, A. J. (2006). A mitogenomic timescale for birds detects variable phylogenetic rates of molecular evolution and refutes the standard molecular clock. *Mol. Biol. Evol.* 23:9. doi: 10.1093/molbev/msl038
- Prum, R. O., Berv, J. S., Dornburg, A., Field, D. J., Townsend, J. P., Lemmon, E. M., et al. (2015). A comprehensive phylogeny of birds (Aves) using targeted next-generation DNA sequencing. *Nature* 526, 569–573. doi: 10.1038/nature15697
- Pycraft, W. P. (1900). On the morphology and phylogeny of the Palaeognathae (Ratitae and Crypturi) and Neognathae (Carinatae). *Trans. Zool. Soc. Lond.* 15, 149–290. doi: 10.1111/j.1096-3642.1900.tb00023.x
- Rasmussen, D. T., Olson, S. L., and Simons, E. L. (1987). *Fossil Birds from the Oligocene Jebel Qatrani Formation, Fayum Province, Egypt*. Washington, DC: Smithsonian Institution, 7–8.
- Reddy, S., Kimball, R. T., Pandey, A., Hosner, P. A., Braun, M. J., Hackett, S. J., et al. (2017). Why do phylogenomic data sets yield conflicting trees? Data type influences the avian tree of life more than taxon sampling. *Syst. Biol.* 66:5. doi: 10.1093/sysbio/syx041
- Shoshoni Language Project (2018). *Shoshoni Dictionary*. Available online at: <https://shoshoniproject.utah.edu/language-materials/shoshoni-dictionary/dictionary.php> (accessed August 6, 2020).
- Sibley, C. G., Ahlquist, J. E., and Monroe, B. L. Jr. (1988). A classification of the living birds of the world based on DNA–DNA hybridization studies. *Auk* 105, 409–423. doi: 10.1093/auk/105.3.409
- Smith, M. E., Chamberlain, K. R., Singer, B. S., and Carroll, A. R. (2010). Eocene clocks agree: coeval 40Ar/39Ar, U–Pb, and astronomical ages from the Green River Formation. *J. Geol.* 38:6. doi: 10.1130/G30630.1
- Smith, N. A. (2011). *Systematics and Evolution of Extinct and Extant Pan-Alcidae (Aves, Charadriiformes): Combined Phylogenetic Analyses, Divergence Estimation, and Paleoclimatic Interactions*. Ph. D. Dissertation, The University of Texas at Austin, Austin, TX.
- Smith, N. A. (2013). A new species of Threskiornithidae-like bird (Aves, Ciconiiformes) from the Green river formation (Eocene) of Wyoming. *J. Vertebr. Paleontol.* 33:2. doi: 10.1080/02724634.2012.722898
- Smith, N. A. (2015). Sixteen vetted fossil calibrations for divergence dating of Charadriiformes (Aves, Neognathae). *Palaeontol. Electron.* 18.1.4FC, 1–18. doi: 10.26879/410
- Smith, N. A., and Clarke, J. A. (2015). Systematics and evolution of the Pan-Alcidae (Aves, Charadriiformes). *J. Avian Biol.* 45, 001–016. doi: 10.1111/jav.00487
- Storer, R. W. (1971). “Adaptive radiation of birds,” in *Avian Biology*, Vol. 1, eds D. S. Farner and J. R. King (New York: Academic Press), 149–188.
- Strauch, J. G. (1978). The phylogeny of the Charadriiformes (Aves): a new estimate using the method of character compatibility analysis. *Trans. Zool. Soc. Lond.* 34, 263–345. doi: 10.1111/j.1096-3642.1978.tb00375.x
- Swofford, D. L. (2002). *PAUP* Phylogenetic Analysis Using Parsimony (* and Other Methods)*. Version 4.0a164 (X86). Sunderland, MA: Sinauer Associates.
- Thomas, A. L. R. (1993). On the aerodynamics of birds' tails. *Philos. Trans. R. Soc. B* 340:1294. doi: 10.1098/rstb.1993.0079
- Thomas, A. L. R., and Balmford, A. (1995). How natural selection shapes birds' tails. *Am. Nat.* 146:6. doi: 10.1086/285828
- van Tuinen, M., and Hedges, S. B. (2001). Calibration of avian molecular clocks. *Mol. Biol. Evol.* 18:2. doi: 10.1093/oxfordjournals.molbev.a003794
- Wang, M., Mayr, G., Zhang, J., and Zhou, Z. (2012). Two new skeletons of the enigmatic, rail-like avian taxon *Songzia* Hou, 1990 (Songziidae) from the early Eocene of China. *Alcheringa Aust. J. Paleontol.* 36:4. doi: 10.1080/03115518.2012.673302
- Weidig, I. (2010). New birds from the lower eocene green river formation, North America,” in Proceedings of the VII International meeting of the society of avian paleontology and evolution, eds W. E. Boles, T. H. Worthy. *Rec. Aust. Mus.* 62:1. doi: 10.3853/j.0067-1975.62.2010.1544
- Zeffer, A., Christoffer, J. L., and Marmebro, A. (2003). Functional correlation between habitat use and leg morphology in birds (Aves). *Biol. J. Linn. Soc.* 79, 461–484. doi: 10.1046/j.1095-8312.2003.00200.x
- Zusi, R. L. (1984). A functional and evolutionary analysis of rhynchokinesis in birds. *Smithson. Contrib. Zool.* 395, 1–40. doi: 10.5479/si.00810282.395

Conflict of Interest: The authors declare that the research was conducted in the absence of any commercial or financial relationships that could be construed as a potential conflict of interest.

The handling editor declared a past co-authorship with the authors.

Copyright © 2020 Musser and Clarke. This is an open-access article distributed under the terms of the Creative Commons Attribution License (CC BY). The use, distribution or reproduction in other forums is permitted, provided the original author(s) and the copyright owner(s) are credited and that the original publication in this journal is cited, in accordance with accepted academic practice. No use, distribution or reproduction is permitted which does not comply with these terms.



Erratum: An Exceptionally Preserved Specimen From the Green River Formation Elucidates Complex Phenotypic Evolution in Gruiformes and Charadriiformes

OPEN ACCESS

Approved by:

Frontiers Editorial Office,
Frontiers Media SA, Switzerland

*Correspondence:

Frontiers Production Office
production.office@frontiersin.org

Specialty section:

This article was submitted to
Paleontology,
a section of the journal
Frontiers in Ecology and Evolution

Received: 20 November 2020

Accepted: 20 November 2020

Published: 10 December 2020

Citation:

Frontiers Production Office (2020)
Erratum: An Exceptionally Preserved
Specimen From the Green River
Formation Elucidates Complex
Phenotypic Evolution in Gruiformes
and Charadriiformes.
Front. Ecol. Evol. 8:631591.
doi: 10.3389/fevo.2020.631591

Frontiers Production Office*

Frontiers Media SA, Lausanne, Switzerland

Keywords: avian phylogeny, Neoaves, Eocene, feathers, fossil, divergence time estimation, morphology

An Erratum on

An Exceptionally Preserved Specimen From the Green River Formation Elucidates Complex Phenotypic Evolution in Gruiformes and Charadriiformes

by Musser, G., and Clarke, J. A. (2020). *Front. Ecol. Evol.* 8:559929. doi: 10.3389/fevo.2020.559929

Due to a production error, the following accession numbers were omitted in error:

Zoobank Identifier: urn:lsid:zoobank.org:pub:57238342-B0D2-4764-8F6C-79205EB14F1A

Genus: urn:lsid:zoobank.org:act:8B1CD8D4-6C0F-4535-B1B2-C87286D6234B

Species: urn:lsid:zoobank.org:act:7E917BC1-DCC7-4046-B7FE-14A9537E2F06.

The publisher apologizes for this mistake. The original article has been updated.

Copyright © 2020 Frontiers Production Office. This is an open-access article distributed under the terms of the Creative Commons Attribution License (CC BY). The use, distribution or reproduction in other forums is permitted, provided the original author(s) and the copyright owner(s) are credited and that the original publication in this journal is cited, in accordance with accepted academic practice. No use, distribution or reproduction is permitted which does not comply with these terms.



Multiple Functional Solutions During Flightless to Flight-Capable Transitions

Ashley M. Heers*, Stephanie L. Varghese, Leila K. Hatier and Jeremiah J. Cabrera

Department of Biological Sciences, California State University Los Angeles, Los Angeles, CA, United States

OPEN ACCESS

Edited by:

Corwin Sullivan,
University of Alberta, Canada

Reviewed by:

Zhiheng Li,
Chinese Academy of Sciences, China
Elizabeth Anne Freedman Fowler,
Dickinson State University,
United States

*Correspondence:

Ashley M. Heers
ashmheers@gmail.com

Specialty section:

This article was submitted to
Paleontology,
a section of the journal
Frontiers in Ecology and Evolution

Received: 17 June 2020

Accepted: 16 November 2020

Published: 10 February 2021

Citation:

Heers AM, Varghese SL, Hatier LK
and Cabrera JJ (2021) Multiple
Functional Solutions During Flightless
to Flight-Capable Transitions.
Front. Ecol. Evol. 8:573411.
doi: 10.3389/fevo.2020.573411

The evolution of avian flight is one of the great transformations in vertebrate history, marked by striking anatomical changes that presumably help meet the demands of aerial locomotion. These changes did not occur simultaneously, and are challenging to decipher. Although extinct theropods are most often compared to adult birds, studies show that developing birds can uniquely address certain challenges and provide powerful insights into the evolution of avian flight: unlike adults, immature birds have rudimentary, somewhat “dinosaur-like” flight apparatuses and can reveal relationships between form, function, performance, and behavior during flightless to flight-capable transitions. Here, we focus on the musculoskeletal apparatus and use CT scans coupled with a three-dimensional musculoskeletal modeling approach to analyze how ontogenetic changes in skeletal anatomy influence muscle size, leverage, orientation, and corresponding function during the development of flight in a precocial ground bird (*Alectoris chukar*). Our results demonstrate that immature and adult birds use different functional solutions to execute similar locomotor behaviors: in spite of dramatic changes in skeletal morphology, muscle paths and subsequent functions are largely maintained through ontogeny, because shifts in one bone are offset by changes in others. These findings help provide a viable mechanism for how extinct winged theropods with rudimentary pectoral skeletons might have achieved bird-like behaviors before acquiring fully bird-like anatomies. These findings also emphasize the importance of a holistic, whole-body perspective, and the need for extant validation of extinct behaviors and performance. As empirical studies on locomotor ontogeny accumulate, it is becoming apparent that traditional, isolated interpretations of skeletal anatomy mask the reality that integrated whole systems function in frequently unexpected yet effective ways. Collaborative and integrative efforts that address this challenge will surely strengthen our exploration of life and its evolutionary history.

Keywords: flight, locomotion, ontogeny, evolution, bird, avian, theropod, musculoskeletal modeling

INTRODUCTION

Locomotion is an integral element in the lives of most vertebrates, and reconstructing locomotor behaviors in fossil taxa is crucial for understanding many evolutionary transitions. Form-function relationships in extant organisms are key to deciphering anatomical features in extinct organisms and fundamental to this process. For example, attributes such as posture, muscle morphology,

and potential joint movements and corresponding locomotor behaviors can be inferred, to varying degrees, based on physical principles and relationships derived from extant homologs or analogs (Hutchinson and Garcia, 2002; Jasinowski et al., 2006; Pierce et al., 2012; Brassey et al., 2017; Otero et al., 2017). However, most fossils lack a living counterpart with an identical suite of morphological features, and are often characterized by mosaics of ancestral and derived anatomical structures. Assessing locomotor capacity in light of these differences is challenging. Although techniques such as musculoskeletal modeling can account for anatomical differences, all methods of inferring functional attributes of extinct organisms must be validated—for example, by constructing models of extant organisms to establish that inferred characteristics, like muscle function or locomotor capacity, match known values (Hutchinson, 2011). Understanding the functional implications of evolutionary transformations therefore requires a thorough exploration of form-function relationships in extant organisms.

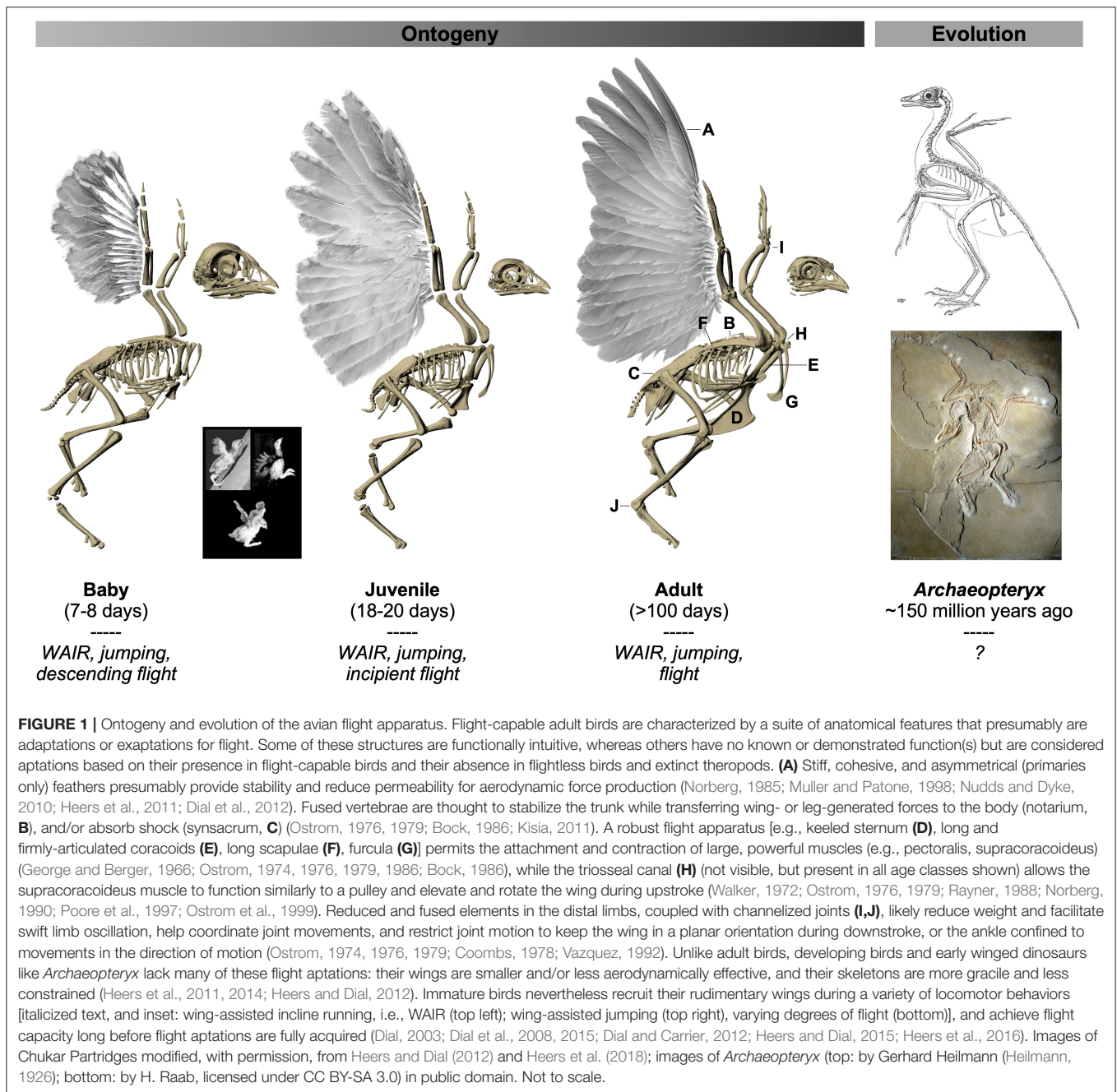
One of evolution's great and puzzling transformations is the acquisition of flight in the theropod-avian lineage. Flight is the most power-demanding mode of locomotion (Alexander, 2002), and its evolution has culminated in a suite of specializations that presumably are adaptations or exaptations (Gould and Vrba, 1982) for meeting aerial challenges. The most conspicuous of these specializations—large wings with asymmetrical primary feathers and a robust pectoral skeleton anchoring large flight muscles—are generally present in volant birds and absent in flightless ones, and have long been viewed as hallmarks of flight capacity. However, these hallmarks did not evolve simultaneously. Feathers appeared very early in the theropod lineage, initially as down-like filaments (Coelurosauria or earlier) that were later complemented by pennaceous feathers arranged as “protowings” on the distal forelimb (Pennaraptora). Larger and more bird-like “wings” appeared among paravians, and fully modern feathers were probably present in ornithurines (Norell and Xu, 2005; Foth et al., 2014; Godefroit et al., 2014; Lefèvre et al., 2020; Rauhut and Foth, 2020; Xu, 2020). In contrast to this early (albeit complex) emergence of feathers, changes in the skeletal apparatus occurred much later. For example, *Microaptor*, *Archaeopteryx*, and many other paravians and early avialans had relatively bird-like wings yet lacked the robust pectoral apparatus and specialized forelimb of extant volant birds (Ostrom, 1976; Xu et al., 2003; Wellnhofer, 2009; Zheng et al., 2014; Mayr, 2017) (but see Nudds and Dyke, 2010; Longrich et al., 2012; Nudds, 2014, for discussion of feather morphology). Theropod fossils thus reveal that bird-like wings appeared before bird-like skeletons (Decicchi et al., 2016), and deciphering the functional attributes of these unique, “transitional” fossils is extremely challenging.

Although extinct theropods like *Archaeopteryx* have most often been compared to extant flight-capable or flightless adult birds, a growing number of studies demonstrate that developing birds can uniquely address certain challenges and provide powerful insights into the evolution of avian flight (Dial, 2003; Heers and Dial, 2012; Heers et al., 2014, 2016). Unlike adult birds, immature birds have rudimentary, somewhat “dinosaur-like” wings coupled with less developed pectoral girdles, and rely on unique pre-flight behaviors that bridge the transition from

leg-based terrestrial locomotion to wing-based aerial locomotion (Figure 1). For example, developing birds recruit their growing wings to flap-run up inclines [wing-assisted incline running, i.e., WAIR (Dial, 2003)], improve jumping performance (Heers and Dial, 2015), slow aerial descents (Dial et al., 2008), and/or swim to safety (Dial and Carrier, 2012). Though the skeletons of these immature birds are not identical to those of extinct theropods, many of the skeletal features that changed during the evolution of flight change in similar fashion during the development of flight. For instance, preliminary observations suggest that in both cases, elements of the pectoral girdle (sternum, coracoid, scapula, furcula) increase in relative size and/or change orientation, while the humerus acquires a more complex shape due to enlargement of muscle attachment sites and deflection of the humeral head (Ostrom et al., 1999; Heers and Dial, 2012; Mayr, 2017; Rauhut et al., 2019; Serrano et al., 2020). Such changes might be expected to influence locomotion by affecting muscle size, leverage (moment arm length), and orientation (Hutchinson and Garcia, 2002; Hutchinson et al., 2005; Jasinowski et al., 2006; Brassey et al., 2017; Otero et al., 2017), as well as flapping kinematics and range of motion (Jenkins, 1993; Pierce et al., 2012). By examining how skeletal ontogeny relates to muscle function and wing movement in developing birds, we may therefore gain insight into the functional implications of similar skeletal changes that occurred during the evolution of flight. In short, developing birds can uniquely contribute to our understanding of avian evolution by revealing relationships between form, function, performance, and behavior during flightless to flight-capable transitions.

Previous work on form-function relationships has tended to focus on anatomical structures in isolation [e.g., wings (Burgers and Chiappe, 1999; Nudds and Dyke, 2010), tails (Gatesy and Dial, 1996), muscles (Poore et al., 1997), joints (Jenkins, 1993)], and often from a static, two-dimensional perspective. Such studies have provided valuable information and a strong foundation for further analyses. However, locomotion is a highly dynamic, three-dimensional behavior that involves the entire body. In order to build upon previous work and gain more quantitative insight into the functional implications of skeletal evolution, techniques that provide a more dynamic, holistic, and three-dimensional perspective are required.

Here, we use CT scans coupled with a three-dimensional musculoskeletal modeling approach to analyze how ontogenetic changes in skeletal anatomy—the pectoral girdle and humerus—influence muscle size, leverage, orientation, and locomotor function during the development of flight in a precocial ground bird, the Chukar Partridge (*Alectoris chukar*). Chukars are a well-studied model system for exploring locomotor ontogeny. At hatching, chicks have somewhat “dinosaur-like” anatomy and are entirely dependent on leg-based locomotion, but within a few days they begin to recruit their wings to jump and to flap-run up inclines (WAIR), then control their descent back down (Figure 1). As their anatomy becomes more bird-like and wing performance improves, chukars are able to flap-run up steeper slopes, jump higher, and eventually fly (Dial, 2003; Dial et al., 2006, 2008; Tobalske and Dial, 2007; Heers et al., 2011, 2016; Heers and Dial, 2012, 2015). This study focuses on three age classes (7–8 days, herein “baby”: wings used for WAIR, jumping, and descending flight; 18–20 days, herein “juvenile”:



wings used for WAIR, jumping, and incipient flight; >100 days, herein “adult”: wings used for WAIR, jumping, and flight) and builds upon previous work to quantitatively explore relationships between skeletal anatomy and muscle morphology and function during flightless to flight-capable transitions.

MATERIALS AND METHODS

Skeletal Reconstructions, Scaling, and Alignment

We imported image slices from previously collected CT scans of baby, juvenile, and adult chukars (1 bird per age class)

(Heers et al., 2016, 2018) into Mimics software (Materialise, Inc.; Leuven, Belgium) and used density thresholds to isolate skeletal elements of the pectoral apparatus and forelimb. The sternum, coracoids, scapulae, furcula, and humeri for each bird were then exported as STL files and imported into 3-matic (Materialise, Inc.; Leuven, Belgium) for analysis. Because birds varied substantially in size (34.6 g baby → 500 g adult) and were scanned in different positions, we scaled and aligned each specimen prior to analysis. Immature (baby and juvenile) birds were scaled to adult size by using the “Measure Distance” tool in 3-matic to measure the length of the notarium (i.e., summed length of the bodies of the thoracic vertebrae that fuse into the notarium)

and calculate scale factors, which were checked by overlaying the notaria of the scaled baby and juvenile specimens and confirming that their scaled sizes matched that of the adult. We chose to scale by notarium length partially because the vertebral body components are completely ossified in immature birds (and thus completely visible in CT data), and partially because notarium length provides a proxy for body size that is independent of limb size. Following scaling, the pectoral girdle of each specimen was oriented with the notarium in a horizontal plane and the keel in a vertical plane. Humeri were oriented with the shaft and the deltopectoral crest in a horizontal plane.

Bone Measurements

Following scaling and alignment, we used 3-matic coupled with measurements of freshly dissected and/or cleared and stained specimens to quantify relative changes in bone size, orientation, and complexity. Staining methods for visualizing cartilage in CT (Gignac et al., 2016) were not an option at the time scans were taken, but may simplify future work following this workflow. Where applicable, measurements of the left and right side were averaged for ontogenetic comparisons. Sketches of different measurements are included with graphs (see Results).

Bone Size

- **Sternum.** Because the keel of immature birds is largely cartilaginous, we used freshly dissected specimens of the same age class (one 7–8 day bird, one 18–20 day bird) to help quantify changes in keel size. The sterna of the dissected specimens were photographed in lateral view and then scaled to the size of the baby or juvenile skeletal model by aligning the ossified portions of the keel, coracoid, and furcula with those in the skeletal model (ossified and cartilaginous components are visually distinguishable during dissection). The “scaled” photographs of the baby and juvenile bird, along with a lateral view of the adult bird exported from 3-matic, were then imported into ImageJ (National Institutes of Health, Bethesda, MD, USA) and the area of the keel was outlined and measured. Note that for other bones (below) we used cleared and stained specimens rather than freshly dissected specimens, partially because cartilage and bone are more distinguishable and partially because cartilage rapidly shrinks following dissection and thus must be photographed immediately. However, we found that the most accurate way to scale the keels of additional specimens to those of the skeletal models was to scale and align based on the entire pectoral girdle rather than the keel alone, since the keel increases in size more rapidly than other bones (i.e., since a slightly older bird may have a similar coracoid and scapula but a larger keel). Visualizing the entire pectoral girdle simultaneously was not possible with cleared and stained specimens because they collapsed on themselves when we attempted to photograph the pectoral girdle in lateral view.

For the remaining bones of the flight apparatus, we measured their lengths in 3-matic and then adjusted the measurements to account for cartilage in immature birds, using cleared and stained specimens (one 7–8 day bird, one 18–20 day bird).

To confirm the validity of our cartilage adjustments, we also used X-ray Reconstruction of Moving Morphology (“XROMM”; xromm.org) to measure distances between joints during *in vivo* flapping kinematics. Previous work had aligned skeletal models (like those here) with x-ray videos of flapping birds to determine *in vivo* flapping postures (Heers et al., 2016). Cartilage was not visible in the skeletal models or the x-rays, but by estimating the positions of the shoulder and elbow joints as halfway between the humerus and glenoid (shoulder joint) or humerus and radius/ulna (elbow joint), we were able to measure the distance between these two joints as a proxy for humerus length. These measurements were nearly identical to those measured and adjusted in 3-matic (below).

- **Coracoids.** For each specimen, the left and right coracoids were fit with a cylinder using the “Analytical Cylinder” tool, and the length of the cylinder was measured. To account for cartilaginous components that were not visible in the baby and juvenile skeletal models, we additionally photographed the coracoid of a cleared and stained specimen for each age class, imported the photograph into ImageJ, measured the total length as well as the ossified length, and used this to adjust our measurements in 3-matic:

$$\text{total length}_{3m} = \text{ossified length}_{3m} \times \frac{\text{total length}_{cs}}{\text{ossified length}_{cs}} \quad (1)$$

where $3m$ refers to lengths of skeletal models measured in 3-matic and cs refers to lengths measured for cleared and stained specimens in ImageJ.

- **Furcula.** The furcula appeared to be nearly completely ossified and was only measured in 3-matic. We used the “Measure Distance” tool to measure the distance between the ventral extreme of the hypocleidum and the left and right proximal extremes adjacent to the coracoid, and defined the average of these distances as the length of the furcula.
- **Scapulae.** The lengths of the left and right scapulae were measured in 3-matic using the same “Measure Distance” tool to quantify the straight-line distance between the cranial end (coracoid process of Ghetie et al., 1976) and the caudal tip of the scapula. As with the coracoid, we accounted for cartilage by photographing the scapula of a cleared and stained specimen for both immature age classes, measuring total vs. ossified lengths in ImageJ, and using those measurements to calculate the true lengths of the scapulae (Equation 1).
- **Humeri.** To measure the lengths of the left and right humeri, we created two parallel, vertical planes, aligned one plane with the proximal end (humeral head) and one with the distal end [ventral or “ulnaris” condyle (Ghetie et al., 1976; Baumel and Witmer, 1993)] of each humerus, and measured the distance between the two planes (same tool as above). Cartilage was accounted for as described above (Equation 1).
- **Deltopectoral crest of humerus (DPC).** The length of the DPC was quantified as a percentage of humeral length, by measuring the distance between the humeral head and the distal end of the DPC, and dividing this measurement by the distance between the humeral head and the distal end of the humerus [ventral or “ulnaris” condyle (Ghetie et al., 1976;

Baumel and Witmer, 1993)]. Both measurements were taken parallel to the shaft of the humerus. For immature birds, we used photographs of the cleared and stained specimens and took measurements in ImageJ; for the adult bird we used 3-matic. Cleared and stained measurements were very similar to measurements made in 3-matic using *in vivo* postures derived from XROMM (Heers et al., 2016), as described above for the humerus.

- **Total forelimb length.** To measure total forelimb length, we imported the remainder of the forelimb (radius, ulna, manus) into 3-matic and positioned each bone in mid-downstroke posture, as recorded during *in vivo* flapping using XROMM (Heers et al., 2016). Because XROMM involves matching bone models with bone x-rays, these *in vivo* positions correctly position the ossified portions of each bone, such that the gaps between bones represent missing cartilage. To measure total forelimb length, we therefore used the *in vivo* positions to measure the distances between the shoulder and elbow joints, elbow and wrist joints, and wrist joint and tip of the manus (completely ossified), by creating two planes for each set of joints (one plane at each joint, perpendicular to bones in question) and measuring the distance between them. The sum of these distances was defined as the total forelimb length. Total forelimb length could also have been measured using cleared and stained specimens to account for missing cartilage, but this would have involved more measurements (i.e., 3-matic plus cleared and stained adjustments with Equation 1) and thus more potential for error.

Bone Orientation

With the exception of the glenoid, bone orientations were quantified solely in 3-matic.

- **Coracoid angle.** We define “coracoid angle” as the obtuse angle between a horizontal plane and the shaft of the coracoid. As described above, we used the “Analytical Cylinder” tool to fit cylinders to the left and right coracoids, and then measured the angle between each cylinder and a horizontal plane, using the “Measure Angle” tool.
- **Scapulocoracoid angle.** The scapulocoracoid angle is the angle between the scapula and coracoid. We used the coracoid cylinders described above to represent each coracoid. For each scapula, we first fitted an arc (“Create Arc” tool) to the ventral edge of the bone, and then fit a cylinder to the portion of the arc that intersected the cylinder of the coracoid. Finally, we measured the angle between the coracoid cylinder and the scapula cylinder to determine the scapulocoracoid angle.
- **Furculocoracoid angle.** We define “furculocoracoid angle” as the angle between the furcula and the coracoids. Again, we used the coracoid cylinders described above to represent each coracoid. We used a plane to quantify the orientation of the furcula (“Datum Plane” tool with 3 points: cranial surface of intersection between left and right clavicles and hypocleidum + cranial surfaces of clavicles at articulations with the coracoids). We then used the “Measure Angle” tool to quantify the angle between the plane of the furcula and each

coracoid cylinder, and took the average of these measurements as the furculocoracoid angle.

- **Glenoid.** The glenoid is partially cartilaginous, especially in immature birds. To quantify the orientation of this structure, we therefore photographed the shoulder joint in dissected specimens in lateral view, as described for the sternum in section *Bone Size* above (glenoid difficult to photograph in cleared and stained specimens). Photographs were aligned to skeletal models (i.e., with the vertebral column horizontal), then measured. For each bird we took two measurements with respect to a horizontal plane: the angle made by a line connecting the dorsal surfaces of the labra of the scapula and coracoid, and the angle made by a line connecting the ventral surfaces of the labra of the scapula and coracoid. These two measurements were averaged for each bird. We did not notice any other obvious, evolutionarily-relevant differences (i.e., whether glenoid was directed more vertically in older birds).

Bone Complexity

The humerus becomes more complex through avian ontogeny and evolution. To capture some of this complexity, we quantified three conspicuous morphological features, in 3-matic.

- **Deflection of humeral head.** We measured the deflection of the humeral head away from the humeral shaft in ventral view, because the deltopectoral crest makes measurements in dorsal view more challenging. For the left and right humeri of each bird, a vertical plane was created, aligned with the shaft of the humerus, and positioned at the intersection between the midline (long axis) of the shaft and the distal end of the deltopectoral crest. This plane was then duplicated, and rotated until it intersected the center of the humeral head. We measured the angle between these two planes (“Measure Angle” tool) to quantify deflection of the humeral head.
- **Depth of deltopectoral crest (DPC).** Although the DPC is partially cartilaginous in immature birds, dissected and cleared and stained specimens show that the pectoralis and supracoracoideus insert mainly on the ossified portions of this structure. We therefore measured the maximal depth of the ossified DPC in 3-matic. This is an underestimate of the size in immature birds, but functionally more relevant. To measure the depth of the DPC on left and right humeri, we created a vertical plane on the cranial surface of the proximal humerus (“Datum Plane” tool), duplicated the plane, aligned the duplicate to the edge of the DPC at its maximal width, and measured the distance between the two planes.
- **Offset of margo caudalis.** The margo caudalis is a muscle attachment site on the caudal surface of the proximal humerus that grows away from the long axis of the humerus as the bicipital crest expands through ontogeny. To quantify this offset on left and right humeri, we created two horizontal planes: one passing through the dorsal surface of the shaft of the humerus, parallel to the long axis of the bone, and one passing through the margo caudalis. The distance between these planes was defined as the offset or expansion of the margo caudalis.

Muscle Analysis

To explore relationships between skeletal and muscular development, we used previously collected data and musculoskeletal models (Heers and Dial, 2015; Heers et al., 2016, 2018) to document ontogenetic changes in muscle mass, as well as the leverage (moment arm length) and orientation or “pull” of shoulder muscles during wing-assisted incline running (WAIR). All of these studies used the same age classes (7–8 day baby, 18–20 day juvenile, >100 day adult) and, as much as possible, the same specimens.

Muscle Mass

Muscle masses were obtained by dissecting birds (three birds per age class). For full details, see (Heers and Dial, 2015).

Muscle Leverage (Moment Arm Length)

The length of a moment arm is defined as the perpendicular distance between a muscle’s line of action and the joint it acts upon. Moment arms determine how muscle force is transformed into limb motion: a muscle’s effect is the product of its force multiplied by its moment arm. Thus, the longer the moment arm, the greater the muscle leverage. We analyzed moment arms that were previously calculated using musculoskeletal models (made in SIMM, i.e., Software for Interactive Musculoskeletal Modeling; Musculographics, Inc, CA; <http://www.musculographics.com/>) and simulations [done in OpenSim; <https://opensim.stanford.edu/> (Delp et al., 2007)] of WAIR. For full details, see (Heers et al., 2018).

Muscle Orientation (Direction of Pull)

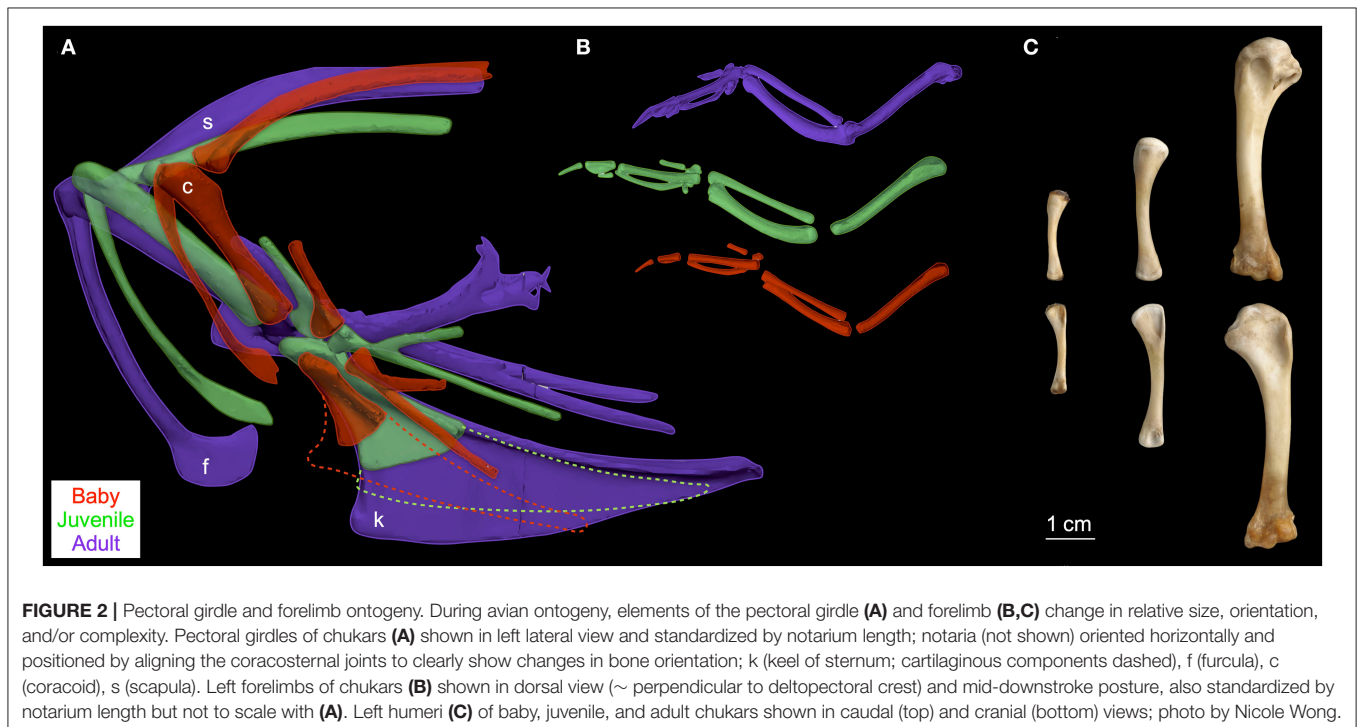
Although each muscle has one moment arm per joint, this three-dimensional moment arm can be decomposed into z, y, and x

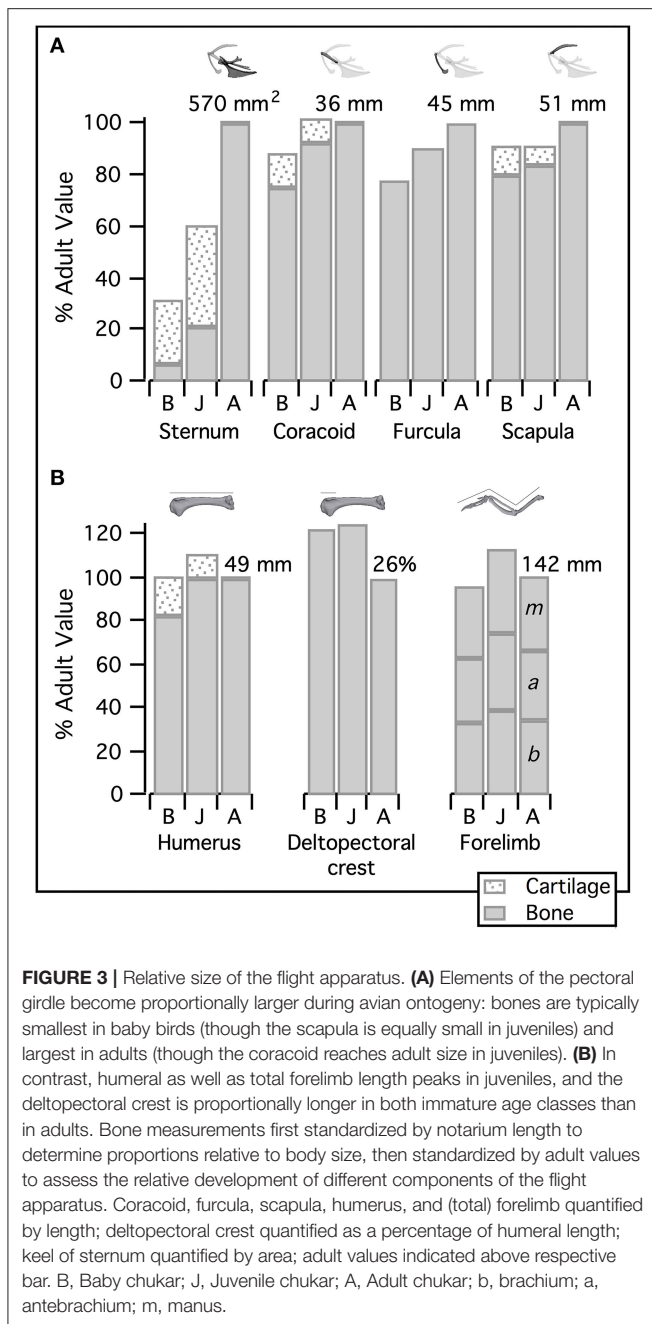
vectors to determine a muscle’s leverage in different directions [i.e., elevation/depression (z) vs. protraction/retraction (y) vs. long axis rotation (x)]. To assess each shoulder muscle’s direction of pull, we calculated the average vector sum of each muscle’s z (elevation/depression) and y (protraction/retraction) moment arms, under three conditions: *in vivo* kinematics during maximal effort WAIR, adult kinematics during WAIR, and a standardized downstroke position (for downstroke muscles) or upstroke position (for upstroke muscles). Ontogenetic differences in muscle pull during *in vivo* kinematics could result from anatomical or kinematic differences, whereas differences during adult and/or standardized kinematics would result solely from anatomical differences.

RESULTS

Bones Change Dramatically in Size, Orientation, and Complexity During Bird Development

Elements of the flight apparatus in 7–8 day old (“baby”), 18–20 day old (“juvenile”), and adult chukars differ substantially in relative size, orientation, and complexity (**Figure 2**). When standardized by notarium length, components of the pectoral girdle (coracoid, scapula, furcula, and especially sternum) increase in size during ontogeny (**Figure 3A**), whereas the humerus and forelimb are proportionally longest in the juvenile bird and the deltopectoral crest is proportionally long in both immature age classes (**Figure 3B**). Bones of the pectoral girdle also change in orientation. During ontogeny, the keel of the sternum shifts $\sim 15^\circ$, from a slightly more vertical orientation to an orientation more parallel to the vertebral column. This





is partially due to a shift in the angle of the sternum and partially due to greater growth in the anterior portion of the keel (Figure 2). The angles between the coracoid and body axis, and coracoid and furcula, increase through ontogeny, while the scapulocoracoid angle decreases and the glenoid becomes more parallel to the vertebral column (Figure 4). Simultaneously, the humerus becomes more complex (Figures 2, 5): muscle attachment sites like the deltopectoral crest become more pronounced, the bicipital crest expands, and the humeral head is deflected away from the shaft and becomes more globular.

Ontogenetic Changes in Skeletal Anatomy Do Not Result in Very Different Flapping Kinematics, at Least During Wing-Assisted Incline Running (WAIR)

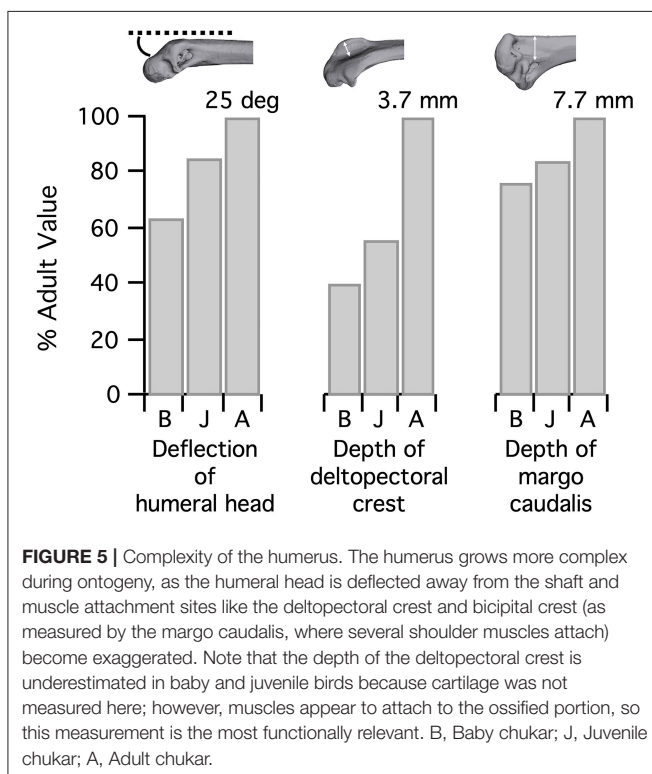
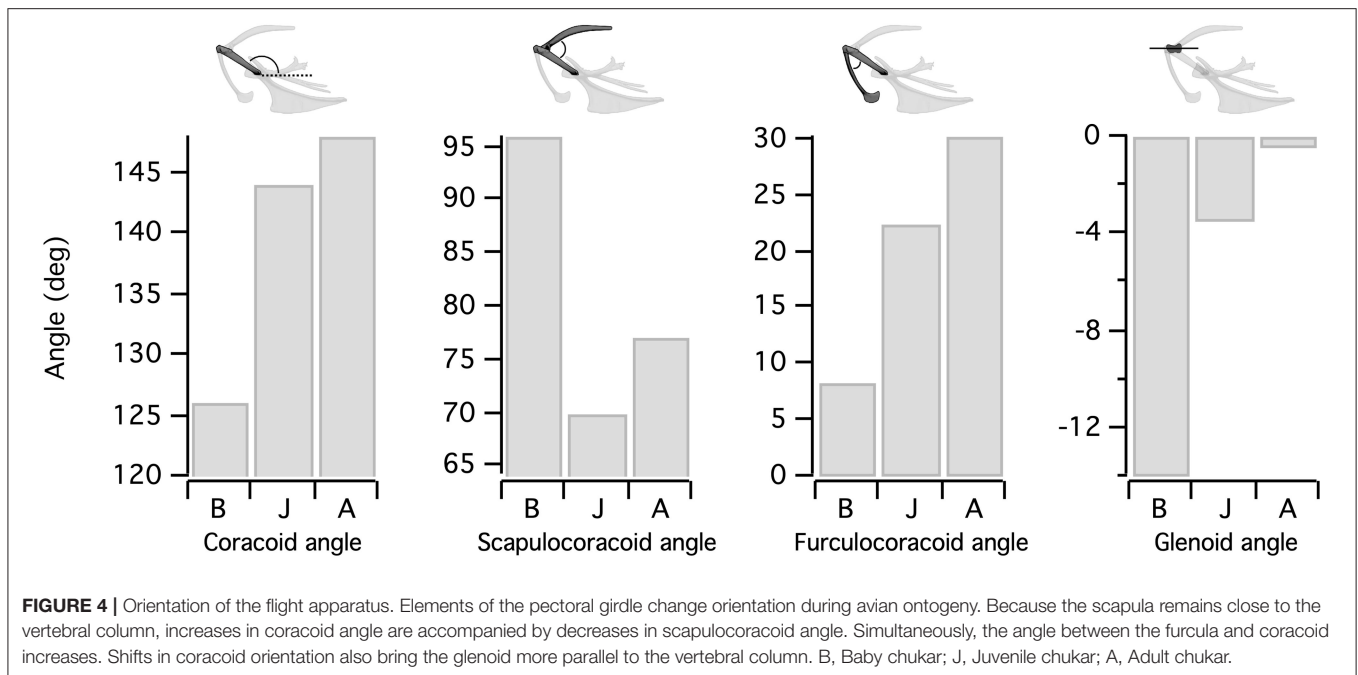
Though differences in skeletal anatomy might be expected to result in different flapping kinematics, due to differing muscle and/or joint morphology, previous work demonstrates that during maximal effort wing-assisted incline running, developing and adult chukars have very similar kinematics (Heers et al., 2016). Differences that do exist may compensate for the underdeveloped flight apparatus of immature birds (below).

Ontogenetic Changes in Skeletal Anatomy Are Associated With Increases in Muscle Mass and Leverage (Moment Arm Length), but Not Necessarily Orientation or Function

Differences in skeletal anatomy might also be expected to influence muscle morphology. Consistent with this expectation, relative muscle mass (% body mass) increases through ontogeny (Figure 6). These increases are most substantial in muscles that originate from the pectoral girdle (e.g., pectoralis, supracoracoideus) and drive shoulder movements (~30% of adult values in baby chukars capable of WAIR, ~60% of adult values in juvenile chukars capable of incipient flight). Relative moment arm lengths—and thus muscle leverage—show a more complicated pattern. When standardized by notarium length, moment arms about the z (elevation-depression) and y (protraction-retraction) axes show a general increase through ontogeny but tend to peak in juveniles (for 6 out of 10 muscles about z axis, 7 about y axis), whereas moment arms for long axis rotation (x) tend to increase through ontogeny and peak in adults (for 6 out of 10 muscles) (Figure 7). The proportionally large z and y moment arms in the juvenile are likely an outcome of its proportionally long forelimbs and deltopectoral crest (Figures 2, 3B), whereas the large x moment arms in the adult probably result from skeletal features like the deflected humeral head, expanded bicipital crest, and wider deltopectoral crest, all of which shift muscle attachment sites away from the long axis of the humerus (Figures 2, 5) (Heers et al., 2018).

In contrast to the substantial changes observed in muscle mass and leverage, average muscle moment arm orientations during flapping are fairly consistent in chukars (i.e., muscles pull in similar directions through ontogeny). Though many shoulder muscles show small changes coincident with shifts in bone orientation and/or complexity (Table 1), moment arm orientations for the two most important flight muscles—the pectoralis and the supracoracoideus—do not appear to shift in conjunction with shifts in bone orientation:

- **Supracoracoideus** (main upstroke muscle; origin on sternum, coracoid, and coracoclavicular membrane; insertion on dorsal surface of deltopectoral crest via triosseal canal). The supracoracoideus appears to pull more dorsally in juveniles than in babies or adults, irrespective of kinematics (Table 1). The proportionally long forelimbs



of juveniles—combined with the proportionally long deltopectoral crest (**Figure 3B**)—presumably enhance elevation. If this interpretation is correct, the more dorsal pull of the supracoracoideus in juveniles results from differences in bone size rather than differences in bone orientation.

The long humerus and deltopectoral crest of juveniles also enhance pectoralis leverage, although not above adult values, potentially due to other changes that enhance pectoralis leverage in adults (below).

- Pectoralis (main downstroke muscle; origin on sternum, ribs, furcula, and sternocoracoclavicular membrane; insertion on ventral surface of deltopectoral crest).** During *in vivo* kinematics for maximal effort WAIR, the pectoralis appears to pull more caudally in immature birds (**Table 1**, column A). However, this difference is largely eliminated when kinematics are standardized (columns B, C), especially during the start of the downstroke when the pectoralis is active (column C). This indicates that differences in moment arm orientation observed during *in vivo* kinematics are due to subtle differences in flapping kinematics rather than anatomy. Kinematic differences do not appear to result from restrictions or differences in joint morphology—immature chukars actually have a greater range of motion than adults (due to their less ossified and more flexible joints) (Heers et al., 2016), and the glenoid is more steeply angled away from the vertebral column (**Figure 4**) indicating that, if anything, the wing would be expected to move more cranially during the downstroke rather than more caudally. Kinematic subtleties also do not appear to optimize muscle leverage for elevation/depression or protraction/retraction, but may improve leverage for long axis rotation, especially in baby birds that have less complex humeri and therefore less leverage for rotation (**Figure 8A**). In addition, kinematic differences may serve to improve aerodynamic performance (**Figure 8B**). Previous work demonstrates that the wings of developing chukars produce proportionally more drag than the wings of adults (Heers et al., 2011). During WAIR, baby chukars adopt a more

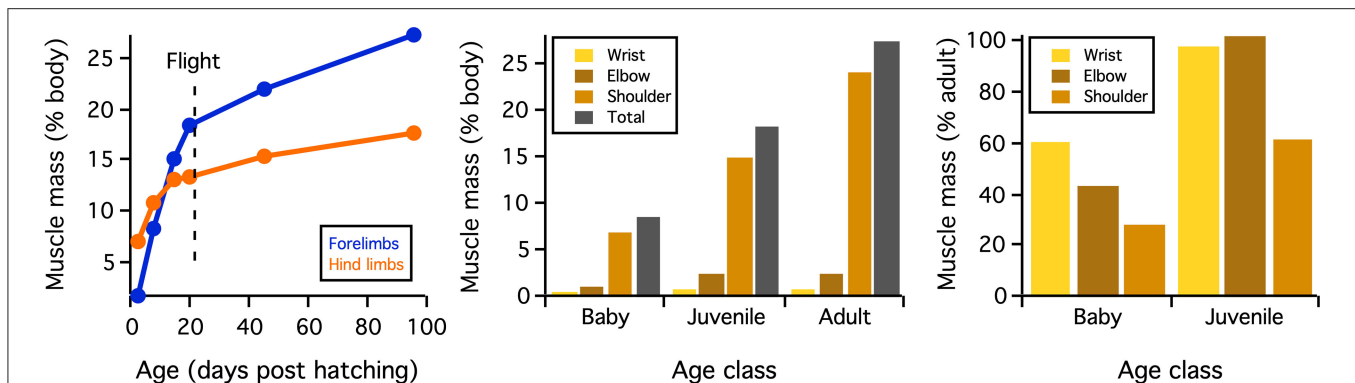


FIGURE 6 | Muscle mass. When standardized by body mass, muscle mass increases through ontogeny. These increases are most extreme for shoulder muscles that originate from the pectoral girdle (Figure 3A) and drive shoulder movements. Figure from Heers et al. (2018).

vertical global stroke plane angle (102° vs. 110° in older birds), such that drag contributes substantially to weight support (Jackson et al., 2009; Heers et al., 2011). This steep stroke plane angle results at least partially from the more pitched posture of younger birds (Heers et al., 2016), but probably also from the more caudally-directed pull of the pectoralis during *in vivo* kinematics. In short, ontogenetic differences in pectoralis pull during *in vivo* flapping kinematics do not appear to result from ontogenetic shifts in skeletal anatomy, but may be adaptive in improving muscle leverage (for rotation) and aerodynamic performance in young birds with draggy wings.

Given that bones of the pectoral girdle show substantial changes in orientation during ontogeny, the fact that these changes do not seem to be associated with changes in orientation of the supracoracoideus or the pectoralis is, at first glance, surprising. For example, as the sternum becomes more parallel to the vertebral column and the angle of the coracoid increases during ontogeny, the pectoralis and supracoracoideus might be expected to take on a more cranio-caudal orientation as their origins shift more caudally to the coracosternal joint and their insertions shift cranially to it (Figure 2). In reality, however, the glenoid, furcula, and scapula maintain their positions relative to the vertebral column through ontogeny (Figure 9), because shifts in coracoid angle are counteracted by changes in furculocoracoid and scapulocoracoid angles (i.e., the coracoid changes orientation but the furcula and scapula do not). Simultaneously, the cranial portion of the keel expands more than the caudal portion and at least partially counteracts ontogenetic shifts in sternum orientation. Thus, as the coracoid changes orientation and positions the growing sternum more caudally, the furcula and cranial portion of the keel expand and maintain the cranial origins of the supracoracoideus and especially the pectoralis. Coupled with the triosseal canal, which helps constrain the supracoracoideus, these skeletal changes allow for an expansion of muscle attachment sites (keel, interosseous membranes) and increases in muscle mass, without changes in muscle function. In short, muscle paths converge near the shoulder joint and functions (Table 1; Table 2 in Heers et al., 2018) remain

similar through ontogeny, in spite of underlying changes in the skeletal apparatus.

DISCUSSION

The evolution of avian flight is one of the great transformations in vertebrate history, marked by striking anatomical changes that presumably are adaptations or exaptations (Gould and Vrba, 1982) (“aptations”) for meeting the demands of aerial locomotion (Figure 1). Some of these aptations are functionally intuitive—for example, the keel of the sternum clearly provides a large attachment site for important flight muscles, while the triosseal canal constrains the tendon of the supracoracoideus muscle. However, many aptations are categorized as such based on their presence in flight-capable birds and their absence in flightless birds and extinct theropods, with no known or demonstrated function(s). For instance, the angle between the scapula and the coracoid is acute (or close to acute) in volant birds but obtuse in avian embryos and secondarily flightless birds (Livezey, 1989, 2003, 2008), and these differences have been used to discuss potential flight capacity in extinct organisms (Olson and Feduccia, 1979; Feduccia, 1986; Chatterjee and Templin, 2003). Yet the functional relevance of this angle has not been demonstrated. Similarly, the humerus of modern birds shows greater complexity (more exaggerated muscle attachment sites, globular and deflected head) than the humeri of extinct theropods like *Archaeopteryx*. Though the degree of complexity is likely related to muscle morphology and function, and/or to flight kinematics, these ideas have not been assessed. In short, the avian body plan is highly specialized for flight, and though widely discussed, many specializations are not well-understood.

Skeletal Anatomy vs. Muscle Morphology

To better understand how changes in the pectoral girdle and humerus influence muscle morphology and function during flightless to flight-capable transitions, we quantified how ontogenetic changes in bone size, orientation, and complexity influence muscle size, leverage, and orientation or pull in a developing ground bird, the Chukar Partridge. The skeletons of developing birds are not identical to those of extinct theropods

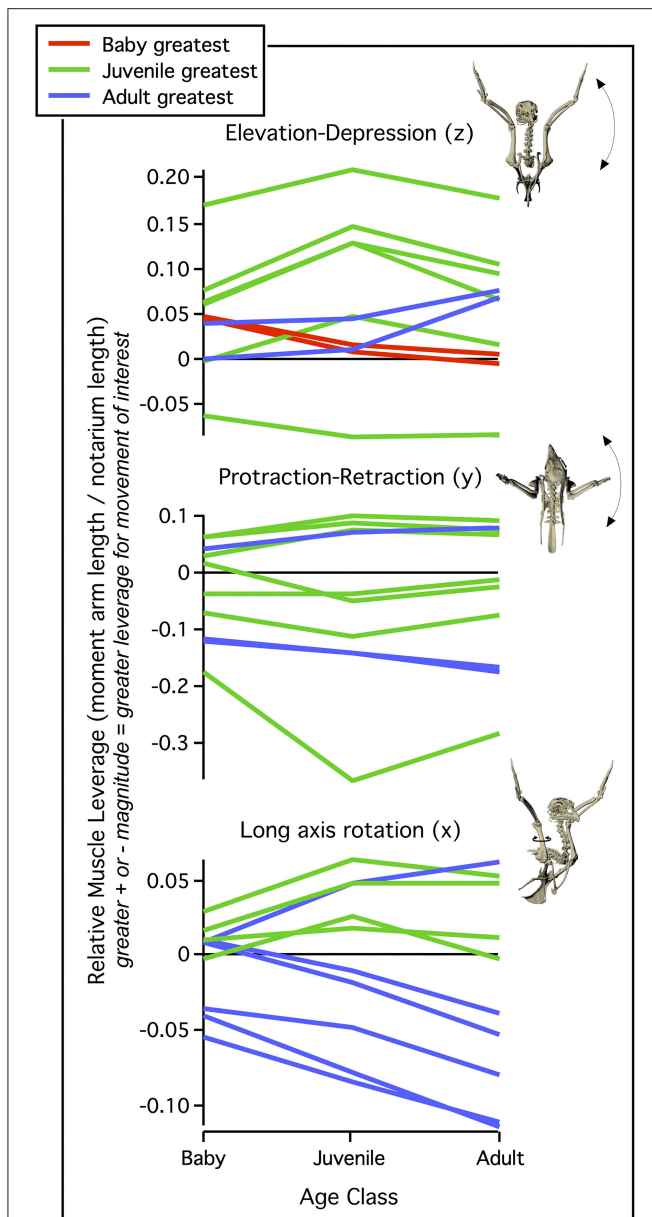


FIGURE 7 | Muscle leverage (moment arm length). When standardized by notarium length, moment arm lengths generally increase through ontogeny but show different developmental patterns, depending on the direction of motion. Muscle leverage for elevation/depression (z axis) and protraction/retraction (y axis) tends to peak in juveniles, most likely due to their proportionally long forelimbs and deltopectoral crests (Figures 2, 3B). In contrast, moment arms for long axis rotation (x axis) tend to peak in adults, whose exaggerated muscle attachment sites help pull muscles away from the long axis of the humerus (Figures 2, 5). Each line represents the relative moment arm length (leverage) for one shoulder muscle about the z, y, or x axis, during maximal effort wing-assisted incline running (WAIR) in chukars. Figure modified from Heers et al. (2018).

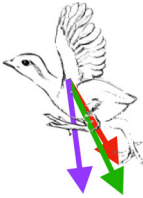


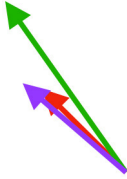
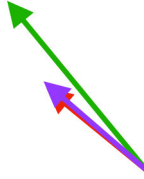
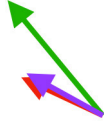
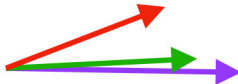






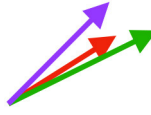
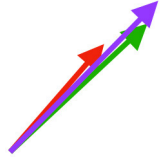

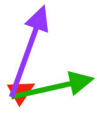
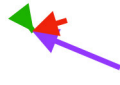
but nevertheless can provide important functional insights, because many features that changed during the evolution of flight also change during the development of flight, which allows their form-function relationships to be assessed. Our results

demonstrate that, like the evolution of flight, the development of flight is accompanied by striking changes in skeletal anatomy (Figures 1, 2). When standardized by body (notarium) length, elements of the chukar flight apparatus increase in relative size (Figure 3) and complexity (Figure 5) during ontogeny, while simultaneously changing substantially in orientation (Figure 4):

- The sternum grows larger and more parallel to the vertebral column as it ossifies. This element is often not preserved in extinct paravians (Zheng et al., 2014), perhaps due to late ossification during ontogeny and/or cartilage decay (Figure 10). If reconstructions showing a small, more vertically-angled sternum (similar to that of secondarily flightless birds; e.g., Chiappe and Dyke, 2006; Hartman, 2013; Xu and Qin, 2017) are correct, then a similar shift occurred during the evolution of flight.
- The coracoid angle increases, the scapulocoracoid angle decreases, and the coracoid and scapula lengthen. All of these changes are readily apparent in the fossil record (e.g., Figure 4 in Jenkins, 1993), albeit to a greater degree (e.g., the coracoid lengthens much more between paravians and modern birds than between hatchling and adult birds).
- The furcula grows longer and the angle between the coracoid and furcula increases. Both of these changes can be observed in the fossil record (see reconstructions in Chiappe and Dyke, 2006), albeit again on a more striking scale.
- The forelimb increases in length but is proportionally longest in juveniles, whereas the deltopectoral crest is proportionally long in both baby and juvenile birds. Growth of the bicapital crest, elaboration of muscle attachment sites, and deflection and expansion of the humeral head simultaneously contribute to increases in complexity. Many of these changes occurred during the evolution of flight as well: the forelimb lengthens, even after the appearance of wings (Middleton and Gatesy, 2000; Dececchi and Larsson, 2013), the humeral head becomes more deflected (Rauhut et al., 2019), and bone complexity generally increases. The size of the deltopectoral crest has been related to flight style in *Sapeornis* (Serrano and Chiappe, 2017), but its relative proportions have not been assessed in other extinct taxa.

Whether on ontogenetic or evolutionary timescales, these transitions in skeletal anatomy change the size, position, and/or orientation of joint surfaces and/or muscle attachment sites, and therefore might be expected to influence muscle size, leverage, and orientation. Consistent with this expectation, relative muscle mass (Figure 6) and relative muscle leverage (Figure 7) generally increase through ontogeny, although moment arms for elevation-depression and protraction-retraction tend to peak in juveniles, likely due to their proportionally long forelimbs and deltopectoral crests (Heers et al., 2018). As anticipated, ontogenetic changes in skeletal anatomy also result in slight shifts in orientation for some shoulder muscles. However, for the two most important flight muscles—the pectoralis and supracoracoideus—muscle paths and subsequent functions (Table 1; Table 2 in Heers et al., 2018) remain similar in spite of

TABLE 1 | Muscle orientations and pull.

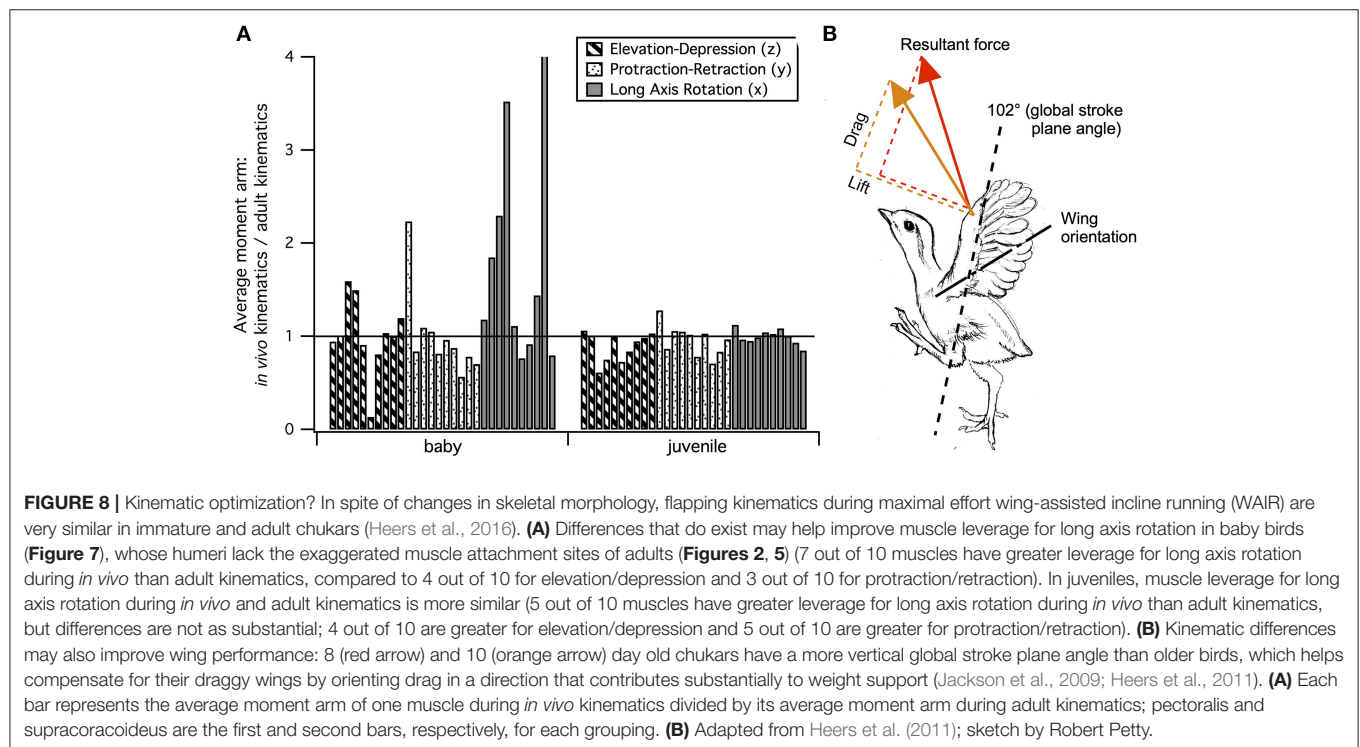
| Muscle | (A) <i>In vivo</i> kinematics, maximal effort WAIR | (B) Same kinematics (adult maximal effort WAIR) | (C) Standardized position | Trends in muscle orientation? | Function |
|-----------------------------------------------------------------------------------------------------|-------------------------------------------------------------------------------------|-------------------------------------------------------------------------------------|--------------------------------------------------------------------------------------|----------------------------------------------------------------------------------------------------------------------------------------------------------------------|--------------------------------------------------------------------------------------|
| P Origin on sternum, ribs, furcula, and sternocoracoclavicular membrane; insertion on DPC |  |  |  | Pulls more caudally in immature birds during <i>in vivo</i> kinematics, but no differences when kinematics are standardized | Downstroke: decelerates then depresses, pronates, and mainly retracts humerus |
| S Origin on sternum, coracoid, and coracoclavicular membrane; insertion on DPC |  |  |  | Pulls more dorsally in juvenile, potentially due to long humerus and DPC | Upstroke: decelerates then elevates and supinates humerus |
| CB Origin near base of coracoid; insertion on margo caudalis of humerus |  |  |  | Pull more caudally and less dorsally in older birds: as coracoid angle increases, the CB and SbC shift to a more craniocaudal orientation and retraction is enhanced | Downstroke: mainly decelerate and retract humerus |
| SbC |  |  |  | | |
| SbS Origin on scapula; insertion on margo caudalis or bicipital crest of humerus |  |  |  | Pull more dorsally in adults, potentially due to expansion of the bicipital crest | Downstroke, but contribution not substantial |
| SHC |  |  |  | | Helps decelerate, stabilize, elevate, and retract or protract humerus, esp. in adult |

(Continued)

TABLE 1 | Continued

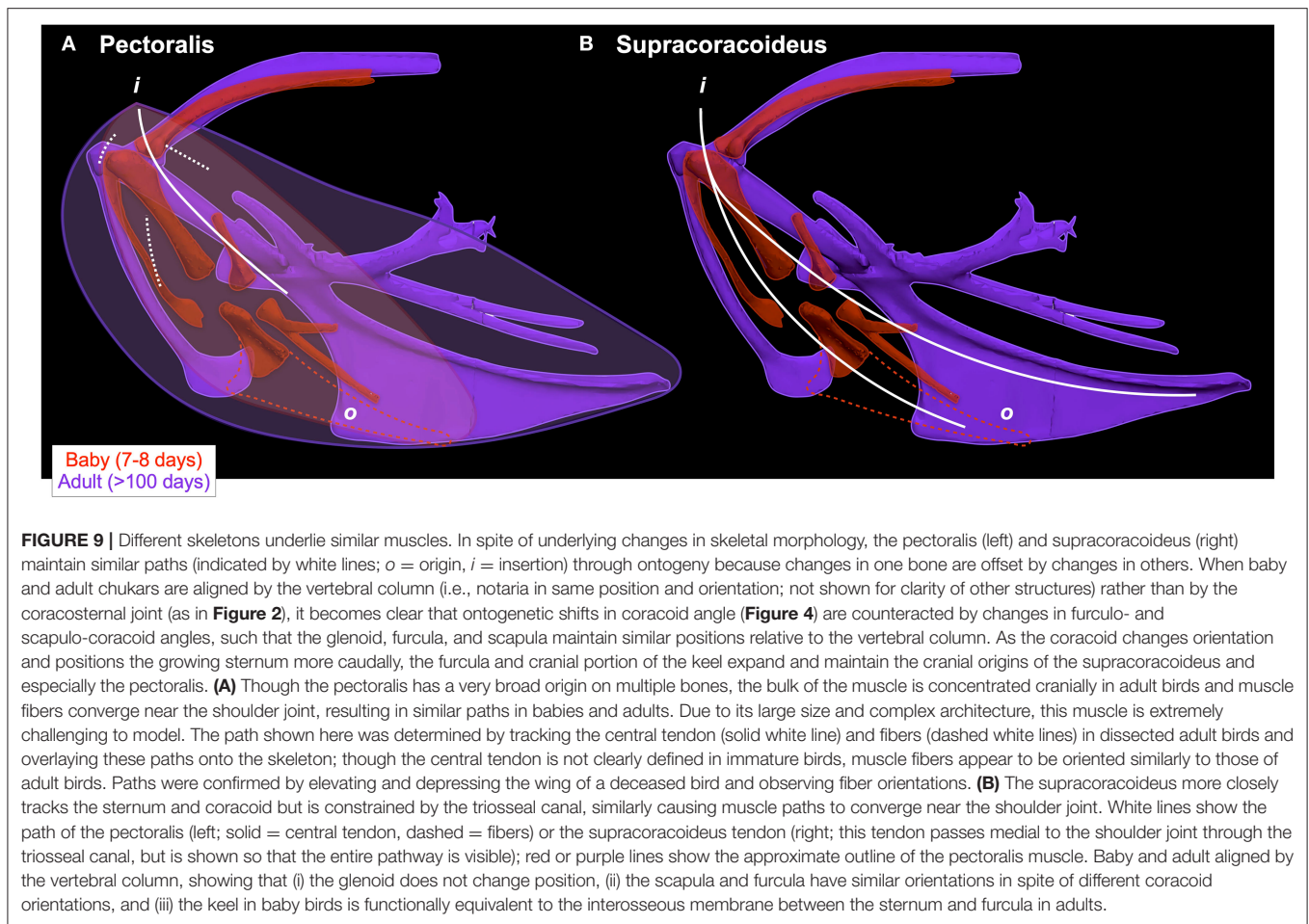
| Muscle | (A) <i>In vivo</i> kinematics, maximal effort WAIR | (B) Same kinematics (adult maximal effort WAIR) | (C) Standardized position | Trends in muscle orientation? | Function |
|------------------------------------------------------------------------|----------------------------------------------------|-------------------------------------------------|---------------------------|--------------------------------------------------------------------------------------------------------------|------------------------------------------------------------------------|
| LD Origin on vertebral column, insertion on humeral shaft | | | | Pulls more caudally in older birds, possibly due to deflection of humeral head and humeral length (juvenile) | Decelerates, stabilizes, elevates, and retracts humerus |
| DM Origin medial to triosseal canal; insertion on humeral shaft | | | | No major trends | Upstroke: decelerates then elevates humerus; protraction or retraction |

Vector sums of the average *z* (elevation/depression) and *y* (protraction/retraction) moment arms simulated under various conditions (columns A–C) show the net pull of muscles in baby (red), juvenile (green), and adult (purple) chukars. Moment arms shown in left lateral view with vertebral column oriented horizontally. Column A: vector sums of average *z* and *y* moment arms during *in vivo* kinematics for maximal effort wing-assisted incline running show how muscle pull varies due to anatomy and/or kinematics; Column B: vector sums of average *z* and *y* moment arms during adult kinematics for maximal effort wing-assisted incline running show how muscle pull varies due to anatomy only; Column C: vector sums of *z* and *y* moment arms in a standardized position (start of downstroke for downstroke muscles; start of upstroke for upstroke muscles) show how muscle pull varies due to anatomy only, at a point in the stroke cycle when muscles are most active; Functions based on moment arms and measured (Dial, 1992) and simulated (Heers et al., 2018) activations. *P*, Pectoralis; *S*, Supracoracoideus; *CB*, Coracobrachialis posterior; *SbC*, Subcoracoideus; *SbS*, Subscapularis; *SHC*, Scapulohumeralis caudalis; *LD*, Latissimus dorsi; *DM*, Deltoides major; *DPC*, deltopectoral crest of humerus. *LD* at 1/3 scale.



underlying changes in the skeletal apparatus. This is surprising, because the pectoralis and supracoracoideus might be expected to take on a more cranio-caudal orientation as the sternum becomes

more parallel to the vertebral column and the coracoid changes orientation (Figure 2). However, our results demonstrate that, in chukars, developmental shifts in one bone are counteracted



by developmental shifts in others: changes in furculocoracoid and scapulocoracoid angles counteract changes in coracoid angle, such that the glenoid, furcula, and scapula maintain their positions relative to the vertebral column (**Figure 9**). As the coracoid changes orientation and displaces the growing sternum more caudally, the furcula and cranial portion of the keel expand and maintain the cranial positions of the supracoracoideus and especially the pectoralis. These changes allow for increases in muscle mass without changes in muscle function, because muscle paths converge near the shoulder joint and remain similar through ontogeny in spite of underlying skeletal changes (**Figure 9**). Collectively, such findings may suggest that evolutionary changes in skeletal anatomy were associated with increases in muscle size and leverage, but perhaps only minor changes in orientation or pull of the pectoralis and supracoracoideus [but see discussions of the triosseal canal (Ostrom, 1976; Mayr, 2017)]. In short, multiple skeletal solutions yield similar muscle pathways.

Our results also provide explanations for why adaptations like humeral complexity and scapulocoracoid angle are related to flight capability. Humeral complexity increases both during ontogeny and evolution, as muscle attachment sites become more exaggerated and the humeral head is deflected. Skeletal features

that are most exaggerated in adult birds—the deflected humeral head, expanded bicipital crest, and generally more complex bone processes—likely improve muscle leverage (moment arms) for long axis rotation (**Figures 2, 5, 7**) by shifting muscle attachment sites away from the long axis of the humerus (Heers et al., 2018). Greater muscle leverage likely improves wing control and may facilitate rapid wing turnaround. For example, the supracoracoideus rapidly supinates the humerus at the start of upstroke (Poore et al., 1997), and although the underdeveloped flight apparatus of baby birds does not prevent them from flapping their wings, this function may be enhanced in older birds as increases in bone complexity improve the supracoracoideus' leverage for rotation.

Whereas increases in humeral complexity likely enhance muscle leverage, the angle between the scapula and coracoid appears to be related to muscle size. As the coracoid angle increases, the scapulocoracoid angle decreases, because the scapula and the glenoid maintain their positions with respect to the vertebral column. This shift in coracoid orientation shifts the sternum to a more caudal position as it grows, and thereby expands the origin of the pectoralis and supracoracoideus caudally (**Figure 9**). Simultaneously, the furculocoracoid angle increases and the cranial portion of the keel hypertrophies,



FIGURE 10 | Cartilaginous keel. The cartilaginous keel of immature birds quickly shrinks and deforms following dissection, is completely degraded by skeletal preparation (warm water bath with protein-digesting enzymes, or dermestid beetles) (inset), and thus would easily be lost in the fossil record.

thereby maintaining the cranial origins of the supracoracoideus and especially the pectoralis. Together, these shifts expand muscle attachment areas and allow for increases in muscle mass while maintaining similar muscle paths (**Figure 9**). Thus, assessing scapulocoracoid angles is assessing only part of the story—in reality, the coracoid shifts to allow for expansion of muscle attachment sites, while both the scapula and the furcula maintain similar positions and help preserve muscle function. Changes in one bone cannot be analyzed independently of changes in others, reiterating that the functional relevance of many flight adaptations is best understood through the lens of a more whole-body perspective.

Skeletal Anatomy vs. Flapping Kinematics

In spite of developmental changes in skeletal anatomy, previous work demonstrates that flapping kinematics in immature and adult chukars are very similar during maximal effort wing-assisted incline running (Heers et al., 2016). Differences that do exist do not appear to be directly caused by developmental changes in skeletal anatomy, but may help compensate for poorer muscle leverage in long axis rotation (**Figure 8A**), especially in baby birds with less complex humeri (**Figures 2, 5**). Kinematic differences may also serve to improve locomotor

performance in young birds with draggy wings (**Figure 8B**)—the pectoralis pulls the wing more caudally in baby and juvenile chukars (**Table 1**) and helps direct drag in a direction that contributes substantially to weight support (Heers et al., 2011). Thus, although flapping kinematics are very similar overall, differences that exist appear to be adaptive for optimizing rotational leverage and aerodynamic performance in young birds with developing flight apparatuses. In conjunction with previous work, these findings show that it is difficult to predict or understand kinematics from skeletal morphology alone, and that similar and effective flapping movements can be produced by animals with very different wings and musculoskeletal apparatuses.

Compensation

This study builds upon previous work demonstrating that developing animals can achieve high levels of locomotor performance by compensating for underdeveloped locomotor structures (Carrier, 1996; Herrel and Gibb, 2006; Dial et al., 2015). Baby (7–8 day) chukars appear to compensate both kinematically and behaviorally. Flapping kinematics appear to improve muscle leverage for long axis rotation and orient drag in a direction that supports body weight (**Figure 8**) (Heers et al., 2011). Behaviorally, locomotor performance is improved by recruiting wings and legs cooperatively (Dial, 2003; Dial et al., 2015; Heers and Dial, 2015). Such wing-leg cooperation also enhances performance in juvenile (18–20 day) birds. However, juvenile chukars are just becoming flight-capable, and, at this critical stage, anatomical features appear to play an additional and important compensatory role. Incipiently volant juveniles compensate for small flight muscles (**Figure 6**) with proportionally long forelimbs and deltopectoral crests (**Figures 2, 3B**), and compensate for less aerodynamically effective feathers by having longer feathers and small bodies (low wing loading) (Jackson et al., 2009; Heers et al., 2011, 2018). In short, anatomic, kinematic, and behavioral compensations allow immature ground birds to acquire flight capacity long before flight adaptations are fully developed, playing a key role in avian ontogeny and perhaps a similar role in avian evolution. Flight apparatuses are functional throughout their development—even at rudimentary, more “dinosaur-like” stages.

Collectively

Our results demonstrate that developing and adult ground birds use different functional solutions to execute similar locomotor behaviors. Muscle paths and subsequent functions are largely maintained through ontogeny in spite of dramatic changes in skeletal morphology because shifts in one bone are offset by changes in others. Future studies could build upon this work by examining ontogenetic changes in birds with different life history or locomotor strategies, and by using such data to help reconstruct the musculoskeletal apparatuses of avian predecessors. These preliminary findings nevertheless suggest a possible mechanism for how extinct winged theropods with rudimentary pectoral apparatuses might have achieved bird-like behaviors before acquiring fully bird-like anatomies. These findings also emphasize:

1. *The importance of a holistic, whole-body perspective on locomotor performance.* Though highly specialized for flight, many aspects of the avian body plan are not well-understood, potentially because they have been viewed in isolation [e.g., scapulocoracoid angle, “What use is half a wing?” (Mivart, 1871)]. Our understanding will be incomplete and possibly misleading unless we consider the entire locomotor apparatus (skeleton + muscles + feathers; wings + legs) on multiple levels (form, function, performance, behavior, ecology).
2. *The need for extant validation of extinct behaviors and performance.* Although powerful techniques for modeling locomotion in extinct organisms are available and constantly improving (see citations in Pittman et al., 2020), all workflows for inferring function must be validated (Hutchinson, 2011), because animals often do not work the way we expect them to (e.g., developing birds fly long before flight adaptations are fully developed; similar muscle paths in spite of different skeletal morphologies). Understanding locomotor evolution requires a thorough exploration of locomotion in extant organisms.
3. *The power of ontogeny.* Developing birds offer a unique and powerful contribution to studies on avian evolution—only among developing birds can we quantitatively explore real relationships between form, function, performance, and behavior during flightless to flight-capable transitions.

As empirical studies on locomotor ontogeny accumulate, it is becoming apparent that traditional, isolated interpretations of skeletal anatomy mask the reality that integrated whole systems function in frequently unexpected yet effective ways. This perspective is challenging to incorporate into evolutionary studies, because it requires establishing relationships between form, function, performance, behavior, and ecology in extant organisms, and validating workflows for inferring such relationships in extinct organisms. But without such a

perspective, our inferences are incomplete and sometimes misleading. Collaborative and integrative efforts that address this challenge will surely strengthen our exploration of life and its evolutionary history.

DATA AVAILABILITY STATEMENT

The original contributions presented in the study are included in the article/supplementary materials, further inquiries can be directed to the corresponding author/s.

ETHICS STATEMENT

The animal study was reviewed and approved by University of Montana Institutional Animal Care and Use Committee and the Royal Veterinary College Ethics and Welfare Committee.

AUTHOR CONTRIBUTIONS

AH, SV, LH, and JC helped collect and analyze data. Manuscript written by AH. All authors contributed to the article and approved the submitted version.

FUNDING

This project was supported by a New Investigator grant from the California State University Program for Education and Research in Biotechnology (CSUPERB).

ACKNOWLEDGMENTS

We thank CSUPERB for funding this project, and Ken Dial, Jeffery Rankin, editor Corwin Sullivan, and manuscript reviewers for their time and feedback.

REFERENCES

- Alexander, R. M. (2002). The merits and implications of travel by swimming, flight and running for animals of different sizes. *Integr. Comp. Biol.* 42, 1060–1064. doi: 10.1093/icb/42.5.1060
- Baumel, J. J., and Witmer, L. M. (1993). “Osteologia,” in *Handbook of Avian Anatomy: Nomina Anatomica Avium*, eds J. J. Baumel, A. S. King, J. E. Breazile, H. E. Evans, and J. C. Vanden Berge (Cambridge, MA: Nuttall Ornithological Club), 45–132.
- Bock, W. (1986). The arboreal origin of avian flight. *Mem. Calif. Acad. Sci.* 8, 57–72.
- Brassey, C. A., Maidment, S. C. R., and Barrett, P. M. (2017). Muscle moment arm analyses applied to vertebrate paleontology: a case study using *Stegosaurus stenops* Marsh, 1887. *J. Vertebr. Paleontol.* 37:e1361432. doi: 10.1080/02724634.2017.1361432
- Burgers, P., and Chiappe, L. M. (1999). The wing of Archaeopteryx as a primary thrust generator. *Nature* 399, 60–62. doi: 10.1038/19967
- Carrier, D. R. (1996). Ontogenetic limits on locomotor performance. *Physiol. Zool.* 69, 467–488.
- Chatterjee, S., and Templin, R. J. (2003). The flight of Archaeopteryx. *Naturwissenschaften* 90, 27–32. doi: 10.1007/s00114-002-0385-0
- Chiappe, L. M., and Dyke, G. J. (2006). The early evolutionary history of birds. *J. Paleontol. Soc.* 22, 133–151.
- Coombs, W. P. (1978). Theoretical aspects of cursorial adaptations in Dinosaurs. *Q. Rev. Biol.* 53, 393–418.
- Dececchi, T. A., and Larsson, H. C. E. (2013). Body and limb size dissociation at the origin of birds: uncoupling allometric constraints across a macroevolutionary transition. *Evolution* 67, 2741–2752. doi: 10.1111/evo.12150
- Dececchi, T. A., Larsson, H. C. E., and Habib, M. B. (2016). The wings before the bird: an evaluation of flapping-based locomotory hypotheses in bird antecedents. *PeerJ* 4:e2159. doi: 10.7717/peerj.2159
- Delp, S. L., Anderson, F. C., Arnold, A. S., Loan, P., Habib, A., John, C. T., et al. (2007). OpenSim: open-source software to create and analyze dynamic simulations of movement. *IEEE Trans. Biomed. Eng.* 54, 1940–1950. doi: 10.1109/TBME.2007.901024
- Dial, K. P. (1992). Activity patterns of the wing muscles of the Pigeon (*Columba livia*) during different modes of flight. *J. Exp. Zool.* 262, 357–373.
- Dial, K. P. (2003). Wing-assisted incline running and the evolution of flight. *Science* 299, 402–404. doi: 10.1126/science.1078237
- Dial, K. P., Heers, A. M., and Dial, T. R. (2015). “Ontogenetic and evolutionary transformations: the ecological significance of rudimentary structures,” in *Great Transformations in Vertebrate Evolution*, eds K. P. Dial, N. Shubin, and E. L. Brainerd (Chicago, IL: University of Chicago Press), 283–301.

- Dial, K. P., Jackson, B. E., and Segre, P. (2008). A fundamental avian wing-stroke provides a new perspective on the evolution of flight. *Nature* 451, 985–989. doi: 10.1038/nature06517
- Dial, K. P., Randall, R. J., and Dial, T. R. (2006). What use is half a wing in the ecology and evolution of birds? *Bioscience* 56, 437–445. doi: 10.1641/0006-3568(2006)056[0437:WUIHAW]2.0.CO;2
- Dial, T. R., and Carrier, D. R. (2012). Precocial hindlimbs and altricial forelimbs: partitioning ontogenetic strategies in Mallard ducks (*Anas platyrhynchos*). *J. Exp. Biol.* 215, 3703–3710. doi: 10.1242/jeb.057380
- Dial, T. R., Heers, A. M., and Tobalske, B. W. (2012). Ontogeny of aerodynamics in mallards: comparative performance and developmental implications. *J. Exp. Biol.* 215, 3693–3702. doi: 10.1242/jeb.062018
- Feduccia, A. (1986). The scapulocoracoid of flightless birds: a primitive avian character similar to that of theropods. *Ibis* 128, 128–132. doi: 10.1111/j.1474-919X.1986.tb02099.x
- Foth, C., Tischlinger, H., and Rahut, O. W. M. (2014). New specimen of Archaeopteryx provides insights into the evolution of pennaceous feathers. *Nature* 511, 79–82. doi: 10.1038/nature13467
- Gatesy, S. M., and Dial, K. P. (1996). From frond to fan: Archaeopteryx and the evolution of short-tailed birds. *Evolution* 50, 2037–2048.
- George, J. C., and Berger, A. J. (1966). *Avian Myology, 1st Edn.* New York, NY: Academic Press.
- Ghetie, V., Chitescu, S. t., Cotofan, V., and Hildebrand, A. (1976). *Anatomical Atlas of Domestic Birds*. Bucharest: Editura Academiei Republicii Socialiste Romania.
- Gignac, P. M., Kley, N. J., Clarke, J. A., Colbert, M. W., Morhardt, A. C., Cerio, D., et al. (2016). Diffusible iodine-based contrast-enhanced computed tomography (diceCT): an emerging tool for rapid, high-resolution, 3-D imaging of metazoan soft tissues. *J. Anat.* 228, 889–909. doi: 10.1111/joa.12449
- Godefroit, P., Sinitisa, S. M., Dhoulilly, D., Bolotsky, Y. L., Sizov, A. V., McNamara, M. E., et al. (2014). A Jurassic ornithischian dinosaur from Siberia with both feathers and scales. *Science* 345, 451–455. doi: 10.1126/science.1253351
- Gould, S. J., and Vrba, E. S. (1982). Exaptation-A Missing Term in the Science of Form. *Paleobiology* 8, 4–15.
- Hartman, S. (2013). *Scott Hartman's Skeletal Drawing*. Available online at: <https://www.skeletaldrawing.com/theropods/archaeopteryx>
- Heers, A. M., Baier, D. B., Jackson, B. E., and Dial, K. P. (2016). Flapping before flight: high resolution, three-dimensional skeletal kinematics of wings and legs during avian development. *PLoS ONE* 11:e0153446. doi: 10.1371/journal.pone.0153446
- Heers, A. M., and Dial, K. P. (2012). From extant to extinct: locomotor ontogeny and the evolution of avian flight. *Trends Ecol. Evol.* 27, 296–305. doi: 10.1016/j.tree.2011.12.003
- Heers, A. M., and Dial, K. P. (2015). Wings versus legs in the avian bauplan: development and evolution of alternative locomotor strategies. *Evolution* 69, 305–320. doi: 10.1111/evo.12576
- Heers, A. M., Dial, K. P., and Tobalske, B. W. (2014). From baby birds to feathered dinosaurs: incipient wings and the evolution of flight. *Paleobiology* 40, 459–476. doi: 10.1666/13057
- Heers, A. M., Rankin, J. W., and Hutchinson, J. R. (2018). Building a bird: musculoskeletal modeling and simulation of wing-assisted incline running during avian ontogeny. *Front. Bioeng. Biotechnol.* 6:140. doi: 10.3389/fbioe.2018.00140
- Heers, A. M., Tobalske, B. W., and Dial, K. P. (2011). Ontogeny of lift and drag production in ground birds. *J. Exp. Biol.* 214, 717–725. doi: 10.1242/jeb.051177
- Heilmann, G. (1926). *The Origin of Birds*. London: Witherby.
- Herrel, A., and Gibb, A. C. (2006). Ontogeny of performance in vertebrates. *Physiol. Biochem. Zool.* 79, 1–6. doi: 10.1086/498196
- Hutchinson, J. R. (2011). On the inference of function from structure using biomechanical modelling and simulation of extinct organisms. *Biol. Lett.* 8, 115–118. doi: 10.1098/rsbl.2011.0399
- Hutchinson, J. R., Anderson, F. C., Blemker, S. S., and Delp, S. L. (2005). Analysis of hindlimb muscle moment arms in Tyrannosaurus rex using a three-dimensional musculoskeletal computer model: implications for stance, gait, and speed. *Paleobiology* 31, 676–701. doi: 10.1666/0094-8373(2005)031[0676:AOHMMMA]2.0.CO;2
- Hutchinson, J. R., and Garcia, M. (2002). Tyrannosaurus was not a fast runner. *Nature* 415, 1018–1021. doi: 10.1038/4151018a
- Jackson, B. E., Segre, P., and Dial, K. P. (2009). Precocial development of locomotor performance in a ground-dwelling bird (*Alectoris chukar*): negotiating a three-dimensional terrestrial environment. *Proc. R. Soc. B Biol. Sci.* 276, 3457–3466. doi: 10.1098/rspb.2009.0794
- Jasinowski, S. C., Russell, A. P., and Currie, P. J. (2006). An integrative phylogenetic and extrapolatory approach to the reconstruction of dromaeosaur (Theropoda: Eumaniraptora) shoulder musculature. *Zool. J. Linn. Soc.* 146, 301–344. doi: 10.1111/j.1096-3642.2006.00200.x
- Jenkins, F. A. (1993). The evolution of the avian shoulder joint. *Am. J. Sci.* 293, 253–267. doi: 10.2475/ajs.293.A.253
- Kisia, S. M. (2011). *Vertebrates: Structures and Functions*. Boca Raton, FL: CRC Press.
- Lefèvre, U., Cau, A., Hu, D., and Godefroit, P. (2020). “Feather Evolution in Pennaraptora,” in *The Evolution of Feathers: From Their Origin to the Present*, eds C. Foth and O. W. M. Rahut (Springer), 103–118.
- Livezey, B. C. (1989). Flightlessness in Grebes (Aves, Podicipedidae): its independent evolution in three genera. *Evolution* 43, 29–54. doi: 10.1111/j.1558-5646.1989.tb04205.x
- Livezey, B. C. (2003). *Evolution of Flightlessness in Rails (Gruiformes: Rallidae): Phylogenetic, Ecomorphological, and Ontogenetic Perspectives*. Lawrence, KS: American Ornithologists' Union.
- Livezey, B. C. (2008). Flightlessness in the Galápagos cormorant (*Compsohalieus [Nannopterum] harrisi*): heterochrony, gigantism and specialization. *Zool. J. Linn. Soc.* 105, 155–224. doi: 10.1111/j.1096-3642.1992.tb01229.x
- Longrich, N. R., Vinther, J., Meng, Q., Li, Q., and Russell, A. P. (2012). Primitive wing feather arrangement in *Archaeopteryx lithographica* and *Anchiornis huxleyi*. *Curr. Biol.* 22, 2262–2267. doi: 10.1016/j.cub.2012.09.052
- Mayr, G. (2017). Pectoral girdle morphology of Mesozoic birds and the evolution of the avian supracoracoideus muscle. *J. Ornithol.* 158, 859–867. doi: 10.1007/s10336-017-1451-x
- Middleton, K. M., and Gatesy, S. M. (2000). Theropod forelimb design and evolution. *Zool. J. Linn. Soc.* 128, 149–187. doi: 10.1006/zjls.1998.0193
- Mivart, S. G. J. (1871). *On the Genesis of Species*. New York, NY: Appleton.
- Muller, W., and Patone, G. (1998). Air transmissivity of feathers. *J. Exp. Biol.* 201, 2591–2599.
- Norberg, R. A. (1985). “Function of vane asymmetry and shaft curvature in bird flight feathers; inferences on flight ability of Archaeopteryx,” in *The Beginnings of Birds*, eds J. H. Ostrom, M. K. Hecht, G. Viohl, and P. Wellnhofer (Eichstatt: Jura Museum), 303–318.
- Norberg, U. M. (1990). *Vertebrate Flight: Mechanics, Physiology, Morphology, Ecology and Evolution*. Berlin: Springer-Verlag.
- Norell, M. A., and Xu, X. (2005). Feathered dinosaurs. *Annu. Rev. Earth Planet. Sci.* 33, 277–299. doi: 10.1146/annurev.earth.33.092203.122511
- Nudds, R. L. (2014). Reassessment of the wing feathers of Archaeopteryx lithographica suggests no robust evidence for the presence of elongated dorsal wing coverts. *PLoS ONE* 9:e93963. doi: 10.1371/journal.pone.0093963
- Nudds, R. L., and Dyke, G. J. (2010). Narrow primary feather rachises in confuciusornis and archaeopteryx suggest poor flight ability. *Science* 328, 887–889. doi: 10.1126/science.1188895
- Olson, S. L., and Feduccia, A. (1979). Flight capability and the pectoral girdle of Archaeopteryx. *Nature* 278, 247–248. doi: 10.1038/278247a0
- Ostrom, J. H. (1974). Archaeopteryx and the origin of flight. *Q. Rev. Biol.* 49, 27–47.
- Ostrom, J. H. (1976). Some hypothetical anatomical stages in the evolution of avian flight. *Smithson. Contrib. Paleobiol.* 27, 1–21.
- Ostrom, J. H. (1979). Bird flight: how did it begin? *Am. Sci.* 67, 46–56.
- Ostrom, J. H. (1986). The cursorial origin of avian flight. *Mem. Calif. Acad. Sci.* 8, 73–81.
- Ostrom, J. H., Poore, S. O., and Goslow, G. E. (1999). Humeral rotation and wrist supination; important functional complex for the evolution of powered flight in birds? *Smithson. Contrib. Paleobiol.* 89, 301–309.
- Otero, A., Allen, V., Pol, D., and Hutchinson, J. R. (2017). Forelimb muscle and joint actions in Archosauria: insights from *Crocodylus johnstoni* (Pseudosuchia) and *Mussaurus patagonicus* (Sauropodomorpha). *PeerJ* 5:e3976. doi: 10.7717/peerj.3976
- Pierce, S. E., Clack, J. A., and Hutchinson, J. R. (2012). Three-dimensional limb joint mobility in the early tetrapod *Ichthyostega*. *Nature* 486, 523–526. doi: 10.1038/nature11124

- Pittman, M., Heers, A. M., Serrano, F. J., Field, D. J., Habib, M. B., Dececchi, T. A., et al. (2020). Methods of studying early theropod flight. *Bull. Am. Mus. Nat. Hist.* 440, 277–294.
- Poore, S. O., Ashcroft, A., Sánchez-Haiman, A., and Goslow, G. E. (1997). The contractile properties of the *M. supracoracoideus* in the pigeon and starling: a case for long-axis rotation of the humerus. *J. Exp. Biol.* 200, 2987–3002.
- Rauhut, O. W., Tischlinger, H., and Foth, C. (2019). A non-archaeopterygid avialan theropod from the Late Jurassic of southern Germany. *eLife* 8:e43789. doi: 10.7554/eLife.43789
- Rauhut, O. W. M., and Foth, C. (2020). “The origin of birds: current consensus, controversy, and the occurrence of feathers,” in *The Evolution of Feathers: From Their Origin to the Present*, eds C. Foth and O. W. M. Rauhut (Springer), 27–46.
- Rayner, J. M. V. (1988). The evolution of vertebrate flight. *Biol. J. Linn. Soc.* 34, 269–287. doi: 10.1111/j.1095-8312.1988.tb01963.x
- Serrano, F. J., and Chiappe, L. M. (2017). Aerodynamic modelling of a Cretaceous bird reveals thermal soaring capabilities during early avian evolution. *J. R. Soc. Interface* 14:20170182. doi: 10.1098/rsif.2017.0182
- Serrano, J. F., Costa-Pérez, M., Navalón, G., and Martín-Serra, A. (2020). Morphological disparity of the humerus in modern birds. *Diversity* 12:173. doi: 10.3390/d12050173
- Tobalske, B. W., and Dial, K. P. (2007). Aerodynamics of wing-assisted incline running in birds. *J. Exp. Biol.* 210, 1742–1751. doi: 10.1242/jeb.001701
- Vazquez, R. J. (1992). Functional osteology of the avian wrist and the evolution of flapping flight. *J. Morphol.* 211, 259–268.
- Walker, A. D. (1972). New light on the Origin of Birds and Crocodiles. *Nature* 237, 257–263. doi: 10.1038/237257a0
- Wellnhofer, P. (2009). *Archaeopteryx: The Icon of Evolution*. Munich: Pfeil Verlag.
- Xu, X. (2020). “Filamentous integuments in nonavian theropods and their kin: advances and future perspectives for understanding the evolution of feathers,” in *The Evolution of Feathers: From Their Origin to the Present* (Cham: Springer), 67–78.
- Xu, X., and Qin, Z.-C. (2017). A new tiny dromaeosaurid dinosaur from the Lower Cretaceous Jehol Group of western Liaoning and niche differentiation among the Jehol dromaeosaurids. *Vertebr. Palasiat.* 55, 129–144.
- Xu, X., Zhou, Z., Wang, X., Kuang, X., Zhang, F., and Du, X. (2003). Four-winged dinosaurs from China. *Nature* 421, 335–340. doi: 10.1038/nature01342
- Zheng, X., O'Connor, J., Wang, X., Wang, M., Zhang, X., and Zhou, Z. (2014). On the absence of sternal elements in Anchiornis (Paraves) and Sapeornis (Aves) and the complex early evolution of the avian sternum. *Proc. Natl. Acad. Sci. U.S.A.* 111, 13900–13905. doi: 10.1073/pnas.1411070111

Conflict of Interest: The authors declare that the research was conducted in the absence of any commercial or financial relationships that could be construed as a potential conflict of interest.

Copyright © 2021 Heers, Varghese, Hatier and Cabrera. This is an open-access article distributed under the terms of the Creative Commons Attribution License (CC BY). The use, distribution or reproduction in other forums is permitted, provided the original author(s) and the copyright owner(s) are credited and that the original publication in this journal is cited, in accordance with accepted academic practice. No use, distribution or reproduction is permitted which does not comply with these terms.



Investigating Possible Gastroliths in a Referred Specimen of *Bohaiornis guoi* (Aves: Enantiornithes)

Shumin Liu^{1,2*}, Zhiheng Li^{1,3}, Alida M. Bailleul^{1,3}, Min Wang^{1,3} and Jingmai O'Connor^{1,3,4*}

¹Key Laboratory of Vertebrate Evolution and Human Origins, Institute of Vertebrate Paleontology and Paleoanthropology, Chinese Academy of Sciences, Beijing, China, ²University of the Chinese Academy of Sciences, Beijing, China, ³CAS Center for Excellence in Life and Paleoenvironment, Beijing, China, ⁴Field Museum of Natural History, Chicago, IL, United States

OPEN ACCESS

Edited by:

Martin Daniel Ezcurra,
Museo Argentino de Ciencias
Naturales Bernardino Rivadavia,
Argentina

Reviewed by:

Ignacio Cerda,
Consejo Nacional de Investigaciones
Científicas y Técnicas, Argentina
Federico Agnolin,
Museo Argentino de Ciencias
Naturales Bernardino Rivadavia,
Argentina

*Correspondence:

Shumin Liu
liushumin@ivpp.ac.cn
Jingmai O'Connor
jingmai.oconnor@gmail.com

Specialty section:

This article was submitted to
Paleontology,
a section of the journal
Frontiers in Earth Science

Received: 30 November 2020

Accepted: 25 January 2021

Published: 19 February 2021

Citation:

Liu S, Li Z, Bailleul AM, Wang M and
O'Connor J (2021) Investigating
Possible Gastroliths in a Referred
Specimen of *Bohaiornis guoi* (Aves:
Enantiornithes).
Front. Earth Sci. 9:635727.
doi: 10.3389/feart.2021.635727

Gastroliths, where preserved, can provide indirect evidence regarding diet in extinct avian and non-avian dinosaurs. Masses of gastroliths consistent with the presence of a gastric mill are preserved in many Early Cretaceous Jehol birds mostly belonging to the Ornithuromorpha. Gastroliths are also present in basal birds *Sapeornis* and *Jeholornis* in which herbivory is supported by direct evidence these taxa consumed seeds in the form of crop or stomach contents. Although gastroliths have been correlated with herbivory in non-avian dinosaurs, the presence of gastroliths and bone together in *Ambopteryx* calls this association in to question. Despite being known from greater numbers of specimens than other avian lineages, no unequivocal direct or indirect evidence of diet has been recovered from Jehol deposits for the Enantiornithes. A referred specimen of *Bohaiornis guoi* IVPP V17963 was described as preserving a small number of gastroliths interpreted as rangle, gastroliths whose function is cleaning the stomach in extant raptorial birds. However, based on comparison with gastroliths in other Jehol birds, it has alternatively been suggested that the identified structures are not ingested stones at all but some unusual mineral precipitate. Considering the limited evidence regarding diet in Enantiornithes and the importance of accurately identifying the traces in *Bohaiornis* in order to understand the enantiornithine digestive system, we extracted two samples of these purported gastroliths and explored these traces using computerized laminography scanning, scanning electron microscopy, energy dispersive x-ray spectroscopy, ground sections, and body size to gastral mass regressions. Similar analyses were conducted on gastroliths extracted from undisputed gastral masses of two Jehol ornithuromorphs and the non-avian pennaraptoran *Caudipteryx*. The combined results contradict the hypothesis that these traces are gastroliths and supports the interpretation they are mineral precipitate, most likely authigenic quartz (chalcedony). Although authigenesis is commonly responsible for the preservation of soft tissues, it is unclear if these traces record part of the tissues of this *Bohaiornis*. This study highlights the importance of a multidisciplinary approach in understanding unusual traces in the fossil record and reveal a previously unidentified taphonomic phenomenon in fossils from Jehol deposits.

Keywords: gastrolith, Enantiornithes, SEM, rangle, authigenic mineral, siliceous mineral, EDS

INTRODUCTION

The digestive system of living birds is highly modified to meet the high caloric demand of flight within an aerodynamically light weight structure (Gill, 2007). Highly efficient food processing capabilities provide birds with the necessary calories to support powered flight, the most energetically costly form of vertebrate locomotion. The neornithine digestive system is characterized by several unique features not found in crocodylians, the other extant clade of archosaurs: many modern birds possess a crop, an expansion of the esophagus used to temporarily store excess food; and the stomach is divided into two chambers (Gill, 2007). The cranial chamber, the proventriculus, produces acid to dissolve ingested items, and is especially large in carnivorous raptorial birds who chemically digest their food. The caudal chamber, the ventriculus or gizzard, in many taxa has a specialized grinding function in which a large number of stones are intentionally ingested to aid in the digestion of hard food items (e.g., seeds, insects) forming a structure referred to as a gastric mill (Duke, 1986). Notably, although raptorial birds lack a gastric mill, they have also been observed intentionally ingesting stones (Albuquerque, 1982). This small number of stones is referred to as *rangle* and is thought to help clean the digestive system (Fox, 1976).

Most data currently available concerning the diversity and physiology of Cretaceous birds comes from the Lower Cretaceous volcanoclastic Jehol deposits in north-eastern China (Xu et al., 2020). These Lagerstätten have produced an abundance of fossil birds whose small and hollow bones only rarely survive diagenesis in most other depositional environments. Most reported specimens are largely complete and articulated and many preserve rare traces such as soft tissues (e.g., feathers, lungs, ovarian remains) (Ji et al., 1998; O'Connor et al., 2013; Wang et al., 2018) and ingested remains (e.g., stomach and crop contents) (Zheng et al., 2011; O'Connor, 2019).

Large numbers of gastroliths preserved in the abdominal cavity of some dinosaur groups suggests these taxa had evolved a gastric mill (Ji et al., 1998; Zhou and Wang, 2000; Ji et al., 2003; Wings, 2007; Cerda, 2008; Varricchio et al., 2008; Xu et al., 2009; Makovicky et al., 2011; Choiniere et al., 2012; Wang et al., 2019). The phylogenetic distribution of these groups suggests that the two-part stomach evolved early in the Dinosauria. Large clusters of gastroliths consistent with their identification as gizzard stones forming a gastric mill have been described in the long bony tailed bird *Jeholornis* (O'Connor et al., 2018), the basal pygostylian *Sapeornis* (Zhou and Zhang, 2003; Zheng et al., 2011), and numerous Jehol ornithuromorphs (e.g., *Archaeorhynchus*, *Eogranivora*, *Bellulornis*, *Changzuornis* and *Iteravis*) (Zhou and Zhang, 2006; Zhou et al., 2013; Zhou et al., 2014; Wang et al., 2016b; Huang et al., 2016; Wang and Zhou, 2016; Wang et al., 2018; Zheng et al., 2018). Interpretations that gastral masses were utilized to digest hard plant material is supported by direct evidence of ingested seeds in three lineages (*Sapeornis*, *Jeholornis*, and *Eogranivora*) (Zhou and Zhang, 2002; Zheng et al., 2011; O'Connor et al., 2018; Zheng et al., 2018). However, ornithuromorphs preserve a diversity of gastral mass morphotypes and the presence of gastroliths and an herbivorous

diet may not strictly correlate in this clade, as is true of Neornithes (O'Connor, 2019). This is somewhat supported by a pellet apparently containing bone found associated with the holotype of *Iteravis* (O'Connor and Zhou, 2019).

Enantiornithines are considered the dominant clade of Cretaceous land birds (O'Connor, 2009; O'Connor et al., 2011; Wang and Zhou, 2017a). Specimens referable to this group account for approximately half of all known Cretaceous birds. Although they have a global distribution being recovered from every continent with the exception of Antarctica (O'Connor et al., 2011), the largest source of enantiornithine fossils is the Jehol Biota, where hundreds if not thousands of specimens have been collected (Zhou, 2006). The remains of enantiornithines in the Huajiyi Formation, the oldest geologic unit preserving the Jehol Biota, represents their earliest known record (Wang et al., 2017); the diversity of enantiornithines increases in younger deposits of the Jehol Biota, being most diverse in the Jiufotang Formation (Wang and Zhou, 2017b).

The most diverse clade of enantiornithines is the Bohaiornithidae, which includes six taxa: *Bohaiornis guoi*, *Paraboaiornis martini*, *Shenqiornis mengi*, *Sulcavis geeorum*, *Longsunguis kurochkini*, and *Zhouornis hani* (Wang et al., 2010; Wang et al., 2014; Zhang et al., 2014; Li et al., 2015). This group is characterized by their fairly large size, robust dentition, and large pedal claws.

Exceptional specimens from the Jehol Biota have allowed scientists to begin to reconstruct the structure of the digestive system in basal birds. These specimens indicate that a digestive system similar to Neornithes (modern birds) in terms of structure and digestive abilities is present in the Ornithuromorpha (O'Connor, 2019). With the exception of the fact teeth are retained by some taxa, the digestive system of Jehol ornithuromorphs appears similar to that of modern birds in the presence of crop and grinding gizzard and the capacity for bidirectional peristalsis including the regurgitation of pellets (Wang et al., 2016a; Zheng et al., 2018).

No unequivocal record of gastrolith use in the Enantiornithes exists so far. The only described specimen purportedly preserving this feature is a referred specimen of *Bohaiornis* IVPP V17963 (Li et al., 2015). This specimen preserves two small masses of rounded objects that are superficially similar to gastroliths (Figures 1A,C). Based on their small size and low number, Li et al. (2015) interpreted these traces as gastroliths and likened them to *rangle*, the small numbers of stones intentionally ingested by extant raptorial birds (Fox, 1976; Li et al., 2015). However, based on comparison with gastroliths preserved in other Jehol birds, O'Connor (2019) argued that these traces did not represent stones but rather some strange form of mineral precipitate (O'Connor, 2019). Understanding these traces will lead to a better understanding of diet, behavior, and digestive function in enantiornithines. In order to test these two competing hypotheses, we utilized scanning electron microscopy (SEM), energy dispersive spectroscopy (EDS), traditional histology, computed laminography (CL) and the relationship between body mass and gastrolith mass in birds to further investigate the identity of the purported gastroliths in *Bohaiornis* IVPP V17963.

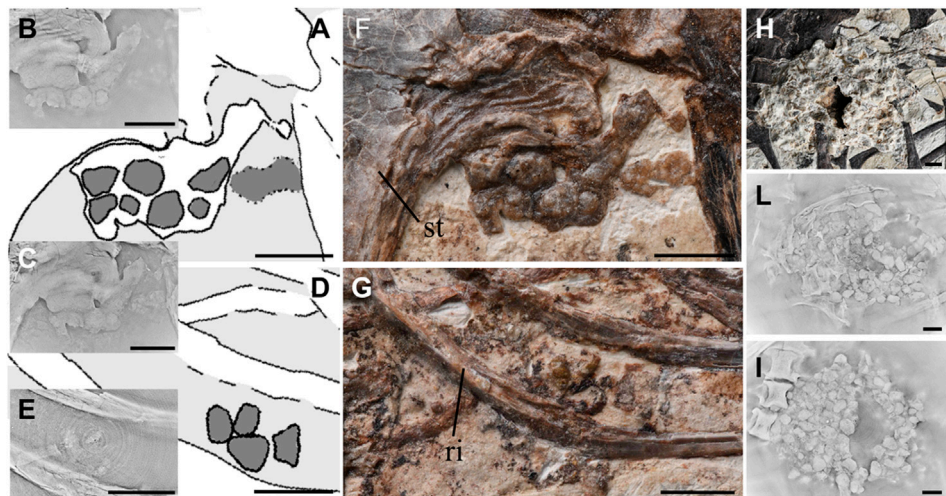


FIGURE 1 | Description and comparison of purported gastroliths and true gizzard stones further illuminated with the aid of CL. (A,D). Line drawing from Li et al. (2015) of the purported gastroliths of *Bohaiornis* IVPP V17963 near the sternum (A) and between the thoracic ribs (D) (Li et al., 2015); (B,C). CL scans results of gastroliths depicted in (A) from two different levels showing the interconnectedness of the purported gastroliths; (E). CL scans result corresponding to (D) depicting the weak impressions of the purported gastroliths; (F). Photograph of purported gastroliths of *Bohaiornis* IVPP V17963 near the sternum; (G). Photograph of purported gastroliths of *Bohaiornis* IVPP V17963 between two thoracic ribs; (H). Photograph of the gastral mass preserved *Archaeorhynchus* IVPP V17075; (L,I). Two location of CL scans corresponding to (H), both revealing distinctly separated individual gastroliths. Anatomical abbreviations: st, sternum; ri, rib. Scale bar equals five millimeters.

METHODS

Bohaiornis IVPP V17963 was studied first under direct observation and then CL scanned at $7.83\ \mu\text{m}$ resolution using the Xm-Tracer-CL-160 at the Institute of Vertebrate Paleontology and Paleoanthropology (IVPP). Two samples of the purported gastroliths were then extracted for additional analysis. Definitive gastroliths from *Archaeorhynchus* IVPP V17075 were also CL scanned at $18.71\ \mu\text{m}$ resolution. Gastroliths were extracted from *Archaeorhynchus* IVPP V17075, *Iteravis* IVPP V23346 and *Caudipteryx* STM (Shandong Tianyu Museum of Nature) 4–5 for detailed comparative analysis.

GROUND-SECTIONING Ground sections were made from the extracted gastroliths of all four specimens.

All extracted gastrolith samples were embedded in EXAKT Technovit 7,200 1-component resin, placed in a vacuum for 1 h to remove bubbles, and then cured for a minimum of 8 h in the EXAKT Technovit 7,200. The resin blocks were cut using an EXAKT 300CP accurate circular saw. The samples were then ground down using 500# sand paper until the sample was exposed and then polish with 4,000# sand paper, both using the EXAKT 400CS grinding system.

The blocks were placed back in the vacuum for 5 min after which they were adhered to slides and placed under UV light for 10 min. The slides were further polished until the desired optical contrast was reached at approximately $45\ \mu\text{m}$ thickness.

The slides were observed using a Leica DM-RX polarized light microscope under both normal and polarized light. Pictures are taken with a DS-Fi3 camera using the software NIS-Element v4.60.

SEM-EDS SEM images were taken using the Merlin Compact Ultra-high resolution field scanning electron microscope at the

Chinese Academy of Geological Sciences (Beijing, China) using FEI Quanta 450 (FEG) at 20 kv. Samples were coated in gold prior to imaging and EDS line scanning and mapping scanning.

Body:gastrolith mass correlation Measurements of *Bohaiornis* IVPP V17963 were taken from Li et al. (2015). The regression formula for estimating birds body mass was adopted from Serrano et al. (2015). Correlations between body mass and gastrolith mass in birds were taken from Wings (2007). Numerous methods for estimating body mass of stem birds have been developed (Butler and Goseami, 2008; Liu et al., 2012; Field et al., 2013; Serrano et al., 2015; Serrano et al., 2016). The methods by Serrano et al. (2015) utilized data acquired from modern birds to build multiple regression functions for each of the major stem avian lineages. This model has greater predictive strength and applicability (Serrano et al., 2015). We used the regressions of Serrano et al. (2015) to estimate the body mass of *Bohaiornis* IVPP V17963 in order to determine if the purported gastroliths are proportionate to the bird's body mass (Table 1).

RESULTS

Raw Morphology

As described by Li et al. (2015), *Bohaiornis* IVPP V17963 preserves a small number of stone-like objects in two clusters: one located near the sternum and the other between two thoracic ribs approximately level with the cranial end of the synsacrum (Figure 1) (Li et al., 2015). The color of these purported gastroliths is a dark brown (Figures 1F,G) that is very similar to the bone preserved in *Bohaiornis*, which is unusual when

TABLE 1 | Data and formula to calculate the body mass of *Bohaiornis guoi* IVPP V17963.

| Data needed of bone | Full name of bone | Length (mm) | Log (length) | References |
|-------------------------------|------------------------------------------------------------------------------------------------------------------------------------------------------------------|-------------|--------------|------------------------|
| HL | Length of humerus | 51.95 | 1.715585552 | (Li et al., 2015) |
| bcL | Length of bicipital crest | 7.63 | 0.882524538 | |
| dHW | Dorsoventral width of distal humerus | 4.4 | 0.643452676 | |
| UL | Length of ulna | 52.39 | 1.719248398 | |
| dUW | Craniocaudal width at midshaft of ulna | 4.24 | 0.627365857 | |
| TL | Length of tibiotarsus | 51.25 | 1.70969387 | (Serrano et al., 2015) |
| Multiple regression functions | $\log BM = \log a + b_1 \log x_1 + b_2 \log x_2 \dots + b_p \log x_p$ | | | |
| Enantiornithes | $-2.626 (\pm 0.284) + 1.528 (\pm 0.436) HL + 0.34 (\pm 0.312) bcL + 0.828 (\pm 0.427) dHW - 1.451 (\pm 0.386) UL + 0.811 (\pm 0.448) dUW + 0.378 (\pm 0.201) TL$ | | | |

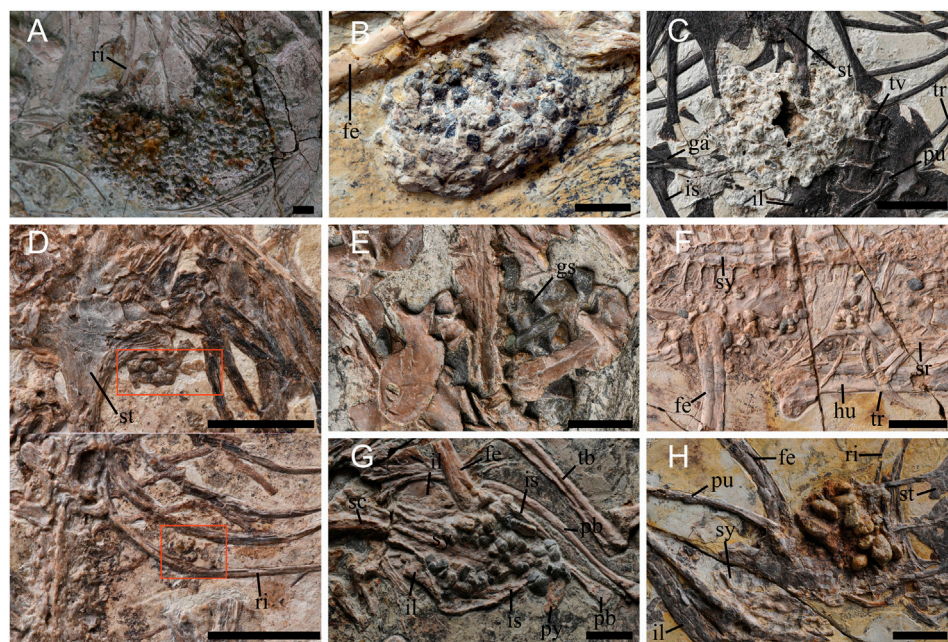


FIGURE 2 | Comparison of purported gastral masses in Early Cretaceous Jehol paravians and birds. (A). *Caudipteryx* STM4-5 (Oviraptorosauria); (B). *Jeholornis* STM2-15 (Jeholomithiformes); (C). *Archaeorhynchus* IVPP V17075 (Ornithuromorpha); (D). *Bohaiornis* IVPP V17963 (Enantiornithes); (E). *Iteravis* IVPP V23346 (Ornithuromorpha); (F). *Archaeorhynchus* IVPP V14287 (Ornithuromorpha); (G). *Dingavis* IVPP V20284 (Ornithuromorpha); (H). *Bellulornis* IVPP V17970 (Ornithuromorpha); Anatomical abbreviations: fe, femur; ga, gastralia; gs, gastroliths; hu, humerus; il, ilium; is, ischium; pb, pubes; pu, pubis; py, pygostyle; ri, rib; sc, scapula; sr, sternal rib; st, sternum; sy, synsacrum; tb, tibiotarsus; tr, thoracic rib; tv, thoracic vertebra. Scale bar equals 1 cm.

compared to other gastral masses found in Jehol birds in which the gastroliths are often a range of colors and are typically clearly distinct from the color of the fossilized bone (Figure 2). The purported gastroliths near the sternum superficially appear to be very rounded and circular.

When observing the mass of purported gastroliths adjacent to the sternum, two spherical structures are visible just below the purported caudal margin of the sternum. These are clearly visible under direct observation (Figure 1A) and in some CL scan slices (Figure 1B). An additional two slightly smaller spherical structures are visible below the two larger structures (Figure 1A) but again are not visible in all CL slices (Figure 1C). The CL data reveals that all of the purported gastroliths are connected, in some cases even with

areas adjacent that were previously interpreted as bone continuous with the sternum. Although superficially circular structures are visible, these represent areas of higher relief and upon closer examination the purported gastroliths from a large amorphous structure that varies in thickness, without distinct boundaries (Figures 1A,C). This includes areas located adjacent to the purported gastroliths that were not identified as gastroliths by Li et al. (2015), but exhibit a similar morphology both through direct observation and in the CL scans (Figures 1A,C) suggesting they have a similar taphonomic origin.

The group of purported gastroliths located between two thoracic ribs are smaller and ill defined (Figure 1D). They are only faintly visible in the CL scans (Figure 1E). These more distally

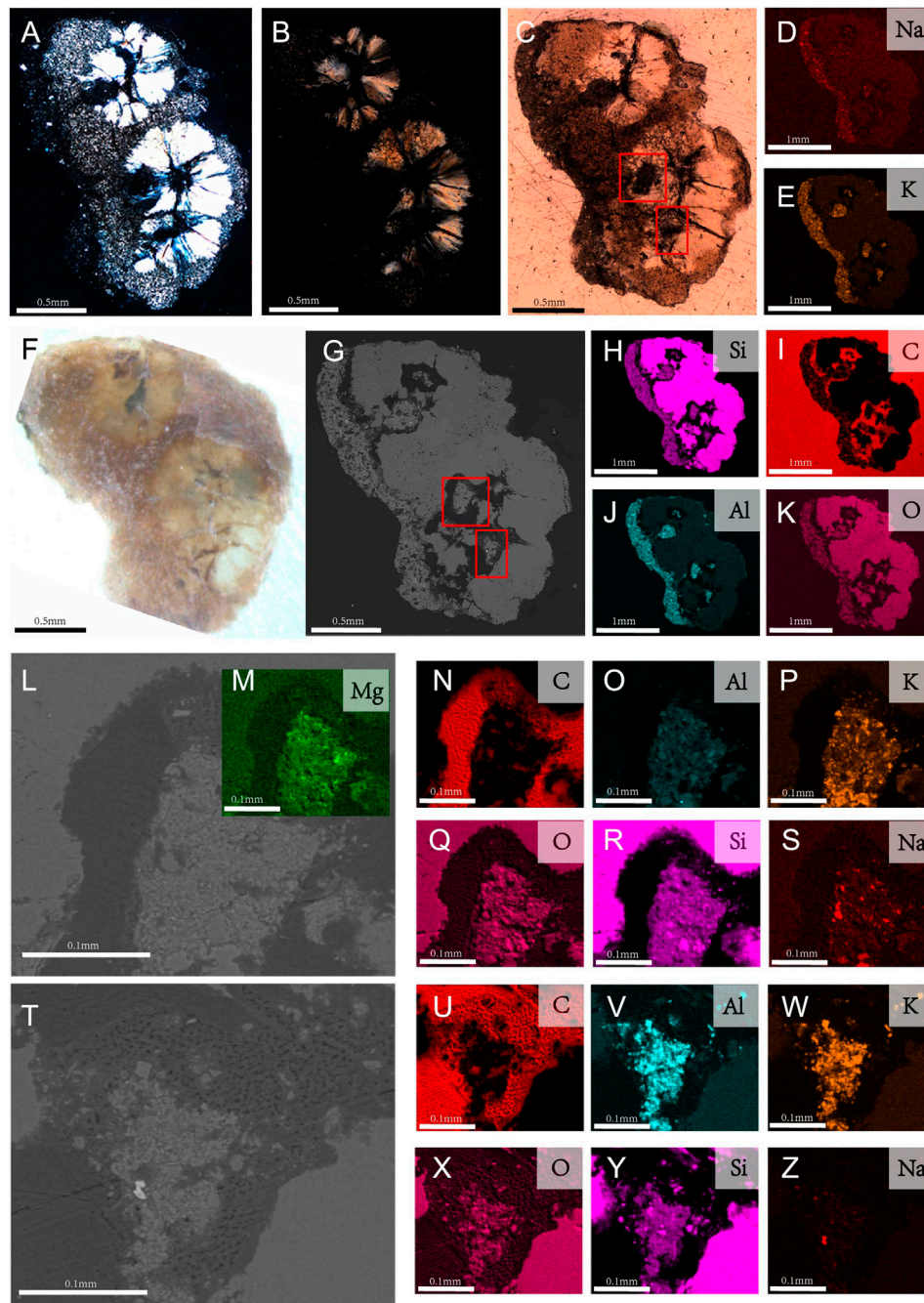


FIGURE 3 | Lithology results and EDS element mapping of the ground-sections of the purported gastroliths of *Bohaiornis guoi* IVPP V17963. **(A,B)**. Photographs under polarized light through microscope; **(A)**. In high brightness; **(B)**. In low brightness; **(C)**. Photograph under natural light; **(D,E,H-K)**. Elemental mapping results of the whole slide. Its major elements include sodium (Na), potassium (K), silicon (Si), carbon (C), aluminum (Al), oxygen (O); **(F)**. Photograph under Stereo Microscope; **(G)**. SEM photograph. **(I-Z)**. Close up photographs of intermediate region of purported gastroliths; Close up regions **(L,T)** are the regions boxed in **(C,G)**. **(M-S)**. Elements mapping of **(L)**; **(U-Z)**. Elements mapping of **(T)**.

located purported gastroliths are much thinner (visible in 55 CL slices) compared to those near the sternum (visible in 164 slices).

In comparison, gastroliths preserved in *Archaeorhynchus* IVPP V17075 (**Figures 1F-H,2C**) form a tight circular aggregate and are embedded in some matrix that has not been

prepared away to completely reveal the surfaces of the gastroliths, as in some other specimens (*Archaeorhynchus* IVPP V17091). The individual stones can be seen readily distinguished in the CL scans. The white material surrounding the gastroliths has a lower density compared to the gastroliths themselves.

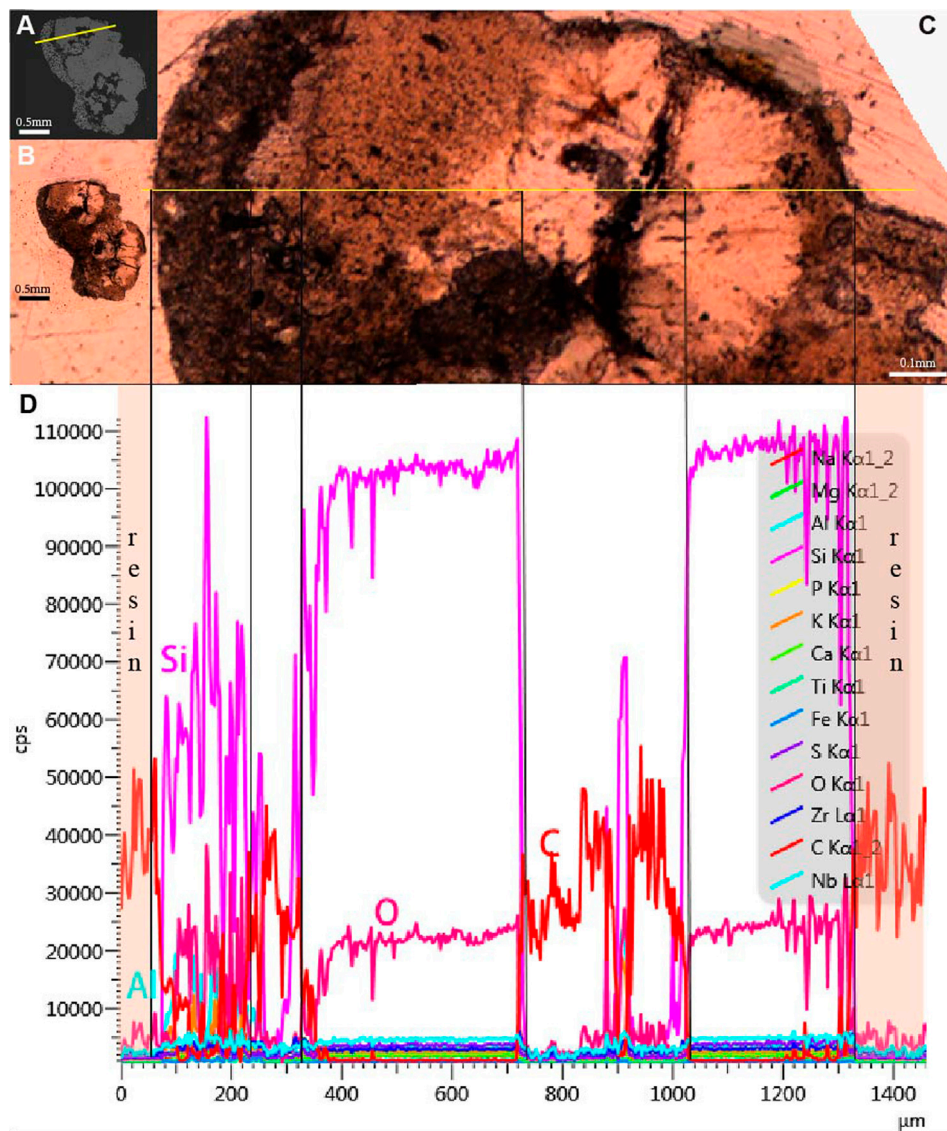


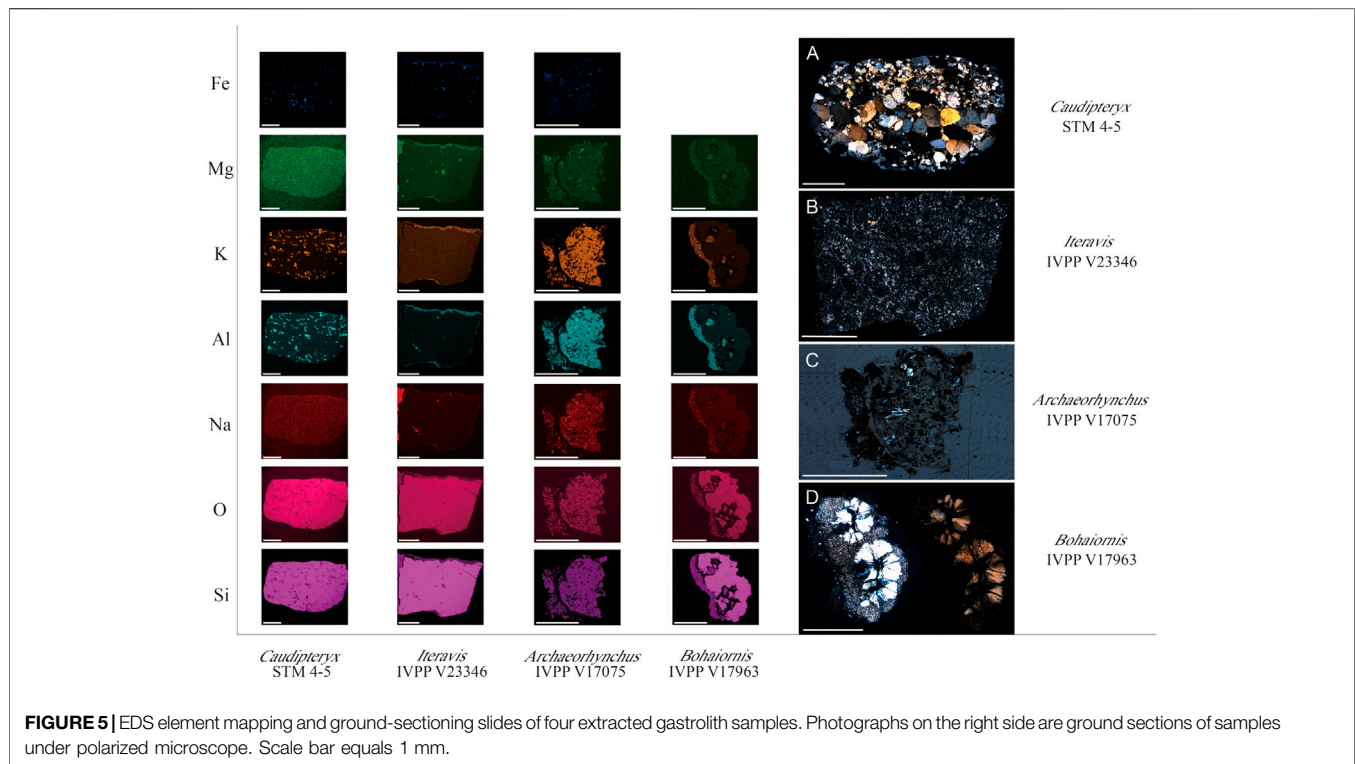
FIGURE 4 | EDS profile of the purported gastroliths extracted from *Bohaiornis guoi* IVPP V17963. **(A)**, SEM photograph with yellow line indicating where the EDS profile was taken; **(B)**, Ground section under microscope with natural light; **(C)**, Enlargement of the cross-section marked in A with the cross-section leveled horizontal; **(D)**, The EDS profile of the line marked in A and C revealing the chemical composition of major elements of the sample in counts per second (cps). Content of Si, O in the interior part are higher than that in the exterior part and in the intermediate region. Content of C in the intermediate region are the same as that of the resin.

The morphology of the gastroliths in *Caudipteryx* STM4-5 (**Figure 2A**) are similar to those preserved in *Archaeorhynchus* IVPP V17075, although much of the fine-grained white material in which the *Archaeorhynchus* gastroliths are embedded has been removed, presumably during mechanical preparation in order to expose the surface of the gastral mass. The mass is crescent-shaped with the convex margin facing the ventral surface of the body and a mineralized reddish layer covers parts of the exposed surface. Gastroliths in *Iteravis* IVPP V23346 (**Figure 2E**) are scattered—not preserved in close association with each other forming an aggregate. The individual gastroliths are black, polished, and mostly subrounded to rounded with moderate sphericity, although

some gastroliths exhibit a subrectangular morphology. The same morphology is observed in *Dingavis* IVPP V20284 (Zhou et al., 2014).

Analyses of Purported Gastroliths of *Bohaiornis guoi* IVPP V17963

Two purported gastroliths, revealed by CL scans to be connected, were extracted and cut into ground sections (**Figures 3A,B,F**). The ground sections reveal that the two circular structures, with diameter of 0.683 mm and 0.793 mm respectively, each consist of fibral-like chalcedony (**Figures 3H,K**) in a spherulitic arrangement which are embedded in a microcrystalline matrix



(Figures 3A,B). The fibers radiate from the central dark region, forming four to five petal-shaped crystals (Figure 3C). The circular structures exhibit order I aurantium of the highest interference color and the fibers exhibit radiated extinction under cross polarized light (Figures 3A,B). The outer region lining one margin of the quartz spherulites consists of a fine-grained matrix (Figure 3C).

The purported gastroliths are embedded in carbon (C) resin (Figure 3I). Carbon can also be observed within the purported gastroliths which may suggest some original organic material formed the nucleus on which the quartz fibers precipitated (Figures 3I,N,U). However, the possibility that the C in the intermediate region is resin that permeated into the sample during ground-sectioning can't be excluded (Figure 3). The EDS profile of the purported gastroliths may support interpretations that the C in the internal region is from the resin because it shows the same high content of C as the resin surrounding the sample (Figure 4). However, the fact that light does not penetrate these regions as it does in the resin surrounding the sample may support the alternative hypothesis that the C is original organic material. This internal C surrounds small pockets that contain Magnesium (Mg), Aluminium (Al), Potassium (K), and traces of Sodium (Na) in addition to Silica (Si) and Oxygen (O) (Figures 3M–Z). The microcrystalline region that forms the left outer margin of the two purported gastroliths (as pictured in Figure 3) similarly contains Aluminum (Al), Potassium (K), and traces of Sodium (Na) in addition to Silica (Si) and Oxygen (O) (Figures 3D,E,H,J,K). Despite their similar element content, the morphology of the inner pockets and the outer left margin under the microscope are completely different with the inner pockets being black in thin

section, without light passing through, whereas the external margin has a microcrystalline morphology.

Analyses and Comparison of Paravian Gastroliths

The gastrolith ground section from *Caudipteryx* STM4-5 was identified under the microscope as fine-grained sandstone, which consists of small quartz particles and a minor portion of mica (Figure 5A). The long axis of mineral particle size ranges from 0.1 mm to 0.4 mm. The quartz particles are characterized by an order I yellowish white interference color and parallel extinction in cross polarized light. The gastrolith extracted from *Iteravis* IVPP V23346 was identified as consisting entirely of quartzite, with the main minerals being quartz and the main component being cement (Figure 5B); the long axis of the mineral particle size measures approximately 0.025 mm, and minerals exhibit an even distribution with quartz accounting for approximately 50%. The gastrolith extracted from *Archaeorhynchus* IVPP V17075 was identified as an igneous rock containing feldspar and biotite, with a porphyritic structure (Figure 5C); the main body of gastrolith is groundmass with serious weathering traces and some brownish substances. Minerals show order I white of the highest interference color and oblique extinction in cross polarized light. These features indicate that their source is probably weathered basalt.

The elemental composition of the gastrolith from *Caudipteryx* STM4-5 has an even distribution from the interior to exterior. The gastrolith primarily consists of Si, O and Na, with smaller amounts of Al, K, Mg and Fe (Figure 5A). The gastrolith

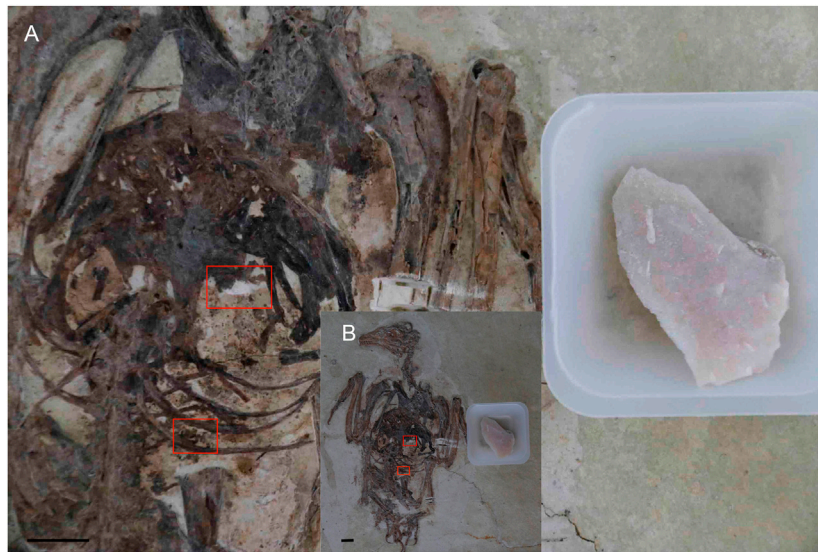


FIGURE 6 | Volume comparison between the purported gastroliths of *Bohaiornis guoi* IVPP V17963 and a 3.09 g piece of chert. Red rectangle indicates areas where the purported gastroliths occur. **(A)** close up photograph; **(B)** photograph of the entire specimen. Scale bar equals 1 cm.

extracted from *Iteravis* IVPP V23346 mainly contains Si and O, with small amounts of Na, Al, Mg and Fe. Some regions along the edge form a thin layer that contains less Si and O and more Al, Mg and Na compared to the main body of the gastrolith. The *Archaeorhynchus* IVPP V17075 gastrolith is also composed primarily of Si and O, with Al, Mg, Na and K content higher than that of the other gastroliths studied here (**Figure 5C**).

EDS indicates the most common elements among the four samples analyzed here are Si and O, which have the highest content of all the identified elements in all the studied samples. Gastroliths of *Caudipteryx* STM4-5 and *Iteravis* IVPP V23346 are rock types in which quartz is the main component. The gastrolith of *Archaeorhynchus* IVPP V17075 is an igneous rock composed of Si and O. All samples also contain Na, Al, K and Mg. The samples from *Iteravis* IVPP V23346 and *Bohaiornis* IVPP V17963 both exhibit an outer layer on some margins that has a higher content of Mg, K, Al, and Na compared to the main body of the gastrolith. None of the true gastroliths show similar internal structures high in C and other minerals like that observed in the purported gastroliths extracted from *Bohaiornis*.

Size Correlation

The body mass of *Bohaiornis* IVPP V17963 is estimated to be approximately 308 g based on measurements in Li et al. (2015). Published data indicates that gastroliths mass account for 1% of the body mass, so the gastroliths of *Bohaiornis* should measure 3.08 g (Wings, 2004). Reports of range in New Zealand falcons (*Falco novaeseelandiae*) indicate the stones account for about 3.3% of the body mass in females and 3.0% in males (Fox, 1976). This would suggest that if the purported gastroliths in *Bohaiornis* IVPP V17963 represent range they should have a mass of approximately 10.14 g. Since the entire purported gastral mass of *Bohaiornis* could not be extracted, we compared the mass in

the fossils to a piece of chert (**Figure 6**). The chemical composition of chert is mainly Si and O, which has a density of 2.53 g/cm^3 which is higher than that of pure quartz. The chert sample weighing 3.09 g is much bigger than the combined volume of the purported gastroliths, which suggests the weight of purported gastroliths are far less than 3.08 g. Therefore, the purported gastroliths do not satisfy the relationship ratio between gastrolith mass and body mass, either as range or as gizzard stones.

It is possible that the preserved mass of “purported gastroliths” is incomplete and that some gastroliths were taphonomically lost. However, even to meet 1% of the body mass (one third the expected mass if these traces are indeed range), the purported gastral mass would have to be several orders of magnitude greater. Such a loss of gastrolith mass is highly unlikely in light of the fact that *Bohaiornis* IVPP V17963 is largely complete, even preserving delicate bones like gastralia (Li et al., 2015), and articulated, suggested minimal disruption of the carcass after death, consistent with a majority of described specimens from the Jehol, which are preserved in a static (low energy) lacustrine environment (Zhang and Miman, 2003).

DISCUSSION AND COMPARISON

Despite the large number of recovered specimens, traces of diet in enantiornithines (Aves: Ornithothoraces) are very rare (Sanz et al., 1996; Dala Vecchia and Chiappe, 2002; Cau and Arduini, 2008; Li et al., 2015; Wang et al., 2016a). Such traces have only been reported in two Jehol specimens both of which have subsequently been questioned in the literature (O'Connor, 2019; O'Connor and Zhou, 2019). Structures in *Bohaiornis* IVPP V17963 identified as gastroliths ingested for use as range, a

specific form of gastral mass utilized by raptorial birds to clean the digestive system (Li et al., 2015), were alternatively interpreted as some form of mineral precipitate (O'Connor, 2019). In order to shed new light on this academic debate, we utilized numerous methods including CL scans, ground-sections, lithology analysis, and SEM-EDS on samples extracted from IVPP V17963 and two other Jehol birds (*Iteravis* IVPP V23346 and *Archaeorhynchus* IVPP V17075) and one non-avian pennaraptoran (oviraptorosaur *Caudipteryx* STM4-5) with distinct masses of gastroliths interpreted without controversy as forming a gastric mill. We consider the various lines of evidence independently below.

Anatomical Location

The preserved location of the purported gastral mass in *Bohaiornis* IVPP V17963 is consistent with their original identification that they are ingested stones. The purported gastroliths occur in two places, one patch along the caudal margin of the sternum and a second patch more distally located between two thoracic ribs, approximately level with the cranial margin of the synsacrum. This is generally consistent with the position of the stomachs. If these two patches are mineral precipitate, the mechanism responsible for the silicification of only these two small patches of soft tissue and the tissues they may represent are equally unknown.

Comparison of Gastral Mass and Macroscopic Gastrolith Morphology

Superficially, gastral mass morphology in Jehol paravians can be roughly divided into three types: 1) a large number of proportionately small gastroliths that are tightly aggregated together, presumably held together by stomach contents due to the tightly packed nature of their association *in vivo*—this morphology is observed in *Caudipteryx* (Figure 2A) (Ji et al., 1998; Zhou and Wang, 2000; Zhou et al., 2000), *Jeholornis* (Figure 2B) (O'Connor et al., 2018), and *Archaeorhynchus* (STM7-11, IVPP V17075, IVPP V17091) (Zhou et al., 2013; Wang et al., 2018); 2) a small number of proportionately larger stones found in loose association—this morphology is observed in *Iteravis* IVPP V23346 (Figure 2E), *Dingavis* IVPP V20284 (Figure 2G) (O'Connor et al., 2016) and *Hongshanornis* DNHM D2945 (Chiappe et al., 2014); and 3) a small number of proportionately larger stones preserved tightly compacted together, protruding from the surface of the slab—this morphology is observed in *Bellulornis* IVPP V17970 (Figure 2H) (Wang et al., 2016b). In addition, this gastral mass morphology is also found in *Gansus yumenensis* (Wang et al., 2015) from the Early Cretaceous Xiagou Formation in Gansu Province, northwestern China.

The purported gastroliths in *Bohaiornis* IVPP V17963 are few in number and proportionately smaller, not fitting any of the gastral mass morphology types described above. As observed by O'Connor (2019), they are morphologically distinct from gastral masses preserved in other Early Cretaceous birds (O'Connor, 2019). However, the purported gastral mass in *Bohaiornis* IVPP V17963 was interpreted as rangle, which is morphologically

distinct from gastral masses in herbivorous and omnivorous birds. Thus the, unusual size of the gastral mass does not exclude the original interpretation from being a viable hypothesis. However, although reported by Li et al. (2015) that the amount of stones ingested is typically very small, literature suggests otherwise; rangle reportedly forms a greater percentage of body mass (3–3.3%) (Fox, 1976) than normal gizzard stones (1%) (Wings, 2004). Thus, if these percentages are correct, the size of the mass of purported gastroliths is inconsistent with their interpretation as rangle.

However, upon closer inspection the shape of the purported gastroliths is unusual for gizzard stones. Some of the purported gastroliths superficially appear spherical in shape, similar to the rounded to subrounded gastroliths found in *Caudipteryx*, Mesozoic birds like *Iteravis* and *Archaeorhynchus*, and neornithines. However, closer examination reveals that the purported gastroliths are actually more similar to circular discs, being very thin, and the two superficially separated circular structures in fact form one amorphous structure connected by thinner regions of mineral that lack the spherulitic structure of the silica fibers and contain higher elemental diversity. This connection is visible both in the CL data and in the ground sections. In contrast, although the gastroliths in *Archaeorhynchus* IVPP V17075 are bound together by matrix, the individual gastroliths can be readily distinguished as separate structures in the CL data (Figure 1B). The purported gastroliths located between the two thoracic ribs form only weak impressions (Figures 1D,E) and it is unclear if these are indeed similar structures to the purported gastroliths near the sternum.

Among the purported gastroliths indicated by Li et al. (2015), closer inspection of *Bohaiornis* IVPP V17963 reveals that one is very thin and amorphous, two are thicker and still amorphous, and two, including the sample extracted for analysis, contain within their margins two circular areas of higher relief connected by thinner areas, one forming an overall amorphous shape and the other together forming a subspherical shape (Figure 1).

Gastrolith Lithology Comparison

EDS of the extracted purported gastrolith ground section reveals that the circular structures are silica (SiO₂) fibers in a spherulitic arrangement (Figure 3). The thinner areas connecting these spherules show a more diverse elemental composition, additionally contain Al, K, Na, and small amounts of Mg. Small regions near the center of the quartz spherules show similar elemental compositions (Figures 3, 5). In addition, regions within the spherules appear to contain organic remains as indicated by the presence of C, suggesting the quartz spherules are authigenic. However, at this time we cannot rule out the possibility that the C is contaminant originating from the resin (Figure 4).

Three gastrolith samples were extracted from undisputed gastral masses belonging to both birds (*Iteravis* IVPP V23346 and *Archaeorhynchus* IVPP V17075) and a non-avian dinosaur (*Caudipteryx* STM4-5) for comparative analysis. Elemental and lithological analysis indicate they are also siliceous rocks composed mainly of quartz. Quartz is a hard, relatively

TABLE 2 | Evidence in support of the two competing hypothesis.

| | Gastroliths | Authigenic mineralization |
|-----------------------------------------|--------------------------------------------------------------------------------------------------------------------------------------|----------------------------------------------------------------------------------------------------------------------|
| Location | Identified masses are roughly preserved in the correct anatomical location to be interpreted as ingested gastroliths in the stomach. | Soft tissues that could serve as nucleation points occur throughout the body |
| Chemical composition and microstructure | The purported gastroliths are siliceous, composed primarily of Si and O, consistent with birds gastroliths in modern birds. | Radiating quartz fibrils not found in other studied gastroliths |
| Zonation | <i>Iteravis</i> IVPP V23346 shows similar zonation in chemical composition with external region of higher elemental diversity. | <i>Bohaiornis</i> IVPP V17963 unique in having an internal zone of elemental diversity as well as the presence of C. |
| Macrostructure | Superficially circular | Purported gastroliths connected, forming a single, thin, amorphous structure |
| General shape | | Thickened regions interpreted as individual gastroliths highly irregular in morphology |
| Thickness | | Extremely thin in some regions |
| Gastral mass composition | | Purported gastroliths lack diversity observed in true gastral masses |
| Gastral mass: body mass | | Total mass is far less than 1–3% body mass estimated for true gizzard stones and rangle |

insoluble mineral that retains its angularity until completely ground to a powder (Meinertzhagen, 1954). The fact quartz predominates in the gizzard of extant birds reflects the requirement of gizzard stones that they be insoluble to survive the acid environment of digestive system and hard to resist gastrolith on gastrolith abrasion and thus serve to better grind ingested remains for longer periods of time (Gionfriddo and Best, 1999). These results indicate that the preference for siliceous rocks for ingestion as gastroliths is extended to Mesozoic birds.

Detailed chemical EDS analysis revealed compositional zonation in the purported gastroliths of *Bohaiornis*. Zonation is also somewhat present in the gastrolith of *Iteravis* IVPP V23346 in that along the exterior of one margin of the gastrolith there is a thin layer that shows greater elemental diversity. However, only the sample from *Bohaiornis* has internal zones as well. Observed under the microscope the internal region of *Bohaiornis* IVPP V17963 that contains higher elemental diversity as well as the similarly elementally diverse region also containing C along one margin of the sample both appear much darker than the remainder of the sample. The cause of this zonal structure in *Bohaiornis* IVPP V17963 is unknown. Notably, despite similar results in the EDS elemental mapping, the internal black region of the purported gastroliths in *Bohaiornis* IVPP V17963 appears completely different under the microscope compared to the area external to the quartz spherules that shows similar chemical composition (Figure 3).

Although chemical analyses indicate that the samples from *Bohaiornis* IVPP V17963 and the comparative samples all primarily consist of Si and O, the lithology varies between specimens and the distribution of elements and structure in the purported gastroliths are distinct from the other three samples.

Gastral Mass Proportions

Modern raptors often ingest stones to clean the stomach, which is referred to as rangle (Albuquerque, 1982). The smallest reported diameter of these stones is 7 mm (Fox, 1976). This is much larger than the purported gastroliths in *Bohaiornis* IVPP V17963 which

measure 0.683 mm and 0.793 mm, even accounting for differences in body size between *bohaiornithids* and extant raptors. Rangle mass accounts for approximately 3.3% of the body mass in female New Zealand falcons and 3.0% in males (Fox, 1976). Gastral masses, which consist of gizzard stones (stones used for grinding food as opposed to rangle which is used to clean the stomach), are reportedly proportionately much smaller, forming only 1% predicted of body mass in neornithines (Wings, 2004). The body mass of *Bohaiornis* IVPP V17963 is estimated to be 308 g (Serrano et al., 2015). Compared to both rangle and gastral masses, the purported gastral mass in *Bohaiornis* is very small, much less than the 3.08–10.14 g expected if these indeed represented rangle or gizzard stones. Based on reports from the literature, the diameter of the individual purported gastroliths and their total mass is not comparable to rangle reported in New Zealand falcons. Due to the excellent preservation of *Bohaiornis* IVPP V17963, which is largely complete and articulated, it is unlikely that a large number of gastroliths were originally present and have been subsequently lost during taphonomy.

Mineral Precipitate Origins?

If the structures are not gastroliths ingested for use in the digestive system and indeed some form of mineral precipitate, this begs the question of what conditions produced these structures. Authigenic minerals can be associated with the fossilization of soft tissues (Tomescu et al., 2016). The radially fibrous morphology of the spherulites is consistent with chalcedony. The purported gastroliths record no microstructures identified thus far that would clearly indicate they are silicified soft tissue. However, chalcedony has been reported to replace fossils and to preserve inclusions of original organic material in carbonate rocks (Noble and Stempvoort, 1989) and authigenic quartz is common in organic rich shales (Zhao et al., 2017). The presence of C within the spherules may be indicative of original organic matter, which can reportedly serve as centers of nucleation for authigenic quartz (Noble and Stempvoort, 1989). However, at this time it cannot be ruled out that the C is resin that has somehow infiltrated into the interior of the spherules (Bailleul et al., 2020).

If this is indeed the case, it would indicate that the spherules were not solid, which further suggests that these stones would be unsuitable for use in the digestive system being prone to breaking.

We consider it more likely that this C is original material of *Bohaiornis* IVPP V17963 that has served as a center of nucleation for the precipitation of authigenic quartz in the form of chalcedony. In the absence of histochemical or microstructural data there are numerous candidates for what this tissue may have been based on their anatomical position. It is possible it originated from the m. rectus abdominis that stretched caudally from the sternum, stomach tissue, or epithelium.

CONCLUSION

Further analysis of the purported gastroliths in *Bohaiornis* IVPP V17963 confirms that the traces are unusual when compared to gastroliths found in gastral masses of other Jehol pennraptorans (Table 2). Morphological observation and CL data indicate that the purported gastroliths are interconnected, amorphous in shape with no consistent structure between themselves, and very thin, altogether inconsistent with the morphology of gizzard stones. In addition, the estimated mass of the purported gastroliths is far below that consistent with interpretation they are either gizzard stones or rangle.

Ground sections and EDS reveal that the superficially circular structures of the purported gastroliths are spherulites composed of Si and O. The internal regions of the spherulites and the thin regions connecting them have more diverse elemental compositions forming a zonal morphology in ground section. These structures resemble authigenic quartz. The gastrolith extracted from the oviraptorosaur *Caudipteryx* is fine-grained sandstone; that of *Archaeorhynchus* is volcanic; and that of *Iteravis* is silty mudstone—all stones with high silica content. Zonation similar to that observed in *Bohaiornis* IVPP V17963 is not present in any of the gastroliths with the minor exception of *Iteravis*, in which one margin of the gastrolith preserves a thin layer with similar higher elemental diversity.

Only the chemical composition of the purported gastroliths is consistent with their identification as ingested stones. Consideration of all the new evidence generated from these analyses taken together favors the hypothesis that the

structures in question are not gastroliths. However, as of yet it is unclear what these structures represent or how they formed. Based on the available data we conclude that there is no strong evidence that *Bohaiornis* IVPP V17963 ingested gastroliths to use as rangle similar to extant raptorial birds. However, these unusual interconnected spherulitic quartz structures themselves represent a new structure that deserves further study. The conditions under which these structures formed is as yet unknown. Similar structures may have been overlooked in other specimens. Identification of similar structures in other Jehol fossils and further analysis of these spherulites may shed light on the taphonomic conditions that produced them in the future. However, the fact that such structures have not been widely reported suggests that this is not a common phenomenon. This research represents the first in-depth analysis of gastroliths in Jehol birds using a variety of methods not previously applied to investigate early avian digestive function. This research highlights the importance of a multidisciplinary approach when explore the soft tissue preservation.

DATA AVAILABILITY STATEMENT

The raw data supporting the conclusions of this article will be made available by the authors, without undue reservation.

AUTHOR CONTRIBUTIONS

SL: experiment design; data collection and analysis; manuscript writing. JO'C: designed research; writing and revising the paper. ZL: designed research; provided guidance. AB: data collection. MW: provided specimens.

ACKNOWLEDGMENTS

We thank Wu Qian, Wang Shiyong for useful comments on paper; Cai Jiachen, Zhu Xufeng, Liu Biying for help with mineral identification under microscope; Hou Hongxiang, Zhang Shukang, Fang Gengyu, Wang Xiaomin for help and guidance on experiments; Gao Wei for photographs assistance; Liu Xinzhen for extracting samples.

REFERENCES

- Albuquerque, J. L. B. (1982). Observations on the use of rangle by the Peregrine falcon (*Falco peregrinus tundrius*) wintering in southern Brasil. *Raptor Res.* 16 (3), 91–92.
- Bailleul, A. M., O'Connor, J., Li, Z., Wu, Q., Zhao, T., Martinez Monleon, M. A., et al. (2020). Confirmation of ovarian follicles in an enantiornithine (Aves) from the Jehol Biota using soft tissue analyses. *Commun. Biol.* 3 (1), 399. doi:10.1038/s42003-020-01131-9
- Butler, R. J., and Goswami, A. (2008). Body size evolution in Mesozoic birds: little evidence for Cope's rule. *J. Evol. Biol.* 21 (6), 1673–1682. doi:10.1111/j.1420-9101.2008.01594.x
- Cau, A., and Arduini, P. (2008). *Enantiophoenix electrophyla* gen. et sp. nov. (Aves, Enantiornithes) from the Upper Cretaceous (Cenomanian) of Lebanon and its phylogenetic relationships. *Atti Soc. it. Sci. nat. Museo civ. Stor. nat. Milano* 149 (2), 293–324.
- Cerda, I. A. (2008). Gastroliths in an ornithomimid dinosaur. *Acta Palaeontol. Pol.* 53 (2), 351–355. doi:10.4202/app.2008.0213
- Chiappe, L. M., Zhao, B., O'Connor, J. K., Chunling, G., Wang, X., Habib, M., et al. (2014). A new specimen of the Early Cretaceous bird *Hongshanornis longicresta*: insights into the aerodynamics and diet of a basal ornithomimid. *PeerJ* 2, e234. doi:10.7717/peerj.234
- Choiniere, J. N., Forster, C. A., and Klerk, W. J. d. (2012). New information on *Nqwebasaurus thwazi*, a coelurosaurian theropod from the early cretaceous kirkwood Formation in South Africa. *J. Afr. Earth Sci.* 71–72, 1–17. doi:10.1016/j.jafrearsci.2012.05.005

- Dala Vecchia, F. M. D., and Chiappe, L. M. (2002). First avian skeleton from the Mesozoic of northern Gondwana. *J. Vertebr. Paleontol.* 22 (4), 856–860. doi:10.1671/0272-4634(2002)022[0856:Fasfmi]2.0.Co;2
- Duke, G. E. (1986). “Alimentary canal: anatomy, regulation of feeding, and motility,” in *Avian physiology*. Editor P. D. Sturkie (New York, NY: Springer-Verlag), 269–288.
- Field, D. J., Lynner, C., Brown, C., and Darroch, S. A. (2013). Skeletal correlates for body mass estimation in modern and fossil flying birds. *PLoS One*. 8 (11), e82000. doi:10.1371/journal.pone.0082000
- Fox, N. (1976). *Rangle. Raptor Res.* 10 (2), 61–64.
- Gill, F. B. (2007). *Ornithology*. New York, NY: W. H. Freeman and Company.
- Gionfriddo, J. P., and Best, L. B. (1999). “Grit use by birds: a review,” in *Current ornithology*. Editors V. N. JR, E. D. Ketterson, and C. F. Thompson (New York, NY: Springer Science+Business), 89–148.
- Huang, J., Wang, X., Hu, Y., Liu, J., Peteya, J. A., and Clarke, J. A. (2016). A new ornithurine from the Early Cretaceous of China sheds light on the evolution of early ecological and cranial diversity in birds. *PeerJ* 4, e1765. doi:10.7717/peerj.1765
- Ji, Q., Currie, P. J., Norell, M. A., and Ji, S. A. (1998). Two feathered dinosaurs from northeastern China. *Nature* 393 (25), 753–761. doi:10.1038/31635
- Ji, Q., Norell, M. A., Makovicky, P. J., Gao, K., Ji, S. A., and Yuan, C. (2003). An early ostrich dinosaur and implications for Ornithomimosaur phylogeny. *Am. Mus. Novit.* 3420 (1), 1–19. doi:10.1206/0003-0082(2003)420<0001:Aeodai>2.0.Co;2
- Li, Z., Zhou, Z., Wang, M., and Clarke, J. A. (2015). A new specimen of large-bodied basal enantiornithine *Bohaiornis* from the Early Cretaceous of China and the inference of feeding ecology in mesozoic birds. *J. Paleontol.* 88 (1), 99–108. doi:10.1666/13-052
- Liu, D., Zhou, Z., and Zhang, Y. (2012). Mass estimate and evolutionary trend in Chinese Mesozoic fossil birds. *Vertebr. Palasiat.* 50 (1), 39–52. doi:10.19615/j.cnki.1000-3118.2012.01.006
- Makovicky, P. J., Kilbourne, B. M., Sadleir, R. W., and Norell, M. A. (2011). A new basal ornithomorph (Dinosauria, Ornithischia) from the late cretaceous of Mongolia. *J. Vertebr. Paleontol.* 31 (3), 626–640. doi:10.1080/02724634.2011.557114
- Meinertzhagen, R. (1954). Grit. *Bull. Br. Ornithol. Club* 74, 97–102.
- Noble, J. P. A., and Stempvoort, D. R. V. (1989). Early burial quartz authigenesis in Silurian platform carbonates, New Brunswick, Canada. *J. Sediment. Petrol.* 59 (1), 65–76. doi:10.1306/212F8F1C-2B24-11D7-8648000102C1865D
- O'Connor, J. K. (2009). A systematic review of enantiornithes (aves: Ornithothoraces). PhD thesis. Los Angeles (CA): University of Southern California.
- O'Connor, J. K. (2019). The trophic habits of early birds. *Palaeogeogr. Palaeoclimatol. Palaeoecol.* 513, 178–195. doi:10.1016/j.palaeo.2018.03.006
- O'Connor, J. K., Wang, M., and Hu, H. (2016). A new ornithomorph (Aves) with an elongate rostrum from the Jehol Biota, and the early evolution of rostralization in birds. *J. Syst. Palaeontol.* 14 (11), 939–948. doi:10.1080/14772019.2015.1129518
- O'Connor, J. K., Wang, X., Sullivan, C., Wang, Y., Zheng, X., Hu, H., et al. (2018). First report of gastroliths in the Early Cretaceous basal bird *Jeholornis*. *Cretac. Res.* 84, 200–208. doi:10.1016/j.cretres.2017.10.031
- O'Connor, J. K., Zheng, X., Wang, X., Wang, Y., and Zhou, Z. (2013). Ovarian follicles shed new light on dinosaur reproduction during the transition towards birds. *Natl. Sci. Rev.* 1 (1), 15–17. doi:10.1093/nsr/nwt012
- O'Connor, J. K., and Zhou, Z. (2019). The evolution of the modern avian digestive system: insights from paravian fossils from the Yanliao and Jehol Biotas. *Palaeontology* 63 (1), 13–27. doi:10.1111/pala.12453
- O'Connor, J. K., Chiappe, L. M., and Bell, A. (2011). “Pre-modern birds: avian divergences in the mesozoic,” in *Living Dinosaurs: the evolution history of modern birds*. 1st Edn, Editors G. Dyke and G. Kaiser (Hoboken, NJ: John Wiley & Sons), 40–114.
- Sanz, J. L., Chiappe, L. M., Pérez-Moreno, B. P., Buscalioni, A. D., Moratalla, J. J., Ortega, F., et al. (1996). An Early Cretaceous bird from Spain and its implications for the evolution of avian flight. *Nature* 382 (1), 442–445. doi:10.1038/382442a0
- Serrano, F. J., Palmqvist, P., Chiappe, L. M., and Sanz, J. L. (2016). Inferring flight parameters of Mesozoic avians through multivariate analyses of forelimb elements in their living relatives. *Paleobiology* 43 (1), 144–169. doi:10.1017/pab.2016.35
- Serrano, F. J., Palmqvist, P., and Sanz, J. L. (2015). Multivariate analysis of neognath skeletal measurements: implications for body mass estimation in Mesozoic birds. *Zool. J. Linn. Soc.* 173 (4), 929–955. doi:10.1111/zoj.12215
- Tomescu, A. M. F., Klymiuk, A. A., Matsunaga, K. K. S., Bippus, A. C., and Shelton, G. W. K. (2016). “Microbes and the fossil record: selected topics in paleomicrobiology,” in *Their world: a diversity of microbial environments*. Editor A. A. Klymiuk (New York, NY: Springer International Publishing), 69–169.
- Varricchio, D. J., Sereno, P. C., Zhao, X., Lin, T., Wilson, J. A., and Lyon, G. H. (2008). Mud-trapped herd captures evidence of distinctive dinosaur sociality. *Acta Palaeontol. Pol.* 53 (4), 567–578. doi:10.4202/app.2008.0402
- Wang, M., O'Connor, J. K., Pan, Y., and Zhou, Z. (2017). A bizarre Early Cretaceous enantiornithine bird with unique crural feathers and an ornithomorph plough-shaped pygostyle. *Nat. Commun.* 8, 14141. doi:10.1038/ncomms14141
- Wang, M., O'Connor, J. K., Xu, X., and Zhou, Z. (2019). A new Jurassic scansoriopterygid and the loss of membranous wings in theropod dinosaurs. *Nature* 569 (7755), 256–259. doi:10.1038/s41586-019-1137-z
- Wang, M., Zhou, Z., and Sullivan, C. (2016a). A fish-eating enantiornithine bird from the early cretaceous of China provides evidence of modern avian digestive features. *Curr. Biol.* 26 (9), 1170–1176. doi:10.1016/j.cub.2016.02.055
- Wang, M., Zhou, Z., and Zhou, S. (2016b). A new basal ornithomorph bird (Aves: Ornithothoraces) from the Early Cretaceous of China with implication for morphology of early ornithomorphs. *Zool. J. Linn. Soc.* 176 (1), 207–223. doi:10.1111/zoj.12302
- Wang, M., and Zhou, Z.-H. (2016). A new adult specimen of the basalmost ornithomorph bird *Archaeorhynchus spathula* (Aves: ornithomorphs) and its implications for early avian ontogeny. *J. Syst. Palaeontol.* 15, 1–18. doi:10.1080/14772019.2015.1136968
- Wang, M., Zhou, Z., O'Connor, J. K., and Zelenkov, N. V. (2014). A new diverse enantiornithine family (Bohaiornithidae fam. nov.) from the Lower Cretaceous of China with information from two new species. *Vertebr. Palasiat.* 52 (1), 31–76. doi:10.19615/j.cnki.1000-3118.2014.01.004
- Wang, M., and Zhou, Z. (2017a). “The evolution of birds with implications from new fossil evidences,” in *The biology of the avian respiratory system*. Editor J. N. Maina (New York, NY: Springer International Publishing), 1–26.
- Wang, M., and Zhou, Z. (2017b). A morphological study of the first known piscivorous enantiornithine bird from the Early Cretaceous of China. *J. Vertebr. Paleontol.* 37 (2), e1278702. doi:10.1080/02724634.2017.1278702
- Wang, X., O'Connor, J. K., Maina, J. N., Pan, Y., Wang, M., Wang, Y., et al. (2018). *Archaeorhynchus* preserving significant soft tissue including probable fossilized lungs. *Proc. Natl. Acad. Sci. Unit. States Am.* 115 (45), 11555–11560. doi:10.1073/pnas.1805803115
- Wang, X., O'Connor, J. K., Zhao, B., Chiappe, L. M., Gao, C., and Cheng, X. (2010). New species of enantiornithes (aves: Ornithothoraces) from the qiaotou Formation in northern hebei, China. *Acta Geol. Sin.* 84 (2), 247–256. doi:10.1111/j.1755-6724.2010.00156.x
- Wang, Y., O'Connor, J. K., Li, D., and You, H. (2015). New information on postcranial skeleton of the early cretaceous *Gansus yumenensis* (aves: ornithomorphs). *Hist. Biol.* 28 (5), 666–679. doi:10.1080/08912963.2015.1006217
- Wings, O. (2007). A review of gastrolith function with implications for fossil vertebrates and a revised classification. *Acta Palaeontol. Pol.* 52 (1), 1–16. doi:10.1038/sj.onc.1207250
- Wings, O. (2004). Identification, distribution, and function of gastroliths in dinosaurs and extant birds with emphasis on ostriches (*Struthio camelus*). PhD thesis. Bonn (Germany): Rheinische Friedrich-Wilhelms-Universität.
- Xu, X., Clark, J. M., Mo, J., Choiniere, J., Forster, C. A., Erickson, G. M., et al. (2009). A Jurassic ceratosaur from China helps clarify avian digital homologies. *Nature* 459 (7249), 940–944. doi:10.1038/nature08124
- Xu, X., Zhou, Z., Wang, Y., and Wang, M. (2020). Study on the Jehol Biota: recent advances and future prospects. *Sci. China Earth Sci.* 63, 1–17. doi:10.1007/s11430-019-9509-3
- Zhang and Miman (2003). *The Jehol biota*. Shanghai, China: Shanghai Scientific and Technical Publishers.

- Zhang, Y., O'Connor, J., Di, L., Qingjin, M., Sigurdson, T., and Chiappe, L. M. (2014). New information on the anatomy of the Chinese early cretaceous Bohaiornithidae (aves: enantiornithes) from a subadult specimen of *Zhouornis hani*. *PeerJ* 2, e407. doi:10.7717/peerj.407
- Zhao, J., Jin, Z., Jin, Z., Wen, X., and Geng, Y. (2017). Origin of authigenic quartz in organic-rich shales of the Wufeng and longmaxi formations in the sichuan basin, south China: implications for pore evolution. *J. Nat. Gas Sci. Eng.* 38, 21–38. doi:10.1016/j.jngse.2016.11.037
- Zheng, X., Martin, L. D., Zhou, Z., Burnham, D. A., Zhang, F., and Miao, D. (2011). Fossil evidence of avian crops from the Early Cretaceous of China. *Proc. Natl. Acad. Sci. U.S.A.* 108 (38), 15904–15907. doi:10.1073/pnas.1112694108
- Zheng, X., O'Connor, J. K., Wang, X., Wang, Y., and Zhou, Z. (2018). Reinterpretation of a previously described Jehol bird clarifies early trophic evolution in the ornithuromorpha. *Proc. Biol. Sci.* 285, 20172494. doi:10.1098/rspb.2017.2494
- Zhou, S., O'Connor, J. K., and Wang, M. (2014). A new species from an ornithuromorph (Aves: Ornithothoraces) dominated locality of the Jehol Biota. *Chin. Sci. Bull.* 59 (36), 5366–5378. doi:10.1007/s11434-014-0669-8
- Zhou, S., Zhou, Z., and O'Connor, J. (2013). Anatomy of the basal ornithuromorph bird *Archaeorhynchus spatula* from the early cretaceous of liaoning, China. *J. Vertebr. Paleontol.* 33, 141–152. doi:10.2307/23361078
- Zhou, Z., and Zhang, F. (2002). A long-tailed, seed-eating bird from the Early Cretaceous of China. *Nature* 418, 405. doi:10.1038/nature00930
- Zhou, Z. (2006). Evolutionary radiation of the Jehol Biota: chronological and ecological perspectives. *Geol. J.* 41 (3–4), 377–393. doi:10.1002/gj.1045
- Zhou, Z., and Wang, X. (2000). A new species of *Caudipteryx* from the yixian formation of liaoning northeast China. *Vertebr. Palasiat.* 38 (2), 111–127. doi:10.19615/j.cnki.1000-3118.2000.02.005
- Zhou, Z., Wang, X., Zhang, F., and Xu, X. (2000). Important features of *Caudipteryx*-evidence from two nearly complete new specimens. *Vertebr. Palasiat.* 38 (4), 241–254. doi:10.19615/j.cnki.1000-3118.2000.04.001
- Zhou, Z., and Zhang, F. (2006). A beaked basal ornithurine bird (Aves, Ornithurae) from the Lower Cretaceous of China. *Zool. Scripta.* 35, 363–373. doi:10.1111/j.1463-6409.2006.00234.x
- Zhou, Z., and Zhang, F. (2003). Anatomy of the primitive bird *Sapeornis chaoyangensis* from the early cretaceous of liaoning, China. *Can. J. Earth Sci.* 40 (5), 731–747. doi:10.1139/e03-011

Conflict of Interest: The authors declare that the research was conducted in the absence of any commercial or financial relationships that could be construed as a potential conflict of interest.

Copyright © 2021 Liu, Li, Bailleul, Wang and O'Connor. This is an open-access article distributed under the terms of the Creative Commons Attribution License (CC BY). The use, distribution or reproduction in other forums is permitted, provided the original author(s) and the copyright owner(s) are credited and that the original publication in this journal is cited, in accordance with accepted academic practice. No use, distribution or reproduction is permitted which does not comply with these terms.



Intraskkeletal Osteohistovariability Reveals Complex Growth Strategies in a Late Cretaceous Enantiornithine

Jessie Atterholt^{1,2*}, Ashley W. Poust^{2,3}, Gregory M. Erickson⁴ and Jingmai K. O'Connor⁵

¹Graduate College of Biomedical Sciences, Western University of Health Sciences, Pomona, CA, United States, ²University of California Museum of Paleontology, Berkeley, CA, United States, ³San Diego Natural History Museum, San Diego, CA, United States, ⁴Department of Biological Science, Florida State University, Tallahassee, FL, United States, ⁵Field Museum of Natural History, Chicago, IL, United States

OPEN ACCESS

Edited by:

Fabien Knoll,
Fundacion Agencia Aragonesa para la
Investigacion y el Desarrollo, Spain

Reviewed by:

Andrew Lee,
Midwestern University, United States
Lucas Legendre,
University of Texas at Austin,
United States

*Correspondence:

Jessie Atterholt
jessie.atterholt@gmail.com

Specialty section:

This article was submitted to
Paleontology,
a section of the journal
Frontiers in Earth Science

Received: 10 December 2020

Accepted: 10 February 2021

Published: 23 March 2021

Citation:

Atterholt J, Poust AW, Erickson GM
and O'Connor JK (2021) Intraskkeletal
Osteohistovariability Reveals Complex
Growth Strategies in a Late
Cretaceous Enantiornithine.
Front. Earth Sci. 9:640220.
doi: 10.3389/feart.2021.640220

Most crown-birds experience rapid growth, reaching adult size within a year. Rapid growth strategies evolved within Aves multiple times during the Cretaceous, documented in the Confuciusornithiformes and the Ornithuromorpha. In contrast, osteohistological data suggest the Enantiornithes, the dominant clade of Cretaceous terrestrial birds, were characterized by much slower growth rates that were sustained longer into adulthood. Here we provide evidence for a unique growth strategy involving relatively rapid growth in the Late Cretaceous avisaurid enantiornithine, *Mirarce eatoni*. Multiple appendicular skeletal elements were sectioned for osteohistological analysis. These show remarkable intraskkeletal variation, and high levels of variation even between individual sections. The radius is composed of parallel-fibered bone, similar to histological descriptions in other enantiornithines. Other elements, in contrast, differ markedly from other members of the clade. The humerus is composed of parallel-fibered bone with a middle layer of incipient fibrolamellar bone and several growth lines in the outer circumferential layer and near the endosteal border. The endosteal and periosteal layers of slow-growing bone indicate cyclical variation in growth rates. The femur shows regions of coarse compact cancellous bone and parallel-fibered bone with numerous secondary osteons, and only a single growth line. The tarsometatarsus is predominantly fibrolamellar in texture, with several asymmetrical growth lines located throughout the cortex; this element exhibits strong cortical drift. Growth lines in both the endosteal and periosteal portions of the cortex indicate that, like the humerus, growth rates of this bone varied cyclically. The two phalanges studied here are composed of parallel-fibered bone with extensive evidence of and remodeling over possible regions of coarse compact cancellous bone. Although *Mirarce* is one of the largest known enantiornithines, slow and protracted growth documented in similarly-sized taxa suggests this bone texture is not merely a size-related scaling effect. These findings indicate that by the Late Cretaceous, some enantiornithines had evolved absolutely higher growth rates and more complex life history strategies, in which growth rates varied across the skeleton. Furthermore, a variety of strategies were employed to achieve adult size and morphology, including cycles of slow and fast growth, asymmetrical growth within a single element, and extensive remodeling.

Keywords: histology, mesozoic birds, enantiornithine, growth, life history evolution

INTRODUCTION

When, how, and why the derived rapid growth strategy that characterizes most modern birds evolved in Aves and the Dinosauria is of intense interest to evolutionary biologists (Chinsamy-Turan, 2005; Erickson et al., 2009; Xu et al., 2014; O'Connor et al., 2018). Living birds nearly all reach skeletal maturity within the first year, some achieving adult size in only a matter of weeks (Gill, 2007; Bourdon et al., 2009). In contrast, non-avian dinosaurs took several years to reach adult size, likely achieving reproductive maturity prior to skeletal maturity (Erickson et al., 2007; Lee and Werning, 2008). More rapid growth strategies, whereby skeletal maturity is achieved in a relatively shorter duration of time (here-within referred to simply as rapid growth), apparently evolved multiple times within Aves during the Cretaceous (Zheng et al., 2017; Chinsamy et al., 2020). Non-ornithothoracine stem avian lineages Jeholornithiformes, and Sapeornithiformes preserve lines of arrested growth (LAGs) in the cortex, and like the Archaeopterygidae and non-avian dinosaurs likely achieved reproductive maturity before skeletal maturity (Erickson et al., 2007; O'Connor et al., 2014; Zheng et al., 2014). A similar pattern has been inferred for the Enantiornithes, the dominant clade of Cretaceous land birds, and for early-diverging members of the Ornithuromorpha, the crown-ward clade that includes Neornithes (living birds) (O'Connor et al., 2014; Wang and Zhou, 2016). However, evidence suggests that the Early Cretaceous early-diverging pygostylian *Confuciusornis* evolved more rapid growth independent of and in parallel to the neornithine lineage (Zhang et al., 1998; De Ricqlès et al., 2003; Chinsamy et al., 2020). Similarly, although protracted growth strategies persisted in some Late Cretaceous lineages (Chinsamy et al., 1995), rapid growth evolved in the Ornithuromorpha ~128 Ma and possibly arose multiple times within this clade during the Early Cretaceous (O'Connor et al., 2015; Wang X.-R. et al., 2020). This information highlights the evolutionary lability of avian development.

Here we describe the long bone osteohistology of a large avisaurid enantiornithine, *Mirarce eatoni* (Atterholt et al., 2018), the holotype of which (and only known specimen) represents the most complete enantiornithine from North America. Given the relatively sparse global record of enantiornithines in the Late Cretaceous, this taxon stands to provide new insights into these enigmatic birds (O'Connor et al., 2011). Most post-cranial elements of *Mirarce* are preserved, including partial or complete representatives of all major limb bones, a pygostyle, and a partial sternum. All preserved elements show signs of somatic maturity, including compound bones that are completely fused and periosteal surfaces lacking substantial rugosity from incompletely formed primary osteons (Atterholt et al., 2018).

We describe the osteohistology from ground-sections of the humerus, radius, femur, third metatarsal, and two pedal phalanges—more elements than have been sampled in any previously studied enantiornithine bird, with the exception

of the recent work on Early Cretaceous *Mirusavis* (Wang M. et al., 2020). This provides an opportunity to further explore intraskeletal histovariability in this clade. It is becoming increasingly common that anatomical descriptions include osteohistological data, and although this provides comparative material, these studies typically only sample just one or two elements (Zhang et al., 2013; Wang M. et al., 2014; Hu et al., 2015; Hu and O'Connor, 2017; Wang et al., 2017a). Recent research revealing high intraskeletal variability in bone tissue highlights the importance of studies utilizing greater numbers of bones whenever possible to facilitate interspecific comparisons between homologous elements (e.g., Horner et al., 2000; De Ricqlès et al., 2003; Woodward et al., 2014; Prondvai et al., 2018; Chinsamy et al., 2020; Cullen et al., 2020). As such, we sampled as many elements as permission allowed. Sampling was facilitated by the fact that, while the specimen is three-dimensionally preserved, it is disarticulated and partially fragmented, so minimally destructive samples could be taken along pre-existing breaks. Histological evidence from *Mirarce* indicates that intraskeletal variability is substantial in this taxon. The preserved bone tissue contributes to our understanding of growth strategies in the Enantiornithes and further elucidates the complex patterns of skeletal ontogeny in stem birds.

MATERIALS AND METHODS

Tissue samples from *Mirarce* were extracted from broken elements in order to minimize damage to the specimen, that at the time of sampling was undescribed. Samples were collected from near the mid-shaft diaphyses wherever possible. Because histological features are known to vary between elements (e.g., Horner et al., 1999; Erickson, 2005), samples were taken from five different bones: 1) a fragment from the cranial mid-shaft diaphysis of the right humerus (the left humerus remains completely intact); 2) a piece of the diaphysis of the right radius; 3) the proximal diaphysis of the right femur (the left femur remains completely intact); 4) a portion of the right metatarsal III extracted just proximal to the mid-diaphysis (the left tarsometatarsus is completely intact); and finally 5) two incomplete pedal phalanges (the 1st phalanx from pedal digit II and the 4th from pedal digit IV). The samples from the femur and phalanges represent entire cross sections of the elements, while those of the humerus, radius, and metatarsal represent only portions of their respective cortices. The holotype fossil skeleton and histological sections of *Mirarce* are housed in the University of California Museum of Paleontology, Berkeley, CA, United States (UCMP 139500).

All bone samples were embedded in the polyester resin Epothin (Buehler Ltd., Lake Bluff, IL) and sectioned into 1 mm wafers using a diamond-embedded saw (Isomet low-speed Saw, Buehler Ltd., Lake Bluff, IL). Wafers were mounted using epoxy (2-ton, Devcon, ITW Polymers Adhesives, Danvers, MA) on petrographic microscope slides and ground to

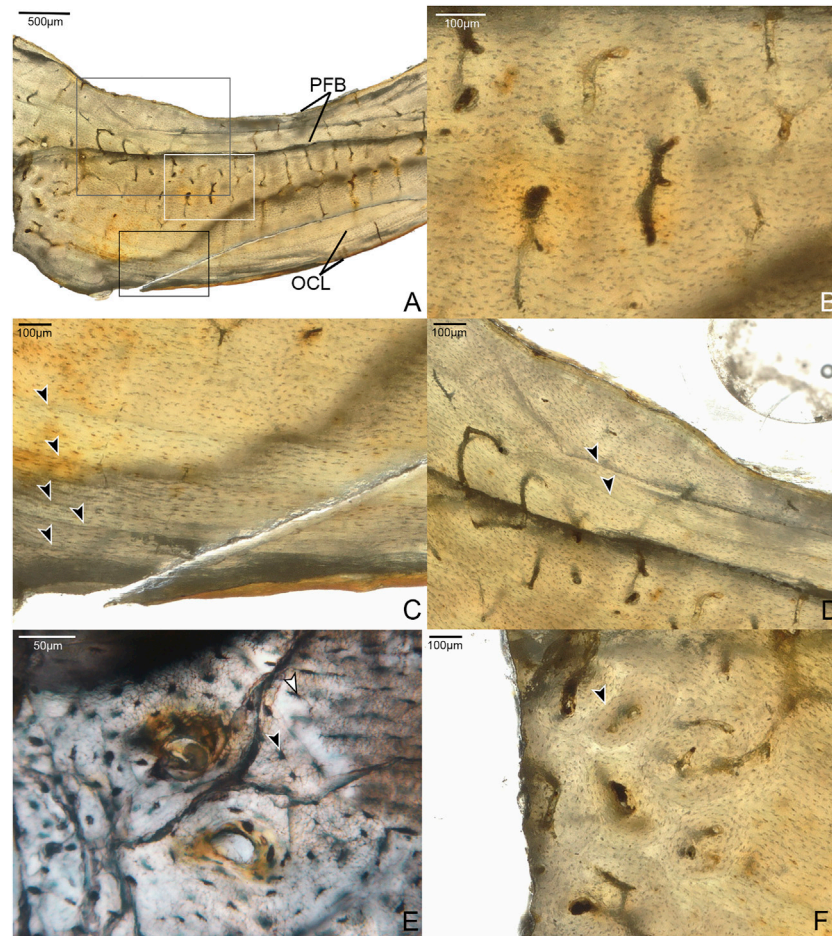


FIGURE 1 | Histological sections of the humerus of *Mirarce eatoni*. **(A)** Fragment of humeral cortex sectioned in this study, composed of a layer of parallel-fibered bone (PFB) and an outer circumferential layer (OCL) surrounding a middle layer of regional fibrolamellar bone and regions of simple vascular canals in woven bone; also, showing a series of LAGs near the periosteal margin, and a moderate level of vascular channels dominated by a reticular and/or radial patterning. 40x, plane light. **(B)** Section in white box of panel A; close-up of simple vascular canals in a region of weakly woven bone. 200x, plane light. **(C)** Section in black box of panel A; close-up of parallel-fibered OCL with growth lines indicated by arrows. 200x, plane light. **(D)** Section in gray box of panel A, showing the double endosteal growth line, separated into two separate lines transitioning from a LAG-like appearance to annulus-like. 100x, plane light. **(E)** Region of incipient fibrolamellar bone with developing primary osteons; image also shows details of canaliculi, and differences in shape and size between osteons in woven bone (black arrow) compared to those in parallel-fibered regions (white arrow). 400x, plane light. **(F)** Region of fibrolamellar bone with mature osteons and some evidence of remodeling (secondary osteon, indicated by arrow). 200x, plane light.

approximately 100 μm thickness using a lap grinder (EcoMet 3, Buehler Ltd., Lake Bluff, IL) with descending grits (260–1,200) of silica-carbide grit paper using water as a lubricant. Slides were photographed using a Keyence VHX-7000 digital imaging microscope and a Nikon digital sight camera (Nikon Inc., Tokyo, Japan) tethered to a petrographic microscope (DS-U3 and DS-Fi2) and captured using the computer program NIS-Elements (Nikon Inc.). Sections were visualized under non-polarized light, linearly polarized light with crossed nicols, and with linearly polarized light with full waveplate compensation. The addition of a waveplate increases the color visibility of linear crystals, such as those of the bioapatite precipitated in vertebrate hard tissues. Under this view the additional colors are created by the orientation of the crystals such that orthogonally oriented fields retard the “slow” and “fast” components of light differently

and appear as opposing color gradients. No colors have been manipulated or altered digitally. Photos were edited in Adobe Photoshop CC (20.0.0; Adobe, San Jose, CA, United States). The terminology used to classify bone tissues follows the precedent of De Ricqlès (1976) and Francillon-Vieillot et al. (1990) as updated by Huttenlocker et al. (2013). Raw images are stored on Zenodo (<https://zenodo.org>).

All measurements were acquired using ImageJ (v.51; National Institute of Health, Bethesda, MD, United States). Cortical diameter (for complete cross-sections) was measured four times along different axes of the element in the transverse plane and averaged to generate a single figure representing this metric. Similarly, cortical thickness is reported as an average of six different measurements across the cortex (medially, laterally, cranially, caudally, and four midpoints

between these regions). Vascular area was calculated by manual outlining and measuring of each vascular pore observable in a given thin section. The total area of these spaces was then calculated and compared to the total cross-sectional area of an element to generate a percentage of vascular porosity.

RESULTS

Humerus

Fragments from the mid-shaft of the cortex of the broken left humerus of *Mirarce* were sectioned. The humeral samples have an average cortical thickness of 1542 μm . Two serial thin sections along the transverse plane of the element were made. Because this element is incomplete, our sampling does not capture the entire bone circumference. The cortex is composed primarily of parallel-fibered bone with regional incipient fibrolamellar bone and shows a thin, weakly-formed outer circumferential layer (OCL) (**Figure 1**). Although there is an endosteal layer of parallel-fibered bone, we do not interpret this as an inner circumferential layer (ICL) because there is no erosional boundary that separates it from the rest of the cortex, and it contains several vascular canals.

The element has mostly simple vascular canals, but developing primary osteons with lamellae in early stages of formation are present (**Figure 1E**). Regional fibrolamellar bone is identified based on areas of relatively high vascular porosity, and a primary matrix composed of randomly oriented woven bone. Because the osteons located in these regions of woven bone do not have distinct lamellae, and contain few osteocyte lacunae, these areas are interpreted as “incipient fibrolamellar bone” *sensu* Woodward et al. (2014). Such regional incipient fibrolamellar bone is also present in small areas of the humerus of adult enantiornithine STM 29-8 (O'Connor et al., 2014), though to a lesser extent than in *Mirarce*. This distinguishes these taxa from others in which the humeral diaphyseal cortices are completely composed of parallel-fibered bone (*Parvavis* IVPP V18586 (Wang M. et al., 2014), *Cruralispennia* IVPP V21711 (Wang et al., 2017b), and *Pterygornis* IVPP V16363 (Wang et al., 2017a)). In the humerus of *Mirarce*, minor remodeling is present, with several secondary osteons observed in the incipient fibrolamellar regions (**Figure 1F**).

There are at least six growth lines near the periosteal margin, although their precise number is obscured by numerous fine cracks in the outer region of the section. The innermost resembles an annulus, while the others are more distinctly formed and appear more like LAGs. Together, these structures corroborate inferences based on gross skeletal morphology that the individual was a somatically mature adult at the time of death (Atterholt et al., 2018).

There is also a growth line near the endosteal margin, that splits in two. Double LAGs (and even triple and quadruple) have been reported in other dinosaurs. Evidence suggests they are prevalent among theropods (e.g., Lee and O'Connor, 2013; Cullen et al., 2014; Evans et al., 2015; Cullen et al., 2020), and also occur in ornithischians (Werning, 2012), albeit more rarely. This is the first report of such a structure in an enantiornithine. In *Mirarce*,

one “branch” grades into a LAG-like distinct line and then transitions into a more annulus-like band of parallel-fibered bone, while the other simply trails off and fades into the surrounding cortical bone.

Vascularization is moderate, with channels concentrated in the middle of the cortex (in the regions of incipient fibrolamellar bone). The vascular canals are primarily longitudinally-oriented in one thin section, while radial and reticulating canals predominate in the consecutive thin section. This highlights the variability and disorganization of vascularity within this element (**Figure 1**). Such variability in canal orientation is unusual for enantiornithines, most of which show exclusively longitudinally-oriented vascularization (e.g., *Zhouornis* CNUVB-0903 (Zhang et al., 2013), STM 29-8 (O'Connor et al., 2014), *Eopengornis* STM24-1 (Wang X. et al., 2014), and *Parvavis* IVPP V18586 (Wang M. et al., 2014)). The areal density of vascular canals is moderate in the preserved portions of the cortex, comprising 4.2 and 1.1% of total cross-sectional area in the reticulated and longitudinally-dominated thin sections, respectively. This is generally higher than, but most similar to, *Zhouornis* CNUVB-0903 (vascular area of 1.57%) and an indeterminant enantiornithine taxon STM 29-8 (vascular area of 1.1%). This vascular area stands in stark contrast to that seen in other enantiornithine humeral sections (e.g., *Parvavis* IVPP V18586 (Wang M. et al., 2014), *Pterygornis* IVPP V16363 (Wang et al., 2017a), and *Cruralispennia* IVPP V21711 (Wang et al., 2017b)), that are nearly or completely avascular (**Table 1**).

Osteocyte lacunae are well-organized, although to a lesser degree in the incipient fibro-lamellar regions, and are extremely small (5–15 μm in length). Fine, intricate canaliculi are also well preserved, forming elaborate communications between neighboring lacunae (**Figure 1**). They differ moderately in shape through different portions of the cortex. In the OCL the osteocyte lacunae are extremely flattened. Within the rest of the cortex, they grade in morphology from rounded and disorganized in the more endosteal portion, where the bone matrix shows an incipient fibro-lamellar texture, to flatter and more organized in the outer half closer to the OCL where the tissue is parallel-fibered.

Radius

A small shard from the mid-shaft of the fragmented right radius was available for sectioning (**Figure 2**). The complete cortex is not captured, but some microstructural features can be discerned. An ICL is present, and at least a portion of the radius is composed of highly-cellular parallel-fibered bone, as inferred from the numerous osteocyte lacunae. This portion of the element also has very low vascularity. These sparsely-distributed canals are mainly simple (i.e., non-osteonal) and longitudinally oriented, although two incipient primary osteons are present (**Figure 2E**). Osteocyte lacunae are disorganized and bulbous relative to the lacunae in the humerus. No OCL is visible, however, the periosteal surface is not preserved in the fragment. One growth line is visible, in the mid-cortical portion of the preserved bone. Antebrachial elements that are composed entirely of slow-growing bone are also reported in the adult enantiornithine *Pterygornis* IVPP V16363 (Wang et al., 2017a) and subadults *Parvavis* IVPP V18586 (Wang M. et al., 2014) and

TABLE 1 | Summary of osteohistological attributes of *Mirarce eatoni* and select other enantiornithines.

| Taxon | Ontogenetic stage | Humerus | Ulna | Femur | Tarsometatarsus | DII, P1 | DIV, PIV |
|------------------------------------|-------------------|--------------------------------------------|------------------------|----------------------------------|--------------------------------|------------------------------|--------------------------------|
| <i>Avimaia</i> (IVPP V25371) | adult | — | — | 0.1% 24.2* PFB GL: 1 | — | — | — |
| <i>Curalispennia</i> (IVPP V21711) | subadult | 0% 19.35 PFB | — | — | — | — | — |
| <i>Eopengornis</i> (STM24-1) | early subadult | 0.9% (38) WB | 2.9% 42.4 WB/PFB | 1.6% 27 WB/IFLB | — | — | — |
| <i>Mirarce</i> (UCMP139500) | adult | 4.2%*; 1.1%* 95.9 PFB/IFLB GL: ~6 | — | 0.9% 89.0 PFB/FLB GL: 1 | 1.7%* 48.1 FLB GL: ~6 | 1.7% 21.7 PFB GL: 1 | 0.9% 12.2 PFB GL: 3-4 |
| <i>Mirusavis</i> (IVPP V18692) | Adult | 0.2% 30.02 PFB GL: 1 | — | 0.3% 27.33 PFB | — | — | — |
| <i>Monoenantius</i> (IVPP V20289) | subadult | — | 3.5% 45.6 FLB | — | — | — | — |
| <i>Parapengornis</i> (IVPP V18687) | young subadult | — | — | 4.3% 39.8 FLB | — | — | — |
| <i>Pterygornis</i> (IVPP V16363) | young adult | 0.6% 33.5 PFB GL: 1 | 0.5% 35.4* PFB | 0.7% 22.3* PFB | — | — | — |
| <i>Parvavis</i> (IVPP V18586) | subadult | 0.3% 18.4 PFB | — | — | — | — | — |
| <i>Zhouornis</i> (CNUVB-0908) | Adult | 1.6%* 50.6 PFB/CCCB GL: 1 | — | 0.4% 44.5 PFB GL: 1 | — | — | — |
| STM 29-8 | Adult | 1.1% 44.7 PFB | — | 0.4% 40.2 PFB GL: 2 | — | — | — |
| MACN-S-01 | adult | — | — | 0%* PFB GL: 4 | — | — | — |
| PVL-4273 | adult | — | — | 0.1%* PFB GL: 5 | — | — | — |

For each element, the following information is given (from top to bottom): measure of approximate vascular porosity (asterisk indicates specimens represented by a fragment of the cortex); measure of total element length, in millimeters (cross indicates estimation); predominant bone tissue for each element (PFB, parallel-fibered bone; WB, woven bone; IFLB, incipient fibrolamellar bone; FLB, fibrolamellar bone; CCCB, compact coarse cancellous bone); and number of growth lines, if present (GL). Measurements of element length are given for the sake of conveying a sense of scale, and reported the most complete side of a given specimen; in some instances (e.g., *Mirarce*, for which only incomplete elements were destructively sampled) this measurement may not be from the element that was sample.

Monoenantius IVPP V20289 (Hu and O'Connor, 2017). This similarity is striking, given the different ontogenetic stages represented by these taxa and differences in the osteohistology of their humeri, suggesting that growth of the radius and ulna slows early in ontogeny relative to other elements in *Mirarce* and other enantiornithines.

Femur

Due to incomplete preservation the left femur was sectioned at the proximal-most portion of the diaphysis (Figure 3). Although

crushed, the entire circumference of the cortex is represented. The femoral cortex is moderately thick compared to the other elements described here, with a tripartite structure composed of an avascular OCL, a mid-cortical zone of coarse compact cancellous bone (CCCB) and parallel-fibered bone with secondary osteons (expressed variably across the cortex), and an ICL consisting primarily of parallel-fibered bone with lamellar bone present in several regions. Although the OCL is primarily parallel-fibered, lamellar bone tissue is also present in some areas. The medial and cranial cortical portions of the femur are twice as

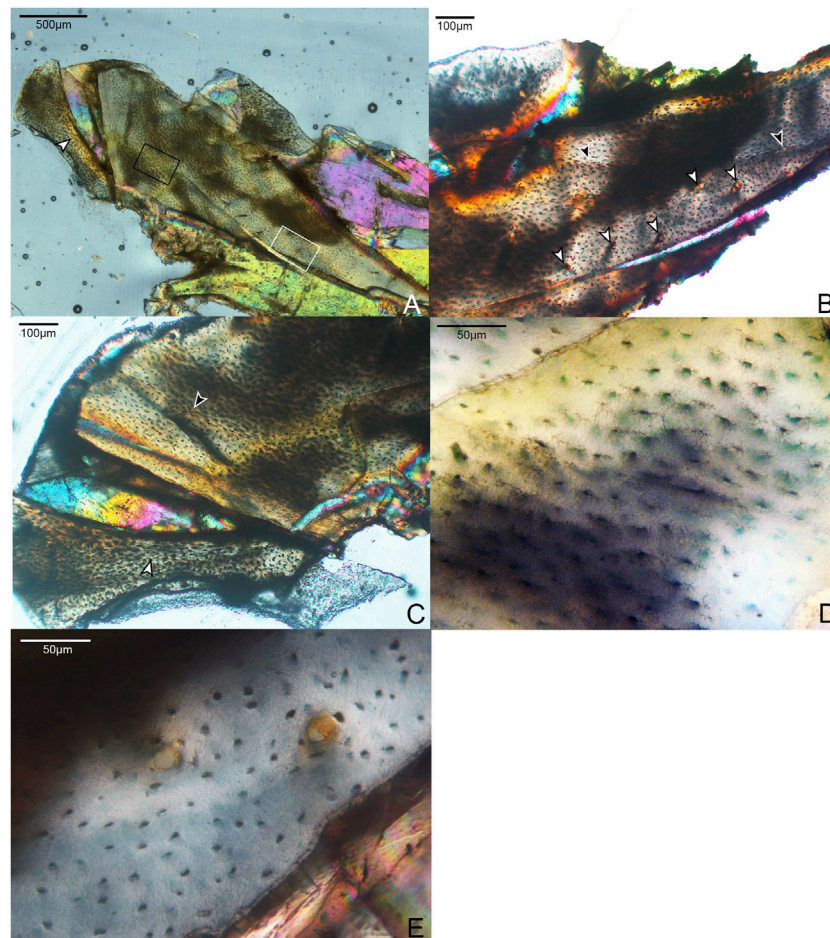


FIGURE 2 | Histological section through the radius of *Mirace eatoni*. **(A)** Section showing entire radial fragment sectioned in this study. It is composed of weakly vascularized parallel-fibered bone. 40x, polarized light. White arrow indicates the ICL. **(B)** Close-up of histological section showing details of the growth line (black arrows) and the few vascular channels (white arrows); some are simple canals, while others are incipient or mature primary osteons. 100x, plane light. **(C)** Portion of radial section showing the main and displaced fragments. On the main fragment, the black arrow indicates a growth line. On the displaced fragment, the white arrow indicates the border of the ICL. **(D)** Area in black box of Panel A, an avascular, parallel-fibered region of the radial cortex showing morphological details of the lacunae and fully developed canaliculi. 400x, plane light. **(E)** Area in white box of panel A, parallel-fibered bone of the radius, showing two incipient primary osteons. 400x, plane light.

thick as the lateral side and are excavated by several large cavities that vary in size and shape, ranging from circular ($\sim 50\text{--}70\text{ }\mu\text{m}$ diameter) to more elongate and irregular ($\sim 180 \times 90\text{ }\mu\text{m}$). These cavities are lined with parallel-fibered or lamellar bone. We posit that these were canals continuous with nutrient foramina open on the surface of the element, where neurovascular bundles passed through the bone. The relatively high concentration of these structures in this section is possibly the result of the proximal diaphyseal location of the sampling (Wang X.-R. et al., 2020).

The texture of the middle cortical layer of the femur varies across the section. CCCB is prominent in the lateral and caudal regions (Figure 3B,C), as indicated by the numerous, irregularly shaped structures resembling osteons and the variously-oriented bands of parallel-fibered bone (interstitial lamellae). It is not unexpected to see this tissue type in such abundance given the proximal sampling of the femoral shaft, which represents a former metaphyseal region that later became incorporated into the diaphysis as the femur grew in length (Enlow, 1963). Similarly,

Zhang et al. (2013) report the presence of CCCB in a distally thin-sectioned humerus of *Zhouornis* (CNUVB-0903).

Most of the vasculature in this central region appears to consist of well-developed, longitudinally-oriented channels. Some of these are at the center of secondary osteons in a region of remodeling within the CCCB-dominated caudal portion of the cortex. The cranial and medial portions of the cortex show mainly parallel-fibered matrices, also with secondary osteons. Unlike the humerus, the femur lacks anastomosing vascular canals at the plane of section. The OCL and ICL are avascular. Possibly due to the proximal location of our sample, the vascular area of the femur sample, not including the large cavities in the cortex, is approximately double that of other adult enantiornithine femoral samples (Table 1).

Importantly, while the humerus preserves at least six growth lines, only one is visible in the femur. It is located within the inner third of the OCL and only visible in the caudal portion of the cortex. Though this difference might be interpreted as differential

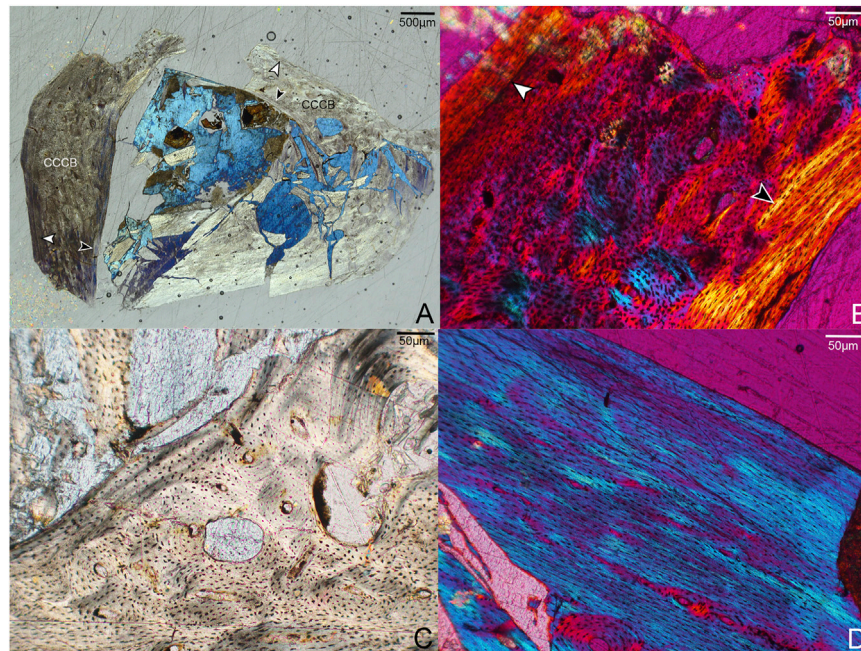


FIGURE 3 | Histological sections through the left femur of *Mirarce eatoni*. **(A)** Section showing entire portion of the left femur; cranial to right, lateral to top. CCCB is widespread in the caudal and lateral regions, closely resembling fibrolamellar bone. Notable are the large cavities in the cranial portion of the cortex. White arrows indicate the OCL; black arrows indicate the ICL. 40x, polarized light. **(B)** Close-up of a portion of the cortex interpreted as CCCB-dominated. The innermost border of the mature ICL is also shown (black arrow). The white arrow indicates a growth line, clearest here in the caudal part of the cortex. 200X, polarized light. **(C)** The large spaces within the cortex, lined with parallel-fibered and lamellar bone. 200x, plane light. **(D)** A parallel-fibered portion of the lateral cortex with low vascular levels. 200x, polarized light.

growth in the fore- and hindlimbs, the proximal position of the section in the femur renders the comparison uncertain. The fact that this structure is only visible in part of the cortex (and not throughout its entire circumference) also speaks to the strong role of cortical drift in the growth and morphological development of the femur. This is similarly suggested by the abundance of CCCB, a tissue type that commonly develops as cortical drift occurs (Heck et al., 2019), in-filling spongy bone to incorporate it into the cortical compacta.

The well-preserved osteocyte lacunae of the femur resemble those in the humerus and other elements in both morphology and distribution. In particular, their organization coincides with differences in bone tissue; bulbous, more-rounded lacunae surrounding primary vascular canals occur in the middle layer of the cortex and grade outward to flattened, circumferentially-aligned lacunae in the OCL.

Metatarsal

Samples from the mid-shaft of the third metatarsal were collected from the broken right tarsometatarsus. The fragment captures the entire plantar half of the cortex. The histology is complex, suggesting varying growth rates, bone resorption, and secondary growth. Generally speaking, it is composed of three layers. The cortical bone has a large area of fibrolamellar tissue that grades outward into parallel-fibered along one side, with a thick ICL of endosteally-derived lamellar bone and a thin OCL of parallel-fibered bone (Figure 4). In the mid-cortical layer,

osteocyte lacunae are round and disorganized with highly elaborated and fully-developed canalicular systems.

In the OCL, there are 2–3 growth lines, that extend only a short distance around the cortex before terminating at the periosteal margin of the bone. Another growth line is present below the OCL, in the middle cortical layer. All of these are distinctly formed and resemble LAGs. Since the morphology of LAGs and annuli grade into each other, we refrain from specifically labeling these structures. Another three growth lines, resembling annuli, are present near the endosteal margin of the bone. The innermost two run a short course before abruptly ending where they were resorbed by the formation of the ICL, while the third traces a path just outside this structure. The strongly laminated, avascular ICL is widest in the middle of the sampled fragment where it forms approximately 20% the thickness of the bone wall, thinning out laterally and medially. The asymmetry of these structures suggests strong cortical drift occurred during the development of this element, emphasizing the complexity of ontogenetic changes in shaping the tarsometatarsus.

Most of the preserved middle layer of bone is highly vascularized by longitudinal canals, mainly forming the central canals of primary osteons, which populate the fibrolamellar layer in high densities. Some oblique canals are also observed (Figure 4B). However, this osteon-dense woven bone grades on one end into a small region of parallel-fibered bone with fewer vascular canals. This further suggests that growth of this element was asymmetrical.

The histological attributes of the metatarsal of *Mirarce* do not closely resemble the metatarsals of *Concornis* LH21006

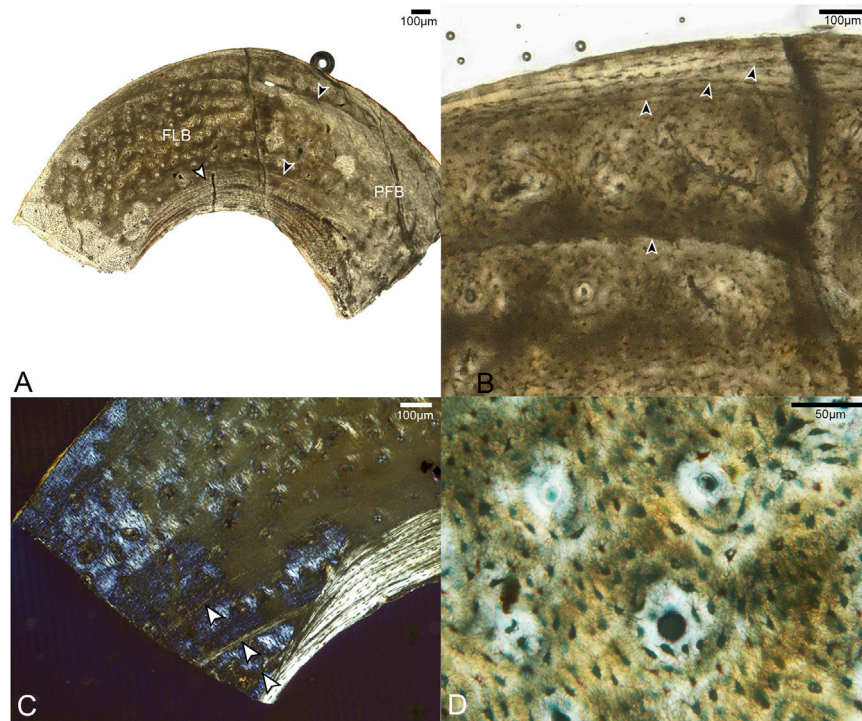


FIGURE 4 | Sections through mid-shaft of the third right metatarsal. **(A)** Image showing entire fragment of the metatarsal. The cortex is composed of a large area of fibrolamellar bone (labeled FLB), which grades into parallel-fibered along one side (indicated by label PFB); it has a thick, asymmetrical ICL composed of lamellar bone (white arrow). Black arrows indicate the clearest growth lines, one near the endosteal and one near the periosteal margin. 40x, plane light. **(B)** A close-up of the cortex showing the crowded growth lines near the periosteal edge of the cortex, and the isolated growth line deeper in the cortex (all indicated by black arrows). 200x, plane light. **(C)** Close-up of the cortex showing three growth lines in the endosteal portion of the fibrolamellar layer, interrupted by the ICL. **(D)** Fibrolamellar portion of the cortex showing microanatomical details of the primary osteons and osteocyte lacunae. 400x, plane light.

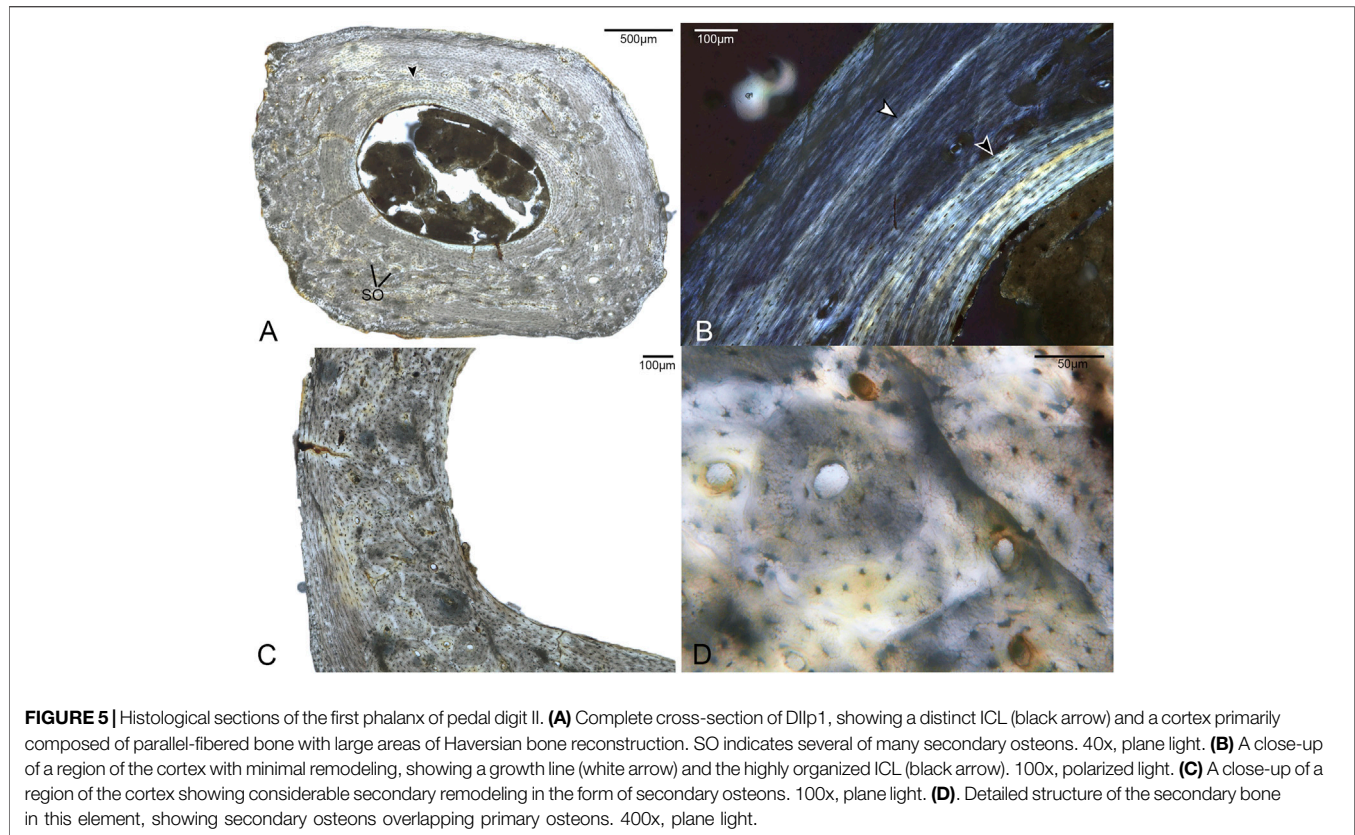
(Cambra-Moo et al., 2006) or *Confuciusornis* NGMC98-8-2 (De Ricqlès et al., 2003) (the only other Cretaceous avians from which metatarsals have been sectioned). In *Confuciusornis* NGMC98-8-2 vascularity is high and the OCL is thin as in *Mirarce*, but compared to *Confuciusornis*, vascularization in *Mirarce* is not exclusively longitudinal in orientation, as some canals show moderate reticulation. In *Concornis* LH21006 the metatarsals are poorly vascularized and consist of a thick cortex of parallel-fibered bone. This stands in contrast to the high vascularity and fibrolamellar texture of the *Mirarce* metatarsal. However, the *Concornis* LH21006 metatarsal section also preserves evidence of remodeling and secondary growth suggesting an early period of rapid growth followed by a major reduction in growth rate as the individual approached somatic maturity. The third metatarsal of *Mirarce* suggests that rapid growth persisted until somatic maturity, only slowing at the time of the formation of the OCL. Nevertheless, we note it is possible that with increased maturity, secondary remodeling comparable to that of *Concornis* LH21006 similarly may have occurred in *Mirarce*.

Pedal Phalanges

Two broken pedal phalanges were sampled at the mid-shaft: the first phalanx of digit II (DIIP1; **Figure 5**) and the fourth phalanx of digit IV (DIVp4; **Figure 6**). The average cortical thickness of

DIIP1 is thinner than that of DIVp4 (**Table 2**). Both pedal phalanges of *Mirarce* are highly vascularized and composed of three distinct layers of tissue: a lamellar ICL of endosteal origin, a middle layer of heavily remodeled bone, and a thin, variably present OCL composed of parallel-fibered bone. In both phalanges, large swaths of the middle are obscured by an expansive, dense Haversian system of longitudinally-oriented secondary osteons (**Figures 5, 6**), with some localized areas of parallel-fibered bone visible. Although difficult to discern due to the degree of remodeling, the bone tissue visible irregularly through the secondary osteons strongly resembles CCCB, with the irregular, wavy occurrences of parallel-fibered bone that presumably were deposited around former trabeculae. Though currently not possible to state with certainty, we posit that the mid-cortical layer of the phalanges was previously dominated by CCCB before undergoing remodeling. This suggests the importance of the role of endosteal resorption, and deposition of secondary endosteal tissue during the shaping and growth of this element. Also, in both phalanges, osteocyte lacunae in the regions of parallel-fibered bone (including in the OCL) are small and flattened. Within the lamellae surrounding the secondary osteons, they are more rounded.

The phalanges were the only elements in this study for which we could examine the complete, uncrushed diaphyseal cross-sections. Notably, there is considerable microanatomical



variation in the cortex of both phalanges (Figures 5, 6). Both exhibit a dense clustering of secondary osteons in the medial and lateral regions of the bone, but these gradually become increasingly sparse near the dorsal portion of the cortex. The phalanges were undergoing extensive, asymmetrical remodeling at the time of the individual's death.

While the two phalanges are broadly similar in terms of microanatomy, there are some minor differences. The bone of DIVp4 is generally more organized in terms of osteocyte position and orientation, to the extent that the parallel-fibered bone of the OCL and middle layer border on lamellar (Figure 6). There are three to four growth lines present in DIVp4, crowded against the periosteal margin of the bone. Additionally, in DIVp4 the secondary remodeling is more concentrated in the lateral and medial portions of the cortex. In DIIP1 a larger proportion of secondary osteons extend from the medial and lateral cortex into the plantar region, and the mid-cortex is interrupted by a single annulus (Figure 5).

DISCUSSION

Enantiornithine life history has been inferred to represent a fairly dramatic departure from relatively rapid growth strategies reported for other Mesozoic stem birds, such as *Confuciusornis* and *Jeholornis* (De Ricqlès et al., 2003; Erickson et al., 2007; Prondvai et al., 2018; Chinsamy et al., 2020). Every previously sampled enantiornithine that can be

considered older than a subadult preserves indications that growth was slow and periodic, as evidenced by a prevalence of parallel-fibered bone. Subsequent studies have revealed higher rates of bone deposition in many enantiornithines across a range of ontogenetic stages compared to that of the first sampled enantiornithines, which revealed avascular parallel fibered bone (Chinsamy and Elzanowski, 2001; Wang M. et al., 2014; Wang X. et al., 2014; Hu et al., 2015; Hu and O'Connor, 2017; Wang et al., 2017a; Knoll et al., 2018), but microanatomy of adult femora still indicates relatively slow growth for a prolonged period of time following reproductive maturity (Zhang et al., 2013; O'Connor et al., 2014; Wang et al., 2017a). The osteohistology of *Mirarce* suggests that at least one lineage of enantiornithines evolved relatively higher growth rates retained later in ontogeny, in the form of intermittent periods of fast post-natal growth in some skeletal elements. However, as in other enantiornithines, growth in *Mirarce* was protracted, as evidenced by the presence of at least six growth lines in the humerus.

The osteohistological variation observed throughout the skeleton of *Mirarce* suggests that, by the Late Cretaceous, some enantiornithine growth strategies evolved to be more nuanced and complex than previously understood. Most major long bone elements in *Mirarce* have a thin, poorly-defined OCL, and the pedal elements show thick, well-developed ICLs. However, beyond these patterns there is considerable microanatomical diversity across the skeleton and the osteohistological characteristics of the middle cortical layers vary greatly. The humerus consists of

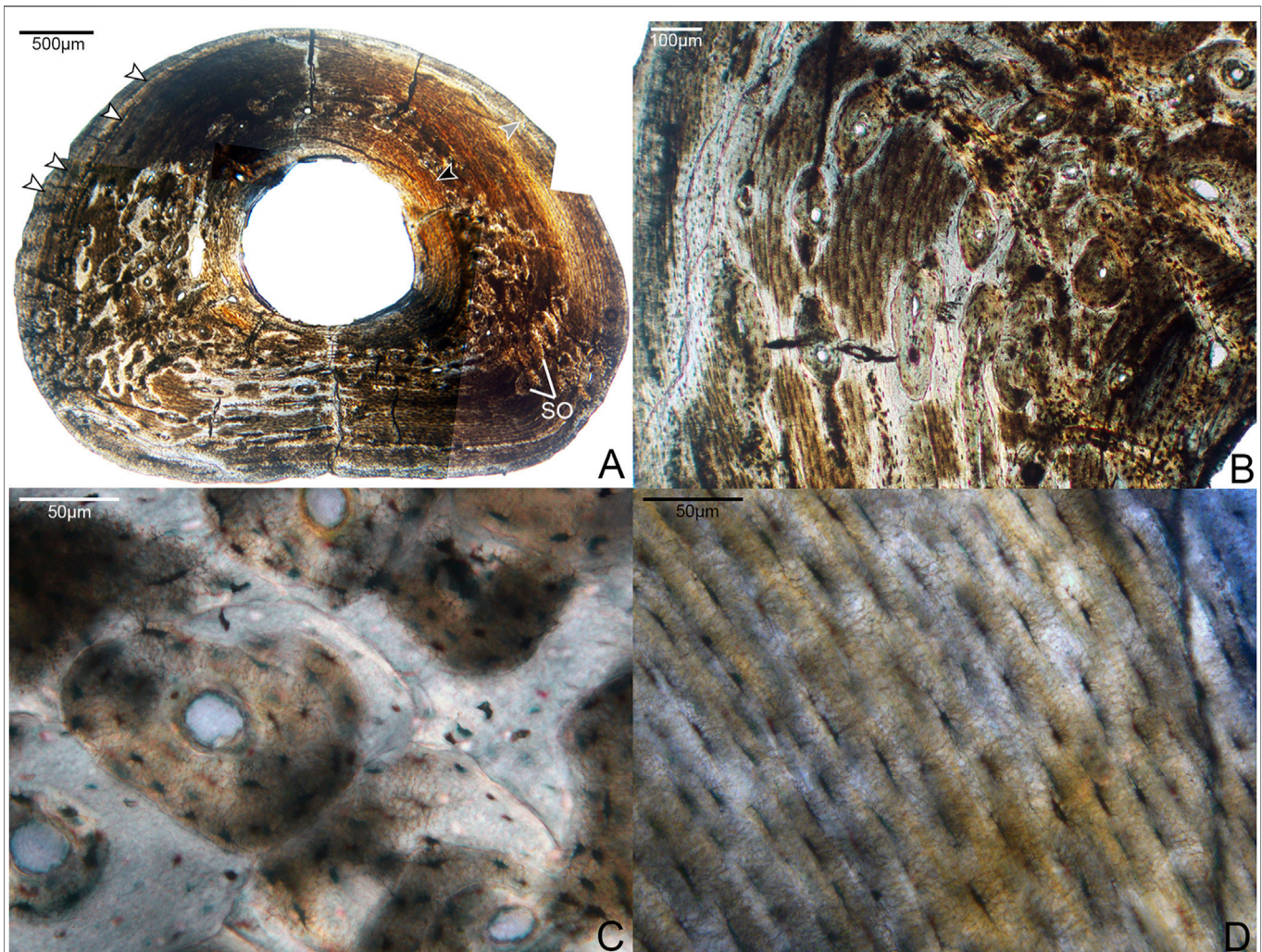


FIGURE 6 | Histological sections of the fourth phalanx of pedal digit IV. **(A)** Complete cross-section of DIIp4, showing a thicker cortex than DIIp2 but otherwise similar organization of tissue: the bone is primarily composed of a parallel-fibered middle layer with large regions of secondary growth, bordered endosteally by a thick, prominent ICL (black arrow) and periosteally by a thin, variably present OCL (gray arrow). White arrows indicate several growth lines, though it is not possible to trace each one entirely around the cortex due to preservational damage. SO indicates several of many secondary osteons. 40x, plane light. **(B)** A close-up of an area of remodeling in the cortex, showing a dense clustering of secondary osteons. 100x, plane light. **(C)** Detailed microanatomy of several secondary osteons present in this element. 400x, plane light. **(D)** Detailed microanatomy of an un-remodeled region of the cortex, composed of parallel-fibered bone with thin, elongate osteocyte lacunae. 400x, plane light.

TABLE 2 | Average cortical diameter and thickness of skeletal elements from *Mirace eatoni* sectioned in this study.

| Element | Average cortical diameter (μm) | Average cortical thickness (μm) |
|----------------------|------------------------------------------------|-------------------------------------------------|
| Humerus | — | 1542 |
| Femur | 5101* | 1392 |
| Metatarsal | — | 1285 |
| Digit II, phalanx I | 1349 | 766 |
| Digit IV, phalanx IV | 2844 | 1090 |

Due to the highly fragmentary nature of the sample from the radius, measurements were not taken. Asterisk indicates estimation.

parallel-fibered and regionally distributed incipient fibrolamellar bone, with unusually high vascular porosity (for a skeletally mature enantiornithine) in one humeral thin section (Table 1). The radius is entirely parallel-fibered. The femur shows regions of CCCB and parallel-fibered bone, with secondary osteons. The metatarsal is predominantly fibrolamellar with a small parallel-fibered region (although this observation is based on an incomplete cortical cross-section). Finally, the phalanges are regionally parallel-fibered with extensive evidence of remodeling obscuring probable regions of CCCB.

The only other stem-avian taxa for which a comparable breadth of elements has been sampled are the Early Cretaceous *Confuciusornis*, and the Early Cretaceous enantiornithine *Mirusavis*. In the case of *Confuciusornis*, the intraskeletal variation observed in *Mirarce* stands in stark contrast to reported histological patterns (De Ricqlès et al., 2003; Chinsamy et al., 2020). *Confuciusornis* exhibits fibrolamellar bone and high levels of vascularity nearly uniformly across all sectioned elements (including the same elements as were sampled in this study). This demonstrates that, although both the *Mirarce* and *Confuciusornis* lineages had relatively elevated growth rates, each lineage was characterized by very different growth strategies, thereby producing very different osteohistological features across the skeleton. Overall, growth in *Confuciusornis* is more similar to that in crown birds, reaching near adult size within the first year such that all LAGs are located in the OCL (De Ricqlès et al., 2003; Chinsamy et al., 2020), whereas elevated bone deposition rates in *Mirarce* were interrupted numerous times prior to achieving skeletal maturity as evidenced by growth lines located within the inner portion of the bone cortex.

The Early Cretaceous enantiornithine *Mirusavis* has also been sampled nearly as extensively as *Mirarce*, with five elements sectioned (humerus, radius, femur, tibiotarsus and scapula) and the entire specimen scanned using computed tomography (Wang M. et al., 2020). The distal hindlimbs are not preserved in *Mirusavis* such that comparison with *Mirarce* can only be made between the humerus, radius, and femur. In contrast to *Mirarce*, the histology in all long bone elements of *Mirusavis* is very consistent, with all sampled cortices composed of parallel fibered bone with little to no vascularization, which consists of simple longitudinal canals where present (Wang M. et al., 2020). The computed tomography scans suggest this bone tissue predominated throughout the entire preserved skeleton. A single LAG is present in the humerus and tibiotarsus but no growth lines are visible in either the radius or femur. Compared to *Mirarce*, growth in *Mirusavis* appears to have been far more consistent between elements. The absence of any indication of remodeling may be due to the relatively more immature ontogenetic stage of this taxon, which was likely still growing despite the fact it was clearly reproductively active, as indicated by the preservation of medullary bone (Wang M. et al., 2020).

While the radius of *Mirarce* exhibits histological characteristics that have come to be expected for enantiornithines (a cortex predominantly composed of parallel-fibered bone with low vascular porosity), other elements of this taxon preserve the first evidence of fibrolamellar/incipient fibrolamellar bone tissue in a somatically mature enantiornithine. This tissue type was previously only known in a perinatal enantiornithine specimen (Chinsamy and Elzanowski, 2001). Although growth rates were apparently not as elevated as those observed in *Confuciusornis* and some ornithuromorphs [e.g., *Iteravis* and *Ichthyornis* (Chinsamy et al., 1998; O'Connor et al., 2015)] the incipient fibrolamellar bone in the humerus and fibrolamellar complex in the tarsometatarsus of *Mirarce* are unique among enantiornithines, thereby increasing the recognized diversity of developmental strategies utilized by this clade.

The humerus of *Mirarce* exhibits a complex and variegated growth pattern. The endosteal and periosteal layers of organized, parallel-fibered bone, together with the growth lines in each of these layers, is indicative of a sustained period of slow growth. The middle layer of incipient fibrolamellar bone in the humerus suggests that this was interrupted by a period of rapid growth. These data reveal a cyclical growth strategy, with a period of slow growth followed by a period of faster growth, and then culminating with a resumption of slow growth. In the OCL, the more numerous growth lines, separated by smaller spaces suggests that this second slowing of growth was more prolonged. It is possible there were additional cycles of slow and fast growth, the traces of which may have been erased by endosteal resorption. This pattern stands in contrast to other enantiornithine taxa, which have humeri with very low levels of vascularity and cortices composed of parallel-fibered bone with either no LAG expression (*Mirusavis* IVPP V18962 (Wang M. et al., 2020), *Parvavis* IVPP V18586 (Wang M. et al., 2014), *Cruralispennia* IVPP V21711 (Wang et al., 2017b), *Pterygornis* IVPP V16363 (Wang et al., 2017a)) or with LAGs in the mid-cortex (STM29-8 (O'Connor et al., 2014)). The overall absence of fibrolamellar bone in these enantiornithines suggest that rapid growth ceased at a much earlier stage in postnatal development. This may also be partially due to differences in body size, since Early Cretaceous enantiornithines were overall much smaller. However, variation in body size cannot explain differences in bone tissue observed between *Mirarce* and similarly sized enantiornithines from the Late Cretaceous Lecho Formation in which the cortical bone consists entirely of avascular parallel-fibered tissue (Chinsamy et al., 1995).

The tarsometatarsus of *Mirarce* shows evidence of a similar cyclical pattern. The middle cortical layer is dominated by fibrolamellar bone, bounded by an OCL containing 2-3 growth lines. There is also evidence of three growth lines in the endosteal portion of the middle layer, that have been partially obscured by endosteal resorption and deposition of the ICL. None of the growth lines present in this element can be traced for any great distance around the cortex, indicating strong cortical drift and asymmetrical growth. This asymmetrical growth is also hinted at by a small parallel-fibered area, which possibly was part of a larger region of this element that was growing more slowly than the portion sectioned in this study. Evidence of asymmetrical growth similarly occurs in the femur, with CCCB concentrated in the lateral and caudal regions. The single growth mark (visible only in the caudal cortex due to cortical drift) is located near the periosteal surface. This element exhibits an OCL, ICL, and middle cortical layer with no additional evidence of the cycles of slow and fast growth seen in the humerus and metatarsal.

The surprising difference in number of growth lines between the femur and the humerus could be accounted for in several ways. If the skeleton was indeed exposed subaerially, lines could have been lost due to flaking. However, our examination of the exterior bone of the femur rules out significant loss of external cortex. The more proximal position of the femoral sample provides a possible alternate explanation. Ossification of avian long bones proceeds from the midshaft, so the more proximal sample might potentially preserve fewer growth marks. However,

if this were the case, one would expect the recovered LAGs in the proximal sample to be the most external, which is not the case here. Another alternative is that additional LAGs were lost due to periosteal resorption, consistent with the evidence of strong cortical drift in the femur. Ultimately, at this juncture we can only suggest that a better understanding of the possibility of differential timing in enantiornithine forelimb/hindlimb development requires additional data.

Taken collectively, these data support previous inferences that enantiornithines did not experience extended periods of very fast, sustained skeletal growth in which skeletal maturity was achieved within the first year as in most modern birds. However, it is not entirely accurate to characterize this entire clade as “slow growing.” Evidence from *Mirarce* indicates that, by the Late Cretaceous, at least one lineage of enantiornithines evolved relatively higher growth rates that were periodically sustained to varying degrees across the skeleton into later ontogenetic stages. Some elements matured very early in ontogeny (the radius); others continued fast growth intermittently into adulthood (the humerus and tarsometatarsus); and still others document high levels of secondary growth and remodeling (the pedal phalanges and portions of the femur). The variation observed in this taxon indicates allometric growth between different elements. This has already been observed in previous studies of both ornithuromorphs and some enantiornithines, in which the pectoral limb elements consistently show signs indicative of faster growth compared to the pelvic limb (O'Connor et al., 2014; Wang and Zhou, 2016). Such allometric growth has similarly been documented in Neornithes (e.g., Carrier and Auriemma, 1992; Prondvai et al., 2020).

Enantiornithine Life History Patterns

Observations from this study allow us to hypothesize several life history trends across Enantiornithes. First, antebrachial elements (the radius and ulna) in adult and late-subadult individuals are almost exclusively characterized by slow-growing bone across taxa and even ontogenetic stages. More generally speaking, these elements are often composed of bone that is more mature relative to the humerus (with a greater proportion of parallel-fibered bone, lower vascularity, and in some cases even lamellar bone). This is the case in *Mirarce*, *Pterygornis* IVPP V16363 (Wang et al., 2017a), subadult *Eopengornis* STM24-1 (Wang X. et al., 2014), and *Mirusavis* IVPP V18692 (Wang M. et al., 2020). The differences in humeral growth may produce ontogenetic differences in the proportions of the forelimb elements (such that the humerus is relatively shorter in juveniles) that reflect phylogenetic underpinnings (the relatively shorter humerus in non-avian non-volant close relatives). Further analyses of enantiornithine intraskkeletal variation across ontogenetic stages, and quantitative assessments of histological maturity, will help parse out answers to these questions of function.

Furthermore, a difference in “maturity” of the humerus and femur also appears to be a common characteristic of the clade Enantiornithes. The humerus often exhibits bone that is less mature and faster growing than the femur, being characterized by relatively higher levels of vascularity, the presence of regional

incipient fibrolamellar bone (in some cases), a comparatively less-developed OCL, and/or and fewer growth lines. Femora, in contrast, often have lower vascularity, no fibrolamellar bone, thicker OCLs, and more growth lines. This pattern persists in most enantiornithines for which the humerus and femur have both been sectioned (e.g., *Zhouornis* CNUVB-0903 (Zhang et al., 2013), STM 29-8 (O'Connor et al., 2014), *Pterygornis* IVPP V16363 (Wang et al., 2017a), and *Eopengornis* STM24-1 (Wang X. et al., 2014)). Furthermore, Prondvai et al. (2018) assign higher “intraskkeletal precocity ranks” to the humerus than the femur in *Eosinopteryx*, *Anchiornis*, and *J. curvipes*; that is, they describe the tissue of the humerus as less functionally mature than that of the femur. Additionally, the humerus was found to be less mature than pelvic limb elements in the dromaeosaurid dinosaurs *Wulong* and *Sinornithosaurus* (Poust et al., 2020). The seemingly widespread occurrence of this pattern suggests it may have deep evolutionary origins.

However, we note that *Mirusavis* appears to break from this larger trend, exhibiting a growth line in the humerus and not the femur. Furthermore, whether *Mirarce* holds to this pattern is currently ambiguous. In terms of certain attributes, the humerus does indeed bear evidence of being faster-growing (e.g., reticulating canals, higher vascular porosity, and regional fibrolamellar bone). On the other hand, this bone has considerably more growth lines than the femur, suggesting that growth of this element had slowed down much earlier. The proximal sampling of the femur and incomplete cross-section of the humeral cortex make meaningful comparisons difficult. This will remain an open question until potential non-destructive histological analysis of the complete humerus and femur of the holotype can be conducted or more specimens become available through future collecting. This question also emphasizes the need for additional histological sectioning of other large-bodied Mesozoic birds.

CONCLUSION

The microanatomy of *Mirarce eatoni* is complex and highly variable both across the skeleton, and even within individual elements. This specimen emphasizes that many categories used to describe microstructural anatomy are in fact part of a spectrum. Fibrolamellar bone may be incipient and may grade into parallel-fibered tissue. Orientation of vascular canals may be predominantly reticular in one thin section, and predominantly longitudinal in the consecutive section. A LAG may grade into an annulus, forming a growth line that is not definitively one or the other. A cross-section of a single element may have large regions of fast-growing bone and large regions of slower-growing bone, leading to asymmetrical growth and the formation of anatomical landmarks at the gross level.

Some skeletal elements of *Mirarce eatoni*, such as the radius, underwent relatively constant, slow growth. Others underwent alternating periods of slow and fast growth, as indicated in the histological patterns of the humerus and tarsometatarsus. Still

others, such as the femur and phalanges, underwent extensive secondary remodeling. Some elements also indicate that asymmetrical growth was an important strategy for achieving adult morphology in this taxon, as seen in the tarsometatarsus and femur. This very possibly was even more common across the skeleton, though our data here are limited by the necessity of sampling only broken bones in the holotype specimen.

This growth strategy appears to represent a marked departure from that of other enantiornithines, which generally appear to have been dominated by slow, steady growth occasionally slowing enough to deposit a growth line. These differences may be partially attributable to body size; *Mirarce* is considerably larger than most of the small, Early Cretaceous enantiornithines that have been sampled. However, it is significant that *Mirarce* also appears to differ substantially from other large-bodied, Late Cretaceous enantiornithines (Chinsamy et al., 1995), although this may be a result of differences in sampling location, as we were forced to sample the femoral diaphysis proximally.

Additional intraskkeletal sampling of other enantiornithines may reveal that the ontogenetic patterns of *Mirarce* were more common in this clade or may provide additional evidence that these are derived traits of the Late Cretaceous taxon. Ultimately, this study emphasizes the importance of understanding intraskkeletal patterns of ontogeny by sampling multiple elements and using this as a basis for making inferences about growth strategies and life-history traits.

DATA AVAILABILITY STATEMENT

The datasets presented in this study can be found in online repositories. The names of the repository/repository and accession number(s) can be found below: Photographs of histological sections of the specimens presented in this paper (both those used in the figures and additional images) are available from Zenodo (<https://zenodo.org>). The original thin-sections can be accessed at the University of California Museum of Paleontology in Berkeley, CA, United States.

REFERENCES

- Atterholt, J., Hutchison, J. H., and O'Connor, J. K. (2018). The most complete enantiornithine from North America and a phylogenetic analysis of the Avisauridae. *PeerJ* 6, e5910. doi:10.7717/peerj.5910
- Bourdon, E., Castanet, J., de Ricqlès, A., Scofield, P., Tennyson, A., Lamrous, H., et al. (2009). Bone growth marks reveal protracted growth in New Zealand kiwi (Aves, Apterygidae). *Biol. Lett.* 5, 639–642. doi:10.1098/rsbl.2009.0310
- Cambra-Moo, O., Buscalioni, Á. D., Cubo, J., Castanet, J., Loth, M.-M., De Margerie, E., et al. (2006). Histological observations of enantiornithine bone (saurischia, Aves) from the lower cretaceous of las hoyas (Spain). *Comptes Rendus Palevol* 5, 685–691. doi:10.1016/j.crpv.2005.12.018
- Carrier, D. R., and Auriemma, J. (1992). A developmental constraint on the fledging time of birds. *Biol. J. Linn. Soc.* 47, 1–17. doi:10.1111/j.1095-8312.1992.tb00656.x
- Chinsamy, A., and Elzanowski, A. (2001). Bone histology. Evolution of growth pattern in birds. *Nature* 412, 402. doi:10.1038/35086650
- Chinsamy, A., Marugán-Lobón, J., Serrano, F. J., and Chiappe, L. (2020). Osteohistology and life history of the basal pygostylian, *Confuciusornis sanctus*. *Anat. Rec. (Hoboken)* 303, 949–962. doi:10.1002/ar.24282
- Chinsamy, A., Chiappe, L. M., and Dodson, P. (1995). Mesozoic avian bone microstructure: physiological implications. *Paleobiology* 21, 561–574. doi:10.1017/s0094837300013543
- Chinsamy-Turan, A. (2005). *The microstructure of dinosaur bone: deciphering biology with fine-scale techniques*. Baltimore: John Wiley & Sons.
- Cullen, T. M., Canale, J. I., Apesteguía, S., Smith, N. D., Hu, D., and Makovicky, P. J. (2020). Osteohistological analyses reveal diverse strategies of theropod dinosaur body-size evolution. *Proc. Biol. Sci.* 287, 20202258. doi:10.1098/rspb.2020.2258
- Cullen, T. M., Evans, D. C., Ryan, M. J., Currie, P. J., and Kobayashi, Y. (2014). Osteohistological variation in growth marks and osteocyte lacunar density in a

AUTHOR CONTRIBUTIONS

JA: Made histological sections, photographed slides, took measurements, made tables and figures, contributed to writing and editing the manuscript. AP: Made histological sections, photographed slides, contributed to writing and editing the manuscript. GE: Made histological sections, contributed to writing and editing the manuscript. JO'C: Contributed to writing and editing the manuscript.

FUNDING

JA was supported by the Joseph Mallard Graduate Fellowship from the Museum of Vertebrate Zoology at the University of California, Berkeley; and the Doris O. and Samuel P. Welles Research Fund from the University of California Museum of Paleontology. JO'C was supported by the Strategic Priority Research Program of the Chinese Academy of Sciences (Grant Number: XDB26000000) and the National Natural Science Foundation (Grant Number: 41688103). AP was supported by a grant from the Jurassic Foundation; and a gift in honor of Jamie Robinson. GE was supported by NSF EAR 0207744 and 1736386.

ACKNOWLEDGMENTS

We thank Pat Holroyd for facilitating this research at the University of California Museum of Paleontology (UCMP). We also are grateful to Diane Erwin for maintaining the histology lab at the UCMP, as well as Seth Finnegan, Sara Kahanamoku, and the Finnegan lab for access to and assistance with the Keyence microscope. We thank Howard Hutchison, who originally discovered the specimen and gave his consent for destructive sampling. Holly Woodward kindly provided helpful ideas and insight regarding histological interpretations of this specimen. We thank Michael Wolf, who was our consulting mineralogist. Finally, we express gratitude to Marvalee Wake, David Lindberg, Rauri Bowie, Sabrina Agarwal and two reviewers who provided very helpful feedback on earlier versions of this work.

- theropod dinosaur (Coelurosauria: ornithomimidae). *BMC Evol. Biol.* 14, 231. doi:10.1186/s12862-014-0231-y
- De Ricqlès, A. J., Padian, K., Horner, J. R., Lamm, E.-T., and Myhrvold, N. (2003). Osteohistology of *Confuciusornis sanctus* (theropoda: Aves). *J. Vertebr. Paleontol.* 23, 373. doi:10.1671/0272-4634(2003)023[0373: oocsta]2.0.co;2
- De Ricqlès, A. (1976). "On bone histology of fossil and living reptiles, with comments on its functional and evolutionary significance," in *Morphology and biology of reptiles*. Editor C. B. Cox. London, United Kingdom: Linnean Society, 123–149.
- Enlow, D. H. (1963). *Principles of bone remodeling: an account of post-natal growth and remodeling processes in long bones and the mandible*. Springfield: Generic.
- Erickson, G. (2005). Assessing dinosaur growth patterns: a microscopic revolution. *Trends Ecol. Evol. (Amst)* 20, 677–684. doi:10.1016/j.tree.2005.08.012
- Erickson, G. M., Curry Rogers, K., Varricchio, D. J., Norell, M. A., and Xu, X. (2007). Growth patterns in brooding dinosaurs reveals the timing of sexual maturity in non-avian dinosaurs and genesis of the avian condition. *Biol. Lett.* 3, 558–561. doi:10.1098/rsbl.2007.0254
- Erickson, G. M., Rauhut, O. W., Zhou, Z., Turner, A. H., Inouye, B. D., Hu, D., et al. (2009). Was dinosaurian physiology inherited by birds? Reconciling slow growth in *Archaeopteryx*. *PLoS One* 4, e7390. doi:10.1371/journal.pone.0007390
- Evans, D. C., Barrett, P. M., Brink, K. S., and Carrano, M. T. (2015). Osteology and bone microstructure of new, small theropod dinosaur material from the early Late Cretaceous of Morocco. *Gondwana Res.* 27, 1034–1041. doi:10.1016/j.gr.2014.03.016
- Francillon-Vieillot, H., De Buffrénil, V., Castanet, J., Géraudie, J., Meunier, F., Sire, J., et al. (1990). "Microstructure and mineralization of vertebrate skeletal tissues," in *Skeletal biomineralization: patterns, processes, and evolutionary trends*. Editor J. G. Carter. New York, NY: Van Nostrand Reinhold, 471–530.
- Gill, F. B. (2007). "Parents and their offspring," in *Ornithology*. Editor F. B. Gill. 3rd Edition (New York, NY: WH Freeman and Company), 467–502.
- Heck, C. T., Varricchio, D. J., Gaudin, T. J., Woodward, H. N., and Horner, J. R. (2019). Ontogenetic changes in the long bone microstructure in the nine-banded armadillo (*Dasypus novemcinctus*). *PLoS One* 14, e0215655. doi:10.1371/journal.pone.0215655
- Horner, J. R., De Ricqlès, A., and Padian, K. (2000). Long bone histology of the hadrosaurid dinosaur *Maiasaura peeblesorum*: growth dynamics and physiology based on an ontogenetic series of skeletal elements. *J. Vertebr. Paleontol.* 20, 115–129. doi:10.1671/0272-4634(2000)020[0115:lbhoth]2.0.co;2
- Horner, J. R., de Ricqlès, A., and Padian, K. (1999). Variation in dinosaur skeletochronology indicators: implications for age assessment and physiology. *Paleobiology* 25, 295–304. doi:10.1017/s0094837300021308
- Hu, H., O'Connor, J. K., and Zhou, Z. (2015). A new species of Pengornithidae (Aves: Enantiornithes) from the Lower Cretaceous of China suggests a specialized scansorial habitat previously unknown in early birds. *PLoS One* 10, e0126791. doi:10.1371/journal.pone.0126791
- Hu, H., and O'Connor, J. K. (2017). First species of Enantiornithes from Sihedang elucidates skeletal development in Early Cretaceous enantiornithines. *J. Syst. Palaeontology* 15, 909–926. doi:10.1080/14772019.2016.1246111
- Huttenlocker, A. K., Woodward, H. N., and Hall, B. K. (2013). "The biology of bone," in *Bone histology of fossil tetrapods*. Editors K. Padian and E.-T. Lamm. Berkeley and Los Angeles: University of California Press, 13–34.
- Knoll, F., Chiappe, L. M., Sanchez, S., Garwood, R. J., Edwards, N. P., Wogelius, R. A., et al. (2018). A diminutive perinate European Enantiornithes reveals an asynchronous ossification pattern in early birds. *Nat. Commun.* 9, 937–939. doi:10.1038/s41467-018-03295-9
- Lee, A. H., and Werning, S. (2008). Sexual maturity in growing dinosaurs does not fit reptilian growth models. *Proc. Natl. Acad. Sci. USA* 105, 582–587. doi:10.1073/pnas.0708903105
- Lee, A. H., and O'Connor, P. M. (2013). Bone histology confirms determinate growth and small body size in the noasaurid theropod *Masiakasaurus* knopfleri. *J. Vertebr. Paleontol.* 33, 865–876. doi:10.1080/02724634.2013.743898
- O'Connor, J. K., Chiappe, L. M., and Bell, A. (2011). "Pre-modern birds: avian divergences in the mesozoic," in *Living dinosaurs: the evolutionary history of modern birds*. Editors G. Dyke and G. Kaiser (New York, NY: John Wiley & Sons, Ltd.), 39–114.
- O'Connor, J. K., Erickson, G. M., Norell, M., Bailleul, A. M., Hu, H., and Zhou, Z. (2018). Medullary bone in an Early Cretaceous enantiornithine bird and discussion regarding its identification in fossils. *Nat. Commun.* 9, 1–8. doi:10.1093/nsr/nwz214
- O'Connor, J. K., Wang, M., Zheng, X.-T., Wang, X.-L., and Zhou, Z.-H. (2014). The histology of two female Early Cretaceous birds. *Vertebrata Palasiatica* 52, 112–128.
- O'Connor, J. K., Wang, M., Zhou, S., and Zhou, Z. (2015). Osteohistology of the lower cretaceous yixian formation ornithuromorph (Aves) *Iteravis huchzermeyeri*. *Palaeontol. Electronica* 18, 1–11. doi:10.26879/520
- Poust, A. W., Gao, C., Varricchio, D. J., Wu, J., and Zhang, F. (2020). A new microraptorine theropod from the Jehol Biota and growth in early dromaeosaurids. *Anat. Rec. (Hoboken)* 303, 963–987. doi:10.1002/ar.24343
- Prondvai, E., Witten, P. E., Abourachid, A., Huysseune, A., and Adriaens, D. (2020). Extensive chondroid bone in juvenile duck limbs hints at accelerated growth mechanism in avian skeletogenesis. *J. Anat.* 236, 463–473. doi:10.1111/joa.13109
- Prondvai, E., Godefroit, P., Adriaens, D., and Hu, D.-Y. (2018). Intraskelatal histovariability, allometric growth patterns, and their functional implications in bird-like dinosaurs. *Scientific Rep.* 8, 1–16. doi:10.1038/s41598-018-20640-6
- Wang, M., Li, Z., and Zhou, Z. (2017a). Insight into the growth pattern and bone fusion of basal birds from an Early Cretaceous enantiornithine bird. *Proc. Natl. Acad. Sci. USA* 114, 11470–11475. doi:10.1073/pnas.1707237114
- Wang, M., O'Connor, J. K., Pan, Y., and Zhou, Z. (2017b). A bizarre Early Cretaceous enantiornithine bird with unique crural feathers and an ornithuromorph plough-shaped pygostyle. *Nat. Commun.* 8, 1–12. doi:10.1038/ncomms14141
- Wang, M., O'Connor, J. K., Bailleul, A. M., and Li, Z. (2020). Evolution and distribution of medullary bone: evidence from a new Early Cretaceous enantiornithine bird. *Natl. Sci. Rev.* 7, 1068–1078. doi:10.1093/nsr/nwz214
- Wang, X.-R., Cau, A., Kundrát, M., Chiappe, L. M., Ji, Q., Wang, Y., et al. (2020). A new advanced ornithuromorph bird from Inner Mongolia documents the northernmost geographic distribution of the Jehol paleornithofauna in China. *Hist. Biol.* doi:10.1080/08912963.2020.1731805
- Wang, M., and Zhou, Z. (2016). A new adult specimen of the basalmost ornithuromorph bird *Archaeorhynchus spatula* (Aves: Ornithuromorpha) and its implications for early avian ontogeny. *J. Syst. Palaeontology* 15, 1–18. doi:10.1080/14772019.2015.1136968
- Wang, M., Zhou, Z., and Xu, G. (2014). The first enantiornithine bird from the Upper Cretaceous of China. *J. Vertebr. Paleontol.* 34, 135–145. doi:10.1080/02724634.2013.794814
- Wang, X., O'Connor, J. K., Zheng, X., Wang, M., Hu, H., and Zhou, Z. (2014). Insights into the evolution of rachis dominated tail feathers from a new basal enantiornithine (Aves: ornithothoraces). *Biol. J. Linn. Soc. Lond.* 113, 805–819. doi:10.1111/bj.12313
- Werning, S. (2012). The ontogenetic osteohistology of *Tenontosaurus tilletti*. *PLoS One* 7, e33539. doi:10.1371/journal.pone.0033539
- Woodward, H. N., Horner, J. R., and Farlow, J. O. (2014). Quantification of intraskelatal histovariability in Alligator mississippiensis and implications for vertebrate osteohistology. *PeerJ* 2, e422. doi:10.7717/peerj.422
- Xu, X., Zhou, Z., Dudley, R., Macken, S., Chuong, C. M., Erickson, G. M., et al. (2014). An integrative approach to understanding bird origins. *Science* 346, 1253293. doi:10.1126/science.1253293
- Zhang, F., Hou, L., and Ouyang, L. (1998). Osteological microstructure of *Confuciusornis*: preliminary report. *Vertebrata Palasiatica* 36, 126–135.
- Zhang, Z., Chiappe, L. M., Han, G., and Chinsamy, A. (2013). A large bird from the Early Cretaceous of China: new information on the skull of

- enantiornithines. *J. Vertebr. Paleontol.* 33, 1176–1189. doi:10.1080/02724634.2013.762708
- Zheng, X., O'Connor, J., Wang, X., Wang, M., Zhang, X., and Zhou, Z. (2014). On the absence of sternal elements in *Anchiornis* (Paraves) and *Sapeornis* (Aves) and the complex early evolution of the avian sternum. *Proc. Natl. Acad. Sci. USA* 111, 13900–13905. doi:10.1073/pnas.1411070111
- Zheng, X., O'Connor, J. K., Wang, X., Pan, Y., Wang, Y., Wang, M., et al. (2017). Exceptional preservation of soft tissue in a new specimen of *Eoconfuciusornis* and its biological implications. *Natl. Sci. Rev.* 4, 441–452. doi:10.1093/nsr/nwx004

Conflict of Interest: The authors declare that the research was conducted in the absence of any commercial or financial relationships that could be construed as a potential conflict of interest.

Copyright © 2021 Atterholt, Poust, Erickson and O'Connor. This is an open-access article distributed under the terms of the Creative Commons Attribution License (CC BY). The use, distribution or reproduction in other forums is permitted, provided the original author(s) and the copyright owner(s) are credited and that the original publication in this journal is cited, in accordance with accepted academic practice. No use, distribution or reproduction is permitted which does not comply with these terms.

GLOSSARY

CNU Capital Normal University, Beijing, China

IVPP Institute of Paleontology and Paleoanthropology, Beijing, China

LH Las Hoyas Collection, Unidad de Paleontología, Universidad Autónoma de Madrid, Madrid, Spain

MACN Sección Paleontología de Vertebrados, Museo Argentino de Ciencias Naturales, Buenos Aires, Argentina

MPCM Museo de Paleontología de Castilla-La Mancha, Cuenca, Spain

NGMC National Geological Museum, Beijing, China

PVL Fundación Instituto Miguel Lillo, Tucumán, Argentina

STM Shandong Tianyu Museum of Nature, Pingyi, China

UCMP University of California Museum of Paleontology, Berkeley, United States

ZPAL Zoological Institute of Palaeobiology of the Polish Academy of Sciences, Warsaw, Poland



Osteohistology of the Scapulocoracoid of *Confuciusornis* and Preliminary Analysis of the Shoulder Joint in Aves

Qian Wu^{1,2,3*}, Alida M. Bailleul^{1,2}, Zhiheng Li^{1,2}, Jingmai O'Connor^{1,2,4*} and Zhonghe Zhou^{1,2}

¹ Key Laboratory of Vertebrate Evolution and Human Origins, Institute of Vertebrate Paleontology and Paleoanthropology, Chinese Academy of Sciences, Beijing, China, ² CAS Center for Excellence in Life and Paleoenvironment, Beijing, China, ³ University of the Chinese Academy of Sciences, Beijing, China, ⁴ Field Museum of Natural History, Chicago, IL, United States

OPEN ACCESS

Edited by:

Haijun Song,
China University of Geosciences,
China

Reviewed by:

Francisco José Serrano,
Natural History Museum of Los
Angeles County, United States

Laura E. Wilson,
Fort Hays State University,
United States

*Correspondence:

Qian Wu
wuqian@ivpp.ac.cn
Jingmai O'Connor
jingmai.oconnor@gmail.com

Specialty section:

This article was submitted to
Paleontology,
a section of the journal
Frontiers in Earth Science

Received: 14 October 2020

Accepted: 25 March 2021

Published: 13 April 2021

Citation:

Wu Q, Bailleul AM, Li Z,
O'Connor J and Zhou Z (2021)
Osteohistology of the
Scapulocoracoid of *Confuciusornis*
and Preliminary Analysis of the
Shoulder Joint in Aves.
Front. Earth Sci. 9:617124.
doi: 10.3389/feart.2021.617124

As key components of the tetrapod pectoral girdle, the scapula and coracoid have played a significant role in the evolution of forelimb locomotion among terrestrial vertebrates. The transition from a rigid fused scapulocoracoid in ancestral non-avian theropods to a presumably more flexible separated scapula-coracoid in early birds is considered to be one of the key morphological transitions related to the rapid refinement of flight. In most Mesozoic birds (e.g., Enantiornithes and Ornithuromorpha) and crown birds the scapula and coracoid are separate (unfused), with few exceptions (e.g., flightless paleognaths). In contrast, in *Confuciusornis*, a basal pygostylian from the Early Cretaceous Jehol Biota known from thousands of specimens, the scapula and coracoid remain plesiomorphically fused. This raises questions regarding the influence of shoulder girdle architecture on the early evolution and refinement of avian flight. The paravian scapula-coracoid joint has never previously been investigated using histology, and thus joint morphology has only been inferred superficially. In order to better understand the evolution of this joint in Mesozoic birds, we make the first histological study of the scapulocoracoid glenoid joint in *Confuciusornis*. The results demonstrate that the scapula and coracoid both consist of cancellous and compact bone, with both fibrolamellar and parallel-fibered structure. A thin layer of calcified cartilage is present on the glenoid fossa surface, representing remnants of the articular surface for the humerus. Both histology and computed tomography reveal that the scapulocoracoid of *Confuciusornis* is fully fused, forming a synostosis. Humeral histology suggests the studied individual was nearing completion of its first year of growth, suggesting the *Confuciusornis* scapulocoracoid fused before skeletal maturity was achieved, as in flightless paleognaths, whereas in the plesiomorphic condition fusion occurs late in ontogeny. We hypothesize the fused scapulocoracoid of *Confuciusornis* is secondarily evolved and suggest the primary factor responsible for this morphology may have been a decrease in mechanical stimulation at the glenoid of *Confuciusornis* relative to other volant birds, linked to the unique flight style of this taxon. Further investigation into the histology of the glenoid joint in other Mesozoic paravians and extant birds will help to clarify the morphological transition of the scapula-coracoid joint in early avian evolution.

Keywords: *Confuciusornis*, histology, scapulocoracoid, pectoral girdle, cretaceous birds

INTRODUCTION

Structural modifications of the scapula and coracoid during the early evolution of Aves are often described as being among the key morphological changes in the early evolution of birds (Chatterjee, 1997; Chiappe and Witmer, 2002; O'Connor et al., 2011). In *Archaeopteryx* the scapula and coracoid are generally regarded as synostosed elements that form a single immobile unit called the scapulocoracoid, a morphology inherited from non-avian dinosaurs (Chiappe and Witmer, 2002). However, these two bones became distinct at an early stage of avian evolution, being already separate in the long boney tailed bird *Jeholornis*, a taxon commonly resolved in cladistic analyses as only more derived than *Archaeopteryx* (Figure 1; Zhou and Zhang, 2002a; O'Connor and Zhou, 2019). The scapula and coracoid to form the glenoid surface for the articulation of the humerus in all tetrapods (Benton, 2014). These elements are key components of the pectoral girdle and have played an important role during the evolution of locomotion in terrestrial vertebrates (Benton, 2014). Therefore, it follows that the change early in avian evolution from fusion between the scapula and coracoid to complete separation of these elements most likely represents a flight adaptation, presumably facilitating greater mobility and more advanced forms of powered flight.

However, as new specimens of *Archaeopteryx* have recently become available, this dichotomy between fused and separate has been shaken, as in most specimens the scapula and coracoid appear to be only sutured [e.g., the Eichstätt specimen (the smallest), Solnhofen specimen (the largest), Munich specimen (Elzanowski, 2001), Daiting specimen (Kundrát et al., 2019), Thermopolis specimen (Mayr et al., 2005), and 12th specimen (Rauhut et al., 2018)]. Synchrotron radiation based computed tomography (CT) scans of the Daiting *Archaeopteryx*, a relatively small specimen, revealed that the scapula and coracoid were closely connected but not fully fused, and the two bones were interpreted as forming a sutural contact (Kundrát et al., 2019). The scapulocoracoid is described as fused (or apparently co-ossified) in the London, Berlin, and Maxberg specimens (Ostrom, 1976), suggesting complete fusion occurred late in the ontogeny of *Archaeopteryx* (Chiappe and Witmer, 2002). Although the specific joint morphology apparently changes with ontogeny, these two bones are firmly articulated and immobile in *Archaeopteryx*, forming a scapulocoracoid complex (Chiappe and Witmer, 2002).

Paraves is the clade of maniraptoran theropods that includes Aves and its closest relatives, the Troodontidae and Dromaeosauridae (Brusatte et al., 2014). In these non-avian paravian clades the morphology of the scapulocoracoid joint appears similar to that observed in *Archaeopteryx*, in which fusion of the scapulocoracoid unit is only found in adult individuals. In the probable troodontid *Anchiornis*, sub-adult specimens (e.g., BMNHC PH822 and IVPP V14378) have an unfused scapula and coracoid (Xu et al., 2009; Pei et al., 2017), whereas these elements are apparently fused in other, presumably adult specimens (LPM-B00169) (Hu et al., 2009). The only known specimen of the probable troodontid *Xiaotingia* (STM 27-2), a presumed adult, has a fused scapulocoracoid (Xu et al., 2011) and

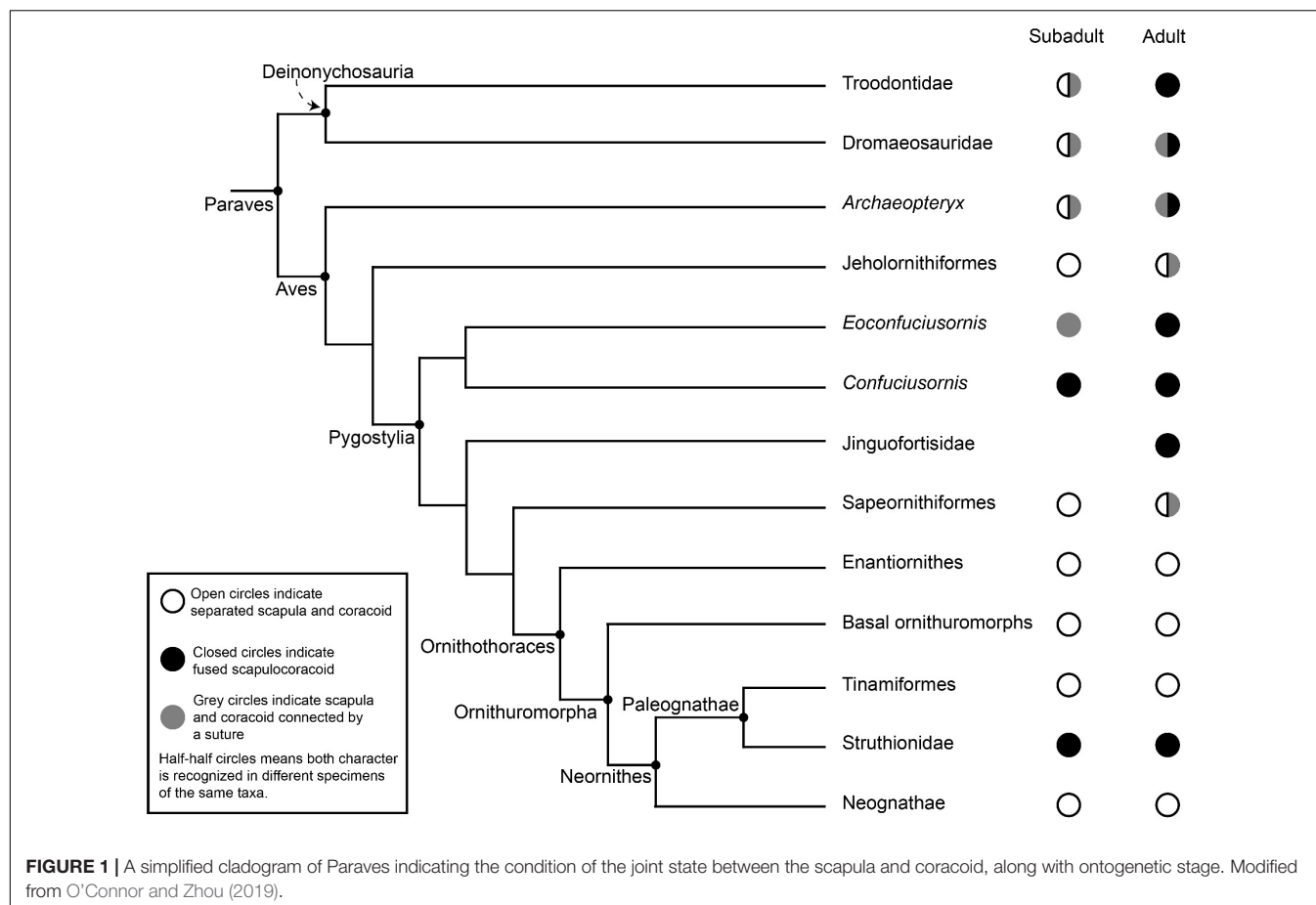
this condition is also reported in the troodontid *Jinfengopteryx* (CAGS-IG-04-0801) (Ji et al., 2005).

Among the Dromaeosauridae, subadult to adult specimens of *Deinonychus* (MOR 1178) (Parsons and Parsons, 2009), *Velociraptor* (IGM 100/986; Parsons and Parsons, 2009), and *Microraptor* (CAGS 20-7-004 and CAGS 20-8-001) (Hwang et al., 2002) reportedly possess fused scapulocoracoids, whereas the two elements are only sutured in obvious juveniles (*Deinonychus* MCZ 8791; Parsons and Parsons, 2015). However, the scapula and coracoid remain connected by a suture in putatively adult specimens of some taxa, including in *Buitreraptor* (MPCA-245) (Makovicky et al., 2005) and *Sinornithosaurus* (IVPP V12811) (Xu et al., 1999). This may suggest that some specimens identified as adults, such as *Deinonychus* (YPM 5236; Parsons and Parsons, 2015), are in fact not fully mature, or that the scapula and coracoid did not become fused in all lineages of dromaeosaurids. It is impossible to differentiate between these hypotheses without relevant histological or CT data, combined with the careful use of suture patterns to assess maturity in these specimens (Bailleul et al., 2016).

Among basal (non-ornithothoracine) lineages of Mesozoic birds, the scapula and coracoid are completely separate in the holotype of *Jeholornis* (Zhou and Zhang, 2002a,b), but in some specimens these bones are preserved firmly articulated (e.g., STM2-19) (O'Connor et al., 2018b) or appear sutured (YFGP-yb2) (Lefèvre et al., 2014). Similarly, in *Sapeornis* (Figure 2) the two elements are tightly joined in the holotype IVPP V12698 (Zhou and Zhang, 2002b, 2003a), but are separate in the subadult specimens DNHMD3078 (Gao et al., 2012), IVPP V13396 (Provini et al., 2008), and HGM-41HIII0405 (Pu et al., 2013).

Confuciusornis is the most common bird in the Jehol Biota, with thousands of specimens reported, mostly from the Yixian Formation (Wang et al., 2019c). Specimens range considerably in size although no clear juveniles are known (humerus length ranging from 41.01 to 78.5 mm; Chiappe et al., 1999, 2008; Zhang et al., 2009; Wang and O'Connor, 2017; Wang et al., 2019c). In all reported specimens of the basal pygostylian *Confuciusornis* the scapulocoracoid is described as fused (Hou, 1997; Chiappe et al., 1999; Ji et al., 1999; Hou et al., 2002; Dalsätt et al., 2006; Zhang et al., 2009; Wang and Zhou, 2018; Wang et al., 2019c), in contrast to the condition in other non-ornithothoracine avians. In the subadult holotype of *Eoconfuciusornis zhengi* IVPP V11977, the oldest and basal-most member of Confuciusornithidae from the Huajiyang Formation, the scapula and coracoid are reportedly only sutured (Zhang et al., 2008a). However, in BMNHC-PH870, an osteologically mature specimen also from the Huajiyang Formation, the scapula and coracoid are reportedly fused (Navalón et al., 2017). This and other potentially ontogenetic differences make it impossible to determine if BMNHC-PH870 is referable to *Eoconfuciusornis* or if it represents another currently unnamed taxon (Navalón et al., 2017).

Despite the enormous number of specimens of *Confuciusornis*, the fact that none reveal an earlier stage in which the scapula and coracoid are sutured or separate appears to represent a distinct departure from other early paravians, in which these elements are only fused in mature, adult specimens. In contrast to other non-ornithomorph paravians, which grew so slowly that they



required several years to reach skeletal maturity (Erickson et al., 2009; Zheng et al., 2014; Prondvai et al., 2018; Shen et al., 2019), *Confuciusornis* had elevated growth rates, reaching near-adult size in the first year of uninterrupted growth (de Ricqlès et al., 2003) after which they continue to grow more slowly for several years forming an outer circumferential layer (OCL) marked by several lines of arrested growth (LAGs) (Chinsamy et al., 2019). This developmental strategy may partly explain the fact the scapulocoracoid is reportedly fused in all known specimens of *Confuciusornis*, a morphology which is otherwise only found in the most mature specimens of taxa with more protracted growth rates (e.g., *Anchiornis*, *Microraptor*, and *Archaeopteryx*). A rapid growth strategy has previously been cited as an explanation for the fusion of the scapulocoracoid in the Jinguoformisidae, a clade of basal pygostylians consisting of two taxa (*Chongmingia* and *Jinguoformis*) each known from a single specimen (Wang et al., 2016, 2018). Histology indicates these two specimens are mature adults (Wang et al., 2016, 2018) making it impossible to determine if the fusion is due to rapid growth, skeletal maturity, or both.

Among neornithines, the scapula and coracoid are typically separate although they are fused into a single scapulocoracoid in some extant flightless taxa including all flightless members of the Paleognathae (the so-called “ratites”), e.g., *Struthio camelus*, *Apteryx australis* (McGowan, 1982),

and *Dromaius novaehollandiae* (Maxwell and Larsson, 2007), and some members of the recently extinct flightless clades the Aepyornithidae, Gastornithidae, and Dinornithiformes (Worthy et al., 2017). Among extant paleognaths, only the volant tinamous (Tinamidae) have separate scapulae and coracoids (Bertelli et al., 2014). The fossil record clearly demonstrates that these two elements were separate in early paleognaths, such as the Paleocene–Middle Eocene Lithornithidae (Torres et al., 2019), indicating that the fused scapulocoracoid of some paleognaths is a derived feature that probably evolved multiple times in this clade along with flightlessness (Faux and Field, 2017). As the wings and sternal carina of Paleocene and Eocene paleognaths were well-developed (Houde, 1986), flightlessness in extant paleognaths is also a derived condition (McNab, 1994; Torres et al., 2019). This suggests that fusion of the scapulocoracoid in neornithines evolved as a consequence of pectoral reduction related to the loss of flight. Notably, in contrast to observations from extinct pennaraptorans, the scapula and coracoid of the ostrich fuse very early on, not via bone but via unmineralized cartilage during embryonic development (day 21) before any extensive ossification has begun (day 22; Maxwell and Larsson, 2009).

Previous studies of neornithines (crown birds) have revealed the developmental trajectory, ossification sequence, regulatory genes, and growth factors of the scapula in embryonic and

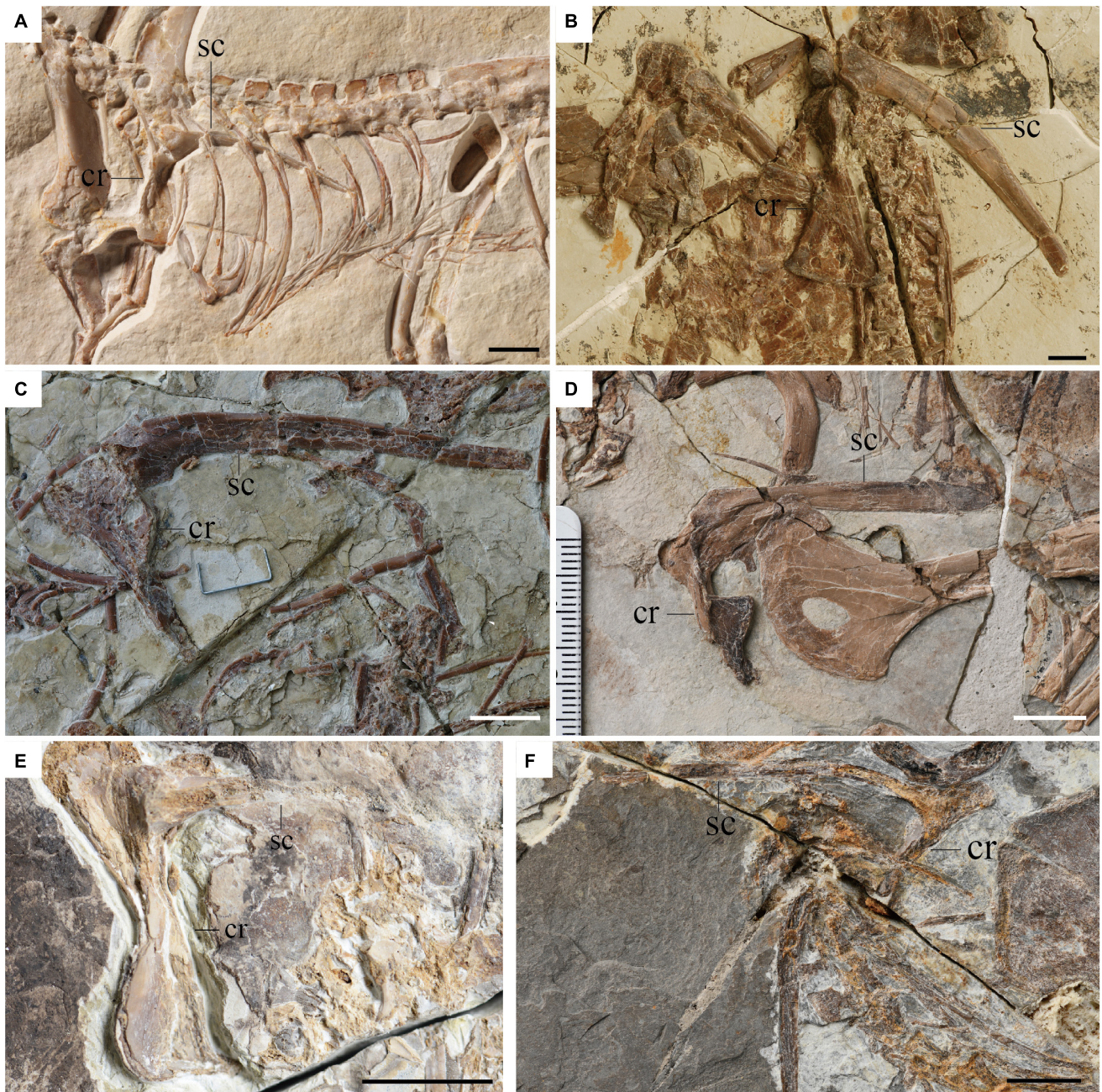


FIGURE 2 | Scapulae and coracoids of basal avialans. **(A)** *Archaeopteryx* Munich specimen; **(B)** *Jeholornis* IVPP V13886 (unpublished specimen); **(C)** *Sapeornis* IVPP V13698 (holotype); **(D)** *Confuciusornis* IVPP V14385; **(E)** *Chongmingia* STM9-9; **(F)** *Jingfuortis* IVPP V24194. Scale bar 1 cm.

early post-hatching growth (Williams, 2003; Sawad et al., 2009; Young et al., 2019). Despite the importance of the scapula-coracoid complex in the pectoral girdle of birds (and in fact in all tetrapods) (Benton, 2014), few histological studies have been conducted on pectoral girdle elements (Russell and Joffe, 1985; Wang et al., 2019a), and the histology of the scapula-coracoid joint has never been reported in any paravian. As a result, the histology of the scapulocoracoid joint is poorly understood even in modern birds. The joint between the

separate scapula and coracoid has been reported in some birds as a syndesmosis (bound together by the Lig. *coracoscapulare interosseum* consisting of elastic cartilage), and in others as an elaborate joint (e.g., *Branta*, *Pelecanus*), in which the articulation is partially synovial and partially syndesmotomic (Baumel and Witmer, 1993). In such a configuration the synovial parts are more mobile than the syndesmoses, as would be expected (Baumel and Witmer, 1993). However, these reports were not accompanied by supporting illustrations.

In extinct organisms descriptions of fusion between elements should be supported with microanatomical evidence, such as histological data, or—at the least—CT data. Surface morphology may suggest a fused joint (i.e., a bony synostosis) even in specimens whose internal anatomy instead reveal the joint to be incompletely fused, retaining either a fibrous suture or some cartilaginous remnants (Bailleul and Horner, 2016). To date, no microanatomical investigation of an apparently fused scapulocoracoid has been conducted on any extinct paravian. Therefore, previous descriptions of purportedly fused scapulocoracoids require re-examination in order to better assess patterns of fusion between these elements. In cases where the two bones are tightly articulated, in particular, it is difficult to determine whether the bones remain separated or if they are actually sutured without investigation of the internal anatomy, as demonstrated in one specimen of *Jeholornis* in which X-rays revealed the presence of a suture (Lefèvre et al., 2014). Here we take a step in this direction by examining the osteohistology of the scapulocoracoid joint morphology in *Confuciusornis*. This joint has never been studied through osteohistology in an extinct theropod until now. We compare the histology to that observed in extant birds in which the scapula and coracoid are fused and unfused, and discuss the underlying factors that may affect fusion of pectoral girdle elements in birds.

Institutional abbreviations. BMNHC, Beijing Museum of Natural History, Beijing, China; CAGS, Chinese Academy of Geological Sciences, Beijing, China; DNHM, Dalian Natural History Museum, Dalian, China; GMV, Geological Museum of China, Beijing, China; HGM, Henan Geological Museum, China; IGM, Mongolian Institute of Geology, Mongolia; IVPP, Institute of Vertebrate Paleontology and Paleoanthropology, Chinese Academy of Sciences, Beijing, China; LPM, Liaoning Paleontological Museum, Liaoning Province, China; MCZ, Museum of Comparative Zoology, Harvard University, Cambridge, MA, United States; MOR, Museum of the Rockies, Bozeman, MT, United States; MPCA, Museo Provincial de Ciencias Naturales, General Roca, Río Negro, Argentina; STM, Shandong Tianyu Museum, Shandong Province, China; YFGP, Yizhou Fossil and Geology Park, Yixian, China; YPM, Yale/Peabody Museum of Natural History, New Haven, CT, United States.

MATERIALS AND METHODS

Specimens

We sectioned the scapulocoracoid through the glenoid of *Confuciusornis* IVPP V11521, a partial skeleton retaining the sternum, ribs, vertebrae, pectoral girdle, pelvis, femora, and tail (Hou et al., 1999). Although this specimen was originally described as the paratype of *Confuciusornis dui* (Hou et al., 1999), it is conservatively referred to *Confuciusornis indet.* After reexamination in the latest analysis concerning the furcula of this same specimen (Wu et al., 2021). The scapulocoracoid is mediolaterally crushed (**Figure 3A**) and the distal part of the scapula is missing. All elements were previously prepared

free from the matrix. The humerus measures 66 mm, which falls within the larger half of the known size range of *Confuciusornis* specimens (humeral length: 41.01–78.5 mm; Chiappe et al., 1999, 2008; Zhang et al., 2009; Wang and O'Connor, 2017; Wang et al., 2019c). As the scapula is incomplete in this specimen, the length of the scapula was not measured.

An adult *Spilopelia chinensis* (Spotted dove) and an 8-day old (post-hatching) *S. camelus* (Common ostrich) were sampled to allow comparison with the scapula-coracoid joint histology in extant birds. The scapulocoracoid of a more mature Common ostrich specimen IVPP OV586 was CT scanned to provide additional comparison. Based on skull length (18 cm), OV586 is estimated to be approximately 6 months old (Castanet et al., 2000; Cuff et al., 2015).

CT Scan of *Confuciusornis* and the Common Ostrich

Prior to cutting, the scapulocoracoid of *Confuciusornis* IVPP V11521 was scanned at Yinghua Testing Co., Ltd., Shanghai, China, using high-resolution micro-computed tomography (μ CT) scanning (Phoenix v | x m) with a detector resolution of 6 μ m per pixel, and three-dimensional reconstructions were created with the software Avizo (version 8.1).

The ostrich scapulocoracoid IVPP OV586 was CT scanned at the Key Laboratory of Vertebrate Evolution and Human Origins at the Institute of Vertebrate Paleontology and Paleoanthropology, Chinese Academy of Sciences, using an industrial CT (mi-CT 450ICT, developed by the Institute of High Energy Physics, Chinese Academy of Sciences) with a detector resolution of 160 μ m per pixel, and three-dimensional reconstructions were created with the software VG studio (version 2.2).

Confuciusornis Ground Sections

The specimen was then embedded in EXAKT Technovit 7200 one-component resin and allowed to dry for 12 h, cut into slices through the glenoid fossa using the CT scans as a guide, and polished until the desired optical contrast was reached (slice thickness \sim 70 μ m). In total, five ground sections were made (also see Wu et al., 2021), observed under natural and polarized light using a Nikon eclipse LV100NPOL, and photographed with a DS-Fi3 camera and the software NIS-Element v4.60. The “photomerge” tool in Adobe Photoshop CS6 was used to reconstruct each section.

Paraffin Section and Staining of Extant Specimens

The shoulder joints of the ostrich and dove were extracted from their thawed carcasses with razor blades and fixed in 10% neutral buffered formalin (NBF) for at least 48 h, then demineralized in HCl and EDTA (JYBL-II, Cat DD0017, Leagene). After demineralization, the samples were embedded following the standard protocol for paraffin sections (Bailleul et al., 2017), dehydrated with a graded series of ethanol solutions (in 70,

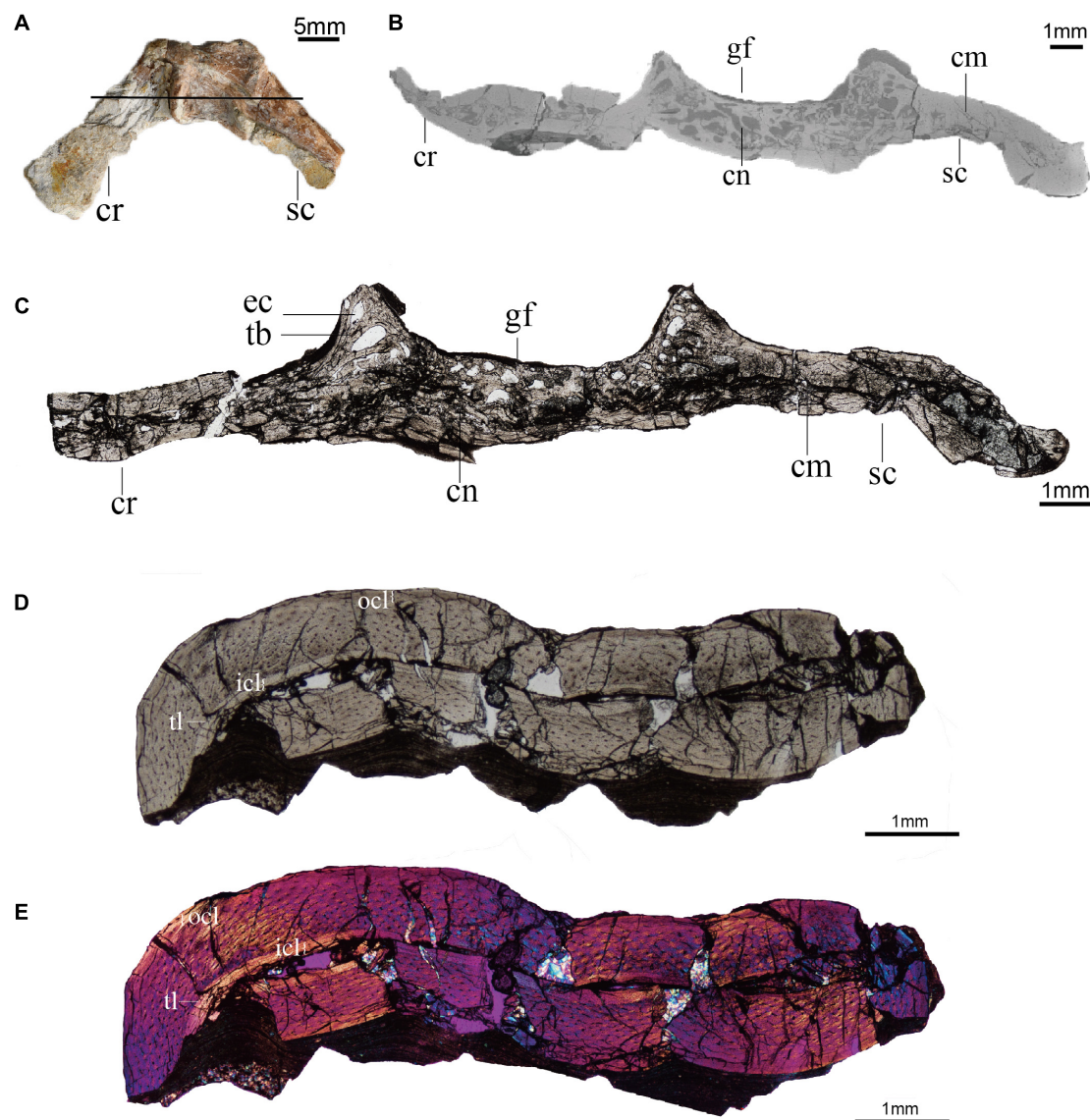


FIGURE 3 | Histology (ground-sections) of *Confuciusornis* (IVPP V11521). **(A)** Gross morphology of the scapulocoracoid; **(B)** CT slice of pectoral girdle indicated by the black line in panel **(A)**; **(C)** Associated histological section indicated by the black line in panel **(A)**, magnified region showing the compact bone connecting the scapula and coracoid is in **Supplementary Figure 1A**; **(D)** histological section of the humerus; **(E)** polarized light image of panel **(D)**. cm, compact bone; cn, cancellous bone; cr, coracoid; ec, erosion cavity; gf, glenoid fossa; icl, inner circumferential layer; ocl, outer circumferential layer; sc, scapula; tb, trabecula; tl, tide line.

80, 90, 95, and 100% EtOH for ~1 h each, and two additional 100% EtOH for ~1 h each), cleared in xylene (three changes for 30 min each), infiltrated in melted paraffin wax, and embedded manually (Paraplast Plus EMS Cat#19216). Samples were sectioned at 5 μ m on a rotary microtome (Leica Biosystems RM2265) and mounted on charged slides (Superfrost Plus, Fisher Scientific).

The selected slices were stained using a modified Masson's trichrome protocol (Witten and Hall, 2003) as follows: deparaffinized with xylene (2 changes for 5 min each), dehydrated with a graded series of ethanol solution (100, 95, 90, 80, 70, and 50% for 1 min each), rinsed in deionized water for 2 min, stained

for 10 min with Mayer's acid hematoxylin (Ruitaibio), rinsed in deionized water for 1 min, stained with Xylidine Ponceau/Acid Fuchsin for 2 min (equal volumes of 0.5% xylidine ponceau 2R CI no. 16150 in 1% acetic acid and 0.5% Acid Fuchsin CI no. 42685 in 1% acetic acid), rinsed for 1 min in deionized water, stained for 4 min with 1% phosphomolybdic acid, rinsed for 1 min in deionized water, stained with light green for 90 s (2% light green CI 42095 in 2% citric acid, diluted 1:10 with deionized water prior to use) and rinsed in deionized water for 1 min. Sections were then dipped twice in 100% ethanol for 10 s, cleared in xylene for 4 min, mounted in Permount and coverslipped.

Terminology

Histological terminology is following Padian and Lamm (2013) and ontogenetic terminology is following Prondvai et al. (2014).

RESULTS

General Osteohistology of *Confuciusornis* IVPP V11521

The scapulocoracoid of IVPP V11521 is crushed, collapsing the medullary cavity. Although distorted by compaction, the medullary cavity can still be identified in the bodies of the scapula and coracoid, both from the remnants of the space itself and from the presence of some cancellous tissue between the walls of cortical bone (Figure 3).

The scapulocoracoid consists of both compact and cancellous bone. The compact bone is mainly distributed in the bodies of the scapula and coracoid, while the cancellous bone is primarily located in the glenoid region (Figures 3B,C). A layer of compact bone connects the bodies of the scapula and coracoid opposite the glenoid on the medial (costal) side of the scapulocoracoid junction (Figures 3B,C and Supplementary Figure 1). The cancellous bone consists of erosion cavities of various sizes separated by trabeculae, similar to the epiphyseal structures and metaphyseal regions of limb bones (de Ricqlès et al., 2003). These features are also visible in the CT scans (Figure 3B).

The cancellous bone in the *Confuciusornis* scapulocoracoid consists of incipient fibrolamellar bone (FLB), and contains reticular to obliquely oriented vascular canals with frequent anastomoses (Figure 4A and Supplementary Figure 2). Densely arranged, plump, oval, haphazardly aligned osteocyte lacunae predominate, although some flatter osteocyte lacunae are aligned parallel to the margins of the erosion cavities (Figure 4B). The compact bone of the scapula and coracoid bodies comprises two layers: a thick inner layer of incipient FLB and a much thinner outer layer of parallel-fibered bone (PFB) (Figures 4C,D and Supplementary Figure 3). There is no clear boundary between the FLB and PFB tissue (Figures 4C,D and Supplementary Figure 3), but polarized light reveals obvious differences in collagen fiber orientation between them (Figure 4D and Supplementary Figure 3). The vascular canals in the FLB are primarily obliquely oriented, and anastomoses can be observed between several canals (Figure 4C). The inner osteocyte lacunae are plump, but the lacunae become progressively flatter and increasingly more arranged in parallel to each other toward the periosteum (Figure 4C and Supplementary Figure 4). The PFB is nearly avascular, with a low density of flat osteocyte lacunae arranged parallel to the periosteal surface (Figure 4C and Supplementary Figure 4). Because the specimen is broken and not a typical long bone mid-shaft section, it is difficult to identify primary osteons in either the cancellous or the compact bone of the scapulocoracoid, but the absence of secondary osteons is clear.

The humerus of *Confuciusornis* IVPP V11521 is also crushed. The midshaft of the humerus consists of compact bone (Figure 3D). An inner circumferential layer (ICL) lines the

medullary cavity, consisting of PFB. The ICL is separated from the thicker FLB layer by a tide line (Figures 3D,E). The majority of the compacta consists of FLB, which gradually transitions into PFB toward the periosteum as the vascular canals and osteocyte lacunae decrease in numbers. As in the scapulocoracoid, no clear boundary between the FLB and PFB layers exists (Figure 3D). The PFB of the ICL is avascular, and the flat osteocyte lacunae and collagen fibers are oriented parallel to the endosteum. The FLB layer is richly vascularized by longitudinal canals, among which are numerous anastomoses (Figure 4G). The outer PFB layer is avascular, and is interpreted as the OCL. This layer is more continuous than in the scapulocoracoid (Figure 3D). LAGs are absent in the OCL (Figures 4G,H) and the FLB mid-cortical bone. In the OCL the osteocyte lacunae are flat and the dense collagen fibers are arranged parallel to the periosteum (Figure 4H), as in the ICL. Primary osteons are abundant in the FLB (Figure 4G and Supplementary Figure 5), but no secondary osteons are visible.

In general, the bone microstructure of the scapulocoracoid and humerus is consistent with observations from previous histological studies of *Confuciusornis*, with both FLB and PFB present (Zhang et al., 1998; de Ricqlès et al., 2003; Erickson et al., 2009; Chinsamy et al., 2019). de Ricqlès et al. (2003) reported that in adult *Confuciusornis* the weight bearing femur undergoes the most remodeling, exhibiting numerous secondary osteons, followed by the humerus in which just a few secondary osteons are present, while the non-load-bearing pygostyle and fibula only have primary osteons (de Ricqlès et al., 2003). However, a recent osteohistology analysis of 14 *Confuciusornis* specimens by Chinsamy et al. (2019) did not report secondary osteons in any element, even in individuals with three to four LAGs and humeral lengths over 65 mm. According to Chinsamy et al. (2019), *Confuciusornis* grew rapidly from early ontogeny until almost adult size, then experienced at least three to four years slow and episodic growth to reach skeletal maturity, indicated by the LAGs in the OCL. In contrast to long bones, no noticeable ICL is visible in the ground sections of the scapulocoracoid. The presence of an OCL in the humerus suggests growth had slowed down by the time of death in this individual, but the absence of LAGs in the OCL indicates that IVPP V11521 had not finished its first year of growth at the time of death.

Histology of the Pectoral Girdle of the Adult Spotted Dove and the Common Ostrich Hatchling

In the adult Spotted dove, the subchondral bone of the scapula and coracoid is composed of densely arranged secondary osteons (Figure 5C). The collagen fibers are oriented in parallel around the central canal of the Haversian system and along the erosion cavities. In some regions the PFB is nearly avascular (Figure 5D). The ossified scapula and coracoid are connected by fibrocartilage (Figures 5C,D), and covered by a single thick layer of articular cartilage, much thicker than that on the humeral head, together forming the glenoid fossa (Figure 5A). The articular cartilage is also more fibrous than the humeral articular cartilage

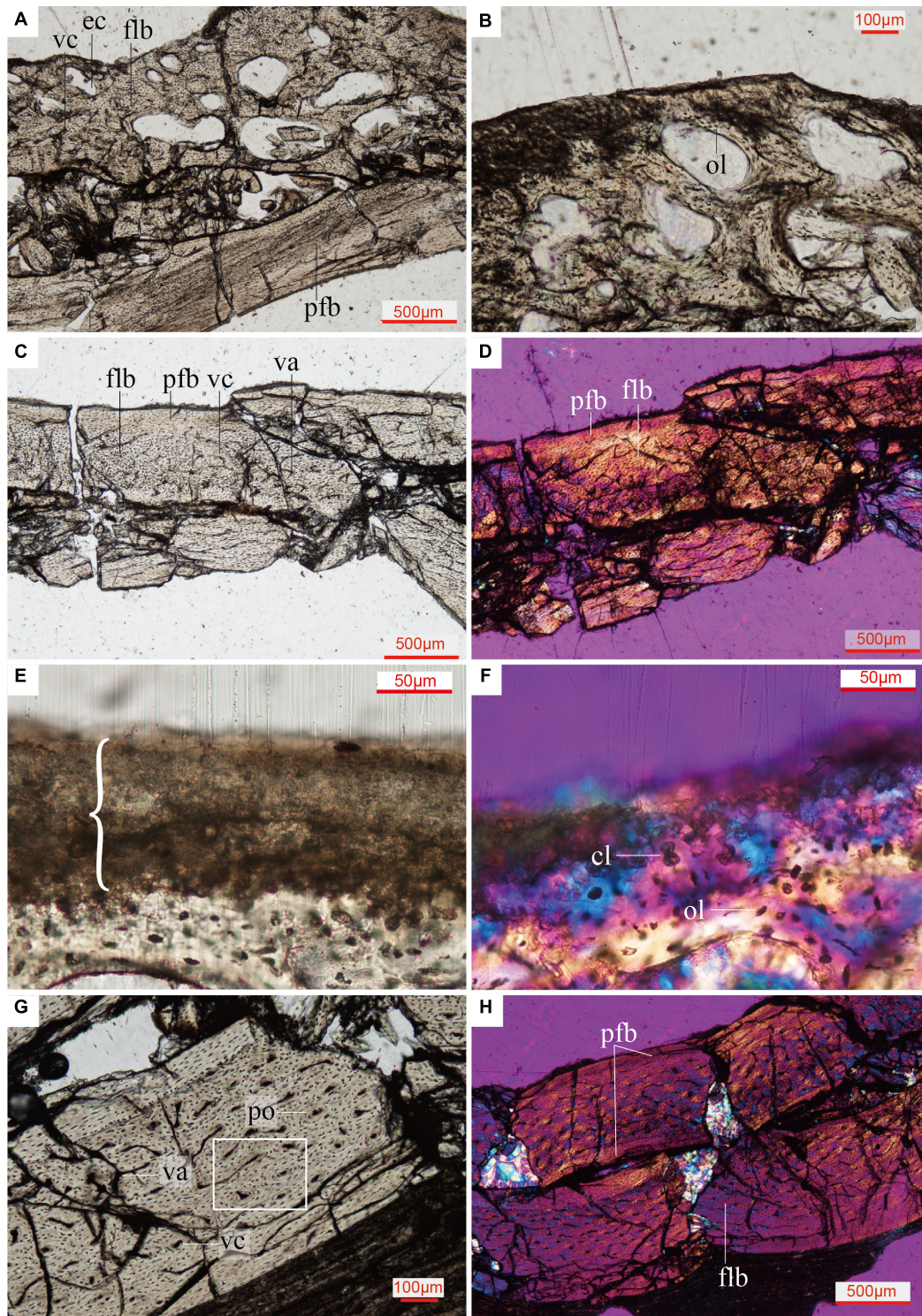


FIGURE 4 | Close up histology (ground-section) of *Confuciusornis* IVPP V11521. **(A)** Osteohistology beneath the glenoid fossa, showing that the cancellous bone consists of fibrolamellar tissue and the compact bone consists of parallel-fibered tissue; **(B)** Osteohistology around the trabeculae and erosion cavities; **(C)** osteohistology of the scapula blade; **(D)** osteohistology of the scapular blade under polarized light; **(E)** brace indicates dark layer without cellular structures, comprising diagenetically altered calcified cartilage, with potential remnants of hyaline cartilage mixed with sediment, location of the section is indicated in **Supplementary Figure 2B**; **(F)** highly diagenetically altered calcified cartilage under polarized light; **(G)** osteohistology of the humerus; **(H)** osteohistology of the humerus under polarized light. cl, chondrocyte lacunae showing a cell-doublet organization; cn, cancellous bone; cr, coracoid; ec, erosion cavity; flb, fibrolamellar bone; gf, glenoid fossa; ol, osteocyte lacunae; pfb, parallel-fibered bone; po, primary osteon; sc, scapula; vc, vascular canals; va, vascular canals anastomose.

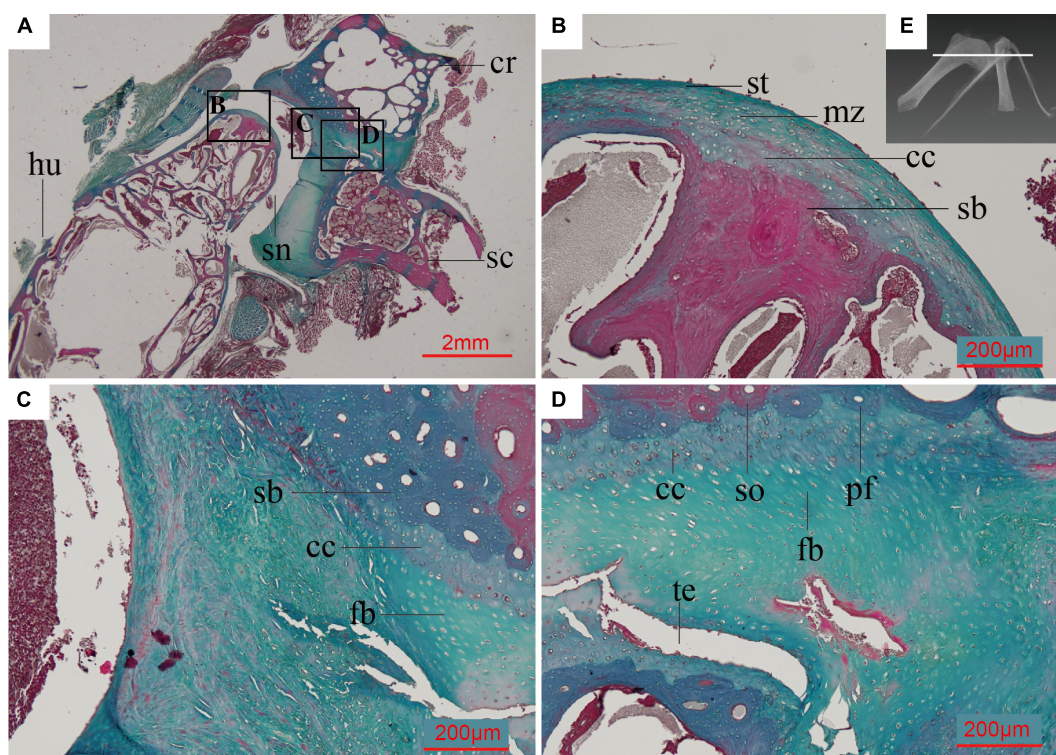


FIGURE 5 | Paraffin thin section showing the histology of the pectoral girdle of an adult *Spilopelia chinensis* (Spotted dove). **(A)** Thin-section of shoulder joint in Spotted dove, indicated by the white line in panel **(E)**. It shows a synovial joint between the humerus and the scapula and coracoid, the latter two technically “separated” and only linked together by some unmineralized fibrocartilage; **(B)** Close-up of left black box in panel **(A)**, showing the histology of the humeral head and its articular cartilage, with its multiple zones; **(C)** Close-up of middle black box in panel **(A)**; **(D)** Close-up of right black box in panel **(A)**, showing the synchondrosis joint formed by fibrocartilage and calcified cartilage between the scapula and coracoid; **(E)** 3D reconstruction of shoulder joint of the Spotted dove. cc, calcified cartilage; cr, coracoid; fb, fibrocartilage; hu, humerus; md, middle zone; pf, parallel-fibered bone; sb, subchondral bone; sc, scapula; sn, synovial cavity; so, secondary osteon; st, superficial tangential zone; te, tear. This slide was stained with a modified Masson’s trichrome.

(Figure 5B), with larger collagen fibers (as indicated by the faintly redder stain; Figure 5D).

The humerus and scapulocoracoid are not fully ossified in the 8-day old (post-hatching) ostrich we sampled. These bones are composed mostly of hyaline cartilage with a few cartilage canals in the bodies of the elements, and newly formed bone tissue along the perichondrium (Figure 6). The glenoid fossa is almost completely cartilage at this ontogenetic stage. Invasive cartilage canals indicate the individual is at an early stage of ossification (Figure 6C).

The scapulocoracoid of IVPP OV586 measures 22 cm in length. Superficially the scapula and coracoid appear fully fused at the level of the glenoid with the acromion process of the scapula also fused to the sternolateral margin of the coracoid (Supplementary Figure 6A). In the CT scans traversing the glenoid fossa, the joint between the scapula and coracoid is composed of an outer layer of compact bone and an inner layer of cancellous bone. Within the cancellous bone the bony trabeculae have a uniform arrangement, with no trace of any gap, osteoid bridge, rugose digitation or remnant of bone wall that would indicate the presence of a suture or cartilage (Supplementary Figure 6B). In contrast, clear remnants of the bony wall are present between the lateral corner of the sternal margin of the

coracoid and the acromion process of scapula indicating fusion between these two parts of the scapula and coracoid was not complete at the time of death (Supplementary Figure 6C). This CT data indicates that the scapula and coracoid at the level of the glenoid fused early in the Common ostrich, well within the first year of postnatal growth, and prior to fusion between the acromion process of scapula and the sternal margin of the coracoid.

Assessment of the Scapulocoracoid Joint of *Confuciusornis*

Although broken, the FLB and PFB matrix of the cancellous bone and compact bone tissue under the glenoid fossa of *Confuciusornis* is continuous and uniform in all the CT scan images and ground sections (Figures 3B,C). There is no evidence of a gap to indicate the presence of a suture (Bailleul et al., 2016). Our preliminary data on the Spotted dove show that the two bones in this taxon are linked together by fibrocartilage, making this joint a synchondrosis (Figure 5). No trace of a cartilaginous connection that would indicate a synchondrosis like that in the Spotted dove can be identified in IVPP V11521. The presence of an ongoing fusion, as would be indicated by the existence of a

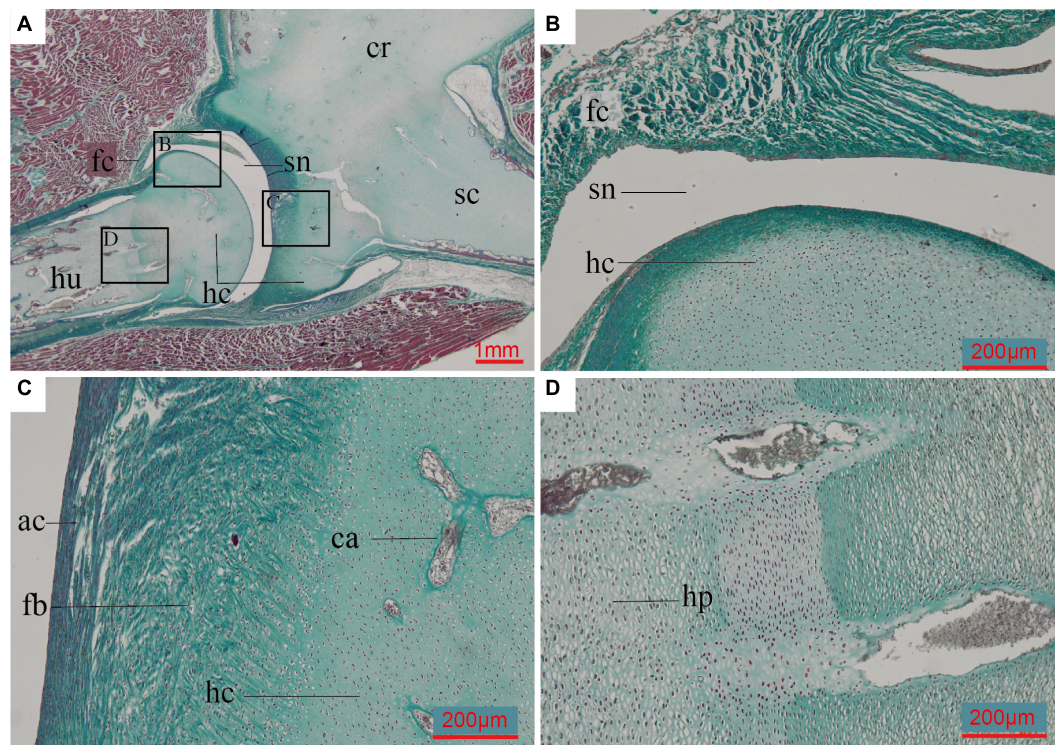


FIGURE 6 | Paraffin thin-section showing the histology of pectoral girdle of an 8-day-old *Struthio camelus* (Common ostrich). (A) Thin-section of the shoulder joint. It shows a synovial joint between the humerus and the already fused (but still mostly unmineralized) cartilaginous scapulocoracoid; (B) Close-up of black box in panel (A), showing the synovial cavity and fibrous capsule of the synovial joint between the humerus and scapulocoracoid, and the hyaline cartilage of the humeral head; (C) Close-up of right black box in panel (A), showing the fibroid surface of the articular surface, hyaline cartilage of the un-ossified scapulocoracoid body, and invasive cartilage canals; (D) Close-up of left black box in panel (A), showing hypertrophic chondrocytes. ac, articular cartilage; ca, cartilage canals; fb, fibrocartilage; fc, fibrous capsule; hc, hyaline cartilage; hp, hypertrophic chondrocytes; sn, synovial cavity. Slide stained with a modified Masson's trichrome.

less mineralized osteoid bridge (Funston et al., 2019) or rugose digitation (Brochu, 1995; Parsons and Parsons, 2015), is also not supported by the evidence. Therefore, we confirm that the scapula and coracoid in *Confuciusornis* IVPP V11521 are completely fused into a bony scapulocoracoid, forming a true synostosis.

Cartilage Histology at the Glenoid of *Confuciusornis*

A thin amorphous brown layer is preserved along the articular surface of the glenoid fossa (Figure 4 and Supplementary Figure 2B). Viewed under transmitted light, this layer is clearly distinct from the bone tissue beneath it (Figure 4E). Under polarized light, this layer is uniformly dark, with no observable cellular structures (Figure 4F). Near this layer, there are some large globular lacunae, distinct from the small fusiform to oval osteocyte lacunae in the bone tissue. A cell-doublet confirms these are chondrocyte lacunae (Figure 4F), which in turn supports identification of this layer as calcified cartilage, most likely representing a remnant of the articular cartilage of the glenoid fossa. Calcified fibrocartilage was also found on the other side of the glenoid cavity of the same specimen, where it articulates with the furcula (Wu et al., 2021). Calcified cartilage tissue has been previously reported

in two specimens of *Confuciusornis* and one of *Yanornis*, also from the Jehol Biota (de Ricqlès et al., 2003; Jiang et al., 2017; Bailleul et al., 2019a). The tissue of the darker layer has been deeply altered histologically by diagenetic processes, and may have been invaded by bacteria post-mortem. In the Spotted dove, the fibrocartilaginous component of the articular cartilage occupies the same position above the calcified cartilage (Figure 5). Compared to calcified cartilage, fossilized hyaline cartilage and fibrocartilage are very rare (Schwarz et al., 2007; Schweitzer, 2011). Further investigation is required (e.g., using SEM and EDS analyses) to determine if any remnants of the hyaline cartilage are also fossilized. Preservation of remnants of fossilized fibrocartilage reported in another specimen of *Confuciusornis* was suggested to be related to pyroclastic flows (Jiang et al., 2014, 2017).

DISCUSSION

Scapulocoracoid Fusion in *Confuciusornis*

Osteohistology has become widely applied in vertebrate paleontology during the last three decades (e.g., see review by Ray et al., 2010; Padian and Lamm, 2013; Bailleul et al., 2019b).

Studying the microstructure of bone can help scientists better understand not only growth-related questions but also functional aspects of the skeleton such as joint morphology and mobility (Bailleul et al., 2019a), and much more (Bailleul et al., 2019b). Over the past three decades, abundant fossil birds have been unearthed from deposits yielding the Early Cretaceous Jehol Biota. As the number of taxa has increased, so has the number of histological studies conducted on these specimens (e.g., de Ricqlès et al., 2003; O'Connor et al., 2014, 2018a; Jiang et al., 2017; Chinsamy et al., 2019). Until recently these histological analyses have focused almost entirely on limb bones in growth related studies. Here we utilize histology to shed light on the morphology of the joint between the scapula and coracoid in *Confuciusornis*. This study represents the first traditional, non-digital osteohistological analysis of the glenoid joint in a Mesozoic theropod, although the histology of this joint has been viewed through virtual thin-sections in the Daiting *Archaeopteryx* (Kundrát et al., 2019) and the scapular corpus has been studied through ground sections in the enantiornithine *Mirusavis* IVPP V18692 (Wang et al., 2019a).

In *Confuciusornis*, a separate scapula and coracoid have not been described in any published specimen, nor can this condition be identified from published descriptions or figures (e.g., holotype IVPP V10918, V10923, V10928, V11308, V13313, V14412, GMV2132-33, DNHM D2454) (Hou et al., 1995; Hou, 1997; Chiappe et al., 1999; Dalsätt et al., 2006; Zhang et al., 2009; Wang et al., 2019c), even in one purportedly immature specimen (IVPP V13172; Wang et al., 2019c). We conducted a survey of 132 unpublished *Confuciusornis* specimens at the Shandong Tianyu Museum of Nature and five unpublished specimens at the IVPP (IVPP V11305, V11548, V11552, V11795, and V13338), and found no specimens that clearly preserved a separate or sutured scapula and coracoid. In contrast, unfused scapulae and coracoids are readily identified in specimens of numerous paravian taxa in which it is evident that these bones only became fused later in ontogeny (e.g., *Anchiornis*, *Microraptor*, *Archaeopteryx*, and *Sapeornis*).

Both CT data and histological analysis of *Confuciusornis* IVPP V11521 confirm the presence of a synostosis joint between the scapula and coracoid (the elements are fully fused)—no traces of a gap, fibrous connection, intervening cartilage, osteoid bridge, or rugose digitation, features which would indicate a suture, synchondrosis or syndesmosis joint, can be identified in the ground sections (Figures 3,4). This study demonstrates that in a large but young specimen of *Confuciusornis*, apparently within the first year of its growth, fusion of the scapulocoracoid was already complete. This indicates that the scapulocoracoid fused relatively early in the ontogeny of *Confuciusornis*, prior to skeletal maturity. Although at this stage interpretations are preliminary, since only a single specimen has been studied, the combined facts that *Confuciusornis* IVPP V11521 preserves no LAGs in the humerus, indicating it is most likely in its first year of growth, yet records no vestiges of ongoing fusion at the scapulocoracoid juncture, strongly suggests that in contrast to other Mesozoic paravians fusion between these elements began early in ontogeny and was completed within the first year, before somatic maturity.

At this time, it is uncertain if the relative early fusion of scapula and coracoid in *Confuciusornis* is due to differences in growth strategy between *Confuciusornis* and most other non-ornithuromorpha paravians, or if there exists some other underlying functional explanation, and how fusion patterns are affected by developmental plasticity. In stark contrast to other non-ornithothoracine paravians, *Confuciusornis* attained the majority of its body mass in the first year, after which it continued to grow at a minimal rate for three to four years, depositing several LAGs in the OCL (Chinsamy et al., 2019). In contrast, other non-ornithuromorpha paravians took several years to reach the same relative body mass (Erickson et al., 2009; Zheng et al., 2014; Prondvai et al., 2018; Shen et al., 2019), and their fossil record is dominated by subadults. A large size range is observed in *Confuciusornis*, but size does not strictly correlate with the number of visible LAGs, an inconsistency interpreted as the result of developmental plasticity (Chinsamy et al., 2019). Similar developmental plasticity has also been documented in other paravians with protracted growth, in that size and osteohistological maturity are not strongly correlated in such taxa (e.g., *Sapeornis*, *Anchiornis*) (Zheng et al., 2014). Despite the abundance of specimens, morphological variation in development has yet to be quantified, but developmental plasticity clearly was present in non-neornithine avians and thus extended well into at least some lineages of the Avetheropoda, contra Griffin and Nesbitt, 2016. *Confuciusornis* IVPP V11521 may be relatively young, but is fairly large (humeral length 66 mm, in the higher end of the documented size range of 41.01–78.5 mm; Chiappe et al., 1999, 2008; Zhang et al., 2009; Wang and O'Connor, 2017; Wang et al., 2019c). Since developmental plasticity can affect character states as well as size (Griffin and Nesbitt, 2016), further sampling both within *Confuciusornis* and across a broader range of paravians is required to shed light on the potential effects of development plasticity on fusion events in this taxon. However, given that fusion is entirely complete between these two elements and no sutured specimens have ever been identified, developmental plasticity is unlikely to strongly affect the conclusion that fusion of the scapulocoracoid occurs early in *Confuciusornis*.

The fused scapulocoracoid in the Jinguoformisidae is hypothesized to reflect the accelerated osteogenesis in this clade, relative to other non-ornithuromorpha birds (Wang et al., 2018). This may also at least partially explain the ubiquitous presence of scapulocoracoid fusion in *Confuciusornis* since it is known this taxon grew more rapidly than other non-ornithuromorpha paravians (Chinsamy et al., 2019). The histology of the limb bones in the only two known jinguoformisid specimens indicates they are mature, so without further data it cannot be determined if fusion in this clade is simply due to ontogenetic maturity. In addition, the exact morphology of the scapulocoracoid joint in jinguoformisids is unknown, as it has never been investigated using high resolution scans or histology. However, the fact that the scapulocoracoid joint is completely fused in *Confuciusornis* IVPP V11521 within the first year of its growth and thus prior to skeletal maturity still represents a departure from the pattern observed in most other paravians, in which fusion only occurs with skeletal maturity, and thus

rapid growth rates in *Confuciusornis* do not fully explain the differences in fusion pattern observed.

The fully synostosed morphology observed in *Confuciusornis* IVPP V11521, together with the absence of any known specimen preserving a suture, suggests the scapula and coracoid fused early in ontogeny, potentially first via cartilage during embryology in a pattern similar to that seen in the Common ostrich (Figure 6). In the ostrich, however, the bones ossify post-hatching from different centers, even though cartilage forms a single unit embryonically (Maxwell and Larsson, 2009). If fossilized, a hatchling ostrich would appear to have separate scapulae and coracoids, despite the unmineralized cartilaginous connection in embryonic life. Morphological observations and CT scans indicate the scapulocoracoid at the level of the glenoid is fully fused in the ostrich specimen IVPP OV586. Although the exact age of this ostrich specimen is unknown, we estimate it to have been a juvenile approximately 6 months old, based on the skull length (18 cm), and the small size of the scapulocoracoid (length 22 cm) compared to that of an adult ostrich specimen (IVPP OV1026, scapulocoracoid length 25 cm). Unfortunately histology cannot be conducted on this specimen to corroborate this estimate. This specimen demonstrates that like *Confuciusornis* the ostrich scapulocoracoid fuses early during postnatal ontogeny, during the first year of growth, well before skeletal maturity is achieved. In order to fully compare the pattern in the Common ostrich with that in *Confuciusornis*, detailed knowledge of the post-hatching ossification pattern in the scapulocoracoid would be required for both taxa. This is further complicated by the fact that fusion of compact bones is heterochronic and may vary among individuals and between species (Brochu, 1995). For example, in crocodilians, the other clade of extant archosaurs, closure of the synchondrosis between the scapula and coracoid begins only after hatching. Closure in immature specimens is reported in *Caiman crocodilus*, *Melanosuchus niger*, and *Paleosuchus palpebrosus*, whereas in *Alligator* closure is considered to be a gerontic character, associated with old age (Brochu, 1995). Without fossils capturing the early ontogenetic stages of *Confuciusornis*, the pattern of fusion in this taxon may never be fully understood.

Shoulder Joint Evolution Across Paraves

In the Spotted dove, a volant neornithine, the separated scapula and coracoid are connected by fibrocartilage, forming a rigid synchondrosis joint (Figure 5). This makes it unclear what the functional difference is between a fused and unfused scapula-coracoid complex in birds, since in both cases the joint is immobile. Another major challenge in understanding the early avian transition from sutured or fused (*Archaeopteryx*, *Jinguoformisidae*, and *Confuciusornis*) to connected by a synchondrosis or completely separated (Ornithothoraces) is that both morphologies occur in volant taxa, both within Aves and among volant non-avian dinosaurs. The scapulocoracoid is fused in the volant dromaeosaurid *Microraptor*, whereas all known specimens of the volant Scansoriopterygidae have separate scapulae and coracoids (although the very limited record of this clade is dominated

by immature individuals) (Zhang et al., 2008b; Xu et al., 2015; Wang et al., 2019b).

The early fusion of the scapulocoracoid in *Confuciusornis*, unlike in most other Cretaceous non-ornithomorph paravians, and the presence of a sutured scapula and coracoid in the holotype of the basal confuciusornithid *Eoconfuciusornis*, may collectively suggest that fusion of the scapulocoracoid in *Confuciusornis* is secondarily derived, as in flightless paleognaths. This hypothesis is somewhat consistent with differences in the morphology of the scapulocoracoid between *Archaeopteryx* and *Sapeornis*, in which the coracoid retains the plesiomorphic axe-shape, and *Jeholornis*, *Confuciusornis*, and ornithothoracines, in which the coracoid is strut-like (O'Connor et al., 2011). An alternative but not mutually exclusive hypothesis is that separation of the scapulocoracoid evolved more than once in early avians, appearing evolving independently in the *Jeholornis* lineage and then again in the lineage including *Sapeornis* and Ornithothoraces. The high degree of homoplasy at this early point in avian evolution, and the absence of early ontogenetic stages in the non-enantiornithine Mesozoic avian fossil record, hinder interpretations. Microanatomical studies of the scapula-coracoid joint in *Sapeornis* and *Jeholornis* will help to elucidate this issue in the future.

Scapulocoracoid fusion in Neornithes is not common. The scapula and coracoid are separate in most neognaths (Figure 5), including several species from different lineages which have secondarily lost flight, such as *Thambetochen chauliodus* (Anatidae; Olson and Wetmore, 1976) and *Strigops habroptilus* (Psittaciformes; Livezey, 1992), and flightless lineages such as the Phorusrhacidae (Alvarenga and Höfling, 2003). A quarter of all extant species in the Rallidae are flightless (Olson, 1973) and in these taxa the scapula and coracoid remain separate although they demarcate an obtuse angle (acute in volant birds), and processes for muscle attachment are reduced (Olson, 1973). This may suggest that following the loss of flight reduction of the scapula-coracoid joint precedes fusion of these elements in neornithines or that fusion of the scapulocoracoid in neornithines is not related to flightlessness as is commonly suggested (e.g., Mayr, 2007; Mayr, 2011). This morphology is primarily found in large flightless taxa (e.g., Dinornithidae, Gastornithidae, "ratites") and thus may potentially be related to body size as well.

Possible Factors Influencing Scapulocoracoid Fusion in Paravians

Several factors affect skeletal fusion. Age and diet can result in fusion among pectoral girdle elements in some living species. Older adult Hoatzin often lay down new bone within connective tissues, resulting in the fusion of parts of the skeleton, probably because of the high calcium content of their vegetarian diet (Kaiser, 2007). In the *Alligator* closure of the synchondrosis between the scapula and coracoid is associated with senescence (Brochu, 1995). This type of effect may explain rare fusion of these elements in taxa like *Archaeopteryx*, but does not explain the condition in *Confuciusornis*.

Soaring frigatebirds and pelicans are among the few volant crown birds that have fused elements in the pectoral girdle. The furcula and sternum are fused in the Spot-billed pelican (*Pelecanus philippensis*; Sathyamoorthy et al., 2012) and in frigatebirds the furcula and coracoid are fused to each other and to the sternum (Kaiser, 2007), but the scapula and coracoid remain separate (Olson, 1977; F. Seranno pers. comm.). Understanding the function of these fused elements may help to elucidate the evolutionary changes in the fusion of the shoulder joint in Mesozoic paravians. Fusion of the axial elements provides rigidity necessary for flight, while fusion of other bones reduces weight while providing strength, all of which are considered advantageous for flight (Kaiser, 2007; Lovette and Fitzpatrick, 2016; Gill et al., 2019). Pectoral fusion may evolve for a number of reasons. For example, fusion of the sternum and furcula in pelicans may be related to the expansion of these elements, which is purportedly a feature that aids in homeostasis (Kaiser, 2007). Frigatebirds are extremely agile and have the lowest wing-loading among all birds (Brooke, 2018). Pectoral fusion in this group may serve to reduce body mass, helping to lower wing-loading while retaining strength, thus reducing the cost of flight (Weimerskirch et al., 2003). This is unlikely the underlying cause of scapulocoracoid fusion in *Confuciusornis*, the skeleton of which is generally robust.

Mechanical stimuli (e.g., weight bearing, movement, and tension) promote chondrogenesis and result in delayed ossification and may also affect joint structure. The asymmetric, enlarged ischiopubic synchondrosis in children forms via delayed ossification, due to mechanical forces being applied asymmetrically by the weight-bearing non-dominant limb (Herneth et al., 2004). In mice, tensile stress will promote the expression of core-binding factor $\alpha 1$ (Cbfa1) and vascular endothelial growth factor (VEGF) in the spheno-occipital synchondrosis (Lei et al., 2008). Even in tendons, tension is required to initiate chondrogenesis (Hall, 2005). In contrast, absence of mechanical stimuli can result in joint fusion. Lack of *in ovo* movement results in fusion of the normally synovial ankle joint in paralyzed chicken embryos (Persson, 1983). In rabbits, intervertebral discs degenerate and are replaced by bone after the transverse processes of the lumbar vertebrae are fixed through surgery (Phillips et al., 2002). Skeletogenesis is sensitive to mechanical stimulation; this reactivity has a possible role in evolution as a source of phenotypic plasticity and the formation of *de novo* skeletal elements from responsive tissues (Müller, 2003). This may suggest that, during the evolution of the confuciusornithiform lineage, these birds experienced less mechanical stimulation of the glenoid than members of avian lineages in which the scapula and coracoid are unfused or fuse only in senescence. This in turn would suggest the existence of important mechanical differences in the flight stroke, or in the forces exerted on the glenoid, between forms in which the scapulocoracoid is sutured and/or fused (at least in mature individuals) (e.g., *Archaeopteryx* and *Confuciusornis*) and taxa in which the two elements are fully separate (e.g., ornithothoracines). Because fusion occurs in both volant (e.g., *Confuciusornis*)

and non-volant taxa (e.g., Struthionidae), however, flight mechanics cannot be the only factor affecting the occurrence of fusion in this joint.

Although the underlying pressures responsible for changes in the joint architecture of the scapulocoracoid are not understood at this time, studies of extant birds hint at the genes that may have been active in producing the two phenotypes. In the chicken, for example, abnormal expression of the Hoxc6 gene may result in fusion of the scapula and coracoid, accompanied by thickening of the scapular head, reduction of the coracoid (resulting in reduction or loss of the supracoracoid process and a shorter, thicker coracoid), loss of the acrocoracoid process, and other malformations of the pectoral girdle elements (Oliver et al., 1990; Williams, 2003). Differences in expression of this gene may have been involved in the transition within Paraves from fusion to separation of the scapula-coracoid complex.

The fusion of the scapulocoracoid in *Confuciusornis* is likely the result of a complex interplay of genetic, mechanical and epigenetic factors and cannot be fully understood from the currently available data.

CONCLUSION AND PERSPECTIVES

Among early paravians in which the scapulocoracoid is fused, *Confuciusornis* is unique in that a synostosis is present in all available and published specimens. In contrast, these bones are fused only in the most mature individuals of other paravians. However, previous descriptions of joint morphology have not utilized microanatomical tools capable of determining the type of joint present with high accuracy. In this first osteohistological study of the scapulocoracoid glenoid joint in a Cretaceous paravian, we demonstrate that the scapulocoracoid is completely fused in *Confuciusornis* IVPP V11521. Humeral histology suggests this specimen was nearing completion of its first year of growth. The bodies of the scapula and coracoid consist of compact bone with an internal FLB layer and outer PFB layer. The bone along the glenoid fossa consists of cancellous FLB. Calcified cartilage is preserved on the articular surface of the glenoid. Both CT data and histology confirm the presence of a synostosed joint and a fully fused scapulocoracoid in IVPP V11521. This evidence suggests the *Confuciusornis* scapulocoracoid fused early in development, before skeletal maturity was achieved. However, further sampling of *Confuciusornis* is required to understand how developmental plasticity may affect the timing of this fusion event. Fusion of the scapulocoracoid in *Confuciusornis* most likely results from a complex interplay of genetic, mechanical and epigenetic factors; we hypothesize the primary factor may be a relative decrease in the amount of mechanical stimulation received by the glenoid of *Confuciusornis* relative to those of other volant birds, as a unique flight style has already been suggested for this taxon. Further investigation into the architecture of the glenoid joint in other Mesozoic paravians, and the timing and pattern of scapulocoracoid fusion in selected extant birds, will help to elucidate the transition from sutured/fused to unfused

and separate that occurs early in avian evolution, and may shed light on flight dynamics in early birds.

DATA AVAILABILITY STATEMENT

The original contributions presented in the study are included in the article/**Supplementary Material**, further inquiries can be directed to the corresponding author/s.

ETHICS STATEMENT

Ethical review and approval was not required for the animal study because the dove specimen is cadaveric when we collect, and the ostrich is collected legally from a commercial ostrich farm.

AUTHOR CONTRIBUTIONS

All authors designed the research, performed the research, and analyzed the data. QW and AB collected the data. QW, AB, JO'C, and ZL wrote the manuscript.

REFERENCES

- Alvarenga, H. M., and Höfling, E. (2003). Systematic revision of the phorusrhacidae (aves: ralliformes). *Papéis Avulsos de Zool.* 43, 55–91. doi: 10.1590/S0031-10492003000400001
- Bailleul, A. M., and Horner, J. R. (2016). Comparative histology of some craniofacial sutures and skull-base synchondroses in non-avian dinosaurs and their extant phylogenetic bracket. *J. Anat.* 229, 252–285.
- Bailleul, A. M., Li, Z., O'Connor, J. K., and Zhou, Z. (2019a). Origin of the avian prefrontal and evidence of a unique form of cranial kinesis in *Cretaceous* ornithomorphs. *Proc. Natl. Acad. Sci.* 116, 24696–24706. doi: 10.1073/pnas.1911820116
- Bailleul, A. M., O'Connor, J. K., and Schweitzer, M. H. (2019b). Dinosaur paleohistology: review, trends and new avenues of investigation. *PeerJ* 2019, 1–45. doi: 10.7717/peerj.7764
- Bailleul, A. M., Scannella, J. B., Horner, J. R., and Evans, D. C. (2016). Fusion patterns in the skulls of modern archosaurs reveal that sutures are ambiguous maturity indicators for the dinosauria. *PLoS One* 11:0147687. doi: 10.1371/journal.pone.0147687
- Bailleul, A. M., Witmer, L. M., and Holliday, C. M. (2017). Cranial joint histology in the mallard duck (*Anas platyrhynchos*): new insights on avian cranial kinesis. *J. Anat.* 230, 444–460. doi: 10.1111/joa.12562
- Baumel, J. J., and Witmer, L. M. (1993). "Osteologia," in *Handbook of avian anatomy: nomina anatomica avium*, Second Edn, eds J. J. Baumel, A. S. King, J. E. Breazile, H. E. Evans, and J. C. Berge (Cambridge: Nuttall Ornithological Club), 45–132.
- Benton, M. J. (2014). *Vertebrate palaeontology*. Hoboken, NJ: John Wiley & Sons.
- Bertelli, S., Chiappe, L. M., and Mayr, G. (2014). Phylogenetic interrelationships of living and extinct Tinamidae, volant palaeognathous birds from the new world. *Zool. J. Linn. Soc.* 172, 145–184. doi: 10.1111/zoj.12156
- Brochu, C. A. (1995). Heterochrony in the crocodylian scapulocoracoid. *J. Herpetol.* 29:464. doi: 10.2307/1565002
- Brooke, M. (2018). *Far From Land: The Mysterious Lives of Seabirds*. Princeton: Princeton University Press.
- Brusatte, S. L., Lloyd, G. T., Wang, S. C., and Norell, M. A. (2014). Gradual assembly of avian body plan culminated in rapid rates of evolution across the dinosaur-bird transition. *Curr. Biol.* 24, 2386–2392. doi: 10.1016/j.cub.2014.08.034

FUNDING

This work has been supported by the National Natural Science Foundation of China (41688103). AB also thanks the CAS-PIFI Program.

ACKNOWLEDGMENTS

We thank Gao Wei for photographing for the specimen, Zhang Shukang for preparing the ground sections, Zhang Limin for facilitating lab access, and Georg Janßen and Oliver Rauhut for providing the photo of the Munich *Archaeopteryx* (Figure 2A), and Holly Woodward for discussing the histology of the *Confuciusornis* specimen, and F. Seranno for discussing the pectoral girdle characters of frigatebirds. We also thank two reviewers for their comments that improved the manuscript.

SUPPLEMENTARY MATERIAL

The Supplementary Material for this article can be found online at: <https://www.frontiersin.org/articles/10.3389/feart.2021.617124/full#supplementary-material>

- Castanet, J., Curry Rogers, K., Cubo, J., and Jacques-Boisard, J. (2000). Periosteal bone growth rates in extant ratites (ostrich and emu). Implications for assessing growth in dinosaurs. *Comptes Rendus de l'Académie des Sci.-Ser. III-Sci. de la Vie* 323, 543–550. doi: 10.1016/S0764-4469(00)00181-5
- Chatterjee, S. (1997). *The Rise of Birds*. Baltimore: Johns Hopkins University Press.
- Chiappe, L. M., Ji, S., Ji, Q., and Norell, M. A. (1999). Anatomy and systematics of the confuciusornithidae (theropoda: aves) from the late mesozoic of northeastern china. *Bull. Am. Museum Nat. Hist.* 242:89.
- Chiappe, L. M., Marugán-Lobón, J., Ji, S., and Zhou, Z. (2008). Life history of a basal bird: morphometrics of the early cretaceous *Confuciusornis*. *Biol. Lett.* 4, 719–723. doi: 10.1098/rsbl.2008.0409
- Chiappe, L. M., and Witmer, L. M. (2002). *Mesozoic birds: above the heads of dinosaurs*. California: University of California Press.
- Chinsamy, A., Marugán-Lobón, J., Serrano, F. J., and Chiappe, L. (2019). Osteohistology and life history of the basal pygostylian, *Confuciusornis sanctus*. *Anat. Rec.* 303, 949–962. doi: 10.1002/ar.24282
- Cuff, A. R., Bright, J. A., and Rayfield, E. J. (2015). Validation experiments on finite element models of an ostrich (*Struthio camelus*) cranium. *PeerJ* 3:e1294. doi: 10.7717/peerj.1294
- Dalsätt, J., Zhou, Z., Zhang, F., and Ericson, P. G. P. (2006). Food remains in *Confuciusornis sanctus* suggest a fish diet. *Naturwissenschaften* 93, 444–446. doi: 10.1007/s00114-006-0125-y
- de Ricqlès, A., Padian, K., Horner, J. R., Lamm, E. T., and Myhrvold, N. (2003). Osteohistology of *Confuciusornis sanctus* (theropoda: aves). *J. Vertebrate Paleontol.* 23, 373–386.
- Elzanowski, A. (2001). A new genus and species for the largest specimen of *Archaeopteryx*. *Acta Palaeontologica Polonica* 46, 519–532.
- Erickson, G. M., Rauhut, O. W. M., Zhou, Z., Turner, A. H., Inouye, B. D., Hu, D., et al. (2009). Was dinosaurian physiology inherited by birds? reconciling slow growth in *Archaeopteryx*. *PLoS One* 4:e7390. doi: 10.1371/journal.pone.0007390
- Faux, C., and Field, D. J. (2017). Distinct developmental pathways underlie independent losses of flight in ratites. *Biol. Lett.* 13:20170234. doi: 10.1098/rsbl.2017.0234
- Funston, G. F., Currie, P. J., Ryan, M. J., and Dong, Z. M. (2019). Birdlike growth and mixed-age flocks in avimimids (theropoda, oviraptorosauria). *Sci. Rep.* 9, 1–21. doi: 10.1038/s41598-019-55038-5

- Gao, C., Chiappe, L. M., Zhang, F., Pomeroy, D. L., Shen, C., Chinsamy, A., et al. (2012). A subadult specimen of the early cretaceous bird *Sapeornis chaoyangensis* and a taxonomic reassessment of sapeornithids. *J. Vertebrate Paleontol.* 32, 1103–1112. doi: 10.1080/02724634.2012.693865
- Gill, F. B., Prum, R. O., and Robinson, S. K. (2019). *Ornithology*, Fourth Edn. New York: W.H. Freeman and Macmillan Learning.
- Griffin, C. T., and Nesbitt, S. J. (2016). Anomalous high variation in postnatal development is ancestral for dinosaurs but lost in birds. *PNAS* 113, 14757–14762. doi: 10.1073/pnas.1613813113
- Hall, B. K. (2005). *Bones and Cartilage: Developmental and Evolutionary Skeletal Biology*. Elsevier.
- Herneth, A. M., Philipp, M. O., Pretterklieber, M. L., Balassy, C., Winkelbauer, F. W., and Beaulieu, C. F. (2004). Asymmetric closure of ischiopubic synchondrosis in pediatric patients: correlation with foot dominance. *Am. J. Roentgenol.* 182, 361–365. doi: 10.2214/ajr.182.2.1820361
- Hou, L. (1997). *Mesozoic birds of China*. Lugu Hsiang, Taiwan: Phoenix Valley Bird Park.
- Hou, L., Martin, L. D., Zhou, Z., Feduccia, A., and Zhang, F. (1999). A diapsid skull in a new species of the primitive bird *Confuciusornis*. *Nature* 399, 679–682.
- Hou, L., Zhou, Z., Gu, Y., and Zhang, H. (1995). *Confuciusornis sanctus*, a new late Jurassic sauriurine bird from china. *Chinese Sci. Bull.* 40, 1545–1551.
- Hou, L., Zhou, Z., Zhang, F., and Gu, Y. (2002). *Mesozoic birds from western Liaoning in China*. Shenyang: Liaoning Science and Technology Publishing House.
- Houde, P. (1986). Ostrich ancestors found in the northern hemisphere suggest new hypothesis of ratite origins. *Nature* 324, 563–565. doi: 10.1038/324563a0
- Hu, D., Hou, L., Zhang, L., and Xu, X. (2009). A pre-*Archaeopteryx* troodontid theropod from china with long feathers on the metatarsus. *Nature* 461, 640–643. doi: 10.1038/nature08322
- Hwang, S. H., Norell, M. A., Ji, Q., and Gao, K. (2002). New specimens of *Microaptor zhaioianus* (theropoda: dromaeosauridae) from northeastern china. *Am. Museum Novitates* 3381, 1–44. doi: 10.1206/0003-00822002381<0001: NSOMZT<2.0.CO;2
- Ji, Q., Chiappe, L. M., and Ji, S. (1999). A new late mesozoic confuciusornithid bird from china. *J. Vertebrate Paleontol.* 19, 1–7. doi: 10.1080/02724634.1999.10011117
- Ji, Q., Ji, S., Lü, J., You, H., Chen, W., Liu, Y., et al. (2005). First avialian bird from china (*Jinfengopteryx elegans* gen. et sp. nov.). *Geol. Bull. China* 24, 197–205.
- Jiang, B., Harlow, G. E., Wohletz, K., Zhou, Z., and Meng, J. (2014). New evidence suggests pyroclastic flows are responsible for the remarkable preservation of the Jehol biota. *Nat. Commun.* 5:3151. doi: 10.1038/ncomms4151
- Jiang, B., Zhao, T., Regnault, S., Edwards, N. P., Kohn, S. C., Li, Z., et al. (2017). Cellular preservation of musculoskeletal specializations in the cretaceous bird *Confuciusornis*. *Nat. Commun.* 8, 1–10. doi: 10.1038/ncomms14779
- Kaiser, G. W. (2007). *The inner bird: anatomy and evolution*. Vancouver: UBC Press.
- Kundrát, M., Nudds, J., Kear, B. P., Lü, J., and Ahlberg, P. (2019). The first specimen of *Archaeopteryx* from the upper jurassic mörsheim formation of germany. *His. Biol.* 31, 3–63. doi: 10.1080/08912963.2018.1518443
- Lefèvre, U., Hu, D., Escuillie, F., Dyke, G., and Godefroit, P. (2014). A new long-tailed basal bird from the lower cretaceous of north-eastern china. *Biol. J. Linn. Soc.* 113, 790–804. doi: 10.1111/bij.12343
- Lei, W. Y., Wong, R. W. K., and Rabie, A. B. M. (2008). Factors regulating endochondral ossification in the spheno-occipital synchondrosis. *Angle Orthod.* 78, 215–220. doi: 10.2319/020707-59.1
- Livezey, B. C. (1992). Morphological corollaries and ecological implications of flightlessness in the kakapo (psittaciformes: *Strigops habroptilus*). *J. Morphol.* 213, 105–145. doi: 10.1002/jmor.1052130108
- Lovette, I. J., and Fitzpatrick, J. W. (2016). *Handbook of Bird Biology*. John Wiley & Sons.
- Makovsky, P. J., Apesteguía, S., and Agnolín, F. L. (2005). The earliest dromaeosaurid theropod from south america. *Nature* 437, 1007–1011. doi: 10.1038/nature03996
- Maxwell, E. E., and Larsson, H. C. E. (2007). Osteology and myology of the wing of the Emu (*Dromaius novaehollandiae*), and its bearing on the evolution of vestigial structures. *J. Morphol.* 268, 423–441.
- Maxwell, E. E., and Larsson, H. C. E. (2009). Comparative ossification sequence and skeletal development of the postcranium of palaeognathous birds (aves: palaeognathae). *Zool. J. Linn. Soc.* 157, 169–196. doi: 10.1111/j.1096-3642.2009.00533.x
- Mayr, G. (2007). The birds from the paleocene fissure filling of walbeck (germany). *J. Vertebr. Paleontol.* 27, 394–408.
- Mayr, G. (2011). Metaves, mirandornithes, strisores and other novelties - a critical review of the higher-level phylogeny of neornithine birds: higher-level phylogeny of birds. *J. Zool. Syst. Evol. Res.* 49, 58–76. doi: 10.1111/j.1439-0469.2010.00586.x
- Mayr, G., Pohl, B., and Peters, D. S. (2005). A well-preserved *Archaeopteryx* specimen with theropod features. *Science* 310, 1483–1486. doi: 10.1126/science.1120331
- McGowan, C. (1982). The wing musculature of the Brown kiwi *Apteryx australis* mantelli and its bearing on ratite affinities. *J. Zool.* 197, 173–219. doi: 10.1111/jzo.1982.197.2.173
- McNab, B. K. (1994). Energy conservation and the evolution of flightlessness in birds. *Am. Nat.* 144, 628–642. doi: 10.1086/285697
- Müller, G. B. (2003). Embryonic motility: environmental influences and evolutionary innovation. *Evol. Dev.* 5, 56–60. doi: 10.1046/j.1525-142x.2003.03009.x
- Navalón, G., Meng, Q., Marugán-Lobón, J., Zhang, Y., Wang, B., Xing, H., et al. (2017). Diversity and evolution of the confuciusornithidae: evidence from a new 131-million-year-old specimen from the huajiyang formation in NE china. *J. Asian Earth Sci.* 152, 12–22. doi: 10.1016/j.jseas.2017.11.005
- O'Connor, J. K., Chiappe, L. M., and Bell, A. (2011). “Pre-modern birds: avian divergences in the Mesozoic,” in *Living Dinosaurs: the Evolutionary History of Birds*, eds G. D. Dyke and G. Kaiser (Hoboken, NJ: Wiley & Sons), 39–114.
- O'Connor, J. K., Erickson, G. M., Norell, M. A., Bailleul, A. M., Hu, H., and Zhou, Z. (2018a). Medullary bone in an early cretaceous enantiornithine bird and discussion regarding its identification in fossils. *Nat. Commun.* 9:5169. doi: 10.1038/s41467-018-07621-z
- O'Connor, J. K., Wang, X.-L., Sullivan, C., Wang, Y., Zheng, X.-T., Hu, H., et al. (2018b). First report of gastroliths in the early cretaceous basal bird *Jeholornis*. *Cretaceous Res.* 84, 200–208.
- O'Connor, J. K., Wang, M., Zheng, X., Wang, X., and Zhou, Z. (2014). The histology of two female early cretaceous birds. *Vertebrata Palasiatica* 52, 112–128.
- O'Connor, J. K., and Zhou, Z. (2019). The evolution of the modern avian digestive system: insights from paravian fossils from the yanliao and jehol biotas. *Palaeontology* 63, 13–27. doi: 10.1111/pala.12453
- Oliver, G., De Robertis, E. M., Wolpert, L., and Tickle, C. (1990). Expression of a homeobox gene in the chick wing bud following application of retinoic acid and grafts of polarizing region tissue. *EMBO J.* 9, 3093–3099. doi: 10.1002/j.1460-2075.1990.tb07506.x
- Olson, S. L. (1973). Evolution of the rails of the south atlantic islands (aves: rallidae). *Smithsonian Contrib. Zool.* 86, 484–485. doi: 10.5479/si.00810282.152
- Olson, S. L. (1977). A lower eocene frigatebird from the green river formation of wyoming (pelecaniformes: fregatidae). *Smithson. Contrib. Paleobiol.* 1–33. doi: 10.5479/si.00810266.35.1 **v
- Olson, S. L., and Wetmore, A. (1976). Preliminary diagnoses of two extraordinary new genera of birds from pleistocene deposits in the hawaiian islands. *Proc. Biol. Soc. Wash.* 89, 247–258.
- Ostrom, J. H. (1976). *Archaeopteryx* and the origin of birds. *Biol. J. Linn. Soc.* 8, 91–182.
- Padian, K., and Lamm, E.-T. (2013). *Bone histology of fossil tetrapods: advancing methods, analysis, and interpretation*. Berkeley: University of California Press.
- Parsons, W. L., and Parsons, K. M. (2009). Further descriptions of the osteology of *Deinonychus antirrhopus* (saurischia, theropoda). *Bull. Buffalo Soc. Nat. Sci.* 38, 43–54.
- Parsons, W. L., and Parsons, K. M. (2015). Morphological variations within the ontogeny of *Deinonychus antirrhopus* (theropoda, dromaeosauridae). *PLoS One* 10:0121476. doi: 10.1371/journal.pone.0121476
- Pei, R., Li, Q., Meng, Q., Norell, M. A., and Gao, K.-Q. (2017). New specimens of *Anchiornis huxleyi* (theropoda: paraves) from the late jurassic of northeastern china. *Bull. Am. Museum Nat. Hist.* 2017, 1–67.
- Persson, M. (1983). The role of movements in the development of sutural and diarthrodial joints tested by long-term paralysis of chick embryos. *J. Anat.* 137, 591–599.

- Phillips, F. M., Reuben, J., and Wetzel, F. T. (2002). Intervertebral disc degeneration adjacent to a lumbar fusion. *J. Bone Joint Sur.* 84:6. doi: 10.1302/0301-620X.84B2.0840289
- Prondvai, E., Godefroit, P., Adriaens, D., and Hu, D. (2018). Intraskelletal histovariability, allometric growth patterns, and their functional implications in bird-like dinosaurs. *Sci. Rep.* 8:258. doi: 10.1038/s41598-017-18218-9
- Prondvai, E., Stein, K. H. W., de Ricqlès, A., and Cubo, J. (2014). Development-based revision of bone tissue classification: the importance of semantics for science. *Biol. J. Linn. Soc. Lond.* 112, 799–816. doi: 10.1111/bij.12323
- Provini, P., Zhou, Z. H., and Zhang, F. (2008). A new species of the basal bird *Sapeornis* from the early cretaceous of liaoning, china. *Vertebrata Palasiatica* 14, **,
- Pu, H.-Y., Chang, H.-L., Lü, J.-C., Wu, Y.-H., Xu, L., Zhang, J.-M., et al. (2013). A new juvenile specimen of *Sapeornis* (pygostylia: aves) from the lower cretaceous of northeast china and allometric scaling of this basal bird. *Paleontol. Res.* 17, 27–38.
- Rauhut, O. W. M., Foth, C., and Tischlinger, H. (2018). The oldest *Archaeopteryx* (theropoda: avialae): a new specimen from the kimmeridgian/tithonian boundary of schamhaupten, bavaria. *PeerJ* 6:e4191. doi: 10.7717/peerj.4191
- Ray, S., Bandyopadhyay, S., and Appana, R. (2010). “Bone Histology of a Kannemeyeriid Dicotylodont Wadiazaurus: Palaeobiological Implications,” in *New Aspects of Mesozoic Biodiversity Lecture Notes in Earth Sciences*, ed. S. Bandyopadhyay (Berlin, Heidelberg: Springer), 73–89.
- Russell, A. P., and Joffe, D. J. (1985). The early development of the quail (*Coturnix c. japonica*) furcula reconsidered. *J. Zool.* 206, 69–81.
- Sathyamoorthy, O. R., Thirumurugan, R., Senthil Kumar, K., and Jayathangaraj, M. G. (2012). Gross anatomical studies on the sternum and clavicle of spot-billed pelican (*Pelecanus philippensis*). *TN J. Vet. Anim. Sci.* 8, 166–170.
- Sawad, A. A., Hana, B. A., and Al-Silawi, A. N. (2009). Morphological study of the skeleton development in chick embryo (*Gallus domesticus*). *Int. J. Poul. Sci.* 8, 710–714. doi: 10.3923/ijps.2009.710.714
- Schwarz, D., Wings, O., and Meyer, C. A. (2007). Super sizing the giants: first cartilage preservation at a sauropod dinosaur limb joint. *J. Geol. Soc.* 164, 61–65. doi: 10.1144/0016-76492006-019
- Schweitzer, M. H. (2011). Soft tissue preservation in terrestrial mesozoic vertebrates. *Ann. Rev. Earth Planetary Sci.* 39, 187–216. doi: 10.1146/annurev-earth-040610-133502
- Shen, C., Lü, J., Gao, C., Hoshino, M., Uesugi, K., and Kundrát, M. (2019). Forearm bone histology of the small theropod *Daliansaurus liaoningensis* (paraves: troodontidae) from the yixian formation, liaoning, china. *His. Biol.* 31, 253–261. doi: 10.1080/08912963.2017.1360296
- Torres, C. R., Norell, M. A., and Clarke, J. A. (2019). Estimating flight style of early eocene stem palaeognath bird *Calciavis grandei* (Lithornithidae). *Anat. Rec.* 303, 1035–1042. doi: 10.1002/ar.24207
- Wang, M., O'Connor, J. K., Bailleul, A. M., and Li, Z. (2019a). Evolution and distribution of medullary bone: evidence from a new early cretaceous enantiornithine bird. *Natl. Sci. Rev.* 7, 1068–1078. doi: 10.1093/nsr/nwz214
- Wang, M., O'Connor, J. K., Xu, X., Zhou, Z., O'Connor, J. K., Xu, X., et al. (2019b). A new Jurassic scansoriopterygid and the loss of membranous wings in theropod dinosaurs. *Nature* 569, 256–259. doi: 10.1038/s41586-019-1137-z
- Wang, M., O'Connor, J. K., and Zhou, Z.-H. (2019c). A taxonomical revision of the confuciusornithiformes (aves: pygostylia). *Vertebrata Palasiatica* 57, 1–37. doi: 10.19615/j.cnki.1000-3118.180530
- Wang, M., Stidham, T. A., and Zhou, Z. (2018). A new clade of basal early cretaceous pygostylan birds and developmental plasticity of the avian shoulder girdle. *Proc. Natl. Acad. Sci.* 115:201812176. doi: 10.1073/pnas.1812176115
- Wang, M., Wang, X., Wang, Y., and Zhou, Z. (2016). A new basal bird from china with implications for morphological diversity in early birds. *Sci. Rep.* 6, 1–12. doi: 10.1038/srep19700
- Wang, M., and Zhou, Z.-H. (2018). A new confuciusornithid (aves: pygostylia) from the early cretaceous increases the morphological disparity of the confuciusornithidae. *Zool. J. Linn. Soc.* 185, 417–430. doi: 10.1093/zoolinnean/zly045
- Wang, W., and O'Connor, J. K. (2017). Morphological coevolution of the pygostyle and tail feathers in early cretaceous birds. *Vertebrata Palasiatica* 55, 289–314.
- Weimerskirch, H., Chastel, O., Barbraud, C., and Tostain, O. (2003). Frigatebirds ride high on thermals. *Nature* 421, 333–334. doi: 10.1038/421333a
- Williams, M. S. (2003). Developmental anomalies of the scapula the most forgotten bone. *Am. J. Med. Genet.* 120A, 583–587. doi: 10.1002/ajmg.a.20091
- Witten, P. E., and Hall, B. K. (2003). Seasonal changes in the lower jaw skeleton in male atlantic salmon (*Salmo salar* L.): remodelling and regression of the kype after spawning. *J. Anat.* 203, 435–450.
- Worthy, T. H., Degrange, F. J., Handley, W. D., and Lee, M. S. Y. Y. (2017). The evolution of giant flightless birds and novel phylogenetic relationships for extinct fowl (aves, galloanseres). *R. Soc. Open Sci.* 4:170975. doi: 10.1098/rsos.170975
- Wu, Q., O'Connor, J., Li, Z.-H., and Bailleul, A. M. (2021). Cartilage on the furculae of living birds and the extinct bird *Confuciusornis*: a preliminary analysis and implications for flight style inferences in Mesozoic birds?. *Vertebr. Palasiat.* 59, 106–124. doi: 10.19615/j.cnki.1000-3118.201222
- Xu, X., Wang, X., and Wu, X. (1999). A dromaeosaurid dinosaur with a filamentous integument from the yixian formation of china. *Nature* 401, 262–266. doi: 10.1038/45769
- Xu, X., You, H., Du, K., and Han, F. (2011). An Archaeopteryx-like theropod from China and the origin of Avialae. *Nature* 475, 465–470. doi: 10.1038/nature10288
- Xu, X., Zhao, Q., Norell, M., Sullivan, C., Hone, D., Erickson, G., et al. (2009). A new feathered maniraptoran dinosaur fossil that fills a morphological gap in avian origin. *Chinese Sci. Bull.* 54, 430–435. doi: 10.1007/s11434-009-0009-6
- Xu, X., Zheng, X., Sullivan, C., Wang, X., Xing, L., Wang, Y., et al. (2015). A bizarre Jurassic maniraptoran theropod with preserved evidence of membranous wings. *Nature* 521, 70–73. doi: 10.1038/nature14423
- Young, M., Selleri, L., and Capellini, T. D. (2019). “Genetics of scapula and pelvis development: An evolutionary perspective,” in *Current Topics in Developmental Biology Organ Development*, ed. D. M. Wellik (Cambridge: Academic Press), 311–349.
- Zhang, F., Hou, L., and Ouyang, L. (1998). Osteological microstructure of *Confuciusornis*: preliminary report. *Vertebrata Palasiatica* 36, 126–135.
- Zhang, F., Zhou, Z., and Benton, M. J. (2008a). A primitive confuciusornithid bird from china and its implications for early avian flight. *Sci. China Ser. D Earth Sci.* 51, 625–639. doi: 10.1007/s11430-008-0050-3
- Zhang, F., Zhou, Z., Xu, X., Wang, X., Sullivan, C., Zhou, Z., et al. (2008b). A bizarre Jurassic maniraptoran from china with elongate ribbon-like feathers. *Nature* 455, 1105–1108. doi: 10.1038/nature07447
- Zhang, Z., Gao, C., Meng, Q., Liu, J., Hou, L., and Zheng, G. (2009). Diversification in an early cretaceous avian genus: evidence from a new species of *Confuciusornis* from china. *J. Ornithol.* 150, 783–790. doi: 10.1007/s10336-009-0399-x
- Zheng, X., O'Connor, J. K., Wang, X., Wang, M., Zhang, X., and Zhou, Z. (2014). On the absence of sternal elements in *Anchiornis* (paraves) and *Sapeornis* (aves) and the complex early evolution of the avian sternum. *Proc. Natl. Acad. Sci.* 111, 13900–13905. doi: 10.1073/pnas.1411070111
- Zhou, Z., and Zhang, F. (2002a). A long-tailed, seed-eating bird from the early cretaceous of china. *Nature* 418, 405–409. doi: 10.1038/nature00930
- Zhou, Z., and Zhang, F. (2002b). Largest bird from the early cretaceous and its implications for the earliest avian ecological diversification. *Naturwissenschaften* 89, 34–38. doi: 10.1007/s00114-001-0276-9
- Zhou, Z., and Zhang, F. (2003a). Anatomy of the primitive bird *Sapeornis chaoyangensis* from the early cretaceous of liaoning, china. *Can. J. Earth Sci.* 40, 731–747. doi: 10.1139/e03-011
- Zhou, Z., and Zhang, F. (2003b). *Jeholornis* compared to *Archaeopteryx*, with a new understanding of the earliest avian evolution. *Naturwissenschaften* 90, 220–225. doi: 10.1007/s00114-003-0416-5

Conflict of Interest: The authors declare that the research was conducted in the absence of any commercial or financial relationships that could be construed as a potential conflict of interest.

Copyright © 2021 Wu, Bailleul, Li, O'Connor and Zhou. This is an open-access article distributed under the terms of the Creative Commons Attribution License (CC BY). The use, distribution or reproduction in other forums is permitted, provided the original author(s) and the copyright owner(s) are credited and that the original publication in this journal is cited, in accordance with accepted academic practice. No use, distribution or reproduction is permitted which does not comply with these terms.



A Juvenile Specimen of *Archaeorhynchus* Sheds New Light on the Ontogeny of Basal Euornithines

Christian Foth^{1*}, Shiying Wang², Frederik Spindler³, Youhai Lin⁴ and Rui Yang⁴

¹Department of Geosciences, University of Fribourg, Fribourg, Switzerland, ²Institute of Vertebrate Paleontology and Paleoanthropology (CAS), Beijing, China, ³Dinosaur Museum Altmühltal, Denkendorf, Germany, ⁴Western Liaoning Museum of Paleontology, Liaoning Technical University, Fuxin, China

OPEN ACCESS

Edited by:

Corwin Sullivan,
University of Alberta, Canada

Reviewed by:

Sebastian Apesteguía,
Consejo Nacional de Investigaciones
Científicas y Técnicas (CONICET),
Argentina

Jingmai Kathleen O'Connor,
Field Museum of Natural History,
United States

*Correspondence:

Christian Foth
christian.foth@gmx.net

Specialty section:

This article was submitted to
Paleontology,
a section of the journal
Frontiers in Earth Science

Received: 09 September 2020

Accepted: 18 February 2021

Published: 16 April 2021

Citation:

Foth C, Wang S, Spindler F, Lin Y and
Yang R (2021) A Juvenile Specimen of
Archaeorhynchus Sheds New Light on
the Ontogeny of Basal Euornithines.
Front. Earth Sci. 9:604520.
doi: 10.3389/feart.2021.604520

The ontogenetic development of extant birds is characterized by rapid growth, bone fusion and an early onset of flight ability. In contrast, little is known about how these ontogenetic traits evolved in the bird stem lineage, and the available data pertains primarily to Enantiornithes. Here, we describe an almost complete skeleton of a juvenile euornithine bird (LNTU-WLMP-18) from the Early Cretaceous Jiufotang Formation (Aptian), which was discovered near Lamadong Town (Jianchang County, Liaoning, China). Despite its completeness, bone preservation is rather poor. Thus, to increase the contrast between bone tissue and matrix, we used cyan-red-based autofluorescence photography. The specimen is more or less articulated and exposed in ventral aspect. The jaws are edentulous, the coracoid bears a procoracoid process, and the ischium lacks a proximodorsal process. The pedal unguals are short and barely curved, indicating a ground-dwelling lifestyle. Feathers, including long primaries, are present as carbonized traces. Several characters indicate that LNTU-WLMP-18 is a juvenile: the bone surface has a coarsely striated texture and no fusion is evident between the carpals and metacarpals, between the tibia and the astragalus and calcaneum, or among the metatarsals. Although juvenile characters have the potential to impede accurate identification of the specimen, morphological comparisons and cladistic analysis identify LNTU-WLMP-18 as most likely referable to the basal euornithine *Archaeorhynchus*, which would make the specimen the first juvenile bird from the Jehol Group that could be assigned to a specific taxon. Based on its size and the incomplete ossification of the bone surface, LNTU-WLMP-18 represents the smallest and therefore youngest known individual of this genus. A statistical comparison of limb proportions shows that the forelimbs of LNTU-WLMP-18 are significantly shorter than the hindlimbs, while the forelimbs are longer than the hindlimbs in subadult and adult individuals. This is different from the situation in some Enantiornithes, in which the forelimbs exceed the length of the hindlimbs even in hatchlings. Similar to Enantiornithes, *Archaeorhynchus* probably exhibit an early onset of flight ability, as indicated by the extensive wing plumage in LNTU-WLMP-18. Finally, the lack of gastroliths in the visceral cavity might indicate a dietary shift in *Archaeorhynchus* during ontogeny. As a small-bodied, ground-dwelling, seed-eating bird with a precocial ontogeny, *Archaeorhynchus* filled an ecological niche that later allowed early crown birds to survive the K-Pg mass extinction.

Keywords: Euornithes, ontogeny, Early Cretaceous, China, bird evolution

INTRODUCTION

Extant birds differ from other extant groups of amniotes (with the exception of Chiroptera) in having a unique anatomical bauplan that enables active aerial locomotion (Brown 1963; Herzog 1968). In addition, they are characterized by a pattern of ontogenetic development that includes rapid growth, extensive bone fusion and onset of flight ability within the first weeks or months after hatching (Starck and Ricklefs, 1998a; Wang et al., 2019a; Plateau and Foth, 2020). The discovery of numerous ancestral birds from the Early Cretaceous of China (Benton et al., 2008; Zhou et al., 2010; Chiappe and Meng, 2016) and Spain (Sanz et al., 2002; Sanz et al., 2016) has provided new insights into the origin of modern birds and the evolution of feathers and flight (see Mayr, 2017; Wang and Zhou, 2017a; O'Connor, 2020 for summary), and to a lesser degree also into the evolution of their unique developmental mode. Macroevolutionary comparisons, for instance, indicate that the skull shape and small body size of extant birds probably result from paedomorphosis (i.e., the conservation of ancestral juvenile features in adults) nested deep in the evolution of Coelurosauria (Bhullar et al., 2012; Benson et al., 2014; Foth et al., 2016). In contrast, the intensity of bone fusion observed in this group and the rapidity of their growth reflect peramorphic heterochrony (i.e., the developmental exaggeration of ancestral adult traits), evolving within Ornithothoraces (Scheyer et al., 2010; Wang et al., 2017b; Plateau and Foth, 2020). Due to the rarity of juvenile avialan fossils, little is known about how these particular ontogenetic traits evolved in detail. Most available information comes from Enantiornithes (e.g., Elzanowski, 1981; Sanz et al., 1997; Chiappe et al., 2007; Xing et al., 2017; Kaye et al., 2019), an extinct subclade of ornithothoracines that represents the most diverse group of avialan stem birds during the Cretaceous (Wang and Zhou, 2017a). Enantiornithes show relatively slow skeletal growth (when compared with extant birds) in combination with an early onset of fledging, indicating a highly precocial developmental mode (Elzanowski, 1981; Sanz et al., 1997; Chiappe et al., 2007; Kurochkin et al., 2013). However, except for a limited number of specimens of *Gobipteryx* (Elzanowski, 1981), the juvenile enantiornithines that have been reported to date cannot be referred to any particular species. Thus, the documented ontogenetic changes represent only very general patterns.

Here, we describe the fossil remains of a juvenile avialan from the Early Cretaceous Jiufotang Formation (Aptian), which can be classified as a basal member of Euornithes (the ornithothoracine subclade that includes extant birds), and most likely a juvenile representative of the genus *Archaeorhynchus* (Zhou and Zhang, 2006). This new find allows for deep comparisons of juvenile morphology among enantiornithines, euornithines and more basal members of Avialae, giving new insights into the ontogenetic development of Mesozoic birds.

Geological Settings

The fossil described in this paper was collected by Prof. Yang Rui in the town of Lamadong, 21 km southwest of Jianchang,

Jianchang County, Liaoning, China. The locality exposes the lower part of the Jiufotang Formation, which is Aptian (Early Cretaceous) in age (see Zhang et al., 2007; Cao and He, 2019) (Figure 1).

MATERIAL AND METHODS

Material

The specimen represents a single slab containing the remains of an immature bird fossil. It was found and mechanically prepared by one of the authors (YR). The counter slab was unfortunately lost, and is therefore not available for study. The specimen is housed at the Western Liaoning Museum of Paleontology (WLMP) of the Liaoning Technical University in Fuxin (LNTU), and stored under the collection number LNTU-WLMP-Yang Rui-18 (Figure 2; Table 1).

Autofluorescence Imaging

For photo documentation, we used a cyan-red-based autofluorescence technique (Figure 2B; Figures 3A,B) which increased the contrast between fossilized hard and soft tissues and the matrix, emphasizing delicate structures, cracks and preparation artifacts that were at best poorly discernible under visible light (Haug et al., 2011; Haug and Haug, 2011; Foth et al., 2020). The investigation was performed with a Canon EOS 600D camera and a Canon Macro Photo Lens MP-E 65 mm, equipped with a red filter foil taken from cyan-red stereo spectacles. The complementary cyan filter foil was attached to three LED light sources. After the specimen was excited by cyan light, only the emitted red light passed readily through the complementary red camera filter, while light of other wavelengths was mostly blocked (Haug et al., 2011; Haug and Haug, 2011). To increase the signal, the autofluorescence images were modified by deleting the blue and/or green color channels in Adobe Photoshop CC 19.0 (Adobe Inc.) to increase the contrast between fluorescent and non-fluorescent structures.

Phylogenetic Analysis

For taxonomic identification, we added LNTU-WLMP-18 to the phylogenetic dataset recently published by Zheng et al. (2018). Characters that pertain specifically to the adult condition were scored as inapplicable for LNTU-WLMP-18. The species sample in the dataset was modified, following a recent taxonomic revision of Confuciusornithidae that found *Jinzhourornis yixianensis* to be a junior synonym of *Confuciusornis sanctus* (Wang et al., 2019a). Furthermore, *Didactylus jii* was treated as a junior synonym of *Sapeornis chaoyangensis*, following Gao et al. (2012). The updated dataset consisted of 62 terminal taxa scored for 245 characters (see Supplementary Files S1, S2) and was analyzed using the software TNT 1.5 (Goloboff, Farris and Nixon, 2008; Goloboff and Catalano, 2016), using equal weights and implied weights ($K = 12$; Goloboff et al., 2018) through a heuristic search of 1,000 replicates of Wagner trees, followed by TBR (tree bisection and reconnection) branch swapping.

Statistics

Limb proportions of LNTU-WLMP-18 were compared with those of previously described *Archaeorhynchus* specimens (see

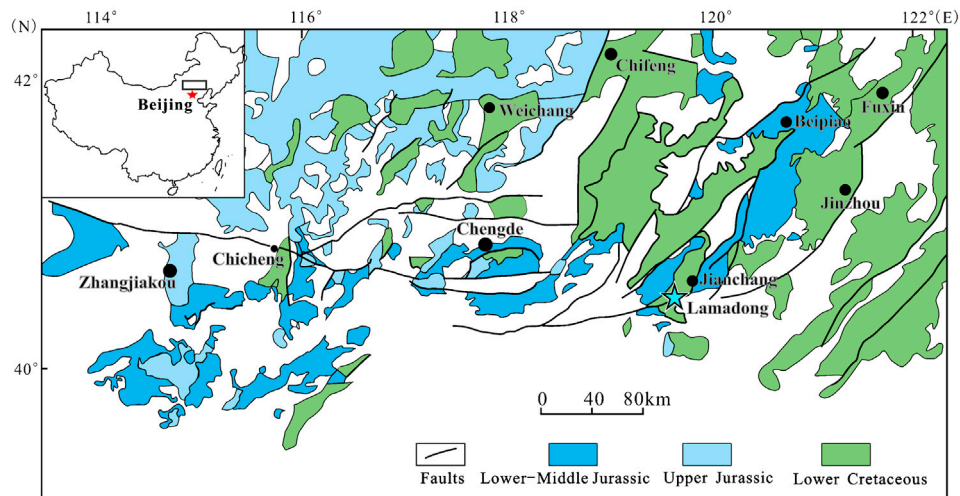


FIGURE 1 | Geological map of northeastern China (western Liaoning, northern Hebei and adjacent Inner Mongolia), showing the distribution of Late Mesozoic terrestrial strata and the geographic locality of LNTU-WLMP-18 near Lamadong Town (turquoise star). Modified after (Liu et al., 2012).

discussion for taxonomic classification) using the one sample *t*-test, which allows estimations of the probability that the two sets of values represent the same population (Table 2). Significant differences in limb proportions between LNTU-WLMP-18 and other *Archaeorhynchus* specimens can be interpreted as potential ontogenetic changes. Furthermore, we compared the ontogenetic changes in the lengths of the forelimb (defined by the length of the humerus and ulna) and hindlimb (defined by the length of the femur and tibia) in *Archaeorhynchus*, *Archaeopteryx* (data from Rauhut et al., 2018) and *Confuciusornis* (data from Chiappe et al., 2008), using ordinary least squares (OLS) regression analysis. Equality in the slopes of the single ontogenetic trajectories was investigated using a one-way ANCOVA, which tests for equality of means between univariate groups, using *F* statistics (Hammer and Harper, 2006). The tests were performed with the software PAST 3.21 (Hammer et al., 2001).

Anatomical Nomenclature

Following the argument of Wilson (2006), we applied the anatomical and directional terms commonly used in anatomical descriptions of non-avian dinosaurs, rather than rigorously using the anatomical terms recommended in the *Nomina Anatomica Avium* by Baumel and Witmer (1993). However, the latter are for anatomical structures that are typical for extant birds, but not present in non-avian dinosaurs. One major conflict between the two different nomenclatures pertains to the digit identity of extant birds and non-avian tetanurans. While the three-fingered hand of tetanurans evolved through the successive reduction of digits V and IV in early theropod evolution, leaving digits I to III (e.g., Rauhut, 2003), embryological studies on the limb development of birds indicate digit primordia are most appropriately identified as II to IV (e.g., Hinchliffe and Hecht, 1984; Burke and Feduccia, 1997). This contradiction between palaeontological and embryological data renewed the controversy regarding the

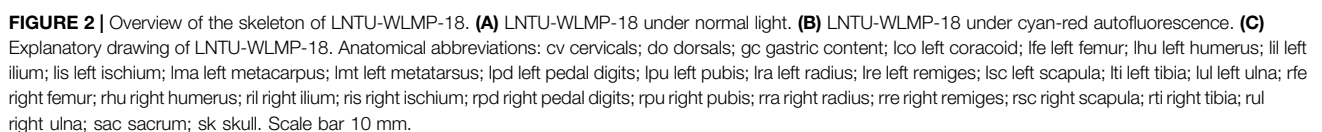
dinosaur origin of birds (Burke and Feduccia, 1997; Feduccia et al., 2005). To avoid this conflict in digit numbering, Baumel and Witmer (1993) suggested calling the three fingers of extant birds the alular digit, major digit and minor digit. However, new developmental studies indicate a decoupling of the digit anlagen from the molecular mechanisms that pattern them. This frameshift results in an imposition of digit identities I, II and III on the digit anlagen II, III, and IV (e.g., Wagner and Gauthier, 1999; Vargas and Fallon, 2005; Tamura et al., 2011; Young et al., 2011), which is further supported by recent anatomical comparisons among theropod manus throughout evolution (e.g., Bever et al., 2011; Guinard, 2015). Therefore, we apply the general digit nomenclature of non-avian theropods to highlight the dinosaur origin of extant birds. Furthermore, we prefer the terms “anterior” and “posterior” over “cranial” and “caudal” (as the latter terms could be potentially confused with anatomical regions of the skeleton), and refer to the different sides of long bones according to their orientation in the resting pose in a theropod dinosaur.

Anatomical Description

Due to general uncertainty regarding the taxonomic classification of juvenile specimens in the fossil record, especially within the clade Avialae, the morphology of LNTU-WLMP-18 is described at face value and compared with other bird species from the Jehol Group. The reasons, why this specimen most likely represents a juvenile of the euornithine bird *Archaeorhynchus* are documented in the Discussion, on the basis of detailed anatomical comparisons with various euornithine bird species and a phylogenetic analysis. After the taxonomic evaluation, morphological differences with other *Archaeorhynchus* specimens are discussed from the perspective of ontogeny.

General Preservation

Only the main slab of the specimen is available for study, while the counter slab is missing. The specimen is exposed in



In ventral view, the neck appears bent ventrally to the left side, while the head is exposed in right lateral aspect. The skeleton is more or less articulated, although some elements are displaced. The temporal region of the skull is disarticulated, but still in association with the rest of the cranium. The left humerus is rotated about its long axis and the right foot is incomplete and

TABLE 1 | Skeletal measurements of LNTU-WLMP-18 and other specimens of *Archaeorhynchus spathula*. *estimated values.

| mm | LNTU-WLMP-18 | | IVPP V14287 | IVPP V17075 Zhou et al. (2013) | IVPP V17091 | IVPP V20312 Wang et al. (2016) |
|--------------------|--------------|-------|-------------|-----------------------------------|-------------|-----------------------------------|
| | Left | Right | | | | |
| Skull | >22.0 | — | — | — | — | — |
| Scapula | >14.5 | >15.0 | 46 | 46 | 43 | — |
| Coracoid | 8.0* | — | 20 | 20 | 19 | — |
| Humerus | 20.5 | 22.0 | 54 | 53 | 49 | 59.1 |
| Deltpectoral crest | NA | 10.0* | — | — | — | — |
| Ulna | 21.0 | 21.0 | 57 | 58 | 54 | 61.3 |
| Radius | 20.0 | 20.0* | 56 | 55 | 52 | 60.3 |
| Mc I | 3.0 | — | 6 | 6 | 5 | 7.2 |
| Mc II | 11.0 | — | 25 | 25 | 23 | — |
| Mc III | >7.5 | — | 24 | 23 | 21 | — |
| MP I-1 | 5.0 | — | 10.5 | 10 | 9 | — |
| PII-2 | 0.6* | — | — | 12 | 10 | — |
| Ilium | >16 | 20.5* | — | — | — | — |
| Pubis | >12.5 | >16.0 | 37 | 28 | 30 | — |
| Ischium | >8.0 | 10.0 | 20 | 17 | 14 | — |
| Femur | 21.0 | 21.5 | 37 | 36 | 34 | — |
| Tibia | 23.0 | >18.0 | 43 | 42 | 39 | 44.9 |
| Mt I | 1.0 | — | — | — | — | — |
| Mt II | 10.0 | — | — | — | — | — |
| Mt III | 11.5 | — | 20 | 22 | 19 | 21.6 |
| Mt IV | 10.0 | — | — | — | — | — |
| PP I-1 | 1.5 | — | — | — | — | — |
| PP I-2 (U) | 1.0 | — | — | — | — | — |
| PP II-1 | 3.5* | — | — | 6 | 5.5 | — |
| PP II-2 | 2.5* | — | — | 5 | 4 | — |
| PP II-3 (U) | 3.0* | — | — | 5 | 4 | — |
| PP III-1 | 4.0 | — | — | 6.5 | 6 | — |
| PP III-2 | 2.5 | — | — | 5 | 5 | — |
| PP III-3 | 2.5* | — | — | 4 | 4 | — |
| PP III-4 (U) | 2.5* | — | — | 5 | 4 | — |
| PP IV-1 | 2.5* | — | — | 5 | 4.5 | — |
| PP IV-2 | 2.0* | — | — | 3 | 3.5 | — |
| PP IV-3 | 2.0* | — | — | 2.5 | 3 | — |
| PP IV-4 | 2.0* | — | — | 2 | 3 | — |
| PP IV-5 (U) | 2.0 | — | — | 4 | 3.5 | — |

disarticulated from the tibia. However, phalangeal elements of the right foot can be found next to the right forelimb. Despite the general completeness of the specimen, some bones are hidden or missing, including various skull bones and the furcula, sternum (or anlagen for sternal ossification, see Zheng et al., 2012), sternal ribs, gastralia, right coracoid, right manus, and right metatarsus. Due to the loss of the counter slab, it is uncertain whether these bones were originally present or not. Unfortunately, the preservation of the remaining bones is rather poor. The limb bones are generally crushed and often split in half, so that the original cortical surface is not visible. However, these splits occur primarily in the midshaft regions of the bones, while the cortical surface of the proximal and distal ends remains intact (Figure 3). In addition, the specimen preserves the remains of the wing plumage and gut contents.

Ontogenetic Stage

Several characters indicate that LNTU-WLMP-18 is still a juvenile individual, which impedes taxonomic identification. As in extant birds and early juvenile non-avian theropods (Tumarkin-Deratzian et al., 2006; Chiappe and Göhlich, 2010;

Dal Sasso and Manuco, 2011; Rahut et al., 2012; Hone et al., 2016), the bone surface has a coarsely striated texture, which is associated with a high degree of vascularity resulting from increased rates of bone growth. Furthermore, the specimen lacks fusion between the carpals and metacarpals, among the tibia, astragalus, and calcaneum, and among the metatarsal bones, which are interpreted as juvenile characters in Ornithothoraces (e.g., Wang et al., 2017a; Wang and Zhou 2017b).

Skull

The skull of LNTU-WLMP-18 is heavily crushed (Figures 4A,B). During splitting of the rock, many skull bones were damaged or were lost with the counter slab. Consequently, the lacrimal, jugal, postorbital, squamosal, quadratojugal, quadrate, and palatal bones, as well as the basicranium, cannot be identified. Only the right **premaxilla** is exposed. LNTU-WLMP-18 possesses a short to moderately long edentulous beak (Figures 3A, 4A,B), as in euornithines like *Archaeorhynchus* (Zhou and Zhang, 2006; Zhou et al., 2013), *Eogranivora* (Zheng et al., 2018), and *Schizoura* (Zhou et al., 2012). The premaxilla tapers anteriorly, with the nasal (frontal) process and maxillary

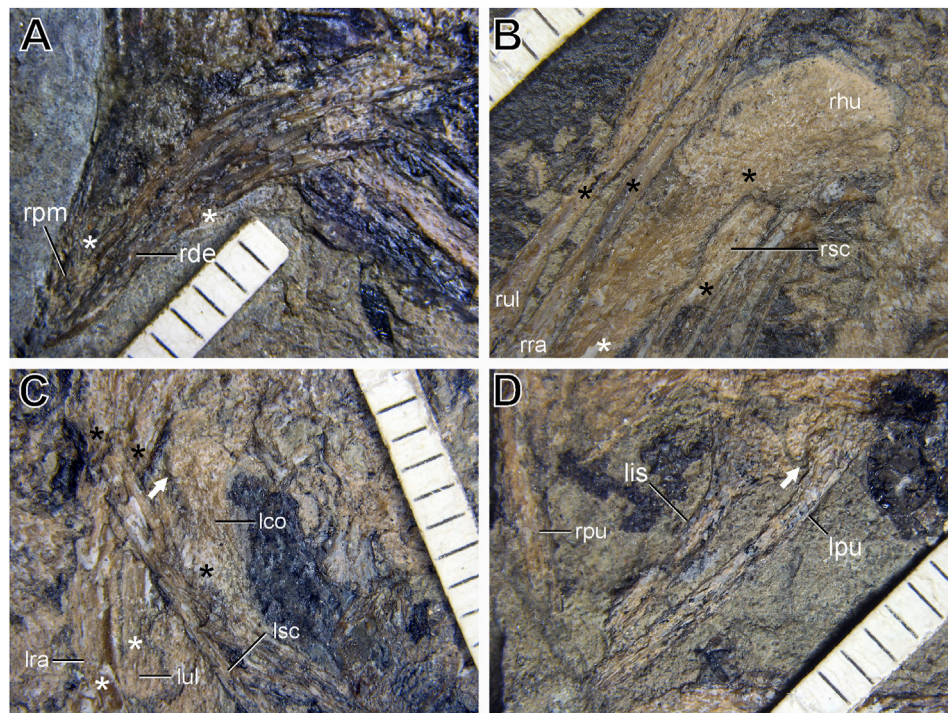


FIGURE 3 | Details of preservation of LNTU-WLMP-18 under normal light. White asterisks highlight regions, where long bones are split in half. Black asterisks highlight the original cortical structure of bones. **(A)** Close-up of the beak. **(B)** Close-up of the right forelimb. **(C)** Close-up of the left coracoid and forelimb. The white arrow highlights the procoracoid process of the coracoid. **(D)** Close-up of the pelvis. The white arrow highlights the ventral fossa between the ischial peduncle and pubic shaft. Anatomical abbreviations: lco left coracoid; lis left ischium; lpu left pubis; lra left radius; lsc left scapula; lul left ulna; rde right dentary; rhu right humerus; rpm right premaxilla; rpu right pubis; rra right radius; rsc right scapula; rul right ulna.

TABLE 2 | Comparison of skeletal proportions and statistical differences (*t*-test) between LNTU-WLMP-18 and other specimens *Archaeorhynchus spathula*. Comparisons with significant differences are shown in bold.

| | LNTU-WLMP-18 | IVPP V17091 | IVPP V14287 | IVPP V17075 | IVPP V20312 | <i>t</i> -value | <i>p</i> -value |
|----------------------------|--------------|-------------|-------------|-------------|-------------|-----------------|------------------|
| Forelimb/Hindlimb | 0.973 | 1.370 | 1.360 | 1.360 | 1.378 | 90.080 | <0.001 |
| Ulna/Humerus | 0.988 | 1.102 | 1.056 | 1.094 | 1.020 | 4.230 | 0.024 |
| Metacarpal-I/Humerus | 0.141 | 0.102 | 0.111 | 0.113 | 0.122 | -7.128 | 0.006 |
| Metacarpal-I/Ulna | 0.143 | 0.093 | 0.105 | 0.103 | 0.119 | -6.870 | 0.006 |
| Metacarpal-I/Metacarpal-II | 0.273 | 0.217 | 0.240 | 0.240 | 0.277 | -2.387 | 0.097 |
| Metacarpal-II/Humerus | 0.518 | 0.469 | 0.463 | 0.472 | 0.440 | -7.780 | 0.004 |
| Metacarpal-II/Ulna | 0.524 | 0.426 | 0.439 | 0.431 | 0.431 | -34.310 | <0.001 |
| Tibia/Femur | 1.082 | 1.147 | 1.162 | 1.167 | 1.151 | 16.260 | <0.001 |
| Metatarsus-III/Femur | 0.494 | 0.559 | 0.541 | 0.611 | 0.554 | 4.640 | 0.019 |
| Metatarsus/Tibia | 0.457 | 0.487 | 0.465 | 0.524 | 0.481 | 2.640 | 0.077 |

process diverging at an angle of approximately 20°. In (sub-)adult specimens of *Archaeorhynchus*, for instance, this angle measures approximately 30° (Zhou and Zhang, 2006; Zhou et al., 2013). The nasal (frontal) process is slender and elongated, forming the dorsal border of the external naris. Likewise, the length of the premaxillary body (measured as the distance between the anterior tip of the premaxilla and the anterior margin of the external naris) is considerable, measuring about 42% of the total length of the dorsal margin of the premaxilla (measured as the distance between the anterior tip and posterior end of the nasal

process). The premaxillary body contributes the acute anterior apex of the external naris. The premaxilla is still in articulation with the anterior end of the maxilla, but due to compression, the suture between the two elements cannot be traced. Under autofluorescent light, a weak red light signal representing an upwardly directed process is detectable (Figure 4B), which could be either the ascending process of the maxilla or the anteroventral process of the right nasal that separates the external naris from the antorbital fenestra. Ventral to the nasal process of the premaxilla and dorsal to the possible ascending process of the

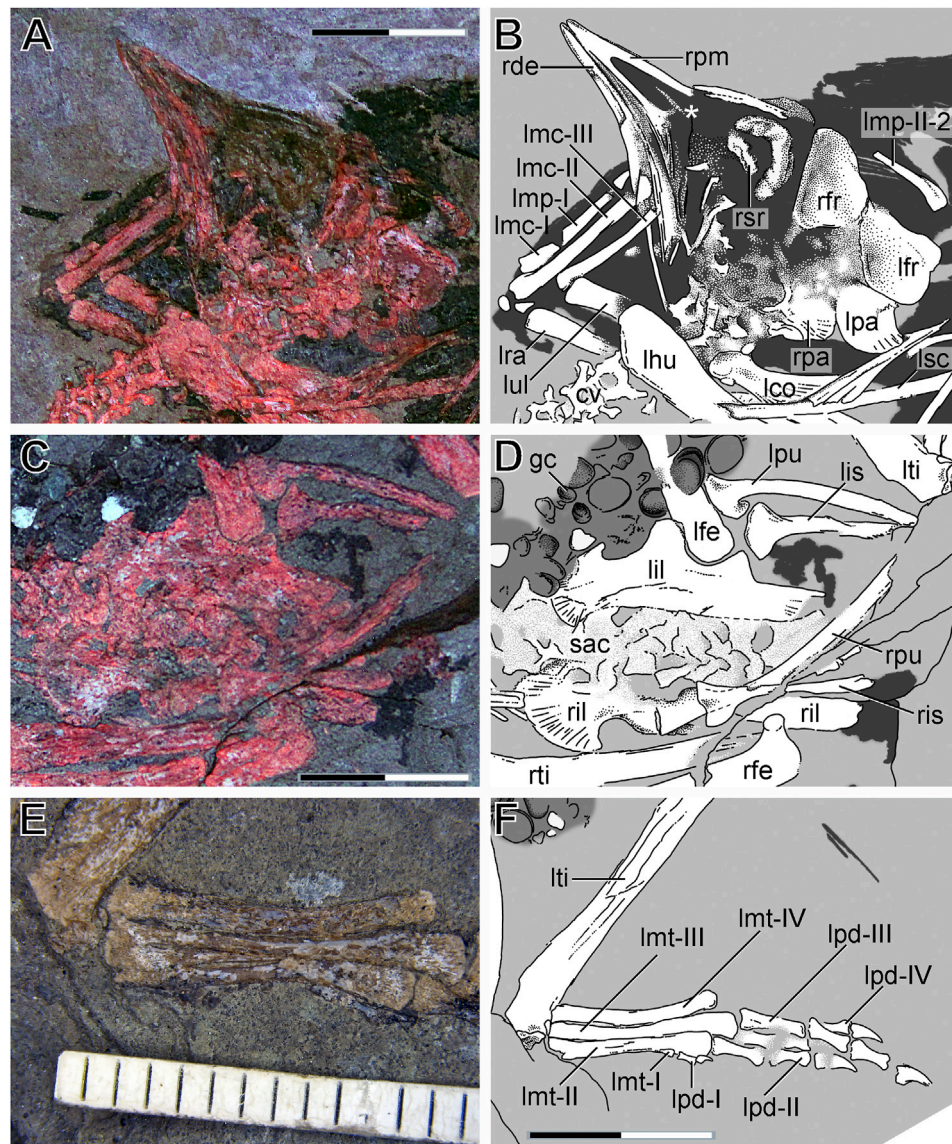


FIGURE 4 | Anatomical details of LNTU-WLMP-18. **(A)** Skull and left manus under cyan-red autofluorescence. **(B)** Explanatory drawing of the skull and left manus. The white asterisk marks the possible remains of the ascending process of the maxilla and the nasal body. **(C)** Pelvis and sacrum under cyan-red autofluorescence. **(D)** Explanatory drawing of the pelvis and sacrum. **(E)** Left metatarsus under normal light. **(F)** Explanatory drawing of the left foot. Anatomical abbreviations: cv cervicals; gc gastric content; lco left coracoid; lfe left femur; lfr left frontal; lhu left humerus; lil left ilium; lis left ischium; lmc left metacarpal; lmp left manual phalanx; lmt left metatarsus; lpa left parietal; lpd left pedal digits; lpu left pubis; lra left radius; lsc left scapula; lti left tibia; lul left ulna; rde right dentary; rfe right femur; rfr right frontal; ril right ilium; ris right ischium; rpa right parietal; rpm right premaxilla; rpu right pubis; rsr right scleral ring; rti right tibia; sac sacrum. Scale bar 10 mm.

maxilla, a further weak autofluorescence signal is present, which may correspond to remains of the nasal body. If these interpretations are correct, the two signals indicate the posterior and dorsal limits of the external naris.

The **frontals** are not fused to each other (**Figures 4A,B**), which represents the usual condition in non-ornithurine birds, including adult specimens of *Archaeorhynchus* (Wang et al., 2016; Plateau and Foth, 2020). The right frontal bone is more or less complete and exposed in laterodorsal view. As typical for avialans (e.g., Zhou et al., 2013; Wang et al., 2017a; Rauhut et al., 2018), it is elongated, forming the majority of the skull roof and

the dorsal margin of the orbit. It narrows anteriorly and is still in articulation with the nasal process of the premaxilla, and the contact zone between both bones is marked by a distinct kink. The posterior portion of the right frontal, which is broken off and slightly displaced ventrally, is laterally expanded. The lateral margin of the posterior portion of the frontal bears an orbital rim, which is slightly offset from the dorsal roof of the frontals. Due to poor preservation, the anterior extent of the rim cannot be judged.

Posterior to the right frontal, remains of the left frontal are visible, with the element's concave ventral surface exposed.

Although the jugal and postorbital are missing, it is clear that the orbit was enlarged and rounded. In the center of the orbit, remains of a **sclerotic ring** are preserved (**Figures 4A,B**). While the dorsal half of the ring is more or less intact, the ventral part has suffered some damage. Ventral to the frontals, both **parietals** are preserved, and are fused neither to the frontals nor to each other. As with the frontals, the right element shows the external surface, while the right shows the internal one. Both elements are roughly square, but due to crushing and overlap with the anterior cervicals, no further details can be described. The absence of the postorbital bone could reflect imperfect preservation, but as this bone was lost independently in the enantiornithine and euornithine lineages (see e.g., Zhou and Zhang, 2006; O'Connor et al., 2010; Zhou et al., 2012; Zhou et al., 2014), its absence could also be genuine.

More than two-thirds of the **mandible** is preserved, with the posterior end missing (**Figures 4A,B**). In *Archaeorhynchus* the posterior end of the dentary is unforked (Zhou and Zhang, 2006; Zhou et al., 2013). Like in many other Jehol birds (Zhou and Zhang, 2006; O'Connor and Chiappe, 2011; O'Connor et al., 2011; Wang et al., 2017b), the ventral margin of the mandible is concave in shape. Only the anteriormost tip and the posterior end of the right **dentary** are preserved, while the mid-section is missing. Consequently, the left dentary is exposed in medial view, making it impossible to evaluate if the specimen possessed a longitudinal lateral groove with small foramina, as described for *Archaeorhynchus* and *Schizoura* (Zhou and Zhang, 2006; Zhou et al., 2012; Zhou et al., 2013). Nonetheless, the dentaries appear to be slender, spatulate, and edentulous as in *Archaeorhynchus* and *Schizoura* (Zhou and Zhang, 2006; Zhou et al., 2012; Zhou et al., 2013). Due to poor preservation, the remnants of the posterior part of the mandible are difficult to identify. Two small fragments lying posterior to the dentary probably represent the right **surangular** and **angular** in lateral view, while the posterior-most fragment might include remains of the right **prearticular** and the medial part of the left surangular (**Figures 4A,B**). However, nothing can be said about their morphology or that of the jaw joint.

Axial Skeleton

The vertebral column is poorly preserved. The more anterior cervicals are covered by the left humerus or intermixed with the crushed temporal skull bones so that nothing can be said about their anatomy or exact number (**Figures 4A,B**). The last seven posterior **cervical vertebrae** are preserved in association, but are no longer in full articulation. Due to rotation and displacement, one articular surface is exposed on each cervical, but it is not clear whether the anterior or posterior surface is exposed. The intense compression hampers morphological interpretation of the cervicals. Consequently, exact identification of particular processes is not possible. Due to the almost pentaradial arrangement of the processes, however, it is clear that the cervicals bear carotid processes, similar to *Archaeorhynchus*, *Schizoura*, and other Euornithes (Zhou et al., 2012; Zhou et al., 2013; Wang et al., 2016). The exposed neural canals are enlarged and rounded.

The **dorsals** and sacral series have both suffered much damage (**Figure 2**), and little can therefore be said about their morphology. The dorsal vertebrae seem not to be fused together, similar to other Early Cretaceous ornithothoracine birds (Clarke et al., 2006; Zhou and Zhang, 2006; Zhou et al., 2012; Zhou et al., 2014; Chiappe et al., 2020). Fine gaps between the vertebrae indicate that this was also true of the sacrals (**Figures 4C,D**). Due to damage and compaction, the exact number of sacrals cannot be determined. Neither **caudal vertebrae** nor a **pygostyle** are visible under normal light, although autofluorescent signals indicate that the fragmentary remains of some anterior caudals are present next to the right pubic shaft.

There is no indication of free **cervical ribs**. Many of the **dorsal ribs** are preserved in articulation with the dorsal section of the vertebral column. The ribs are long and straight and show no signs of **uncinate processes**, which are present in adult *Archaeorhynchus* (Zhou and Zhang, 2006) and many other Pygostylia (Chiappe et al., 1999; Zhang et al., 2001; Clarke et al., 2006; Wang et al., 2015). No **sternal ribs** or **gastralria** were identified.

Pectoral Girdle

Neither the **furcula** nor the **sternal elements** are preserved. This is also the case for the anterior and posterior ends of the left **scapula**. The anterior end of the right scapula is hidden by the overlying humerus, while the posterior end is not preserved. Thus, the only visible parts of the scapulae are the midshafts, which are very slender and straight. This is different from the condition in (sub-)adult specimens of *Archaeorhynchus* (Zhou and Zhang, 2006; Zhou et al., 2013) and other euornithine birds (Clarke et al., 2006; Chiappe et al., 2014; Wang et al., 2015), in which the shaft is slightly curved. The left **coracoid** is exposed in anterior view and lies in close association with the anterior end of the left scapula and the proximal end of the left humerus (**Figure 3C**). As preserved, the scapula and coracoid are unfused, which is the typical situation for Early Cretaceous ornithothoracine birds (Serenio et al., 2002; Clarke et al., 2006; Zhou and Zhang, 2006; Wang et al., 2016; Chiappe et al., 2020). The coracoid is a strut-like element. The omal end is relatively broad and forms a flattened, oval surface that faces laterally and might represent the articular facet for the scapula. Below the coracoid head a small, blunt tubercle is present on the medial side, which represents the procoracoid process (**Figure 3C**). This process is also present in *Archaeorhynchus* (Zhou et al., 2013), *Archaeornithura* (Wang et al., 2015), *Eogranivora* (Zheng et al., 2018) and *Yixianornis* (Clarke et al., 2006). The mid-section of the shaft is slightly constricted. Distally, the coracoid shaft expands drastically on the lateral side, while the medial expansion is minor. The lateral margin is almost straight and is longer than the medial one, similar to the condition in adult specimens of *Archaeorhynchus* (Zhou and Zhang, 2006). The distal expansion of the coracoid shaft indicates the presence of a broad contact zone for the sternum, but the actual sternal margin is damaged and cannot be evaluated (**Figures 4A,B**).

Forelimbs

Both forelimbs are preserved. The left **humerus** is turned 180° about its long axis, lying next to the dorsal column and exposing its posterior surface. The right humerus is preserved in natural position, exposed in anterior aspect (**Figure 2**). Proximally, the humeral head is craniocaudally convex and the internal tuberosity is not well developed. The small deltopectoral crest is only visible in the right element. As preserved, the crest measures more than one-third the length of the humerus, but its anterior margin is broken off, so that the actual shape cannot be evaluated. The middle part of the humeral shaft is almost straight, while the distal end is slightly expanded (**Figure 2**). The **ulna** is longer than the **radius**, but both bones are slightly shorter than the humerus, in contrast to (sub-) adult specimens of *Archaeorhynchus* (Zhou et al., 2012; Zhou et al., 2013) and many other euornithine birds (e.g., *Iteravis*, Zhou et al., 2014; *Bellulia*, Wang et al., 2016; *Eogranivora*, Zheng et al., 2018). The right ulna and radius are visible over their entire length, while the left elements are partly covered by the neck and by the left humerus, scapula and coracoid, so that only the proximal and distal ends are visible. As is evident from the right forelimb, the proximal end of the ulna is slightly expanded, but a distinct olecranon process is lacking as is typical for maniraptorans (Rauhut, 2003). The proximal half of the ulna is slightly bowed, and an interosseous cleft separates the ulna and radius over most of their length. The distal half of the ulnar shaft is almost straight, while the distal end is slightly expanded. In both forelimbs, the radius is displaced anteriorly with respect to the ulna. The former bone is straight and relatively thick, being more than half as wide as the ulna in the midshaft region (**Figures 2, 3D**).

Only the proximal portion of the left **manus** is preserved, and the phalanges of the second (major) and third (minor) digit are covered by the skull (**Figures 4A,B**). Two ossified **carpal** elements can be identified, lying proximal to metacarpals II and III. They are similar in size and not fused to the metacarpals or to each other. This condition resembles the morphology of subadult specimens of *Archaeorhynchus* (Zhou et al., 2013), while adult specimens of ornithothoracine birds (including *Archaeorhynchus*) usually form a fused carpometacarpus (Wang et al., 2016; Wang et al., 2017b). Based on their positions, they most likely represent the semilunate carpal and the ulnare (Zhou et al., 2013). Traces in the rock might indicate that the radiale was also once present. A fourth carpal x (see Zhou et al., 2013) cannot be identified. **Metacarpals** I and III are slightly displaced distally, and are not in line with the proximal end of metacarpal II. The metacarpal elements are not fused to each other. The distal ends of metacarpal II and III are covered by the mandible, but the distal end of metacarpal II is visible due to a break in the jaw. Metacarpal I (the alular metacarpal) is short and rectangular, measuring less than one-third of the length of metacarpal II. No signs of additional processes, such as an extensor process or a pisiform process, can be identified. Metacarpal II is the most robust element in the metacarpus, and is almost straight. Its distal end is slightly expanded compared to the midshaft. Metacarpal III is approximately half as wide as metacarpal II. As its distal end is covered by

the lower jaw, its actual length cannot be estimated. However, the bone is slightly bowed, forming a long intermetacarpal space. As preserved, the metacarpus of LNTU-WLMP-18 therefore resembles that of subadult individuals of *Archaeorhynchus* (Zhou et al., 2013).

Only in the first digit are the phalanges preserved in articulation (**Figures 4A,B**). The first **phalanx** of digit I is almost twice as long as metacarpal I. The remains of the first ungual indicate that this element was short and lacked a prominent flexor tubercle. It is very likely, also not certain that the first digit failed to reach the distal end of metacarpal II. As stated above, the phalanges of the second and third digits are covered by the skull. However, a single splint of bone preserved above the frontal (**Figures 4A,B**) might represent phalanx II-2. This bone measures approximately half the length of metacarpal II and shows a very distinct shape, with one end significantly expanded compared to the other. In ornithothoracine birds, the proximal third of phalanx II-2 exhibits a small posterior flange (e.g., *Archaeorhynchus*, Zhou et al., 2013; *Yanornis*, Wang et al., 2013b; *Sinornis*, Sereno et al., 2002), which could correspond to the expansion found in the element in question.

Pelvic Girdle

Both **ilia** are preserved, and exposed in medial view (**Figures 4C,D**). They are still in association with the sacrum, but not fused to the vertebrae. The right ilium is more or less complete, but its acetabular region is covered by the right pubis and ilium, and is separated from the postacetabulum by a deep crack in the matrix. In the left ilium the acetabular region is intact, but the anterior end of the preacetabulum is partly covered by gut contents (see below), while the posterior end of the postacetabulum is damaged. The preacetabulum seems to be as long as, or slightly longer than, the postacetabulum, but the exact ratio cannot be measured with certainty due to poor preservation. As in other euornithines, including subadult *Archaeorhynchus*, the preacetabulum is approximately twice as high as the postacetabulum (Zhou et al., 2013; Zhou et al., 2014). The preacetabulum possesses an rounded anterior margin, and shows a ventral expansion in the form of a prominent hook as seen in subadult specimens of *Archaeorhynchus* (Zhou et al., 2013), but also *Dingavis* (O'Connor et al., 2016), *Eogranivora* (Zheng et al., 2018), *Schizoura* (Zhou et al., 2012), and *Yixianornis* (Clarke et al., 2006). Furthermore, the preacetabular blade shows a radial pattern of strong striations. The pubic peduncle is longer and more massive than the triangular ischial peduncle. The postacetabulum is almost rectangular, with a blunt posterior end. This differs from the situation in *Iteravis* (Zhou et al., 2014), but resembles the condition in adult *Archaeorhynchus* (Zhou and Zhang, 2006).

The **pubes** are incomplete, missing the distal ends (**Figures 3D, 4C,D**). The left pubis seems to be exposed in lateral view, the right element in anterior view. The latter is still in contact with the left ilium, while the left pubis is slightly displaced posteriorly. The iliac peduncle of the left pubis shows a small anterior projection, and the peduncle's ventral margin bears a small embayment (**Figure 3D**). While such embayment is usually absent in

pygostylians, *Archaeopteryx* (Foth et al., 2014, Extended Data Figure 2 and *Rahonavis* (Forster et al., 2020, Figure 31) display a similar morphology. In more basal theropods, this structure is described as an obturator notch (Rauhut, 2003). In the (sub-) adult *Archaeorhynchus* specimen IVPP V17075, the proximal end of the pubis is exposed in anteromedial view, showing no sign of an obturator notch. While the iliac peduncle of the pubis in this specimen is rather massive, the ischial peduncle is a thin, plate-like structure that fuses with the proximal end of the pubic shaft (Zhou et al., 2013). Beneath the right iliac peduncle of LNTU-WLMP-18, a small section of pubic shaft is broken away so that the underlying ischium is exposed. The pubic shafts are slender, and bowed both posteriorly and medially. Nothing can be said about the distal end of the pubic shaft, but based on the displacement of the left pubis, the distal ends must have been unfused, similar to the condition in (sub-)adult specimens of *Archaeorhynchus* (Zhou et al., 2013; Wang et al., 2016). However, the pubes probably contacted each other, as suggested by their curvature.

Both **ischia** are present (Figures 4C,D). The right ischium is complete, although the midshaft is interrupted by a crack in the slab. In the left ischium, the distal end is slightly broken. The ischium is shorter than the pubis, measuring about half the length of the ilium. The proximal end that forms the peduncles for the ilium and the pubis is short and broad, lacking the additional proximodorsal process present in many enantiornithines (e.g., Wang et al., 2010; Li et al., 2012; Hu et al., 2015; Wang and Zhou, 2017c) and more basal birds (e.g., Chiappe et al., 1999; Zhou and Zhang, 2002a; Zhou and Zhang, 2002b; Wellnhofer, 2009; Wang et al., 2018a). The shaft is simply straight, having a blunt distal end. Thus, the ischium resembles that of subadult specimens of *Archaeorhynchus* (Zhou et al., 2013) in possessing neither a strut-like proximodorsal process nor a gradual distal dorsal expansion along the shaft as in more advanced euornithines, like *Yixianornis* (Clarke et al., 2006), *Schizoura* (Zhou et al., 2012), *Iteravis* (Zhou et al., 2014) or *Dingavis* (O'Connor et al., 2016).

Hindlimbs

Both hindlimbs are present, and are more or less complete apart from the fragmentary preservation of the right foot. The left **femur** is still in articulation with the iliac portion of the acetabulum, lying perpendicular to the main body axis with the medial side visible (Figure 2). In contrast, the right femur lies parallel to the body axis, exposing the posterior surface. The femur is approximately as long as the humerus, whereas the humerus is longer than the femur in most other Pygostylia, including (sub-)adult specimens of *Archaeorhynchus* (Zhou and Zhang, 2002b; Zhou et al., 2012; Zhou et al., 2013; O'Connor et al., 2016). The femoral head is ball-shaped, and the neck is short (Figure 4D). The dorsal margin of the femur is convex from anterior view, and the greater trochanter is continuous with the lesser trochanter as in other pygostylians (Chiappe et al., 1999). The femoral shaft is relatively robust and straight, in contrast to most Paraves, where the shaft is curved (Norell and Makovicky, 1999; Zhou and Zhang, 2006; Clarke

et al., 2006; O'Connor et al., 2011; Rauhut et al., 2018). In posterior view, the distal end of the femur is slightly expanded lateromedially with a small concavity interrupting the ventral margin. In medial view the distal end appears rounded, with a minor posterior expansion. This expansion probably represents the remains of the distal condyles, but due to preservation not much more can be said about their morphology.

The right **tibia** lies medially to the corresponding femur, paralleling the body axis, and exhibiting its anterior surface. Approximately two-thirds of the tibia is preserved, with the distal end missing. Slightly disarticulated from the femur, the left tibia is complete, being slightly longer than the femur. The bone is exposed in posteromedial view. The proximal end of the tibia is lateromedially expanded. The shaft is straight, while the distal end does not show any distinctive features apart from a minor expansion (Figure 2). No **fibula** was identified. Fragmentary bone remains distal to the tibia might represent the **astragalus** (Figures 4E,F), in which cases the proximal tarsals would seem not to be fused with the tibia to form a tibiotarsus. This morphology resembles the condition seen in subadult specimens of *Archaeorhynchus* (Zhou and Zhang 2006; Zhou et al., 2013), but all three bones are fused to each other in adults (Wang et al., 2016).

Only the left **metatarsus**, which is exposed in anterior view, is completely preserved and still in articulation with the tibia. A short metatarsal I, whose shaft is triangular and expands into the distal condyle, articulates at the distal third of metatarsal II. As in subadult specimens of *Archaeorhynchus* (Zhou et al., 2013), metatarsals II–IV are unfused to each other along their entire lengths (Figures 4E,F), while adult specimens show proximal fusion among the metatarsal bones (Wang and Zhou 2017b). Proximally, all three metatarsals end at the same level. Metatarsal II is approximately as long and as wide as metatarsal IV, as in for instance *Longicrusavis* (O'Connor et al., 2010) or *Sapeornis* (Gao et al., 2012), while metatarsal III is the longest. In most *Archaeorhynchus* specimens, metatarsal II is shorter than metatarsal IV (Zhou and Zhang, 2006; Zhou et al., 2013), while in IVPP V20312, both metatarsal bones have almost the same length (Wang et al., 2016). Although the proximal and distal ends of metatarsal III are approximately as wide as those of the other metatarsals, the midshaft is slightly pinched. While the shaft of metatarsal III is almost straight, metatarsals II and IV are slightly curved medially and laterally direction, respectively. The distal trochleae of all three elements are slightly expanded. No remains of distal tarsals or metatarsal V can be identified.

The **pedal digits** of the left foot are preserved in articulation, with the fourth digit partly covered by the third (Figure 4F). Next to the right ulna, further phalanges are preserved in partial articulation. Based on their size they do not belong to the manus, and they are identified here as pedal phalanges of the right foot. The first phalanx of left digit I is longer than the corresponding metatarsus and ungual I. The phalanges of digits II to IV are relatively robust with the proximal elements being longer than the more distal ones. The pedal unguals are short and not strongly curved, with only small flexor tubercles at their proximal ends, as is typical for ground-dwelling birds (Hedrick et al., 2019).

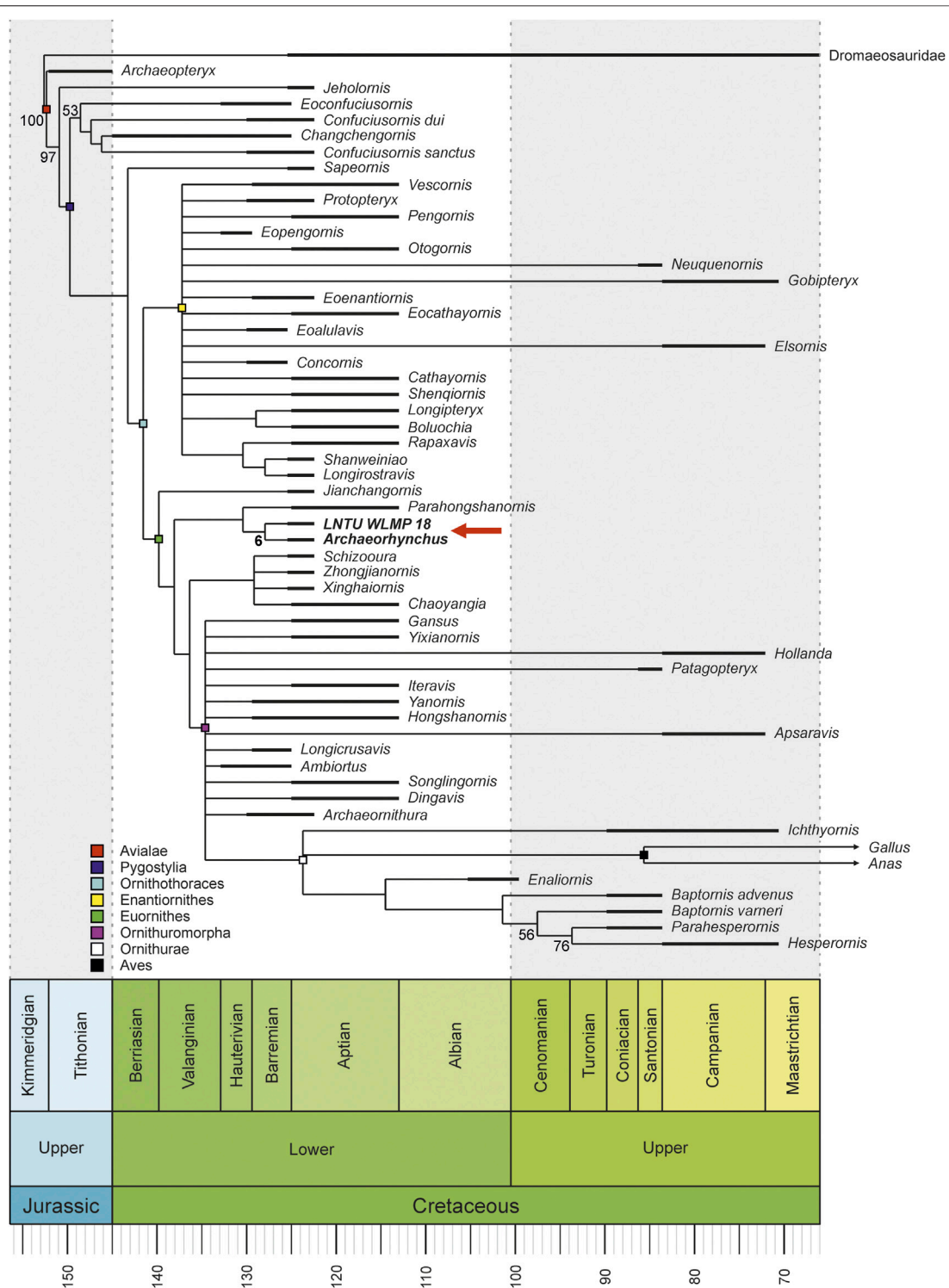


FIGURE 5 | Time-calibrated, reduced consensus tree (12,102 MPTs; length 900 steps) under equally weighted parsimony, showing the phylogenetic position of LNTU-WLMP-18 as sister taxon to *Archaeorhynchus*. Numbers at the nodes are bootstrap values for clades with more than 50% support. The support for the *Archaeorhynchus*–LNTU-WLMP-18 clade is also shown.

Feathers

The feathers are present as carbonized traces, but their preservation is rather poor (**Figure 2**). The plumage of the left

wing provides the most detail. The primaries are long, and partly covered by the skull. Outlines of single feathers can be identified, but their actual morphology cannot be described. Dark patches

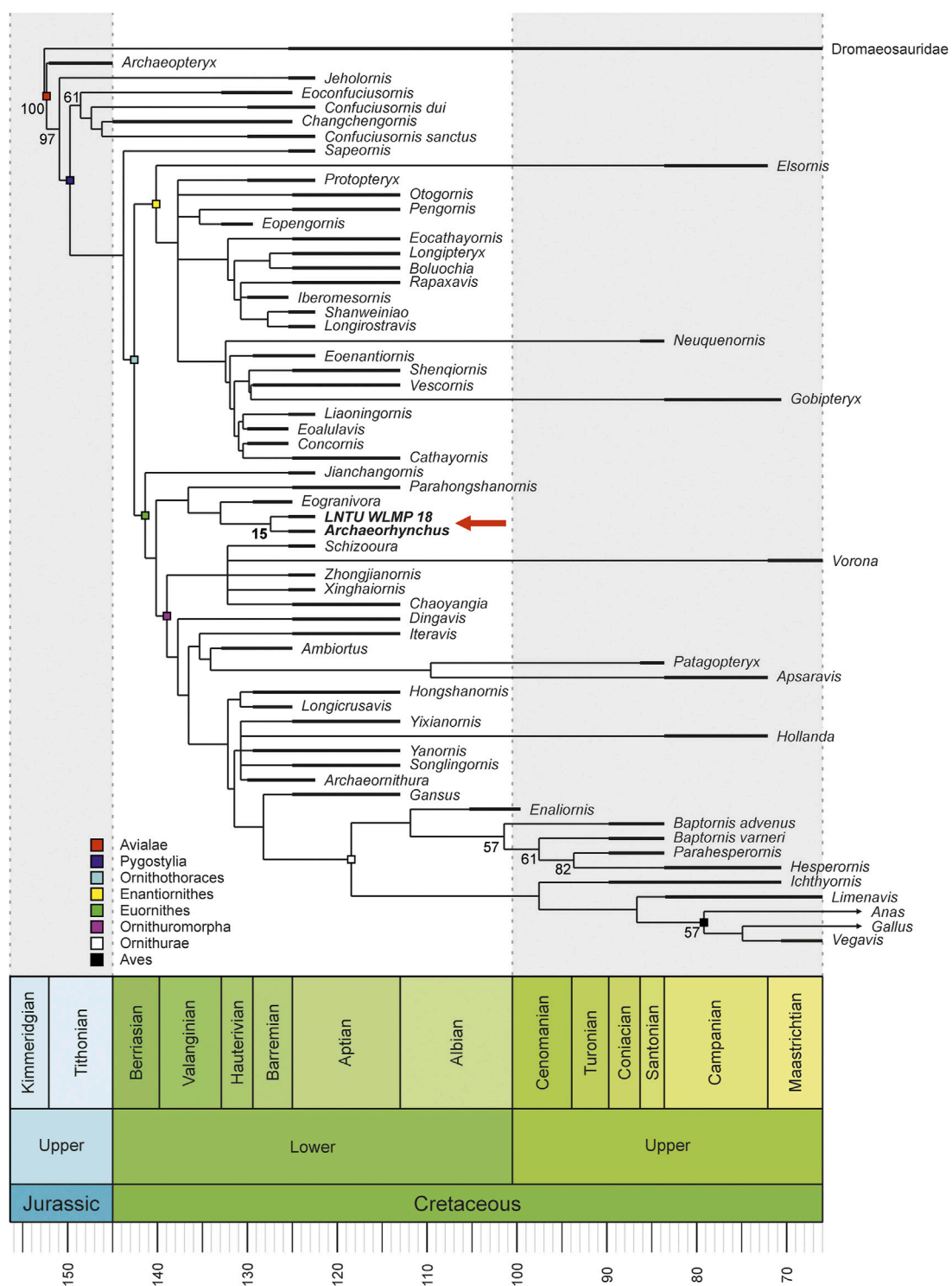


FIGURE 6 | Time-calibrated, strict consensus tree (125 MPTs; length 35.88411 steps) under implied-weighted parsimony, showing the phylogenetic position of LNTU-WLMP-18 as sister taxon to *Archaeorhynchus*. Numbers at the nodes are bootstrap values for clades with more than 50% support. The support for the *Archaeorhynchus*–LNTU-WLMP-18 clade is also shown.

situated posterior to the skull most likely represent remains of the secondaries. As preserved, they are approximately half as long as the primaries. The right wing plumage is also partly preserved. Small traces in the pelvic region may represent either body plumage or remains of the rectrices.

Intestinal Contents

A dark rope-like trace is preserved in the posterior portion of the torso, and probably represents the remains of gut contents (Figure 2). The structure is proportionally wider than intestinal tracts known from *Yanornis* (Zheng et al., 2014), but it is not possible to determine if the trace is formed by one intestinal loop or several ones that partially overlap each other. The supposed intestine contains small, round dark coaly and whitish clayey elements that measure between 1 and 2 mm in diameter (Figures 4C,D). They probably represent remains of ingested propagules of plants, e.g., round fruits, seeds, ovules, or parts thereof (see Mayr et al., 2020). In contrast to euornithine birds, including *Archaeorhynchus* (Zhou et al., 2004; Zhou and Zhang, 2006; Zhou et al., 2013; Chiappe et al., 2014; Zheng et al., 2018), no gastroliths, which could have helped processing ingested food, can be identified.

DISCUSSION

Taxonomic Identification of LNTU-WLMP-18

The phylogenetic analysis with equally weighted characters resulted in 12,102 trees with a length of 900 steps (Figure 5). Implied weighting resulted in 125 equally parsimonious trees with a length of 35,884,11 steps (Figure 6). In both analyses, LNTU-WLMP-18 was identified as a member of the Euornithes based on the presence of a procoracoid process on the coracoid (char. 89; Wang et al., 2016). Further anatomical features supporting the placement of LNTU-WLMP-18 within euornithines are the rounded deltopectoral crest (O'Connor and Zelenkov, 2013) and coplanar proximal ends of metatarsals II–IV (Wang et al., 2016), and the absence of a tubercle on the dorsal face of metatarsal II (Chiappe, 2002). Within euornithines, LNTU-WLMP-18 was found to be the sister taxon to *Archaeorhynchus*, and this pairing formed a clade with *Parahongshanornis* and *Eogranivora*. The following characters support this clade: ratio between the diameters of the radial and ulnar shaft larger than 0.70 (char. 145), ischium without a proximodorsal process (char. 191), and metatarsal II approximately equal in distal extent to metatarsal IV (char. 236). Close affiliation to *Archaeorhynchus* is supported by an expanded sternolateral corner of the coracoid (char. 95), a humerus whose proximal and distal ends are expanded and nearly in the same plane (char. 121), an alular digit that does not extend distally beyond metacarpal II (char. 168), a weakly co-ossified tibia, calcaneum, and astragalus (char. 209), and a hallucal claw that is smaller than the other pedal claws (char. 243). Nevertheless, statistical support for this phylogeny is generally low, as the

clade of LNTU-WLMP-18 and *Archaeorhynchus* is only supported by a bootstrap value of 15.

When compared with other edentulous euornithines from the Jehol Group, LNTU-WLMP-18 differs from *Eogranivora* in having a relatively short tibiotarsus compared to the femur (Zheng et al., 2018), and from *Dingavis*, *Schizoooura*, *Xinghaiornis* and *Zhongjianornis* in having a relatively short tibiotarsus and metatarsus (Zhou et al., 2012; Wang et al., 2013a; Zhou et al., 2014; O'Connor et al., 2016; see also *Archaeornithura*; Wang et al., 2015; *Parahongshanornis*; Li et al., 2011). LNTU-WLMP-18 differs from *Dingavis*, *Xinghaiornis* and *Zhongjianornis* in having a relatively short beak (Wang et al., 2013a; Zhou et al., 2014; O'Connor et al., 2016). Furthermore, LNTU-WLMP-18 is different from *Schizoooura* and *Zhongjianornis* in having a small deltopectoral crest (Zhou et al., 2012; Zhou et al., 2014). Finally, LNTU-WLMP-18 is different from *Eogranivora* (Zheng et al., 2018), *Dingavis* (O'Connor et al., 2016) and *Archaeornithura* (Wang et al., 2015) in having a short metatarsal I and pedal digit I. LNTU-WLMP-18 lacks a dorsomedially oriented bluntly triangular process on the pubis (present in *Eogranivora*, Zheng et al., 2018), and a posterior intermediate expansion on the ischium (present in *Schizoooura*, Zhou et al., 2012; *Archaeornithura*, Wang et al., 2015; and *Chaoyangia*, O'Connor and Zhou, 2013). Thus, based on the results of the phylogenetic analysis and comparisons with edentulous birds from the Jehol Group, we identify LNTU-WLMP-18 as a juvenile *Archaeorhynchus*, which would make it the ontogenetically youngest individual of this genus described so far based on its size and incompletely ossified bone surfaces (Zhou et al., 2013). Although the specimen is not sufficiently well preserved for all diagnostic characters of *Archaeorhynchus* to be evaluated (see emended diagnosis in Wang et al., 2016), the following characters support our identification: the upper and lower jaws are toothless; the dentary is spatulate; and the lateral margin of the coracoid is longer than the medial margin. The identification is further supported by similarities in manual and pelvic morphology (see above). Based on the femur length, LNTU-WLMP-18 is approximately 62.5 percent the size of the second smallest individual (IVPP V17091) and 54.5 percent the size of the largest specimen (IVPP V20312) (Table 1). Character differences with other specimens of *Archaeorhynchus* (listed below) are interpreted as ontogenetic variation and do not justify the establishment of a new taxon.

Ontogenetic Variation in *Archaeorhynchus*

Several ontogenetic studies on Mesozoic birds have been published so far, but are primarily restricted to Enantiornithes (Elzanowski, 1981; Sanz et al., 1997; Cambra-Moo et al., 2006; Chiappe et al., 2007; Kurochkin et al., 2013; Xing et al., 2017; Knoll et al., 2018; Xing et al., 2018; Kaye et al., 2019). The ontogeny of enantiornithine birds is characterized by relatively slow skeletal growth, but early onset of fledging that precedes skeletal maturation and indicates a highly precocial developmental mode (Elzanowski, 1981; Sanz et al., 1997;

Chiappe et al., 2007; Kurochkin et al., 2013; Knoll et al., 2018). However, interspecific comparison of osteogenesis in the sternum and pygostyle indicates great variation in the tempo of skeletal development, in relation to size, within Enantiornithes (Knoll et al., 2018). Knowledge of ontogenetic trends among Early Cretaceous euornithines was previously based solely on one adult and four subadult specimens of *Archaeorhynchus* (Zhou and Zhang, 2006; Zhou et al., 2013; Wang and Zhou 2017b; Wang et al., 2018). As LNTU-WLMP-18 is the first known juvenile euornithine that can be assigned to a particular genus, the specimen helps to improve our knowledge of early ontogeny not only in *Archaeorhynchus*, but among early euornithines in general.

The bone histology of *Archaeorhynchus* reveals relatively slow growth, with more than three years needed to reach skeletal maturity (Wang and Zhou, 2017b). This is different from the growth patterns found in other Early Cretaceous euornithines, like *Iteravis* (O'Connor et al., 2015) and *Yanornis* (J. Wang et al., 2019), and from the growth of extant birds (Ricklefs 1968; Scheyer et al., 2010), but similar to Enantiornithes (Chinsamy et al., 1994; O'Connor et al., 2014). Previous studies have demonstrated that *Archaeorhynchus* shows distinct morphological changes even in its late ontogeny. The sternum of adult individuals differs from that of subadults in being proportionally longer, and in having fan-shaped zyphoid processes and a proportionally more elongated xiphoid process at the posterior end (Wang and Zhou, 2017b). This indicates that the process of sternal ossification in *Archaeorhynchus* was not completed until an advanced postnatal developmental stage. *Archaeorhynchus* also shows late ontogenetic fusion of the pygostyle, the carpometacarpus, the tibiotarsus and the proximal end of the tarsometatarsus (Zhou et al., 2013; Wang and Zhou, 2017b). This differs from the situation in extant birds, in which fusion of bones happens relatively early during postnatal development (e.g., Schepelmann, 1990). This precocious fusion process is probably driven by the accelerated growth pattern of extant birds (Starck and Ricklefs, 1998a; Scheyer et al., 2010). Unfortunately, the new specimen cannot provide new information on the ossification pattern of the sternum or the pygostyle, as these elements are not preserved. As in subadult specimens of this genus, the carpometacarpus, tibiotarsus and tarsometatarsus are not yet developed due to lack of fusion (see above). Similarly, the sacral vertebrae of LNTU-WLMP-18 are still unfused with each other and the ilia. However, the first four of the seven sacra of the subadult specimen IVPP V17075 form a synsacrum (Zhou et al., 2013), while in the holotype IVPP V14287, which is only slightly bigger than IVPP V17075, all seven sacra are fused into a synsacrum (Zhou and Zhang, 2006). This indicates that the sacral region of *Archaeorhynchus* shows an earlier onset of fusion than the distal limb elements, as is also the case in Enantiornithes (Hu and O'Connor 2017).

Although the skulls of the various known specimens of *Archaeorhynchus* are incomplete or badly crushed, the premaxilla (including the nasal process) is estimated to account for a slightly smaller proportion of total skull length

in LNTU-WLMP-18 (c. 36 percent) than in IVPP V17075 (c. 42 percent). Although these measurements have to be interpreted with caution, the proportional differences, if correct, could indicate the presence of a relatively shorter beak in the younger individual, as is typical for juveniles birds in general (e.g., Sosa and Hospitaleche, 2018; Piro and Hospitaleche, 2019). Differences in limb proportions can be more reliably identified. The forelimbs of LNTU-WLMP-18 are significantly shorter relative to the hindlimbs (t -value: 90.08; p -value: < 0.0001) than in the other known individuals, which all have almost identical proportions (**Figure 7A**). Relative to humeral length, the ulna of LNTU-WLMP-18 is significantly shorter than in other individuals (t -value: 4.23; p -value: 0.024), while metacarpals I and II are significantly longer (Mc-I: t -value: -7.13 ; p -value: 0.006; Mc-II: t -value: -7.78 ; p -value: 0.004). While the length ratio between the tibia and metatarsal III is more or less similar in all *Archaeorhynchus* individuals (t -value: 2.64; p -value: 0.077), the femur of LNTU-WLMP-18 is unusually long in comparison to the tibia (t -value: 16.26; p -value: < 0.001) and metatarsal III (t -value: 4.64; p -value: 0.019). These results indicate 1) that the forelimbs of *Archaeorhynchus* increased in length during ontogeny, and b) that proportions within the forelimb change more during ontogeny than proportions within the hindlimb (**Table 2**). This is similar to the situation in *Archaeopteryx* (Wellnhofer, 1974), but different to that in the enantiornithine hatchlings of *Gobipipus* and *Gobipteryx*, in which the forelimbs are already longer than the hindlimbs (Elzanowski, 1981; Kurochkin et al., 2013). However, in other Enantiornithes the ratios are more similar to LNTU-WLMP-18 (Chiappe et al., 2007). As in early juvenile Enantiornithes, LNTU-WLMP-18 possesses straight scapulae and femora (Elzanowski, 1981; Chiappe et al., 2007; Kurochkin et al., 2013), while in subadult and adult individuals of *Archaeorhynchus* these elements are curved (Zhou and Zhang, 2006; Zhou et al., 2013; Wang et al., 2016).

The rib morphology of LNTU-WLMP-18 indicates that uncinat processes also developed later in ontogeny. These processes are present in the holotype of *Archaeorhynchus* (Zhou and Zhang, 2006), but are described as being absent in subadult individuals (Zhou et al., 2013). However, Zhou et al. (2013) mention the presence of short and robust gastralia in IVPP V17075 and IVPP V14287. In both specimens, these bones are associated with the thoracic ribs, and in IVPP V17075, the elements of the left side are even aligned with each other in an anteroposteriorly directed pattern. Therefore, we speculate that these short, robust elements are in fact uncinat processes, indicating the presence of these structures in subadult individuals of this genus. Furthermore, the morphology of the humerus reveals that the deltopectoral crest was weakly developed in early juveniles, but grew more prominent during ontogeny. Finally, LNTU-WLMP-18 differs from other *Archaeorhynchus* specimens in having a ventral embayment between the ischial peduncle and the proximal end of the pubic shaft, which resembles the obturator notch in non-pygostylian theropods (Rauhut, 2003). In (sub)adult individuals the plate-like ischial peduncle is continuous with the proximal end of the pubic shaft (Zhou et al., 2013). Due to the preservation, we cannot fully rule out the possibility that this fossa results from breakage. If this

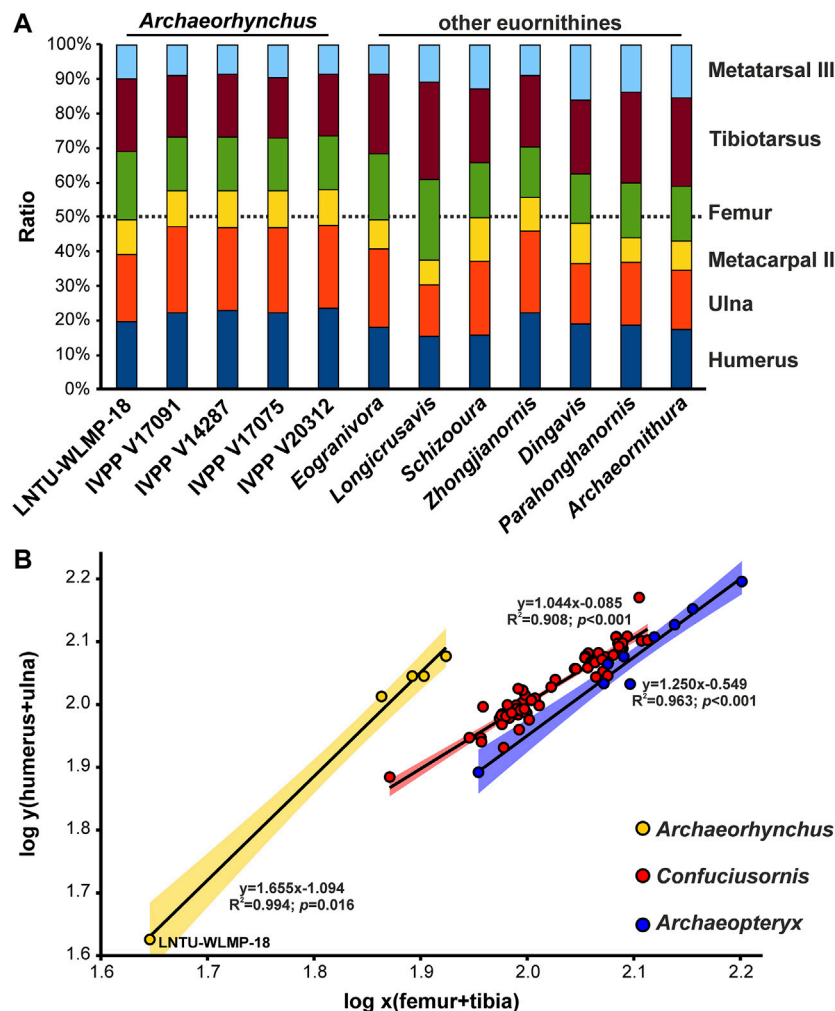


FIGURE 7 | Limb proportions of Early Cretaceous Euornithines. **(A)** Histogram comparing the limb proportions of LNTU-WLMP-18 with those of different *Archaeorhynchus* specimens and other euornithine species. **(B)** Ordinary linear regression between log-transformed forelimb and hindlimb element lengths comparing *Archaeorhynchus* (including LNTU-WLMP-18), *Confuciusornis* (see Chiappe et al., 2008) and *Archaeopteryx* (see Rauhut et al., 2018).

structure is genuine, this would be an ontogenetic character change that recapitulated a corresponding character change during evolution. However, further early juvenile ornithothoracine bird specimens from the Early Cretaceous will be needed to evaluate this hypothesis.

Examining the ontogenetic trajectory of ratio between forelimb and hindlimb length, the slope for *Archaeorhynchus* is significantly different from that for *Archaeopteryx* (F -value: 7.315; p -value: 0.022) or *Confuciusornis* (F -value: 25.970; p -value: <0.001), showing strong positive ontogenetic allometry (slope: 1.655; R^2 : 0.994; p -value: 0.016) of the forelimb relative to the hindlimb. *Archaeopteryx* shows also positive allometry (slope: 1.250; R^2 : 0.963; p -value: <0.001), while in *Confuciusornis* the forelimb is almost isometric to the hindlimb (slope: 1.044; R^2 : 0.908; p -value: <0.001). Nevertheless, the trajectory slopes of *Archaeopteryx* and *Confuciusornis* are statistically indistinguishable (F -value: 1.950; p -value: 0.167) (Figure 7B).

Despite the small body size and weak degree of bone fusion, the extensive wing plumage of LNTU-WLMP-18 indicates that the specimen was already fledged, implying an early onset of flight ability in the ontogeny of basal euornithines, as in Enantiornithes and extant birds (Carrier and Auriemma, 1992). In contrast to extant birds, fledging and skeletal maturity were not ontogenetically synchronized in basal Euornithes and Enantiornithes. In fact, based on femoral length, LNTU-WLMP-18 had no more than 22% of the body mass of IVPP V14287 (see Field et al., 2013 for body mass estimation) (Figure 8). Thus, the early onset of fledging in early Ornithothoraces did not interfere with their ancestral growth pattern. Whether *Archaeorhynchus* was also precocial cannot be answered with absolute certainty, as this requires the discovery of earlier ontogenetic stages close to hatching. However, the relatively long hindlimbs, the short first pedal phalanx and the generally slight curvature of the pedal claws indicate that LNTU-



FIGURE 8 | Reconstruction of *Archaeorhynchus* growth stages, with the new juvenile LNTU-WLMP-18 on the left. Note the nearly adult-like proportions of the wing bones and primary feathers, even though the trunk is only about half as long as in an adult. Subadult stage in the center reconstructed from IVPP V14287, 17,075, 17,091, and STM7-11 (Zhou and Zhang, 2006; Zhou et al., 2013; Wang et al., 2018b; respectively), with still unfused metacarpals. Adult stage on the right reflecting IVPP V20312 (Wang et al., 2016), with plumage inferred from subadults. Scale bar in cm.

WLMP-18 was ground-dwelling rather than arboreal. A similar mode of life is also suggested for (sub-)adult individuals of *Archaeorhynchus* (Zhou and Zhang, 2006; Zhou et al., 2013; Wang et al., 2016) and other Early Cretaceous ornithuromorph euornithines (Zhou and Zhang, 2005; Bell and Chiappe, 2011; Wang et al., 2016). Together with relatively early onset of fledging, a precocial ontogeny is more likely than an altricial one (Starck and Ricklefs, 1998b). Finally, the fossilized intestinal remains indicate that early juveniles of *Archaeorhynchus* fed on plant propagules, most likely seeds or seed-containing fruits (Mayr et al., 2020). Studies on modern seed-eating birds indicate that individuals at different ontogenetic stages may prefer seeds of differing sizes (Kear, 1962; Newton, 1967; Díaz, 1996). The fact that LNTU-WLMP-18 lacks gastroliths, in contrast to larger specimens of *Archaeorhynchus* (Zhou and Zhang, 2006; Zhou et al., 2013; Wang et al., 2016), might indicate a dietary shift through ontogeny. Being seed-eating and ground-dwelling, *Archaeorhynchus* differs in its ecological adaptations from most Enantiornithes, but filled an ecological niche that may have allowed basal crown birds to survive the K-Pg mass extinction (Field et al., 2018).

REFERENCES

Baumel, J. J., and Witmer, L. M. (1993). "Osteologia," in *Handbook of avian anatomy*. Editors J. J. Baumel, A. S. King, J. E. Breazile, H. E. Evans, and

DATA AVAILABILITY STATEMENT

The original contributions presented in the study are included in the article/**Supplementary Material**, further inquiries can be directed to the corresponding author.

ETHICS STATEMENT

Ethical review and approval was not required for the animal study because the specimen studied is a fossil of an animal that died 125 Myrs ago.

AUTHOR CONTRIBUTIONS

FC, WS, SF, LY, and YR designed the project. FC, WS, SF, LY and YR performed the research. FC, WS, and SF wrote the manuscript. All authors contributed to the article and approved the submitted version.

FUNDING

This research was supported by the Swiss National Science Foundation (PZ00P2_174040 to CF), the German Science Foundation (FO 1005/2-1 to CF) and the Liaoning Technical University of Fuxin.

ACKNOWLEDGMENTS

Michael Völker and Raimund Albersdörfer (both Dinosaur Museum Altmühltal, Denkendorf, Germany) are thanked for sponsoring the research trip (to FS). We are furthermore grateful to Liang Bing and Han Jun for hosting us at the Liaoning Technical University (Fuxin, China). We further thank Sebastian Apesteguia and Jingmai O'Connor for their critical reviews and Walter Joyce and Corwin Sullivan for proofreading. Finally, we thank the editors Jingmai O'Connor, Corwin Sullivan and Daniel Field for the invitation to contribute to the article collection "Early Avian Evolution" in *Frontiers in Earth Science*.

SUPPLEMENTARY MATERIAL

The Supplementary Material for this article can be found online at: <https://www.frontiersin.org/articles/10.3389/feart.2021.604520/full#supplementary-material>.

J. C. Vanden Berge (Cambridge, MA: Nuttall Ornithological Club), 45–132.

Bell, A., and Chiappe, L. M. (2011). Statistical approach for inferring ecology of Mesozoic birds. *J. Syst. Palaeontology* 9, 119–133. doi:10.1080/14772019.2010.525536

- Benson, R. B. J., Campione, N. E., Carrano, M. T., Mannion, P. D., Sullivan, C., Upchurch, P., et al. (2014). Rates of dinosaur body mass evolution indicate 170 million years of sustained ecological innovation on the avian stem lineage. *Plos Biol.* 12, e1001853. doi:10.1371/journal.pbio.1001853
- Benton, M. J., Zhou, Z., Orr, P. J., Zhang, F., and Kearns, S. L. (2008). The remarkable fossils from the Early Cretaceous Jehol Biota of China and how they have changed our knowledge of Mesozoic life. *Proc. Geol. Assoc.* 119, 209–228. doi:10.1111/j.1525-142x.2011.00478.x
- Bever, G. S., Gauthier, J. A., and Wagner, G. P. (2011). Finding the frame shift: digit loss, developmental variability, and the origin of the avian hand. *Evol. Dev.* 13, 269–279. doi:10.1111/j.1525-142x.2011.00478.x
- Bhullar, B.-A. S., Marugán-Lobón, J., Racimo, F., Bever, G. S., Rowe, T. B., Norell, M. A., et al. (2012). Birds have paedomorphic dinosaur skulls. *Nature* 487, 223–226. doi:10.1038/nature11146
- Brown, R. H. J. (1963). The flight of birds. *Biol. Rev.* 38, 460–489. doi:10.1111/j.1469-185x.1963.tb00790.x
- Burke, A. C., and Feduccia, A. (1997). Developmental patterns and the identification of homologies in the avian hand. *Science* 278, 666–668. doi:10.1126/science.278.5338.666
- Cambrá-Moo, O., Chamero, B., Marugán-Lobón, J., Delclós, X., Poyato-Ariza, F. J., and Buscalioni, A. D. (2006). Estimating the ontogenetic status of an enantiornithine bird from the lower barremian of el montsec, central pyrenees, Spain. *Estud. Geológicas* 62, 241–248. doi:10.3989/egool.0662123
- Cao, H., and He, W. (2019). Correlation of carbon isotope stratigraphy and paleoenvironmental conditions in the Cretaceous Jehol Group, northeastern China. *Int. Geology. Rev.* 62, 113–128. doi:10.1080/00206814.2019.1681303
- Carrier, D. R., and Auriemma, J. (1992). A developmental constraint on the fledging time of birds. *Biol. J. Linn. Soc.* 47, 61–77. doi:10.1111/j.1095-8312.1992.tb00656.x
- Chiappe, L. M. (2002). “Basal bird phylogeny: problems and solutions,” in *Mesozoic birds: above the heads of dinosaurs*. Editors L. M. Chiappe and L. M. Witmer (Berkeley, CA: University of California Press), 448–472.
- Chiappe, L. M., Di, L., Serrano, F. J., Yuguang, Z., and Meng, Q. (2020). Anatomy and flight performance of the early enantiornithine bird *Proteropteryx fengningensis*: information from new specimens of the early cretaceous huajiyang formation of China. *Anat. Rec.* 303, 716–731. doi:10.1002/ar.24322
- Chiappe, L. M., and Göhlich, U. B. (2010). Anatomy of *Juravenator starki* (theropoda: Coelurosauria) from the late jurassic of Germany. *N. Jb. Geol. Paläont. Abh.* 258, 257–296. doi:10.1127/0077-7749/2010/0125
- Chiappe, L. M., Ji, S., Ji, Q., and Norell, M. A. (1999). Anatomy and systematics of the Confuciusornithidae (theropoda: aves) from the late mesozoic of northeastern China. *Bull. Am. Mus. Nat. Hist.* 242, 1–89.
- Chiappe, L. M., Marugán-Lobón, J., Ji, S. a., and Zhou, Z. (2008). Life history of a basal bird: morphometrics of the Early Cretaceous *Confuciusornis*. *Biol. Lett.* 4, 719–723. doi:10.1098/rsbl.2008.0409
- Chiappe, L. M., and Meng, Q. (2016). *Birds of stone*. Baltimore, MD: Johns Hopkins University Press.
- Chiappe, L. M., Shu'an, J., and Qiang, J. (2007). Juvenile birds from the Early Cretaceous of China: implications for enantiornithine ontogeny. *Am. Mus. Novitates* 3594, 1–49. doi:10.1206/0003-0082(2007)3594[1jbftec]2.0.co;2
- Chiappe, L. M., Zhao, B., O'Connor, J. K., Chunling, G., Wang, X., Habib, M., et al. (2014). A new specimen of the Early Cretaceous bird *Hongshanornis longicresta*: insights into the aerodynamics and diet of a basal ornithuromorph. *PeerJ* 2, e234. doi:10.7717/peerj.234
- Chinsamy, A., Chiappe, L. M., and Dodson, P. (1994). Growth rings in Mesozoic birds. *Nature* 368, 196–197. doi:10.1038/368196a0
- Clarke, J. A., Zhou, Z., and Zhang, F. (2006). Insight into the evolution of avian flight from a new clade of Early Cretaceous ornithurines from China and the morphology of *Yixianornis grabaui*. *J. Anat.* 208, 287–308. doi:10.1111/j.1469-7580.2006.00534.x
- Dal Sasso, C., and Maganuco, S. (2011). *Scipionyx samniticus* (theropoda: compsognathidae) from the lower cretaceous of Italy. Osteology, ontogenetic assessment, phylogeny, soft tissue anatomy, taphonomy and paleobiology. *Hist. Biol.* 37, 1–281.
- Díaz, M. (1996). Food choice by seed-eating birds in relation to seed chemistry. *Comp. Biochem. Physiol. A: Physiol.* 113, 239–246. doi:10.1016/0300-9629(95)02093-4
- Elzanowski, A. (1981). Embryonic bird skeletons from the late cretaceous of Mongolia. *Palaeontol. Pol.* 42, 147–179.
- Feduccia, A., Lingham-Soliar, T., and Hinchliffe, J. R. (2005). Do feathered dinosaurs exist? Testing the hypothesis on neontological and paleontological evidence. *J. Morphol.* 266, 125–166. doi:10.1002/jmor.10382
- Field, D. J., Bercovici, A., Berv, J. S., Dunn, R., Fastovsky, D. E., Lyson, T. R., et al. (2018). Early evolution of modern birds structured by global forest collapse at the End-Cretaceous mass extinction. *Curr. Biol.* 28, P1825–P1831. doi:10.1016/j.cub.2018.04.062
- Field, D. J., Lynner, C., Brown, C., and Darroch, S. A. F. (2013). Skeletal correlates for body mass estimation in modern and fossil flying birds. *PLoS One* 8, e82000. doi:10.1371/journal.pone.0082000
- Forster, C. A., O'Connor, P. M., Chiappe, L. M., and Turner, A. H. (2020). The osteology of the Late Cretaceous paravian *Rahonavis ostromi* from Madagascar. *Palaeontol. Electron.* 23, 147–176. doi:10.26879/793
- Foth, C., Haug, C., Haug, J. T., Tischlinger, H., and Rahuhut, O. W. M. (2020). “Two of a feather: a comparison of the preserved integument in the juvenile theropod dinosaurs *Sciuromimus* and *Juravenator* from the Kimmeridgian Torleite Formation of southern Germany,” in *The evolution of feathers*. Editors C. Foth and O. W. M. Rahuhut (Basingstoke, United Kingdom: Springer Nature), 79–101.
- Foth, C., Hedrick, B. P., and Ezcurra, M. D. (2016). Cranial ontogenetic variation in early saurischians and the role of heterochrony in the diversification of predatory dinosaurs. *PeerJ* 4, e1589. doi:10.7717/peerj.1589
- Foth, C., Tischlinger, H., and Rahuhut, O. W. M. (2014). New specimen of *Archaeopteryx* provides insights into the evolution of pennaceous feathers. *Nature* 511, 79–82. doi:10.1038/nature13467
- Gao, C., Chiappe, L. M., Zhang, F., Pomeroy, D. L., Shen, C., Chinsamy, A., et al. (2012). A subadult specimen of the Early Cretaceous bird *Sapeornis chaoyangensis* and a taxonomic reassessment of sapeornithids. *J. Vertebr. Paleontol.* 32, 1103–1112. doi:10.1080/02724634.2012.693865
- Goloboff, P. A., and Catalano, S. A. (2016). TNT version 1.5, including a full implementation of phylogenetic morphometrics. *Cladistics* 32, 221–238. doi:10.1111/cla.12160
- Goloboff, P. A., Farris, J. S., and Nixon, K. C. (2008). TNT, a free program for phylogenetic analysis. *Cladistics* 24, 774–786. doi:10.1111/j.1096-0031.2008.00217.x
- Goloboff, P. A., Torres, A., and Arias, J. S. (2018). Weighted parsimony outperforms other methods of phylogenetic inference under models appropriate for morphology. *Cladistics* 34, 407–437. doi:10.1111/cla.12205
- Guinard, G. (2015). *Limusaurus inextricabilis* (Theropoda: ceratosauria) gives a hand to evolutionary teratology: a complementary view on avian manual digits identities. *Zool. J. Linn. Soc.* 176, 674–685. doi:10.1111/zoj.12329
- Hammer, O., and Harper, D. A. T. (2006). *Paleontological data analysis*. Malden, MA: Blackwell Publishing.
- Hammer, O., Harper, D. A. T., and Ryan, P. D. (2001). PAST: paleontological statistics software package for education and data analysis. *Palaeontol. Electron.* 4, 9.
- Haug, J. T., and Haug, C. (2011). Fossilien unter langwelligem Licht: grün-Orange-Fluoreszenz an makroskopischen Objekten. *Archaeopteryx* 29, 20–23.
- Haug, J. T., Haug, C., Kutschera, V., Mayer, G., Maas, A., Liebau, S., et al. (2011). Autofluorescence imaging, an excellent tool for comparative morphology. *J. Microsc.* 244, 259–272. doi:10.1111/j.1365-2818.2011.03534.x
- Hedrick, B. P., Cordero, S. A., Zanno, L. E., Noto, C., and Dodson, P. (2019). Quantifying shape and ecology in avian pedal claws: the relationship between the bony core and keratinous sheath. *Ecol. Evol.* 9, 11545–11556. doi:10.1002/ece3.5507
- Herzog, K. (1968). *Anatomie und Flugbiologie der Vögel*. Jena, Germany: Gustav Fischer Verlag.
- Hinchliffe, J. R., and Hecht, M. K. (1984). Homology of the bird wing skeleton. *Evol. Biol.* 18, 21–39. doi:10.1007/978-1-4615-6977-0_2
- Hone, D. W. E., Farke, A. A., and Wedel, M. J. (2016). Ontogeny and the fossil record: what, if anything, is an adult dinosaur? *Biol. Lett.* 12, 20150947. doi:10.1098/rsbl.2015.0947
- Hu, D., Liu, Y., Li, J., Xu, X., and Hou, L. (2015). *Yuanjiaawaornis viriosus*, gen. et sp. nov., a large enantiornithine bird from the Lower Cretaceous of western Liaoning, China. *Cretaceous Res.* 55, 210–219. doi:10.1016/j.cretres.2015.02.013

- Hu, H., and O'Connor, J. K. (2017). First species of Enantiornithes from Sihedang elucidates skeletal development in Early Cretaceous enantiornithines. *J. Syst. Palaeontology* 15, 909–926. doi:10.1080/14772019.2016.1246111
- Kaye, T. G., Pittman, M., Marugán-Lobón, J., Martín-Abad, H., Sanz, J. L., and Buscalioni, A. D. (2019). Fully fledged enantiornithine hatchling revealed by Laser-Stimulated Fluorescence supports precocial nesting behavior. *Sci. Rep.* 9, 5006. doi:10.1038/s41598-019-41423-7
- Kear, J. (1962). Food selection in finches with special reference to the interspecific differences. *J. Zool.* 138, 163–204. doi:10.1111/j.1469-7998.1962.tb05694.x
- Knoll, F., Chiappe, L. M., Sanchez, S., Garwood, R. J., Edwards, N. P., Wogelius, R. A., et al. (2018). A diminutive perinate European Enantiornithes reveals an asynchronous ossification pattern in early birds. *Nat. Commun.* 9, 937. doi:10.1038/s41467-018-03295-9
- Kurochkin, E. N., Chatterjee, S., and Mikhailov, K. E. (2013). An embryonic enantiornithine bird and associated eggs from the Cretaceous of Mongolia. *Paleontol. J.* 47, 1252–1269. doi:10.1134/s0013030113110087
- Li, L., Jin, W., Xi, Z., and Shilin, H. (2012). A new enantiornithine bird from the lower cretaceous Jiufotang Formation in jinzhou area, western liaoning province, China. *Acta Geol. Sin.* 86, 1039–1044. doi:10.1111/j.1755-6724.2012.00729.x
- Li, L., Wang, J., and Hou, S. (2011). A new ornithurine bird (hongshanornithidae) from the jiufotang formation of chaoyang, liaoning, China. *Vertebr. Palasiat.* 49, 195–200.
- Liu, Y.-Q., Kuang, H.-W., Jiang, X.-J., Peng, N., Xu, H., and Sun, H.-Y. (2012). Timing of the earliest known feathered dinosaurs and transitional pterosaurs older than the Jehol Biota. *Palaeogeogr. Palaeoclimatol. Palaeoecol.* 323–325, 1–12. doi:10.1016/j.palaeo.2012.01.017
- Mayr, G. (2017). *Avian evolution*. Chichester, United Kingdom: John Wiley.
- Mayr, G., Kaye, T. G., Pittman, M., Saitta, E. T., and Pott, C. (2020). Reanalysis of putative ovarian follicles suggests that Early Cretaceous birds were feeding not breeding. *Sci. Rep.* 10, 19035. doi:10.1038/s41598-020-76078-2
- Newton, I. (1967). The adaptive radiation and feeding ecology of some British finches. *Ibis* 109, 33–96. doi:10.1111/j.1474-919X.1967.tb00005.x
- Norell, M. A., and Makovicky, P. J. (1999). Important features of the dromaeosaurid skeleton II: information from newly collected specimens of *Velociraptor mongoliensis*. *Am. Mus. Novit.* 3282, 1–45.
- O'Connor, J. K. (2020). The plumage of basal birds. *The evolution of feathers* Editors C. Foth and O. W. M. Rauhut (Cham. Springer Nature), 147–172.
- O'Connor, J. K., and Chiappe, L. M. (2011). A revision of enantiornithine (Aves: Ornithothoraces) skull morphology. *J. Syst. Palaeontol.* 9, 135–157. doi:10.1080/14772019.2010.526639
- O'Connor, J. K., Chiappe, L. M., Gao, C., and Zhao, B. (2011). Anatomy of the early cretaceous enantiornithine bird *Rapaxavis pani*. *Acta Palaeontol. Pol.* 56, 463–475. doi:10.4202/app.2010.0047
- O'Connor, J. K., Gao, K., and Chiappe, L. M. (2010). A new ornithuromorph (Aves: Ornithothoraces) bird from the Jehol Group indicative of higher-level diversity. *J. Vertebr. Paleontol.* 30, 311–321. doi:10.1080/02724631003617498
- O'Connor, J. K., Wang, M., and Hu, H. (2016). A new ornithuromorph (Aves) with an elongate rostrum from the Jehol Biota, and the early evolution of rostralization in birds. *J. Syst. Palaeontol.* 14, 939–948. doi:10.1080/14772019.2015.1129518
- O'Connor, J. K., Wang, M., Zheng, X., Wang, X., and Zhou, Z. (2014). The histology of two female Early Cretaceous birds. *Vertebr. Palasiat.* 52, 112–128.
- O'Connor, J. K., Wang, M., Zhou, S., and Zhou, Z. (2015). Osteohistology of the lower cretaceous yixian formation ornithuromorph (aves) *Iteravis huchzermeyeri*. *Palaeontol. Electron.* 18, 1–11. doi:10.26879/520
- O'Connor, J. K., and Zelenkov, N. V. (2013). The phylogenetic position of *Ambiortus*: comparison with other Mesozoic birds from Asia. *Paleontol. J.* 47, 1270–1281. doi:10.1134/S0013030113110063
- O'Connor, J. K., and Zhou, Z. (2013). A redescription of *Chaoyangia beishanensis* (Aves) and a comprehensive phylogeny of Mesozoic birds. *J. Syst. Palaeontol.* 11, 889–906. doi:10.1080/14772019.2012.690455
- Piro, A., and Acosta Hospitaleche, C. (2019). Skull morphology and ontogenetic variation of the southern giant petrel *Macronectes giganteus* (aves: procellariiformes). *Polar Biol.* 42, 27–45. doi:10.1007/s00300-018-2397-z
- Plateau, O., and Foth, C. (2020). Birds have peramorphic skulls, too: anatomical network analyses reveal oppositional heterochronies in avian skull evolution. *Commun. Biol.* 3, 195. doi:10.1038/s42003-020-0914-4
- Rauhut, O. W. M., Foth, C., Tischlinger, H., and Norell, M. A. (2012). Exceptionally preserved juvenile megalosauroid theropod dinosaur with filamentous integument from the Late Jurassic of Germany. *Proc. Natl. Acad. Sci.* 109, 11746–11751. doi:10.1073/pnas.1203238109
- Rauhut, O. W. M., Foth, C., and Tischlinger, H. (2018). The oldest *Archaeopteryx* (theropoda: avialae): a new specimen from the kimmeridgian/tithonian boundary of schamhaupten, bavaria. *PeerJ* 6, e4191. doi:10.7717/peerj.4191
- Rauhut, O. W. M. (2003). The interrelationships and evolution of basal theropod dinosaurs. *Spec. Pap. Palaeontol.* 69, 1–213.
- Ricklefs, R. E. (1968). Patterns of growth in birds. *Ibis* 110, 419–451. doi:10.1111/j.1474-919X.1968.tb00058.x
- Sanz, J. L., Chamero, B., Chiappe, L. M., Marugán-Lobón, J., O'Connor, J. K., Ortega, F., et al. (2016). “Aves,” in *Las hoyas. A cretaceous wetland*. Editors F. J. Poyato-Ariza and A. D. Buscalioni (Munich, Germany: Verlag Dr. Friedrich Pfeil), 183–189.
- Sanz, J. L., Chiappe, L. M., Pérez-Moreno, B. P., Moratalla, J. J., Hernández-Carrasquilla, F., Buscalioni, A. D., et al. (1997). A nestling bird from the Lower Cretaceous of Spain: implications for avian skull and neck evolution. *Science* 276, 1543–1546. doi:10.1126/science.276.5318.1543
- Sanz, J. L., Pérez-Moreno, B. P., Chiappe, L. M., and Buscalioni, A. D. (2002). “The birds from the lower cretaceous of las hoyas (province of cuenca, Spain),” in *In mesozoic birds: Above the Heads of dinosaurs*. Editors L. M. Chiappe and L. M. Witmer (Berkeley, CA: University of California Press), 209–267.
- Schepelmann, K. (1990). Erythropoietic bone marrow in the pigeon: development of its distribution and volume during growth and pneumatization of bones. *J. Morphol.* 203, 21–34. doi:10.1002/jmor.1052030104
- Scheyer, T. M., Klein, N., and Sander, P. M. (2010). Developmental palaeontology of Reptilia as revealed by histological studies. *Semin. Cel Developmental Biol.* 21, 462–470. doi:10.1016/j.semcdb.2009.11.005
- Sereno, P. C., Rao, C., and Li, J. (2002). “*Sinornis santensis* (aves: Enantiornithes) from the early cretaceous of northeastern China,” in *Mesozoic birds: Above the heads of Dinosaurs*. Editors L. M. Chiappe and L. M. Witmer (Berkeley, CA: University of California Press), 184–208.
- Sosa, M. A., and Acosta Hospitaleche, C. (2018). Ontogenetic variations of the head of *Aptenodytes forsteri* (Aves, Sphenisciformes): muscular and skull morphology. *Polar Biol.* 41, 225–235. doi:10.1007/s00300-017-2183-3
- Starck, J. M., and Ricklefs, R. E. (1998a). *Avian growth and development*. New York, NY: Oxford University Press.
- Starck, J. M., and Ricklefs, R. E. (1998b). “Patterns of development: the altricial-precocial spectrum,” in *Avian growth and development. Evolution in the altricial precocial spectrum*. Editors J. M. Starck and R. E. Ricklefs (New York, NY: Oxford University Press), 3–30.
- Tamura, K., Nomura, N., Seki, R., Yonei-Tamura, S., and Yokoyama, H. (2011). Embryological evidence identifies wing digits in birds as digits 1, 2, and 3. *Science* 331, 753–757. doi:10.1126/science.1198229
- Tumarkin-Deratzian, A. R., Vann, D. R., and Dodson, P. (2006). Bone surface texture as an ontogenetic indicator in long bones of the Canada goose *Branta canadensis* (Anseriformes: anatidae). *Zool. J. Linn. Soc.* 148, 133–168. doi:10.1111/j.1096-3642.2006.00232.x
- Vargas, A. O., and Fallon, J. F. (2005). Birds have dinosaur wings: the molecular evidence. *J. Exp. Zool.* 304B, 86–90. doi:10.1002/jez.b.21023
- Wagner, G. P., and Gauthier, J. A. (1999). 1,2,3 = 2,3,4: a solution to the problem of the homology of the digits in the avian hand. *Proc. Natl. Acad. Sci.* 96, 5111–5116. doi:10.1073/pnas.96.9.5111
- Wang, J., Hao, X., Kundrát, M., Liu, Z., Uesugi, K., Jurašková, Z., et al. (2019b). Bone tissue histology of the Early Cretaceous bird *Yanornis*: evidence for a diphyletic origin of modern avian growth strategies within Ornithuromorpha. *Hist. Biol.* 32, 1422. doi:10.1080/08912963.2019.1593405
- Wang, M., Li, Z., and Zhou, Z. (2017b). Insight into the growth pattern and bone fusion of basal birds from an Early Cretaceous enantiornithine bird. *Proc. Natl. Acad. Sci. U.S.A.* 114, 11470–11475. doi:10.1073/pnas.1707237114
- Wang, M., O'Connor, J. K., and Zhou, Z. (2019a). A taxonomical revision of the confuciusornithiformes (aves: Pygostylia). *Vertebr. Palasiat.* 57, 1–37. doi:10.19615/j.cnki.1000-3118.180530

- Wang, M., Stidham, T. A., and Zhou, Z. (2018a). A new clade of basal Early Cretaceous pygostylian birds and developmental plasticity of the avian shoulder girdle. *Proc. Natl. Acad. Sci. USA* 115, 10708–10713. doi:10.1073/pnas.1812176115
- Wang, M., Zheng, X., O'Connor, J. K., Lloyd, G. T., Wang, X., Wang, Y., et al. (2015). The oldest record of Ornithuromorpha from the early cretaceous of China. *Nat. Commun.* 6, 6987. doi:10.1038/ncomms7987
- Wang, M., and Zhou, Z. (2017c). A morphological study of the first known piscivorous enantiornithine bird from the Early Cretaceous of China. *J. Vertebr. Paleontol.* 37, e1278702. doi:10.1080/02724634.2017.1278702
- Wang, M., and Zhou, Z. (2017b). A new adult specimen of the basalmost ornithuromorph bird *Archaeorhynchus spathula* (Aves: ornithuromorpha) and its implications for early avian ontogeny. *J. Syst. Palaeontology* 15, 1–18. doi:10.1080/14772019.2015.1136968
- Wang, M., and Zhou, Z. (2017a). “The evolution of birds with implications from new fossil evidences,” in *The biology of the avian respiratory system*. Editor J. N. Maina (Basingstoke, United Kingdom: Springer Nature), 1–26.
- Wang, M., and Zhou, Z. (2017b). A new basal ornithuromorph bird (Aves: Ornithothoraces) from the Early Cretaceous of China with implication for morphology of early Ornithuromorpha. *Zool. J. Linn. Soc.* 176, 207–223. doi:10.1111/zooj.12302
- Wang, X., Chiappe, L. M., Teng, F., and Ji, Q. (2013a). *Xinghaiornis lini* (Aves: Ornithothoraces) from the early cretaceous of liaoning: an example of the evolutionary mosaic in early birds. *Acta Geol. Sin.* 87, 686–689. doi:10.1111/1755-6724.12080
- Wang, X., Ji, Q., Teng, F., and Jin, K. (2013b). A new species of *Yanornis* (aves: ornithurae) from the lower cretaceous strata of yixian, liaoning province. *Geol. Bull. China* 32, 601–606.
- Wang, X., O'Connor, J. K., Zhao, B., Chiappe, L. M., Gao, C., and Cheng, X. (2010). New species of Enantiornithes (aves: Ornithothoraces) from the qiaotou formation in northern Hebei, China. *Acta Geol. Sin.* 84, 247–256. doi:10.1111/j.1755-6724.2010.00156.x
- Wang, X., O'Connor, J. K., Maina, J. N., Pan, Y., Wang, M., Wang, Y., et al. (2018). Archaeorhynchus preserving significant soft tissue including probable fossilized lungs. *Proc. Natl. Acad. Sci. USA* 115, 11555–11560. doi:10.1073/pnas.1805803115
- Wang, Y., Hu, H., O'Connor, J. K., Wang, M., Xu, X., Zhou, Z., et al. (2017). A previously undescribed specimen reveals new information on the dentition of *Sapeornis chaoyangensis*. *Cretaceous Res.* 74, 1–10. doi:10.1016/j.cretres.2016.12.012
- Wellnhofer, P. (2009). *Archaeopteryx: the icon of evolution*. München, Germany: Verlag Dr. Friedrich Pfeil.
- Wellnhofer, P. (1974). Das fünfte skelettexemplar von *Archaeopteryx*. *Palaeontogr. Abt. A* 147, 169–216.
- Wilson, J. A. (2006). Anatomical nomenclature of fossil vertebrates: standardized terms or “lingua franca”? *J. Vertebr. Paleontol.* 26, 511–518. doi:10.1671/0272-4634(2006)26[511:anofvs]2.0.co;2
- Xing, L., O'Connor, J. K., McKellar, R. C., Chiappe, L. M., Bai, M., Tseng, K., et al. (2018). A flattened enantiornithine in mid-Cretaceous Burmese amber: morphology and preservation. *Sci. Bull.* 63, 235–243. doi:10.1016/j.scib.2018.01.019
- Xing, L., O'Connor, J. K., McKellar, R. C., Chiappe, L. M., Tseng, K., Li, G., et al. (2017). A mid-Cretaceous enantiornithine (Aves) hatchling preserved in Burmese amber with unusual plumage. *Gondwana Res.* 49, 264–277. doi:10.1016/j.gr.2017.06.001
- Young, R. L., Bever, G. S., Wang, Z., and Wagner, G. P. (2011). Identity of the avian wing digits: problems resolved and unsolved. *Dev. Dyn.* 240, 1042–1053. doi:10.1002/dvdy.22595
- Zhang, F., Zhou, Z., Hou, L., and Gu, G. (2001). Early diversification of birds: evidence from a new opposite bird. *Chin.Sci.Bull.* 46, 945–949. doi:10.1007/bf02900473
- Zhang, L., Yang, Y., Zhang, L., Guo, S., Wang, W., and Zheng, S. (2007). Precious fossil-bearing beds of the lower cretaceous Jiufotang Formation in western liaoning province, China. *Acta Geol. Sin.* 81, 357–364.
- Zheng, X., O'Connor, J. K., Wang, X., Wang, Y., and Zhou, Z. (2018). Reinterpretation of a previously described Jehol bird clarifies early trophic evolution in the Ornithuromorpha. *Proc. R. Soc. B.* 285, 20172494. doi:10.1098/rspb.2017.2494
- Zheng, X., O'Connor, J. K., Huchzermeyer, F., Wang, X., Wang, Y., Zhang, X., et al. (2014). New specimens of *Yanornis* indicate a piscivorous diet and modern alimentary canal. *PLoS One* 9, e95036. doi:10.1371/journal.pone.0095036
- Zheng, X., Wang, X., O'Connor, J. K., and Zhou, Z. (2012). Insight into the early evolution of the avian sternum from juvenile enantiornithines. *Nat. Commun.* 3, 1116. doi:10.1038/ncomms2104
- Zhou, S., O'Connor, J. K., and Wang, M. (2014). A new species from an ornithuromorph (Aves: Ornithothoraces) dominated locality of the Jehol Biota. *Chin. Sci. Bull.* 59, 5366–5378. doi:10.1007/s11434-014-0669-8
- Zhou, S., Zhou, Z., and O'Connor, J. K. (2012). A new basal beaked ornithurine bird from the Lower Cretaceous of western Liaoning, China. *Vertebr. Palasiat.* 50, 9–24.
- Zhou, S., Zhou, Z., and O'Connor, J. K. (2013). Anatomy of the basal ornithuromorph bird *Archaeorhynchus spathula* from the Early Cretaceous of Liaoning, China. *J. Vertebr. Paleontol.* 33, 141–152. doi:10.1080/02724634.2012.714431
- Zhou, Z., Clarke, J., Zhang, F., and Wings, O. (2004). Gastroliths in *Yanornis*: an indication of the earliest radical diet-switching and gizzard plasticity in the lineage leading to living birds?. *Naturwissenschaften* 91, 571–574. doi:10.1007/s00114-004-0567-z
- Zhou, Z., Li, F. Z. Z., and Li, Z. (2010). A new Lower Cretaceous bird from China and tooth reduction in early avian evolution. *Proc. R. Soc. B* 277, 219–227. doi:10.1098/rspb.2009.0885
- Zhou, Z., and Zhang, F. (2006). A beaked basal ornithurine bird (Aves, Ornithurae) from the Lower Cretaceous of China. *Zool Scripta* 35, 363–373. doi:10.1111/j.1463-6409.2006.00234.x
- Zhou, Z., and Zhang, F. (2002a). A long-tailed, seed-eating bird from the Early Cretaceous of China. *Nature* 418, 405–409. doi:10.1038/nature00930
- Zhou, Z., and Zhang, F. (2005). Discovery of an ornithurine bird and its implication for Early Cretaceous avian radiation. *Proc. Natl. Acad. Sci.* 102. doi:10.1073/pnas.0507106102
- Zhou, Z., and Zhang, F. (2002b). Largest bird from the Early Cretaceous and its implications for the earliest avian ecological diversification. *Naturwissenschaften* 89, 34–38. doi:10.1007/s00114-001-0276-9

Conflict of Interest: The authors declare that the research was conducted in the absence of any commercial or financial relationships that could be construed as a potential conflict of interest.

Copyright © 2021 Foth, Wang, Spindler, Lin and Yang. This is an open-access article distributed under the terms of the Creative Commons Attribution License (CC BY). The use, distribution or reproduction in other forums is permitted, provided the original author(s) and the copyright owner(s) are credited and that the original publication in this journal is cited, in accordance with accepted academic practice. No use, distribution or reproduction is permitted which does not comply with these terms.



The True Identity of Putative Tooth Alveoli in a Cenozoic Crown Bird, the Gastornithid *Omorhamphus*

Antoine Louchart^{1*}, Bhart-Anjan Bhullar², Ségolène Riamon¹ and Daniel J. Field^{3*}

¹ Univ Lyon, UCBL, ENSL, UJM, CNRS, LGL-TPE, University of Lyon, Villeurbanne, France, ² Department of Geology and Geophysics, Peabody Museum of Natural History, Yale University, New Haven, CT, United States, ³ Department of Earth Sciences, University of Cambridge, Cambridge, United Kingdom

OPEN ACCESS

Edited by:

Fabien Knoll,
Fundacion Agencia Aragonesa para la
Investigacion y el Desarrollo, Spain

Reviewed by:

Aaron R. H. LeBlanc,
University of Alberta, Canada
Andrew H. Lee,
Midwestern University, United States
Edina Prondvai,
University of Birmingham,
United Kingdom

*Correspondence:

Antoine Louchart
antoine.louchart@ens-lyon.fr
Daniel J. Field
djf70@cam.ac.uk

Specialty section:

This article was submitted to
Paleontology,
a section of the journal
Frontiers in Earth Science

Received: 31 January 2021

Accepted: 16 April 2021

Published: 13 May 2021

Citation:

Louchart A, Bhullar B-A,
Riamon S and Field DJ (2021) The
True Identity of Putative Tooth Alveoli
in a Cenozoic Crown Bird,
the Gastornithid *Omorhamphus*.
Front. Earth Sci. 9:661699.
doi: 10.3389/feart.2021.661699

All extant birds are toothless, and recent molecular evidence suggests that edentulism in extant birds is the product of a single evolutionary transition to toothlessness on the line to crown birds in the Cretaceous. However, a fossil crown bird premaxilla from the Palaeogene of North America (assigned to the gastornithid *Omorhamphus storchi*) has been interpreted as bearing alveoli for teeth, an observation that would cast doubt on a single loss of teeth preceding the extant avian radiation. However, the identity of these putative alveoli has never been reinvestigated in detail. Here, we re-examine this problematic juvenile specimen, using non-invasive x-ray microtomography, enabling the assessment of the true identity of the large, alveolus-like pits on the ventral side of this premaxilla. Although superficially alveolus-like, we illustrate that these pits represent openings of large neurovascular canals communicating with both the medullary cavity as well as other canals opening along the dorsal and lateral surfaces of the upper jaw, and that none of these openings appear to represent tooth alveoli. Further, we demonstrate that claims of an adult gastornithid specimen (*Gastornis parisiensis*) exhibiting tooth alveoli are similarly unfounded. By rejecting the hypothesis of dentition in these gastornithids, we eliminate any lingering uncertainty regarding the persistence of teeth within the avian crown group. We illustrate the presence of similar large vascular openings along the ventral surface of the beak of juvenile *Gastornis russelli/parisiensis*, and smaller versions in the juvenile premaxillae of *Sylviornis neocaledoniae*. We suggest that the large vascular canals in gastornithid specimens such as *O. storchi* are a feature associated with rapid growth of the juvenile beak, allowing the attainment of a large and dorsoventrally deep beak early in ontogeny. This may have enabled young gastornithids to become autonomous early, consistent with a presumably precocial developmental strategy.

Keywords: Aves, beak, bone, Gastornithidae, Neornithes, ontogeny, *Sylviornis*, x-ray microtomography

INTRODUCTION

Virtually all known representatives of the avian crown group, extant and extinct, are edentulous, with estimates suggesting a single transition to toothlessness in the ancestors of crown birds between 116 and 88 Ma (Louchart and Viriot, 2011; Meredith et al., 2014; Brocklehurst and Field, 2021). The only hitherto unchallenged example of a crown bird exhibiting tooth alveoli is

a juvenile jaw specimen from the early Eocene of Wyoming (Sinclair, 1928; Lambrecht, 1930). This enigmatic specimen, referred to *Omorhamphus storchii*, therefore has important potential to inform our understanding of the evolutionary dynamics of avian dentition. However, since its initial descriptions the identity of these pits has not been revisited. The juvenile premaxilla, which bears distinctive pits in the jaw tomia interpreted as tooth alveoli, is associated with several other skeletal elements, and the specimen was assigned to Gastornithidae (previously known as Diatrymidae; Sinclair, 1928; Lambrecht, 1930). Hence, these holes were purported evidence that at least juveniles of *O. storchii* possessed teeth (Lambrecht, 1930), an interpretation that has not been critically evaluated.

Tooth alveoli in *Omorhamphus storchii* would represent the only known evidence of teeth in a crown bird, and would challenge current interpretations of the evolutionary history of avian tooth reduction (Dumont et al., 2016; Brocklehurst and Field, 2021). However, the *O. storchii* specimen in question appears to be skeletally immature, which might suggest the presence of teeth only in juveniles, as is the case in the extant platypus (*Ornithorhynchus anatinus*), a monotreme mammal in which adults are toothless (Grant and Fanning, 2007), or the ceratosaurian theropod dinosaur *Limusaurus*, in which the dentition was reduced throughout ontogeny leading to a toothless adult (Wang et al., 2017). Given the striking degree of homoplasy in the pattern of tooth reduction along the avian stem lineage throughout the Mesozoic (e.g., Louchart and Viriot, 2011; Brocklehurst and Field, 2021), the possibility of such homoplasy extending into the avian crown group during the Cenozoic demands investigation. Here, we redescribe the fossil jaw element of *O. storchii* in question, which represents the rostral portion of the premaxilla. We use high-resolution X-ray microtomography (μ CT) to non-destructively investigate the internal structure of the bone, and re-evaluate previous interpretations of this specimen, which suggested that the holes in the premaxillary tomia might represent (Sinclair, 1928), or surely did represent (Lambrecht, 1930), tooth alveoli. These arguments were based only on external shape similarity between some of the pits in the *O. storchii* tomia with the tooth alveoli of typical thecodont vertebrates, and their similar position along the tomia (Sinclair, 1928; Lambrecht, 1930). Therefore, our application of μ CT scanning allows us to evaluate the internal morphology of this specimen for the first time.

MATERIALS AND METHODS

YPM 13106, a rostral portion of the premaxilla of *Omorhamphus storchii*, from the Lower Gray Bull Formation, early Eocene, Bighorn Basin, Wyoming. The fragment is ca. 51 mm long rostrocaudally, 22 mm at its widest point from right lateral edge to left lateral edge, and 36 mm at its deepest point dorsoventrally. We conservatively apply the binomen *Omorhamphus storchii* throughout this manuscript, rather than accepting its proposed synonymization with *Gastornis giganteus* (Andors, 1992), since there is no unambiguous evidence that the associated juvenile bones referred to *O. storchii* represent the same species as

G. giganteus, which is known only from adult specimens, with no known associations of the two taxa.

We also examined the external morphology of juvenile upper beaks attributed to a gastornithid (MNHN-R2583; *Gastornis russelli/parisiensis*; early Eocene, France), and a sylvornithid (MNHN-NCP-220, 242, 263 and 290; *Sylviornis neocaledoniae*; Holocene, New Caledonia), as well as adult beaks of *Gastornis laurenti* (MHNT.PAL.2013.15.1; early Eocene, France) and *Sylviornis neocaledoniae* (NCP-242 and a partial unnumbered specimen; Holocene, New Caledonia).

X-ray microtomography was performed at the University of Texas High-Resolution X-ray CT Facility. Three-dimensional reconstructions of the premaxilla were generated from 16-bit TIFF stacks from a scan of the complete fossil. Scan parameters were as follows: NSI scanner, Feinfocus source, high power, 200 kV, 0.14 mA, 1 aluminum filter, Perkin Elmer detector, 0.25 pF gain, 1 fps (999.911 ms integration time), no binning, no flip, source to object 218.58 mm, source to detector 1316.527 mm, continuous CT scan, no frames averaged, 0 skip frames, 3600 projections, 6 gain calibrations, 5 mm calibration phantom, data range [−10, 100] (grayscale range adjusted from NSI defaults), beam-hardening correction = 0.3. Voxel size = 0.0302 mm. Total slices = 1813. Then, three-dimensional reconstructions were generated from 16-bit stacks from a central region of the fossil, in order to reach better resolution parameters. Scan parameters were as follows: NSI scanner, Feinfocus source, high power, 210 kV, 0.12 mA, 1 aluminum filter, Perkin Elmer detector, 0.25 pF gain, 1 fps (999.911 ms integration time), no binning, no flip, source to object 133.754 mm, source to detector 1316.527 mm, continuous CT scan, no frames averaged, 0 skip frames, 5400 projections, 6 gain calibrations, 0.762 mm calibration phantom, data range [−10, 600] (grayscale range adjusted from NSI defaults), beam-hardening correction = 0.25, voxel size = 0.0109 mm, total slices = 1683.

RESULTS

Examination of the μ CT reconstruction and the actual *Omorhamphus* specimen reveals that the pits in the premaxillary tomia originally interpreted as tooth alveoli exhibit different shapes in ventral view (**Figure 1**). The more rostrally positioned pits on the ventral surface of the premaxilla are rostrocaudally elongated ellipses. This apparent elongation appears to be the product of canals with circular cross-sections contacting the ventral surface of the premaxilla obliquely, whereas more caudally positioned pits are nearly orthogonal to the palatal surface, resulting in circular openings. The pits are situated on the palatal surface of the premaxilla, just medial to the tomia, which are eroded. The four principal pits visible on the left side, from rostral-most to caudal-most, comprise (**Figure 1C**): (a) a large pit (2.5 mm in mediolateral diameter) with an oblong opening; (b) a smaller pit (2 mm mediolateral diameter) with a circular opening which is also the lateral-most pit; (c) a ~2 mm mediolateral diameter pit, with a slightly elongated opening; and (d) a ~2 mm mediolateral diameter pit, with a more rounded opening. The three visible pits on the right

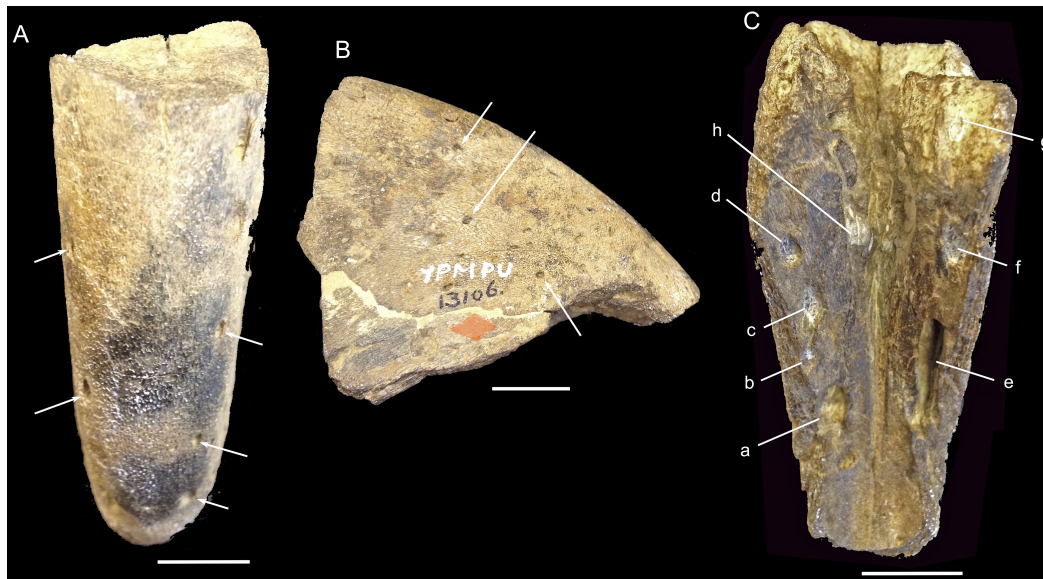


FIGURE 1 | External views of *Omorhamphus storchii* YPM 13106 (rostral part of juvenile premaxilla). **(A)** Dorsal view. **(B)** Right lateral view. **(C)** Ventral view. (a–g) Large openings visible in ventral view **(C)** on lateral sides of the palate just medial to the eroded tomia (a–d, left side; e–g, right side; h, median-left). The ventral pits are obturated by sediment, except the large oblique pit (labeled e). Several medium-sized foramina are visible (white arrows) on the dorsal and lateral sides **(A,B)**. Scale bars, 10 mm.

side, from rostral-most to caudal-most, comprise: (e) a large pit (2.5 mm mediolateral diameter) with the most rostrocaudally elongated opening (10 mm), with its associated internal canal positioned at the most acute angle to the palatal surface; (f) and (g) two larger pits (~2.5 mm in mediolateral diameter) with rounder openings (the more caudally situated pit's palatal opening is incomplete due to specimen damage). An additional large opening is also situated far more medially, slightly left of the midline of the palatal surface (h). All of the pits are obturated by sediment, except for the large, oblique pit on the right side (e).

X-ray μ CT reveals that, despite the superficially alveolus-like appearance of some of these pits, all represent the openings of deep canals that communicate with other neurovascular canals and medullary cavities within the premaxilla (Figures 2, 3, Supplementary 3D File and Supplementary Figure 1). Among the vascular canals that communicate with the seven large pits studied here are medium-sized canals that open on the dorsal surface of the premaxilla, some dorsal openings being as large as the ventral “alveolus-like” pits (Figures 1A,B, Supplementary 3D File and Supplementary Figure 1). Based on digital examination of the internal structure of the bone, no visible differences in bone structure are apparent between the areas surrounding the seven canals and the rest of the jaw bone (Figure 4).

Peripherally, the bone of the premaxilla comprises vascular canals with no apparent preferential orientation within the cortex, merging together and into a medulla toward the center of the premaxilla with a rather spongy structure composed of trabeculae. Elongated cavities lacking trabeculae are located near the tomial edges of the premaxilla, not far from the occlusal surface and oriented parallel to the tomia. The vascular canals, and cavities within the spongy part of the bone, communicate both with these elongated cavities and with the surface of the

cortex (Supplementary 3D File and Supplementary Figure 1). The cortical bone structure is consistent with juvenile bone in an active growth phase, and as such the canals are likely to represent simple primary canals (and some possible primary osteons) (see Francillon-Vieillot et al., 1990; Starck and Chinsamy, 2002). The bone is highly vascularized, secondary osteons have not started to colonize the bone thickness, and no fundamental external system (lamellar or avascular bone with parallel fibers) exists at the periphery; instead, numerous osteocyte lacunae are visible on the surface (periphery) (Figure 4). All of these observations are consistent with a juvenile stage of premaxillary bone development, concordant with the highly “fibrous” external texture of the element.

DISCUSSION

Our μ CT data reveal that all seven of the more tomially positioned pits in the palatal surface of the premaxilla are neurovascular canals (not merely the rostralmost pit on the right side as suggested by Sinclair, 1928), with six of these canals now obturated by sediment. In addition, an eighth large pit positioned toward the midline of the palate is similar to the others, and appears to represent another vascular canal opening. The position of this opening far from the tomia adds evidence for the absence of any association between these pits and the purported presence of dentition. These vascular canals are large in diameter throughout their length, without abrupt constrictions, and communicate with the medullary cavities as well as smaller vascular canals within the bone. Tooth alveoli do communicate with neurovascular canals, but these are markedly narrower than the alveoli themselves (see, e.g., Ferreira-Cardoso et al., 2019). If these pits corresponded to tooth alveoli, the following structures

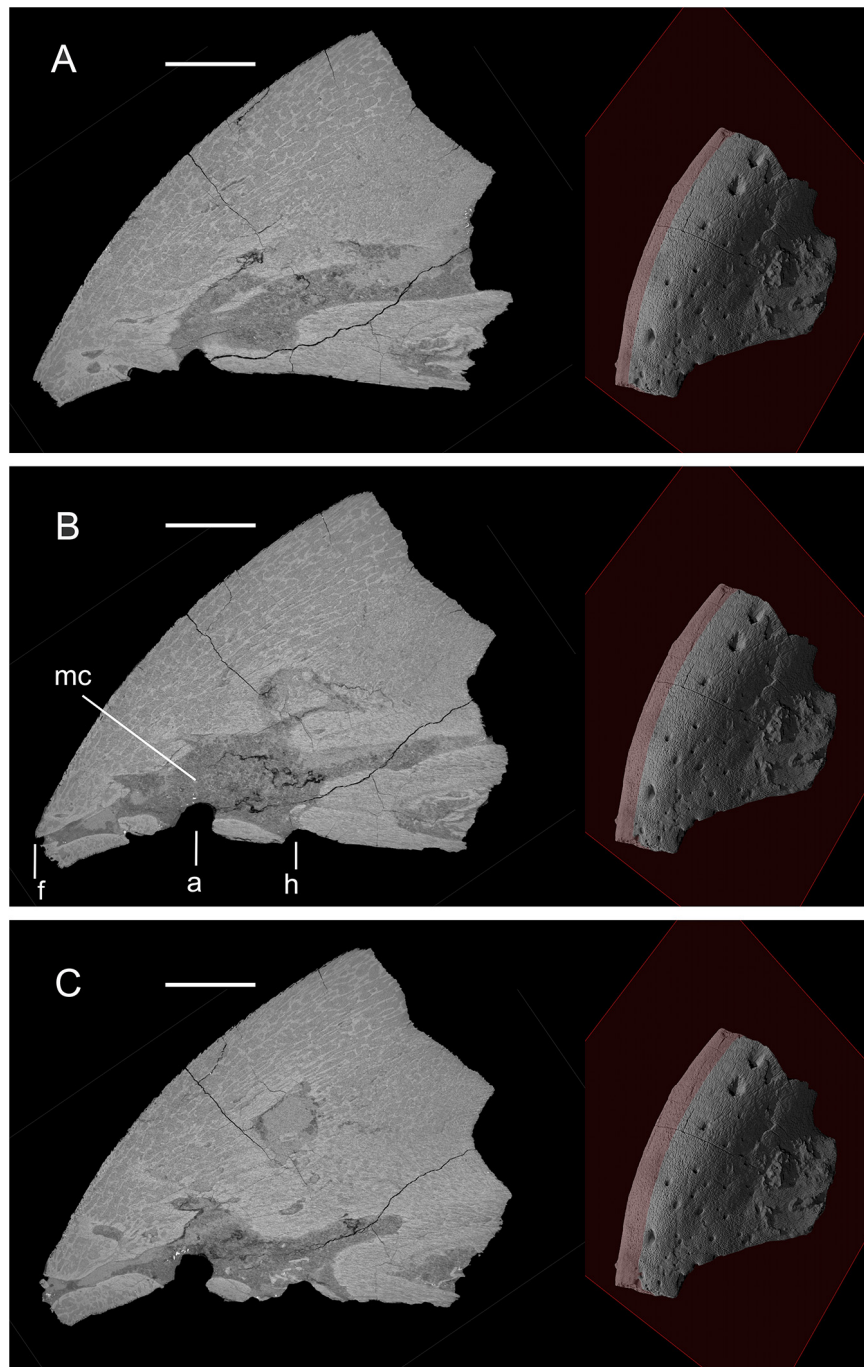


FIGURE 2 | Three parasagittal sections through the premaxilla of YPM 13106, showing communications between canals and with the medullary cavity. Plane of parasagittal section moves toward the left from **(A)** through **(B)** and **(C)**. The position of the plane is shown to the right of each section. Two of the large ventral pits (a, h) (see **Figure 1**) appear to communicate with the medullary cavity (mc), and a dorsal distal foramen (f). Scale bars, 10 mm.

would be expected to be observed surrounding the pits in birds (Dumont et al., 2016), or in non-avian archosaurs or mammals (LeBlanc et al., 2017; Funston et al., 2019): differentiated alveolar bone forming the internal wall of every cavity, traces of tooth buds of replacement teeth, and traces of Sharpey's fibers. None of these features are discernible in the premaxilla of *Omorhamphus*.

Moreover, alveoli (or remnants thereof) would also be expected to exhibit less irregular shapes and sizes than the pits observed in *Omorhamphus*. The absence of visible differentiation in structure between the bone surrounding the seven pits and the rest of the jaw bone is concordant with the identification of these structures as particularly large vascular canals. Finally, the location of these



FIGURE 3 | Nine parallel transverse sections through the premaxilla of YPM 13106. The planes of section are shown on the upper right corner of each virtual section. **(A–I)** The sections proceed from more caudal to more rostral. R, right side of a section. L, left side of a section. The succession of section planes (separated by ca. 2.2 mm) reveal connections between the large ventral openings (here a, b, c, e; see **Figure 1**), the medullary cavity (mc) and vascular canal openings, or foramina (f) to the dorsal and lateral sides of the premaxilla. Scale bars, 5 mm.

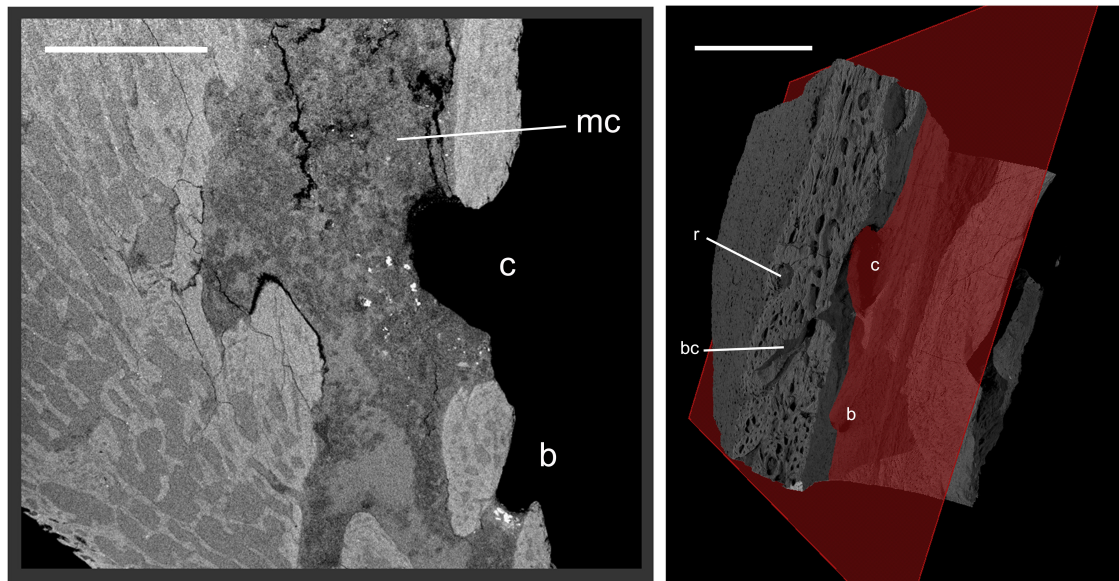


FIGURE 4 | Closeup view in parasagittal section through the premaxilla of YPM 13106. The position of the plane of section is indicated on the right panel (ventro-lateral left view in volume). The regions surrounding the canals (and the cavity with which they communicate), including at openings on the palatal surface (b, c) (see **Figure 1**), show no difference in structure with the rest of the bone. The numerous smallest cavities visible in section and all over the surface (left side of specimen on right panel) are osteocyte lacunae. bc, branched canal; mc, medullary cavity; r, resorption pit corresponding to the site of a possible future secondary osteon. Scale bars, 5 mm.

large canals differs from those of typical tooth alveoli, given that they are positioned with an irregular alignment mesial to the jaw tomia instead of regularly alongside the tomia. Hence, none of these pits can reasonably be interpreted as tooth alveoli, contrary to the heretofore unchallenged suggestion by Sinclair (1928) and assertion by Lambrecht (1930). The recognition that these putative gastornithid tooth alveoli have remained misidentified for nearly a century is reminiscent of the recent observation that bony ridges surrounding the lingual groove on the mandibles of caenagnathid theropods also do not represent vestiges of tooth-bearing structures (Funston et al., 2019).

Purported tooth alveoli in “*Gastornis parisiensis*” (formerly *Gastornis edwardsii*) were additionally noted by Lambrecht (1930). Sinclair (1928) had already mentioned that the beak margins of this species, of which all known specimens comprise adults described by Lemoine (1881), exhibit perforations similar to what he observed in *O. storchii*. But Lambrecht (1930) went further and was affirmative that the *G. parisiensis* premaxilla and mandible exhibit distinct alveoli for teeth along the tomia, based on figures from two plates in Lemoine (1881: plates 9, 10). On the other hand, concerning the premaxilla, Lemoine (1881) himself interpreted these holes as the openings of large vascular canals, and not as tooth alveoli. Since then, however, Martin (1992) demonstrated that the rostral and mandibular components concerned were non-avian in origin (and were instead probably attributable to turtles), along with numerous other elements in Lemoine’s reconstruction.

In his re-evaluation of Lemoine’s gastornithid description and reconstruction, Martin (1992) considered a tarsometatarsus to represent a new species, *G. russelli*. We examined the

beak tentatively assigned to this species (specimen R2583, Reims collection) (**Figures 5A,C**). Supporting the suggestion by Bourdon et al. (2016), it appears to be attributable to a juvenile on the basis of the fibrous nature of its bone surface, which was not mentioned by Martin (1992). However, it appears to be more ontogenetically advanced than the beak of *O. storchii*, since the surface aspect is less fibrous and smoother than in the latter. In addition, the *Omorhamphus* beak, although fragmentary, is obviously smaller and less compressed laterally than R2583, in line with a markedly less advanced growth stage. The juvenile status of R2583 specimen may account for its relatively small beak, compared with known adult *Gastornis* beaks, suggesting that it could belong to a larger species such as *G. parisiensis*. Incidentally, although this was also the suggestion of Bourdon et al. (2016), recent recognition that the holotype tarsometatarsus of *G. russelli* is actually much larger than stated by Martin (1992) emphasizes the potential compatibility of the juvenile maxilla R2583 with *G. russelli* (Mourer-Chauviré and Bourdon, 2020). Mesial to the tomia of this juvenile *Gastornis* beak from Reims are several large vascular foramina (**Figure 5C**), similar to those of *Omorhamphus storchii* described above and found at similar locations along the jaw. The identical aspect and irregular size and position of the openings in R2583 indicate that they are of the same nature as those of *O. storchii*. The presence of very large vascular canals in juvenile beaks may therefore be constant in gastornithids, from both sides of the Atlantic, whereas it is undocumented in other birds.

In sum, this work affirms that there is no evidence for the occurrence of teeth in any crown birds, living or extinct, and

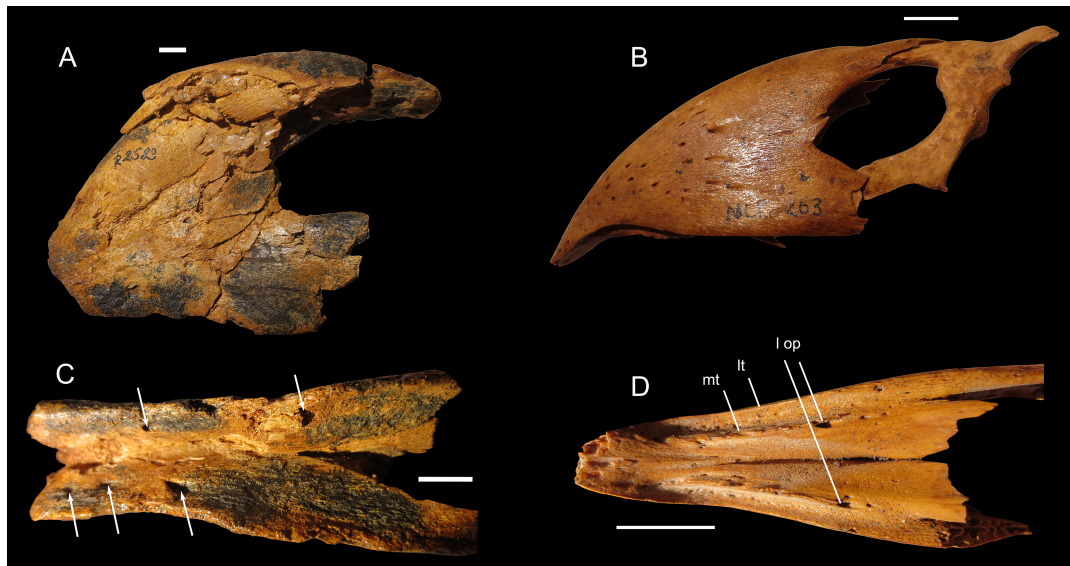


FIGURE 5 | Juvenile upper beaks of *Gastornis russelli/parisiensis* R2583 **(A,C)** and *Sylviornis neocaledoniae* NCP-263 **(B,D)**. **(A,B)** Left lateral views. **(C,D)** Ventral views. White arrows in **(C)** indicate large pits similar to those in *Omorhamphus storchii*, which are also vascular openings. In **(D)**: lt, lateral tomial crest; mt, medial tomial crest; l op, large openings of vascular canals. Scale bars, 10 mm.

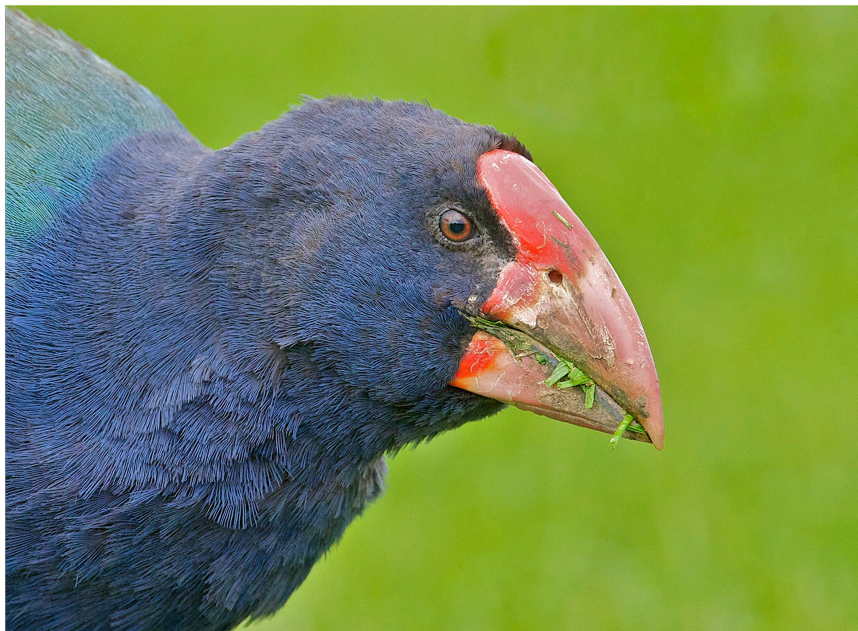


FIGURE 6 | Closeup of the head of the extant New Zealand Takahe (*Porphyrio mantelli*). The general proportions of the bill are comparable to those of the vastly larger-bodied extinct neornithine clade Gastornithidae. Photo by DF.

thus that avian dentition does not appear to have persisted into the Cenozoic. This supports the hypothesis of a single transition to neornithine toothlessness among the close ancestors of crown birds, pre-dating the Cretaceous-Paleogene transition as corroborated by the earliest-known probable crown bird fossils (Chatterjee, 2000; Louchart and Viriot, 2011; Meredith et al., 2014; Field et al., 2020; Brocklehurst and Field, 2021). An

apparently reminiscent example is that of rather irregular large canals opening on the occlusal side of the mandibles of adult anteaters (Mammalia: Vermilingua), interpreted as evolutionary remnants of tooth alveoli in these edentulous mammals. These canals may be associated with a sensory role in conjunction with a mandibular keratinous pad (Ferreira-Cardoso et al., 2019). In such case, canals convey nerves as well as blood vessels, and

are therefore truly neurovascular. Nevertheless, this example differs from that of gastornithids in that it is found in adult anteaters, whereas in gastornithids these pits are only evident in juveniles. Moreover, if these pits were associated with a sensory role in gastornithids, the restriction of these structures to juveniles would be puzzling, and without known extant analogs. Therefore, although we cannot entirely exclude the possibility that these canals housed nerves in addition to vasculature, we propose an alternative hypothesis whereby these large canals in juvenile gastornithid premaxillae were more explicitly associated with blood vessels.

Compared with non-gastornithid Neornithes, the juvenile gastornithid premaxillae examined here exhibit unusually large vascular canals on the sides of the palatal surface, both in terms of their absolute size and in relation to the dimensions of the beak. These may reasonably be explained by rapid growth of the extremely large beaks of gastornithids. Gastornithids were large, flightless birds, and have been interpreted as plant-eating relatives of Anseriformes or Galliformes (Andors, 1992; Angst et al., 2014; Worthy et al., 2017). These birds exhibited some of the largest-known beaks in avian evolutionary history, together with some phorusrhacids and dromornithids. Gastornithid beaks were relatively short, laterally compressed, and dorsoventrally deep, in some ways resembling much larger versions of the beak of the extant New Zealand Takahe (*Porphyrio mantelli*; Gruiformes: Rallidae) (Figure 6). Another extinct fossil galloanseran showing a deep, laterally compressed and curved beak is the large, flightless galliform *Sylviornis neocaledoniae*, of New Caledonia. Comparisons between *Gastornis* and *Sylviornis* are therefore interesting, and made possible by the existence of beaks deriving from juvenile specimens of *Sylviornis*. Most of the vascular foramina in juvenile *Sylviornis* beaks in dorsal view are small, becoming more densely spaced toward the rostral end, as in *Omorhamphus*. In palatal view, juvenile *S. neocaledoniae* exhibit smaller vascular openings than do *O. storchii* and juvenile *Gastornis* (Figure 5), both in terms of absolute size and relative to beak dimensions. Unlike *O. storchii* and *Gastornis*, however, *S. neocaledoniae* exhibits double bony tomia (lateral tomia and mesial tomia) in both juvenile and adult specimens (Mourer-Chauviré and Balouet, 2005). The largest vascular openings in juvenile specimens of *Sylviornis* are positioned at the caudal end of the mesial tomia (Figure 5D). The vascular openings of adult *S. neocaledoniae* beaks in palatal view are much reduced, and of comparable proportions to those of many extant birds with particularly large beaks (e.g., large macaws, storks, shoebill, large birds of prey, hornbills, and toucans; orig. obs.). The two largest foramina of juveniles are no longer visible in the beaks of adults. In juvenile *S. neocaledoniae* the vascular openings are of relatively small size, and the number of larger vascular openings is reduced compared with *Gastornis* sp. of similar ontogenetic stage (and the even younger material attributed to *Omorhamphus storchii*). This suggests reduced vascularization during beak growth in *S. neocaledoniae* relative to *O. storchii* and *Gastornis*, which may be related to the smaller absolute and relative size of the beak in adult *Sylviornis*.

A precocial developmental strategy and early behavioral autonomy can be hypothesized for gastornithids based on their hypothesized phylogenetic placement as stem group

Anseriformes (Andors, 1992) or stem group Galliformes (see Worthy et al., 2017). Extant representatives of Anseriformes, and its extant sister clade Galliformes, exhibit developmental strategies ranging from precocial to superprecocial (the latter characterizing Megapodiidae, the sister clade to all other extant galliforms; Starck and Ricklefs, 1998; Botelho and Faunes, 2015; Prum et al., 2015). Hatchlings of extant precocial bird taxa encompass a range of feeding behaviors, including complete feeding autonomy, parental guidance, and short-term direct parental feeding (Starck and Ricklefs, 1998; Botelho and Faunes, 2015). Although presumably precocial, young gastornithids may not have been fully autonomous feeders, and a period of parental feeding assistance may have preceded the acquisition of full feeding autonomy, associated with the attainment of a mature beak. Among precocial birds the intermediate phase between hatching and full feeding autonomy tends to be short (Starck and Ricklefs, 1998). The large relative and absolute dimensions of adult gastornithid beaks (maximum depth of the premaxilla may reach 18 cm in adult *Gastornis giganteus*) may therefore have been attained fairly rapidly following hatching. This may have been achieved through rapid growth rates early in ontogeny, allowing adult-like, autonomous feeding in relatively young birds. Hence, the beaks of juvenile gastornithids may have required substantial vascularization in order to yield sufficient blood flux for rapid bone accretion. A general relationship between vascularization and growth rate exists (see Francillon-Vieillot et al., 1990; Starck and Chinsamy, 2002), which could suggest that the particularly large localized canals in *O. storchii* and R2583 (both juveniles) are related to rapid growth rates. In bird bones, the intensity of remodeling by Haversian bone tissue in adults is correlated with the intensity of blood flow and size of vascular canals (Allan et al., 2014). A similar relationship between intensity of primary bone accretion and the size of vascular canals during juvenile growth is therefore to be expected.

Upon reaching adult size, the larger vascular canals observed in juvenile beaks of gastornithids (and to a lesser extent in *Sylviornis*) presumably decreased in size with the obturation of primary osteons and simple canals through internal bone apposition, reducing their diameter and the dimensions of openings to the cortical surface. This mechanism is often observed in vertebrates (Francillon-Vieillot et al., 1990; Polig and Jee, 1990; Starck and Chinsamy, 2002) though data on bird beak growth series in general are scarce.

In adult beaks of *Gastornis* (*G. giganteus*, *G. laurenti*), rather small dorsal pits are still present in lateral view, but only toward the rostral end of the beak, while deep grooves are present over most of the dorsal surface of the beak (Bourdon et al., 2016); such grooves are absent in juvenile specimens (*Omorhamphus* and R2583). The latter grooves also characterize adult *Sylviornis* beaks (Mourer-Chauviré and Balouet, 2005) as opposed to juvenile ones (Figure 5B). The remnant pits on the rostral part of adult beaks can be compared with those visible in several extant birds, including those of some ratites which have been interpreted as being related to a sensory bill tip organ (Crole and Soley, 2017; du Toit et al., 2020). The deep grooves in adult *Gastornis* and *Sylviornis* are vascular grooves on the surface of the bone that

have been interpreted as necessary to maintain and nourish a thick rhamphotheca (Mourer-Chauviré and Balouet, 2005) and their exclusive presence in adults presumably indicates that their formation took place after the cessation of primary bone growth. Therefore, it may be that a thickening of the beak rhamphotheca concomitantly occurred only after beak growth was completed. Beak rhamphotheca protects the underlying facial bones from damage, and is continuously replaced starting from its living base – becoming keratinized with growth toward the outer surface in order to prevent wear. The thickening of gastornithid beak rhamphotheca in adults may therefore have been related to a diet that incorporated hard or abrasive food items.

DATA AVAILABILITY STATEMENT

The datasets presented in this study can be found in online repositories. The names of the repository/repositories and accession number(s) can be found below: The scan data for *Omorhamphus storchii* generated for this study, as well as three dimensional volumetric reconstructions, are deposited online and available on Zenodo (doi: 10.5281/zenodo.4670739).

AUTHOR CONTRIBUTIONS

AL, B-AB, and DF designed the research. AL wrote the original manuscript and prepared figures with inputs from

B-AB, SR, and DF. SR segmented the canal system. All authors conducted the analyses, collected the data, and reviewed and edited the manuscript.

FUNDING

DF acknowledges support from the UKRI Future Leaders Fellowship MR/S032177/1 and a Royal Society Research Grant (RGS/R2/192390).

ACKNOWLEDGMENTS

We thank Matthew Colbert for scanning the specimen, Cécile Mourer-Chauviré for discussions and access to *Gastornis* material under study by herself and Estelle Bourdon, Ronan Allain, and Claire Sagne for access to *Gastornis* and *Sylviornis* material in the MNHN (Paris), comments on bone microstructure from Vivian de Buffrénil, and helpful comments from ARL, EP, and AHL, which improved the manuscript.

SUPPLEMENTARY MATERIAL

The Supplementary Material for this article can be found online at: <https://www.frontiersin.org/articles/10.3389/feart.2021.661699/full#supplementary-material>

REFERENCES

- Allan, G. H., Cassey, P., Snelling, E. P., Maloney, S. K., and Seymour, R. S. (2014). Blood flow for bone remodelling correlates with locomotion in living and extinct birds. *J. Exp. Biol.* 217, 2956–2962. doi: 10.1242/jeb.102889
- Andors, A. V. (1992). Reappraisal of the Eocene groundbird *Diatryma* (Aves: Anserimorphae). *Nat. Hist. Mus. Los Angeles Cty. Sci. Ser.* 36, 109–125.
- Angst, D., Lécuyer, C., Amiot, R., Buffetaut, E., Fourel, F., Martineau, F., et al. (2014). Isotopic and anatomical evidence of an herbivorous diet in the early Tertiary giant bird *Gastornis*, implications for the structure of Paleocene terrestrial ecosystems. *Naturwissenschaften* 101, 313–322. doi: 10.1007/s00114-014-1158-2
- Botelho, J. F., and Faunes, M. (2015). The evolution of developmental modes in the new Avian phylogenetic tree. *Evol. Dev.* 17, 221–223. doi: 10.1111/ede.12126
- Bourdon, E., Mourer-Chauviré, C., and Laurent, Y. (2016). Early Eocene birds from La Borie, southern France. *Acta Palaeontol. Polon.* 61, 175–190.
- Brocklehurst, N., and Field, D. J. (2021). Macroevolutionary dynamics of dentition in Mesozoic birds reveal no long-term selection towards tooth loss. *iScience* 24, 102243. doi: 10.1016/j.isci.2021.102243
- Chatterjee, S. (2000). “The morphology and systematics of *Polarornis*, a Cretaceous loon (Aves: Gaviidae) from Antarctica,” in *Proceedings of the 5th Symposium of the Society of Avian Paleontology and Evolution*, Vol. 1, eds Z. Zhou and F. Zhang (Beijing: Science Press), 125–155.
- Crole, M. R., and Soley, J. T. (2017). Bony pits in the Ostrich (*Struthio camelus*) and Emu (*Dromaius novaehollandiae*) bill tip. *Anat. Rec.* 300, 1705–1715. doi: 10.1002/ar.23594
- du Toit, C. J., Chinsamy, A., and Cunningham, S. J. (2020). Cretaceous origins of the vibrotactile bill-tip organ in birds. *Proc. R. Soc. B* 287, 20202322. doi: 10.1098/rspb.2020.2322
- Dumont, M., Tafforeau, P., Bertin, T., Bhullar, B. A., Field, D., Schulp, A., et al. (2016). Synchrotron imaging of dentition provides insights into the biology of *Hesperornis* and *Ichthyornis*, the “last” toothed birds. *BMC Evol. Biol.* 16:178. doi: 10.1186/s12862-016-0753-6
- Ferreira-Cardoso, S., Delsuc, F., and Hautier, L. (2019). Evolutionary tinkering of the mandibular canal linked to convergent regression of teeth in placental mammals. *Curr. Biol.* 29, 468–475. doi: 10.1016/j.cub.2018.12.023
- Field, D. J., Benito, J., Chen, A., Jagt, J. W. M., and Ksepka, D. T. (2020). Late Cretaceous neornithine from Europe illuminates the origins of crown birds. *Nature* 579, 397–401. doi: 10.1038/s41586-020-2096-0
- Francillon-Vieillot, H., de Buffrénil, V., Castanet, J., Géraudie, J., Meunier, F. J., Sire, J. Y., et al. (1990). “Microstructure and mineralization of vertebrate skeletal tissues,” in *Skeletal Biomineralization: Patterns, Processes and Evolutionary Trends*, Vol. 1, ed. J. G. Carter (New York, NY: Van Nostrand Reinhold), 471–530. doi: 10.1007/978-1-4899-5740-5_20
- Funston, G. F., Wilkinson, R. D., Simon, D. J., LeBlanc, A. R. H., Wosik, M., and Currie, P. J. (2019). Histology of caenagnathid (*Theropoda*, *Oviraptorosauria*) dentaries and implications for development, ontogenetic edentulism, and taxonomy. *Anat. Rec.* 303, 918–934. doi: 10.1002/ar.24205
- Grant, T., and Fanning, D. (2007). *Platypus*. Collingwood, Vic: CSIRO Publishing.
- Lambrech, K. (1930). Studien über fossile Riesenvögel. *Geol. Hung. Ser. Palaeontol.* 7, 1–37. doi: 10.1159/000397953
- LeBlanc, A. R. H., Brink, K. S., Cullen, T. M., and Reisz, R. R. (2017). Evolutionary implications of tooth attachment versus tooth implantation: a case study using dinosaur, crocodilian, and mammal teeth. *J. Vertebr. Paleontol.* 37:e1354006. doi: 10.1080/02724634.2017.1354006
- Lemoine, V. (1881). *Recherches sur les Oiseaux Fossiles des Terrains Tertiaires Inférieurs des Environs de Reims, Part II*. Reims: F. Keller, 75–170.
- Louchart, A., and Viriot, L. (2011). From snout to beak: the loss of teeth in birds. *Trends Ecol. Evol.* 26, 663–673. doi: 10.1016/j.tree.2011.09.004
- Martin, L. D. (1992). The status of the late Paleocene birds *Gastornis* and *Remiornis*. *Nat. Hist. Mus. Los Angeles Cty. Sci. Ser.* 36, 97–108.
- Meredith, R. W., Zhang, G., Gilbert, M. T. P., Jarvis, E. D., and Springer, M. S. (2014). Evidence for a single loss of mineralized teeth in the common avian ancestor. *Science* 346, 1254390. doi: 10.1126/science.1254390

- Mourer-Chauviré, C., and Balouet, J. C. (2005). Description of the skull of the genus *Sylviornis* Poplin, 1980 (*Aves*, *Galliformes*, *Sylviornithidae* new family), a giant extinct bird from the Holocene of New Caledonia. *Monogr. Soc. Hist. Nat. Balears* 12, 205–218.
- Mourer-Chauviré, C., and Bourdon, E. (2020). Description of a new species of *Gastornis* (*Aves*, *Gastornithiformes*) from the Early Eocene of La Borie, Southwestern France. *Geobios* 63, 39–46. doi: 10.1016/j.geobios.2020.10.002
- Polig, E., and Jee, W. S. S. (1990). A model of osteon closure in cortical bone. *Calcif. Tissue Int.* 47, 261–269. doi: 10.1007/bf02555907
- Prum, R. O., Berv, J. S., Dornburg, A., Field, D. J., Townsend, J. P., Lemmon, E. M., et al. (2015). A comprehensive phylogeny of birds (*Aves*) using targeted next generation DNA sequencing. *Nature* 526, 569–573. doi: 10.1038/nature15697
- Sinclair, W. J. (1928). *Omorhamphus*, a new flightless bird from the lower Eocene of Wyoming. *Proc. Amer. Phil. Soc.* 67, 51–65.
- Starck, J. M., and Chinsamy, A. (2002). Bone microstructure and developmental plasticity in birds and other dinosaurs. *J. Morphol.* 254, 232–246. doi: 10.1002/jmor.10029
- Starck, J. M., and Ricklefs, R. E. (1998). “Patterns of development: the altricial-precocial spectrum,” in *Avian Growth and Development: Evolution within the Altricial-Precocial Spectrum*, eds J. M. Starck and R. E. Ricklefs (Oxford: Oxford University Press), 3–30. doi: 10.1002/zoo.1430110103
- Wang, S., Stiegler, J., Amiot, R., Wang, X., Du, G. H., Clark, J. M., et al. (2017). Extreme ontogenetic changes in a ceratosaurian theropod. *Curr. Biol.* 27, 144–148. doi: 10.1016/j.cub.2016.10.043
- Worthy, T. H., Degrange, F. J., Handley, W. D., and Lee, M. S. (2017). The evolution of giant flightless birds and novel phylogenetic relationships for extinct fowl (*Aves*, *Galloanseres*). *R. Soc. Open Sci.* 4, 170975. doi: 10.1098/rsos.170975

Conflict of Interest: The authors declare that the research was conducted in the absence of any commercial or financial relationships that could be construed as a potential conflict of interest.

Copyright © 2021 Louchart, Bhullar, Riamon and Field. This is an open-access article distributed under the terms of the Creative Commons Attribution License (CC BY). The use, distribution or reproduction in other forums is permitted, provided the original author(s) and the copyright owner(s) are credited and that the original publication in this journal is cited, in accordance with accepted academic practice. No use, distribution or reproduction is permitted which does not comply with these terms.



Comments on the Morphology of Basal Paravian Shoulder Girdle: New Data Based on Unenlagiid Theropods and Paleognath Birds

Fernando E. Novas^{1*}, Matías J. Motta¹, Federico L. Agnolín^{1,2*}, Sebastián Rozadilla¹, Gastón E. Lo Coco¹ and Federico Brissón Egli¹

¹CONICET-Laboratorio de Anatomía Comparada y Evolución de Los Vertebrados, Museo Argentino de Ciencias Naturales "Bernardino Rivadavia", Buenos Aires, Argentina, ²Fundación de Historia Natural "Félix de Azara", Universidad Maimónides, Buenos Aires, Argentina

OPEN ACCESS

Edited by:

Jingmai Kathleen O'Connor,
Field Museum of Natural History,
United States

Reviewed by:

Alexander Wilhelm Armin Kellner,
Federal University of Rio De Janeiro,
Brazil

David Marjanović,
Museum of Natural History Berlin
(MfN), Germany
Thomas Dececchi,
Mount Marty College, United States

*Correspondence:

Fernando E. Novas
fernovas@yahoo.com.ar
Federico L. Agnolín
fedeagnolin@yahoo.com.ar

Specialty section:

This article was submitted to
Paleontology,
a section of the journal
Frontiers in Earth Science

Received: 31 January 2021

Accepted: 04 May 2021

Published: 25 May 2021

Citation:

Novas FE, Motta MJ, Agnolín FL,
Rozadilla S, Lo Coco GE and
Brissón Egli F (2021) Comments on the
Morphology of Basal Paravian
Shoulder Girdle: New Data Based on
Unenlagiid Theropods and
Paleognath Birds.
Front. Earth Sci. 9:662167.
doi: 10.3389/feart.2021.662167

In 1976 John Ostrom published an enlightening paper about the anatomical transformations in the shoulder girdle and forelimb elements along the origin of birds. Most of his ideas were based on comparing *Archaeopteryx lithographica* with the extant New World vulture *Cathartes aura*. Ostrom offered innovative ideas about range of movements and function of wing elements in the basal bird *Archaeopteryx*. Further, he explored anatomical transformations that may have occurred at early stages of the evolution of flight and established several hypothetical steps toward the acquisition of flapping flight in modern birds. Since then, however, our understanding of paravian diversity and anatomy has increased dramatically. Based on novel information derived from recent experiments, and currently available anatomical evidence of basal paravians, the present paper aims to review some important topics on pectoral girdle anatomy related to flight origins. Further, a brief analysis of pectoral girdle osteology and myology of the extant paleognath *Rhea americana* is also included with the aim to test whether Ostrom's ideas still remain valid under this new context, based on available phylogenetic and anatomical frameworks.

Keywords: *Archaeopteryx*, hypothetical stages, flight origins, pectoral girdle, Ostrom

INTRODUCTION

The origin and early evolution of birds and flight are one of the most debated topics on evolutionary biology. By the 1970 and 1980 decades the work of several authors, but most notably the contributions by John Ostrom (1928–2005), were essential to the building of the modern theory of bird origins (Witmer, 2002). In 1976, Ostrom published a detailed comparison between the early bird *Archaeopteryx lithographica* and the extant New World vulture *Cathartes aura*, entitled "Some hypothetical anatomical stages in the evolution of avian flight". In this contribution he speculated about the anatomical transformations and evolutionary steps in the shoulder girdle and forelimb during avian evolution, taking *Archaeopteryx* as the "starting point" of this sequence of evolutionary changes. Ostrom offered ideas about range of movements and function of limb elements in *Archaeopteryx*. He gave special importance to the modifications of the dinosaurian "biceps tubercle" (homologous with the modern avian acrocoracoid process) and its direct relation with the course of one of the main wing elevators, the *m. supracoracoideus*. Ostrom clearly

demonstrated the absence in *Archaeopteryx* of such anatomical and functional adaptations, considering this taxon as representative of a “pre-flying stage”. Within this interpretive framework Ostrom also recognized a series of “hypothetical stages” in the transformation of the pectoral girdle between the ancestral stage, as represented by *Archaeopteryx*, and the highly modified girdle of living flying birds.

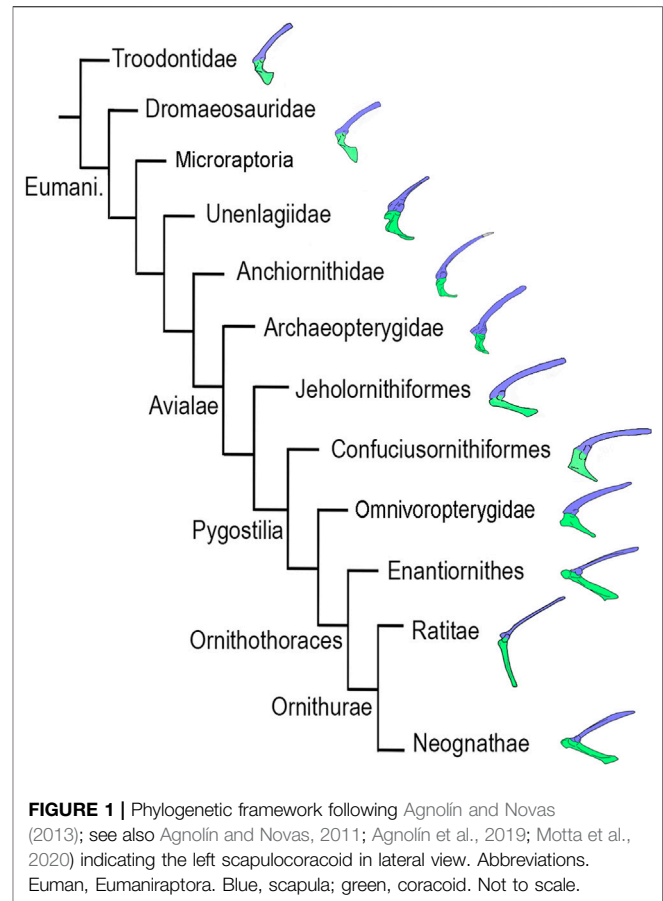
More than four decades have passed since Ostrom’s seminal contribution, and a lot of novel anatomical, biomechanical, and phylogenetic information on extinct and extant theropods has become available. Further, in the last decades the number of bird-like theropods and basal birds has dramatically increased (Witmer, 1991; Witmer, 2002; Chiappe and Vargas, 2003; Xu et al., 2014; Brusatte et al., 2015; Cau et al., 2017).

The aim of the present paper is to emphasize the anatomical similarities of some key features of the pectoral girdle in basal paravians, basal avialans and extant flightless paleognaths. Specifically, comparisons are detailed with the Greater Rhea (*Rhea americana*), and we provide a brief description of its musculature with the goal of comparing it with the inferred musculature of basal paravians. The shoulder girdle of large secondarily flightless paleognaths like *R. americana* may have partially converged on the condition of primarily flightless theropods, and indeed our comparison finds features, like the locations of muscle attachment sites and gross morphology of the bones, that can easily be interpreted in the light of the Greater Rhea. With all this information at hand we briefly re-analyze here the “hypothetical stages” in the acquisition of bird flight as originally proposed by Ostrom.

MATERIAL AND METHODS

Phylogenetic Framework

We follow the phylogenetic framework proposed by Agnolín and Novas (2013); (see also Agnolín and Novas, 2011; Agnolín et al., 2019; Motta et al., 2020) in which Deinonychosauria is interpreted as a non-monophyletic group, and Dromaeosauridae is formed by *Velociraptor*, *Dromaeosaurus*, *Deinonychus*, and taxa more closely related to them than to *Microraptor*, *Unenlagia*, *Rahonavis* or *Archaeopteryx*. *Microraptor* and *Unenlagiidae* are interpreted to form successively closer relatives of the clade Avialae (Figure 1). The clade Scansoriopterygidae is excluded from Paraves following Agnolín and Novas (2013); (see also O’Connor and Sullivan, 2014). The paravian clade including Dromaeosauridae and Avialae, but not Troodontidae, is termed Eumaniraptora (see discussion in Padian et al., 1999). Our interpretative scheme about the phylogenetic relationships among basal paravians departs from others (e.g., Norell and Clarke, 2001; Makovicky et al., 2005; Xu and Kim, 2011; Turner et al., 2012; Gianechini et al., 2017; Lefèvre et al., 2017; Pei et al., 2017; Hartman et al., 2019; Cau, 2020; Pei et al., 2020) in that we propose that Troodontidae, Dromaeosauridae, *Microraptor*, *Unenlagiidae* and *Anchiornithidae* form successively closer relatives of Avialae. We choose to follow this scheme, because a detailed overview of other phylogenetic analyses (e.g., TWIG) resulted in



poorly resolved phylogenetic relationships among derived paravians (Agnolín et al., 2019).

In the present contribution we do not include the basal bird clade Jinguoortidae, as represented by *Jinguoortis* and *Chongmingia* (Wang et al., 2016; Wang et al., 2018), because the reconstructions and interpretations on the pectoral girdle in both genera are problematic. This is due to the incomplete and bidimensional preservation of the specimens.

We also do not include detailed analysis of the scapulocoracoid morphology of *Jeholornis*. Since its discovery, the coracoid of *Jeholornis* has been usually described as robust and strut-like (Zhou and Zhang, 2003a), but the deformation of the available specimens makes recognition of several anatomical features very difficult. Due to the differential preservation of each available coracoid (Wang et al., 2020), the recognition of anatomical details is not certain.

The pectoral girdle of flightless paleognaths was considered the best living analog to compare with the anatomy of extinct paravians (Feduccia, 1986; Novas et al., 2020). We will pay special attention to those morphological traits of flightless paleognaths that look closer to early diverging paravians than to flying avians. We are aware, however, that these birds are secondarily flightless, being descendants of flying avian ancestors (Yonezawa et al., 2017; Sackton et al., 2019), and that flightless paleognaths are sharply distinguished from the remaining avians (as well as from extinct early diverging paravians) in several anatomical traits. It is

clear to us that, regardless of which pennaraptoran phylogenetic tree is followed, the osteological similarities between *Rhea* and basal paravians (e.g., *Buitreraptor*, *Archaeopteryx*) are analogous, and not strict homologies. In any case, the *Rhea* shoulder girdle (see Novas et al., 2020) joins models previously studied by several authors (Dial et al., 1991; Baier et al., 2007), and we believe that we cannot ignore the information yielded by the anatomy of this bird and its possible implications on the origin of flight.

Nomenclature

The anatomical nomenclature follows Baumel et al. (1993) and the abbreviations used in the text are as follows: m (musculus), mm (musculi) and p (pars). Because the “coracoid tuberosity” or “biceps tubercle” in theropods is considered by most authors as homologous with the modern avian “acrocoracoid process” (Ostrom, 1976), we only employ the latter term throughout the text.

We follow Jasinowski et al. (2006) in that the *m. coracobrachialis brevis* is a homologue to the *m. coracobrachialis cranialis*.

We use the form Unenlagiidae (Agnolín and Novas, 2011, 2013; Motta et al., 2020) instead of the form Unenlagiinae that has been employed by several authors (Makovicky et al., 2005; Turner et al., 2007; Turner et al., 2012; Brusatte et al., 2015; Cau et al., 2017; Rahut et al., 2018; Pei et al., 2020). The name Dromaeosauridae is instead restricted to the paravian Laurasian clade including *Dromaeosaurus* but not *Passer* and *Troodon* (see Agnolín et al., 2019). The Late Cretaceous Malagasy taxon *Rahonavis ostromi* (Forster et al., 1998) is here considered outside of Dromaeosauridae, following recent interpretations (e.g., O'Connor et al., 2011; Agnolín and Novas, 2013; Godefroit et al., 2013; Lefèvre et al., 2017; Novas et al., 2018; Motta et al., 2020).

Scapulocoracoid Position

The discussion on the position of the pectoral girdle in extinct theropods has not been continued since Senter (2006). Despite the lack of agreement, and the sake of clarity and for comparative purposes, we opt to place paravian scapulocoracoids with the scapular blade oriented in an almost horizontal position, with a slight ventral inclination of its anterior extremity, in a way similar to what is seen in living flying birds.

Data Collection

The specimens of *Rhea americana* were not stored for more than six months, and only those muscles and body parts that were in good condition were considered for the study. Before the dissection, each specimen was defrosted in the fridge (4–5°C). We dissected the wing muscles of both sides. The wing muscle data was available in two specimens (MACN-Or 9428, 9583). Following a classical anatomical approach of describing wing musculature, we removed each muscle and documented the origin and insertion sites of principal muscles of the shoulder girdle that originated on the acrocoracoid process, as well as their general features and appearance. We manipulated the muscles in order to observe the movement ratios in the wing.

Institutional Abbreviations

IVPP, Institute of Vertebrate Paleontology and Paleoanthropology, Beijing, China; MACN-Or, Museo Argentino de Ciencias

Naturales Bernardino Rivadavia, sección Ornitología, Buenos Aires, Argentina; MPCA, Museo Provincial Carlos Ameghino, Cipolletti, Río Negro, Argentina; MPCN-PV, Museo Provincial de Ciencias Naturales, General Roca, Río Negro, Argentina.

Anatomical Abbreviations

Acr pr, acromion process; acroc pr, acrocoracoid process; acroc-acr lig, acrocoraco-acromial ligament; BB, *m. biceps brachii*; CBB, *m. coracobrachialis brevis*; CBCr, *m. coracobrachialis cranialis*; corac f, coracoid foramen; fur, furcula; gl, glenoid; h, humerus; P, *m. pectoralis*; post cor pr, posterior coracoid process; pro pr, procoracoid process; SC, *m. supracoracoideus*; sc canal, supracoracoid canal; trioss canal, triosseal canal.

RESULTS

Elsewhere (Novas et al., 2020) we preliminarily analyzed the pectoral girdle and forearm of extant non-tinamid paleognaths, emphasizing some similarities with early diverging paravians (i.e., *Archaeopteryx*, *Buitreraptor*). Main similarities concern the subvertical orientation of the glenoid cavity and poor development of acrocoracoid process, which may reflect similar postural activities of the forelimbs not only in paravians, but also in non-avian pennaraptorans. We present here a summary description of the main muscle masses of the shoulder girdle of the Greater Rhea (*Rhea americana*), specifically those muscles that originate on the coracoid and acrocoracoid (i.e., *mm. pectoralis*, *supracoracoideus*, *biceps brachii*, and *coracobrachialis cranialis*), also constituting the most important muscles for the movement of the wing.

Myology of the Shoulder Girdle of the Greater Rhea (*Rhea americana*)

M. pectoralis (P, **Figure 2**). In *Rhea* this muscle has only one belly as it also occurs in some specimens of *Struthio* and most neognaths (Jasinowski et al., 2006). This muscle has a fleshy origin on the anterolateral surface of coracoid. In accordance with Beddard (1898) and Lowe (1928), the origin of the *m. pectoralis* in *Rhea* does not reach the sternum or the ribs, a condition contrasting with the notable expansion of the *m. pectoralis* in tinamous and neognaths (Baumel et al., 1993; Jasinowski et al., 2006; Suzuki et al., 2014).

The function of the *m. pectoralis* in *Rhea* is to protract and abduct the arm, when the wing is unfolded. This function is similar to that in *Struthio* (Jasinowski et al., 2006), but it is different from neognaths in which the *m. pectoralis* is the main adductor and depressor of the arm (Raikow, 1985; Dial, 1992; Baumel et al., 1993). Ostrom (1976) indicated that the *m. pectoralis* in “Carinatae” birds is the main adductor/depressor of the humerus during flapping flight, and the same function was inferred for *Archaeopteryx*. Based on information afforded by *Rhea*, we believe that *m. pectoralis* in *Archaeopteryx* also played a role of protractor and adductor of the arm.

M. supracoracoideus (SC, **Figure 2**). In *Rhea* this muscle is fleshy and fan-shaped, originating on the medial portion of the

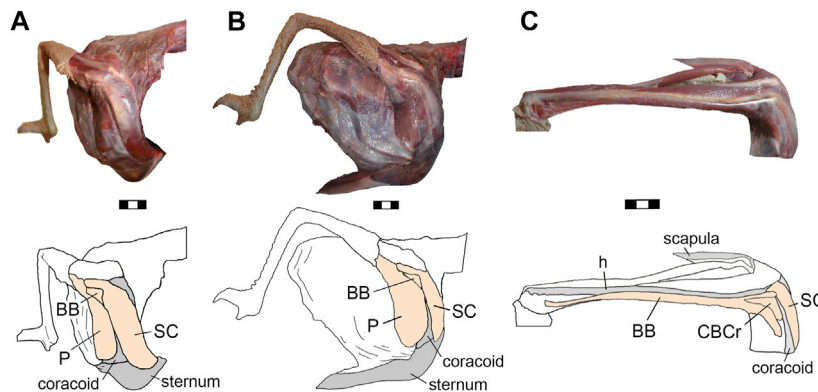


FIGURE 2 | *Rhea americana*, photographs and schematic drawings of selected muscles of right shoulder girdle in anterolateral (A) and lateral (B) views, and proximal humerus in lateral (C) view. Abbreviations: h, humerus; BB, *m. biceps brachii*; CBCr, *m. coracobrachialis cranialis*; P, *m. pectoralis*; SC, *m. supracoracoideus*. The bones were shaded in gray and the muscles in orange. Scale bars 3 cm.

anterior surface of the coracoid, on the *processus procoracoideus*, on the coracoid membrane [homologous with the sternocoracoclavicular membrane of neognaths, according to Baumel et al. (1993) and Livezey and Zusi (2007)], and on the small cranial area of the sternum (close to the sternal-coracoidal articulation).

In specimen MACN-Or 9428 of *Rhea americana* the origin area of the *m. supracoracoideus* is smaller than in other individuals and lacks contact with the sternum, suggesting that this muscle has considerable intraspecific variation. In other paleognaths, like *Struthio* and *Dromaius*, the area of origin of the *m. supracoracoideus* only includes the coracoid (Jasinoski et al., 2006; Maxwell and Larsson, 2007), while in extant flying birds the origin is variable but large, usually including the ventral surface of the sternum, the lateral and basal part of the sternal carina, the lateral margin of the furcula, the sternocoracoclavicular membrane, the medial portion of the coracoid and the *processus procoracoideus* (Baumel et al., 1993; Jasinoski et al., 2006; Suzuki et al., 2014; Lo Coco et al., 2020).

In *Rhea*, the *m. supracoracoideus* runs through the supracoracoideus canal and inserts as a tendon on the dorsal and proximal end of the humerus. In *Struthio*, the insertion of the *m. supracoracoideus* instead is more anteriorly located on the humerus (Jasinoski et al., 2006) while in neognaths the tendon of the *m. supracoracoideus* inserts into the proximal end of the *crista deltopectoralis* (Baumel et al., 1993).

The *m. supracoracoideus* of *Rhea* protracts the humerus and barely elevates it (Novas et al., 2020). In *Struthio*, this muscle protracts the humerus (Jasinoski et al., 2006), while in neognaths and tinamids this muscle is the main elevator of this bone (Raikow, 1985; Dial, 1992; Suzuki et al., 2014). The rotation of the humerus, as occurs in neognathan birds (Dial et al., 1991), has not been observed in *Rhea*. Ostrom (1976) originally inferred for *Archaeopteryx* that the *m. supracoracoideus* produced abduction, a conclusion that is in agreement with the protractor role of this muscle in extant non-tinamid paleognaths.

M. biceps brachii (BB, Figure 2). In *Rhea*, this is a fusiform muscle that has two well-differentiated bellies from its origin

(Lowe, 1928). One belly is tendinous and originates on the *processus acrocoracoideus* of the coracoid, while the other belly is fleshy and originates on the lateral edge of the coracoid (Lowe, 1928). In most neognaths the *m. biceps brachii* also has two bellies with double origins, although in *Rhea* the double origin is present on the coracoid but not on the proximal end of the humerus, like other extant non-tinamid paleognaths (George and Berger, 1966; McGowan, 1982; Jasinoski et al., 2006).

In *Rhea*, the two bellies of the *m. biceps brachii* become fused close to the proximal humerus, and have a strong contact with the skin and the *crista deltopectoralis*. The insertion is double and tendinous into the proximal end of the radius and the ulna, as in most of the neognaths and tinamids (McGowan, 1982; Baumel et al., 1993; Picasso and Mosto, 2018; Lo Coco et al., 2020) but different than *Struthio* (Jasinoski et al., 2006) and *Dromaius* (Maxwell and Larsson, 2007).

The function of the *m. biceps brachii* in *Rhea* is to flex the forearm as in *Struthio* and neognaths (Baumel et al., 1993; Jasinoski et al., 2006). Nevertheless, in *Rhea*, this muscle also abducts and protracts the arm, similar to *Struthio* in which the *m. biceps brachii* protracts the arm to a small degree (Jasinoski et al., 2006). Ostrom (1976) hypothesized for *Archaeopteryx* that the *m. biceps brachii* was a primary flexor of the forearm, but based on extant non-tinamid paleognaths we also hypothesize that it acted to abduct and protract the arm.

M. coracobrachialis. In *Rhea*, only a single belly (i.e., *p. cranialis*, CBCr, Figure 2) of *m. coracobrachialis* is present. This is in congruence with observations in other flightless paleognaths (McGowan, 1982; Jasinoski et al., 2006), but contrasting with neognaths and tinamids in which both *p. cranialis* and *p. caudalis* are present (Hudson et al., 1972; Baumel et al., 1993; Jasinoski et al., 2006; Suzuki et al., 2014). The *m. coracobrachialis cranialis* is a fusiform muscle that originates from the subglenoid fossa (lateral subtriangular area of the omal end of the scapulacoracoid, ventral to the glenoid cavity) and associated tendinous tissue. The insertion is located in a wide area between the *crista deltopectoralis* and the *crista*

bicipitalis of the humerus, similar to the condition present in *Struthio* (Jasinowski et al., 2006). This contrasts with the smaller insertion area observed in neognaths (Baumel et al., 1993; Picasso and Mosto, 2018; Lo Coco et al., 2020).

The function of the *m. coracobrachialis cranialis* in *Rhea* is to protract and adduct the humerus. In *Struthio* and in neognaths the *m. coracobrachialis cranialis* protracts the humerus (Jasinowski et al., 2006). Ostrom (1976) interpreted the *m. coracobrachialis p. cranialis* in *Archaeopteryx* as a primary extensor of the humerus, a role that is in agreement with the protractor role documented in extant non-tinamid paleognaths.

The *m. deltoideus minor* was not observed during the dissection of *Rhea*, in congruence with other non-tinamid paleognaths (Beddard, 1898; Lowe, 1928; McGowan, 1982; Jasinowski et al., 2006). Because this muscle is also absent in crocodiles (Jasinowski et al., 2006) but present in tinamids (Suzuki et al., 2014) and neognaths (Baumel et al., 1993; Picasso and Mosto, 2018; Lo Coco et al., 2020), we assume that it was probably not present in basal paravians and basal birds, and thus, it is not included in present analysis.

DISCUSSION

Ostrom paid attention to the strong anatomical differences between *Archaeopteryx* and the skillful flyers among extant birds. Moreover, no recognized taxon was known in the 1970s to be evolutionarily intermediate between *Archaeopteryx* and birds of modern aspect (e.g., *Ichthyornis*). In the last 40 years, but especially the last 20, the diversity of birds phylogenetically intermediate between *Archaeopteryx* and living birds has considerably expanded, with recognition of many different and speciose new clades (e.g., Jinguoformidae, Jeholornithiformes, Confuciusornithidae, Omnivoropterygidae, Enantiornithes). Also important is the discovery of different non-avian paravian taxa which closely resemble the pectoral morphology of *Archaeopteryx* (i.e., *Buitreraptor*, *Sinornithosaurus*, *Microraptor*), thus indicating that any functional conclusion arrived for *Archaeopteryx* may be also extrapolated for the remaining basal avianraptorans. A third aspect is that the information on postural activities of the wings in flightless paleognath birds has to be taken into account now to discuss the anatomical transformations that may have occurred at early stages of the evolution of flight.

Current knowledge of Mesozoic bird anatomy invites a review of Ostrom's ideas on the evolutionary changes that have occurred in the pectoral girdle from the time of *Archaeopteryx* to extant birds.

Origin of the *M. Supracoracoideus* Pulley

The *m. supracoracoideus* is one of the most important elevator muscles of the wing in extant flying birds (Dial et al., 1991; Mayr, 2017). This muscle arises from the dorsal part of the sternal carina and adjacent body of the sternum. The tendon of the *m. supracoracoideus* passes dorsally through the triosseal canal and inserts on the proximal portion of the dorsomedial surface of humerus (Lowe, 1928). This deflection of the *m.*

supracoracoideus in extant flying birds is due to the well-developed acrocoracoid process, which projects antero-dorso-medially and is located above the level of the glenoid cavity.

Ostrom (1976) proposed that in *Archaeopteryx* the *m. supracoracoideus* must have depressed and adducted laterally the wing because the biceps tubercle (= acrocoracoid process) was much less developed and located well below the level of the glenoid cavity. His main conclusion was that in *Archaeopteryx* the *m. supracoracoideus* acted as a wing depressor, different from its elevator role in living flying birds. Based on comparisons between *Archaeopteryx* and *Cathartes*, Ostrom masterfully hypothesized that the evolutionary elongation of the acrocoracoid process progressively changed the path of the tendon of the *m. supracoracoideus*, modifying its role from a depressor to an elevator of the wing.

We concur with Ostrom in the main conclusions, but some considerations have to be made regarding with the origin of this pulley for the *m. supracoracoideus*, as well as the evolutionary trends of the coracoid in general and the acrocoracoid process in particular, in birds that are closer to the crown than *Archaeopteryx*.

First, the shape, orientation and relative size of the acrocoracoid process in *Archaeopteryx* do not represent an avialan autapomorphy, but a similarly constructed acrocoracoid process is also present in other paravians such as *Buitreraptor*, *Saurornitholestes* and *Microraptor*. In other words, *Archaeopteryx* does not represent an evolutionary "starting point" for this condition, because a closely similar coracoid evolved prior to avian origins. The kind of acrocoracoid process present in *Archaeopteryx* and closely related taxa (*Buitreraptor*, *Saurornitholestes* and *Microraptor*), albeit small with respect to more derived birds, is notably larger when compared with more basal theropods (e.g., ornithomimosaurs, tyrannosauroids, therizinosauroids; Agnolín and Novas, 2013). That means that at the base of Paraves the *m. supracoracoideus* anteriorly protracted the humerus, which was somewhat different from the action performed in early diverging archosaurs (i.e., crocodiles) and retained in basal coelurosaurs, in which the humerus is anteroventrally protracted. In other words, the common ancestor of Paraves (or possibly, Pennaraptora), evolved a large *m. supracoracoideus* with an anteriorly protractive function. This indicates that basal paravians (or more inclusively, pennaraptorans) attained a cranially increased range of movements of their forelimbs compared with non-pennaraptoran theropods. Despite this increase in protracting capabilities (presumably allowing reaching items in front of the animal), we are unable to identify any function of the *m. supracoracoideus* for flying activities.

Manipulation of *m. supracoracoideus* in *Rhea* (Lowe, 1928; Novas et al., 2020) shows that its contraction protracts the humerus, thus supporting Ostrom's interpretation for *Archaeopteryx* and early diverging avialans. Ostrom considered *Archaeopteryx* as representing a pre-flight stage in bird evolution, and the inferred action of the *m. supracoracoideus* is in accordance with his view.

The interesting point here is that three successive clades of early avialans with well-developed wings, Jeholornithiformes,

Confuciusornithidae and Omnivoropterygidae, show a coracoid shape that does not fit with the sequence of progressive transformations expected in Ostrom's hypothetical stages: on the contrary, the coracoids of omnivoropterygids are subquadrangular and notably wide, and those of jeholornithiforms are proportionally much longer than confuciusornithids and omnivoropterygids. Curiously, jeholornithiforms show a coracoidal shape that superficially resembles the strut-like condition of the phylogenetically distant ornithothoracine birds. This indicates that coracoidal evolution and shape at the base of avian tree was more diverse than thought.

Also interesting is the fact that in Jeholornithiformes, Confuciusornithidae and Omnivoropterygidae (Zhou and Zhang, 2003a; Zhou and Zhang, 2003b; Chiappe and Meng, 2016) the acrocoracoid process, albeit more prominent than in *Archaeopteryx* and other basal paravians, still retained a lower position with respect to the glenoid cavity, indicating that the path of the *m. supracoracoideus* was not modified substantially with respect to more basal paravians, but still acted as a humeral protractor. In birds more derived than *Archaeopteryx*, *Confuciusornis* and *Sapeornis*, the coracoid instead became strut-like and the acrocoracoidal process became even more elongate and related with a very deep supracoracoid canal (Mayr, 2017).

Another aspect to be considered concerns the formation of the triosseal foramen and its function. In *Buitreraptor* (MPCA-245; MPCN-PV-598) and *Archaeopteryx* the cranial surface of the coracoid, between the acrocoracoid process and the medial coracoidal margin, exhibits a deep transverse concavity (Novas et al., 2018). This dorsoventral groove is suggestive of a deep canalization of the belly of the *m. supracoracoideus*. The cranial concavity on the coracoid of *Buitreraptor* is in concert with similar modifications on the proximal end of the scapula, from which the acromial process also projects cranially, thus defining a trough on the lateral surface of the proximal scapula (Novas et al., 2018). This trough on the cranial surface of the scapulocoracoid of *Buitreraptor* may represent an initial stage of the formation of the supracoracoidal canal of more derived birds. This suggests a change in anatomy and function of the *m. supracoracoideus* at the base of Eumaniraptora (in contrast, in more basal coelurosaurs the outer surface of the scapulocoracoid is flattened or slightly convex, and such a canal is absent).

In *Rhea* the furcula is lacking and consequently a triosseal canal is absent. However, a supracoracoid canal does exist, being delimited by the acromion process, the acrocoracoid process, and a strong acrocoraco-acromial ligament which connects the acrocoracoidal and acromial processes. The acrocoraco-acromial ligament forms a bridge under which the *m. supracoracoideus* slides. This ligament is also present in modern flying birds, but it is cranially covered by the omal end of the furcula. Ultimately, the foramen through which the tendon of the *m. supracoracoideus* slides is basically the same (and homologous) in both flying and flightless living birds, with the only distinction of the presence or absence of a bony enclosure by the furcula. We suspect that an acrocoraco-acromial ligament

was already present in basal Eumaniraptora, in congruence with the presence of a deep supracoracoidal groove on the cranial surface of the coracoid and the proximal end of the scapula.

Rhea shows a path of the *m. supracoracoideus* tendon that is not present in flying birds. In dorsal view, the coracoid of *Rhea* exhibits a “coracoidal plate” between the glenoid and the acromion process (Figure 3E, portion of the coracoid in red color). This “coracoidal plate” delimits the path of the supracoracoid tendon. In this way, the *m. supracoracoideus* originates at the anterior surface of the coracoid and passes through the supracoracoid canal (homologous to the “triosseal canal”), and finally inserts dorsally into the proximal humerus. This results in movements of the wing that are different from flying birds, because when the *m. supracoracoideus* is contracted, it produces an anterior shift of the wing, contrasting with the dorsal movement of the wing in flying birds where the triosseal canal is well developed. In extant volant birds the triosseal canal opens ventrally and medially to the glenoid (Figure 3F); due to the absence of the “coracoidal plate” the path of the *m. supracoracoideus* runs dorsally (Ostrom, 1976), and not posteriorly as occurs in *Rhea*.

Previous observations lead to the following considerations: the triosseal canal, in the way it is defined by the bony encounter of furcula, scapular acromium and coracoidal acrocoracoid, was absent in *Buitreraptor* and *Archaeopteryx*. Nevertheless, the trough present on the cranial surface of the coracoid and the proximal end of the scapula suggests that: 1) an acrocoraco-acromial ligament connecting the acrocoracoidal and acromial processes was probably present in basal Eumaniraptora; and 2) the *m. supracoracoideus* changed its course running through the supracoracoid canal.

As a corollary of these observations, we must conclude that the change in course of the *m. supracoracoideus* in early paravian evolution did not require the presence of a proper triosseal foramen. It is feasible that as the supracoracoidal sulcus became deeper and its orientation changed from anterodorsal (basal paravians and basal birds) to medial (extant flying birds), the function of the *m. supracoracoideus* changed from protractor to protractor-elevator of the humerus.

In Enantiornithes a true triosseal canal and foramen are not complete. As indicated by reconstructions of the pectoral girdle (Martin, 1995; Mayr, 2017), in Enantiornithes the omal extremity of the furcula articulated with the tip of the acromion of the scapula but the coracoid lacked a bony contact with the furcula. This lack of contact was due to the straight and cranially projected acrocoracoid, different from the hook-like, anteromedially curved acrocoracoid process of extant flying birds. This hook-like process creates a bony contact with the furcula, thus participating in the cranial enclosure of the triosseal canal. It is unknown whether non-carinate birds with a strut-like coracoid possessed a cartilaginous medial prolongation of the simple acrocoracoid process for contacting the furcula.

The basal euornithines *Apsaravis* and *Patagopteryx* (Chiappe, 2002; Clarke and Norell, 2002) also show a similar groove on the proximal end of the scapula, suggesting a similar path of the supracoracoid pulley as that present in enantiornithine birds. In this way, Enantiornithes and probably the basalmost euornithines

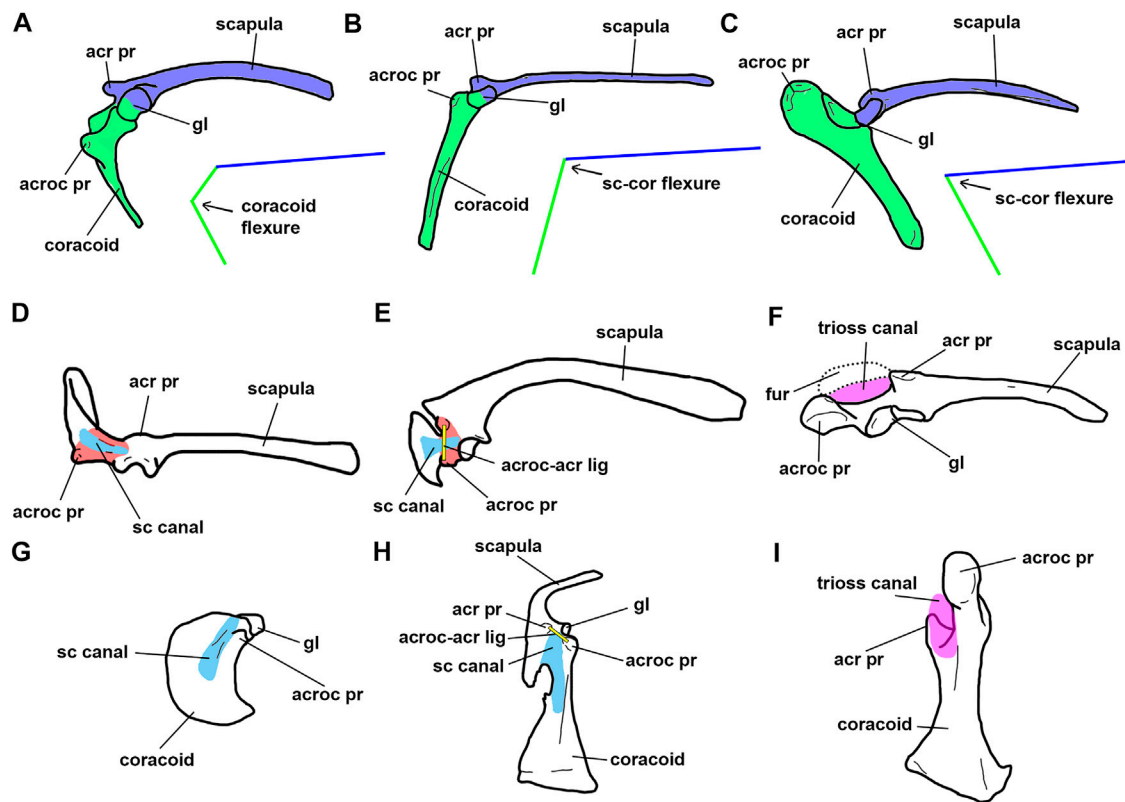


FIGURE 3 | Selected paravian scapulocoracoid in lateral (A–C), dorsal (D–F) and anterior (G–I) views. (A, D, G): *Archaeopteryx lithographica*; (B, E, H), *Rhea americana*; (C, F, I), *Vultur gryphus*. Abbreviations. acr pr, acromion process; acroc pr, acrocoracoid process; acroc-acr lig, acrocoraco-acromial ligament; fur, furcula; gl, glenoid; sc canal, supracoracoid canal; trioss canal, triosseal canal. Blue, scapula; red, coracoid; green, coracoid; light blue, supracoracoid canal; yellow, acrocoraco-acromial ligament; violet, triosseal canal. Not to scale.

had flight mechanics that were different from extant birds (Mayr, 2017).

Classically, the triosseal canal was interpreted as a pulley that deflected the tendon of the *m. supracoracoideus*, such that this muscle became the primary humeral elevator/supinator in the upstroke. However, the path of the supracoracoideus tendon is already deflected in basal paravians by virtue of the presence of a supracoracoid canal. Despite the fact that the triosseal canal of modern birds is the result of the cranial closure of this sulcus, the strong deepening of the canal is the main responsible factor for the change in orientation of the supracoracoideus tendon in neognaths (Figures 3E–H). Mechanically, the supracoracoid sulcus acted almost in the same way with or without the cranial closure by the furcula.

It is possible that the change in the orientation of the *m. supracoracoideus* is mostly the result of the deepening and orientation of the supracoracoid canal, in a way that the muscle tendon changed from tangential to perpendicular to the margin of the glenoid cavity. In fact, it seems that the change in pull direction of this muscle is related with the inclination of the greater axis of the glenoid: in forms with a glenoid cavity that is aligned with the main axis of the scapula, the pull direction of the *m. supracoracoideus* is tangential to the glenoid; in contrast, in those birds in

which the glenoid is subhorizontal, the pull of the *m. supracoracoideus* is perpendicular to the long axis of the glenoid. This change in orientation of the glenoid cavity apparently occurred at the Ornithothoraces node, and resulted in the main difference in humeral movements from mainly protraction in non-ornithothoracine birds to mainly elevation in ornithothoracines (Agnolín et al., 2019; Novas et al., 2020).

In Ornithothoraces the dorsal elongation of the acrocoracoid increased the origin of the *mm. biceps brachii*, *coracobrachialis cranialis* and, probably, *deltoideus minor*. In addition, the acrocoracoid process also offered attachment for the *ligamentum acrocoracohumerale*, which connects the coracoid with the transverse sulcus of the proximal end of the humerus and replaced the plesiomorphic muscle-based system which prevented humeral ventral dislocation (Baier et al., 2007).

In sum, it is here hypothesized that the action of the *m. supracoracoideus* was at first modified with the definition of the supracoracoid canal (in early paravians), and that the capacity for rapid rotation (elevation and supination) of the humerus was acquired later in avian history (probably at the base of Ornithothoraces) with the rotation of the glenoid cavity involving the increase in size of the *m. supracoracoideus* (as expressed by the formation of a keeled sternum; Mayr, 2017).

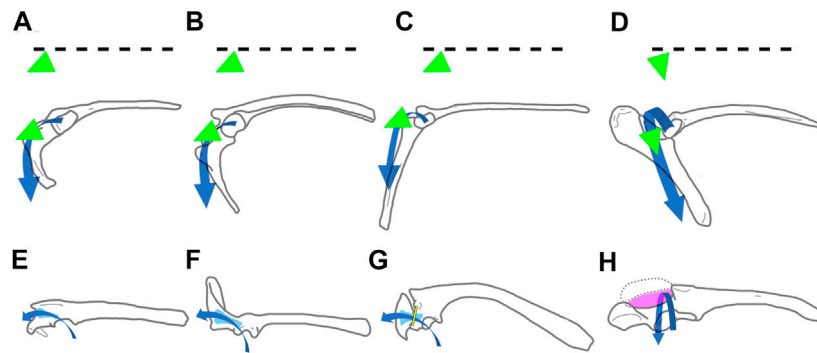


FIGURE 4 | Right scapulocoracoid of selected paravians in lateral (A–D), and dorsal (E–H) views. (A, E), *Buitreraptor gonzalezorum*; (B, F), *Archaeopteryx lithographica*; (C, G), *Rhea americana*; (D, H), *Vultur gryphus*. The broken line indicates the main antero-posterior axis of the scapulocoracoid. Blue, path of the SC; green, first and main action vector of the SC; light blue, supracoracoid canal; yellow, acrocoraco-acromial ligament; violet, triosseal canal. Not to scale.

Changes in Glenoid Orientation

The morphology and orientation of the glenoid cavity apparently has utmost importance in the range of humeral (and then, wing) movements (Jenkins, 1993; Baier et al., 2007; Agnolín et al., 2019). Nevertheless, the effects of the inclination of the greater glenoid axis on wing posture remain poorly explored.

Basal paravians like *Saurornitholestes*, *Buitreraptor*, *Anchiornis*, and *Archaeopteryx* share a similar orientation of the scapular glenoid. One of the main distinctions from flying euornithines is the orientation of the glenoid cavity and the inclination of its major axis, being laterally faced and with a horizontal major axis in flying forms, and laterally facing and with a subvertical major axis in basal paravians. The glenoid cavity in *Rhea*, as in other flightless paleognaths, faces laterally, and its main axis is subvertically oriented (MACN-Or 9428, 9583). In *Rhea* the subvertical orientation of the major axis of the glenoid almost restricts humeral abduction-adduction movements and allows movements in an anteroposterior direction to be more prevalent (Agnolín et al., 2019; Novas et al., 2020). In flightless paleognaths the position of the pectoral girdle “frame” is closer to that of a basal archosaur, rather than a flying euornithine. Morphological similarities among living non-tinamid paleognaths and basal paravians suggest resemblance in forelimb posture and range of movements (Figure 4).

In most theropods the scapular and coracoidal glenoid lips are prominent (Bakker et al., 1992). In basal theropods as *Syntarsus* and *Allosaurus* (Madsen, 1976; Raath, 1978) the scapular lip occupies a much more laterally salient position than the coracoidal lip, whereas in paravians as *Bambiraptor* and *Deinonychus* (Burnham et al., 2000; Ostrom, 1969, 1974) both lips are equally projected outwards. In contrast, in unenlagiids (e.g., *Buitreraptor*) and neognath birds (flying or flightless) the coracoidal lip laterally surpasses the level of the scapular one. Additionally, in basal birds (e.g., *Archaeopteryx*, *Confuciusornis*) the glenoid facet retained the lateral orientation seen in more basal paravians (e.g., *Buitreraptor*), and both sections (scapular and coracoidal) are subequal in size and aligned on the same dorsoventral plane. This lack of a “twisted” glenoid (that is,

without a large coracoidal surface that faces dorsally) suggests that basal birds had not yet attained the same amplitude of forelimb movements, nor the humeral trajectory over the glenoid, as that present in living flying birds (see Novas et al., 2020).

In *Rhea* the acrocoracoid process is poorly developed and separated from the glenoid cavity. A similar condition is present in most basal paravians (e.g., *Bambiraptor*, *Buitreraptor*, *Archaeopteryx*) and basal birds (*Sapeornis*, *Confuciusornis*), in which the acrocoracoid process is differentiated and well separated from the glenoid cavity. On the contrary, in extant flying birds the acrocoracoid process is strongly expanded and is adjacent to the glenoid cavity.

The rotation of the glenoid (from subvertical to horizontal) constitutes the main responsible factor for the range of humeral movements, thus accompanying the direction of the pull of the *m. supracoracoideus*. The dorsal elongation of the acrocoracoid was accompanied by the change in the orientation of the glenoid cavity, of which the cranial (coracoidal) half surpassed the size of the caudal (scapular) half, adopting a horizontal position, and came to be dorsally and slightly posteriorly oriented.

We hypothesize that the strong development of the acrocoracoid process may not be directly correlated with the change in the orientation of the *m. supracoracoideus*, but instead the full rotation of the glenoid cavity had a main role in the change of direction of the *m. supracoracoideus*.

Scapulocoracoid Flexure

In living volant birds the scapula and the coracoid articulate with each other, forming an acute angle (Figure 3C). This scapulocoracoid flexure is variable within a single taxon during ontogeny, and the angle between the main shafts of coracoid and scapula decreases during growth (Heers and Dial, 2012). Contrary, a higher angle (obtuse) between scapula and coracoid is observed in extant and extinct flightless birds, including non-tinamid paleognaths (Figure 3B; Olson, 1973; Livezey, 1989; Agnolín et al., 2019).

In basal paravians (e.g., *Deinonychus*, *Buitreraptor*, *Archaeopteryx*) the scapulocoracoid is remarkably “L”-shaped

when viewed from the side (Paul, 2002). However, in the case of *Buitreraptor* and *Archaeopteryx* this flexure is almost restricted to the coracoid (Figure 3A). In these cases, it is observed that at the level of the acrocoracoid process the coracoid has a strong posterior tilting resulting in an angle of more than 90°. A similar condition is present in basal birds, such as *Sapeornis* and *Confuciusornis*, although this angle is even more acute (Zhou and Zhang, 2003b; Wang et al., 2018). The condition of *Jeholornis* is difficult to discern, because the studied specimens of this avialan (IVPP V13274; IVPP V13553) preserve this bone in dorsal or ventral views, thus presence or absence of such a flexure is difficult to ascertain. In contrast to basal paravians, and more derived birds including Euornithes (e.g., *Rhea*, *Vultur*) and Enantiornithes (Walker and Dyke, 2009), the coracoid tends to be strut-like and lacks any sign of flexure (Figures 3B,C).

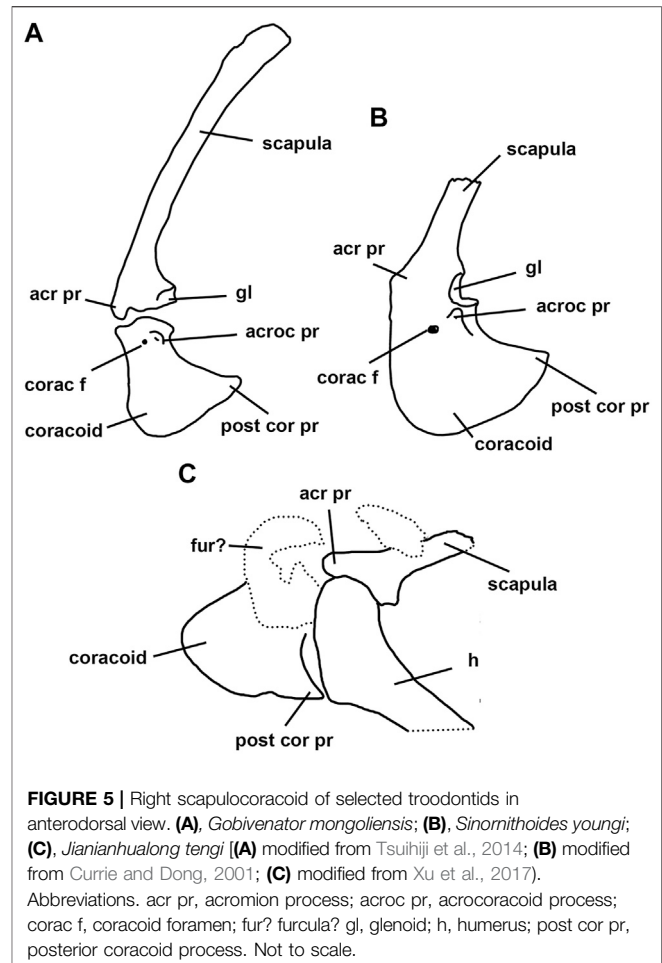
It is worth mention that the existence of an angled scapulocoracoid in basal paravians does not mean that the *m. supracoracoideus* acted exactly in the same way as in Euornithes. In basal paravians such as *Buitreraptor*, *Archaeopteryx*, and *Rhea*, the supracoracoidal canal does not reach the medial margin of the glenoid cavity because is not deep enough and the “coracoidal plate” is still relatively large (Figures 3D,E). In this case the supracoracoideus tendon runs anteriorly on the “coracoidal plate” before inserting into the humerus, and therefore its main action is to protract the humerus. In contrast, in extant flying birds and probably Enantiornithes, the supracoracoideus tendon attaches to the humerus from the medial aspect of the glenoid due to the development of the triosseal canal (Figures 3F,I). This part of the tendon of the *m. supracoracoideus* creates a pulley effect and elevates the humerus.

In whichever way the scapulocoracoid flexure is acquired (in the case of basal paravians due to coracoid tilting, and in the case of Enantiornithes and flying Euornithes by the increased angle between the scapular and coracoid main axes; Figure 3C), this results in an increase of the lever arm of the *m. supracoracoideus*. In this way, such an increase is not only related to the development of the acrocoracoid process, but also the result of the scapulocoracoidal angle.

Variability of Coracoid Morphology Among Basal Paravians

It is important to remark that both coracoid shape and the development of the acrocoracoid process are not uniform among basal paravians. The kind present in *Archaeopteryx* is closely similar to that of *Microraptor*, *Sinornithosaurus*, and *Buitreraptor*, but in *Bambiraptor* (Burnham et al., 2000) the coracoid is notably low and transversely wide, the acrocoracoid process is proportionally smaller than in the above mentioned taxa, and the cranial surface of the coracoid is convex, thus lacking a supracoracoid sulcus as in *Buitreraptor*, for example. This condition described for *Bambiraptor* is also found in all known troodontids, and possibly also occurs in the basal paravian *Anchiornis* (Figures 5, 6).

Remarkably, the troodontid scapulocoracoid lacks most derived features observed in other paravians. The scapulocoracoid of troodontids is completely preserved in a



number of taxa, including *Gobivenator*, *Sinornithoides*, *Mei*, and *Jianianhualong* (Russell and Dong, 1993; Currie and Dong, 2001; Xu et al., 2004; 2017; Tsuihiji et al., 2014; Figure 5).

The coracoid of *Gobivenator* lacks the coracoid flexure described above as typical for basal paravians (e.g., *Buitreraptor*, *Bambiraptor*, *Archaeopteryx*). In this way, the coracoid in troodontids is nearly straight or slightly convex in lateral view. Further, the outer surface of the coracoid lacks any sign of the supracoracoid sulcus present in other paravians.

In sum, basal dromaeosaurids (e.g., *Bambiraptor*) and troodontids lack some derived features that characterize Eumaniraptora, indicating that not all basal pennaraptorans had already evolved forelimb movements that were prerequisites for the acquisition of flight.

Muscle Changes

The *m. supracoracoideus* expanded its origin surface with the dorsoventral elongation of the coracoid, the development of osseous sternal plates and the later emergence of the sternal keel (Mayr, 2017), and by modifying the passage of the supracoracoidal tendon with the change of the depth and orientation of the supracoracoidal canal. Therefore, *m. supracoracoideus* changed its function by the evolutionary

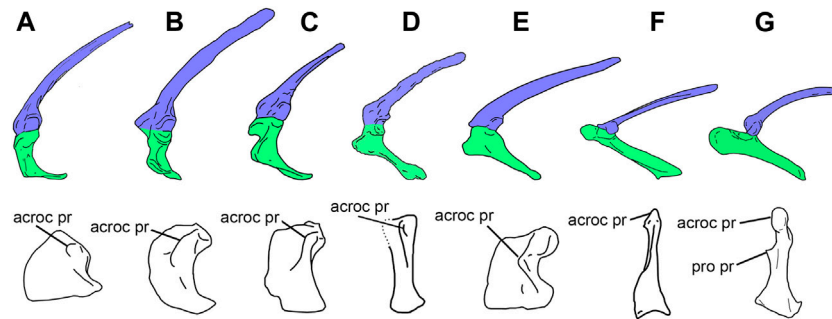


FIGURE 6 | Selected scapulocoracoids and coracoids from the left side in lateral (**top**) and anterolateral (**bottom**) views, showing variation in shape among basal paravians. (**A**), *Anchiornis huxleyi* (Pei et al., 2017); (**B**), *Archaeopteryx lithographica* (London specimen); (**C**), *Buitreraptor gonzalezorum*; (**D**), *Confuciusornis sanctus* (Chiappe and Meng, 2016; the anterolateral view is distorted in the original specimen, and thus, its reconstruction is uncertain); (**E**), *Sapeornis chaoyangensis*; (**F**), Enantiornithine bird (modified from Mayr, 2017); (**G**), *Vultur gryphus*. Scapula shaded in blue, coracoid shaded in green. Abbreviations. acroc pr, acrocoracoid process; pro pr, procoracoid process. Not to scale.

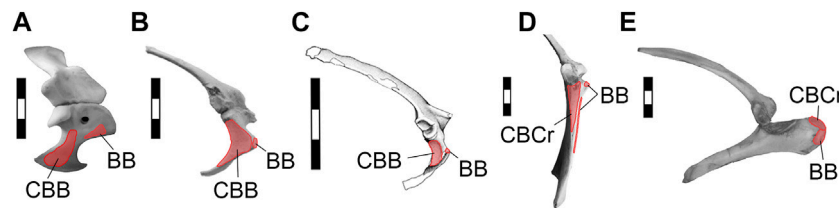


FIGURE 7 | Selected scapulocoracoids from the right side in lateral views, showing the *mm. biceps brachii* and *coracobrachialis* origins. (**A**), *Caiman latirostris*; (**B**), *Archaeopteryx lithographica* (London specimen); (**C**), *Buitreraptor gonzalezorum*; (**D**), *Rhea americana*; (**E**), *Vultur gryphus*. Abbreviations. BB, *m. biceps brachii*; CBB, *m. coracobrachialis brevis*; CBCr, *m. coracobrachialis cranialis*. Light red, muscle origins. Scale bars 3 cm.

modifications that happened in the groups of basal paravians and basal birds.

The *m. pectoralis* also increased its origin area with the expansion of the coracoid and the appearance of osseous sternal plates and the sternal keel. The *m. pectoralis* in basal coelurosaurs and basal birds has been interpreted as a humerus depressor (Ostrom, 1976; Nicholls and Russell, 1985; Jasinoski et al., 2006). Its function was also enhanced by coracoid flexion and/or the flexion between coracoid and scapula.

While the origin of the *m. biceps brachii* has been thought to lie on the top of the acrocoracoid process in basal coelurosaurs (Nicholls and Russell, 1985; Jasinoski et al., 2006) and basal birds (Ostrom, 1976), the origin of the *m. coracobrachialis cranialis* (= *brevis*) was wider on the area of the subglenoid fossa (Nicholls and Russell, 1985). It is interesting to note that although the subglenoid fossa varied in shape and area among basal paravians and basal birds, in these groups the *m. coracobrachialis cranialis* always occupied a caudoventral position to the origin of the *m. biceps brachii*. This condition is shared with *Rhea* but contrasts with the derived attachment seen in flying Euornithes, in which both, *mm. biceps brachii* and *coracobrachialis cranialis*, originate on the acrocoracoid process, the former being dorsal to the latter (Figure 7). The presence of a well-developed subglenoid fossa in the coracoid of *Confuciusornis* (Figure 6) indicates that the plesiomorphic location of the *m. coracobrachialis cranialis* was

retained by early pygostylians and contrasts with the derived attachment of the *mm. biceps brachii* and *coracobrachialis cranialis* present in tinamids and Neognathae (Figure 7).

Although we do not know with certainty the origin area of the *m. biceps brachii*, it was probably located at the tip of the acrocoracoid process in Eumaniraptora. In contrast, the *m. coracobrachialis cranialis* occupied the entire subglenoid fossa in non-avian eumaniraptorans. Thus, we hypothesize that this muscle had a larger area of origin than the one for the *m. biceps brachii* and, therefore, it could have presented greater volume and strength for humerus movements. This interpretation would indicate that *m. coracobrachialis cranialis* had a relevant role in protractor and depressor movements of the humerus and the wing in basal eumaniraptorans.

Implications for Ostrom's (1976) Hypothetical Stages

The main modifications during the transition among basal theropods and paravians include:

- 1) Transverse rotation of the whole scapulocoracoid toward an anterior position on the chest,
- 2) Reduction of the area of origin of the deltoid muscle (mirroring the reduction of the acromion),

- 3) Great development of the *m. supracoracoideus* (probably following the backward expansion of the coracoidal shaft),
- 4) Change in the course of the tendon of the *m. supracoracoideus* that became encased in a supracoracoidal canal,
- 5) Flexure of the scapulocoracoid, increasing the lever arm of the *m. supracoracoideus*.

It is interesting to note that all these modifications occurred prior to the acquisition of the novel glenoid cavity of flying euornithines, which is horizontally oriented and located laterally with respect to the reduced scapular lip.

We have to ask here: what the functional implications of the above enumerated modifications on the movement and posture of the forelimb in basal paravians were? We ignore the response, but all suggest that this set of evolutionary novelties were not related to flying capabilities.

Based on anatomical traits of the pectoral girdle, as well as field observations of non-tinamid paleognath behavior, the wings of non-tinamid paleognaths move predominantly in an anteroposterior direction, lacking the complex and largely dorsoventral wing excursion seen in living neognaths (see Novas et al., 2020). Because of the strong similarities in pectoral girdle structure between flightless paleognaths and basal avialans and paravians such as *Archaeopteryx* and *Buitreraptor*, it can be inferred that the main forelimb movements were from anterodorsal to posteroventral in the latter group. The primitive-looking pectoral girdle of *Archaeopteryx* is in agreement with other lines of evidence, including feather morphology and bone geometry (Feo et al., 2015; Mayr, 2017; Voeten et al., 2018), that suggest that flight capability was poor or absent (as originally advocated by Ostrom, 1976).

As indicated in a previous contribution (Novas et al., 2020), most discussions about flight origin assume that basal birds moved the wings like modern avialans. However, we think that as important as the wing range of motion is the orientation of the wing beat. As suggested by comparisons between *Rhea* and early paravians, the basal bird *Archaeopteryx* had a wing posture different from neognaths, with an arc of movement from anterodorsal to posteroventral, and a main wing surface that was posteroventrally oriented in maximum abduction (Voeten et al., 2018; Novas et al., 2020). This reconstruction of the wing posture suggests that this obliquely oriented wing surface may not have generated enough lift to allow these early birds to be airborne. This is not congruent with previous proposals on which early birds are inferred to be gliders with the wing surface subparallel to the ground (Beebe, 1915; Geist and Feduccia, 2000; Long et al., 2003; Xu et al., 2004; Zhou, 2004; Xu and Zhang, 2005; Longrich, 2006; Chatterjee and Templin, 2007; Hu et al., 2009; Alexander et al., 2010; Hone et al., 2010; Ruben, 2010).

The evolutionary stage represented by the basal pygostylians *Confuciusornis* and *Sapeornis* is functionally intriguing. *Confuciusornis* and *Sapeornis* exhibit enlarged wings of modern aspect, but their pectoral girdles retained the plesiomorphic morphology of more basal paravians, including the subvertical orientation of the major axis of the glenoid cavity and the lack of a “twisted” morphology, and the anteroventral position of the acrocoracoid process. If the basalmost

pygostylians *Confuciusornis* and *Sapeornis* were capable of flying, as their wings suggest, then they lacked the cycle of wing movements around the glenoid of extant flying birds. Reconstruction of the wing beat in these basal birds, with an archaic construction of their shoulder girdles, represents an exciting challenge that needs to be seriously discussed in the years to come.

CONCLUSION

Inspired by Ostrom (1976) research, we evaluated some key-features of pectoral girdle morphology that may have importance in the rise of bird flight.

Important selective forces occurred at the level of Pennaraptora, with modifications of the thorax as a whole and the shoulder girdle in particular, positioning the coracoids over the cranial margin of the sternum (Paul, 2002). The laterally oriented glenoid cavity indicates that pennaraptorans differ from more basal coelurosaurs in having evolved a cranial shift of humeral movements, in agreement with the increase in size of the acrocoracoid process (which mirrors the increase in size and cranial pulling of the *mm. coracobrachialis cranialis* and *biceps brachii*). Explaining the reasons for such modifications is difficult, and we feel unable to envisage relationships with postural activities of the forelimbs other than increased capabilities for hunting, fighting, grasping, etc., but not for flying, although they were antecedents of the avian flight stroke.

Among paravians, the plesiomorphic pectoral girdle morphology is retained by troodontids like *Gobivenator* which lack a scapulocoracoid flexure and supracoracoid groove. More birdlike pectoral girdle features are shared by other basal paravians (i.e., Eumaniraptora) including basal birds such as *Archaeopteryx*, *Confuciusornis* and *Sapeornis*, which exhibit a derived coracoidal flexure and a well-defined supracoracoid sulcus, but retain an acrocoracoid that slightly surpasses the level of the glenoid cranially, and still lack an osseous bridge enclosing the triosseal canal. This combination of features is absent in non-paravian theropods, including troodontids, suggesting that an important change in pectoral girdle anatomy occurred at the base of Eumaniraptora. Possibly, the supracoracoid tendon in eumaniraptorans was housed in a deep supracoracoid sulcus that was roofed by an acrocoraco-acromial ligament, similarly to extant non-tinamid paleognaths.

We found that the *m. supracoracoideus* was much more developed in paravians more derived than troodontids, and that the existence of the tendon of *m. supracoracoideus* was probably diagnostic of eumaniraptorans. It is possible that the change in orientation of this muscle, the most important elevator muscle of the wing in extant birds, occurred not only through the extension of the acrocoracoid process, as Ostrom originally proposed, but by the channeling of the supracoracoidal sulcus and later by the rotation of the glenoid cavity. The increase of the lever arm of the *m. supracoracoideus* may have been increased in tandem with the coracoidal flexure, which is strong in paravians as *Buitreraptor* and *Archaeopteryx*, and even more pronounced in basal birds like *Sapeornis* and *Confuciusornis* (Agnolín et al., 2019).

The shape of the pectoral girdle and orientation of the glenoid of basal eumaniraptorans (including dromaeosaurids, unenlagiids, *Archaeopteryx*) is difficult to interpret both morphologically and functionally. As indicated previously, these early paravians probably had a wing posture similar to that of flightless paleognaths, with an anterodorsal-to-posteroventral arc of movement, and a wing surface that was posteroventrally oriented in maximum abduction.

The triosseal canal, as defined on the basis of bony contacts, was acquired in euornithine birds, but a foramen for the passage of the *m. supracoracoideus* was probably operative earlier (probably at the base of Pennaraptora, as shown by oviraptorosaurs with a cranially turned, pencil-like acromial process of the scapula) and bounded by bone (the acrocoracoid process), ligaments (the acrocoraco-acromial ligament bridging above the *m. supracoracoideus*), and eventually cartilage (the procoracoid process of the coracoid and the proximal end of the furcula).

In ornithothoracine birds the coracoid became even more elongate and lost its internal flexure. However, in enantiornithes and basal euornithines a groove on the proximal end of the scapula probably served for the path for the tendon of the *m. supracoracoideus*. This condition is usually correlated with the absence of a true triosseal canal and foramen. The latter was probably acquired in more derived euornithines as clearly observed in basal forms such as *Yanornis* and *Ichthyornis* (Clarke, 2004).

REFERENCES

- Agnolin, F. L., Motta, M. J., Brissón Egli, F., Lo Coco, G., and Novas, F. E. (2019). Paravian Phylogeny and the Dinosaur-Bird Transition: an Overview. *Front. Earth Sci.* 6, 252. doi:10.3389/feart.2018.00252
- Agnolin, F. L., and Novas, F. E. (2013). *Avian Ancestors: A Review of the Phylogenetic Relationships of the Theropods Unenlagiidae, Microraptoria, Anchiornis and Scansoriopterygidae*. Dordrecht: Springer Science & Business Media, 1–96.
- Agnolin, F. L., and Novas, F. E. (2011). Unenlagiid Theropods: Are They Members of the Dromaeosauridae (Theropoda, Maniraptora)? *Acad. Bras. Ciênc.* 83 (1), 117–162. doi:10.1590/s0001-37652011000100008
- Alexander, D. E., Gong, E., Martin, L. D., Burnham, D. A., and Falk, A. R. (2010). Model Tests of Gliding with Different Hindwing Configurations in the Four-Winged Dromaeosaurid *Microraptor gui*. *Proc. Natl. Acad. Sci.* 107 (7), 2972–2976. doi:10.1073/pnas.0911852107
- Baier, D. B., Gatesy, S. M., and Jenkins, F. A. (2007). A Critical Ligamentous Mechanism in the Evolution of Avian Flight. *Nature* 445 (7125), 307–310. doi:10.1038/nature05435
- Bakker, R. T., Siegwirth, J., Kralis, D., and Filla, J. (1992). *Edmarka rex*, a New, Gigantic Theropod Dinosaur from the Middle Morrison Formation, Late Jurassic of the Como Bluff Outcrop Region. *Hunteria* 2 (9), 1–24.
- Baumel, J. J., King, A. S., Lucas, A. M., Breazile, J. E., Evans, H. E., and Vanden Berge, J. C. (1993). *Handbook of Avian Anatomy: Nomina Anatomica Avium*. U.S.A.: Publ. of the Nuttall Ornithol. Club.
- Beddard, F. E. (1898). *The Structure and Classification of Birds*. London: Longmans, Green and Co.
- Beebe, W. (1915). A Tetrapteryx Stage in the Ancestry of Birds. *Zool. Soc.* 2, 39–52.
- Brusatte, S. L., O'Connor, J. K., and Jarvis, E. D. (2015). The Origin and Diversification of Birds. *Curr. Biol.* 25 (19), R888–R898. doi:10.1016/j.cub.2015.08.003
- Burnham, D. A., Derstler, K. L., Currie, P. J., Bakker, R. T., Zhou, Z., and Ostrom, J. H. (2000). Remarkable New Birdlike Dinosaur (Theropoda: Maniraptora) from the Upper Cretaceous of Montana. *Univ. Kans. Paleontol. Contrib. Pap.* 13, 1–13. doi:10.17161/pcons.1808.3761

DATA AVAILABILITY STATEMENT

The original contributions presented in the study are included in the article/Supplementary Material, further inquiries can be directed to the corresponding authors.

AUTHOR CONTRIBUTIONS

All authors listed have made a substantial, direct, and intellectual contribution to the work and approved it for publication.

ACKNOWLEDGMENTS

X. Xu, C. Muñoz, P. Chafrat, D. Lijmaer, P. Tubaro and S. Bogan for allowing access to osteological collections under their care. We also acknowledge R. Stoll, G. Stoll, M. Isasi, M. Cerroni, A.M. Aranciaga-Rolando and J.A. García Marsà for their help during experimentation with *Rhea americana* as well as for technical support. We thank David Marjanović and two anonymous reviewers for their comments that greatly improved the quality of this paper. We also thank Jingmai O'Connor and Ursula Rabar for their help and patience. We further thank J. O'Connor for inviting us to participate in this special issue. This contribution is part of the PICT 2018-01390 grant to FLA.

- Cau, A., Beyrand, V., Voeten, D. F. A. E., Fernandez, V., Tafforeau, P., Stein, K., et al. (2017). Synchrotron Scanning Reveals Amphibious Ecomorphology in a New Clade of Bird-like Dinosaurs. *Nature* 552 (7685), 395–399. doi:10.1038/nature24679
- Cau, A. (2020). The Body Plan of *Halszkaraptor escuilliei* (Dinosauria, Theropoda) Is Not a Transitional Form along the Evolution of Dromaeosaurid Hypercarnivory. *PeerJ* 8, e8672. doi:10.7717/peerj.8672
- Chatterjee, S., and Templin, R. J. (2007). Biplane Wing Planform and Flight Performance of the Feathered Dinosaur *Microraptor gui*. *Proc. Natl. Acad. Sci.* 104 (5), 1576–1580. doi:10.1073/pnas.0609975104
- Chiappe, L. M., and Meng, Q. (2016). *Birds of Stone: Chinese Avian Fossils from the Age of Dinosaurs*. Baltimore: JHU Press.
- Chiappe, L. M. (2002). "Osteology of the Flightless *Patagopteryx deferrariisi* from the Late Cretaceous of Patagonia (Argentina)," in *Mesozoic Birds: Above the Heads of Dinosaurs*. Editors L. M. Chiappe and L. M. Witmer (California: University of California Press), 281–316.
- Chiappe, L. M., and Vargas, A. (2003). Emplumando dinosaurios: la transición evolutiva de terópodos a aves. *Hornero* 18 (1), 1–11.
- Clarke, J. A. (2004). Morphology, Phylogenetic Taxonomy, and Systematics of *Ichthyornis* and *Apatornis* (Avialae: Ornithurae). *Bull. Am. Mus. Nat. Hist.* 286 (286), 1–179. doi:10.1206/0003-0090(2004)286<0001:mptaso>2.0.co;2
- Clarke, J. A., and Norell, M. A. (2002). The Morphology and Phylogenetic Position of *Apsaravis ukhaana* from the Late Cretaceous of Mongolia. *Am. Mus. Novitates* 3387 (3387), 1–46. doi:10.1206/0003-0082(2002)387<0001:tmappo>2.0.co;2
- Currie, P. J., and Zhiming, D. (2001). New Information on Cretaceous Troodontids (Dinosauria, Theropoda) from the People's Republic of China. *Can. J. Earth Sci.* 38 (12), 1753–1766. doi:10.1139/e01-065
- Dial, K. P. (1992). Avian Forelimb Muscles and Nonsteady Flight: Can Birds Fly without Using the Muscles in Their Wings? *The Auk* 109 (4), 874–885. doi:10.2307/4088162
- Dial, K. P., Goslow, G. E., Jr., and Jenkins, F. A., Jr. (1991). The Functional Anatomy of the Shoulder in the European Starling (*Sturnus vulgaris*). *J. Morphol.* 207 (3), 327–344. doi:10.1002/jmor.1052070309
- Feduccia, A. (1986). The Scapulocoracoid of Flightless Birds: a Primitive Avian Character Similar to that of Theropods. *Ibis* 128, 128–132. doi:10.1111/j.1474-919X.1986.tb02099.x

- Feo, T. J., Field, D. J., and Prum, R. O. (2015). Barb Geometry of Asymmetrical Feathers Reveals a Transitional Morphology in the Evolution of Avian Flight. *Proc. R. Soc. B.* 282 (1803), 20142864. doi:10.1098/rspb.2014.2864
- Forster, C. A., Sampson, S. D., Chiappe, L. M., and Krause, D. W. (1998). The Theropod Ancestry of Birds: New Evidence from the Late Cretaceous of Madagascar. *Sci.* 279, 1915–1919. doi:10.1126/science.279.5358.1915
- Geist, N. R., and Feduccia, A. (2000). Gravity-defying Behaviors: Identifying Models for Protoaves. *Am. Zool.* 40 (4), 664–675. doi:10.1093/icb/40.4.664
- George, J. C., and Berger, A. J. (1966). *Avian Myology*. Cambridge, MA: Academic Press.
- Gianechini, F. A., Makovicky, P. J., and Apesteguía, S. (2017). The Cranial Osteology of *Buitreraptor gonzalezorum* Makovicky, Apesteguía, and Agnolín, 2005 (Theropoda, Dromaeosauridae), from the Late Cretaceous of Patagonia, Argentina. *J. Vertebr. Paleontol.* 37 (1), e1255639. doi:10.1080/02724634.2017.1255639
- Godefroit, P., Cau, A., Dong-Yu, H., Escuillié, F., Wenhao, W., and Dyke, G. (2013). A Jurassic Avialan Dinosaur from China Resolves the Early Phylogenetic History of Birds. *Nature* 498 (7454), 359–362. doi:10.1038/nature12168
- Hartman, S., Mortimer, M., Wahl, W. R., Lomax, D. R., Lippincott, J., and Lovelace, D. M. (2019). A New Paravian Dinosaur from the Late Jurassic of North America Supports a Late Acquisition of Avian Flight. *PeerJ* 7, e7247. doi:10.7717/peerj.7247
- Heers, A. M., and Dial, K. P. (2012). From Extant to Extinct: Locomotor Ontogeny and the Evolution of Avian Flight. *Trends Ecol. Evol.* 27, 296–305. doi:10.1016/j.tree.2011.12.003
- Hone, D. W. E., Tischlinger, H., Xu, X., and Zhang, F. (2010). The Extent of the Preserved Feathers on the Four-Winged Dinosaur *Microraptor gui* under Ultraviolet Light. *PLoS ONE* 5 (2), e9223. doi:10.1371/journal.pone.0009223
- Hu, D., Hou, L., Zhang, L., and Xu, X. (2009). A Pre-archaeopteryx Troodontid Theropod from China with Long Feathers on the Metatarsus. *Nature* 461 (7264), 640–643. doi:10.1038/nature08322
- Hudson, G. E., Schreiweis, D. O., Wang, S. Y., and Lancaster, D. A. (1972). A Numerical Study of the Wing and Leg Muscles of Tinamous (Tinamidae). *Northwest. Sci.* 46, 207–255.
- Jasinowski, S. C., Russell, A. P., and Currie, P. J. (2006). An Integrative Phylogenetic and Extrapolatory Approach to the Reconstruction of Dromaeosaur (Theropoda: Eumaniraptora) Shoulder Musculature. *Zool. J. Linn. Soc.* 146 (3), 301–344. doi:10.1111/j.1096-3642.2006.00200.x
- Jenkins, F. A. (1993). The Evolution of the Avian Shoulder Joint. *Am. J. Sci.* 293, 253–267. doi:10.2475/ajs.293.a.253
- Lefèvre, U., Cau, A., Cincotta, A., Hu, D., Chinsamy, A., Escuillié, F., et al. (2017). A New Jurassic Theropod from China Documents a Transitional Step in the Macrostructure of Feathers. *Sci. Nat.* 104 (9–10), 74. doi:10.1007/s00114-017-1496-y
- Livezey, B. C. (1989). Phylogenetic Relationships and Incipient Flightlessness of the Extinct Auckland Islands Merganser. *Wilson Bull.* 101 (3), 410–435.
- Livezey, B. C., and Zusi, R. L. (2007). Higher-order Phylogeny of Modern Birds (Theropoda, Aves: Neornithes) Based on Comparative Anatomy. II. Analysis and Discussion. *Zool. J. Linn. Soc.* 149 (1), 1–95. doi:10.1111/j.1096-3642.2006.00293.x
- Lo Coco, G. E., Motta, M. J., Mosto, M. C., and Picasso, M. B. (2020). Wing and Tail Myology of *Tyto furcata* (Aves, Tytonidae). *J. Morphol.* 281 (4–5), 450–464. doi:10.1002/jmor.21111
- Long, C. A., Zhang, G. P., George, T. F., and Long, C. F. (2003). Physical Theory, Origin of Flight, and a Synthesis Proposed for Birds. *J. Theor. Biol.* 224, 9–26. doi:10.1016/s0022-5193(03)00116-4
- Longrich, N. (2006). Structure and Function of Hindlimb Feathers in *Archaeopteryx lithographica*. *Paleobiology* 32 (3), 417–431. doi:10.1666/04014.1
- Lowe, P. R. (1928). Studies and Observations Bearing on the Phylogeny of the Ostrich and its Allies. *Proc. Zool. Soc. Lond.* 98, 185–247. doi:10.1111/j.1469-7998.1928.tb07148.x
- Madsen, J. H., Jr. (1976). *Allosaurus fragilis*: a Revised Osteology. *Utah Geol. Mineral. Surv. Bull.* 109, 1–163.
- Makovicky, P. J., Apesteguía, S., and Agnolín, F. L. (2005). The Earliest Dromaeosaurid Theropod from South America. *Nature* 437 (7061), 1007–1011. doi:10.1038/nature03996
- Martin, L. D. (1995). The Enantiornithes: Terrestrial Birds of the Cretaceous. *Cour. Forsch. Senckenberg* 181, 23–36.
- Maxwell, E. E., and Larsson, H. C. E. (2007). Osteology and Myology of the Wing of the Emu (*Dromaius novaehollandiae*), and its Bearing on the Evolution of Vestigial Structures. *J. Morphol.* 268 (5), 423–441. doi:10.1002/jmor.10527
- Mayr, G. (2017). Pectoral Girdle Morphology of Mesozoic Birds and the Evolution of the Avian Supracoracoideus Muscle. *J. Ornithol.* 158 (3), 859–867. doi:10.1007/s10336-017-1451-x
- McGowan, C. (1982). The Wing Musculature of the Brown kiwi *Apteryx australis mantelli* and its Bearing on Ratite Affinities. *J. Zool.* 197 (2), 173–219. doi:10.1111/jzo.1982.197.2.173
- Motta, M. J., Agnolín, F. L., Brissón Egli, F., and Novas, F. E. (2020). New Theropod Dinosaur from the Upper Cretaceous of Patagonia Sheds Light on the Paravian Radiation in Gondwana. *Sci. Nat.* 107 (3), 1–8. doi:10.1007/s00114-020-01682-1
- Nicholls, E. L., and Russell, A. P. (1985). Structure and Function of the Pectoral Girdle and Forelimb of *Struthiomimus altus* (Theropoda: Ornithomimidae). *Palaeontol.* 28, 643–677.
- Norell, M. A., and Clarke, J. A. (2001). Fossil that Fills a Critical Gap in Avian Evolution. *Nature* 409 (6817), 181–184. doi:10.1038/35051563
- Novas, F. E., Agnolín, F., Brissón Egli, F., and Lo Coco, G. E. (2020). Pectoral Girdle Morphology in Early-Diverging Paravians and Living Ratites: Implications for the Origin of Flight. *Bull. Am. Mus. Nat. Hist.* 440 (1), 345–353. doi:10.5531/sd.sp.44
- Novas, F. E., Brissón Egli, F., Agnolín, F. L., Gianechini, F. A., and Cerda, I. (2018). Postcranial Osteology of a New Specimen of *Buitreraptor gonzalezorum* (Theropoda, Unenlagiidae). *Cretaceous Res.* 83, 127–167. doi:10.1016/j.cretres.2017.06.003
- O'Connor, J. K., Chiappe, L. M., and Bell, A. (2011). “Pre-modern Birds: Avian Divergences in the Mesozoic,” in *Living Dinosaurs: The Evolutionary History of Modern Birds*. Editors G. D. Dyke and G. Kaiser (Hoboken, NJ: J. Wiley & Sons), 39–114. doi:10.1002/9781119990475.ch3
- O'Connor, J. K., and Sullivan, C. (2014). Reinterpretation of the Early Cretaceous Maniraptoran (Dinosauria: Theropoda) *Zhongornis haoae* as a Scansoriopterygid-like Non-avian, and Morphological Resemblances between Scansoriopterygids and Basal Oviraptorosaurs. *Vert. Pala.* 52 (1), 3–30.
- Olson, S. L. (1973). Evolution of the Rails of the South Atlantic Islands (Aves: Rallidae). *Smithson. Contrib. Zool.* 152, 1–53. doi:10.5479/si.00810282.152
- Ostrom, J. H. (1969). Osteology of *Deinonychus antirrhopus*, an Unusual Theropod from the Lower Cretaceous of Montana. *Peabody Mus. Bull.* 30, 1–165. doi:10.2307/j.ctvqc6gzz
- Ostrom, J. H. (1974). The Pectoral Girdle and Forelimb Function of *Deinonychus* (Reptilia: Saurischia): a Correction. *Postilla* 165, 1–11.
- Ostrom, V. (1976). The American Experiment in Constitutional Choice. *Public Choice* 27, 1–12. doi:10.1007/bf01718942
- Padian, K., Hutchinson, J. R., and Holtz, T. R. (1999). Phylogenetic Definitions and Nomenclature of the Major Taxonomic Categories of the Carnivorous Dinosauria (Theropoda). *J. Vertebr. Paleontol.* 19 (1), 69–80. doi:10.1080/02724634.1999.10011123
- Paul, G. S. (2002). *Dinosaurs of the Air: The Evolution and Loss of Flight in Dinosaurs and Birds*. Baltimore: JHU Press.
- Pei, R., Li, Q., Meng, Q., Norell, M. A., and Gao, K.-Q. (2017). New Specimens of *Anchiornis huxleyi* (Theropoda: Paraves) from the Late Jurassic of Northeastern China. *Bull. Am. Mus. Nat. Hist.* 411, 1–67. doi:10.1206/0003-0090-411.1.1
- Pei, R., Pittman, M., Goloboff, P. A., Dececchi, T. A., Habib, M. B., Kaye, T. G., et al. (2020). Potential for Powered Flight Neared by Most Close Avialan Relatives, but Few Crossed its Thresholds. *Curr. Biol.* 30 (20), 4033–4046. doi:10.1016/j.cub.2020.06.105
- Picasso, M. B., and Mosto, M. C. (2018). Wing Myology of Caracaras (Aves, Falconiformes): Muscular Features Associated with Flight Behavior. *Vertebr. Zool.* 68 (2), 177–190.
- Raath, M. A. (1978). *The Anatomy of the Triassic Theropod Syntarsus rhodesiensis (Saurischia: Podokesauridae) and a Consideration of its Biology*. PhD Thesis. Grahamstown (Makhanda): Rhodes University, Faculty of Science, Zoology and Entomology.
- Raikow, R. J. (1985). “Locomotor System,” in *Form and Function in Birds*. Editors A. King and J. McLelland (London: Academic Press), 57–147.

- Rauhut, O. W., Foth, C., and Tischlinger, H. (2018). The Oldest *Archaeopteryx* (Theropoda: Avialae): a New Specimen from the Kimmeridgian/Tithonian Boundary of Schamhaupten, Bavaria. *PeerJ* 6, e4191. doi:10.7717/peerj.4191
- Ruben, J. (2010). Paleobiology and the Origins of Avian Flight. *Proc. Natl. Acad. Sci.* 107 (7), 2733–2734. doi:10.1073/pnas.0915099107
- Russell, D. A., and Dong, Z.-M. (1993). A Nearly Complete Skeleton of a New Troodontid Dinosaur from the Early Cretaceous of the Ordos Basin, Inner Mongolia, People's Republic of China. *Can. J. Earth Sci.* 30 (10), 2163–2173. doi:10.1139/e93-187
- Sackton, T. B., Grayson, P., Cloutier, A., Hu, Z., Liu, J. S., Wheeler, N. E., et al. (2019). Convergent Regulatory Evolution and Loss of Flight in Paleognathous Birds. *Science* 364 (6435), 74–78. doi:10.1126/science.aat7244
- Senter, P. (2006). Scapular Orientation in Theropods and Basal Birds, and the Origin of Flapping Flight. *Acta Palaeontol. Pol.* 51 (2), 305–313.
- Suzuki, D., Chiba, K., VanBuren, C. S., and Ohashi, T. (2014). The Appendicular Anatomy of the Elegant Crested Tinamou (*Eudromia elegans*). *Bull. Kitaky. Mus. Nat. Hist. Hum. Histo., Seri. A.* 12, 1–48.
- Tsuihiji, T., Barsbold, R., Watabe, M., Tsogtbaatar, K., Chinzorig, T., Fujiyama, Y., et al. (2014). An Exquisitely Preserved Troodontid Theropod with New Information on the Palatal Structure from the Upper Cretaceous of Mongolia. *Naturwissenschaften* 101 (2), 131–142. doi:10.1007/s00114-014-1143-9
- Turner, A. H., Hwang, S. H., and Norell, M. A. (2007). A Small Derived Theropod from Öösh, Early Cretaceous, Baykhangor, Mongolia. *Am. Mus. Novit.* 2007 (3557), 1–27. doi:10.1206/0003-0082(2007)3557[1:asdtfs]2.0.co;2
- Turner, A. H., Makovicky, P. J., and Norell, M. A. (2012). A Review of Dromaeosaurid Systematics and Paravian Phylogeny. *Bull. Am. Mus. Nat. Hist.* 371 (371), 1–206. doi:10.1206/748.1
- Voeten, D. F., Cubo, J., Margerie, E., Röper, M., Beyrand, V., Bureš, S., et al. (2018). Wing Bone Geometry Reveals Active Flight in *Archaeopteryx*. *Nat. Commun.* 9 (1), 1–9. doi:10.1038/s41467-018-03296-8
- Walker, C. A., and Dyke, G. J. (2009). Euenantiornithine Birds from the Late Cretaceous of El Brete (Argentina). *Irish J. Earth Sci.* 27, 15–62. doi:10.3318/ijes.2010.27.15
- Wang, M., Stidham, T. A., and Zhou, Z. (2018). A New Clade of Basal Early Cretaceous Pygostylian Birds and Developmental Plasticity of the Avian Shoulder Girdle. *Proc. Natl. Acad. Sci. USA* 115 (42), 10708–10713. doi:10.1073/pnas.1812176115
- Wang, M., Wang, X., Wang, Y., and Zhou, Z. (2016). A New Basal Bird from China with Implications for Morphological Diversity in Early Birds. *Sci. Rep.* 6, 19700. doi:10.1038/srep19700
- Wang, X., Huang, J., Kundrát, M., Cau, A., Liu, X., Wang, Y., et al. (2020). A New Jeholornithiform Exhibits the Earliest Appearance of the Fused Sternum and Pelvis in the Evolution of Avialan Dinosaurs. *J. Asian Earth Sci.* 199, 104401. doi:10.1016/j.jseas.2020.104401
- Witmer, L. M. (2002). "The Debate on Avian Ancestry: Phylogeny, Function, and Fossils," in *Mesozoic Birds: Above the Heads of Dinosaurs*. Editors L. M. Chiappe and L. M. Witmer (Berkeley: University of California Press), 3–30.
- Witmer, L. M. (1991). "Perspectives on Avian Origins," in *Origins of the Higher Groups of Tetrapods: Controversy and Consensus*. Editors H. P. Schultze and L. Trueb (Ithaca: Cornell University Press), 427–466.
- Xu, X., Currie, P., Pittman, M., Xing, L., Meng, Q., Lü, J., et al. (2017). Mosaic Evolution in an Asymmetrically Feathered Troodontid Dinosaur with Transitional Features. *Nat. Commun.* 8 (1), 1–12. doi:10.1038/ncomms14972
- Xu, X., and Kim, S. K. (2011). The Early Bird Catches the Worm: New Technologies for the *Caenorhabditis elegans* Toolkit. *Nat. Rev. Genet.* 12 (11), 793–801. doi:10.1038/nrg3050
- Xu, X., Norell, M. A., Kuang, X., Wang, X., Zhao, Q., and Jia, C. (2004). Basal Tyrannosauroids from China and Evidence for Protofeathers in Tyrannosauroids. *Nature* 431, 680–684. doi:10.1038/nature02855
- Xu, X., and Zhang, F. (2005). A New Maniraptoran Dinosaur from China with Long Feathers on the Metatarsus. *Naturwissenschaften* 92, 173–177. doi:10.1007/s00114-004-0604-y
- Xu, X., Zhou, Z., Dudley, R., Mackem, S., Chuong, C. M., Erickson, G. M., et al. (2014). An Integrative Approach to Understanding Bird Origins. *Sci* 346 (6215), 1341. doi:10.1126/science.1253293
- Yonezawa, T., Segawa, T., Mori, H., Campos, P. F., Hongoh, Y., Endo, H., et al. (2017). Phylogenomics and Morphology of Extinct Paleognaths Reveal the Origin and Evolution of the Ratites. *Curr. Biol.* 27 (1), 68–77. doi:10.1016/j.cub.2016.10.029
- Zhou, Z. (2004). The Origin and Early Evolution of Birds: Discoveries, Disputes, and Perspectives from Fossil Evidence. *Naturwissenschaften* 91 (10), 455–471. doi:10.1007/s00114-004-0570-4
- Zhou, Z., and Zhang, F. (2003b). Anatomy of the Primitive Bird *Sapeornis chaoyangensis* from the Early Cretaceous of Liaoning, China. *Can. J. Earth Sci.* 40 (5), 731–747. doi:10.1139/e03-011
- Zhou, Z., and Zhang, F. (2003a). *Jeholornis* Compared to *Archaeopteryx*, with a New Understanding of the Earliest Avian Evolution. *Naturwissenschaften* 90 (5), 220–225. doi:10.1007/s00114-003-0416-5

Conflict of Interest: The authors declare that the research was conducted in the absence of any commercial or financial relationships that could be construed as a potential conflict of interest.

Copyright © 2021 Novas, Motta, Agnolín, Rozadilla, Lo Coco and Brissón Egli. This is an open-access article distributed under the terms of the Creative Commons Attribution License (CC BY). The use, distribution or reproduction in other forums is permitted, provided the original author(s) and the copyright owner(s) are credited and that the original publication in this journal is cited, in accordance with accepted academic practice. No use, distribution or reproduction is permitted which does not comply with these terms.



Exploring the Ecomorphology of Two Cretaceous Enantiornithines With Unique Pedal Morphology

Alexander D. Clark^{1*} and Jingmai K. O'Connor²

¹ Davis College of Agriculture, Natural Resources, and Design, West Virginia University, Morgantown, WV, United States,

² Field Museum of Natural History, Chicago, IL, United States

OPEN ACCESS

Edited by:

Nathalie Bardet,
UMR 7207 Centre de Recherche sur
la Paléobiodiversité et les
Paléoenvironnements (CR2P), France

Reviewed by:

Delphine Angst,
University of Bristol, United Kingdom
Sebastian Apesteguia,
Consejo Nacional de Investigaciones
Científicas y Técnicas (CONICET),
Argentina

*Correspondence:

Alexander D. Clark
ac00040@mix.wvu.edu

Specialty section:

This article was submitted to
Paleontology,
a section of the journal
Frontiers in Ecology and Evolution

Received: 15 January 2021

Accepted: 19 April 2021

Published: 15 June 2021

Citation:

Clark AD and O'Connor JK (2021)
Exploring the Ecomorphology of Two
Cretaceous Enantiornithines With
Unique Pedal Morphology.
Front. Ecol. Evol. 9:654156.
doi: 10.3389/fevo.2021.654156

Recently, ~100 Ma amber from Myanmar has become an important source of information regarding the morphology of Late Cretaceous enantiornithines. Two specimens consisting of partial hindlimbs exhibit unusual morphologies when compared to both extant avian taxa and other Cretaceous enantiornithines. Pedal morphology is extremely ecologically informative in Aves as it represents the interface between body and substrate. These seemingly bizarre pedal morphologies represent adaptations that allowed these birds to utilize certain niches present in their paleoenvironment. Specific ecological niches apply the same general pressures to different species over time, and in doing so, through natural selection, produce morphologies that function much the same, although they may be anatomically dissimilar. As such, extant animals can provide useful information pertaining to the functional morphology of extinct animals, even in the absence of direct analogs, as in the case of these two Hukawng enantiornithines. Comparisons to extant taxa in the same predicted niches of these enantiornithines can be used to either support or contradict previous hypotheses regarding the *in vivo* function of these unique pedal morphologies. *Elektorornis chenguangi* exhibits a hypertrophied third pedal digit, originally interpreted as an appendage used for probing. We support this interpretation, which allows informed speculation as to the cranial anatomy of this taxon since extant animals that probe in woody substrates consistently pair elongate probing structures with a second robust structure that functions as a means to penetrate into this hard substrate. This suggests that the rostrum of *Elektorornis* would have been robust and most likely edentulous. The second specimen YLSNHM01001 exhibits an unusually mediolaterally robust fourth pedal digit, nearly double the width of digit II. Given that no such morphology is present in any other bird in the Mesozoic or Cenozoic we feel the unusual morphology justifies erection of a new taxon, *Fortipesavis prehensilis* gen. et sp. nov. Although distinct, the morphology in *F. prehensilis* resembles the syndactyl condition in some extant avian groups, and we hypothesize the robust digit similarly functioned to increase the surface area of the foot, facilitating grip on perches through increased friction. The necessity for increased grip and the lateral placement of this digit may suggest *F. prehensilis* utilized mobile perches similar to extant kingfishers.

Keywords: enantiornithines, *Elektorornis*, ecomorphology, Burmese amber, morphology, pedal morphology

INTRODUCTION

The Enantiornithes (Walker, 1981) is the dominant clade of Cretaceous land birds and the most diverse recognized clade of non-neornithine birds (Chiappe and Witmer, 2002; O'Connor and Chiappe, 2011). With each new discovery, our understanding of this extinct group's ethology and ecology grows. The vast majority of information regarding this clade comes from the Lower Cretaceous deposits in northeastern China that have produced the Jehol avifauna (Zhou and Zhang, 2007; Zhou and Wang, 2010; O'Connor and Chiappe, 2011). However, during the past 5 years, mid-Cretaceous aged Burmese amber from northern Myanmar has proved to be an unlikely but important source of information regarding this diverse clade (Xing et al., 2016, 2017, 2018a,b, 2019b,c, 2020a,b,c). Together, the record of lithic and amber fossils reveals that enantiornithines had both unique plumages and skeletal morphologies not present among extant avians (Zhang and Zhou, 2000; O'Connor and Chiappe, 2011; O'Connor et al., 2013, 2016a,b). In particular, preservation in amber commonly records particularly fine soft tissue details such as the presence of unusual scutellae scale filaments (SSFs) (Xing et al., 2019c, 2020c), skin texture (Xing et al., 2017, 2018b), and the delicate morphology of ornamental feathers (Xing et al., 2016, 2018a, 2019a, 2020a,b,c,d) that are rarely preserved in lithic fossils, and when preserved, do not record these structures in high fidelity (e.g., ornamental rachis dominated tail feathers).

Two Burmese amber enantiornithine specimens show exceptionally odd pedal morphologies that were described as unique among Aves (Xing et al., 2019b,c). Both specimens were discovered in the Late Albian-Cenomanian deposits (98.8 ± 0.6 Ma) (Shi et al., 2012) of the Angbamo locality, Hukawng Valley, Kachin Province (Tanai Township, Myitkyina District), in northern Myanmar (Figure 1A). The holotype of *Elektorornis chenguangi* (HPG-15-2) consists of an isolated right hindlimb and partial wing integument. The foot exhibits an unusual form of pedal digit elongation in which digit III is substantially longer than the other digits (Xing et al., 2019c). This digit also supports the proportionally longest ungual. This specific morphology is not exhibited among extant birds, nor does an exact analog appear in other living taxa. The second specimen, YLSNHM01001, an indeterminant probable enantiornithine, is even more incomplete with only remnants of digits II–IV preserved and only the skin demarcating the exterior surface of these digits together with portions of feathers belonging to the tail (Xing et al., 2019b). Digit IV is the most robust being mediolaterally expanded relative to the other digits such that digit II is approximately half the mediolateral width of digit IV. Additionally, digit IV exhibits exaggerated plantar pads as compared to most extant perching birds in that the pads are not only robust mediolaterally, but also dorsoventrally thickened such that they are separated by deep clefts.

Although both of these specimens record only partial features of the whole organism, unique morphology is clearly present. Unique morphologies invite speculation as to their *in vivo* function. However, the absence of direct analogs among extant avian taxa hinders attempts to infer the ecomorphological

function of unique features in extinct taxa. Ecological niches have the ability to shape organismal morphology as evolutionary processes give way to physiological alterations (Wainwright, 1991; Bock, 1994; Eduardo et al., 2010; Felice et al., 2019). The morphological solutions to a specific niche's "problems," though not exact across taxa, are typically comparable since they represent a response to a similar set of limitations and pressures. The resultant morphologies can be anatomically disparate but should be functionally similar (Arendt and Reznick, 2008; Stayton, 2008; Pearce, 2012). Therefore, rather than looking for superficially similar morphologies with which to make functional inferences, we can explore a feature through its potential structural benefits.

Both the skeletal structure and soft tissue morphology of the avian foot are functionally important and ecologically informative because these morphologies reveal how the bird interacts with its substrate (Höfling and Abourachid, 2020), and in some groups are highly involved in the acquisition and manipulation of food (Tsang and McDonald, 2018). The placement, shape, length, and robustness of extant bird pedal digits vary greatly, and this variation correlates with ecological habit (Tsang and McDonald, 2018; Gill et al., 2019). Among Neornithes, there are several foot types based on the arrangement of the pedal digits. The most common is the anisodactyl morphology found in perching birds, in which digits II, III, and IV face cranially, and digit I (the hallux) faces caudally, facilitating grip (Lovette and Fitzpatrick, 2016).

Both unusual Burmese enantiornithines were described as arboreal, an ecological niche apparently utilized by the vast majority of enantiornithines, all of which reveal an anisodactyl morphology where pedal remains are recovered (Chiappe and Witmer, 2002). *Elektorornis chenguangi* was further hypothesized to have utilized its elongate third pedal digit to probe for food whereas YLSNHM01001 was hypothesized to be an aerial insectivore using its robust fourth pedal digit to grip its prey (Xing et al., 2019b,c). However, neither initial hypothesis was supported by robust comparisons with a range of taxa. Here we assess these interpretations using additional data and further explore the ecology of each of these birds using inferences drawn from avian morphologies in similar predicted ecological niches. We also explore other extant non-avian taxa with specialized features in our search for potential extant analogs. From this data, we provide more rigorous support for the initially superficial prediction that the unique pedal digit of *E. chenguangi* was being used as a probing device. In the case of YLSNHM01001 we also concur that this taxon was an aerial insectivore, but not for the reasons put forth by Xing et al. (2019b). These observations help us to understand how particular niches have shaped and are shaping organisms morphologically. Such studies will lead to a better understanding of the possible range of morphological adaptations to a particular ecological role and improve inferences regarding how these unusual birds and other extinct animals may have lived. We hypothesize that by observing ecomorphological features found in extant taxa from a functional perspective, we can provide better insights as to the *in vivo* ecology, function, and ethology of unusual morphologies exhibited in enantiornithines.

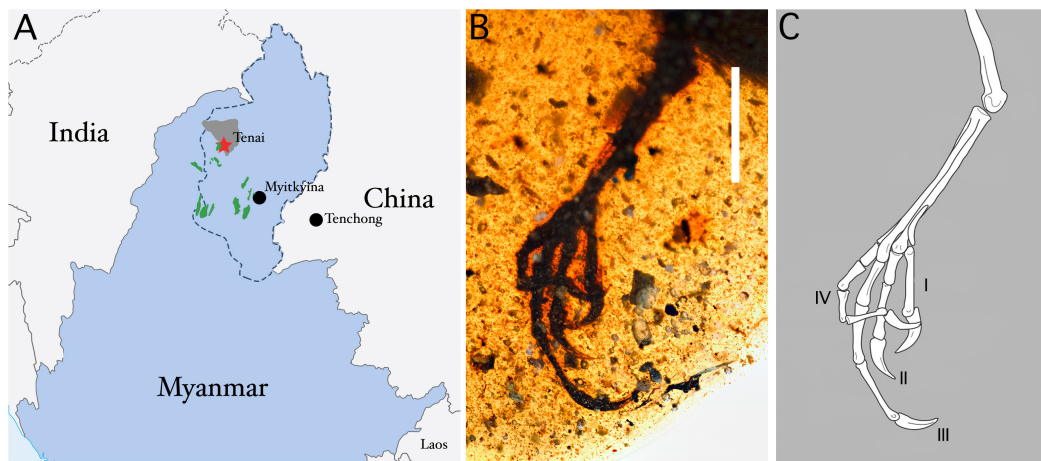


FIGURE 1 | (A) A map of the approximate location of the amber mines in Northern Myanmar where both specimens HPG-15-2 and YLSNHM01001 were discovered. Dark blue dotted outline = Kachin Province, gray shaded area = Hukawng Valley, red star = amber mines, and Tenai (Angbamo locality), green structures = Cretaceous-aged deposits. **(B)** The partial right hindlimb of *Elektorornis chenguangi* encased in amber (specimen HPG-15-2). **(C)** An interpretive osteological line-drawing of the partial right hindlimb of the *Elektorornis chenguangi* specimen, giving a clearer depiction of the proportionally elongated length of digit III. Scale bars = 5 mm. Photographs of specimens HPG-15-2 credited to Lida Xing, used with permission from Jingmai O'Connor.

RESULTS

Elektorornis chenguangi

Elektorornis chenguangi (Figures 1B,C) was interpreted as a tactile prober foraging in a wooded environment (Xing et al., 2019c). Among living avian taxa, the ecological niche of wood-probing is mainly attributed to the avian family Picidae (Winkler et al., 2020a). Within this group, the bill is used for chipping or gouging woody substrate. Once a hole has been created, picids utilize their elongated tongues to then search for and acquire prey items (Winkler et al., 2020a; Figure 2C). In many species, the tongue is additionally equipped with a rostrally sheathed barbed tip to facilitate prey acquisition. Outside the Picidae, there exists another group of birds that may provide a close analog for the proposed probing function of the elongated pedal digit in *E. chenguangi*. *Hemignathus munroi* (“Akiapola”au) (Pratt, 2005) is a Hawaiian honeycreeper that has an unusual beak morphology in which the upper bill is elongated and laterally compressed whereas the lower bill is stout and comparatively shorter (Figure 2D). It uses the lower bill to hammer and gouge into woody substrate. Once an opening has been made near a presumed arthropod cavity, the bird then utilizes its elongated upper bill to probe in search of arthropods. It then manipulates the prey item either by skewering it or by dragging it out into the open where it can more easily direct it back into the mouth (Pratt, 2005).

The ecological niche of probing inside a hard substrate is not limited to Aves. Xing et al. (2019c) compared the predicted ecological niche of *E. chenguangi* to the prosimian mammal *Daubentonia madagascariensis* (Aye-aye), which gnaws into woody substrate and uses its elongate manus and unique, thin third manual digit to probe in woody matter for arthropods (Soligo, 2005; Figure 2A). Similarly, the marsupial *Dactylopsila trivirgata* (Striped possum) gnaws into woody substrate and

removes arthropods with both its elongated tongue and an elongated fourth manual digit (Van Dyck, 1983; Handasyde and Martin, 1996; Figure 2B).

YLSNHM01001

The specimen preserves an outline of digits II, III, and IV (Figures 3A–C). Digit I is not preserved but it most-likely faced caudally, opposing digits II–IV in an anisodactyl arrangement (Xing et al., 2019b). The fourth digit is the most robust, measuring nearly twice the mediolateral width of digit II. The plantar pads of digit IV appear exaggerated, exhibiting ventral extensions from the plantar surface of the pes similar to some members of the orders Accipitriformes, Piciformes, and Psittaciformes (Figure 4D). Only the outline of digit II’s ungual is preserved, therefore the shape and size of the digits III and IV unguals are unknown. The single preserved ungual is large, elongate, and recurved, supporting both an arboreal ecology and probable referral to the enantiornithines (Xing et al., 2019b).

The graduated arrangement of the pedal digits with the narrowest digit located medially and the widest digit laterally placed most closely resembles the syndactyl (e.g., Alcedinidae, Meropidae) morphology. In most anisodactyl species that exhibit the syndactyl condition, it is primarily the soft tissue encasing digits III and IV that are fused such that these two digits share mediolaterally wide plantar pads whereas in zygodactyl syndactyl birds (e.g., Rhamphastidae) it is only digits II and III that are fused. In syndactyl birds, fusion of the pedal digits may be limited to the proximal portions or complete, such that the two digits are fused along their entire length forming a singular enlarged plantar surface (Winkler et al., 2020b). YLSNHM01001 does not exhibit a syndactyl condition, but the extreme width of the fourth digit in this specimen is strongly reminiscent of the fused digits III and IV in extant anisodactyl-syndactyl birds and this may suggest similarities *in vivo* function.

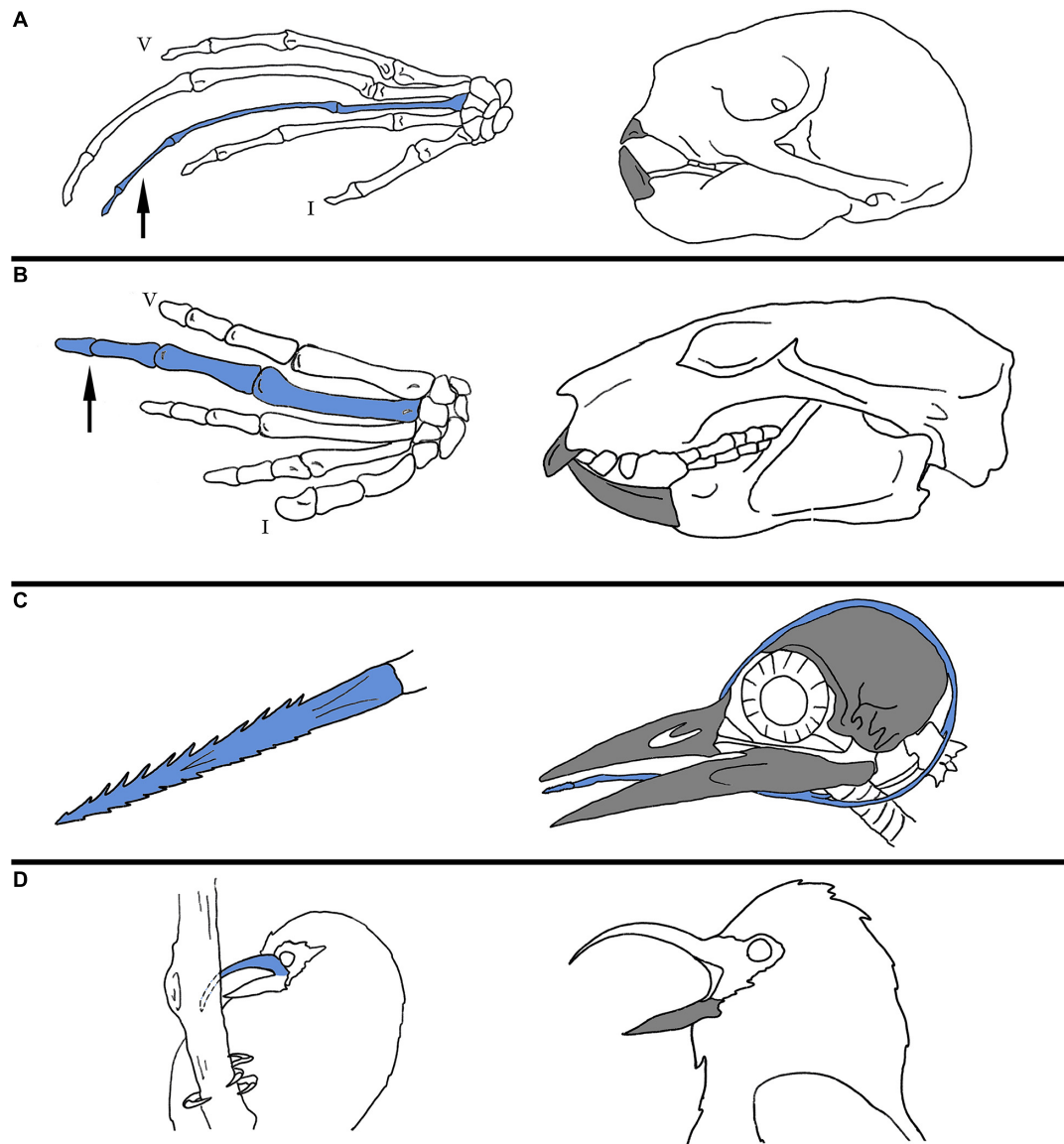


FIGURE 2 | In all known extant taxa that bore into and probe within hard substrate (e.g., wood), the “tool” used to extract prey items are accompanied by a structure that first allows entry into the hard substrate. The left column exhibits the morphologies used to probe and extract prey items (shaded blue), while the right column shows the morphologies used to break into the hard substrate (shaded gray). **(A)** The Aye-aye (*Daubentonia madagascariensis*) and the **(B)** Striped Possum (*Dactylopsila trivirgata*) both exhibit elongate manual digits used to probe in holes made in wood created by specialized rostromedially angled incisors which gnaw away woody material. The arrows indicate the specific digit used to probe. **(C)** Insectivorous woodpecker species exhibit distally barbed tips of the tongue covered in thick sheaths in order to skewer prey items within cavities which are accessed by gouging made possible by a robust conical bill and cushioned cranium. **(D)** The “Akiapola”au (*Hemignathus munroi*) probes with its distally tapered flexible upper bill, while the bottom robust bill, reminiscent to that of most woodpeckers, facilitates wood gouging with its straight, wedge-like shape. Line illustrations not drawn to scale.

Syndactyly primarily occurs in arboreal birds and has evolved multiple times, also being exhibited in two unique families of Passeriformes, the Calyptomenidae and Eurylaimidae (colloquially known as broadbills) (Winkler et al., 2020b,d,e,f,g), as well as in the Phoeniculidae (wood hoopoes), and even some members of the Trochilidae (hummingbirds) (Botelho et al., 2015). However, in these groups fusion is minimal, typically with only the proximal portion of digits III and IV conjoined. Increasing the plantar surface of the foot increases

friction with the substrate and thus improves grip during perching (Höfling and Abourachid, 2020). Predominant among anisodactyl-syndactyl birds in which digits III and IV are joined through soft tissue, thus increasing the surface area of the lateral portion of the foot similar to the condition in YLSNHM01001, are the Alcedinidae (kingfishers) and Meropidae (bee-eaters), both groups that forage from frequently mobile perches that require increased grip (Backus et al., 2015). The deep interpad sulci like those observed in YLSNHM01001 are also

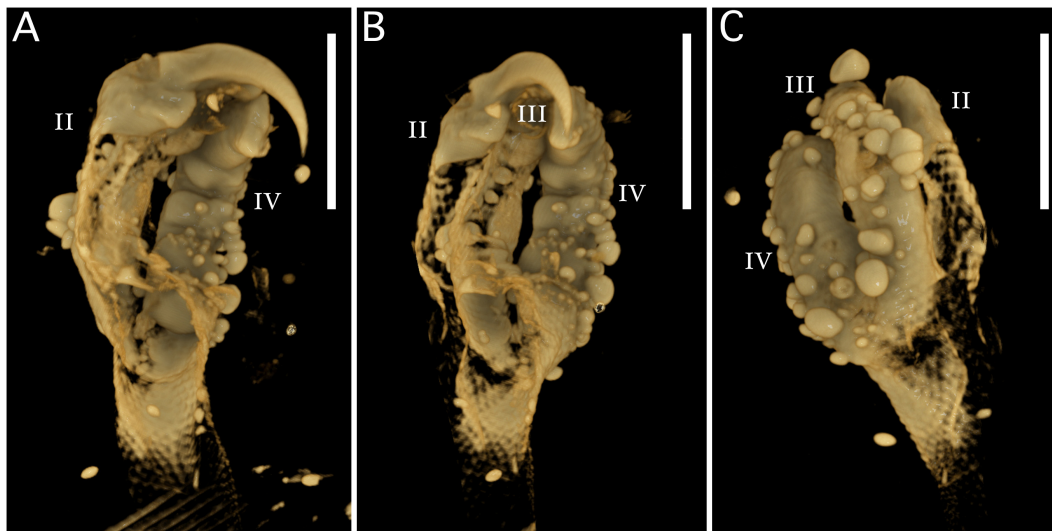


FIGURE 3 | The external surface of the partial left pes of YLSNHM01001 in (A) medial, (B) ventral, and (C) dorsal views. Note digit I (hallux) is missing from the specimen but is assumed to be a feature based on known enantiornithine pedal morphology. Scale bars = 5 mm, (A–C) Photographs of specimen YLSNHM01001 credited to Lida Xing, used with permission from Jingmai O'Connor.

found in some arboreal taxa including some syndactyl species (Höfling and Abourachid, 2020).

DISCUSSION

The avian foot represents the interface between the body and substrate and in some groups is highly involved in prey acquisition and object manipulation (Tsang and McDonald, 2018; Höfling and Abourachid, 2020). As such, the foot can be highly informative with regards to ecology. Recently, two enantiornithines from the Late Cretaceous ~100 Ma Burmese Hukawng avifauna were described with unique pedal morphologies not observed in any other bird, living or extinct (Xing et al., 2019b,c). Given the ecological diversity of modern birds and the shape of Cretaceous ecosystems, it is very likely that these enantiornithine taxa exploited ecological niches utilized by neornithines today. However, the unique morphologies observed in these two specimens suggest that these Cretaceous enantiornithines evolved their own adaptations different than those evolved by neornithines through which they exploited similar niches. Although each specimen preserves a pedal morphology not found among the approximately 10,000 species of extant birds (Neornithes), the ecological functions of these unique foot morphologies can be discussed through ecomorphological predictions and comparisons with potentially functionally analogous structures in extant taxa, not limited to other birds. Organisms have clearly changed over time, but the various “problems” or environmental pressures they experience as a result of exploiting resources in similar niches acquired through comparable ecological roles leads to the evolution of similar “solutions” or structures with comparable functions (Arendt and Reznick, 2008; Stayton, 2008; Pearce, 2012). Thus, behavioral inferences of extinct species based on unique

morphologies can be explored through detailed comparisons of functional morphology.

Elektorornis chenguangi

Elektorornis chenguangi (Xing et al., 2019c) exhibits a novel appendicular appendage in which the third pedal digit has been greatly elongated such that it is approximately double the length of digit II. Among birds, digit III is most commonly the longest digit in the foot, but the proportions observed in *E. chenguangi* and the specific morphological trait of a singularly elongated pedal digit is not found in any extant bird, nor does a directly similar structure appear elsewhere in any extant non-avian taxa (Figures 5B–D). Xing et al. (2019c) made two predictions regarding the function of the elongate third digit: that it increased the arboreal function of the foot and that it may be a trophic adaptation, or served both functions. Here we examine these two predictions and provide additional support for interpretations that this digit was involved in a probing foraging behavior.

Many extant birds have proportionally elongated pedal digits such as members of the Charadriiformes and Passeriformes. However, in these groups all digits are proportionally elongated. In passeriforms, digital elongation serves to improve grip, facilitating perching behavior (Lovette and Fitzpatrick, 2016). Charadriiform pedal digits have become proportionally elongate in order to increase surface area to facilitate walking over soft substrates. Notably, many charadriiforms probe for food. However, members of this group utilize unique bill morphologies to probe within the soft substrate upon which they walk (Lovette and Fitzpatrick, 2016). *Elektorornis chenguangi* exhibits only a single cranially facing elongated pedal digit paired with an elongate hallux and large, recurved claws, morphologies all absent in extant charadriiforms, dispelling the possibility that this specialized pes morphology was for increased surface area when



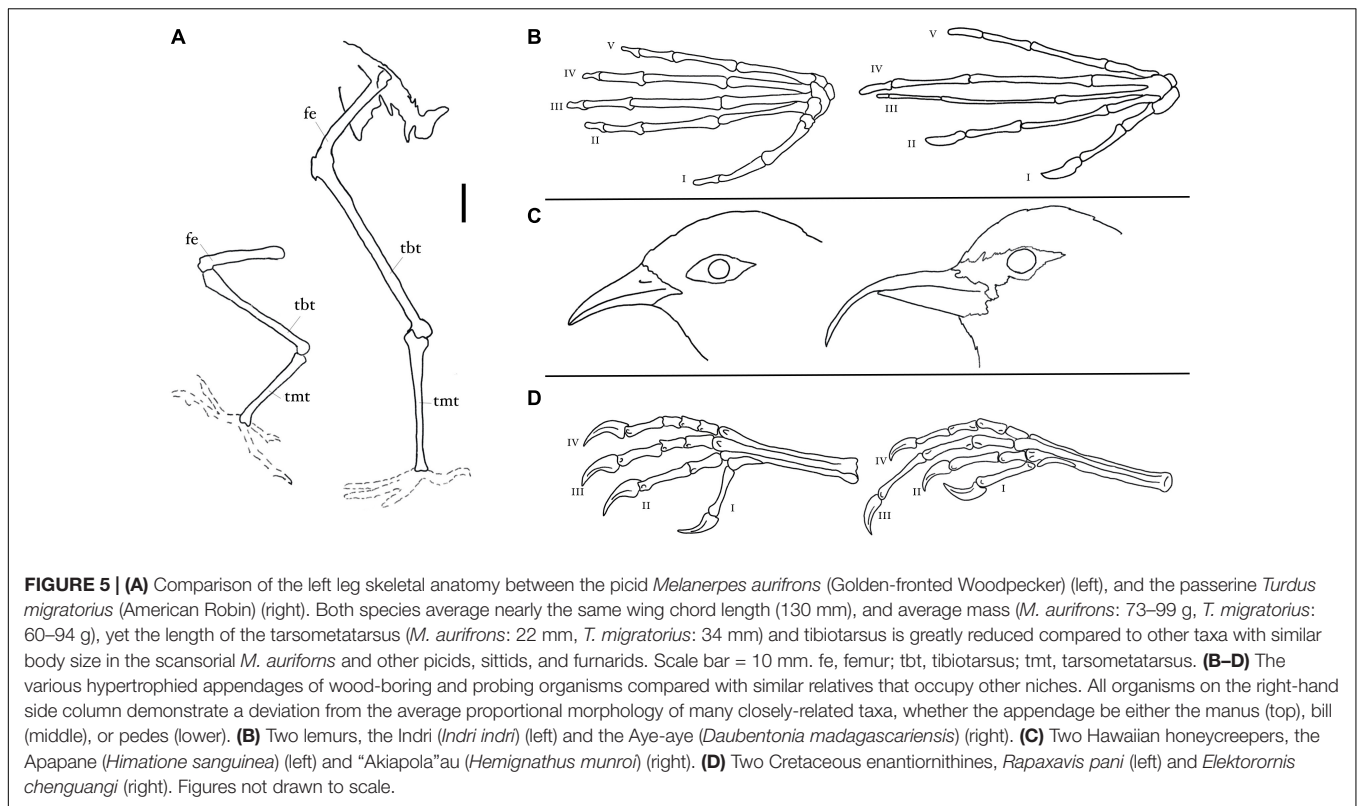
FIGURE 4 | (A) An in-life reconstruction of *Fortipesavis prehendens*' pedes. The most robust digit is laterally placed on each pes and the plantar pads exhibit a slight pebbly texture. **(B)** The amber mold of *Fortipesavis prehendens* in medial view, with focus on the reticulatae textured plantar pads of digit II. Inset shows larger image of plantar pad texture as signaled by the white arrow. Scale bar = 5 mm. Photo of specimen YLSNHM01001 credited to Lida Xing, used with permission from Jingmai O'Connor. **(C)** In-life reconstruction exhibiting the same posture as the amber specimen, exhibiting the textured plantar pads similar to the texture seen in other extant avian pedes **(D)** such as members of the Psittacidae (*Ara chloropterus*) (top) and Ramphastidae (*Rhampastos toco*) (bottom).

walking over soft surfaces. This pedal morphology also makes it highly unlikely that *E. chenguangi* could both probe with its elongated third pedal digit and maintain balance on soft terrain without also sinking. Therefore, the possibility that *E. chenguangi* probed in a soft substrate can also be ruled out.

Like other enantiornithines, the anisodactyl foot of *E. chenguangi* appears to be adapted for arboreality as the proportionally long hallux and long, pointed, and recurved unguis are features consistent with an arboreal lifestyle in birds and are present in all known enantiornithines (O'Connor, 2012; Lovette and Fitzpatrick, 2016; Xing et al., 2019c). Furthermore, in *E. chenguangi* and other enantiornithines, the penultimate phalanges are the longest non-ungual phalanges within each digit, a morphology statistically linked to an arboreal

lifestyle, whereas a terrestrial ecology as in charadriiforms is indicated by phalanges that become progressively shorter distally in each digit (Hopson, 2001). Xing et al. (2019c) hypothesized that the elongated third digit aided in gripping perches since the reversed hallux in this taxon is also proportionately elongate relative to other enantiornithines and considered these two features together to indicate increased arboreal function relative to other enantiornithines.

Xing et al. (2019c) noted that arboreal skinks also display elongated digits, which similarly provide for increased grip. Skinks with longer digits were shown to move with greater agility on the ground and were also able to climb trees faster than similar species with comparatively shorter digits (Huang, 2006). The comparative increase in speed is most likely attributable



to increased surface area and subsequently, greater traction. However, in the studied skinks all digits were elongated, not a singular elongated digit like that in *E. chenguangi*. Lizards that are primarily arboreal tend to have proportionally longer digits, while those with more terrestrial lifestyles have shorter digits (Losos et al., 2006). However, for lizards that live in arboreal settings, digit length is less important than total appendicular length with shorter limbs being a better indicator of an arboreal lifestyle (Losos et al., 2006).

A similar pattern is also observed in birds. Evolution in crown birds facing the “problem” of stability in an arboreal environment overcome this physiological issue in a similar way. When grip strength becomes a priority in arboreal and scansorial species, the metatarsus and tibiotarsus either evolve to decrease in length, shortening the hindlimb, or the hindlimbs become overall stouter in proportion to the body as seen in most members of the families Picidae, Sittidae, and Furnariidae, and even rare cases in the Parulidae (Hoyo et al., 1992; **Figure 5A**). Any morphological change that brings the body closer to the branch or trunk, and thus lowers the center of gravity, is advantageous for balance and stability (Grant, 1966; Schulenberg, 1983; Zeffer and Norberg, 2002; Zeffer et al., 2002). *Elektorornis chenguangi*, like other enantiornithines, has a proportionally long tibiotarsus and tarsometatarsus (Xing et al., 2019c; Falk et al., 2020). Proportionally long appendicular bones are not well-suited for lowering the center of gravity closer to the perching surface for birds, so the need for greater stability in an arboreal or scansorial context is most likely not the evolutionary cause of *E. chenguangi*’s elongated pedal digit.

The second prediction by Xing et al. (2019c) was that the elongate third pedal digit of *E. chenguangi* represents a tactile probing structure used in foraging behaviors. The authors hypothesized that the foot would aid in, or be the primary means of, food acquisition. Xing et al. (2019c) compared the odd digit morphology of *E. chenguangi* to another organism that has a somewhat similar structure, the extant Madagascan prosimian *Dau. madagascariensis*, a species of lemur colloquially known as the Aye-aye. Although there exists no direct analog, since no extant taxon probes with its feet, the manual digits of *Dau. madagascariensis* and elongated appendages in other mammals and some crown birds may still aid in understanding the ecological function of the unique appendage in *E. chenguangi*.

The manual digits in *Dau. madagascariensis* are elongated relative to most other prosimians and the third digit has been drastically diminished in robustness relative to the rest of the manual digits (**Figures 3B, 4A**). This thin third digit is used to probe for grubs and other arthropods within openings in woody matter created using its powerful jaw muscles and specialized dentition (Jouffroy, 1975; Milliken et al., 1991; Feistner et al., 1994; Erickson et al., 1998). The fourth digit is the longest, followed by the third digit, neither of which is twice the length of digit II (Soligo, 2005). Another potential mammalian analog, the marsupial *Dac. trivirgata* (Striped possum), gnaws into hard woody substrates with its rostromedially placed incisors and uses both its elongated tongue and elongated fourth manual digit to probe for prey (Van Dyck, 1983; Handasyde and Martin, 1996). Upon closer inspection, the proportions of the hand in *Dau. madagascariensis* and *Dac. trivirgata* are actually quite

disparate from those in the foot of *E. chenguangi* (Figures 5B,D). However, these three taxa share the presence of some form of digital elongation, which in the two extant mammals, direct observation demonstrates are wood-probing adaptations.

Birds are unlikely to evolve manual probing structures like those seen in mammals since their manual digits are reduced and consolidated to form a sturdy surface for the attachment of the primary flight feathers. However, within crown birds there are still examples of taxa that probe for food that may also be relevant to ecological interpretations regarding *E. chenguangi*. In extant birds, the wood-probing niche is primarily utilized by the Picidae family which, like *Dau. madagascariensis*, are percussive foragers (Lovette and Fitzpatrick, 2016). Picids bore holes in woody matter with their bills and probe with their elongated, barbed tongues, which in some species are tipped with a keratinous sheath with recurved spines (Lovette and Fitzpatrick, 2016). Pict tongues resemble harpoons and work in a similar fashion (Figure 2C).

The wood-probing niche is also present in the Hawaiian archipelago avifauna, in which a specific group of Hawaiian honeycreepers have elongated a part of their body in order to probe, presumably similar to *E. chenguangi*. The Hawaiian honeycreeper genus *Hemignathus* is divided into two subgenera: *Akialoa* and *Hemignathus*. All members but one are now either critically endangered, thought to be extinct, or are known to be extinct (Pratt, 2005). Although a majority of species belonging to these two subgenera primarily picked and gleaned in and under flakes of bark, and occasionally, at the base of native plant leaves (Pratt, 2005), one species probes in wood—the sole remaining member of this group *H. munroi* (“Akiapola”au), found only on the Big Island of Hawai’i in the Hawaiian archipelago. The lower bill of *H. munroi* is very short, thick, and stout when compared to the upper bill which is long, laterally compressed, and tapers as it extends distally to a short point (Figure 5C). *Hemignathus munroi* uses its stout lower bill to hammer and gouge holes into woody matter and then probes these openings using its elongate upper bill (Perkins, 1903; Munro, 1960; Hoyo et al., 1992, 2002; Ralph and Fancy, 1996).

The behavior and tools organisms have evolved in order to exploit the wood-probing niche, while sometimes appearing physically dissimilar, are similar in their function, being elongate and with some degree of flexibility. In extant wood-probers we see several structures that have become adapted for this role: the upper bill in *H. munroi*, the tongue in many picids, and manual digits in *Dau. madagascariensis* and *Dac. trivirgata*. If correctly interpreted, *E. chenguangi*, adds pedal digits to the diversity of known probing structures. Unique to the enantiornithines, *E. chenguangi* is the only member of the clade to exhibit a digit III that is 120% the length of metatarsal III, and 118% the length digit II (Table 1). As in other elongated appendages evolved for the purpose of probing after a surface has been bored into, proportional differences are evident when compared to closely related non-probing taxa (Table 1).

These structures vary in their degree of flexibility and versatility. Even though the tongue contains small bones (the hyoids), with the exception of the keratinized tip in some taxa, the extended portion of the tongue is not a rigid structure, and is much more flexible and pliable than an elongated pedal digit in

which bending is limited to the location of the interphalangeal joints and their range of motion. This may also explain the relative greater diversity (as a measure of success) in the Picidae compared to these other wood-probing groups that rely on less versatile structures. Among extant probers, elongated digits (as opposed to hypertrophied cranial features like bills and tongues), are only observed in wood-probing mammals (Milliken et al., 1991; Handasyde and Martin, 1996). Thus, it appears that *E. chenguangi* evolved a more mammalian-style, rather than avian, means of probing. Although mammals utilize their forelimb digits, these are reduced and modified for flight in birds and thus cannot be adapted into specialized feeding structures in taxa that retain their volancy. Notably, in ornithothoracines, the hand is reduced and consolidated in a way that appears irreversible since no flightless bird has evolved elongated manual digits (McCall et al., 1998; Nudds and Davidson, 2010).

A common pattern emerges among extant taxa that have evolved to acquire prey within a wood substrate by means of an elongated and flexible appendage. In addition to the elongated structure used for extraction, all extant wood-probers have also evolved a means to enter this hard substrate. This pattern is observed in both birds (Munro, 1960; Hoyo et al., 1992, 2002; Ralph and Fancy, 1996; Pratt, 2005; Winkler et al., 2020a) and mammals (Jouffroy, 1975; Van Dyck, 1983; Milliken et al., 1991; Feistner et al., 1994; Handasyde and Martin, 1996; Erickson et al., 1998). Entering the hard substrate entails creating an opening near where the prey resides, which requires a robust structure (e.g., teeth and jaw musculature, thick bill). Among mammals, in both *Dau. madagascariensis* and *Dac. trivirgata*, access into the hard wood substrate is achieved through a pair of specialized rostromedially placed incisors, similar to rodents, paired with robust jaw muscles (Morris et al., 2018). Similarly, although not feeding within a wood-substrate, members of the families Myrmecophagidae (ant-eaters) and Orycteropodidae (aardvarks) remove hard substrates (arthropod mounds) with their robust forelimbs in order to access their prey with specialized elongated tongues (Sesoko et al., 2015; Casali et al., 2017; Legendre and Botha-Brink, 2018). In extant avian wood-probers, picids have evolved dense skulls and a suite of other features including reinforced cervical vertebrae that aid in the hammering and subsequent removal of woody matter (Lovette and Fitzpatrick, 2016), whereas the honeycreeper *H. munroi* has evolved a stocky, dense, lower bill that allows it to hammer into wood.

Elektorornis chenguangi would likely be physiologically capable of picking under flakes of bark or into branch junctions with its hypertrophied digit in search of prey items, yet we find this ecology less likely. Extant bird groups that pick underneath and in-between hard surfaces such as bark or glean from or within soft surfaces such as leaf clumps or mud, typically do so with an elongated bill in which the upper and lower portions are subequal (Lovette and Fitzpatrick, 2016) (e.g., the families Furnariidae, Certhiidae, Sittidae, Neosittidae, and Climacteridae). Rostral elongation is possible in enantiornithines, as evidenced from the Early Cretaceous Longipteryidae (Zhang et al., 2001; O'Connor et al., 2009). Therefore, unless the mouth was modified for a different specific behavior, it would be inefficient to forage with the foot only to then move the food

TABLE 1 | (Top) Comparisons of pedal digit proportions between Cretaceous aves and (Bottom) upper and lower bill lengths in eight species of Hawaiian honeycreeper.

| Taxon | Specimen | Digit III/ Metatarsal III | Digit I/ Digit III | Digit II/ Digit III | | |
|-------------------------------------------------------|---------------------|---------------------------|-----------------------|-------------------------|---------------------------------|-------------|
| Pedal proportion comparisons of Cretaceous aves | | | | | | |
| <i>Jeholornis</i> | IVPP V13886 | 1.11 | 0.42 | 0.8 | | |
| <i>Sapeornis</i> | 41HIII0405 | 1.16 | 0.7 | 0.8 | | |
| <i>Bohaiornis</i> | LPM B00167 | 1.41 | 0.43 | 0.75 | | |
| <i>Sinornis</i> | BPV 538a | 1.27 | 0.5 | 0.71 | | |
| <i>Junornis</i> | BMNHC-PH-919 | 1.15 | 0.47 | 0.67 | | |
| <i>Rapaxavis</i> | DNHM 2522 | 0.97 | 0.65 | 0.89 | | |
| <i>Iteravis</i> | IVPP V18958 | 1.1 | 0.32 | 0.79 | | |
| <i>Elektorornis</i> | HPG-15-2 | 1.2 | 0.51 | 0.59 | | |
| Taxon | Common Name | Ex. Culmen (mm) | Mandible (mm) | Ex. Culmen/ Mandible | Difference in Bill Tips (mm) | Tarsus (mm) |
| Comparisons in similarly-sized Hawaiian Honeycreepers | | | | | | |
| <i>Hemignathus wilsoni</i> | Akiapola'au | 26.61 ± 4.1 (male) | | | | 25.06 ± 2.8 |
| <i>Hemignathus wilsoni</i> (CMNH 55430) | Akiapola'au | 21.2 | 11.63 | 0.548 | 8.39 | |
| <i>Hemignathus wilsoni</i> (CMNH 55431) | Akiapola'au | 23.89 | 14.09 | 0.589 | 9.39 | |
| <i>Chloroderepanis virens</i> | Hawaii' Amakihi | 14.3 ± 1.8 (male) | | | | 22.4 ± 2.3 |
| <i>Chloroderepanis virens</i> (CMNH 55439) | Hawaii' Amakihi | 14.86 | 9.48 | 0.637 | 0.1 | |
| <i>Chloroderepanis virens</i> (CMNH 55438) | Hawaii' Amakihi | 13.8 | 10.16 | 0.736 | −0.2 | |
| <i>Chloroderepanis flava</i> | Oahu' Amakihi | 15.2 ± 0.09 (male) | | | | 20.2 ± 0.09 |
| <i>Chloroderepanis flava</i> (CMNH 55443) | Oahu' Amakihi | 13.95 | 10.2 | 0.731 | −0.01 | |
| <i>Chloroderepanis flava</i> (CMNH 55444) | Oahu' Amakihi | 12.61 | 9.56 | 0.758 | 0.61 | |
| <i>Himatione sanguinea</i> | Apapane | 15.8 ± 0.18 (male) | | | | 23.5 ± 0.22 |
| <i>Himatione sanguinea</i> (CMNH 55435) | Apapane | 17.24 | 12.37 | 0.717 | −0.35 | |
| <i>Himatione sanguinea</i> (CMNH 91505) | Apapane | 16.13 | 11.7 | 0.725 | 0.51 | |
| <i>Drepanis coccinea</i> | I'iwi | 25.0 ± 0.63 (male) | | | | 25.2 ± 0.47 |
| <i>Drepanis coccinea</i> (CMNH 55433) | I'iwi | 27.45 | 18.23 | 0.664 | 1.46 | |
| <i>Drepanis coccinea</i> (CMNH 55432) | I'iwi | 27.78 | 18.7 | 0.673 | 0.18 | |
| <i>Akialoa obscura</i> | Lesser Akialoa | 40.1 ± 2.64 (male) | | | 4.9 ± 1.20 | 21.6 ± 0.72 |
| <i>Akialoa obscura</i> (CMNH 55429) | Lesser Akialoa | 37.18 | 26.75 | 0.719 | 5.19 | |
| <i>Akialoa obscura</i> (CMNH 55428) | Lesser Akialoa | 37.77 | Specimen damaged | Specimen damaged | Specimen damaged | |
| <i>Akialoa stejnegeri</i> | Kauai Akialoa | 60.8 ± 2.52 (male) | | | 6.4 ± 2.38 | 24.9 ± 1.40 |
| <i>Akialoa stejnegeri</i> (CMNH 55427) | Kauai Akialoa | 51.58 | 39 | 0.756 | 4.99 | NA |
| <i>Akialoa stejnegeri</i> (CMNH 118048) | Kauai Akialoa | 56.45 | 44.92 | 0.795 | 4.3 | NA |
| <i>Himatione fraithii</i> (CMNH 102721) | Laysan Honeycreeper | 13.63 | 10.01 | 0.734 | 0.64 | NA |

Exposed culmen was measured from the tip of the bill to where culmen meets feathers at proximal base of the rhamphotheca. Mandible was measured from mandible bill tip to where the rhamphotheca meets the skin at proximal base of the bill in a straight linear line. Difference in bill tip was the measurement from upper bill tip to lower bill tip with the bill closed. Measurements of bill tip differences and upper and lower bill length differences vary due to the highly curved nature of many honeycreeper bills. Measurements accompanied by variations acquired from the Cornell Lab of Ornithology Birds of the World online database.

to the mouth after acquisition. Among extant wood probers, the evolution of an additional specialized probing appendage is found only in taxa in which the mouth apparatus is already serving another function, such as gnawing as exhibited in *Dau. madagascariensis* and *Dac. trivirgata*, and gouging as demonstrated in picids (Figures 2A–C). *Hemignathus munroi* represents an odd intermediate with half of the beak serving to gouge while the other serves as a probing device (Figure 2D).

This pairing of structures observed in extant wood-probers allows us to make predictions regarding the anatomy of *E. chenguangi*, of which only the hindlimb is known (Figures 1B,C). If the hypothesis that *E. chenguangi* was a

tactile wood-prober is correct, then this species most likely also required a means of removing woody substrate prior to prey acquisition. Therefore, we hypothesize *E. chenguangi* may have possessed a unique rostral morphology that aided in either prying or gouging hard substrates, the two primary methods utilized by extant birds to enter bark or woody substrate in order to access arthropod cavities (Mountainspring, 1987; Zusi, 1989; Simon et al., 2020; Winkler et al., 2020a). Enantiornithines varied in their cranial morphology with respect to rostral length, dentition, and presence of a complete infratemporal bar, which has led to inferences that members of this clade occupied a variety of ecological niches (O'Connor, 2019; O'Connor et al., 2020). At

least one Late Cretaceous documented taxon was edentulous (Chiappe et al., 2001). This indicates that enantiornithines had the genetic potential to utilize a variety of rostral morphologies.

In addition to their specialized bill morphology, picids possess a complex suite of other specialized cranial and cervical features to cope with the impact generated by their boring behavior (Winkler et al., 2020a). Since this level of anatomical specialization is not recognized in any Cretaceous enantiornithine or other non-neornithine avian group, this suggests that it was very unlikely that *E. chenguangi* would be able to bore in a manner similar to picids. If *E. chenguangi* utilized a prying behavior as a means to enter woody substrates, we would predict an overall robust bill with a dorsoventrally and mediolaterally widened base and robust dentaries (Zusi, 1989; Simon et al., 2020). Alternatively, if a gouging action was utilized we might expect to find a rostral morphology characterized by a sub-conical, distally tapering bill with minimal curvature (e.g., picids).

We predict that with either rostral morphology (prying or gouging) *E. chenguangi* was likely edentulous or partial edentulous, with teeth—if present—caudally restricted. Both behaviors involve considerable force and the small, delicate teeth of most Cretaceous enantiornithines would most likely interfere with this behavior and/or become damaged. Furthermore, if the elongated pedal digit was the means of prey acquisition, teeth may not have been necessary. It has been demonstrated that in birds under a relax of evolutionary pressure teeth are rapidly lost (Louchart and Viriot, 2011; Li et al., 2020). Altogether, we suggest *E. chenguangi* was most likely edentulous. These predictions, based on niche associated morphologies as seen in extant taxa, allow for not only for more scientifically accurate reconstructions, but also for possible identification of fragmentary material from the Hukawng recovered in the future. Should cranial material be recovered for *E. chenguangi* and a robust rostral morphology is not present, functional interpretations of the elongate third pedal digit as a wood-probing structure would be unsupported and the role of the elongate third pedal digit would need to be reassessed.

Xing et al. (2019c) did not specify a particular mode of probing although the comparison with *Dau. madagascariensis* indirectly suggests probing in wood and the suggestion that the SSFs had a tactile function may further suggest probing in an enclosed, hidden environment in which visually guided probing is not possible. *Elektorornis chenguangi* exhibits SSFs on the tarsometatarsus and pedal digits. These unusual integumentary structures are also present in other Burmese amber enantiornithines (Xing et al., 2017, 2019a, 2020b,c,d). Although their primary function is still unclear, it has been suggested that they served a mechanosensory function (Xing et al., 2019c). These structures are present dorsally, laterally, and ventrally on other phalanges, but concentrated clusters of them can be found near the apex of digit III, just before the ungual. Similar structures are present, though less extensively, on the distal end of digit IV. Clustered groups of SSFs could represent areas of increased sensory sensitivity, which could aid in probing for prey. Tactile signals indicating an arthropod occupant within a cavity might have been the primary means of prey detection for *E. chenguangi* once the digit was inserted into a cavity. Herbst

corpuscles, which would presumably be associated with the SSFs if they indeed had a sensory function, occur in greater abundance in the bill tip organ of taxa that forage using their rostra to probe soft substrate (Cunningham et al., 2010, 2013). Some animals that forage in similar environments in which visual cues are not the primary means of food acquisition display similar appendages that are used for tactile signals. In addition to the avian bill tip organ (Cunningham et al., 2010, 2013), biological structures like catfish barbules, and some species of birds' rectal bristles are used for sensory purposes to locate prey (Kapoor and Bhargava, 1967; Lovette and Fitzpatrick, 2016). However, with many Burmese amber enantiornithines exhibiting pedal SSFs, with some even present on the tarsus (Xing et al., 2020b), these structures may also be a widespread feature that assisted in stability or balance when perched. Potentially, their sensory function involved in stability and balance made the evolution of the elongate third pedal as a probing mechanism possible. Histology of the SSFs may shed light on their function in the future.

YLSNHM01001

Inferences regarding YLSNHM01001 are limited due to the only preserved remains being a mold of a single pes in amber. However, this mold is preserved in high-fidelity, and the observed features are quite unique. This specimen is characterized by digits that progressively become mediolaterally wider laterally on the foot such that the fourth pedal digit is twice the mediolateral width of the second (Xing et al., 2019b). Similar to *E. chenguangi*, there is no extant bird that exhibits the same pedal morphology that can serve as a direct analog for the morphology observed in YLSNHM01001 (Xing et al., 2019b). Although the external morphology of digits II, III, and IV are preserved, digit I, which most likely formed a caudally-facing hallux, is not preserved, hindering interpretations. The robust fourth pedal digit is atypical for enantiornithines (Chiappe and Walker, 2002; **Figure 4A**). In other enantiornithines, digits II and III are usually equally robust (digit IV being slightly more delicate), or the second digit is slightly more robust, as in bohaiornithids (Wang et al., 2014). In YLSNHM01001, the plantar pads of digit IV appear hypertrophied, exhibiting greater size and depth than in the adjacent digits. The digit II ungual is the only one preserved, so the shape and size of the unguals on the remaining preserved digits are unknown (**Figures 3A–C**). As in most other Hukawng enantiornithines, this specimen also exhibits SSFs (Xing et al., 2019b, 2020b). Although preservation is limited, the proportions of digit IV relative to digits II and III distinguish this specimen from all other known avians, therefore we feel justified in erecting a new taxon based on this specimen (see section “Systematic Paleontology”) *Fortipesavis prehensens* gen. et sp. nov.

Xing et al. (2019b) suggested a possible raptorial ecological niche for *F. prehensens* due to the size and slight “pebbly” reticulae texture on the plantar pad of digit II which is moderately similar to some extant birds of prey (**Figure 4B**; Xing et al., 2019b). However, the plantar pad texture is more reminiscent of non-raptorial birds such as those in the families Phasianidae, Ramphastidae, and Psittacidae, exhibiting flattened sub-circular reticulae rather than the often-observed ventrally exaggerated

and finely textured plantar pads of birds of prey (**Figures 4B–D**). Additionally, the lateral placement of the most robust digit is in fact dissimilar to the pedal morphology of most extant raptorial birds. In almost all birds of prey the most robust and often shortest digits are the medial digits I or II (Lovette and Fitzpatrick, 2016). This morphology positions the body mass on top of the prey, increasing stability and facilitating grip, and thus decreasing the likelihood of the prey escaping (Fowler et al., 2009; Tsang et al., 2019). This behavior has also been predicted for dromaeosaurids which share with extant raptorial birds a similar pes morphology in which the medial digit II is the most robust (Fowler et al., 2011). In contrast, having the most robust digit, intended for hunting or pinning prey, on the lateral side of the foot relative to the body, would most likely result in instability and decrease the pressure exerted by the body mass applied to the prey item.

In a rare example and exception among extant raptors, in *Pandion haliaetus* (Osprey) the fourth digit is typically the most robust. However, *P. haliaetus* has a unique foot structure in which the typical raptor anisodactyl morphology used by the bird when engaged in perching behavior, transforms into a zygodactyl morphology during prey capture through caudal rotation of the fourth digit. This rotation of the fourth digit provides added grip, necessary for maintaining hold of the slippery laterally compressed bodies of fish, *P. haliaetus*' prey of choice (Bierregaard et al., 2020). The plantar surface of the pedal digits of this piscivorous raptor are covered in spicules which provide additional grip similar to the lingual papillae on the tongues of penguins which also feed on fish (Kobayashi et al., 1998; Allen et al., 2018). The soft tissue morphology *F.prehendens* is also inconsistent with interpretations regarding raptorial function. In general, the plantar pad papillae are far more exaggerated, an adaption for dispersing pressure, with a sharp texture that increases grip (Lovette and Fitzpatrick, 2016; Höfling and Abourachid, 2020). Furthermore, the interpad sulci are more weakly defined compared to *F.prehendens* (Höfling and Abourachid, 2020).

Although inconsistent with gripping prey, the medial to lateral graduated order of the digital diameters in *F.prehendens* still provides important clues as to the *in vivo* function of this unusual pedal morphology. Members of the avian order Podicipediformes exhibit enlarged lateral pedal digits, which are additionally lobate, a morphology that facilitates diving and swimming (Winkler et al., 2020c). However, *F.prehendens* clearly does not exhibit an aquatic pes morphology, lacking lobate digits, webbing, or short pedal unguals. In some extant birds with the zygodactyl foot morphology (e.g., family Ramphastidae and order Psittaciformes), the most robust or longest digit is located laterally on the foot, but because the fourth digit is reversed, it is digit II or III that is the most robust. This pes morphology has multiple functional benefits, including facilitating grip, object manipulation, and stability on moving perches (Lovette and Fitzpatrick, 2016). In *F.prehendens*, digits II–IV appear to be facing cranially, preserved flexed in a gripping morphology. The absence of indications of deformation strongly suggests a zygodactyl morphology was not present in *F.prehendens*.

As hypothesized by Xing et al. (2019b), it seems most likely that *F.prehendens* was anisodactyl, as in all other known enantiornithines. Various groups of extant birds have a modified anisodactyl morphology known as syndactyly in which pedal digits, typically III and IV, are either partially or completely fused such that the digits in some groups are nearly completely encased in tissue forming a single structure (e.g., Coraciiformes, Bucerotiformes) (Bock and Miller, 1959). The condition of syndactyly is not restricted to anisodactyl pedes, but also appears minimally in some zygodactyl (e.g., picids, ramphastids, capitonids) and heterodactyl (e.g., trogonids) species (Höfling and Abourachid, 2020); however, the syndactyl condition is most commonly used to described anisodactyl morphologies with some degree of fusion between the three cranially facing pedal digits (**Table 2**).

In such taxa, the two cranially-facing lateral digits function as one enlarged laterally-placed digit, which may share mechanical similarities with the morphology observed in *F.prehendens* (**Figure 4A**). The evolutionary origin behind syndactyly in birds is as yet undetermined, although it is clear it has evolved multiple times, possibly for different reasons in at least some occurrences. In general, this morphology increases the surface area of the foot which in turn increases friction and thus increases grip (Höfling and Abourachid, 2020). The anisodactyl, heterodactyl, and zygodactyl foot morphology and syndactyl variants of these pedal arrangements are considered to be adaptations for perching, each with their own particular benefit (Bock and Miller, 1959).

Two families belonging to the order Coraciiformes are characterized by an anisodactyl-syndactyl foot morphology and hunt from frequently mobile perches (e.g., swaying branches): the Meropidae (bee-eaters) and the Alcedinidae (kingfishers). In both groups the extent of the syndactyl fusion varies but most commonly digit II is minimally joined to digit III along the length of the proximal phalanx and digits III and IV are extensively joined such that only the penultimate phalanges are free. Meropids are generally small birds and hunt insects, whereas alcedinids are a predominately piscivorous group and occupy a larger size range compared to meropids.

Alcedinids employ a hunting strategy that includes waiting on perches near water or over streams, which often move and sway, either being blown by the wind, or erratically moved by the water current. Some meropids also hunt near rivers but in general this group utilizes open environments prone to wind (Hoyo et al., 2001). Hunting from mobile surfaces requires adaptations that provide greater stability such as head stabilization, so that a successful trajectory to a prey item can be achieved (Wallman and Letelier, 1993; Katzir et al., 2001, 2018; Ochs et al., 2017). In the coraciiforms with the anisodactyl-syndactyl morphology, greater stability is achieved through the fusion of pedal digits, which allows for less pedal movement [also accompanied by a reduction in musculature for the outer digits (Backus et al., 2015)] and a laterally placed expanded plantar surface with which to grasp surfaces which produces a firmer grip on mobile, and occasionally thin, perches through increased surface friction (Bock and Miller, 1959; Höfling and Abourachid, 2020). Similarly, the pedal morphology exhibited by *F.prehendens* increases the lateral surface area of the foot in contact with the perch which may

TABLE 2 | List of 14 neornithine families in which syndactyly occurs.

| Family | Genus | Foot morphology | Level of fusion (proximal, partial, distal) | Ecological niche |
|---------------------------------|-----------------------|------------------------|---------------------------------------------|--------------------------------------------------------------|
| Alcedinidae (Kingfishers) | <i>Alcedo</i> | Anisodactyl-Syndactyl | Partial (III and IV) | Riparian, aquatic vertebrates and invertebrates |
| | <i>Ceyx</i> | Anisodactyl-Syndactyl | Partial (III and IV) | Riparian, aquatic vertebrates and invertebrates |
| | <i>Corythornis</i> | Anisodactyl-Syndactyl | Partial (III and IV) | Riparian, aquatic vertebrates and invertebrates |
| | <i>Ispidina</i> | Anisodactyl-Syndactyl | Partial (III and IV) | Riparian, aquatic vertebrates and invertebrates |
| | <i>Lacedo</i> | Anisodactyl-Syndactyl | Partial (III and IV) | Arboreal, carnivorous (vertebrate and invertebrate) |
| | <i>Dacelo</i> | Anisodactyl-Syndactyl | Partial (III and IV) | Arboreal, carnivorous (vertebrate and invertebrate) |
| | <i>Clytocex</i> | Anisodactyl-Syndactyl | Partial (III and IV) | Arboreal, carnivorous (vertebrate and invertebrate) |
| | <i>Cittura</i> | Anisodactyl-Syndactyl | Partial (III and IV) | Arboreal, carnivorous (vertebrate and invertebrate) |
| | <i>Pelargopsis</i> | Anisodactyl-Syndactyl | Partial (III and IV) | Riparian, aquatic vertebrates and invertebrates |
| | <i>Halycon</i> | Anisodactyl-Syndactyl | Partial (III and IV) | Arboreal-riparian, carnivorous (vertebrate and invertebrate) |
| | <i>Tordiramphus</i> | Anisodactyl-Syndactyl | Partial (III and IV) | Arboreal-riparian, carnivorous (vertebrate and invertebrate) |
| | <i>Caridonax</i> | Anisodactyl-Syndactyl | Partial (III and IV) | Arboreal, carnivorous (vertebrate and invertebrate) |
| | <i>Melidora</i> | Anisodactyl-Syndactyl | Partial (III and IV) | Arboreal-riparian, carnivorous (vertebrate and invertebrate) |
| | <i>Actenoides</i> | Anisodactyl-Syndactyl | Partial (III and IV) | Arboreal-riparian, carnivorous (vertebrate and invertebrate) |
| | <i>Syma</i> | Anisodactyl-Syndactyl | Partial (III and IV) | Arboreal, carnivorous (vertebrate and invertebrate) |
| | <i>Tanyptera</i> | Anisodactyl-Syndactyl | Partial (III and IV) | Arboreal-riparian, carnivorous (vertebrate and invertebrate) |
| | <i>Megaceryle</i> | Anisodactyl-Syndactyl | Distal (III and IV) | Riparian, aquatic vertebrates and invertebrates |
| | <i>Ceryle</i> | Anisodactyl-Syndactyl | Partial (III and IV) | Riparian, aquatic vertebrates and invertebrates |
| | <i>Chloroceryle</i> | Anisodactyl-Syndactyl | Distal (III and IV) | Riparian, aquatic vertebrates and invertebrates |
| Meropidae (Bee-eaters) | <i>Nyctornis</i> | Anisodactyl-Syndactyl | Proximal-Partial (III and IV) | Arboreal, insectivorous |
| | <i>Meropogon</i> | Anisodactyl-Syndactyl | Proximal-Partial (III and IV) | Arboreal, insectivorous |
| | <i>Merops</i> | Anisodactyl-Syndactyl | Proximal-Partial (III and IV) | Arboreal, insectivorous |
| Ramphastidae (Toucans) | <i>Aulacorhynchus</i> | Zygodactyl-Syndactyl | Proximal (II and III) | Arboreal. Omnivorous (fruits, invertebrates, vertebrates) |
| | <i>Andigena</i> | Zygodactyl-Syndactyl | Proximal (II and III) | Arboreal, frugivorous, occasional invertebrates |
| | <i>Pteroglossus</i> | Zygodactyl-Syndactyl | Proximal (II and III) | Arboreal, omnivorous (fruits, invertebrates, vertebrates) |
| | <i>Selenidera</i> | Zygodactyl-Syndactyl | Proximal (II and III) | Arboreal, omnivorous (fruits, invertebrates, vertebrates) |
| | <i>Ramphastos</i> | Zygodactyl-Syndactyl | Proximal (II and III) | Arboreal, omnivorous (fruits, invertebrates, vertebrates) |
| Trogonidae (Trogons) | <i>Euptilotis</i> | Heterodactyl-Syndactyl | Proximal (III and IV) | Arboreal, primarily frugivorous, occasional invert and vert |
| | <i>Pharomachrus</i> | Heterodactyl-Syndactyl | Proximal (III and IV) | Arboreal, primarily frugivorous, occasional invert and vert |
| | <i>Priotelus</i> | Heterodactyl-Syndactyl | Proximal (III and IV) | Arboreal, primarily frugivorous, occasional invert and vert |
| | <i>Trogon</i> | Heterodactyl-Syndactyl | Proximal (III and IV) | Arboreal, primarily frugivorous, occasional invert and vert |
| | <i>Apaloderma</i> | Heterodactyl-Syndactyl | Proximal (III and IV) | Arboreal, primarily frugivorous, occasional invert and vert |
| | <i>Harpactes</i> | Heterodactyl-Syndactyl | Proximal (III and IV) | Arboreal, primarily frugivorous, occasional invert and vert |
| Capitonidae (New World Barbets) | <i>Capito</i> | Zygodactyl-Syndactyl | Proximal (II and III) | Arboreal, generalist (frugivorous, insectivorous) |
| | <i>Eubucco</i> | Zygodactyl-Syndactyl | Proximal (II and III) | Arboreal, generalist (frugivorous, insectivorous) |

(Continued)

TABLE 2 | Continued

| Family | Genus | Foot morphology | Level of fusion (proximal, partial, distal) | Ecological niche |
|-------------------------------------|--------------------------|-----------------------|---------------------------------------------------|-------------------------------------------------------------|
| Calyptomenidae (African Broadbills) | <i>Smithornis</i> | Anisodactyl-Syndactyl | Proximal (II and III) | Arboreal, primarily frugivorous, occasional invert and vert |
| | <i>Calyptomera</i> | Anisodactyl-Syndactyl | Proximal (III and IV) | Arboreal, primarily frugivorous, occasional invert and vert |
| Eurylaimidae (Asian Broadbills) | <i>Cymbirhynchus</i> | Anisodactyl-Syndactyl | Proximal (III and IV) | Arboreal, omnivorous (fruits, invertebrates, vertebrates) |
| | <i>Psarisomus</i> | Anisodactyl-Syndactyl | Proximal (III and IV) | Arboreal, omnivorous (fruits, invertebrates, vertebrates) |
| | <i>Serilophus</i> | Anisodactyl-Syndactyl | Proximal (III and IV) | Arboreal, omnivorous (fruits, invertebrates, vertebrates) |
| | <i>Eurylaimus</i> | Anisodactyl-Syndactyl | Proximal (III and IV) | Arboreal, omnivorous (fruits, invertebrates, vertebrates) |
| | <i>Corydon</i> | Anisodactyl-Syndactyl | Proximal (III and IV) | Arboreal, omnivorous (fruits, invertebrates, vertebrates) |
| | <i>Pseudocalyptomena</i> | Anisodactyl-Syndactyl | Proximal (III and IV) | Arboreal, omnivorous (fruits, invertebrates, vertebrates) |
| | | | | |
| Phoeniculidae (Wood Hoopoes) | <i>Phoeniculus</i> | Anisodactyl-Syndactyl | Partial (III and IV) | Arboreal, insectivorous |
| | <i>Rhinopomastus</i> | Anisodactyl-Syndactyl | Partial (III and IV) | Arboreal, insectivorous |
| Bucerotidae (Hornbills) | <i>Lophoceros</i> | Zygodactyl-Syndactyl | Proximal (II and III) | Arboreal, omnivorous (fruits, invertebrates, vertebrates) |
| | <i>Tockus</i> | Zygodactyl-Syndactyl | Proximal (II and III) | Arboreal, omnivorous (fruits, invertebrates, vertebrates) |
| | <i>Berenicornis</i> | Zygodactyl-Syndactyl | Proximal (II and III) | Arboreal, omnivorous (fruits, invertebrates, vertebrates) |
| | <i>Horizocerus</i> | Zygodactyl-Syndactyl | Proximal (II and III) | Arboreal, omnivorous (fruits, invertebrates, vertebrates) |
| | <i>Ceratogymna</i> | Zygodactyl-Syndactyl | Proximal (II and III) | Arboreal, omnivorous (fruits, invertebrates, vertebrates) |
| | <i>Bycanistes</i> | Zygodactyl-Syndactyl | Proximal (II and III) | Arboreal, omnivorous (fruits, invertebrates, vertebrates) |
| | <i>Buceros</i> | Zygodactyl-Syndactyl | Proximal (II and III) | Arboreal, omnivorous (fruits, invertebrates, vertebrates) |
| | <i>Anorrhinus</i> | Zygodactyl-Syndactyl | Proximal (II and III) | Arboreal, omnivorous (fruits, invertebrates, vertebrates) |
| | <i>Ocyceros</i> | Zygodactyl-Syndactyl | Proximal (II and III) | Arboreal, omnivorous (fruits, invertebrates, vertebrates) |
| | <i>Anthracoceros</i> | Zygodactyl-Syndactyl | Proximal (II and III) | Arboreal, omnivorous (fruits, invertebrates, vertebrates) |
| | <i>Aceros</i> | Zygodactyl-Syndactyl | Proximal (II and III) | Arboreal, omnivorous (fruits, invertebrates, vertebrates) |
| | <i>Rhyticeros</i> | Zygodactyl-Syndactyl | Proximal (II and III) | Arboreal, omnivorous (fruits, invertebrates, vertebrates) |
| | <i>Rhabdotorrhinus</i> | Zygodactyl-Syndactyl | Proximal (II and III) | Arboreal, omnivorous (fruits, invertebrates, vertebrates) |
| | <i>Penelopides</i> | Zygodactyl-Syndactyl | Proximal (II and III) | Arboreal, omnivorous (fruits, invertebrates, vertebrates) |
| | | | | |
| | | | | |
| | | | | |
| | | | | |
| | | | | |
| | | | | |
| | | | | |
| Bucconidae (Puffbirds) | <i>Notharchus</i> | Zygodactyl-Syndactyl | Proximal (II and III) | Arboreal, primarily carnivorous, occasional frugivorous |
| | <i>Bucco</i> | Zygodactyl-Syndactyl | Proximal (II and III) | Arboreal, primarily carnivorous, occasional frugivorous |
| | <i>Nystalus</i> | Zygodactyl-Syndactyl | Proximal (II and III) | Arboreal, primarily carnivorous, occasional frugivorous |
| | <i>Hypnelus</i> | Zygodactyl-Syndactyl | Proximal (II and III) | Arboreal, primarily carnivorous, occasional frugivorous |
| | <i>Malacoptila</i> | Zygodactyl-Syndactyl | Proximal (II and III) | Arboreal, primarily carnivorous, occasional frugivorous |

(Continued)

TABLE 2 | Continued

| Family | Genus | Foot morphology | Level of fusion (proximal, partial, distal) | Ecological niche |
|----------------------------|--------------------------|-----------------------|-------------------------------------------------|---------------------------------------------------------------------------|
| Galbulidae (Jacamars) | <i>Micromonacha</i> | Zygodactyl-Syndactyl | Proximal (II and III) | Arboreal, primarily carnivorous, occasional frugivorous |
| | <i>Nonnula</i> | Zygodactyl-Syndactyl | Proximal (II and III) | Arboreal, primarily carnivorous, occasional frugivorous |
| | <i>Hapaloptila</i> | Zygodactyl-Syndactyl | Proximal (II and III) | Arboreal, primarily carnivorous, occasional frugivorous |
| | <i>Monasa</i> | Zygodactyl-Syndactyl | Proximal (II and III) | Arboreal, primarily carnivorous, occasional frugivorous |
| | <i>Chelidoptera</i> | Zygodactyl-Syndactyl | Proximal (II and III) | Arboreal, primarily carnivorous, occasional frugivorous |
| | <i>Galbalcyrrhynchus</i> | Zygodactyl-Syndactyl | Proximal (II and III) | Arboreal, insectivorous |
| | <i>Brachygalba</i> | Zygodactyl-Syndactyl | Proximal (II and III) | Arboreal, insectivorous |
| | <i>Jacamaalcyon</i> | Zygodactyl-Syndactyl | Proximal (II and III) | Arboreal, insectivorous |
| | <i>Galbula</i> | Zygodactyl-Syndactyl | Proximal (II and III) | Arboreal, insectivorous |
| | <i>Jacamerops</i> | Zygodactyl-Syndactyl | Proximal (II and III) | Arboreal, insectivorous |
| Picidae (Woodpeckers) | 33 Genera total | Zygodactyl-Syndactyl | Proximal (II and III) Very limited | Scansorial, primarily insectivorous |
| Cuculidae (Cuckoos) | 33 Genera total | Zygodactyl-Syndactyl | Partial (II and III) Partial fusions present | Arboreal, primarily carnivorous (invert and vert), occasional frugivorous |
| Trochilidae (Hummingbirds) | 107 Genera total | Anisodactyl-Syndactyl | Many show incredibly limited to no fusion | Arboreal, mainly volant, primarily nectivorous, also insectivorous |
| | <i>Rhamphodon</i> | Anisodactyl-Syndactyl | Partial (III and IV) | Arboreal, mainly volant, primarily nectivorous, also insectivorous |
| | <i>Eupetomena</i> | Anisodactyl-Syndactyl | Partial (III and IV) | Arboreal, mainly volant, primarily nectivorous, also insectivorous |
| | <i>Ensifera</i> | Anisodactyl-Syndactyl | Partial (III and IV) | Arboreal, mainly volant, primarily nectivorous, also insectivorous |

suggest this taxon also exploited an ecological niche that required a firmer grasp than non-specialized arboreal birds with a typically proportioned anisodactyl pedes could provide, such as mobile perches (Höfling and Abourachid, 2020).

Both meropids and alcedinids have proportionally small pedes. Notably, the preserved traces in *F. prehensens* holotype also suggest a proportionally small pedes. The distal portions of the metatarsals appear quite thick, possibly indicating relatively robust, stout legs, which are not observed in other enantiornithines preserved in amber also associated with soft tissue (Xing et al., 2017, 2020c,d; Winkler et al., 2020b,d,e). This functional speculation supports interpretations that a reversed hallux was present, as in meropids and alcedinids. Syndactyl birds also commonly have exaggerated interpad sulci (Höfling and Abourachid, 2020) like that is *F. prehensens*, a morphology that is clearly absent in other Burmese amber enantiornithines in which the soft tissue can be observed (Xing et al., 2020c,d). These exaggerated pads likely aided in increasing surface area, which increased surface contact, and therefore increased friction.

In light of existing interpretations regarding diet in other enantiornithines (O'Connor, 2019), it is possible that *F. prehensens* was an aerial insectivore as originally hypothesized similar to extant meropids and eurylaimids. However, in contrast to the original interpretation which inferred the foot was adapted

for grasping prey (Xing et al., 2019b), we hypothesize the foot is adapted for increased stability while possibly utilizing mobile perches and that the rostrum would most likely have been the means of prey acquisition. A piscivorous diet similar to alcedinids is also consistent with the paleoenvironment of the Burmese amber, which is interpreted as a mangrove forest. However, *F. prehensens* is much smaller than most alcedinids which may suggest an insectivorous diet is more likely. The accrual of additional skeletal remains, in particular pertaining to the skull, may shed additional information on the specific niche utilized by this enantiornithine lineage (Zhang et al., 2001; Wang and Zhou, 2017). A diversity of bill morphologies are observed among extant syndactyl birds with piscivorous and insectivorous diets ranging from elongate and slender (e.g., Meropidae) to stout and wide (e.g., Calyptomenidae and Eurylaimidae) preventing us from making predictions regarding the rostral morphology of *F. prehensens*.

It is notable that among neornithines, specialized foot morphologies such as heterodactyl, zygodactyl and syndactyl-anisodactyl are limited to altricial birds and all syndactyl neornithines are all regarded as super-altricial (Botelho et al., 2015). In contrast, enantiornithines are considered highly precocial (Zhou and Zhang, 2004; Xing et al., 2017). Although often described as super-precocial, in fact enantiornithines do not

really fit into the neornithine altricial-precocial spectrum, being small arboreal birds that were likely independent and volant upon hatching and thus unlike the extant super-precocial megapodes which are primarily cursorial birds (Xing et al., 2017). A highly precocial developmental strategy is inferred wherever there is evidence of early developmental stages and appears to have been widespread in the Enantiornithes. Such a developmental strategy may have excluded enantiornithines from evolving specialized foot morphologies like those observed in altricial neornithines, thus forcing them to evolve alternative strategies to cope with certain environments, such as the proportionately mediolaterally wide digit observed in *F. prehensens*.

Although syndactyly has evolved multiple times during avian evolution, it appears to be a synapomorphy of Eucavities, so named for their tendency to nest in cavities or burrows, and it occurs most extensively in members of this clade (Yuri et al., 2013). Although this morphology and this behavior have both been secondarily lost in some lineages (e.g., members of Bucerotidae utilizing rotted holes or damaged trunks from large broken branches), it is commonly inferred that syndactyly facilitates active excavation of burrows in soft substrate (Winkler et al., 2020c). The increased plantar surface of the pedes makes for a useful spade during the process of shoveling out dirt, mud, or sand, along with the bill in some members of this group (Winkler et al., 2020b). Notably, some members within the families Gabulidae (Jacamars), and Capitonidae (Barbets) exhibit a modified syndactyl-zygodactyl foot morphology, which aids in the shoveling of substrate during burrow excavation (Hoyo et al., 2002), thus revealing that there may be a positive correlation between pedal syndactyl morphology and burrow excavation across not just eucavities, but throughout the neornithines. In most extant examples, when creating a burrow, the foot is positioned either on the parasagittal plane pushing substrate out, or ventrally in relation to the animal, allowing the material to pass underneath the body when excavating. Having the widest portion of the foot located laterally, rather than medially, facilitates this movement of the substrate out of the burrow or cavity in relation to the bird. Although *F. prehensens* similarly exhibits an enlarged laterally placed plantar surface relative to the morphology found in other enantiornithines, it is unlikely that it utilized this morphology in moving substrate during burrow or cavity construction. Members of the Eucavities are altricial, their cavities providing added protection for their highly dependent offspring (Hoyo et al., 2002), whereas evidence indicates enantiornithines were precocial and laid their eggs partially exposed in soft sediments near water (Varricchio and Jackson, 2016; Bailleul et al., 2019).

Reconstructing the Burmese Avifauna

The Hukawng is thought to have been part of the *Trans-Tethyan* island arc—an isolated island setting, separated from the mainland of what is now the Asian continent (Westerweel et al., 2019). These two species of morphologically specialized enantiornithines further support the prediction that geographically isolated settings (i.e., islands) have the capability to produce an array of unique and specialized fauna, particularly in birds, that exhibit morphologies disparate from other related

mainland species (e.g., Hawaiian archipelago, New Guinea, Galapagos Islands) (Pratt, 2005). Like other geographically isolated settings, various niches have been adopted with unique evolutionary responses to environmental pressures. On most continents, picids dominate the wood boring and probing niche, while on isolated islands like the Hawaiian archipelago and the Galapagos islands, this niche has been filled by other bird species either by a hypertrophied hetero-bill (*Hemignathus munroi*) and even with tool use (*Camarhynchus pallidus*). Similarly, these isolated Cretaceous *Trans-tethyan* islands may have been free of boring/probing taxa found on the continent, allowing this niche to become utilized by enantiornithine birds. The unique way in which this niche was utilized by enantiornithines, through an elongated pedal digit, contributes to the diversity of vertebrate probing structures evolved through time.

Although the vast majority of known enantiornithine taxa appear to be arboreal on the basis of pedal morphology, this clade does exhibit ecological diversity. In the Early Cretaceous this diversity can be observed in the variation of cranial and dental morphologies found in the Jehol avifauna (O'Connor and Chiappe, 2011) whereas in the Late Cretaceous diversity is expressed through variation in the tarsometatarsus (Chiappe, 1993). Our revised ethological inferences regarding these two unusual Hukawng birds strengthen the prediction that the enantiornithines were a clade capable of high morphological diversification.

Despite the fact the remains of these two taxa represent only a small portion of each bird, they still exhibit morphologies unique among all previously known avian and non-avian taxa (i.e., elongate pedal digit for probing and mediolaterally enlarged lateral pedal digit presumed for greater stability while perched). Re-evaluation of these taxa helps to create a better understanding of both the biodiversity of the Burmese avifauna and the ways in which enantiornithines adapted to fill ecological roles.

The recognition of these specialized forms also reveals a pattern of avian faunal structure evolution similar to that observed in isolated settings today. Changes in morphology and behavior from mainland counterparts, often times with alterations in the latter affecting the former, further facilitate unique morphological responses allowing for greater ecological niche expansion (Scott et al., 2003; Pratt, 2005). Isolation-caused evolutionary changes, according to Bock (1970), begin with allopatric speciation due to an array of open niches, which gives way to secondary sympatry, and finally results in further diverged speciation events of differing ethologies and ecologies (Bock, 1970; Pratt, 2005). This clear demonstration of unique morphologies and subsequent predicted accompanying behavior in these two enantiornithines, supports the pattern that geographically isolated evolutionary pressures can produce unique physiological adaptations in birds, and that these patterns extended back into the Cretaceous.

Systematic Paleontology

Aves Linnaeus 1758

Ornithothoraces Chiappe, 1995

Enantiornithines Walker, 1981

Fortipesavis prehensens gen. et sp. nov. (Figures 3A–C).

Holotype

YLSNHM01001, external mold of digits II–IV and distalmost portion of left tarsometatarsus preserved in amber (Xing et al., 2019b). Middle-upper Albian, 98.8 ± 0.06 Ma (Wright et al., 1996; Shi et al., 2012; Xing et al., 2019b).

Etymology

The generic name *Fortipesavis*, derives from “*Fortipes*,” Latin compound for strong-footed, “*avis*,” Latin meaning bird. The specific name “*prehendens*” comes from the Latin verb to grip or grasp. “*Fortipesavisprehendens*,” Latin for gripping strong-footed bird.

Diagnosis

Small bird with the unique combination of the following features: mediolateral width of digit IV greater than digit III, and that of digit III greater than that of digit II, such that the mediolateral width of digit IV is twice that of digit II (autapomorphy); plantar pads of digit IV mediolaterally wider than they are craniocaudally long and located between phalangeal joints; exaggerated plantar pads of digit IV separated by deep clefts; and digit II ungual long, recurved and sharply tapered.

CONCLUSION

Taxa utilizing the same ecological niche tend to evolve morphological structures with similar functions that are often superficially reminiscent (e.g., elongated structures used for probing). Morphological differences in functionally homologous structures between groups are likely due to natural selection modifying the morphology of a particular organism, limited by the existing structures of each particular group (e.g., the wings of volant birds cannot be modified into elaborate probing structures). Two enantiornithines known entirely from hindlimb material preserved in mid-Cretaceous amber exhibit unusual morphologies that have no obvious analogs among extant taxa. Here we explore previous predictions regarding the ecological niches of these two taxa, through additional comparative information from a wider range of extant taxa. We provide further support for the inferences regarding the probing ecology of *E. chenguangi*, for which we consider a wood-probing ecology most likely, and further predict the bill was robust and edentulous allowing this taxon to create openings in hard wood substrate. Crown birds that probe in hard substrates do so with the bill and/or tongue, whereas mammals primarily probe with manual digits. Thus, if predictions regarding *E. chenguangi* are correct, the ecological adaptations for probing utilized by this taxon are unique among all known animals but are more similar to mammalian wood-probers than to extant avians that utilize this niche. Further comparison between raptorial birds and *F.prehendens* does not support the original interpretation that this species was a predator that relied on its pedes for prey capture. The laterally robust foot morphology is more reminiscent of the syndactyl condition and suggests this species utilized thin, mobile perches that required increased grip and stability. These results help

us elucidate habitat structure in the mid-Cretaceous tropical forests of Myanmar. This study supports interpretations that the enantiornithines were ecologically diverse and employed unique morphologies to thrive in roles utilized by birds today. This study demonstrates the utility of comparative data derived from extant taxa in making ecomorphological inferences regarding extinct taxa. Additional discoveries will reveal the accuracy of these interpretations, which will in turn improve the accuracy of future predictions regarding Cretaceous enantiornithine ecology and behavior, specifically in the unusual Burmese avifauna. Continued study and understanding of how ecology shapes morphology in extant taxa will continue to aid paleontologists in understanding the incredible diversity and behavior of extinct organisms.

DATA AVAILABILITY STATEMENT

The original contributions presented in the study are included in the article/**Supplementary Material**, further inquiries can be directed to the corresponding author/s.

AUTHOR CONTRIBUTIONS

AC was responsible for primary investigation, conceptualization, data curation, and original draft authorship. JO'C was responsible for investigation, methodology, supervision, and draft editor. Both authors contributed to the article and approved the submitted version.

ACKNOWLEDGMENTS

We would like to thank Ville Sinkkonen for his work as a paleoartist, and for working with us in order to bring *Fortipesavisprehendens* to life. We would also like to thank Steve Rogers at the Carnegie Museum in Pittsburgh and the staff within the ornithology collections at the Field Museum at Chicago for access to specimens. We would further like to thank USGS biologist Paul Banko for aid in locating historical Hawaiian honeycreeper measurements. The new taxon's genus and species catalog number from Zoobank.org is urn:lsid:zoobank.org:pub:C7C3F5C0-CBD8-42C0-A6F2-231CA2D1C0D1.

SUPPLEMENTARY MATERIAL

The Supplementary Material for this article can be found online at: <https://www.frontiersin.org/articles/10.3389/fevo.2021.654156/full#supplementary-material>

Supplementary Figure 1 | A ternary diagram plotting seven species of similarly-sized Hawaiian honeycreepers. Bt.Diff, bill tip differences; ExC.M, exposed culmen length to mandible length ratio. The large disparity in upper and lower bill morphologies of the *H. wilsoni* is present even though similar tarsus lengths are fairly consistent throughout the measured species.

REFERENCES

- Allen, L. L., Morrison, K. L., Scott, W. A. E., Shinn, S., Haltiner, A. M., and Doherty, M. J. (2018). Differences between stance and foot preference evident in Osprey (*Pandion haliaetus*) fish holding during movement. *Brain Behav.* 8:e01126. doi: 10.1002/brb3.1126
- Arendt, J., and Reznick, D. (2008). Convergence and parallelism reconsidered: what have we learned about the genetics of adaptation? *Trends Ecol. Evol.* 23, 26–32. doi: 10.1016/j.tree.2007.09.011
- Backus, S. B., Sustaita, D., Odhner, L. U., and Dollar, A. M. (2015). Mechanical analysis of avian feet: multiarticular muscles in grasping and perching. *R. Soc. Open Sci.* 2:140350. doi: 10.1098/rsos.140350
- Bailleul, A. M., O'Connor, J., Zhang, S., Li, Z., Wang, Q., Lamanna, M. C., et al. (2019). An Early Cretaceous enantiornithine (Aves) preserving an unlaid egg and probable medullary bone. *Nat. Commun.* 10:1275. doi: 10.1038/s41467-019-09259-x
- Bierregaard, R. O., Poole, A. F., Martell, M. S., Pyle, P., and Patten, M. A. (2020). "Osprey (*Pandion haliaetus*), version 1.0," in *Birds of the World*, ed. P. G. Rodewald (Ithaca, NY: Cornell Lab of Ornithology).
- Bock, W., and Miller, W. D. (1959). The scansorial foot of the woodpeckers, with comments on the evolution of perching and climbing feet in birds. *Am. Mus. Novit.* 1931, 1–45.
- Bock, W. J. (1970). Microevolutionary sequences as a fundamental concept in macroevolutionary models. *Evolution* 24, 704–722. doi: 10.2307/2406551
- Bock, W. J. (1994). Concepts and methods in ecomorphology. *J. Biosci.* 19, 403–413. doi: 10.1007/bf02703177
- Botelho, J. F., Smith-Paredes, D., and Vargas, A. O. (2015). Altriciality and the evolution of Toe orientation in birds. *Evol. Biol.* 42, 502–510. doi: 10.1007/s11692-015-9334-7
- Casali, D. M., Martins-Santos, E., Santos, A. L. Q., Miranda, F. R., Mahecha, G. A. B., and Perini, F. A. (2017). Morphology of the tongue of Vermilingua (*Xenarthra*: Pilosa) and evolutionary considerations: casali et al. *J. Morphol.* 278, 1380–1399. doi: 10.1002/jmor.20718
- Chiappe, L., Norell, M., and Clark, J. (2001). A New Skull of *Gobipteryx minuta* (Aves:Enantiornithines) from the cretaceous of the gobi desert. *Am. Mus. Novit.* 2001, 1–5. doi: 10.1206/0003-0082(2001)346<0001:ansogm>2.0.co;2
- Chiappe, L. M. (1993). Enantiornithine (Aves) tarsometatarsi from the cretaceous lecho formation of Northwest Argentina. *Am. Mus. Novit.* 3083, 1–27.
- Chiappe, L. M. (1995). The first 85 million years of avian evolution. *Nature* 378, 349–355.
- Chiappe, L. M., and Walker, C. A. (2002). "Skeletal morphology and systematics of the Cretaceous Euenantiornithines (Ornithothoraces: Enantiornithes)," in *Mesozoic birds: Above the Heads of Dinosaurs*, eds L. M. Chiappe and L. M. Witmer (Berkeley, CA: University of California Press), 240–267.
- Chiappe, L. M., and Witmer, L. M. eds (2002). *Mesozoic birds: Above the Heads of Dinosaurs*. Berkeley, CA: University of California Press.
- Cunningham, S. J., Alley, M. R., Castro, I., Potter, M. A., Cunningham, M., and Pyne, M. J. (2010). bill morphology of ibises suggests a remote-tactile sensory system for prey detection. *Auk* 127, 308–316. doi: 10.1525/auk.2009.09117
- Cunningham, S. J., Corfield, J. R., Iwaniuk, A. N., Castro, I., Alley, M. R., Birkhead, T. R., et al. (2013). the anatomy of the bill tip of kiwi and associated somatosensory regions of the brain: comparisons with shorebirds. *PLoS One* 8:e80036. doi: 10.1371/journal.pone.0080036
- Eduardo, J., Bicudo, P. W., Buttemer, W. A., Chappell, M. A., Pearson, J. T., and Bech, C. (2010). *Ecological and Environmental Physiology of Birds*. Oxford: Oxford University Press.
- Erickson, C. J., Nowicki, S., Dollar, L., and Goehring, N. (1998). Percussive Foraging: stimuli for prey location by aye-ayes (*Daubentonia madagascariensis*). *Int. J. Primatol.* 19, 111–122.
- Falk, A. R., Lamsdell, J. C., and Gong, E. (2020). Principal component analysis of avian hind limb and foot morphometrics and the relationship between ecology and phylogeny. *Paleobiology* 2020, 1–23. doi: 10.1017/pab.2020.39
- Feistner, A. T. C., Price, E. C., and Milliken, G. W. (1994). Preliminary observations on hand preference for tapping, digit-feeding and food-holding in captive aye-ayes (*Daubentonia madagascariensis*). *Folia Primatol.* 62, 136–141. doi: 10.1159/000156770
- Felice, R. N., Tobias, J. A., Pigot, A. L., and Goswami, A. (2019). Dietary niche and the evolution of cranial morphology in birds. *Proc. R. Soc. B* 286:20182677. doi: 10.1098/rspb.2018.2677
- Fowler, D. W., Freedman, E. A., and Scannella, J. B. (2009). Predatory Functional morphology in raptors: interdigital variation in talon size is related to prey restraint and immobilization technique. *PLoS One* 4:e7999. doi: 10.1371/journal.pone.0007999
- Fowler, D. W., Freedman, E. A., Scannella, J. B., and Kambic, R. E. (2011). The predatory ecology of deinonychus and the origin of flapping in birds. *PLoS One* 6:e28964. doi: 10.1371/journal.pone.0028964
- Gill, F. B., Prum, R. O., and Robinson, S. K. (2019). in *Ornithology*, 4 Edn, ed. W. H. Freeman (New York NY: Macmillan Learning).
- Grant, P. (1966). Further Information on the relative length of the tarsus in land birds. post. *Peabody Mus. Nat. Hist.* 98, 1–13. doi: 10.3838/jjo.47.1
- Handasyde, K., and Martin, R. (1996). Field observations of the common striped possum (*Dactylopsila trivirgata*) in North Queensland. *Wildlife Res.* 23:755. doi: 10.1071/wr9960755
- Höfling, E., and Abourachid, A. (2020). The skin of birds' feet: morphological adaptations of the plantar surface. *J. Morphol.* 282, 88–97. doi: 10.1002/jmor.21284
- Hopson, J. (2001). "Ecomorphology of avian and nonavian theropod phalangeal proportions: implications for the arboreal versus terrestrial origin of bird flight. New perspectives on the origin and early evolution of birds," in *Proceedings of the International Symposium in Honor of John H. (Paris: Ostrum).*
- Hoyo, J., del Burn, H., Collar, N., and Fuller, E. (Eds.) (2002). *Jacamars to Woodpeckers, Handbook of the Birds of the World*. Barcelona: Lynx Edicions.
- Hoyo, J., Elliot, A., and Sargatal, J. (Eds.) (2001). *Mousebirds to Hornbills, Handbook of the Birds of the World*. Barcelona: Lynx Edicions.
- Hoyo, J., Elliot, A., Sargatal, J., and Cabot, J. (Eds.) (1992). *Handbook of the Birds of the World*. Barcelona: Lynx Edicions.
- Huang, W.-S. (2006). Ecological characteristics of the skink, *Mabuya longicaudata*, on a tropical east Asian island. *Copeia* 2006, 293–300. doi: 10.1643/0045-8511(2006)6[293:ecotsm]2.0.co;2
- Jouffroy, F. K. (1975). "Osteology and myology of the lemuriform postcranial skeleton," in *Lemur Biology*, eds I. Tattersall and R. W. Sussaman (New York NY: Plenum Press), 149–191. doi: 10.1007/978-1-4684-2121-7_9
- Kapoor, B. G., and Bhargava, S. C. (1967). A study on the barbels of a marine catfish, *arius thalassinus*. *Jap. J. Lchthyol.* 14, 201–298.
- Katzir, G., Berman, D., Nathan, M., and Weihs, D. (2018). Sustained hovering, head stabilization and vision through the water surface in the Pied kingfisher (*Ceryle rudis*). *bioRxiv*[Preprint] doi: 10.1101/409201
- Katzir, G., Schechtman, E., Carmi, N., and Weihs, D. (2001). Head Stabilization in Herons. *J. Comparat. Physiol. A* 187, 423–432. doi: 10.1007/s003590100210
- Kobayashi, K., Kumakura, M., Yoshimura, K., Inatomi, M., and Asami, T. (1998). Fine structure of the tongue and lingual papillae of the penguin. *Arch. Histol. Cytol.* 61, 37–46. doi: 10.1679/aohc.61.37
- Legendre, L. J., and Botha-Brink, J. (2018). Digging the compromise: investigating the link between limb bone histology and fossoriality in the aardvark (*Orycteropus afer*). *PeerJ* 6:e5216. doi: 10.7717/peerj.5216
- Li, Z., Wang, C.-C., Wang, M., Chiang, C.-C., Wang, Y., Zheng, X., et al. (2020). Ultramicrostructural reductions in teeth: implications for dietary transition from non-avian dinosaurs to birds. *BMC Evol. Biol.* 20:46.
- Losos, J. B., Schoener, T. W., Langerhans, R. B., and Spiller, D. A. (2006). Rapid temporal reversal in predator-driven natural selection. *Science (New York, N.Y.)* 314:1111. doi: 10.1126/science.1133584
- Louchart, A., and Viriot, L. (2011). From snout to beak: the loss of teeth in birds. *Trends Ecol Evol* 26:663–673. doi: 10.1016/j.tree.2011.09.004
- Lovette, I. J., and Fitzpatrick, J. W. eds (2016). *Handbook of Bird Biology*, 3 Edn. Nashville, TN: John Wiley & Sons.
- McCall, R. A., Nee, S., and Harvey, P. H. (1998). The role of wing length in the evolution of avian flightlessness. *Evol. Ecol.* 12, 569–580. doi: 10.1023/a:1006508826501
- Milliken, G. W., Ward, J. P., and Erickson, C. J. (1991). Independent digit control in foraging by the aye-aye (*Daubentonia madagascariensis*). *Folia Primatologica* 56, 219–224. doi: 10.1159/000156551

- Morris, P. J. R., Cobb, S. N. F., and Cox, P. G. (2018). Convergent evolution in the Euarchontoglires. *Biol. Lett.* 14:20180366. doi: 10.1098/rsbl.2018.0366
- Mountainspring, S. (1987). Ecology. *Behav. Conserv. Maui Parrotbill. Condor* 89, 24–39.
- Munro, G. C. (1960). *Birds of Hawai'i*. Charles E. Rutland, VT: Tuttle Company.
- Nudds, R. L., and Davidson, J. S. (2010). A shortening of the manus precedes the attenuation of other wing-bone elements in the evolution of flightlessness in birds. *Acta Zool.* 91, 115–122. doi: 10.1111/j.1463-6395.2009.00391.x
- Ochs, M. F., Zamani, M., Gomes, G. M. R., de Oliveira Neto, R. C., and Kane, S. A. (2017). Sneak peek: raptors search for prey using stochastic head turns. *Auk* 134, 104–115. doi: 10.1642/auk-15-230.1
- O'Connor, J. (2012). A Revised Look at. *Vertebrata Palasiatica: Liaoningornis Longidigitrus*, 25–37.
- O'Connor, J. K. (2019). The trophic habits of early birds. *palaeogeography, palaeoclimatology. Palaeoecology* 513, 178–195. doi: 10.1016/j.palaeo.2018.03.006
- O'Connor, J. K., and Chiappe, L. M. (2011). A revision of enantiornithine (Aves: Ornithothoraces) skull morphology. *J. Syst. Palaeontol.* 9, 135–157. doi: 10.1080/14772019.2010.526639
- O'Connor, J. K., Li, D.-Q., Lamanna, M. C., Wang, M., Harris, J. D., Atterholt, J., et al. (2016a). A new early cretaceous enantiornithine (Aves, Ornithothoraces) from northwestern China with elaborate tail ornamentation. *J. Vertebrate Paleontol.* 36:e1054035. doi: 10.1080/02724634.2015.1054035
- O'Connor, J. K., Wang, X., Chiappe, L. M., Gao, C., Meng, Q., Cheng, X., et al. (2009). Phylogenetic support for a specialized clade of cretaceous enantiornithine birds with information from a new species. *J. Vertebrate Paleontol.* 29, 188–204. doi: 10.1080/02724634.2009.10010371
- O'Connor, J. K., Wang, X., Zheng, X., Hu, H., Zhang, X., and Zhou, Z. (2016b). An Enantiornithine with a fan-shaped tail, and the evolution of the rectricial complex in early birds. *Curr. Biol.* 26, 114–119. doi: 10.1016/j.cub.2015.11.036
- O'Connor, J. K., Zhang, Y., Chiappe, L. M., Meng, Q., Quanguo, L., and Di, L. (2013). A new enantiornithine from the yixian formation with the first recognized avian enamel specialization. *J. Vertebrate Paleontol.* 33, 1–12. doi: 10.1080/02724634.2012.719176
- O'Connor, P. M., Turner, A. H., Groenke, J. R., Felice, R. N., Rogers, R. R., Krause, D. W., et al. (2020). Late cretaceous bird from Madagascar reveals unique development of beaks. *Nature* 588, 272–276.
- Pearce, T. (2012). Convergence and parallelism in evolution: a neo-gouldian account. *Br. J. Phil. Sci.* 63, 429–448. doi: 10.1093/bjps/axr046
- Perkins, R. C. L. (1903). in *Fauna Hawaiiensis, Vertebrata*, Vol. I, ed. D. Sharp (Cambridge: Cambridge University Press).
- Pratt, H. D. (2005). *The Hawaiian Honeycreepers: Drepanidinae*. London: Oxford University Press.
- Ralph, C. J., and Fancy, S. G. (1996). Aspects of the life history and foraging ecology of the endangered akiapolaau. *Condor* 98, 312–321. doi: 10.2307/1369149
- Schulenberg, T. (1983). Foraging behavior, eco-morphology, and systematics of some antshrikes (Formicariidae: Thamnomanes). *Wilson Bull.* 95, 505–521.
- Scott, S. N., Clegg, S. M., Simon, P. B., Kikkawa, J., and Owens, P. F. (2003). Morphological shifts in island-dwelling birds: the roles of generalist foraging and niche expansion. *Evolution* 57, 2147–2156. doi: 10.1554/03-021
- Sesoko, N. F., Rahal, S. C., Bortolini, Z., de Souza, L. P., Vulcano, L. C., Monteiro, F. O. B., et al. (2015). SKELETAL MORPHOLOGY OF THE FORELIMB OF MYRMECOPHAGA TRIDACTYLA. *J. Zoo Wildlife Med.* 46, 713–722.
- Shi, G. G., Harlow, G. E., Wang, J., Wang, J., Yang, M., Yang, M., et al. (2012). Age constraint on Burmese amber based on U-Pb dating of zircons. *Cretac. Res.* 37, 155–163. doi: 10.1016/j.cretres.2012.03.014
- Simon, J. C., Baker, P. E., and Baker, H. (2020). “Maui Parrotbill (Pseudonestor xanthophrys), version 1.0,” in *Birds of the World*, eds A. F. Poole and F. B. Gill (Ithaca, NY: Cornell Lab of Ornithology).
- Soligo, C. (2005). Anatomy of the hand and arm in daubentonina madagascariensis: a functional and phylogenetic outlook. *Folia Primatol.* 76, 262–300. doi: 10.1159/000088034
- Stayton, C. T. (2008). Is convergence surprising? An examination of the frequency of convergence in simulated datasets. *J. Theor. Biol.* 252, 1–14. doi: 10.1016/j.jtbi.2008.01.008
- Tsang, L. R., and McDonald, P. G. (2018). A comparative study of avian pes morphotypes, and the functional implications of Australian raptor pedal flexibility. *Emu Austral. Ornithol.* 119, 14–23. doi: 10.1080/01584197.2018.1483203
- Tsang, L. R., Wilson, L. A. B., Ledogar, J., Wroe, S., Attard, M., and Sansalone, G. (2019). Raptor talon shape and biomechanical performance are controlled by relative prey size but not by allometry. *Sci. Rep.* 9:7076.
- Van Dyck, S. (1983). in *Striped Possum. Complete Book of Australian Mammals*, ed. R. Strahan (Sydney: The Australian Museum of Angus and Robertson), 144.
- Varricchio, D. J., and Jackson, F. D. (2016). Reproduction in Mesozoic birds and evolution of the modern avian reproductive mode. *Auk* 133, 654–684. doi: 10.1642/AUK-15-216
- Wainwright, P. C. (1991). Ecomorphology: experimental functional anatomy for ecological problems. *Am. Zool.* 31, 680–693. doi: 10.1093/icb/31.4.680
- Walker, C. A. (1981). New subclass of birds from the Cretaceous of South America. *Nature* 292, 51–53. doi: 10.1038/292051a0
- Wallman, J., and Letelier, J.-C. (1993). “Eye movements, head movements, and gaze stabilization in birds,” in *Vision, Brain, and Behavior in Birds*, eds H. P. Zeigler and H.-J. Bischof (Cambridge MA: The MIT Press), 245–263.
- Wang, M., and Zhou, Z. (2017). A morphological study of the first known piscivorous enantiornithine bird from the Early Cretaceous of China. *J. Vertebrate Paleontol.* 37:e1278702. doi: 10.1080/02724634.2017.1278702
- Wang, M., Zhou, Z.-H., O'Connor, J. K., and Zelenkov, N. V. (2014). A new diverse enantiornithine family (*Bohaiornithidae* fam. nov.) from the Lower Cretaceous of China with information from two new species. *Vertebrata Palasiatica*. 2014, 31–76.
- Westerweel, J., Roperch, P., Licht, A., Dupont-Nivet, G., Win, Z., Poblete, F., et al. (2019). Burma Terrane part of the trans-tethyan arc during collision with India according to palaeomagnetic data. *Nat. Geosci.* 12, 863–868. doi: 10.1038/s41561-019-0443-2
- Winkler, D. W., Billerman, S. M., and Lovette, I. J. (2020a). “Woodpeckers (Picidae), version 1.0,” in *Birds of the World*, eds S. M. Billerman, B. K. Keeney, P. G. Rodewald, and T. S. Schulenberg (Ithaca, NY: Cornell Lab of Ornithology).
- Winkler, D. W., Billerman, S. M., and Lovette, I. J. (2020b). “Kingfishers (Alcedinidae), version 1.0,” in *Birds of the World*, eds S. M. Billerman, B. K. Keeney, P. G. Rodewald, and T. S. Schulenberg (Ithaca, NY: Cornell Lab of Ornithology).
- Winkler, D. W., Billerman, S. M., and Lovette, I. J. (2020c). “Grebes (Podicipedidae), version 1.0,” in *Birds of the World*, eds S. M. Billerman, B. K. Keeney, P. G. Rodewald, and T. S. Schulenberg (Ithaca, NY: Cornell Lab of Ornithology).
- Winkler, D. W., Billerman, S. M., and Lovette, I. J. (2020d). “Bee-eaters (Meropidae), version 1.0,” in *Birds of the World*, eds S. M. Billerman, B. K. Keeney, P. G. Rodewald, and T. S. Schulenberg (Ithaca, NY: Cornell Lab of Ornithology).
- Winkler, D. W., Billerman, S. M., and Lovette, I. J. (2020e). “Hornbills (Bucerotidae), version 1.0,” in *Birds of the World*, eds S. M. Billerman, B. K. Keeney, P. G. Rodewald, and T. S. Schulenberg (Ithaca, NY: Cornell Lab of Ornithology).
- Winkler, D. W., Billerman, S. M., and Lovette, I. J. (2020f). “Asian and grauer's Broadbills (Eurylaimidae), version 1.0,” in *Birds of the World*, eds S. M. Billerman, B. K. Keeney, P. G. Rodewald, and T. S. Schulenberg (Ithaca, NY: Cornell Lab of Ornithology).
- Winkler, D. W., Billerman, S. M., and Lovette, I. J. (2020g). “African and green broadbills (Calyptomenidae), version 1.0,” in *Birds of the World*, eds S. M. Billerman, B. K. Keeney, P. G. Rodewald, and T. S. Schulenberg (Ithaca, NY: Cornell Lab of Ornithology).
- Wright, C. W., Callomon, J. H., and Howarth, M. K. (1996). “Cretaceous ammonioidea,” in *Treatise on Invertebrate Paleontology. Part I. Mollusca 4 (Revised)*, ed. R. L. Kaesler (Boulder: Geological Society of America), 362.
- Xing, L., Cockx, P., and McKellar, R. C. (2020a). Disassociated feathers in Burmese amber shed new light on mid-Cretaceous dinosaurs and avifauna. *Gondwana Res.* 82, 241–253. doi: 10.1016/j.jgr.2019.12.017
- Xing, L., Cockx, P., McKellar, R. C., and O'Connor, J. (2018a). Ornamental feathers in Cretaceous Burmese amber: resolving the enigma of rachis-dominated feather structure. *J. Palaeogeogr.* 7:13.
- Xing, L., Cockx, P., O'Connor, J. K., and McKellar, R. C. (2020b). A newly discovered enantiornithine foot preserved in mid-Cretaceous Burmese amber. *Palaeontomology* 3, 212–219. doi: 10.11646/palaeontomology.3.2.11

- Xing, L., McKellar, R. C., and O'Connor, J. K. (2020c). An unusually large bird wing in mid-Cretaceous Burmese amber. *Cretac. Res.* 110:104412. doi: 10.1016/j.cretres.2020.104412
- Xing, L., McKellar, R. C., O'Connor, J. K., Bai, M., Tseng, K., and Chiappe, L. M. (2019a). A fully feathered enantiornithine foot and wing fragment preserved in mid-Cretaceous Burmese amber. *Sci. Rep.* 9:927.
- Xing, L., McKellar, R. C., O'Connor, J. K., Niu, K., and Mai, H. (2019b). A mid-Cretaceous enantiornithine foot and tail feather preserved in Burmese amber. *Sci. Rep.* 9:15513.
- Xing, L., McKellar, R. C., Wang, M., Bai, M., O'Connor, J. K., Benton, M. J., et al. (2016). Mummified precocial bird wings in mid-Cretaceous Burmese amber. *Nat. Commun.* 7:12089.
- Xing, L., O'Connor, J. K., Chiappe, L. M., McKellar, R. C., Carroll, N., Hu, H., et al. (2019c). A new enantiornithine bird with unusual pedal proportions found in Amber. *Curr. Biol.* 29:2594. doi: 10.1016/j.cub.2019.07.042
- Xing, L., O'Connor, J. K., McKellar, R. C., Chiappe, L. M., Bai, M., Tseng, K., et al. (2018b). A flattened enantiornithine in mid-Cretaceous Burmese amber: morphology and preservation. *Sci. Bull.* 63, 235–243. doi: 10.1016/j.scib.2018.01.019
- Xing, L., O'Connor, J. K., McKellar, R. C., Chiappe, L. M., Tseng, K., Li, G., et al. (2017). A mid-Cretaceous enantiornithine (Aves) hatchling preserved in Burmese amber with unusual plumage. *Gondwana Res.* 49, 264–277. doi: 10.1016/j.gr.2017.06.001
- Xing, L., O'Connor, J. K., Niu, K., Cockx, P., Mai, H., and McKellar, R. C. (2020d). A New Enantiornithine (Aves) Preserved in Mid Cretaceous Burmese amber contributes to growing diversity of cretaceous plumage patterns. *Front. Earth Sci.* 8:264.
- Yuri, T., Kimball, R., Harshman, J., Bowie, R., Braun, M., Chojnowski, J., et al. (2013). Parsimony and Model-Based Analyses of Indels in avian nuclear genes reveal congruent and incongruent phylogenetic signals. *Biology* 2, 419–444. doi: 10.3390/biology2010419
- Zeffer, A., Johansson, C., and Marmebro, A. (2002). Functional correlation between habitat use and leg morphology in birds (Aves). *Biol. J. Linn. Soc.* 79, 461–484. doi: 10.1046/j.1095-8312.2003.00200.x
- Zeffer, A., and Norberg, M. (2002). Leg morphology and locomotion in birds: requirements for force and speed during ankle flexion. *J. Exp. Biol.* 206, 1085–1097. doi: 10.1242/jeb.00208
- Zhang, F., and Zhou, Z. (2000). A primitive enantiornithine bird and the origin of feathers. *Science* 290, 1955–1959. doi: 10.1126/science.290.5498.1955
- Zhang, F., Zhou, Z., Hou, L., and Gu, G. (2001). Early diversification of birds: Evidence from a new opposite bird. *Kexue tongbao [Chin. Sci. Bull.]* 46, 945–949. doi: 10.1007/bf02900473
- Zhou, Z., and Wang, Y. (2010). Vertebrate diversity of the Jehol Biota as compared with other lagerstätten. *Sci. China Earth Sci.* 53, 1894–1907. doi: 10.1007/s11430-010-4094-9
- Zhou, Z., and Zhang, F. (2004). A Precocial avian embryo from the lower cretaceous of china. *Science* 306, 653–653. doi: 10.1126/science.1100000
- Zhou, Z., and Zhang, F. (2007). Mesozoic birds of China—a synoptic review. *Front. Biol. China* 2, 1–14. doi: 10.1007/s11515-007-0001-y
- Zusi, R. (1989). A modified jaw muscle in the maui parrotbill (*Pseudonestor: Drepanididae*). *Condor* 91, 716–720. doi: 10.2307/1368125

Conflict of Interest: The authors declare that the research was conducted in the absence of any commercial or financial relationships that could be construed as a potential conflict of interest.

Copyright © 2021 Clark and O'Connor. This is an open-access article distributed under the terms of the Creative Commons Attribution License (CC BY). The use, distribution or reproduction in other forums is permitted, provided the original author(s) and the copyright owner(s) are credited and that the original publication in this journal is cited, in accordance with accepted academic practice. No use, distribution or reproduction is permitted which does not comply with these terms.



Quantitative Analysis of Morphometric Data of Pre-modern Birds: Phylogenetic Versus Ecological Signal

Alyssa Bell^{1,2*}, Jesús Marugán-Lobón^{1,3}, Guillermo Navalón^{3,4}, Sergio M. Nebreda³, John DiGiuldo² and Luis M. Chiappe¹

¹The Dinosaur Institute, Natural History Museum of Los Angeles County, Los Angeles, CA, United States, ²Department of Biological Sciences, California Polytechnic State University, Pomona, CA, United States, ³Unidad de Paleontología, Departamento de Biología, Universidad Autónoma de Madrid, Madrid, Spain, ⁴Department of Earth Sciences, University of Oxford, Oxford, United Kingdom

OPEN ACCESS

Edited by:

Corwin Sullivan,
University of Alberta, Canada

Reviewed by:

Federico Agnolin,
Museo Argentino de Ciencias
Naturales Bernardino Rivadavia,
Argentina
Raúl Orencio Gómez,
University of Buenos Aires, Argentina

*Correspondence:

Alyssa Bell
abell@nhm.org

Specialty section:

This article was submitted to
Paleontology,
a section of the journal
Frontiers in Earth Science

Received: 02 February 2021

Accepted: 18 June 2021

Published: 06 July 2021

Citation:

Bell A, Marugán-Lobón J, Navalón G, Nebreda SM, DiGiuldo J and Chiappe LM (2021) Quantitative Analysis of Morphometric Data of Pre-modern Birds: Phylogenetic Versus Ecological Signal.
Front. Earth Sci. 9:663342.
doi: 10.3389/feart.2021.663342

Birds are one of the most diverse clades of extant terrestrial vertebrates, a diversity that first arose during the Mesozoic as a multitude of lineages of pre-neornithine (stem) birds appeared but did not survive into the Cenozoic Era. Modern birds (Neornithes) inhabit an extensive array of ecologically distinct habitats and have specific and varied foraging strategies. Likewise, the morphological disparity among Mesozoic lineages appears to underscore a significant degree of ecological diversity, yet attempts to determine lineage-specific ecologies have mainly been limited to superficial narratives. In recent years, numerous studies have used various morphometric proxies to interpret the paleoecology of Mesozoic bird lineages, but largely without evaluating the interplay between ecological and phylogenetic signals. Moreover, most studies of this sort transform the original data into logarithms to control dimensionality, underestimating the biases induced upon such transformations. The goal of this study is to quantitatively address the ecomorphology of crown-group Neornithes using a dense sample of raw forelimb and hindlimb measurements, and to examine if such results can be used to infer the ecologies of Mesozoic bird lineages. To that end, scaling of limb measurements and ecological data from modern birds was assessed statistically using phylogenetic comparative methods, followed by the inclusion of fossil taxa. A strong relationship was recovered between humerus and hindlimb allometric scaling and phylogeny. Our results indicate that while some ecological classes of modern birds can be discriminated from each other, phylogenetic signature can overwhelm ecological signal in morphometric data, potentially limiting the inferences that can be made from ecomorphological studies. Furthermore, we found differential scaling of leg bones among Early Cretaceous enantiornithines and ornithuromorphs, a result hinting that habitat partitioning among different lineages could be a pervasive phenomenon in avian evolution.

Keywords: aves, mesozoic birds, neornithes, enantiornithes, ornithuromorpha, ecology, ecomorphology, phylogeny

INTRODUCTION

Modern birds comprise one of the most diverse clades of vertebrates alive today, yet members of this crown group, the Neornithes, are poorly represented in the fossil record before the Tertiary (Fountaine et al., 2005; Brocklehurst et al., 2012; Field et al., 2020). Instead, a wealth of pre-Tertiary fossils reveals the existence of numerous Mesozoic lineages outside of the crown clade Neornithes (Brusatte et al., 2015; Mayr 2016; Wang and Zhou 2017; Chiappe 2018; Chiappe and Bell 2020). These stem lineages represent an enormous diversity of forms, from the long-legged, cursorial *Hollanda* (Bell et al., 2010) to the long-winged, soaring *Sapeornis* (Serrano and Chiappe 2017), and from the small, flighted enantiornithines (O'Connor and Chiappe 2011; Liu et al., 2017) to the large, flightless hesperornithiforms (Bell and Chiappe 2016). This diversity in form has hinted at the possibility that collectively these stems birds could have approached the spectacular ecological diversity we see today in modern birds (Chiappe 2018).

Evidence for this impressive ecological diversity comes from a range of sources, such as specimens that preserve gut contents, which provide first-hand evidence of what some of these birds ate, yielding direction information regarding their lifestyles. Additionally, a number of pre-modern birds exhibit specific morphological features that can be interpreted as indicators of a particular lifestyle. A classic example of this sort of ecomorphological inference pertains to the hesperornithiforms, whose many skeletal similarities to modern loons and grebes have long led to interpretations of an aquatic, foot-propelled diving lifestyle (i.e., Marsh 1880; Bell et al., 2019). Aside from the hesperornithiforms, which were flightless, recent studies have revealed that stem birds evolved most flight modes (e.g., soaring, flap and glide, bounding, and continuous flapping) typical of modern birds (Serrano and Chiappe 2017; Serrano et al., 2017). Finally, because the relationship between morphological traits and ecological characteristics is not always straightforward, quantitative analysis of comparative datasets for modern and fossil birds is a promising avenue of inquiry.

As our understanding of Mesozoic avian diversity has grown through the study of individual taxa, some generalizations have been proposed as well. One study of the Early Cretaceous Jehol Biota found ecological diversity was low in comparison to taxonomic diversity, (Mitchell and Makovicky 2014). The study in question, however, focused exclusively on the Jehol Biota and used a very limited number of taxa from that assemblage. A number of studies have posited a trophic bias among Early Cretaceous birds, with gut contents, facial morphology, tooth patterns and form, and other indicators of diet or ecological niche suggesting that many enantiornithines from this time period may have had an arboreal lifestyle and an insectivorous diet (although there are notable counterexamples among the longipterygids; see O'Connor et al., 2011), while ornithuromorphs are more commonly interpreted as land-dwellers or amphibious birds that ate fish or probed the substrate in search of crustaceans and worms (Zhou 2006; Wang et al., 2013; Field et al., 2018; O'Connor 2019; Wang et al., 2020). These generalizations, however, are far from certain,

and to date quantitative data has not been used to test these observations.

This study will first summarize the literature that has explored ecological diversity in Mesozoic birds and then present a new ecomorphological analysis of the largest database of modern and fossil birds collected to date. The results from these avenues of research demonstrate the enormous diversity of pre-modern birds, as well as a number of difficulties in reconstructing an animal's ecology from fossil remains, including important ways that data transformations alter results and can obscure underlying scaling relationships.

Previous Analyses of Mesozoic Avian Ecology

The past twenty years has seen a wealth of literature aimed at better understanding the ecology of Mesozoic birds. Studies have varied from qualitative or quantitative ecological assessments of specific taxa (i.e., You et al., 2006; Chiappe et al., 2007; Bell et al., 2010; Hu et al., 2015) to quantitative analyses of large datasets of modern and Mesozoic birds as well as non-avian theropods (i.e., Gatesy and Middleton 1997; Hopson 2001; Nudds et al., 2004; Bell and Chiappe 2011; Falk et al., 2020). Quantitative analyses that include Mesozoic birds have explored the use of a wide variety of data as proxies or indicators of ecological niche occupation: cortical bone thickness (Habib and Ruff 2008), furcula shape (Close and Rayfield 2012), curvature of the pedal ungual phalanges (Pike and Maitland 2004; Glen and Bennett 2007; Cobb and Sellers 2020), and various measurements of the forelimb and/or hindlimb (i.e., Nudds et al., 2004; Bell and Chiappe 2011; Wang et al., 2011; Falk et al., 2020). These studies have built on a substantial body of ecomorphological work on modern taxa (see reviews by Bock 1994; Tobias et al., 2020), particularly modern birds (e.g., Barbosa 1993; Hertel 1995; Zeffer 2002; Felice et al., 2019; Navalón et al., 2019; Sheard et al., 2020).

Ecological Inferences for Individual Taxa

A number of studies have used specific morphological features to infer the ecological habits of individual Mesozoic birds or clades. For instance, the inferred aquatic lifestyle of hesperornithiforms is based on a number of osteological features, such as the expanded fourth trochlea of the tarsometatarsus, extreme reduction of the forelimb, and expansion of the tibiotarsal cnemial crests and patella (Bell et al., 2019). Another classic example is the inference that enantiornithines occupied a wide variety of ecological niches, which rests on specific morphological features such as anisodactyly (indicating perching and arboreality) in *Sinornis*, *Concornis*, and *Neuquenornis*, and wading adaptations in the pedal morphology of *Lectavis* and *Yungavolucis* (Chiappe and Walker 2002).

More recently, the presence of expanded cnemial crests on the tibiotarsus, proximal displacement of metatarsal II, extremely elongate toes, proximal phalanges that are more elongate than the distal phalanges, unrecurved unguals with large flexor tubercles, and potentially webbed feet were all identified as morphological features indicative of an aquatic habitat in the ornithurine *Gansus*

(You et al., 2006). Similarly, the long leg bones of *Hongshanornis* and *Jianchangornis* were used without formal analysis to propose an aquatic lifestyle (*Hongshanornis*; Zhou and Zhang 2005) and a terrestrial lifestyle (*Jianchangornis*; Zhou et al., 2009) lifestyle for these taxa. Another example of an ecological inference for a specific taxon is the flightless, terrestrial lifestyle posited for *Patagopteryx*, based on extreme reduction of the wing (Alvarenga and Bonaparte 1992; Chiappe 2002). Additionally, an extremely short and broad pygostyle, unique among Mesozoic birds but seen in modern woodpeckers, was used to infer a scansorial lifestyle for *Parapengornis* (Hu et al., 2015).

Moving beyond osteology, the growing record of Cretaceous avian ichnofossils has provided evidence for ecological niche diversification. Sites in the Korean peninsula have revealed feeding traces (probing and others) similar to those left by mud probers and spoonbills (Kim et al., 2012). Likewise, a variety of tracks from these sites and others have been interpreted as belonging to web-footed (e.g., Lim et al., 2000) and terrestrial or climbing (e.g., Lockley et al., 2007) birds. Today, a global record of fossil traces (Lockley and Harris 2010) reinforces the skeletal evidence indicating that birds evolved a significant level of ecological diversity as early as the Early Cretaceous. While assigning specific trackmakers to these trace fossils is not possible to date, the existence of specialized ecological features in what were likely stem lineages points to a degree of diversification in these early birds that might have approached that seen in modern birds today.

A final line of evidence bearing on the ecology of individual specimens comes from the gut contents of particularly well-preserved individuals. O'Connor (2019) reviewed the fossil record of gut contents in Mesozoic birds, taking advantage of the exceptional preservation of numerous species with gut contents preserved in the Lower Cretaceous Jehol Lagerstätte of China. This analysis identified a variety of trophic guilds among early birds, including granivores (e.g., *Jeholornis*, *Sapeornis*), piscivores (e.g., *Yanornis*), and birds that fed on invertebrates (*Eoalulavis*) (O'Connor 2019). The elongate, thin rostrum and mandible of *Longirostravis* (Hou et al., 2004) and *Xinghaiornis* (Wang et al., 2013) has been used to infer a shore-dwelling, mud-probing lifestyle for both these birds.

While the presence of specific morphological features or preserved gut contents can make interpreting the ecology of some taxa relatively straightforward, in many cases such clear ecological indicators are not preserved in the fossil record.

Statistical Analyses of Individual Elements

In order to elucidate the complex relationships among morphology, function and ecology, a second type of paleoecological study has focused on quantitative analysis of the morphology of single elements, to evaluate them as proxies for particular aspects of avian ecology. An advantage of this approach is the ability to include fragmentary specimens, provided the focal element is preserved. The ungual phalanges or claws of birds have been used qualitatively by several studies as an indicator of ecological habit in modern birds (Richardson 1942; Yalden 1985; Peters and Görgner 1992). The first study to include a Mesozoic bird in a quantitative analysis focused on the interior

curvature of the claws on the third toe and the manus of *Archaeopteryx* and modern birds (Feduccia 1993). The results of this study were interpreted as indicating an arboreal lifestyle for *Archaeopteryx* (Feduccia 1993). Other studies have expanded on Feduccia's work by examining the scaling relationship of body mass with pedal claw shape, finding that while claw size appears to scale geometrically with body mass in most birds, the degree of overlap among most ecological groups made assigning specific ecological niches to fossil birds, such as *Archaeopteryx*, problematic (Pike and Maitland 2004). Glen and Bennett (2007) refined Feduccia (1993) ecological categories as segments of a continuum from completely arboreal (woodpeckers) to completely terrestrial (ostriches), and included multiple Mesozoic birds as well as non-avian theropods in the analysis. The results indicated that limited curvature of the pedal claw was the ancestral state in theropods, and most Mesozoic birds displayed pedal claw geometry consistent with a primarily terrestrial lifestyle (Glen and Bennett 2007). More recently, linear discriminant analysis of a large quantitative dataset of the curvature of the pedal ungual of modern and stem birds as well as non-avian theropods predicted an arboreal lifestyle for *Archaeopteryx* and *Microraptor*, and a predatory lifestyle for *Confuciusornis* (Cobb and Sellers 2020). However, a recent study has identified the remains of conifer cones among the gut contents of the confuciusornithid *Eoconfuciusornis*, thus casting doubts on the latter interpretation (Mayr et al., 2020).

The furcula has also been proposed as an indicator of ecology in modern birds, as the shape of the furcula varies widely across birds and is closely involved in the musculature of the flight apparatus (Hui 2002). Close and Rayfield (2012) expanded on Hui (2002) study of modern birds by performing an eigenshape analysis on the furcula of modern birds, sorted into five categories on the basis of flight style, as well as those of Mesozoic birds and non-avian theropods. This study found that Mesozoic ornithurines shared morphospace with modern flapping and flap-gliding birds, while all other Mesozoic taxa occurred at either the fringes of or outside the morphospace defined by modern birds (Close and Rayfield 2012).

Analyses of Multiple Elements

A large body of literature uses length comparisons of multiple elements in concert to correlate morphology with ecology in modern and Mesozoic birds. While individual studies usually vary in the choice of analyses and the elements included, all use similar methods. The morphospace occupied by modern birds is generally visualized using ternary diagrams or plots derived from Principal Components Analysis (PCA), which summarize the total variation described by the data. The location of the Mesozoic taxa in relation to that of modern birds in the morphospace is then described, although explicit statistical inferences are needed before drawing conclusions regarding ecological features. Ecological partitioning is often investigated by assigning modern taxa to ecological categories. Datasets can include measurements of the wing, leg, or toes, or some combination of those parts of the skeleton. Ecological bin choices vary widely across studies, ranging across general "terrestrial" and "arboreal"

categories, specific descriptions of flight styles, and categories of habitat usage.

Wing Measurements

One of the primary areas of interest in early bird research is the evolution of flight and the flight capabilities of Mesozoic birds. Stemming from this is the reconstruction of flight strategies used by Mesozoic birds, and investigation of how varying flight capabilities can be tied to ecological role. While a discussion of the literature on the evolution of flight is beyond the scope of this review, a number of papers specifically address the correlation of morphometric data from the wing with flight styles associated with specific ecological niches in modern birds. Two main types of data have been utilized thus far in the literature: relative lengths of the main skeletal elements of the wing (humerus + ulna/radius + manus/carpometacarpus) and relative lengths of the skeletal elements and primary feathers (humerus + ulna/radius + manus/carpometacarpus + primary feathers).

One of the earliest studies of the correlation between form and function in the wings of ancient and modern birds was undertaken by Middleton and Gatesy (2000). In this study, ternary diagrams were utilized to visualize the measurements of modern and Mesozoic birds and non-avian theropods in morphospace (Middleton and Gatesy 2000). Mesozoic taxa fell within a small portion of the morphospace defined by modern birds, with the chosen ecological groups not overlapping substantially in the morphospace. A later study that followed these methods expanded the analysis to include a wider variety of enantiornithine birds, as well as hindlimb data (Dyke and Nudds 2009; as forelimb and hindlimb data were analyzed separately, the hindlimb data will be discussed below with other studies of the hindlimb). This study also found that most Mesozoic birds overlapped in morphospace with modern birds, but specific ecological characterizations were not used (Dyke and Nudds 2009). Furthermore, this study highlighted the importance of body mass in ecologic interpretation. For example, while the Early Cretaceous *Otogornis* falls near hummingbirds and swifts in the morphospace, the large size of *Otogornis* as compared to hummingbirds makes a similar flight strategy and ecology unlikely (Dyke and Nudds 2009).

A number of studies have focused on the use of the brachial index (BI: humerus length/ulna length) as an indicator of flight capability or style, and as a correlate of ecological role. Such research initially focused on disparity in BI across modern and fossil birds (Nudds et al., 2004), and subsequently refining correlations between BI and ecological niche partitioning (Chiappe et al., 2007; Nudds et al., 2007). Nudds et al. (2007) found that BI varied among three groups of modern birds, classified according to flight style. Chiappe et al. (2007) used BI to infer a flightless lifestyle for the Late Cretaceous bird *Elsornis*.

In addition to the lengths of the skeletal elements of the wing, some studies have considered the length of the primary feathers, which contribute to the overall dimensions and aerodynamic properties of the wings in modern birds. Nudds et al. (2007) found a negative scaling relationship between primary feather

length and total arm length in modern birds, but also noted that differences in the lengths of all elements could function to alter the relative positions of joints, thus affecting wing kinematics and flight style. Research incorporating Mesozoic birds identified relatively short primary feathers as the ancestral state in theropods, and correlated disparity in the ratio of feather length to total arm length with the ecological divergence of modern birds (Wang et al., 2011). Further research found that variation in proportional primary feather lengths was correlated with flight style and could therefore be used to predict flight style in Mesozoic birds (Wang et al., 2011). A later study contradicted these results, finding that feather length did not alter the positioning of taxa in morphospace (comparing analyses which did and did not include primary feather length) and that wing data were insufficient to distinguish flight styles among modern birds (Chan et al., 2012).

One final line of research investigating the flight modalities of stem birds is based on the combined analysis of linear measurements of the wing skeletal elements and the length of the longest primary feather (Serrano et al., 2017), structures which are often preserved among the spectacular avifauna from the Jehol Biota of northeastern China (Chiappe and Meng 2016). Serrano et al. (2017) approach used multivariate models that made possible the accurate determination of key aerodynamic parameters (wing loading and aspect ratio) in a variety of stem birds. The strength of these predictions was supported by the fact that the variables used in their study showed similar scaling patterns in both modern and stem birds, as well as the similarity of the results obtained from the multivariate models to measurements from fossils preserving wing outlines (e.g., wing surface area and wing aspect ratio). The methodology designed by Serrano et al. (2017) has been applied to a variety of stem taxa (e.g., *Sapeornis*, *Confuciusornis*, various enantiornithines), indicating that these birds collectively covered much of the spectrum of fundamental flight modes seen in modern birds (e.g., soaring, gliding, flap and glide, soaring) (Serrano and Chiappe 2017; Serrano et al., 2017; Chiappe et al., 2019). Studies by Serrano and collaborators have clearly shown that stem birds had already evolved a diversity of flight modalities, with the accompanying implied ecological diversity, by the Early Cretaceous. Additional work has focused on specific taxa; for example, authors have proposed *Sapeornis* was most likely a thermal soaring bird (Serrano and Chiappe 2017) and that bohaiornithids were likely continuous flapping birds (Chiappe et al., 2019). While significantly advancing our understanding of the flight properties of stem birds, these interpretations do not consider the significant musculoskeletal differences with respect to modern birds, or how such differences may have influenced flight performance. However, the stark differences in musculoskeletal arrangement of the flight apparatus between modern and stem birds (e.g., Chiappe and Meng 2016; Mayr 2017) calls into question the validity of some of these direct ecomorphological inferences and suggests we might need a deeper knowledge of the mechanics of the wingstroke in pre-modern birds.

Hindlimb Measurements

A variety of studies have focused on the hindlimb instead of the wing as a correlate of ecological role in modern and ancient birds. One early study found birds to occupy a much broader hindlimb morphospace than non-avian theropods, suggesting that reliance on the wing allowed adaptive changes in the hindlimb that might correlate with ecological diversity (Gatesy and Middleton 1997). Later work, however, found that Mesozoic enantiornithine birds only partially overlapped in morphospace with modern birds and in general displayed less variation in hindlimb measurements, suggesting less ecological diversity among the group (Dyke and Nudds 2009).

Another study successfully used the proportions of the pedal phalanges of the third toe to separate terrestrial from arboreal modern birds (Hopson 2001). Subsequent studies utilized toe proportions to identify *Hongshanornis* (Zhou and Zhang 2005), *Jianchangornis* (Zhou et al., 2009), and *Archaeorhynchus* (Zhou et al., 2013) as terrestrial. A later study that expanded the original database of Hopson (2001), confirmed the initial findings, and inferred *Hollandia* as a terrestrial bird (Bell et al., 2010).

While some of these studies covered a broad swath of the phylogeny of early birds, Bell et al. (2019) focused on a narrower clade, the hesperornithiforms. These authors utilized a database of 15 measurements from the hindlimb (exclusive of the foot) of modern foot-propelled divers as well as the extinct Hesperornithiformes to investigate morphometric variation among avian families that had convergently evolved foot-propelled diving, while focusing on the extinct hesperornithiforms. Their results revealed that loons and grebes often clustered together in morphospace, as did cormorants and diving ducks, with hesperornithiforms sometimes occupying a unique area of the morphospace and sometimes overlapping with diving ducks or cormorants, depending upon which element was considered. In contrast to the conventional analogy between hesperornithiforms and living loons and grebes, Bell et al. (2019) demonstrated that hesperornithiforms are closer in morphospace (and perhaps functionally, with regard to foot-propelled locomotion) to diving ducks and cormorants.

Wing and Hindlimb Measurements

While a large number of studies have analyzed the wing and hindlimb separately, as discussed above, relatively few studies have examined the wing and hindlimb in combination. One of the first studies to do this focused on the use of CT data to measure the cortical thickness of the humerus and femur of modern birds, finding this sort of structural data to be more useful than element length one at identifying the primary force generator (wing vs. leg) (Habib and Ruff 2008). This study had the benefit of requiring only two elements for analysis, but was limited in requiring three-dimensional preservation.

Two studies to date have combined wing and hindlimb data from both modern and stem birds. Hinic-Frlog and Motani (2009) successfully combined a wide variety of skeletal measurements to sort modern aquatic birds into several locomotor-based ecological categories and confirm the

interpretation of *Hesperornis* as a foot-propelled diver. Bell and Chiappe (2011) demonstrated the division in morphospace of modern birds into several ecological categories based on foraging strategies and specified possible ecological niches for a number of Mesozoic birds.

Phylogenetic Signal in Morphometric Data

The degree to which evolutionary history contributes to the observed variation in morphometric datasets for modern and stem birds is often overlooked. The majority of quantitative studies described above did not control for phylogeny in their analyses of morphometric data. Some recent analyses have identified a significant phylogenetic signature in modern avian morphometric datasets, thus indicating the importance of including such methods in ecomorphological studies.

While various wing metrics have been used to infer flight styles or foraging strategies, as described above, Wang and Clarke (2015) analyzed wing shape and covert feather patterning in modern birds, finding that both wing shape variation and the extent of covert feather patterning were significantly correlated with phylogeny, but only weakly correlated with flight style. A study of airspeed in modern taxa also identified a strong phylogenetic signal (Alerstam et al., 2007).

A number of ecomorphological studies have focused on the utility of various skull and beak measurements for distinguishing foraging strategies or trophic guilds among modern birds. Benson et al. (2017) identified correlations between the size of the vestibular system and body mass as well as allometric changes in the shape of semicircular canals. The latter, however, exhibited a strong phylogenetic, and evidence for a link between flight style and labyrinth shape was ambiguous. Felice and Goswami (2018) identified a significant phylogenetic signal in three-dimensional geometric morphometric data on cranial shape in modern birds. Using this same dataset, Felice et al. (2019) found that, among modern birds, cranial morphology was poorly predicted by diet when phylogenetically transformed trait values were used. The beak is the region of the skull directly in contact with objects in the environment and might therefore be expected to be more strongly adapted to interacting with particular food items than other cranial regions. However, Navalón et al. (2019) found only a weak link between beak morphology and trophic ecology. This relationship seems to be more complex than often assumed (Gill 1995) and riddled with both trade-offs (the beak is used for many tasks beyond feeding) and many-to-one relationships between feeding autecology and morphology (a single beak shape could be associated with disparate ecologies).

A broad study that investigated a variety of morphological metrics of modern birds, including beak parameters, body size, tail remiges length, and tarsus size, found that increasing the number of morphometric dimensions in models increased their predictive abilities, but that foraging niches were less predictable than trophic levels or niches, with phylogenetic signal accounting for a significant portion of the match between phenotype models and trophic niches (Pigot et al., 2020).

Taken together, these studies highlight the importance of evaluating phylogenetic signal in morphometric data, something the majority of previous studies of Mesozoic avian

ecomorphology did not do. An exception to this trend is a recent preliminary analysis by Falk et al. (2020) of approximately 60 modern and Mesozoic bird species, which found a significant phylogenetic signal in hindlimb length data, whether analyzed in terms of leg and foot modules or included in a combined analysis.

The present study therefore analyzes measurements of the forelimb and hindlimb in modern and Mesozoic birds in order to quantify the role of phylogenetic signal in these morphometric data, and examines the possibility of using this large dataset to infer the ecology of Mesozoic birds.

MATERIALS AND METHODS

Because most prior work in avian paleoecomorphology has not taken phylogenetic hypotheses into account when developing ecological niche hypotheses for Mesozoic birds, this study aims to incorporate phylogenetic independent contrasts into an analysis of a large database of forelimb and hindlimb measurements from both modern and extinct birds in order to identify trends in the skeletal proportions of the limb that may have significance for inferring the ecology of extinct birds.

Morphometric Data

The data used in this analysis constitute an expansion of a previous database developed by Bell and Chiappe (2011), with 107 modern taxa added to more fully represent the phylogenetic diversity of Neornithes (**Supplemental Table S1**). Measurements of modern taxa were taken from the skeletal collections of the Ornithology Department at the Natural History Museum of Los Angeles County (NHMLAC). Length measurements were collected from the forelimb (humerus, ulna, radius, and carpometacarpus) and hindlimb (femur, tibiotarsus, tarsometatarsus, and phalanges I–III of pedal digit III). All measurements were taken from the same side of a single individual for each species. Measurements were taken from 583 modern bird species representing 28 orders (see **Supplemental Table S1**). Species were selected for inclusion based on availability in the collection of the NHMLAC, with the intent of sampling as broad a range of modern avian diversity (both phylogenetic and ecological) as possible.

Mesozoic taxa were added to the database using measurements reported in the primary literature or gathered from photographs using ImageJ (Schneider et al., 2012), with inclusion limited to taxa for which the full set of measurements listed above were available. Twenty-four taxa were added to the 16 taxa in the database of Bell and Chiappe (2011), for a total of 42 Mesozoic taxa (see **Supplemental Table S1** for complete list of specimens included).

Foraging Strategies

Modern taxa were assigned to one of eight foraging strategies, as defined by Bell et al. (2010) and Bell and Chiappe (2011). Classification into foraging categories was made on the basis of the ecological descriptions provided in Hoyo (2007). When necessary, the primary literature was consulted for clarification on specific habits. It is understood that the birds used in this study

are not limited to the behavior described by the bins below. Rather, the foraging bins are designed to describe the primary means by which the bird obtains food, as follows.

1. Terrestrial foragers: birds that forage on the ground, such as roadrunners or ostriches. Birds in this category gather food primarily or entirely through leg-powered foraging or stalking, thus presumably experiencing selective pressures for improved hindlimb performance. This category is not restricted to flightless birds.
2. Arboreal foragers: birds that forage in trees, such as woodpeckers or some species of parrot. Birds in this category perform activities such as fruit/seed collection or bark probing in trees. Selective pressures experienced by birds in this category might favor traits which enhance perching capabilities or short vertical flights.
3. Aerial foragers: birds that forage during flight, as well as birds that utilize flight to capture prey, such as hummingbirds or hawks. Birds in this category utilize flight to either spot food (whether live or carrion), or engage in foraging activities such as hawking, in which prey is captured on the wing. Selective pressures experienced by birds in this category would favor enhanced forelimb development for flight capabilities such as soaring or hovering.
4. Foot-propelled divers: birds that carry out extended powered dives underwater using their legs for propulsion, such as grebes or loons. Selective pressures on these birds might favor hindlimb adaptations for swimming.
5. Wing-propelled divers: birds that carry out extended powered dives underwater using their wings for propulsion, such as penguins or auks. Selective pressures on these birds might favor forelimb adaptations for swimming.
6. Dabblers: birds that primarily swim on the surface of the water while foraging and only briefly (if at all) submerge, such as dabbling ducks. Birds in this category engage in a different style of swimming than foot or wing-propelled divers, and are therefore expected to experience different selective pressures.
7. Waders: birds that forage for food walking in shallow water, such as spoonbills or flamingoes. These birds have many foraging behaviors in common with the terrestrial foragers described above, and are therefore expected to experience very different selective pressures from aquatic birds that swim or dive.

Phylogenetic Categories

All avian taxa were clustered into one of 14 phylogenetic categories that correspond to clades supported by most current phylogenetic hypotheses (Jarvis et al., 2014; Prum et al., 2015; Wang et al., 2016): non-ornithothoracines, Enantiornithes, stem Ornithuromorpha (exclusive of Neornithes), Palaeognathae, Galloanserae, Strisores, Otidimorphae, Columbimorphae, Gruiformes, Mirandornithes, Ardeae, Charadriiformes, Telluraves (exclusive of passerines), Passeriformes.

This categorization was undertaken to subdivide the taxa in the morphometric database into a manageable number of clades that each retained a statistically meaningful sample size.

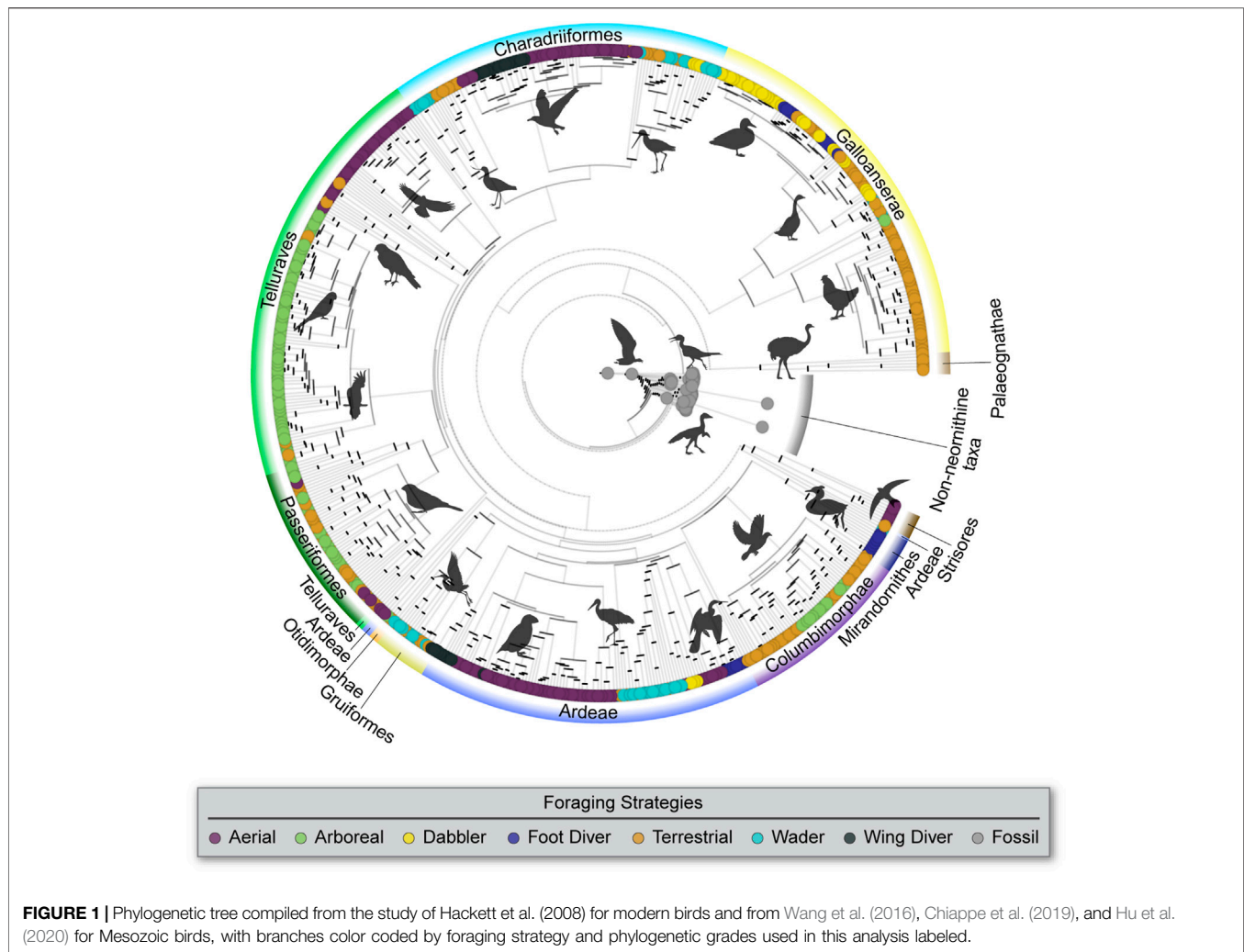


FIGURE 1 | Phylogenetic tree compiled from the study of Hackett et al. (2008) for modern birds and from Wang et al. (2016), Chiappe et al. (2019), and Hu et al. (2020) for Mesozoic birds, with branches color coded by foraging strategy and phylogenetic grades used in this analysis labeled.

Phylogenetic Hypothesis

An informal supertree was constructed by combining two phylogenies. First, for the modern birds in the database, a maximum clade credibility (MCC) time-calibrated consensus tree was generated using TreeAnnotator (Rambaut and Drummond 2015) from a population of 10,000 Hackett's all species trees (see www.birdtree.org and Jetz et al., 2012 for further details on these source trees) (Figure 1). Branch lengths were set equal to "Common ancestor" node heights. Second, for stem birds, the topology was constructed following recent phylogenetic hypotheses (Wang et al., 2016; Chiappe et al., 2019; Hu et al., 2020), with branch lengths calibrated using stratigraphic range data with the function `bin_timePaleoPhy` from the R package `palaeotree` (Bapst and Wagner 2019). Finally, the two phylogenies were integrated, taking the stem bird phylogeny as the receptor and rooting the modern bird phylogeny in the Neornithes terminal branch of the former using the interactive function `bind.tree` from the R package "ape" (Paradis and Schliep 2019). The phylogeny of modern birds was placed within the stem bird phylogeny at the neornithine node

divergence time that was obtained from the original calibration (Jetz et al., 2012).

Statistical Analyses

All statistical analyses were conducted in R (R Core Team 2020). To account for the several orders of magnitude of size variation among lineages, all measurement length data were \log_{10} -transformed. All analyses were conducted using both raw length and \log_{10} -transformed data to gain insight about the biases introduced by each kind of data.

A Principal Components Analysis (PCA) was run to summarize the variation in skeletal element proportions among the birds in the database. Regular and phylogenetic least squares (PGLS) regressions were used to explore the allometric scaling among the main limb elements between the following pairs of bones: femur-humerus (interlimb proportions), femur-tibiotarsus (upper leg proportions), and tibiotarsus-tarsometatarsus (lower leg proportions). Allometric slopes were then compared among all possible pairs of foraging and phylogenetic groups. These analyses were done using `procD.pgls` and pairwise functions from the

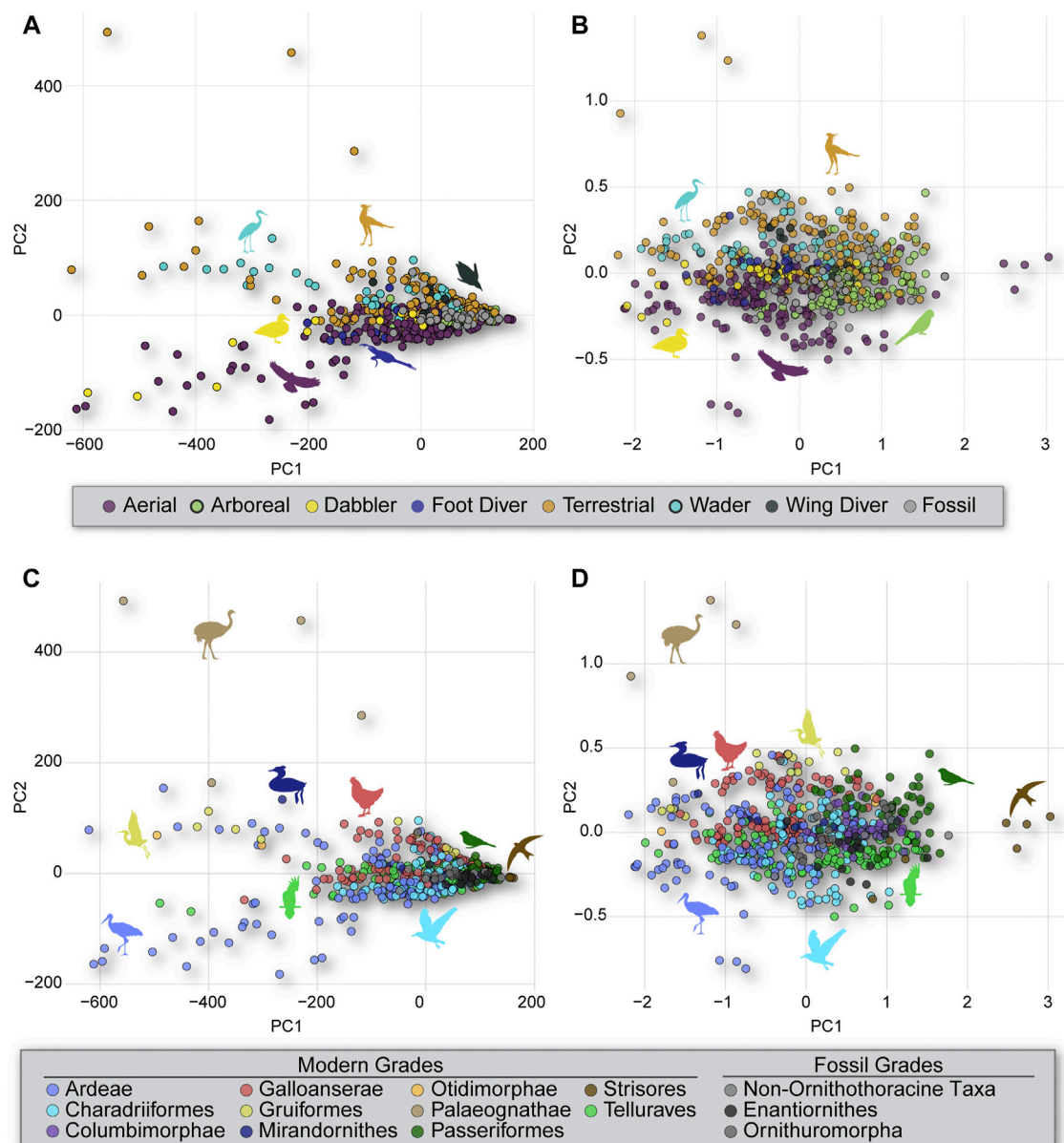


FIGURE 2 | PCA results of untransformed (A) and \log_{10} -transformed (B) morphometric data color-coded by foraging strategy. The same data color coded by clade, with untransformed (C) and \log_{10} -transformed (D) morphometric data. Notice how the raw data shown in (A,C) clearly display slope differences reflecting the scaling patterns between dimensions (PCs), whereas the \log_{10} -transformed data in (B,D) obscure those relationships.

packages geomorph (Adams and Otárola-Castillo 2013) and RRPP (Collyer and Adams 2018), respectively. For the foraging groups, regression scores were plotted by taxa, such that the data were projected onto the coefficients of the regression fit, each dot representing a unique taxon colored by its foraging strategy. For the sake of clarity, only the regression lines were plotted for the 14 phylogenetic groups, such that the data were projected by their predicted values onto the regression lines for these phylogenetic groups, showing the allometric slopes for the various groups clearer.

The phylogenetic signal in the morphometric data was measured by calculating Blomberg's K (Blomberg et al., 2003) for the entire dataset as well as for the femur/humerus, femur/tibiotarsus, and tibiotarsus/tarsometatarsus proportions, using the function *physignal* from the package *phytools* (Revell 2012). Empirical values were then compared with the predicted value of $K = 1$ for a constant Brownian Motion model of evolution for all the tree, which assumes diffusive evolution in which lineages exhibit no strong tendency to evolve toward certain trait values. Values of K less than one indicate weaker phylogenetic signal than expected and values

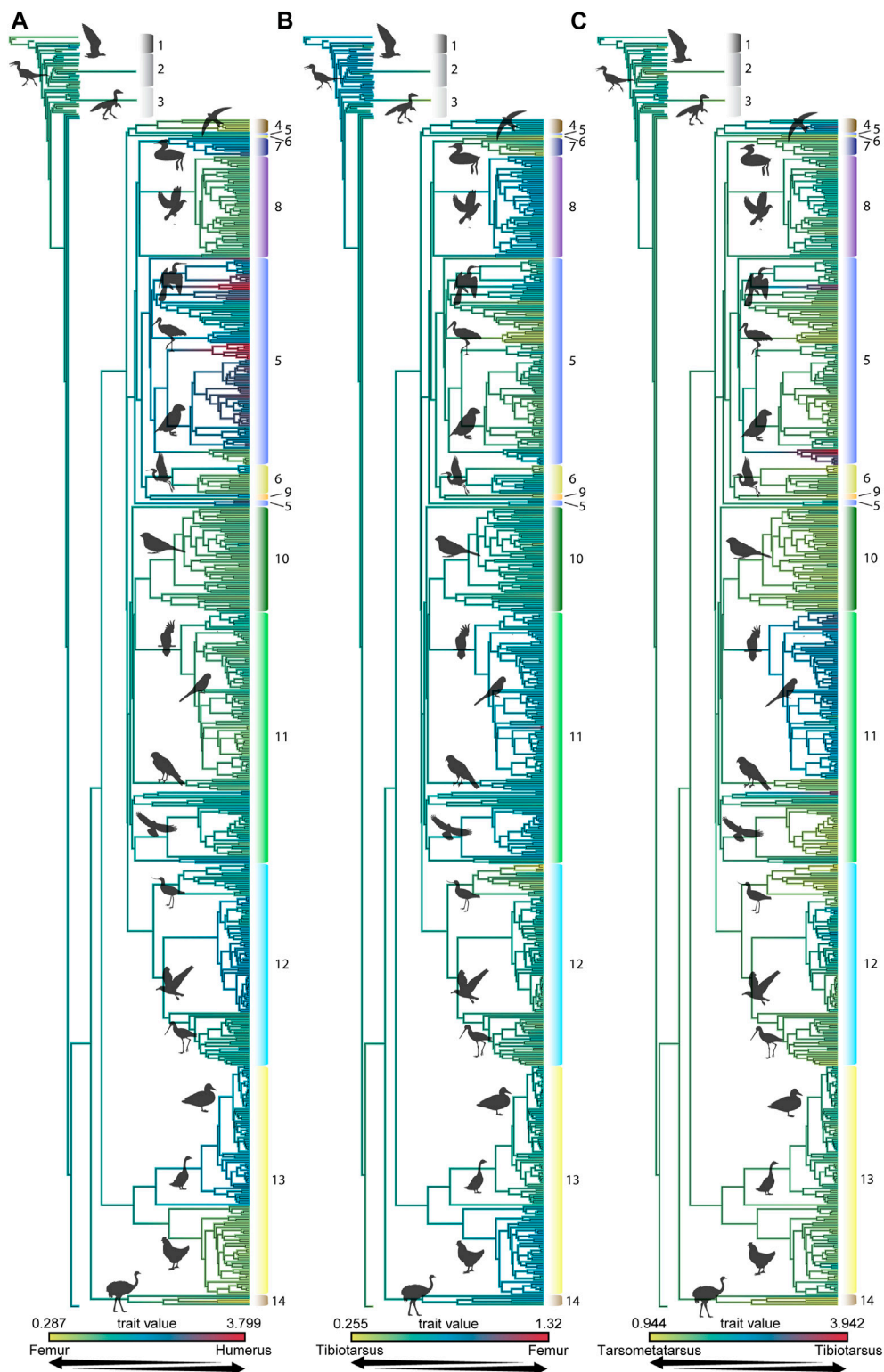


FIGURE 3 | Proportions of the untransformed lengths of the humerus to femur (**A**), femur to tibiotarsus (**B**), and tibiotarsus to tarsometatarsus (**C**) mapped onto the phylogeny created for this analysis. Phylogenetic grade numbers are as follows: 1 Non-ornithothoracine taxa, 2 Enantiornithes, 3 Ornithuromorpha, 4 Strisores, 5 Ardeae, 6 Gruiformes, 7 Mirandornithes, 8 Columbimorphae, 9 Otidimorphae, 10 Passeriformes, 11 Telluraves, 12 Charadriiformes, 13 Galloanserae, 14 Palaeognathae.

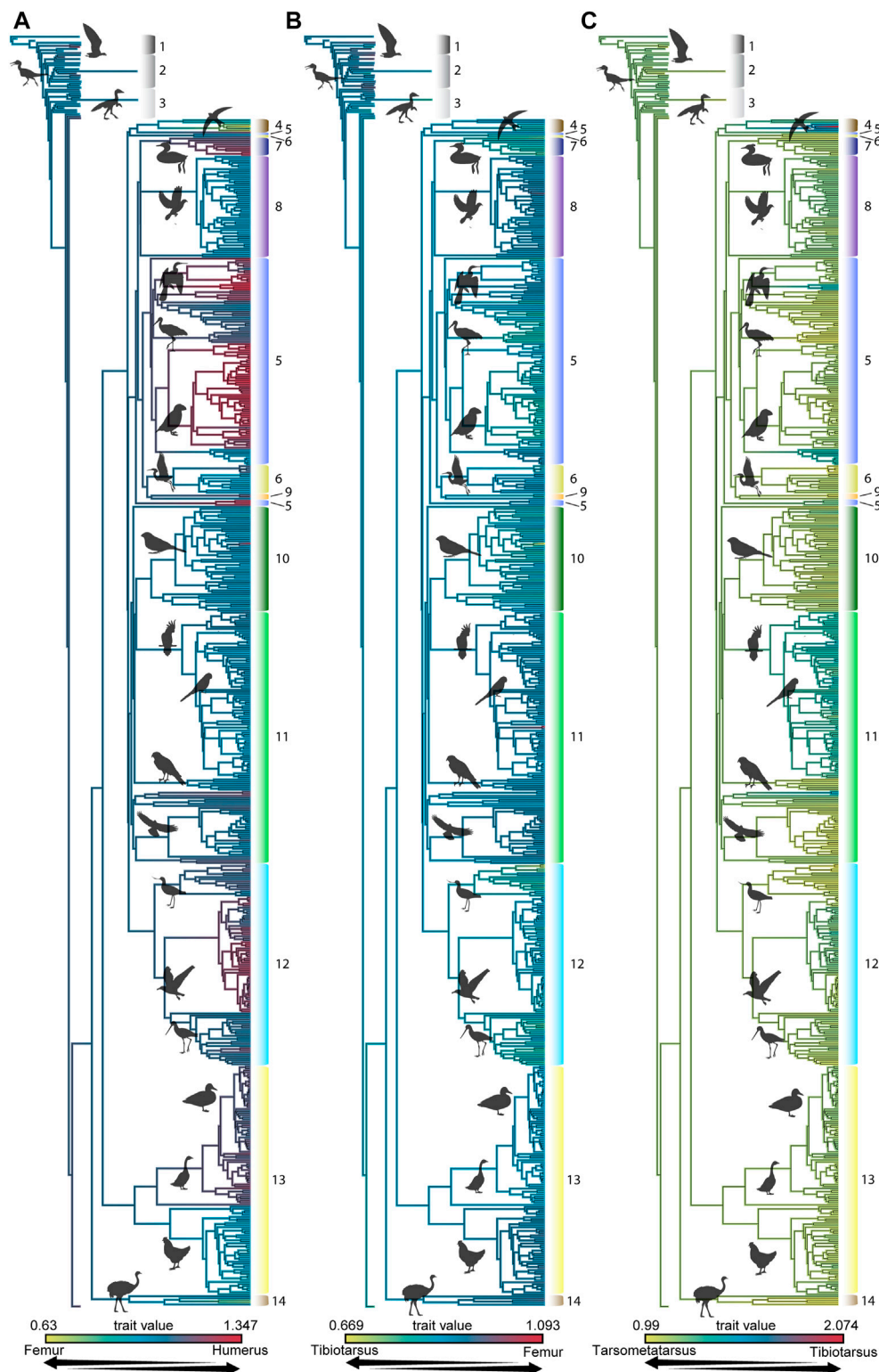


FIGURE 4 | Proportions of the \log_{10} -transformed lengths of the humerus to femur **(A)**, femur to tibiotarsus **(B)**, and tibiotarsus to tarsometatarsus **(C)** mapped onto the phylogeny created for this analysis. Phylogenetic grade numbers are as follows: 1 Non-ornithothoracine taxa, 2 Enantiornithes, 3 Ornithuromorpha, 4 Strisores, 5 Ardeae, 6 Gruiformes, 7 Mirandornithes, 8 Columbimorphae, 9 Otidimorphae, 10 Passeriformes, 11 Telluraves, 12 Charadriiformes, 13 Galloanserae, 14 Palaeognathae.

close to or surpassing one indicate stronger phylogenetic signal than expected. To further visualize the phylogenetic structure of our proportional data we plotted the values of the three proportions over our phylogeny using the function `contMap` from the package `phytools` (Revell 2012).

RESULTS

Principal Components Analysis

PCA results (Figure 2) show little separation among birds with different foraging strategies in morphospace. This is largely true for both untransformed (Figure 2) and \log_{10} -transformed (Figure 2) data. An exception is the separation of most waders and terrestrial birds from most aerial and dabbling birds along PC2. This separation is seen more clearly in the untransformed data than in the \log_{10} -transformed data. Mesozoic taxa largely fall within the region of morphospace where ecological groups overlap; however, *Patagopteryx* does plot outside that region, in the area occupied by modern waders and terrestrial birds. Phylogenetic groups exhibit a similar pattern but with even greater overlap in morphospace. Paleognaths were mostly separated from the other taxa and some members of Ardeae fall outside of the main cluster of birds into a unique area of morphospace for both the untransformed (Figure 2) and \log_{10} -transformed (Figure 2) data. Some members of Strisores and Passeriformes also fall into unique regions of the morphospace when considering \log_{10} -transformed data, but they fall closer to the main cluster of birds when using untransformed data.

Phylogenetic Signal

Blomberg's *K* (Blomberg et al., 2003) was calculated for all morphometric data in order to assess the overall phylogenetic signal in these data. This analysis returned a *K*-value of 0.4753 for the untransformed data and a *K*-value of 0.5175 for the \log_{10} -transformed data. This indicates a weak phylogenetic signal overall, but the *K*-values for individual elements varied, as described below. This highlights the importance of considering skeletal elements separately when assessing the covariation of phylogeny and morphometric patterns, rather than simply treating the data as a whole.

Interlimb Proportions and Scaling

The influence of phylogeny on the observed morphometric patterns is indicated by the *K*-values determined in this study and can be readily visualized using heatmaps of interlimb proportions mapped onto the consensus phylogeny used in this study (Figures 3, 4) or by mapping foraging strategy onto phylogeny (Figure 1). The proportion of the femur to the humerus exhibits a very high degree of phylogenetic signal [*K* = 1.669 and 1.456, for untransformed (Figure 3) and \log_{10} -transformed (Figure 4) data, respectively]. This indicates that most variation in the proportion between these two bones can be attributed to lineage-specific factors or allometry, and should not be straightforwardly interpreted as representing an ecomorphological signal. This notwithstanding, further

scrutiny of this pattern reveals that certain aerial birds like frigatebirds and tubenoses (albatrosses, shearwaters, fulmars), as well as foot propelled-divers like loons and grebes exhibit the most extreme values, having very large humeri but comparatively very short femora (Figure 5). Some phylogenetic analyses place these birds in a clade with Charadriiformes called Aequorlornithes (e.g., Prum et al., 2015), and so it is unsurprising that they are the most allometrically distinct with regard to interlimb scaling proportions (Figure 5; Supplemental Tables S2 and S3). Further confirming this pattern, dabblers, aerial foragers, and foot-propelled divers are the most statistically distinctive foraging groups, although this varies depending on whether untransformed or \log_{10} -transformed data are used, indicating differences in overall size are an important factor affecting this allometric pattern (Figure 5; Supplemental Tables S2 and S4).

Upper Leg Proportions and Scaling

The proportion of the femur to the tibiotarsus does not exhibit significant phylogenetic signal [*K* = 0.274 and 0.293, for untransformed (Figure 3) and \log_{10} -transformed (Figure 4) data, respectively], unlike the proportion of the femur to the humerus *g* described above. Ecomorphologically, the most extreme values of this proportional index are among very long-legged taxa with a wading foraging strategy, such as storks and herons (Ardeae), wading birds (Charadriiformes), and flamingoes (Mirandornithes) (Figure 6). The slopes for all these clades roughly align, and deviate from those for clades that forage primarily arboreally or terrestrially (Telluraves, Columbimorphae, Passeriformes) (Figure 6; Supplemental Tables S2 and S3). However, many of these differences collapse when using the \log_{10} -transformed data, indicating differences in total size are an important factor defining this allometric scaling (Figure 6). The general pattern is confirmed in three of seven of the pairwise comparisons, with aerial foragers being statistically distinct from the other foraging groups, as these taxa are more short-legged in general (Supplemental Tables S2 and S4). Arboreal taxa could be distinguished from many of the other groups (such as aerial, terrestrial, and wading groups) using raw data but not with \log_{10} -transformed data, revealing that these taxa tend to be very small in overall size (Supplemental Tables S2 and S4).

Enantiornithines exhibit significant differences in slope from many clades of modern birds and ornithuromorphs, and near significant differences from non-ornithothoracines. However, their regression line nearly overlaps that for modern passerines. This suggests stark differences in ecology among enantiornithines and ornithuromorphs in Mesozoic ecosystems, particularly during the Early Cretaceous.

Lower Leg Proportions and Scaling

The proportion of the tibiotarsus to the tarsometatarsus also exhibits a weak phylogenetic signal [*K* = 0.660 and 0.616 for untransformed (Figure 3) and \log_{10} -transformed (Figure 4) data, respectively]. Penguins and frigatebirds (Ardeae), parrots (Telluraves), and hummingbirds (Strisores) exhibit the most extreme values, and some long-legged taxa like ratites

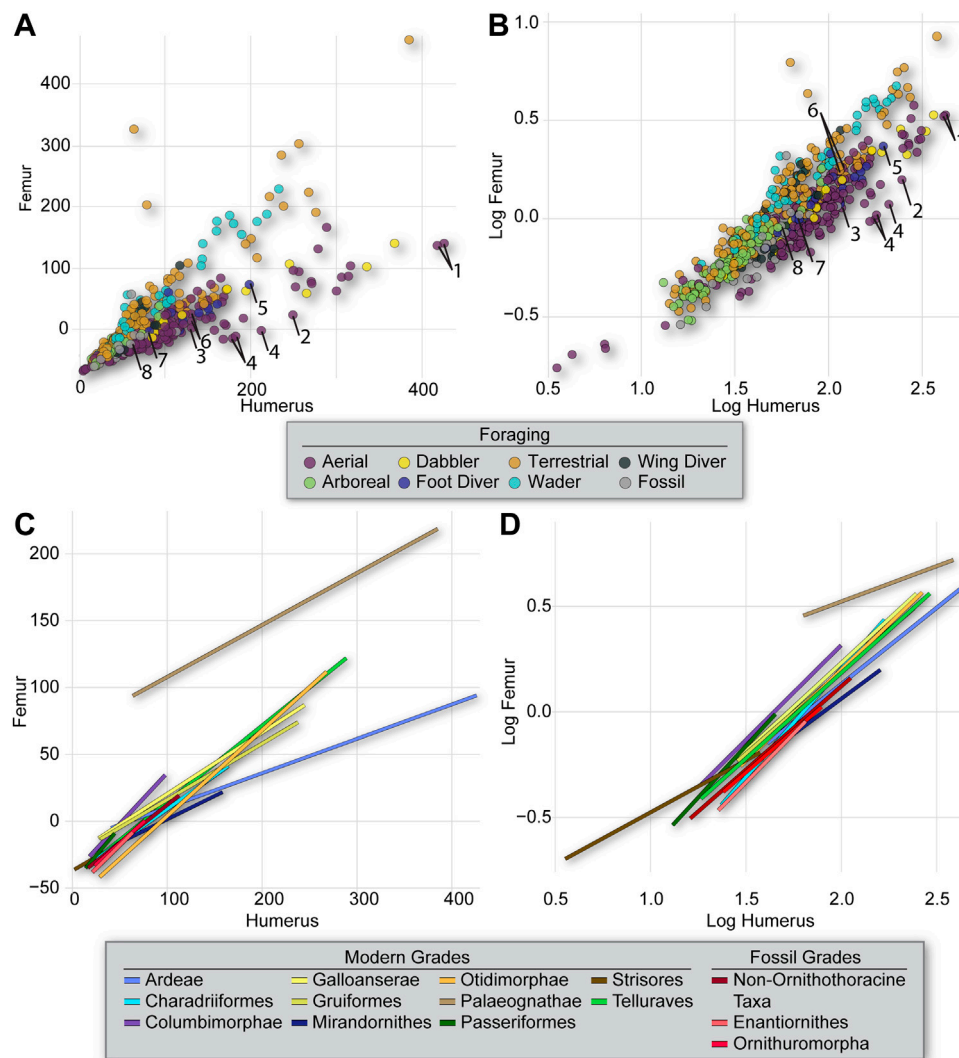


FIGURE 5 | Interlimb proportions (humerus vs. femur) from all specimens coded by foraging strategy (A,B) and slopes for phylogenetic groupings (C,D) resulting from the PGLS regression of the untransformed (A,C) and log₁₀-transformed (B,D) data. Notice clear differences among the regression slopes for the foraging groups and clades when using untransformed data (A,C) and their collapse when using log₁₀-transformed data (B,D). Taxa are numbered as follows in (A,B): Tubenoses-1 *Diomedea*, 2 *Phoebastria*, 3 *Calonectris*; Frigatebird-4 *Fregata*; Loon-5 *Gavia*; Grebe-6 *Aechmophorus*, 7 *Podiceps*, 8 *Rollandia*.

(Palaeognathae) or storks (Charadriiformes) exhibit extreme values in the other direction (Figure 7). As expected from the diverse phylogenetic positions of these taxa, there are practically no significant differences in scaling among the phylogenetic groups when considering the log₁₀-transformed data, with only Strisores differing from other clades (Supplemental Tables S2 and S3). Similarly, the only statistically significant differences in slope evident from the log₁₀-transformed data separate terrestrial and wading birds from all other foraging ecologies (i.e., dabbler, arboreal, aerial, plunge divers, and foot- and wing-propelled divers). When considering raw data, many more significant differences between clades and foraging groups emerge, as most groups exhibit idiosyncratic scaling relationships in which total size is a defining factor.

When considering the proportions of the lower limb, none of the groups of Mesozoic birds (non-ornithothoracine taxa, enantiornithines, ornithuromorphs) exhibit slopes that differ significantly from those for other groups of birds included in this analysis.

DISCUSSION

Our results are largely consistent in general patterns of morphospace occupation among lineages and foraging groups with previous studies that included a similar range of taxa (for example, Dyke and Nudds 2009; Bell et al., 2010; Bell and Chiappe 2011; Falk et al., 2020). All these studies found most avian taxa clustered together in morphospace,

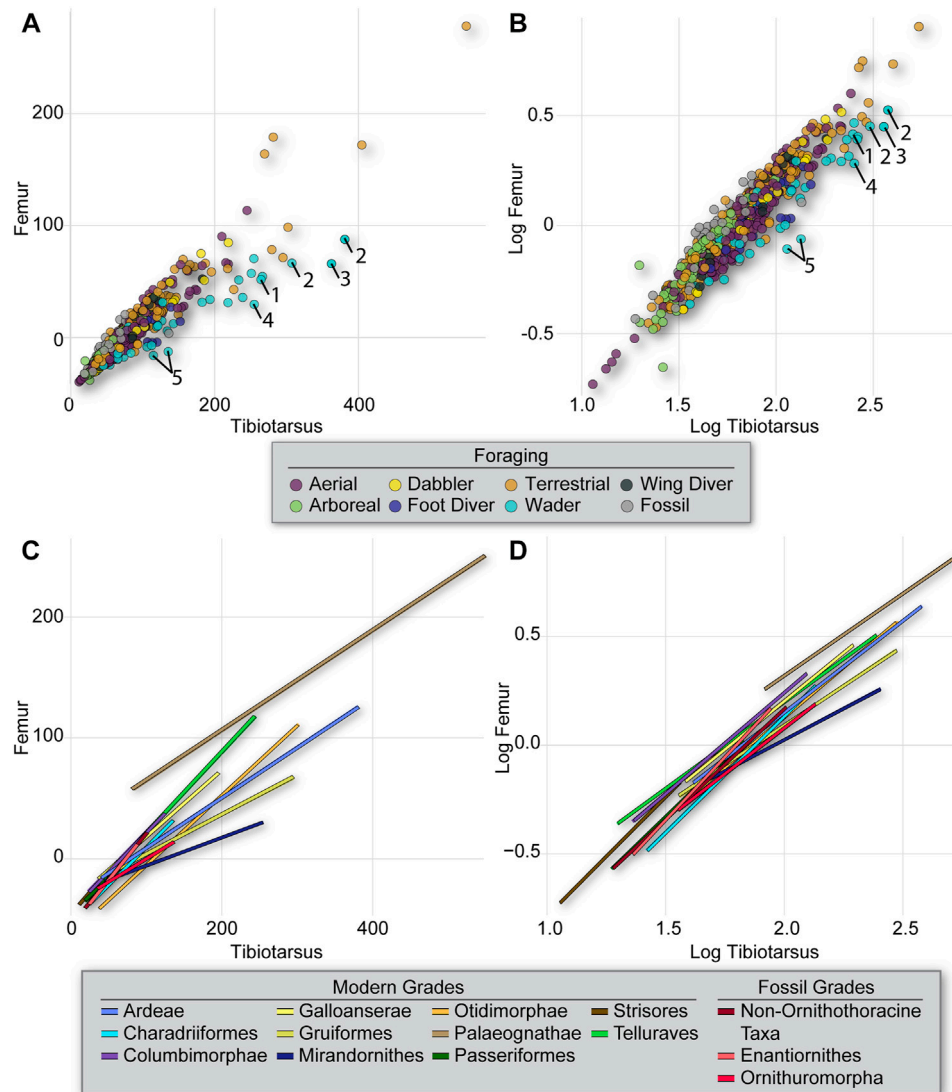


FIGURE 6 | Intralimb upper-leg proportions (femur vs. tibiotarsus) from all specimens coded by foraging strategy (A,B) and slopes for phylogenetic groupings (C,D) resulting from the PGLS regression of the untransformed (A,C) and log₁₀-transformed (B,D) data. As in Figure 5, slope differences collapse when using log₁₀-transformed data, confounding results. Taxa are numbered as follows in (A,B): Storks–1 *Ciconia*, 2 *Leptoptilos*, 3 *Ephippiorhynchus*; Flamingo–4 *Phoeniconaias*; Stilt–5 *Himantopus*.

regardless of ecology, with only small regions of morphospace in which specific ecological niches were isolated. The only taxa whose positions in morphospace may actually result from shared ecology are the terrestrial and wading birds, as these taxa belong to a variety of clades. Their shared morphospace may thus reflect similar selective pressures that drive elongation of the hindlimb for walking in grass or shallow water, foraging strategies that might be functionally similar. Other similarities in morphospace occupation, such as the overlap of dabbling and aerial birds, likely reflect the close relationship of the taxa in question. For example, all of the dabblers and aerial foragers that plot together outside of the common central morphospace are members of the same clade (Ardeae) (Figure 2).

As described above, our results indicate varying degrees of phylogenetic signal in inter- and intra-limb proportions (Figure 3). Proportions among pairs of elements are generally consistent within clades, and only rarely is intra-clade variation high. Several clades included in our analyses exhibit a variety of foraging strategies among their constituent taxa but little variation in element ratios. One example of this is the Charadriiformes, which are generally thought of as wading or shore birds, but actually encompass taxa with diverse foraging strategies, including wing propelled divers, aerial hunters, terrestrial birds, waders, and dabblers. Despite these differences in foraging style, the phylogenetic map of the humerus:femur ratio shows less variation than is present among the different clades considered in this study (Figure 3).

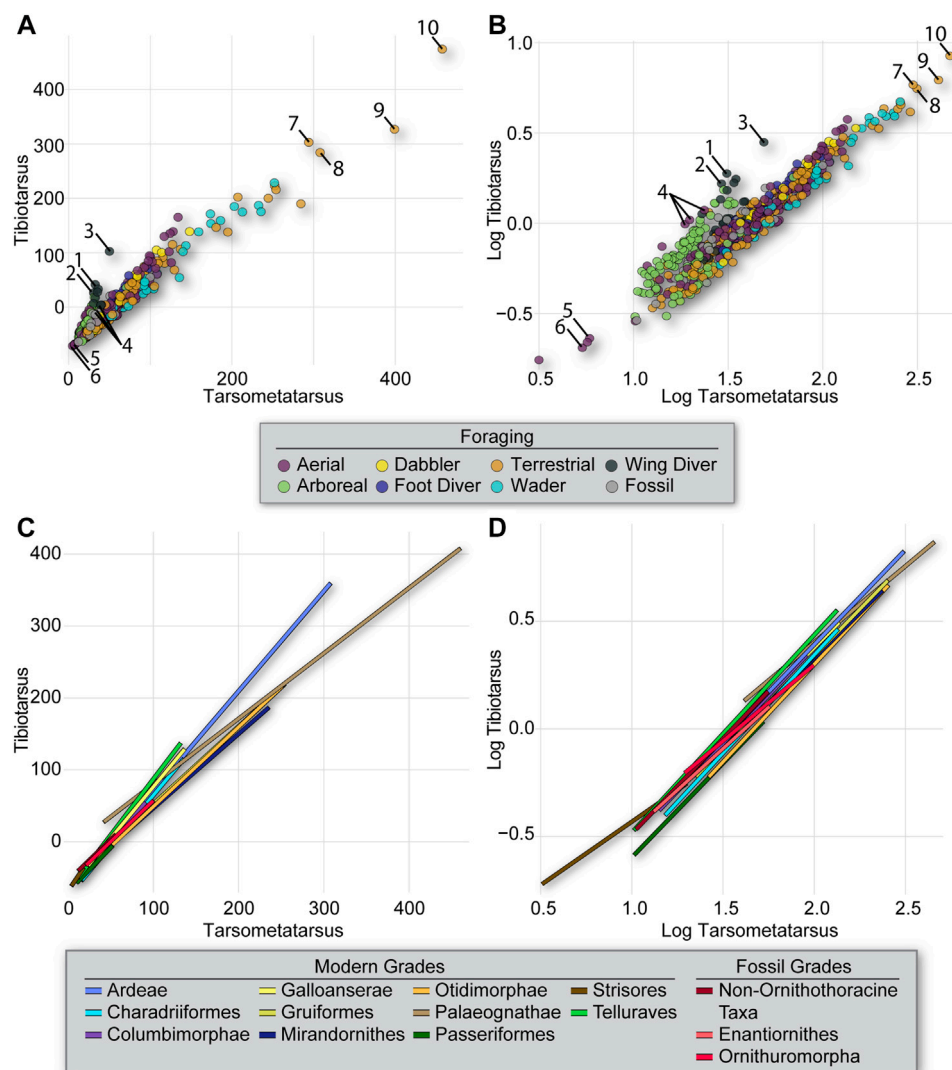


FIGURE 7 | Intralimb lower-leg proportions (tibiotalus vs tarsometatarsus) from all specimens coded by foraging strategy (A,B) and slopes for phylogenetic groupings (C,D) resulting from the PGLS regression of the untransformed (A,C) and log₁₀-transformed (B,D) data. As in Figure 5, slope differences collapse when using log₁₀-transformed data, confounding results. Taxa are numbered as follows in (A,B): Penguins–1 *Pygoscelis*, 2 *Eudyptes*, 3 *Aptenodytes*; Frigatebird–4 *Fregata*; Hummingbirds–5 *Aphantochoa*, 6 *Archilochus*; Storks–7 *Leptoptilos*, 8 *Epihippiorhynchus*; Ratites–9 *Dromaius*, 10 *Struthio*.

An example of this is the similar (and extreme) humerus:femur proportion values seen in both the aerial foraging frigatebirds and tubenoses and the foot-propelled diving loons. These birds all belong to the Ardeae, and thus may share an elongate humerus and proportionally reduced femur as a result of their close evolutionary relationship, despite having very different ecological habits.

However, we found some scaling differences among foraging groups regardless of phylogeny. Proportional relationships between the long bones of the hindlimb (femur:tibiotalus and tibiotalus:tarsometatarsus) were associated with low K-values, indicating weak phylogenetic signal. For example, the upper leg proportion reveals differences among several foraging strategies when pairwise comparisons are made between foraging groups (Supplemental Table S4). Foot-propelled divers, waders, and

terrestrial birds show significant differences from all other foraging strategies, but not from each other, in this proportion. When considered together, these three foraging strategies encompass a phylogenetically diverse sample of the birds included in this dataset, including members of each of the 13 clades used in this study except Strisores. This well-supported difference in scaling between birds that use their hindlimbs for foraging in some way and all other birds is intriguing. When considering the lower leg proportions, wing-propelled divers differ significantly from all other foraging groups. Wing-propelled diving birds are represented by penguins (Ardeae) and alcids (Charadriiformes) in this dataset, clades that are not particularly closely related (Figure 1).

Previous studies concur in detecting generalities about the contribution of phylogeny and ecology to variation in skeletal

morphometrics in birds. However, most such investigations have been relatively inconclusive regarding the biological contributions of the variables to such patterns, or in other words, regarding the real relationships among the original variables underlying the findings. This may occur because the original variables have been transformed into logarithms in an effort to constrain large size variation (i.e., dimensionality; Reymont et al., 1984; Sokal and Rohlf 2012), and hence accommodate scale by equalizing variances (Bryant 1989). What most authors fail to recognize, however, is that such transformation introduces a systematic bias into estimates of scaling coefficients, which is very rarely acknowledged, corrected, or reported (LaBarbera 1989). This situation is especially worrying when multivariate approaches are utilized, particularly PCA, because ecological processes may lead to scaling effects that render log-transformation inappropriate, as such methods are affected by any scale-dependent variation (Bryant 1989). By analyzing (and illustrating) the real scaling patterns among the original variables, our results have demonstrated that logarithmically transformed traits hide or at least obfuscate the ecological and evolutionary circumstances that lead to the observed scaling patterns, inevitably affecting the biological and ecological information that can be gained for paleobiological inference.

Our results support the interpretation that phylogenetic history strongly covaries with ecology in Neornithes. Therefore, although limb skeletal scaling patterns vary in several respects among lineages and/or foraging groups, the strong covariation implies that morphometric data on long bones have limited utility for identification of ecological trends at macroevolutionary scales in birds. Despite this, one interesting trend that is apparent in these analyses is the divergent scaling of the femur and tibiotarsus between enantiornithines and ornithuromorphs (**Figure 6** and **Supplemental Table S3**). Furthermore, enantiornithines do not differ significantly from non-ornithothoracine taxa with regard to this ratio, but ornithuromorphs do. This implies a deep divergence between ornithuromorph and non-ornithuromorph taxa in upper hindlimb scaling patterns. To our knowledge, this is the first time quantitative evidence for such a distinction between ornithuromorphs and other stem birds, some of which may have been sympatric, has been adduced. The vast majority of stem birds in the present dataset come from the Jehol Biota. For example, 11 enantiornithines, six ornithuromorphs, and five non-ornithothoracine taxa in the current dataset have all been reported from the Jiufotang Formation, one of the geologic units containing the Jehol Biota. Previously, qualitative studies of the Jehol birds have proposed a stark difference in ecology between enantiornithines and ornithuromorphs based primarily on inferred trophic niches, with enantiornithines purportedly specialized for arboreal niches and ornithuromorphs specialized for land-based or amphibious niches (primarily terrestrial or wading niches) (Hopson 2001; Zhou 2006; O'Connor 2012; O'Connor 2019; Field et al., 2018). The quantitative differences in the proportions of the upper

hindlimb bones identified here may relate to this previously proposed niche partitioning.

Furthermore, comparison of the results obtained from untransformed and log-transformed data highlights how data transformations can obscure real scaling relationships among the original variables in an analysis; for instance, using such treated data, past studies (Gatesy and Middleton 1997; Middleton and Gatesy 2000; Hopson 2001; Benson et al., 2017; Falk et al., 2020) detected that morphometric differences adhere to phylogeny, but the use of log-transformed data obscured that proportional relationships in skeletal elements are largely phylogenetic. This, in turn, implies that 1) ecology only latently underlies morphological differences at macroevolutionary scales such as those presented in this paper and thus, 2) any ecomorphological approximation based on function needs to be performed with careful consideration of phylogenetic context. This indicates that the numerous previous studies that have relied upon multivariate methods to draw inferences regarding the foraging strategies of stem birds without the proper data and without duly considering phylogenetic context should be viewed cautiously. Such caution does not imply that ecomorphological studies have no utility in the study of Mesozoic birds; rather, it highlights the importance of using appropriate methods that take into account the phylogenetic structure of the data (i.e., Wang and Clarke 2015; Falk et al., 2020; Pigot et al., 2020). Additionally, these results highlight the variability in phylogenetic signal obtained from different combinations of variables, with the humerus:femur proportion showing a much higher phylogenetic signal than the tibiotarsus:tarsometatarsus proportion. The variation in phylogenetic signal among different limb element ratios has not been previously demonstrated. Future work utilizing different types of morphometric data may identify morphometric proxies that are less tied to phylogenetic history.

DATA AVAILABILITY STATEMENT

The original contribution presented in the study are included in the article/**Supplementary Material**, further inquiries can be directed to the corresponding author.

AUTHOR CONTRIBUTIONS

The division of labor for this study was as follows: AB developed the database and supervised the collection of modern bird measurements, conducted the literature review, authored the introduction and database methods section of this paper, finalized the statistical methods, results, and discussion sections of this paper, developed initial drafts of figures, and coordinated all work among co-authors; JM, GN, and SN carried out the statistical analyses; JD collected the Mesozoic birds data and conducted the preliminary statistical assessments; and LC acquired funding, assisted with overall

project design, and provided specimen photographs for inclusion in the database. All authors contributed to writing and reviewing the manuscript.

FUNDING

This research was funded by generous donations of Gretchen Augustyn to the Dinosaur Institute of the NHMLA. SMN is funded by a FPI-UAM 2019 predoctoral grant from the Universidad Autónoma de Madrid. GN is funded by the European Union's Horizon 2020 research and innovation program 2014–2018 under grant agreement 677774 (European Research Council (ERC) Starting Grant: TEMPO).

REFERENCES

- Adams, D. C., and Otárola-Castillo, E. (2013). Geomorph: Anrpackage for the Collection and Analysis of Geometric Morphometric Shape Data. *Methods Ecol. Evol.* 4 (April), 393–399. doi:10.1111/2041-210X.12035
- Alerstam, T., Rosén, M., Bäckman, J., Ericson, P. G. P., Hellgren, O., and Hellgren, O. (2007). Flight Speeds Among Bird Species: Allometric and Phylogenetic Effects. *Plos Biol.* 5 (8), e197. doi:10.1371/journal.pbio.0050197
- Alvarenga, H. M. F., and Bonaparte, J. F. (1992). "A New Flightless Land Bird from the Cretaceous of Patagonia." *Natural History Museum Of Los Angeles County. Sci. Ser.* 36, 51–64.
- Bapst, D. W., and Wagner, P. (2019). *Paleotree: An R Package for Paleontological and Phylogenetic Analyses of Evolution*. Available at: <https://CRAN.Rproject.org/package=paleotree>.
- Barbosa, A. (1993). Morphometric Variation of the Hindlimb of Waders and its Evolutionary Implications. *Ardeola* 40 (1), 65–75.
- Bell, A., and Chiappe, L. M. (2016). A Species-Level Phylogeny of the Cretaceous Hesperornithiformes (Aves: Ornithuromorpha): Implications for Body Size Evolution Amongst the Earliest Diving Birds. *J. Syst. Palaeontology* 14 (3), 239–251. doi:10.1080/14772019.2015.1036141
- Bell, A., and Chiappe, L. M. (2011). Statistical Approach for Inferring Ecology of Mesozoic Birds. *J. Syst. Palaeontology* 9 (1), 119–133. doi:10.1080/14772019.2010.525536
- Bell, A. K., Chiappe, L. M., Erickson, G. M., Suzuki, S., Erickson, G. M., Suzuki, S., et al. (2010). Description and Ecologic Analysis of Hollanda Luceria, a Late Cretaceous Bird from the Gobi Desert (Mongolia). *Cretaceous Res.* 31 (1), 16–26. doi:10.1016/j.cretres.2009.09.001
- Bell, A., Wu, Y.-H., and Chiappe, L. M. (2019). Morphometric Comparison of the Hesperornithiformes and Modern Diving Birds. *Palaeogeogr. Palaeoclimatol. Palaeoecol.* 513, 196–207. doi:10.1016/j.palaeo.2017.12.010
- Benson, R. B. J., Starmer-Jones, E., Close, R. A., and Walsh, S. A. (2017). Comparative Analysis of Vestibular Ecomorphology in Birds. *J. Anat.* 231 (6), 990–1018. doi:10.1111/joa.12726
- Blomberg, S. P., Garland, T., and Ives, A. R. (2003). Testing for Phylogenetic Signal in Comparative Data: Behavioral Traits Are More Labile. *Evolution* 57 (4), 717–745. doi:10.1111/j.0014-3820.2003.tb00285.x
- Bock, W. J. (1994). Concepts and Methods in Ecomorphology. *J. Biosci.* 19 (4), 403–413. doi:10.1007/bf02703177
- Brocklehurst, N., Paul, U., Mannion, P. D., and O'Connor, J. (2012). The Completeness of the Fossil Record of Mesozoic Birds: Implications for Early Avian Evolution. *PLoS One* 7 (6), e39056. doi:10.1371/journal.pone.0039056
- Brusatte, S. L., O'Connor, J. K., and Jarvis, E. D. (2015). The Origin and Diversification of Birds. *Curr. Biol.* 25 (19), R888–R898. doi:10.1016/j.cub.2015.08.003
- Bryant, E. H. (1989). *Multivariate Morphometrics of Bottlenecked Populations. Evolutionary Biology of Transient Unstable Populations*. NY: New York, Springer, 19–31.

ACKNOWLEDGMENTS

The authors would like to thank the interns of Proyecto Dinosaurios, who assisted in the collection of portions of the modern bird database, and Stephanie Abramowicz, who photographed fossil specimens and contributed to the figures for this paper.

SUPPLEMENTARY MATERIAL

The Supplementary Material for this article can be found online at: <https://www.frontiersin.org/articles/10.3389/feart.2021.663342/full#supplementary-material>

- Chan, N. R., Dyke, G. J., and Benton, M. J. (2012). Primary Feather Lengths May Not Be Important for Inferring the Flight Styles of Mesozoic Birds. *Lethaia* 46 (September), 146–153. doi:10.1111/j.1502-3931.2012.00325.x
- Chiappe, L. M., and Bell, A. (2020). *Mesozoic Birds. Encyclopedia of Life Sciences American Cancer Society, Wiley-Blackwell, NJ: Hoboken, American Cancer Society*, 549–557. doi:10.1002/9780470015902.a0029218
- Chiappe, L. M., Suzuki, S., Dyke, G. J., Watabe, M., Tsogtbaatar, K., and Barsbold, R. (2007). A New Enantiornithine Bird from the Late Cretaceous of the Gobi Desert. *J. Syst. Palaeontology* 5 (2), 193–208. doi:10.1017/S1477201906001969
- Chiappe, L. M., and Witmer, L. M. (2002). "Osteology of the Flightless Patagopteryx Deferrariisi from the Late Cretaceous of Patagonia (Argentina)," in *Mesozoic Birds: Above the Heads of Dinosaurs*. Editor L. M. Chiappe (Berkeley, California: University of California Press), 281A316.
- Chiappe, L. M. (2018). Origin and Early Evolution. in *Ornithology: Foundation, Analysis, and Application*, 9.
- Chiappe, L. M., Meng, Q., Serrano, F., Sigurdson, T., Wang, M., Bell, A., et al. (2019). New Bohaiornis-like Bird from the Early Cretaceous of China: Enantiornithine Interrelationships and Flight Performance. *PeerJ* 7, e7846. doi:10.7717/peerj.7846
- Chiappe, L. M., and Meng, Q. (2016). *Birds of Stone: Chinese Avian Fossils from the Age of Dinosaurs*. Baltimore, MD: JHU Press.
- Chiappe, L. M., and Walker, C. A. (2002). Skeletal Morphology and Systematics of the Cretaceous Euenantiornithes (Ornithothoraces: Enantiornithes). *Mesozoic Birds: Above the Heads of Dinosaurs*, CA: Berkeley, University of California Press, 240–267.
- Close, R. A., and Rayfield, E. J. (2012). Functional Morphometric Analysis of the Furcula in Mesozoic Birds. *PLoS One* 7 (5), e36664. doi:10.1371/journal.pone.0036664
- Cobb, S. E., and Sellers, W. I. (2020). Inferring Lifestyle for Aves and Theropoda: A Model Based on Curvatures of Extant Avian Ungual Bones. *Plos One* 15 (2), e0211173. doi:10.1371/journal.pone.0211173
- Collyer, M. L., and Adams, D. C. (2018). RRPP: An R Package for Fitting Linear Models to High-dimensional Data Using Residual Randomization. *Methods Ecol. Evol.* 9 (7), 1772–1779. doi:10.1111/2041-210x.13029
- Dyke, G. J., and Nudds, R. L. (2009). The Fossil Record and Limb Disparity of Enantiornithines, the Dominant Flying Birds of the Cretaceous. *Lethaia* 42 (June), 248–254. doi:10.1111/j.1502-3931.2008.00135.x
- Falk, A. R., Lamsdell, J. C., and Gong, E. (2020). Principal Component Analysis of Avian Hind Limb and Foot Morphometrics and the Relationship between Ecology and Phylogeny. *Paleobiology*, 47, 1–23. doi:10.1017/pab.2020.39
- Feduccia, A. (1993). Evidence from Claw Geometry Indicating Arboreal Habits of Archaeopteryx. *Science* 259 (5096), 790–793. doi:10.1126/science.259.5096.790
- Felice, R. N., and Goswami, A. (2018). Developmental Origins of Mosaic Evolution in the Avian Cranium. *Proc. Natl. Acad. Sci. USA*. 115 (3), 555–560. doi:10.1073/pnas.1716437115
- Felice, R. N., Tobias, J. A., Pigot, A. L., and Goswami, A. (2019). Dietary Niche and the Evolution of Cranial Morphology in Birds. *Proc. R. Soc. B*. 286, 20182677. doi:10.1098/rspb.2018.2677

- Field, D. J., Benito, J., Chen, A., Jagt, J. W. M., and Ksepka, D. T. (2020). Late Cretaceous Neornithine from Europe Illuminates the Origins of Crown Birds. *Nature* 579 (7799), 397–401. doi:10.1038/s41586-020-2096-0
- Field, D. J., Bercovici, A., Berv, J. S., Dunn, R., Fastovsky, D. E., Lyson, T. R., et al. (2018). Early Evolution of Modern Birds Structured by Global Forest Collapse at the End-Cretaceous Mass Extinction. *Curr. Biol.* 28 (11), 1825–1831. doi:10.1016/j.cub.2018.04.062
- Fountaine, T. M. R., Benton, M. J., Dyke, G. J., and Nudds, R. L. (2005). The Quality of the Fossil Record of Mesozoic Birds. *Proc. R. Soc. B.* 272 (1560), 289–294. doi:10.1098/rspb.2004.2923
- Gatesy, S. M., and Middleton, K. M. (1997). Bipedalism, Flight, and the Evolution of Theropod Locomotor Diversity. *J. Vertebr. Paleontol.* 17 (2), 308–329. doi:10.1080/02724634.1997.10010977
- Gill, F. B. (1995). *Ornithology*. NY: New York, Macmillan. doi:10.1007/978-1-349-13596-7
- Glen, C. L., and Bennett, M. B. (2007). Foraging Modes of Mesozoic Birds and Non-avian Theropods. *Curr. Biol.* 17 (21), R911–R912. doi:10.1016/j.cub.2007.09.026
- Habib, M. B., and Ruff, C. B. (2008). The Effects of Locomotion on the Structural Characteristics of Avian Limb Bones. *Zoolog. J. Linn. Soc.* 153 (3), 601–624. doi:10.1111/j.1096-3642.2008.00402.x
- Hertel, F. (1995). Ecomorphological Indicators of Feeding Behavior in Recent and Fossil Raptors. *The Auk* 112 (4), 890–903. doi:10.2307/4089021
- Hinic-Frlog, Sanja, and Motani, R. (2009). Relationship between Osteology and Aquatic Locomotion in Birds: Determining Modes of Locomotion in Extinct Ornithurae. *J. Evol. Biol.* 23 (December), 372–385. doi:10.1111/j.1420-9101.2009.01909.x
- Hopson, J. A. (2001). Ecomorphology of Avian and Nonavian Theropod Phalangeal Proportions: Implications for the Arboreal versus Terrestrial Origin of Bird Flight. In Gauthier, J., and Gall, L., in *New Perspectives on the Origin and Early Evolution of Birds: Proceedings of the International Symposium in Honor of John H. Ostrom*. Peabody Museum of Natural History, CT: New Haven, Yale University, 211–235.
- Hou, L., Chiappe, L. M., Zhang, F., and Chuong, C.-M. (2004). New Early Cretaceous Fossil from China Documents a Novel Trophic Specialization for Mesozoic Birds. *Naturwissenschaften* 91 (1), 22–25. doi:10.1007/s00114-003-0489-1
- Hoyo, J. d. (2007). *Buteo Books: Handbook of Birds of the World*. Available at: <https://www.buteobooks.com/category/HBW.html>.
- Hu, H., O'Connor, J. K., and Zhou, Z. (2015). A New Species of Pengornithidae (Aves: Enantiornithes) from the Lower Cretaceous of China Suggests a Specialized Scansorial Habitat Previously Unknown in Early Birds. *PLoS One* 10 (6), e0126791. doi:10.1371/journal.pone.0126791
- Hu, H., O'Connor, J. K., Wang, M., Wroe, S., and McDonald, P. G. (2020). New Anatomical Information on the Bohaiornithid Longsunguis and the Presence of a Plesiomorphic Diapsid Skull in Enantiornithes. *J. Syst. Palaeontology* 18 (18), 1481–1495. doi:10.1080/14772019.2020.1748133
- Hui, C. A. (2002). Avian Furcula Morphology May Indicate Relationships of Flight Requirements Among Birds. *J. Morphol.* 251 (3), 284–293. doi:10.1002/jmor.1089
- Jarvis, E. D., Mirarab, S., Aberer, A. J., Li, B., Houde, P., Li, C., et al. (2014). Whole-Genome Analyses Resolve Early Branches in the Tree of Life of Modern Birds. *Science* 346 (6215), 1320–1331. doi:10.1126/science.1253451
- Jetz, W., Thomas, G. H., Joy, J. B., Hartmann, K., and Moores, A. O. (2012). The Global Diversity of Birds in Space and Time. *Nature* 491 (7424), 444–448. doi:10.1038/nature11631
- Kim, J. Y., Lockley, M. G., Seo, S. J., Kim, K. S., Kim, S. H., and Baek, K. S. (2012). A Paradise of Mesozoic Birds: The World's Richest and Most Diverse Cretaceous Bird Track Assemblage from the Early Cretaceous Haman Formation of the Gajin Tracksite, Jinju, Korea. *Ichnos* 19 (1–2), 28–42. doi:10.1080/10420940.2012.660414
- LaBarbera, M. (1989). Analyzing Body Size as a Factor in Ecology and Evolution. *Annu. Rev. Ecol. Syst.* 20 (1), 97–117. doi:10.1146/annurev.es.20.110189.000525
- Lim, J.-D., Zhou, Z., Martin, L. D., Baek, K.-S., and Yang, S.-Y. (2000). The Oldest Known Tracks of Web-Footed Birds from the Lower Cretaceous of South Korea. *Naturwissenschaften* 87 (6), 256–259. doi:10.1007/s001140050715
- Liu, Di., Chiappe, L. M., Serrano, F., Habib, M., Zhang, Y., and Meng, Q. (2017). Flight Aerodynamics in Enantiornithines: Information from a New Chinese Early Cretaceous Bird. *PLoS One* 12 (10), e0184637. doi:10.1371/journal.pone.0184637
- Lockley, M. G., and Harris, J. D. (2010). On the Trail of Early Birds: A Review of the Fossil Footprint Record of Avian Morphological and Behavioral Evolution. In Ulrich, P. K. and Willett, J. H. *Trends in Ornithology Research*, NY: New York, Nova Science Publishers, Inc. 1–63.
- Lockley, M. G., Li, R., Harris, J. D., Matsukawa, M., and Liu, M. (2007). Earliest Zygodactyl Bird Feet: Evidence from Early Cretaceous Roadrunner-like Tracks. *Naturwissenschaften* 94 (8), 657–665. doi:10.1007/s00114-007-0239-x
- Marsh, O. C. (1880). *Odontornithes: A Monograph on the Extinct Toothed Birds of North America*, Vol. 1. Washington, DC: Museum.
- Mayr, G. (2016). *Avian Evolution: The Fossil Record of Birds and its Paleobiological Significance*. NJ: Hoboken, John Wiley & Sons. doi:10.1002/9781119020677
- Mayr, G., Kaye, T. G., Pittman, M., Saitta, E. T., and Pott, C. (2020). Reanalysis of Putative Ovarian Follicles Suggests that Early Cretaceous Birds Were Feeding Not Breeding. *Scientific Rep.* 10 (1), 1–10. doi:10.1038/s41598-020-76078-2
- Mayr, G. (2017). Pectoral Girdle Morphology of Mesozoic Birds and the Evolution of the Avian Supracoracoideus Muscle. *J. Ornithology* 158 (3), 859–867. doi:10.1007/s10336-017-1451-x
- Middleton, K. M., and Gatesy, S. M. (2000). Theropod Forelimb Design and Evolution. *Zoolog. J. Linn. Soc.* 128 (2), 149–187. doi:10.1006/zjls.1998.019310.1111/j.1096-3642.2000.tb00160.x
- Mitchell, J. S., and Makovicky, P. J. (2014). Low Ecological Disparity in Early Cretaceous Birds. *Proc. R. Soc. B.* 281 (1787), 20140608. doi:10.1098/rspb.2014.0608
- Navalón, G., Bright, J. A., Marugán-Lobón, J., and Rayfield, E. J. (2019). The Evolutionary Relationship Among Beak Shape, Mechanical Advantage, and Feeding Ecology in Modern Birds*. *Evolution* 73 (3), 422–435. doi:10.1111/evo.13655
- Nudds, R. L., Dyke, G. J., and Rayner, J. M. V. (2007). Avian Brachial Index and Wing Kinematics: Putting Movement Back into Bones. *J. Zoolog.* 272 (2), 218–226. doi:10.1111/j.1469-7998.2006.00261.x
- Nudds, R. L., Dyke, G. J., and Rayner, J. M. V. (2004). Forelimb Proportions and the Evolutionary Radiation of Neornithes. *Proc. R. Soc. Lond. B* 271 (Suppl. 1_5), S324–S327. doi:10.1098/rsbl.2004.0167
- O'Connor, J. K., and Chiappe, L. M. (2011). A Revision of Enantiornithine (Aves: Ornithothoraces) Skull Morphology. *J. Syst. Palaeontology* 9 (1), 135–157. doi:10.1080/14772019.2010.526639
- O'Connor, J. K. (2019). The Trophic Habits of Early Birds. *Palaeogeogr. Palaeoclimatol. Palaeoecol.* 513, 178–195. doi:10.1016/j.palaeo.2018.03.006
- O'Connor, J. K. (2012). A Revised Look at Liaoningornis Longidigitrus (Aves). *Vertebrata Palasiatica* 50, 25–37. doi:10.1007/s10336-017-1451-x
- O'Connor, J. K., Chiappe, L. M., Gao, C., and Zhao, B. (2011). Anatomy of the Early Cretaceous Enantiornithine Bird Rapaxavis Pani. *Acta Palaeontologica Pol.* 56 (3), 463–475. doi:10.4202/app.2010.0047
- Paradis, E., and Schliep, K. (2019). Ape 5.0: An Environment for Modern Phylogenetics and Evolutionary Analyses in R. *Bioinformatics* 35 (3), 526–528. doi:10.1093/bioinformatics/bty633
- Peters, D. S., and Görgner, E. (1992). "A Comparative Study on the Claws of Archaeopteryx," in *Papers in Avian Paleontology Honoring Pierce Brodkorb*. Editor K. C. Campbell (CA: Los Angeles, Natural History Museum of Los Angeles County Science Series), 36, 29–37.
- Pigot, A. L., Miller, E. T., Bregman, T. P., Freeman, B. G., Roll, U., Seddon, N., et al. (2020). Macroevolutionary Convergence Connects Morphological Form to Ecological Function in Birds. *Nat. Ecol. Evol.* 4 (2), 230–239. doi:10.1038/s41559-019-1070-4
- Pike, A. V. L., and Maitland, D. P. (2004). Scaling of Bird Claws. *J. Zoolog.* 262 (1), 73–81. doi:10.1017/s0952836903004382
- Prum, R. O., Berv, J. S., Dornburg, A., Field, D. J., Townsend, J. P., Lemmon, E. M., et al. (2015). A Comprehensive Phylogeny of Birds (Aves) Using Targeted Next-Generation DNA Sequencing. *Nature* 526 (7574), 569–573. doi:10.1038/nature15697
- R Core Team (2020). *R: A Language and Environment for Statistical Computing*. Vienna, Austria: R Foundation for Statistical Computing. <https://www.R-project.org>.
- Rambaut, A., and Drummond, A. (2015). *TreeAnnotator v1.8.2: MCMC Output Analysis*. <http://beast.bio.ed.ac.uk>.

- Revell, L. J. (2012). Phytools: An R Package for Phylogenetic Comparative Biology (And Other Things). *Methods Ecol. Evol.* 3 (2), 217–223. doi:10.1111/j.2041-210X.2011.00169.x
- Reyment, R. A., Blackith, R. E., and Campbell, N. A. (1984). *Multivariate Morphometrics*, Vol. 10. MA: Cambridge, Academic Press.
- Richardson, F. (1942). *Adaptive Modifications for Tree-Trunk Foraging in Birds*. University of California Publications in Zoology. 46 (4). Available at: <http://paper/Adaptive-modifications-for-tree-trunk-foraging-in-Richardson/9755cedcf873177efcc883a22360d32b71551cd2>
- Schneider, C. A., Rasband, W. S., and Eliceiri, K. W. (2012). NIH Image to ImageJ: 25 Years of Image Analysis. *Nat. Methods* 9 (7), 671–675. doi:10.1038/nmeth.2089
- Serrano, F. J., and Chiappe, L. M. (2017). Aerodynamic Modelling of a Cretaceous Bird Reveals Thermal Soaring Capabilities during Early Avian Evolution. *J. R. Soc. Interf.* 14 (132), 20170182. doi:10.1098/rsif.2017.0182
- Serrano, F. J., Palmqvist, P., Chiappe, L. M., and Sanz, J. L. (2017). Inferring Flight Parameters of Mesozoic Avians through Multivariate Analyses of Forelimb Elements in Their Living Relatives. *Paleobiology* 43 (1), 144–169. doi:10.1017/pab.2016.35
- Sheard, C., Neate-Clegg, Neate-Clegg, M. H. C., Aloravainen, N., Jones, S. E. I., Vincent, C., MacGregor, H. E. A., et al. (2020). Ecological Drivers of Global Gradients in Avian Dispersal Inferred from Wing Morphology. *Nat. Commun.* 11 (1), 2463. doi:10.1038/s41467-020-16313-6
- Sokal, R. R., and Rohlf, F. J. (2012). *Biometry*. 4, K Ed. New York: W. H. Freeman.
- Tobias, J. A., Ottenburghs, J., and Pigot, A. L. (2020). Avian Diversity: Speciation, Macroevolution, and Ecological Function. *Annu. Rev. Ecol. Evol. Syst.* 51, 533–560. doi:10.1146/annurev-ecolsys-110218-025023
- Wang, Min., and Zhou, Z. (2017). The Evolution of Birds with Implications from New Fossil Evidences. *The Biology of the Avian Respiratory System*. NY: New York, Springer, 1–26.
- Wang, X., and Clarke, J. A. (2015). The Evolution of Avian Wing Shape and Previously Unrecognized Trends in Covert Feathering. *Proc. R. Soc. B.* 282 (1816), 20151935. doi:10.1098/rspb.2015.1935
- Wang, X., McGowan, A. J., and Dyke, G. J. (2011). Avian Wing Proportions and Flight Styles: First Step towards Predicting the Flight Modes of Mesozoic Birds. *PLOS ONE* 6 (12), e28672. doi:10.1371/journal.pone.0028672
- Wang, X., Cau, A., Kundrát, M., Chiappe, L. M., Ji, Q., Wang, Y., et al. (2020). A New Advanced Ornithuromorph Bird from Inner Mongolia Documents the Northernmost Geographic Distribution of the Jehol Paleornithofauna in China. *Hist. Biol.* 2020, 1–13. doi:10.1080/08912963.2020.1731805
- Wang, X., Luis, C. M., Teng, F., and Qiang, J. (2013). Xinghaiornis Lini (Aves: Ornithothoraces) from the Early Cretaceous of Liaoning: An Example of Evolutionary Mosaic in Early Birds. *Acta Geologica Sinica-English Edition* 87 (3), 686–689. doi:10.1111/1755-6724.12080
- Wang, Y., Wang, M., O'Connor, J. K., Wang, X., Zheng, X., and Zhang, X. (2016). A New Jehol Enantiornithine Bird with Three-Dimensional Preservation and Ovarian Follicles. *J. Vertebr. Paleontol.* 36 (2), e1054496. doi:10.1080/02724634.2015.1054496
- Yalden, D. W. (1985). “Forelimb Function in *Archaeopteryx*,” in *The Beginnings of Birds: Proceedings of the International Archaeopteryx Conference*, Eichstatt, Germany. Editors M. K. Hecht, J. H. Ostrom, G. Viohl, and P. Wellnhofer (Eichstätt). 1984.
- You, H.-L., Lamanna, M. C., Harris, J. D., and Chiappe, L. M. (2006). Jingmai O'Connor, Shu-An Ji, Jun-Chang Lü, Chong-Xi Yuan, Da-Qing Li, and Xing Zhang. A Nearly Modern Amphibious Bird from the Early Cretaceous of Northwestern China. *Science* 312 (5780), 1640–1643. doi:10.1126/science.1126377
- Zeffer, A. (2002). “Ecomorphology of the Hind Limb Bones of Birds”.
- Zhou, S., Zhou, Z., O'Connor, J. K., and O'Connor (2013). Anatomy of the Basal Ornithuromorph bird *Archaeorhynchus Spathula* from the Early Cretaceous of Liaoning, China. *J. Vertebr. Paleontol.* 33 (1), 141–152. doi:10.1080/02724634.2012.714431
- Zhou, Z. (2006). Evolutionary Radiation of the Jehol Biota: Chronological and Ecological Perspectives. *Geol. J.* 41 (3–4), 377–393. doi:10.1002/gj.1045
- Zhou, Z., Zhang, F., and Li, Z. H. (2009). A New Basal Ornithurine Bird (*Jianchangornis Microdonta* Gen. et Sp. Nov.) from the Lower Cretaceous of China. *Vertebrata Palasiatica* 47 (4), 299–310.
- Zhou, Z., and Zhang, F. (2005). “Discovery of an Ornithurine Bird and its Implication for Early Cretaceous Avian Radiation,” in *Proceedings of the National Academy of Sciences*, 102 (52), 18998–19002. doi:10.1073/pnas.0507106102

Conflict of Interest: The authors declare that the research was conducted in the absence of any commercial or financial relationships that could be construed as a potential conflict of interest.

Copyright © 2021 Bell, Marugán-Lobón, Navalón, Nebreda, DiGiulido and Chiappe. This is an open-access article distributed under the terms of the Creative Commons Attribution License (CC BY). The use, distribution or reproduction in other forums is permitted, provided the original author(s) and the copyright owner(s) are credited and that the original publication in this journal is cited, in accordance with accepted academic practice. No use, distribution or reproduction is permitted which does not comply with these terms.

Advantages of publishing in Frontiers



OPEN ACCESS

Articles are free to read
for greatest visibility
and readership



FAST PUBLICATION

Around 90 days
from submission
to decision



HIGH QUALITY PEER-REVIEW

Rigorous, collaborative,
and constructive
peer-review



TRANSPARENT PEER-REVIEW

Editors and reviewers
acknowledged by name
on published articles

Frontiers

Avenue du Tribunal-Fédéral 34
1005 Lausanne | Switzerland

Visit us: www.frontiersin.org

Contact us: frontiersin.org/about/contact



REPRODUCIBILITY OF RESEARCH

Support open data
and methods to enhance
research reproducibility



DIGITAL PUBLISHING

Articles designed
for optimal readership
across devices



FOLLOW US

@frontiersin



IMPACT METRICS

Advanced article metrics
track visibility across
digital media



EXTENSIVE PROMOTION

Marketing
and promotion
of impactful research



LOOP RESEARCH NETWORK

Our network
increases your
article's readership